Late Palaeozoic to Early Mesozoic evolution of the Palaeotethys in Turkey: Insights from the Karaburun Peninsula and the Konya Complex

Dissertation
zur Erlangung des mathematisch-naturwissenschaftlichen Doktorgrades
"Doctor rerum naturalium"
der Georg-August-Universität Göttingen

im Promotionsprogramm Geowissenschaften / Geographie
der Georg-August-University School of Science (GAUSS)

vorgelegt von

Kersten Löwen
aus Lüdenscheid

Göttingen 2018

Betreuungsausschuss

Prof. Dr. Hilmar von Eynatten, Sedimentologie und Umweltgeologie, GZG, Georg-August-Universität Göttingen

PD Dr. Guido Meinhold, Sedimentologie und Umweltgeologie, GZG, Georg-August-Universität Göttingen; School of Geography, Geology and the Environment, Keele University

Mitglieder der Prüfungskommission

Referent: Prof. Dr. Hilmar von Eynatten, Sedimentologie und Umweltgeologie, GZG, Georg-August-Universität Göttingen

Korreferent: PD Dr. Guido Meinhold, Sedimentologie und Umweltgeologie, GZG, Georg-August-Universität Göttingen; School of Geography, Geology and the Environment, Keele University

Weitere Mitglieder der Prüfungskommission

Prof. Dr. Jonas Kley, Strukturgeologie, GZG, Georg-August-Universität Göttingen

Prof. Dr. Volker Thiel, Geobiologie, GZG, Georg-August-Universität Göttingen

Dr. Andreas Kronz, Geochemie, GZG, Georg-August-Universität Göttingen

Dr. Nicole Nolte, Isotopengeologie, GZG, Georg-August-Universität Göttingen

Tag der mündlichen Prüfung: 15.11.2018

Hiermit erkläre ich an Eides statt, die vorliegende Arbeit selbstständig angefertigt zu haben und dabei keine anderen als die von mir angegebenen Quellen und Hilfsmittel benutzt zu haben. Ferner erkläre ich, dass ich nicht anderweitig versucht habe, eine Dissertation einzureichen.

Göttingen, 11. Oktober 2018

Kersten Löwen

Contents

ACKNOWLEDGEMENTS

First of all I would like to thank all members of the department of Sedimentology and Environmental Geology. It was a pleasure to work with such a nice team in a friendly, positive and familiar atmosphere. My special gratitude goes to Guido Meinhold and Hilmar von Eynatten for the possibility of doing this research and for their guidance and patience during the whole time of my thesis.

Many thanks to Guido Meinhold, Arzu Arslan and Talip Güngör for the nice time in the field, for their constructive discussion and their helpful advices. I am also grateful to Irina Ottenbacher, Judit Dunkl and Cornelia Friedrich for their helping hands during sample preparation and laboratory work.

Finally I wish to thank my friends and family for constant encouragement and emotional support during the past four years of my PhD project.

PREFACE

This cumulative doctoral thesis is composed of five chapters. The first chapter presents a short introduction to the main issue of the thesis and outlines the motivation and main objectives. The following chapters 2 to 4 are manuscripts (listed below), which have been published in peer-reviewed international journals. The last chapter is a short synopsis, highlighting the most important results of the study.

Löwen K, Meinhold G, Güngör T (2017) Provenance and tectonic setting of Carboniferous–Triassic sandstones from the Karaburun Peninsula, western Turkey: A multi-method approach with implications for the Palaeotethys evolution. Sedimentary Geology, 375:232–255

Löwen K, Meinhold G, Güngör T, Berndt J (2017) Palaeotethys-related sediments of the Karaburun Peninsula, western Turkey: constraints on provenance and stratigraphy from detrital zircon geochronology. International Journal of Earth Sciences, 8:2771–2796

Löwen K, Meinhold G, Arslan A, Güngör T, Berndt J (2019) Evolution of the Palaeotethys in the Eastern Mediterranean: A multi-method approach to unravel the age, provenance and tectonic setting of the Upper Palaeozoic Konya Complex and its Mesozoic cover sequence (south-central Turkey). International Geology Review, https://doi.org/10.1080/00206814.2019.1616619

ABSTRACT

The greater aim of this PhD thesis is to test the current palaeotectonic models for the Late Palaeozoic to Early Mesozoic evolution of the Palaeotethys in the Eastern Mediterranean. Therefore, siliciclastic rocks from two key areas – the Karaburun Peninsula in western Turkey and the Konya Complex in south-central Turkey – were examined in detail. These occurrences are of special importance as they exhibit virtually unmetamorphosed Palaeozoic and Mesozoic sedimentary successions and their role within the Tethyan realm has previously been interpreted in different ways. This dissent is caused by the lack of provenance data that could provide information to interpret the history of these sediments and to deduce characteristics of their source area. In the present study this issue is addressed by conducting an extensive provenance analysis using multiple techniques including thin-section petrography, whole-rock geochemistry, detrital zircon U–Pb geochronology and single-grain geochemistry (rutile, garnet, Cr-spinel).

After a short introduction into the subject (**Chapter 1**), the new data from both study areas are presented and discussed (**Chapter 2–4**). The focus of **Chapter 2 and 3** was placed on the Karaburun Peninsula in western Turkey. The first manuscript discusses the main compositional features (petrography and bulk-rock geochemistry) of the Late Palaeozoic sequence (Alandere, Küçükbahçe and Dikendağı formations) and the unconformably overlying Triassic rocks (Güvercinlik and Gerence formations and the İdecik unit). These data are combined with single-grain analyses of detrital rutile, garnet and Cr-spinel to unravel the origin and depositional tectonic setting of the studied rocks. In this context, a set of well-established and novel diagrams for the tectonic discrimination of siliciclastic sediments, using major and trace elements was tested. It has been shown that the efficiency of this approach is strongly dependent on the

correct choice of a representative database and is hampered by effects of grain-size and age of the sediments. Overall, provenance sensitive data highlight the importance of felsic, amphibolite- to eclogite-facies source rocks for the studied stratigraphic sequence of the Karaburun Peninsula and indicate the presence of a nearby volcanic arc. To some extent, detritus was also derived from Palaeozoic ophiolites as documented by detrital Cr-spinels which were likely derived from harzburgite and lherzolite rocks (Alandere and Küçükbahçe formations) and podiform chromitites (Gerence Formation). The emphasis in **Chapter 3** was placed on U–Pb ages from detrital zircons from sandstones of the Karaburun Peninsula to constrain their maximum depositional ages and identify possible source areas. Especially the timing of sediment accumulation for the supposedly Ordovician or Early Carboniferous Küçükbahçe and Dikendağı formations is a matter of discussion. The new data have set the limit of maximum sedimentation ages to Late Carboniferous–Early Permian and allowed to present a revised stratigraphic section for the Palaeozoic part of the Karaburun Peninsula. Furthermore, the obtained age spectra have been compared to data from Late Neoproterozoic and Palaeozoic potential igneous source rocks exposed in the Eastern Mediterranean region. In particular, the presence of prominent age populations from 350–450 Ma and 400–500 Ma in some samples provide strong evidence for sediment supply from units of the southern Eurasian margin, which is in agreement with previous reconstructions for the nearby Aegean islands of Chios and Inousses. **Chapter 4** provides an extensive dataset for siliciclastic rocks of the Upper Palaeozoic Konya Complex and its Mesozoic cover sequence in south-central Turkey. The data are discussed to unravel their age, composition and origin and to shed light on the depositional history of the Konya basin. Despite missing evidence in terms of Late Palaeozoic (or younger) zircon populations in samples of the widely exposed Halıcı Formation, a Pennsylvanian–Cisuralian depositional age is inferred from available biostratigraphic data of the mélange. Information on provenance, inferred from the detrital zircon record of these rocks indicate sediment supply from both, units of the southern Eurasian margin but North Gondwana as well. Similar to source rocks for the stratigraphic sequence on the Karaburun Peninsula, our data suggest low- to medium-grade sedimentary sources of felsic character for both, the Halıcı and Ardıçlı formations. However, common components in the Chios–Karaburun units (garnet, Cr-spinel, arc-derived material) are virtually absent in sediments of the Konya Complex. An open question at the end of the study is the

provenance of sediments from the Late Triassic Ardıçlı Formation, even though a very proximal source is most likely.

To conclude, the data from this study support a palaeotectonic model that combines aspects of different reconstructions. Most of the Upper Palaeozoic Chios–Karaburun units were deposited along the southern Eurasian margin in mid-Carboniferous to Early Permian time, whereas parts of the time-equivalent Halıcı Formation of the Konya Complex document sediment supply from North Gondwana as well. Northward directed subduction of Palaeotethys lithosphere was still active during that period but ceased until Late Triassic time, while the nature of the northern Gondwana margin remains controversial.

KURZFASSUNG

Das übergeordnete Ziel dieser Doktorarbeit ist es, die bestehenden paläotektonischen Modelle zur spät-paläozoischen bis früh-mesozoischen Entwicklung der Paläotethys im östlichen Mittelmeerraum zu überprüfen. Zu diesem Zweck sind siliziklastische Gesteine zweier Schlüsselregionen – der Karaburun Halbinsel im Westen der Türkei und des Konya Komplexes in der Süd-Zentral Türkei – detailliert untersucht worden. Diese Regionen sind aufgrund ihrer nahezu nicht metamorphen, sedimentären Gesteine paläozoischen und mesozoischen Alters von besonderer Bedeutung und wurden in Rekonstruktionen der Tethys auf verschiedene Weise interpretiert. Die unterschiedlichen Anschauungen resultieren aus der dünnen Datenbasis, die es nicht erlaubt die Geschichte der Sedimente zu verfolgen und Aussagen über deren Liefergebiet zu treffen. Die vorliegende Arbeit nimmt sich diesem Problem an, indem eine umfassende Liefergebietsanalyse dieser Sedimente durchgeführt wurde. Dafür wurden die Gesteine im Dünnschliff mikroskopisch untersucht, die Gesamtgesteinsgeochemie bestimmt, mineralchemische Analysen (Rutil, Granat, Cr-Spinel) durchgeführt und detritische Zirkone mit U–Pb datiert.

Nach einer kurzen Einführung in das Thema der vorliegenden Arbeit (**Kapitel 1**) werden die neuen Daten beider Arbeitsgebiete präsentiert und diskutiert (**Kapitel 2–4**). Der Schwerpunkt von **Kapitel 2 und 3** war die Karaburun Halbinsel im Westen der Türkei. Im ersten Manuskript werden die Hauptmerkmale (Petrographie und Geochemie) der spät-paläozoischen Abfolge (Alandere, Küçükbahçe and Dikendağı Formationen), sowie der diskordant überlagernden, triassischen Gesteine (Güvercinlik und Gerence Formationen und der İdecik Einheit) diskutiert. Diese Daten werden durch Einzelkorn-Analysen von detritischen Rutilen, Granaten und Cr-Spinellen ergänzt und hinsichtlich der Herkunft und des tektonischen Milieus zur Zeit der Ablagerung der un-

tersuchten Proben diskutiert. Zu diesem Zweck sind eine Reihe von etablierten und neuartigen Diagrammen zur Diskriminierung des tektonischen Milieus von siliziklastischen Gesteinen auf Grundlage ihrer Haupt- und Spurenelementzusammensetzung getestet worden. Wie sich herausgestellt hat, ist die Tauglichkeit dieser Diagramme stark abhängig von der Wahl einer repräsentativen Datenbasis und wird durch weitere, nicht vollständig verstandene Effekte, wie Korngröße und Alter der Gesteine beeinflusst. Zusammenfassend deuten die Daten der gesamten stratigraphischen Abfolge der Karaburun Halbinsel auf ein Liefergebiet mit hauptsächlich felsischen, amphibolit- bis eklogit-faziellen Gesteinen hin und geben Hinweise auf einen nahegelegenen vulkanischen Bogen. Cr-Spinelle von Lherzoliten und Harzburgiten (Alandere and Küçükbahçe Formationen) sowie von podiformen Chromiten (Gerence Formation) belegen, dass ein Teil des Detritus auch von paläozoischen Ophioliten stammt. In **Kapitel 3** wird ein umfassender Datensatz von U–Pb Altern detritischer Zirkone von Sandsteinen der Karaburun Halbinsel präsentiert, um deren maximales Ablagerunsalter zu bestimmen und mögliche Liefergebiete zu identifizieren. Ganz besonders das Ablagerungsalter der scheinbar ordovizischen oder früh-karbonischen Küçükbahçe and Dikendağı Formationen steht zur Diskussion. Mithilfe des neuen Datensatzes konnte das maximale Sedimentationsalter auf das späte Karbon bis frühe Perm eingegrenzt werden und ein überarbeitetes stratigraphisches Profil für den paläozoischen Teil der Karaburun Halbinsel präsentiert werden. Des Weiteren wurden die erhaltenen Altersspektren mit Daten von spät-neoproterozoischen und paläozoischen magmatischen Gesteinen des östlichen Mittelmeerraumes verglichen, die als Liefergesteine in Frage kommen. Besonders die großen Zirkonpopulationen mit Altern von 350–450 Ma und 400–500 Ma in einigen Proben liefern starke Hinweise auf Sedimentzufuhr von Einheiten des südlichen eurasischen Kontinentalrandes. Dies ist mit vorherigen Rekonstruktionen für die angrenzenden ägäischen Inseln Chios und Inousses in Einklang. In **Kapitel 4** wird ein weitreichender Datensatz für siliziklastische Gesteine des oberpaläozoischen Konya Komplexes und seiner mesozoischen Deckeneinheiten in der Süd-Zentral Türkei präsentiert. Die Daten werden hinsichtlich des Alters, der Zusammensetzung und der Herkunft dieser Gesteine diskutiert und sollen Aufschluss über die Entwicklung der Sedimentation im Konya Becken geben. Zwar enthalten die Sedimente, der im Untersuchungsgebiet großflächig aufgeschlossenen Halıcı Formation keine spät-paläozoischen (oder jüngeren) Zirkonpopulationen, doch auf Grundlage der

vorhandenen biostratigraphischen Daten der Mélange wird ein spät-karbonisches bis früh-permisches Ablagerungsalter vermutet. Mit Blick auf das Herkunftsgebiet zeigen die neuen Daten detritischer Zirkone, dass Detritus für Sedimente der Halıcı Formation sowohl von Einheiten des südlichen eurasischen Kontinents, als auch von Nord-Gondwana geliefert wurde. Vergleichbar zur stratigraphischen Abfolge der Karaburun Halbinsel, deutet die Zusammensetzung der Gesteine der Halıcı und Ardıçlı Formationen auf vorwiegend felsische, gering- bis mittelgradig metamorphe Liefergesteine hin. Einige Bestandteile (Granat, Cr-Spinel, vulkanische Gesteinsbruchstücke), die in den Chios–Karaburun Einheiten verbreitet waren, sind in den untersuchten Gesteinen des Konya Komplexes allerdings nahezu nicht vorhanden. Weiterhin unbeantwortet bleibt die Frage nach dem Liefergebiet für Sedimente der spät-triassischen Ardıçlı Formation, wobei eine nahegelegene Herkunft wahrscheinlich ist.

Abschließend bleibt festzuhalten, dass die Daten dieser Studie ein Model unterstützen, dass Elemente verschiedener Rekonstruktionen vereint. Ein Großteil der ober-paläozoischen Chios–Karaburun Einheiten sind während des mittleren Karbon bis zum frühen Perm entlang des südlichen eurasischen Kontinentalrandes abgelagert worden, wohingegen Teile der Halıcı Formation des Konya Komplexes auch Sedimentzufuhr von Nord-Gondwana dokumentieren. Zu dieser Zeit war die nordwärts gerichtete Subduktion der Paläotethys noch immer aktiv, kam aber bis zur späten Trias zum erliegen. Die Art des Kontinentalrandes von Nord-Gondwana bleibt währenddessen weiterhin umstritten.

List of Figures

List of Tables

Chapter 1

Introduction

1 About the project

This PhD thesis was performed at the Geoscience Center of Göttingen University and was done as part of the project 'Late Palaeozoic evolution of Palaeotethys in the Eastern Mediterranean region' with funding of the German Research Foundation (DFG grant ME 3882/3-1) and a Göttingen University start-up funding for young academics (grant to GM). Working on the project has started in September 2014 and began with four weeks of fieldwork in Turkey together with Dr. Guido Meinhold, Dr. Arzu Arslan and Prof. Dr. Talip Güngör (Department of Geological Engineering, Dokuz Eylül University, İzmir), who was the main collaborator in Turkey. During the field campaign fresh samples of siliciclastic sedimentary rocks were collected from the Palaeozoic and Early Mesozoic successions of the two study areas – the Karaburun Peninsula (western Turkey) and the Konya Complex (south-central Turkey) – and stratigraphic relationships of the exposed units were investigated.

2 The Tethyan realm

The present-day geological configuration of continents on Earth is a consequence of continuous plate tectonic reorganisation due to the opening and consumption of oceanic basins, episodic amalgamation and breakup of continental fragments. During the Phanerozoic, the Mediterranean region was strongly affected by the long lasting convergence between the Eurasian and African–Arabian plates and the evolution of the

Tethys oceans. The term Tethys or the Tethys Ocean goes back to the Austrian geologist Eduard Suess (1893) and refers in ancient Greek mythology to the Titan daughter of Uranus and Gaia, sister and consort of Oceanus, Titan god of the sea. It was used to describe a wide oceanic realm in Palaeozoic to Cenozoic time, stretching from the present-day Mediterranean region to the eastern parts of Asia, whose remnants are now found in the Alpine-Himalayan mountain chain.

Even though there is an ongoing debate on the exact timing and closure history of the Tethyan oceans, there is a general consensus on the existence of a Palaeozoic to Early Mesozoic Palaeotethyan ocean, a (mainly) Mesozoic Neotethyan ocean as well as several Palaeozoic and Mesozoic back-arc basins along the active Eurasian margin. The evolution of the Palaeotethys was initiated by the northward drifting of several continental fragments (*Hun superterrane*) away from the Gondwana margin in or before Early Devonian times (e.g., Stampfli and Borel 2002; von Raumer et al. 2002) (Figure 1.1). From the Carboniferous onward, major plate tectonic reorganisation led to the Variscan orogeny and final assembly of the supercontinent Pangea by the collision of Gondwana and Eurasia. This process was accompanied by ongoing northward subduction of Palaeotethys lithosphere and the opening of several Triassic back-arc oceans along the southern Eurasian margin (e.g., Küre, Meliata, Pindos) (Ziegler and Stampfli 2001; Stampfli et al. 2002). At the same time, a new oceanic basin, the Neotethys evolved along the northern Gondwana margin due to the northward drift of the Cimmerian terrane that rifted away from the Afro-Arabian margin and collided with the southern Eurasian margin in Permian–Triassic times (Stampfli and Borel 2002) (Figure 1.1).

However, many different palaeotectonic models have been proposed for the Tethyan realm and there in no consensus on the precise timing of separation and position of peri-Gondwana fragments such as Apulia, Pelagonia, Sakarya or the Anatolide–Tauride Block (e.g., Şengör et al. 1984; Stampfli 2000). For instance, some authors propose northward rifting of a separate Apulian microcontinent from Gondwana during the Late Triassic (e.g., Robertson et al. 1991), whereas others interpret it as part of the Cimmerian terrane that separated from Gondwana after the Late Carboniferous (e.g., Stampfli and Borel 2002.) With respect to the evolution of the Tethyan realm, more specifically the Palaeotethys during that period, the investigation of Palaeozoic and Mesozoic sedimentary successions is of special importance. Such occurrences are scarce in the Eastern Mediterranean, but sedimentary remnants of the former

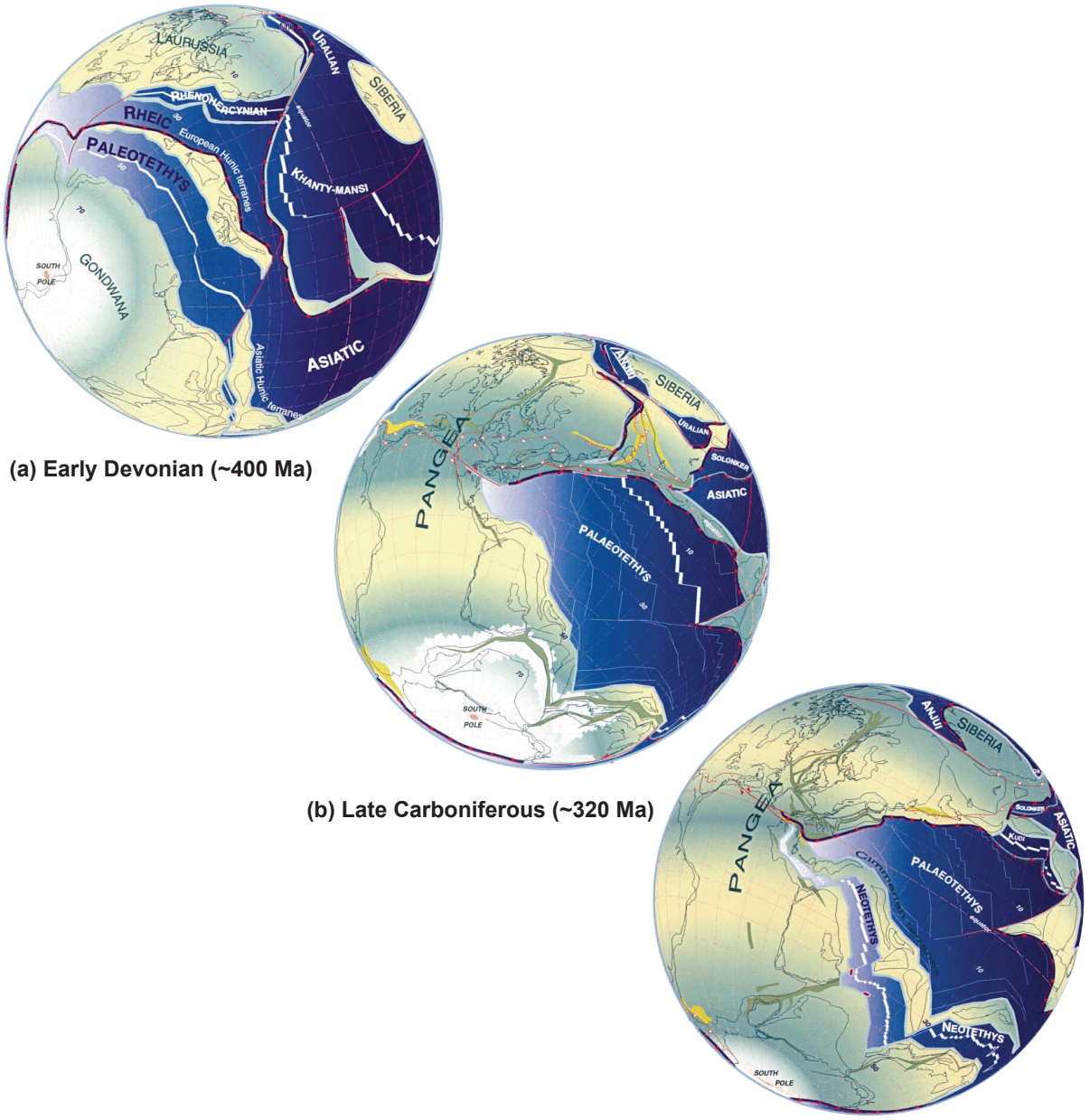

Fig. 1.1: Evolution of the Tethyan realm from Early Devonian to Late Permian (after Stampfli and Borel 2002). **a** Widening of the Palaeotethys in the south and northward drift of the European Hunic terranes in Early Devonian times. **b** Northward subduction of the Palaeotethys and collision of Gondwana with Laurasia in Late Carboniferous time. **c** Opening of the Neotethys to the south and detachment of the Cimmerian terranes in Permian times.

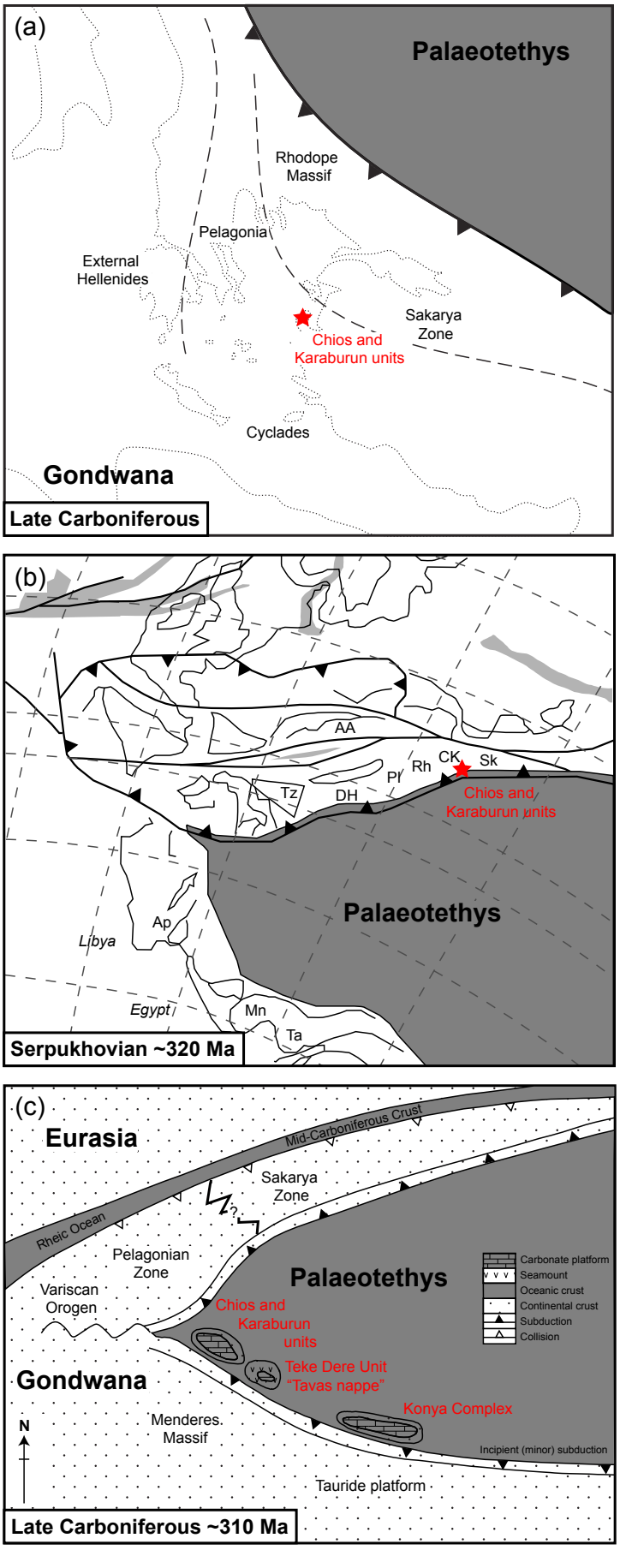

Fig. 1.2: Palaeotectonic reconstructions showing three different models for the location of the study areas during the Late Palaeozoic. **a** The Chios and Karaburun units are located along the northern margin of Gondwana, with the Palaeotethys to the north (modified after Xypolias et al. 2006). **b** The Chios and Karaburun units are located at the southern margin of Eurasia, with the Palaeotethys to the south (modified after Meinhold et al. 2008b). Abbreviations: AA – Austro-Alpine; Ap – Apulia; CK – Chios and Karaburun; DH – Dinarides-Hellenides; Mn – Menderes Massif; Pl – Pelagonian Zone; Rh – Rhodope Massif; Sk – Sakarya Zone; Ta – Taurus; Tz – Tizia. **c** The Chios and Karaburun units are located along the northern margin of Gondwana, with the Palaeotethys to the north (modified after Robertson and Ustaömer 2009b).

Palaeotethyan ocean can be traced on the Greek island of Chios (e.g., Besenecker et al. 1968; Zanchi et al. 2003; Meinhold et al. 2007, 2008b), the Karaburun Peninsula in western Turkey (e.g., Erdoğan et al. 1990; Kozur 1998; Robertson and Pickett 2000) as well as the Konya area in south-central Turkey (Eren et al. 2004) and the Tavas Nappe (Lycian Nappes) in southwest Turkey (Kozur 1998). Their position within the Tethyan realm is controversial and has previously been interpreted in different ways with implications for the Palaeotethys evolution as illustrated in Figure 1.2. Following the interpretation of Xypolias et al. (2006), the occurrence of Carboniferous intrusions within pre-Alpine complexes of the Aegean region (e.g., External Hellenides, Cycladic and Pelagonian basement, NE Greece and NW Turkey) and evidence of Neoproterozoic to Cambrian magmatic events suggest an affiliation of these units (including the Chios and Karaburun units) to the northern Gondwana margin in Late Palaeozoic time (Figure 1.2a). The spatial and temporal distribution of Carboniferous granitoids in the Aegean region in conjunction with their similar geochemical and isotopic signature suggest a close proximity and were interpreted to be related to southward subduction of the Palaeotethys beneath northern Gondwana (e.g., Şengör et al. 1984; Xypolias et al. 2006). Another model follows a palaeogeographic reconstruction of Stampfli and Borel (2002) and Stampfli et al. (2003), in which the above-mentioned characteristics were associated with northward directed subduction of Palaeotethys lithosphere beneath the southern Eurasian margin (Figure 1.2b). A provenance study on the Upper Palaeozoic–Lower Mesozoic clastic successions of Chios by Meinhold et al. (2008b) has shown that sediment was most probably supplied from terranes north of its present-day location (Sakarya Zone, Istanbul Zone, Bulgaria, Serbia) and the Chios and Karaburun units were deposited in close proximity (Figure 1.2b). A third model by Robertson and Ustaömer (2009b) implies dual polarity subduction with a dominant northward direction during the Late Palaeozoic. The Chios and Karaburun units, the Konya Complex and comparable units (Tavas Nappe) were interpreted as continental fragments that rifted from Gondwana in Early Palaeozoic time and were re-accreted to Gondwana as a result of short-lived southward subduction in the Late Carboniferous (Figure 1.2c).

3 Objectives and methodological approach

The main reason hampering a well-grounded interpretation of the Palaeotethyan history in the Eastern Mediterranean is the lack of hard data, for instance provenance data from Late Palaeozoic successions of the few known key areas, such as the Karaburun Peninsula and the Konya Complex in Turkey. As mentioned above, a detailed provenance study was already conducted on Chios Island (Meinhold et al. 2007, 2008a,b). From the Karaburun Peninsula, only a few detrital zircon U–Pb ages are available from the Karareis and Küçükbahçe formations (Rosselet and Stampfli 2003), whilst provenance data from the Konya Complex are lacking completely. In this PhD thesis, therefore, an extensive, multi-parameter provenance analysis was conducted on the Late Palaeozoic and Early Mesozoic sedimentary successions of these two areas to test the current palaeotectonic models for Turkey.

The main objective of sedimentary provenance studies is to reconstruct source area geology and to reveal the history of sediment from the initial erosion of the host rock to the final burial of their detritus (Ibbeken and Schleyer 1991). Sedimentary rocks rarely reflect a direct image of the compositional and textural features of their initial source rock but represent the final product after the detritus was modified by chemical and mechanical processes during transport, deposition and weathering (Johnsson 1993). The initial signature of the source rocks may further be blurred by mixing of material from multiple sources and/or recycling of other sediments that complicate the effort of identifying specific source areas. In this respect, progress in sedimentary provenance analysis has brought up a variety of powerful tools. In modern provenance research bulk-rock techniques are combined with single-grain analysis and varietal studies of heavy minerals and geochronological data. While information from bulk-rock techniques comprise sediment petrography and their chemical and isotopic composition (e.g., Potter 1978; Ingersoll et al. 1984), the study of single-grains focusses on variations (i.e. major and trace element composition, morphology, crystal structure) of specific minerals (e.g., Pober and Faupl 1988; Morton 1991; Zack et al. 2004b; Mange and Morton 2007). Frequently used heavy minerals in this context include rutile, garnet, Cr-spinel, tourmaline as well as amphiboles and pyroxenes that provide insight into their formation history, P–T conditions and the composition and nature of their source rocks.

For the purpose of this study, the siliciclastic sediments were examined by standard

quantitative petrography and geochemical analyses, complemented by single-grain analyses of garnet, rutile and Cr-spinel (if present) and detrital zircon U–Pb geochronology. Garnet is a very common heavy mineral in numerous metamorphic and igneous rocks. Its wide range of major and trace element composition is dependent on its host rock composition and provides information on pressure and temperature conditions during mineral growth (e.g., Wright 1938; Deer et al. 1992; Krippner et al. 2014). Detrital rutile is primarily derived from medium- to high-grade metamorphic rocks (i.e., eclogites, granulites, metasediments) and is commonly used to infer information on source rock lithology (felsic vs. mafic), based on the Cr–Nb system and formation temperatures (Zr-in-rutile thermometry) (e.g., Tomkins et al. 2007; Meinhold 2010; Triebold et al. 2012). Chrome spinel is a stable heavy mineral derived from mafic and ultramafic igneous bodies. Its chemical composition is controlled by several factors and gives insights on the petrogenetic evolution and geodynamic setting of its source rock (e.g., Cookenboo et al. 1997; Kamenetsky et al. 2001). The obtained data are compared to results from the sedimentary sequence on Chios, which are already available and provide valuable information on source area geology and identify the impact of multiple sources. Additionally, this data set was complemented by detrital zircon U–Pb ages that provide constraints on the stratigraphy of the studied units by defining their maximum depositional ages but also serve as a proxy for sedimentary provenance. The obtained age spectra from the examined rocks are compared to available data from the literature of possible source rocks, which were sought in Precambrian and Palaeozoic basement rocks of units located along the southern and northern margins of Palaeotethys, such as SE Europe, Turkey and North Africa.

Chapter 2

Manuscript I: Provenance and tectonic setting of Carboniferous–Triassic sandstones from the Karaburun Peninsula, western Turkey: A multi-method approach with implications for the Palaeotethys evolution

Kersten Löwen[a,*], Guido Meinhold[a,b], Talip Güngör[c]

[a] Abteilung Sedimentologie/Umweltgeologie, Geowissenschaftliches Zentrum Göttingen, Universität Göttingen, Goldschmidtstraße 3, 37077 Göttingen, Germany

[b] School of Geography, Geology and the Environment, Keele University, Keele, Staffordshire, ST5 5BG, UK

[c] Department of Geological Engineering, Dokuz Eylül University, Tınaztepe Campus, 35160 Buca-İzmir, Turkey

[*]e-mail: kersten.loewen@geo.uni-goettingen.de
Tel.: +49 551 399818

Published in: Sedimentary Geology 375 (2017): 232–255

Abstract

Carboniferous–Triassic siliciclastic sediments of the Karaburun Peninsula in western Turkey were studied to unravel their provenance and the tectonic setting of depositional basins within the Palaeotethyan realm. A set of complementary techniques including petrography, bulk-rock geochemistry and single-grain analysis of rutile, garnet and chrome spinel were applied to provide a diverse dataset for testing existing palaeotectonic models using both, established and recently published diagrams. We show that tectonic discrimination diagrams of siliciclastic sediments based on major and trace element whole-rock geochemical data do yield ambiguous results and are only partly in accordance with regional geological events. Chondrite-normalised REE patterns of Upper Palaeozoic samples are characterised by enrichment of LREE and a flat trend towards HREE. The degree of fractionation allows for discrimination between sandstones of Karaburun (La_N/Yb_N = 8.00–14.79) and adjacent Greek islands of Chios (5.82–9.23) and Inousses (7.40–9.95). Petrographic observations and compositional data from single-grain analysis indicate significant supply from low- to medium-grade metamorphic rocks of generally felsic character and minor input of (ultra)mafic detritus. Detrital chrome spinels in the Lower Triassic Gerence Formation are different in composition and shape compared to chrome spinels in Carboniferous–Permian sandstones. They were derived from a very proximal source and exhibit variable, but generally high Cr- and Mg-numbers, consistent with chrome spinels from podiform chromitites that have been formed in an intra-oceanic back-arc setting above a supra-subduction zone. We conclude that most of the Carboniferous–Triassic successions were deposited along the southern active margin of Eurasia in a continental-arc environment during the time period when Palaeotethys diminished in size and finally vanished. Large volumes of detritus were probably derived from rock units located in the present-day

Balkan region and the Sakarya Zone, or equivalent successions that are not present anymore.

Keywords: Petrography; Geochemistry; Mineral chemistry; Palaeotethys; Karaburun Peninsula; Turkey

1 Introduction

The Eastern Mediterranean region is an integral part of the Alpine–Himalayan system and is made up of several continental fragments which document a complex geodynamic history. The major tectonic units and suture zones in western Turkey are, from N to S, the İstanbul Zone, the Sakarya Zone, the İzmir–Ankara Zone, the Menderes Massif, the Lycian Nappes, and the Taurides (Figure 2.1a).

The Late Palaeozoic to Early Mesozoic period in the Eastern Mediterranean region was strongly influenced by the evolution of the Tethyan oceans. The Palaeotethys is considered as an oceanic domain that originated in early to mid-Palaeozoic time separating Gondwana and its detached continental fragments from Eurasia (e.g., Şengör et al. 1984; Stampfli and Borel 2002; Stampfli et al. 2013). Northward drift of the Gondwana-derived Cimmerian continents mostly during the Permian–Triassic and an evolving Neotethys to the south led to subduction of the Palaeotethys, but the timing of final closure remains controversial (e.g., Şengör et al. 1984; Stampfli and Borel 2002; Stampfli et al. 2013).

Chios Island (Greece) and Karaburun Peninisula (W Turkey) are regarded as key areas for understanding the closure history of the Palaeotethys as they exhibit virtually unmetamorphosed Palaeozoic to Mesozoic sedimentary rocks (e.g., Besenecker et al. 1968; Erdoğan et al. 1990; Kozur 1998; Robertson and Pickett 2000; Zanchi et al. 2003; Meinhold et al. 2007, 2008a,b; Robertson and Ustaömer 2009b). Their role within the Palaeotethyan realm has been interpreted in different ways and both the northern margin of Gondwana (e.g., Robertson and Pickett 2000; Robertson and Ustaömer 2009b; Akal et al. 2011) and the southern Eurasian margin (e.g., Stampfli 2000; Stampfli et al. 2003; Moix et al. 2008) have been proposed as palaeopositions for the Late Palaeozoic. This uncertainty is mainly due to the lack of reliable data for testing the various palaeotectonic models. Few available provenance data include detrital zircon U–Pb ages from

both localities as well as bulk-rock geochemistry and compositional data of rutile and chrome spinel from Chios Island that suggest deposition along the southern Eurasian margin in the Late Palaeozoic (Meinhold et al. 2007, 2008a,b; Löwen et al. 2017). Alternatively, other authors propose a northern Gondwana affinity (e.g., Robertson and Pickett 2000; Akal et al. 2011). They refer to similar stratigraphic characteristics (continuous Early Triassic to Late Cretaceous carbonate deposition) of the study area and the Anatolide–Tauride platform while important features of the Pontides (Liassic unconformity and Triassic high-pressure metamorphism) related to the evolution of the Eurasian continent are missing.

The aim of this study is to shed light on the provenance and the depositional tectonic setting of sediments from the Karaburun Peninsula. The reconstruction of source areas will allow us to test current palaeotectonic models and either support or exclude some of those. We present and discuss data from a multi-method approach including data from thin section petrography, whole-rock geochemistry, and single-grain geochemistry of detrital rutile, garnet and Cr-spinel (this study), supplemented by detrital zircon U–Pb ages (Löwen et al. 2017). Samples were taken from siliciclastic sections of Upper Palaeozoic (i.e., Küçükbahçe, Dikendağı and Alandere formations) to Upper Triassic (i.e., İdecik unit, Gerence, and Güvercinlik formations) successions to monitor provenance changes during this important time period when Palaeotethys diminished in size and finally vanished.

2 Geological setting

The Karaburun Peninsula is located in the central, westernmost part of Turkey adjacent to the Aegean Sea (Figure 2.1a). It is part of the İzmir–Ankara Zone, a suture zone separating continental fragments of Eurasian affinity (e.g., units within the Sakarya Zone to the north) from fragments of Gondwana affinity (e.g., Menderes Massif to the south) (e.g., Okay and Tüysüz 1999; Stampfli 2000; Moix et al. 2008). Despite considerable effort – several studies and mappings were carried out in the area during the past >100 years (e.g., Philippson 1911; Kalafatçıoğlu 1961; Erdoğan et al. 1990; Robertson and Pickett 2000; Stampfli et al. 2003; Çakmakoğlu and Bilgin 2006; Robertson and Ustaömer 2009b) – the exact tectono-stratigraphic situation and timing of sediment deposition, especially for the Palaeozoic succession, are not fully understood. By

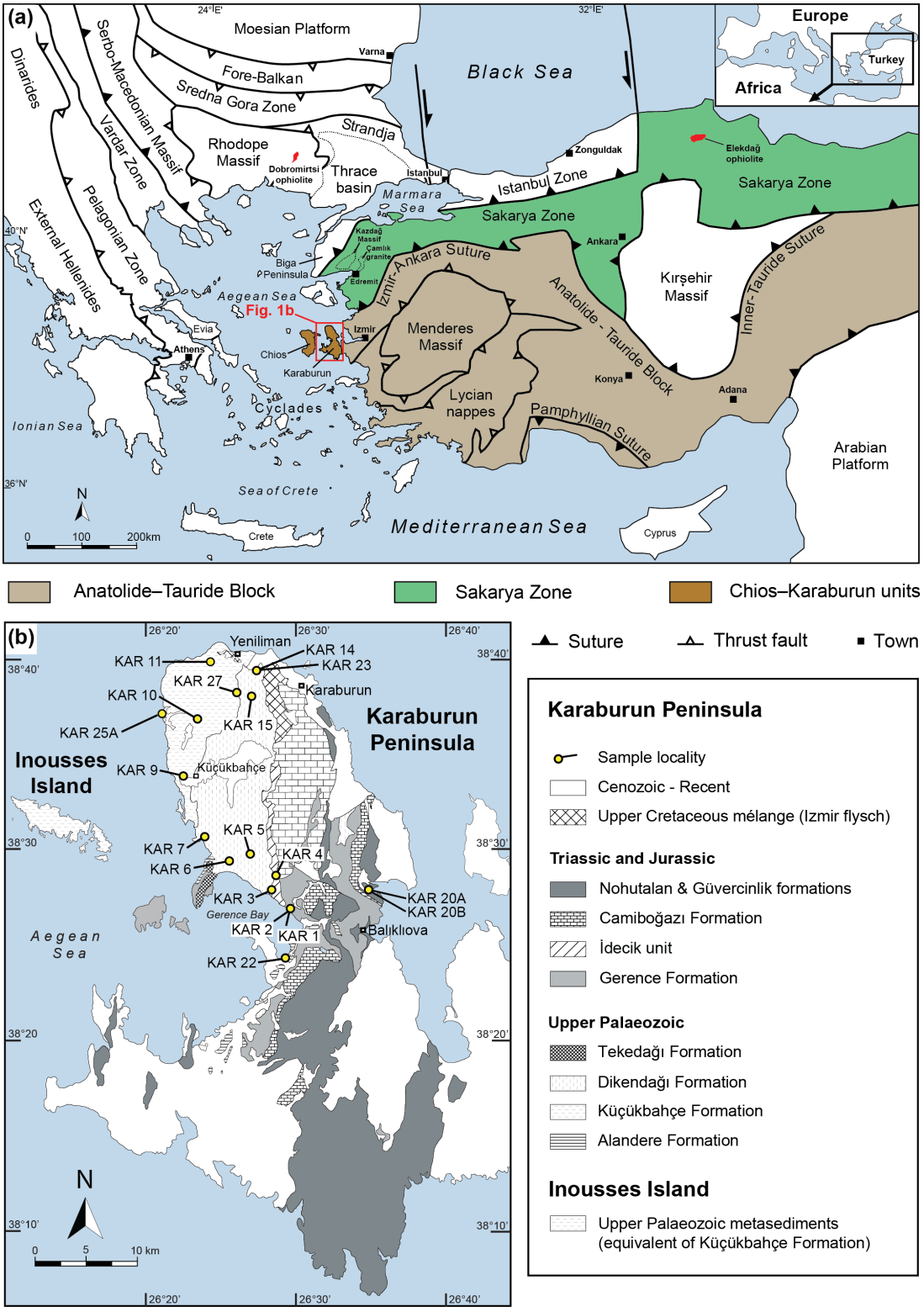

Fig. 2.1: **a** Simplified tectonic map of the Eastern Mediterranean region (compiled and modified after Jacobshagen 1986; Okay and Tüysüz 1999; Okay et al. 2006). The locations of the Dobromirtsi and Elekdağ ophiolite occurrences are after González-Jiménez et al. (2015) and Dönmez et al. (2014), respectively. **b** Simplified geological map of the study area with sample locations. The Karaburun map is modified after Çakmakoğlu and Bilgin (2006) and the Inousses map is modified after Meinhold et al. (2007).

the current state of knowledge large parts of the northwestern Karaburun Peninsula are made up of two main siliciclastic units, the Küçükbahçe and Dikendağı formations. The structurally lower Küçükbahçe Formation is mainly composed of alternating low-grade metamorphosed (turbiditic) sandstones and shales, without any blocks/olistoliths. These sediments are intensely folded and sheared with pronounced schistosity. The upper siliciclastic part is assigned to the Dikendağı Formation, firstly described by Çakmakoğlu and Bilgin (2006). Robertson and Ustaömer (2009b) refer to it as Karaburun mélange. This succession comprises blocks of black chert and pelagic limestones, ranging in age from Silurian to Carboniferous, and poorly dated volcanic rocks embedded in a highly deformed siliciclastic matrix. In the northern outcrop area of the Dikendağı Formation isolated blocks of black chert are rare. Further south large blocks of limestone and folded chert are highly abundant. The blocks have been dated as Silurian to Carboniferous (black chert) and Silurian to Devonian (limestones) by biostratigraphic data (Kozur 1995, 1997, 1998). Main distinctive features compared to the Küçükbahçe Formation are the occurrence of blocks/olistoliths and a very slight schistosity indicative for a lower metamorphic grade. The contact between the Küçükbahçe and Dikendağı formations is tectonic. Two granitoid intrusions crop out in the northern part of the Karaburun Peninsula whose age has been constrained to Early Triassic by a biotite Rb–Sr isochron age of 239.9 $\pm$ 2.4 Ma (Ercan et al. 2000) and zircon U–Pb ages of 244.4 $\pm$ 1.5 Ma (Ustaömer et al. 2016a) and 247.1 $\pm$ 2.0 Ma, respectively (Akal et al. 2011). Local exposures of the Alandere Formation at the southern coast area of Gerence Bay (Figure 2.1b) were interpreted as structurally highest part within the Karaburun mélange by Robertson and Pickett (2000). The Alandere Formation is predominantly composed of fossil-rich, shallow-water limestones and contains sandstones, conglomerates, shales and chert. The age is well constrained by biostratigraphic data to Carboniferous (Serpukhovian–Bashkirian) (Erdoğan et al. 1990, 2000). This whole Palaeozoic succession (i.e., Küçükbahçe, Dikendağı and Alandere formations) was previously also interpreted as Ordovician–Carboniferous sedimentary sequence, separated by gradational contacts (Çakmakoğlu and Bilgin 2006). In contrast, a recent study on detrital zircon ages from these sediments indicates sediment deposition of the Küçükbahçe, and Dikendağı formations probably began in the mid-Carboniferous and continued to at least Pennsylvanian–Cisuralian (Löwen et al. 2017). In the light of these findings a revised stratigraphic section was presented, interpreting this se-

quence as a pile of units deposited in Carboniferous–Early Permian times, separated by tectonic rather than gradational contacts (Figure 2.2).

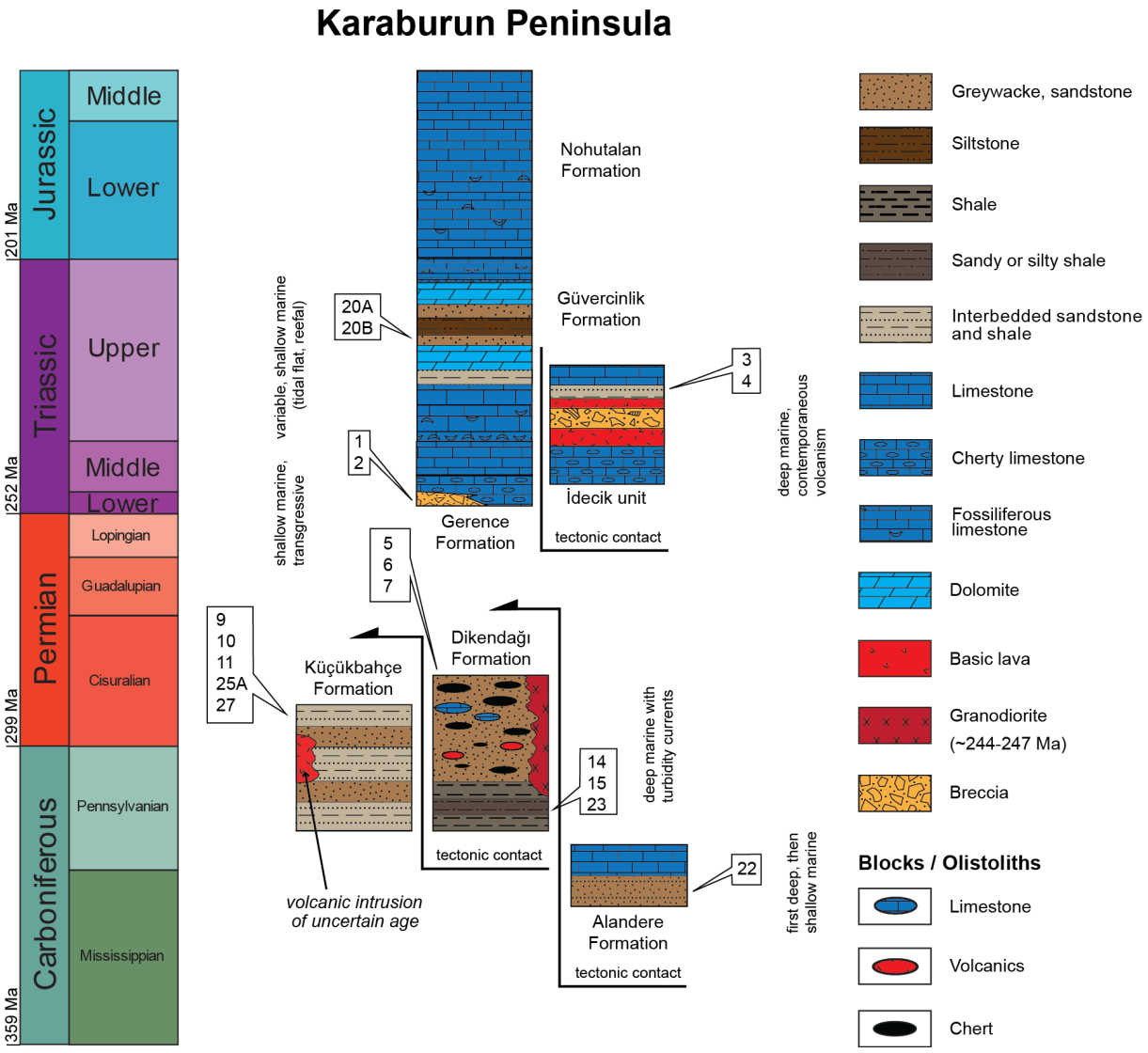

Fig. 2.2: Palaeozoic to Jurassic tectono-stratigraphic section of the Karaburun Peninsula (modified after Löwen et al. 2017). For simplification, the ?Late Permian Tekedağı Formation, consisting of bioclastic limestone, dolomitic limestone, partly oolitic/pisolitic, and limestone with sandstone, siltstone, and marl interfingers (Çakmakoğlu and Bilgin 2006), is not shown here. The Tekedağı Formation is only present in a small area to the NW of Gerence Bay. This formation probably correlates with the stratigraphically younger part of the Permian limestones from the allochthonous Upper Unit of Chios Island. Blocks/olistoliths in the Palaeozoic succession have been described by Kozur (1998) and Robertson and Ustaömer (2009b).

According to Robertson and Pickett (2000) and Robertson and Ustaömer (2009b), the Late Palaeozoic Karaburun mélange is unconformably overlain by a thick sequence dominated by Mesozoic platform carbonates, that make up large parts of the eastern

and southern area of Karaburun Peninsula. This succession is of Early Triassic to Late Cretaceous (Campanian–Maastrichtian) age and is subdivided into several units, including the Gerence Formation, İdecik unit, Camiboğazı Formation and Güvercinlik Formation (Çakmakoğlu and Bilgin 2006). The Gerence Formation unconformably overlies the Karaburun mélange. At its base, it consists of a siliciclastic part dominated by conglomerates with reworked material of underlying formations and intervals of sandstones developing into more carbonate-rich conglomerates at the top. An Early Triassic age has been assigned to this formation by abundant fossils (ammonites, conodonts, foraminifera). This unit is followed by thick-bedded, massive limestones of the Camiboğazı Formation, determined to be of Middle–Late Triassic (Ladinian–Carnian) age (e.g., Brinkmann et al. 1972; Erdoğan et al. 1990, 2000). The gradationally overlying Güvercinlik Formation is a detritic succession of highly mature, red sandstones, conglomerates and fossiliferous (Megalodon bivalves, algae, gastropods) oolitic and dolomitic limestones of Late Triassic age (Stampfli et al. 2003; Çakmakoğlu and Bilgin 2006). Small exposures in the central part of northern Karaburun Peninsula are assigned to the İdecik unit that is tectonically thrust in between the Karaburun mélange and the Gerence Formation. Volcanoclastic rocks, basic lavas, tuffaceous material, limestones and radiolarites of Ladninian–Carnian age are the main constituents of this unit (Çakmakoğlu and Bilgin 2006).

3 Methodology

A total of eighteen siliciclastic sedimentary rocks of Carboniferous to Late Triassic age were collected from the Karaburun Peninsula for petrographic and whole-rock geochemical analysis as well as mineral chemistry of garnet, rutile and chrome spinel. Sample localities are shown in Figure 2.1b, and a list of samples including GPS coordinates and information on conducted analyses is given in Table 2.1. All steps of preparation and geochemical analyses were performed at the Geoscience Center Göttingen (Department of Sedimentology and Environmental Geology and Department of Geochemistry). Samples were cut with a rock saw to have rock slices for thin section preparation. The remaining material was crushed by a jaw crusher and disc mill. Part of the material was grinded to <63 µm by an agate ball mill for whole-rock geochemical analysis. The remaining material was wet-sieved using a mechanical shaker to

separate different grain-size fractions. The 63–250 µm fraction was decarbonated with acetic acid (5%) and heavy minerals were extracted in separation funnels using sodium polytungstate ($Na_6[H_2W_{12}O_{40}]$, ρ = 2.85 g/cm^3).

Thin sections were analysed using a petrographic microscope with an attached point counting stage. At least 300 points were counted for each sample according to the Gazzi-Dickinson method (e.g., Ingersoll et al. 1984). Recorded components include mono- and polycrystalline quartz (Q_m, Q_P), plagioclase (P), alkali feldspar (K-fsp) and lithic fragments (L). Matrix and cement were not counted but estimated using standard charts for visual percentage estimation.

Whole-rock geochemical analyses were carried out using a PANalytical AXIOS Advanced sequential X-ray spectrometer. Fused glass discs were produced by adding Spectromelt® and LiF to the sample powder and melting in platinum crucibles. Loss on ignition (LOI) was determined gravimetrically by stepwise heating to 1000 °C.

Solution inductively coupled plasma mass spectrometry (ICP–MS) for trace element geochemistry was applied to eight samples (at least one from each formation). Sample powder ($\sim$50 mg per sample) was dissolved by PicoTrace® acid digestion system. Analytical procedures were started by pre-reaction with 2 ml HNO_3 at 50 °C overnight. After cooling to room temperature samples were treated with 3 ml HF and 3 ml $HClO_4$ and heated to 150 °C for 8 h during the first pressure phase. For evaporation the digestion vessels were heated to 180 °C for 16 h. After cooling 10 ml H_2O (double deionised), 2 ml HNO_3 and 0.5 ml HCl were added to the samples for the final pressure phase and re-heated to 150 °C for 4 h. Internal standard (100 µl) for ICP–MS analysis was added to the solution after final cooling. Trace element analysis was performed on a ThermoElectron VG PlasmaQuad 2 quadrupole ICP–MS. All analytical data for main and trace element geochemistry are given in the accompanying Supplementary data (see Table A.1).

Mineral chemical analyses of garnet, rutile and chrome spinel were applied to a selection of samples, depending on the presence of the specific minerals, covering formations from mid-Carboniferous to Late Triassic age. Mineral grains were extracted from the 63–250 µm fraction and randomly selected by handpicking under a stereomicroscope and placed on synthetic mounts using an epoxy resin composed of a mixture of Araldite® and hardener (5:1). Prior to analysis, the polished grain mounts were carbon-coated to ensure conductivity. Geochemical measurements were carried out

Table 2.1: GPS coordinates of sample locations and summary of conducted analyses.

Sample	Lithology	Geographic location	Geographic coordinates	QFL	XRF	ICP-MS	EMPA	U-Pb*
Güvercinlik Formation								
KAR20A	Sublitharenite	N of Balıklıova	38°27'51.56"N, 26°35'23.41"E	X	X		X	X
KAR20B	Sublitharenite	N of Balıklıova	38°27'51.56"N, 26°35'23.41"E	X	X	X		X
Gerence Formation								
KAR1	(Feldspathic) Litharenite	Gerence Bay	38°26'41.44"N, 26°30'08.24"E	X	X	X	X	X
KAR2	Lithic subarkose	Gerence Bay	38°26'42.71"N, 26°30'50.86"E	X	X			
İdecik unit								
KAR3	Sublitharenite	N of Gerence Bay	38°27'39.21"N, 26°28'37.59"E	X	X	X	X	X
KAR4	Litharenite	N of Gerence Bay	38°28'24.21"N, 26°28'23.18"E	X	X		X	X
Dikendağı Formation								
KAR5	Sublitharenite	N of Gerence Bay	38°29'39.03"N, 26°27'16.20"E	X	X		X	X
KAR6	Lithic subarkose	N of Gerence Bay	38°29'14.58"N, 26°25'57.37"E	X	X			X
KAR7	Lithic arenite	SW coast of Karaburun Peninsula	38°30'31.44"N, 26°24'17.82"E	X	X	X	X	X
KAR14	Subarkose	SE of Yeniliman	38°39'25.02"N, 26°27'32.04"E	X	X	X		X
KAR15	Subarkose	N Karaburun Peninsula (close to granitoid intrusion)	38°38'00.70"N, 26°27'21.10"E	X	X			X
KAR23	Subarkose	SE of Yeniliman						
Küçükbahçe Formation								
KAR9	Sublitharenite	W of Küçükbahçe	38°33'48.12"N, 26°22'51.24"E	X	X	X		X
KAR10	Subarkose	NW Karaburun Peninsula	38°36'44.64"N, 26°23'40.18"E	X	X		X	X
KAR11	Lithic subarkose	W of Yeniliman	38°39'43.73"N, 26°24'27.59"E	X	X	X		X
KAR25A	Lithic subarkose	NW coast of Karaburun Peninsula	38°37'05.10"N, 26°21'21.36"E	X	X			
KAR27	Sublitharenite	N Karaburun Peninsula; at contact to Dikendagi Formation	38°38'07.78"N, 26°26'34.40"E	X	X		X	X
Alandere Formation								
KAR22	Subarkose	S of Gerence Bay (coast)	38°24'05.34"N, 26°29'43.62"E	X	X	X	X	X

QFL - Petrographic thin-section analysis for conventional QFL classification; XRF - Major and trace element analysis using X-ray fluorescence spectrometry; ICP-MS - Rare earth element analysis using Inductively Coupled Plasma Mass Spectrometry; EMPA - Mineral chemical analysis using an electron microprobe analyzer; U-Pb - Detrital zircon U-Pb geochronology using laser ablation ICP-MS.

* Data from Löwen et al. (2017b)

with a JEOL JXA 8900 RL electron microprobe analyzer (EMPA) equipped with five wavelength dispersive spectrometers. The analytical data, measurement parameters and spectrometer configurations are given in the accompanying Supplementary data (see Tables A.2–A.5).

4 Results

4.1 Petrography

Petrographic analysis included identification of mineral phases and lithic fragments, counting of grains for QFL classification, and estimation of textural maturity based on grain sorting and degree of rounding. Mineralogy and QFL compositions are given in Table 2.2. Classification of siliciclastic sedimentary rocks was done using the relative proportions of quartz, feldspar and lithic fragments (after Mcbride 1963), and additionally based on their chemical composition according to their logarithmic ratios of SiO_2/Al_2O_3 vs. Fe_2O_3/K_2O (Herron 1988) (Figure 2.3). Even though some samples have matrix contents $\geq$15% (Table 2.2) they were not classified as wackes because the origin of this matrix (primary or secondary) is undetermined. An overview of results from petrographic analysis is given in Figure 2.4. With few exceptions, the analysed sandstones are made up of at least 75% quartz and variable amounts of feldspar (mainly plagioclase) and lithic fragments. Feldspar content is generally between 5 and 10% (max. 30%), whereas the amount of rock fragments is highly variable (up to 40%) and usually higher in the Triassic samples (e.g., Gerence Formation and İdecik unit).

The only sample from the Serpukhovian–Bashkirian Alandere Formation (KAR22) is a subarkosic rock, representative of the lower clastic part (Figure 2.1b). The sediment is mainly composed of quartz and plagioclase with minor K-feldspar. Lithic fragments are of primarily volcanic and rare sedimentary origin and carbonate clasts occur sporadically (Figure 2.6a). Non-opaque accessory minerals include zircon, tourmaline, garnet, rutile and chrome spinel. Textural immaturity is indicated by poor sorting and (sub)angular grain shape.

Five samples were collected from the northern, southern and central part of the Küçükbahçe Formation, one of the main siliciclastic units of the Karaburun Peninsula (Figure 2.1b). The fine-medium grained sandstones reveal low textural maturity (moderately to well-sorted, angular to subangular grains) and were classified as

Table 2.2: Mineralogical composition and point counting results of sediments from the Karaburun Peninsula.

Sample	Lithology	Qtz	Pl + Kfs	L	M	Bt	Ms	Chl	Cal	Grt	Cld	Ap	Ep	Tur	Zrn	Amp	Pyx	Rt	Ttn	Cr-Spl
Güvercinlik Formation																				
KAR 20A	Sublitharenite	84	3	13	0	✚	✚	✚	⊙	⊙	–	–	–	⊙	⊙	⊙	⊙	⊙	⊙	–
KAR 20B	Sublitharenite	91	1	8	0	–	–	✚	–	–	–	–	–	⊙	⊙	–	–	⊙	–	–
Gerence Formation																				
KAR 1	(Feldspathic) litharenite	51	10	39	<5	✚	✚	✚	✚	⊙	⊙	⊙	–	⊙	⊙	–	⊙	⊙	⊙	⊙
KAR 2	Lithic subarkose	76	10	14	20	✚	✚	✚	–	–	⊙	–	–	–	⊙	⊙	–	⊙	–	–
İdecik unit																				
KAR 3	Sublitharenite	76	8	16	10	–	✚	–	–	–	–	⊙	–	⊙	⊙	⊙	–	⊙	⊙	–
KAR 4	Litharenite	66	5	29	<5	–	✚	✚	⊙	–	⊙	–	–	⊙	⊙	⊙	–	–	–	–
Dikendağı Formation																				
KAR 5	Sublitharenite	81	9	10	<5	✚	✚	✚	–	–	–	⊙	⊙	⊙	⊙	⊙	–	⊙	⊙	–
KAR 6	Subarkose	77	10	13	5	✚	✚	✚	⊙	–	–	–	–	–	⊙	–	–	–	⊙	–
KAR 7	Lithic arenite	45	29	26	20	✚	✚	✚	⊙	–	–	–	–	⊙	⊙	–	–	⊙	⊙	–
KAR 14	Subarkose	87	9*	4	10	✚	✚	–	–	–	–	⊙	–	⊙	⊙	–	–	⊙	⊙	–
KAR 15	Subarkose	89	10	1	<5	–	✚	✚	–	–	–	–	⊙	–	⊙	⊙	–	–	⊙	–
KAR 23	Subarkose	92	5*	3	15	–	✚	–	–	–	–	–	⊙	⊙	⊙	–	–	⊙	⊙	–
Küçükbahçe Formation																				
KAR 9	Sublitharenite	79	8	13	10	–	✚	–	–	–	⊙	–	–	⊙	⊙	–	–	⊙	–	–
KAR 10	Subarkose	87	9	4	20	–	✚	✚	–	⊙	–	–	–	⊙	⊙	⊙	–	⊙	–	–
KAR 11	Lithic arkose	74	11	15	30	–	✚	⊙	–	–	–	–	–	⊙	⊙	–	–	⊙	⊙	–
KAR 25A	Lithic subarkose	79	10	11	<5	✚	✚	–	–	–	–	–	⊙	⊙	⊙	–	–	–	–	–
KAR 27	Sublitharenite	82	6	12	15	✚	✚	✚	⊙	–	–	–	–	⊙	⊙	–	–	⊙	⊙	⊙
Alandere Formation																				
KAR 22	Subarkose	79	12	9	15	✚	✚	✚	⊙	⊙	⊙	–	–	⊙	⊙	–	–	⊙	–	⊙

✚ present; ⊙ accessory; – not observed; *no Kfs; Abbreviations: Qtz = quartz (in %); Pl = plagioclase (in %); Kfs = K-feldspar (in %); M = matrix (in %); L = lithic fragments; Bt = biotite; Ms = muscovite; Chl = chlorite; Cal = calcite; Grt = garnet; Cld = chloritoid; Ap = apatite; Ep = epidote; Tur = tourmaline; Zrn = zircon; Amp = amphibole; Pyx = pyroxene; Rt = rutile; Ttn = titanite; Cr-Spl = Cr-Spinel.

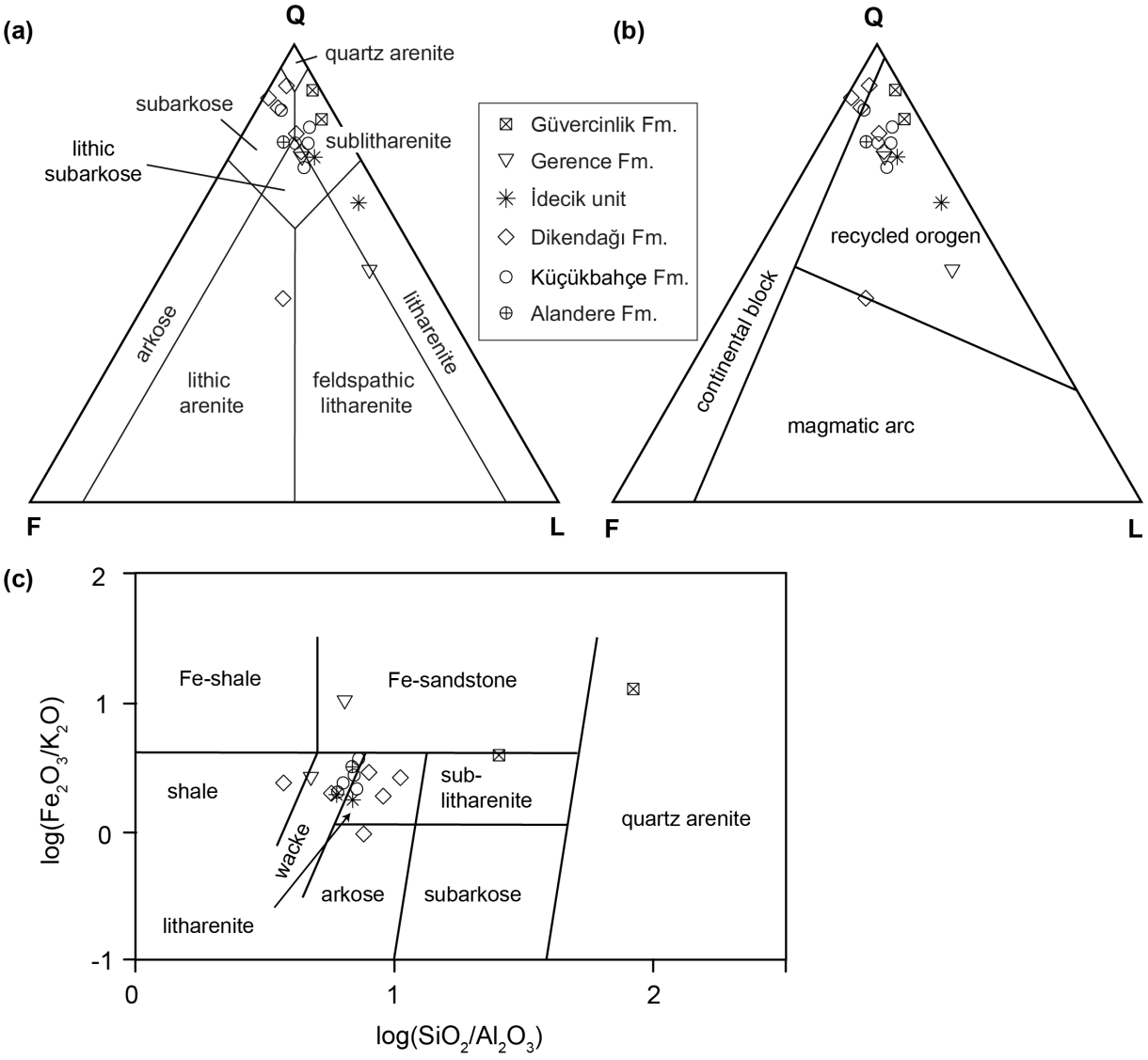

Fig. 2.3: **a** QFL diagram for lithological classification (after Mcbride 1963). **b** Ternary QFL plot for discrimination of tectonic settings (after Dickinson et al. 1983). **c** Chemical classification scheme for siliciclastic sediments (after Herron 1988).

(sub)litharenites and (sub)arkosic rocks. Their texture is often characterised by preferential alignment of slighlty deformed grains and lithic fragments. These clasts occur in low to moderate amounts (4–15%) and were almost entirely derived from sedimentary sources (clastic sedimentary and chert fragments), the exception being one sample (KAR27) with predominant volcanic fragments. Feldspar is equally abundant (6–11%) with plagioclase as the dominant phase. The assemblage of accessory heavy minerals contains mostly tourmaline, zircon and rutile but garnet and chrome spinel exclusively occur in two different samples (KAR9 and KAR27).

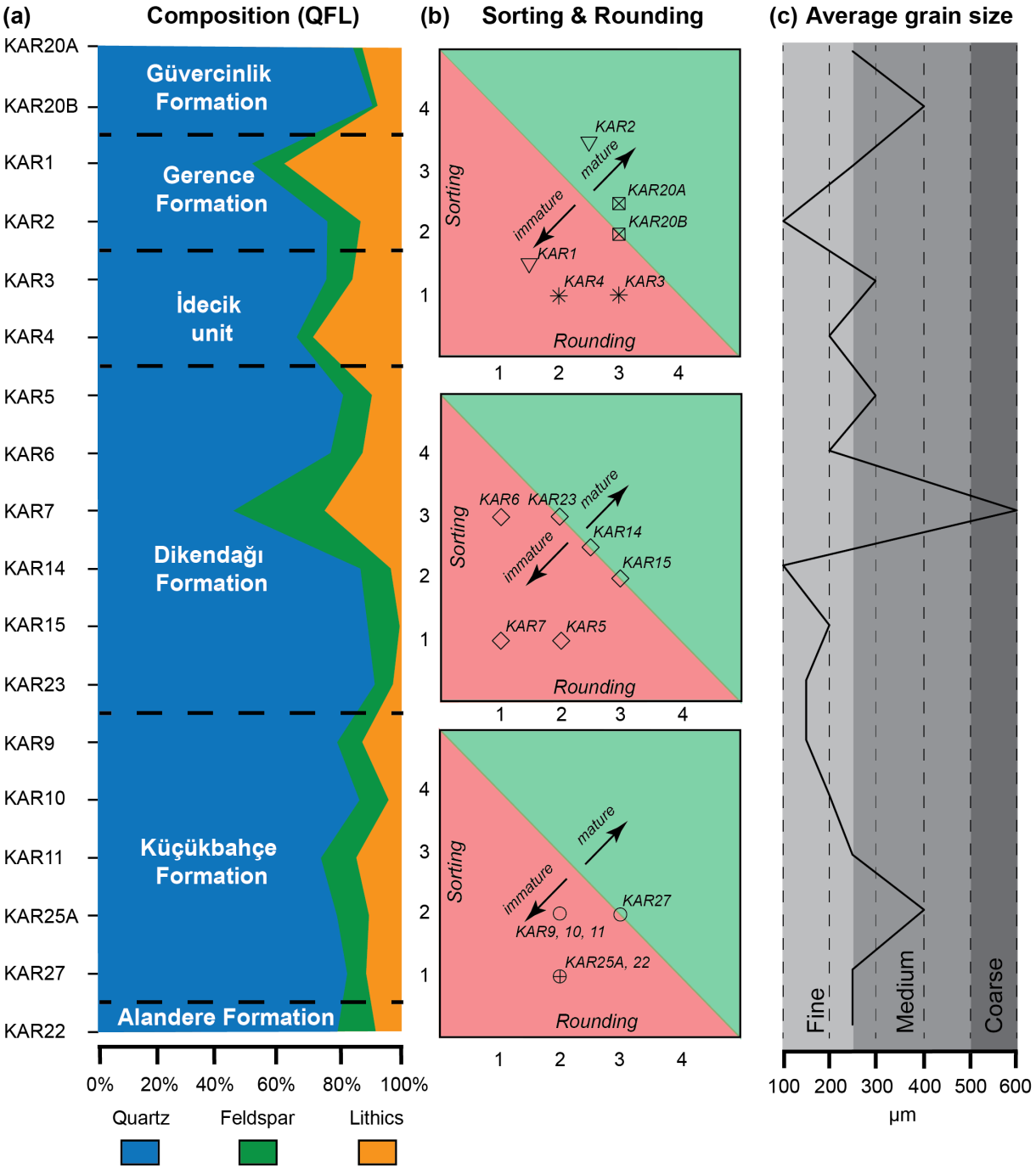

Fig. 2.4: Overview of petrographic analysis of sediments from the Karaburun Peninsula. **a** Percentage of quartz, feldspar and lithic fragments resulting from point couting. **b** Degree of sorting (1 – poorly sorted, 2 – moderately sorted, 3 – well sorted, 4 – very well sorted) and rounding (1 – angular, 2 – subangular, 3 – subrounded, 4 – rounded) were used to estimate maturity. **c** Estimated average grain size.

Six sandstones were collected from the northern and southern part of the Dikendağı Formation, the second main Palaeozoic siliciclastic unit of the Karaburun Peninsula

(Figure 2.1b). In contrast to the comparatively homogeneous Küçükbahçe Formation these samples are characterised by higher compositional variability and generally low textural maturity. Two fine- to medium-grained sediments, a sublitharenite (KAR5) and a lithic subarkose (KAR 6) from the southern part of the formation exhibit moderate amounts of lithic fragments (10–13%) from metapelitic and mafic volcanic rocks (Figure 2.6b). The texture is dominated by poorly- (KAR5) to well-sorted (KAR6) grains of (sub)angular shape (Figure 2.5b). Three fine-grained subarkosic rocks (KAR14, KAR15, KAR23) from the northern part, however, are slightly more mature and contain negligible amounts of lithic sedimentary fragments only (1–4%). Another sample (KAR7), classified as lithic arenite was taken from the southwestern coastal part of the study area. Its particular textural and compositional properties are characterised by considerably coarse and highly variable grain size and angular components. A striking feature is the high abundance of lithic volcanic rock fragments and large, subhedral plagioclase (mainly albite) and K-feldspar crystals (up to 2 mm) (Figures 2.5d, 2.6c). The heavy mineral assemblage of these rocks is dominated by tourmaline, zircon, rutile and titanite but garnet and chrome spinel are absent.

From the İdecik unit, two samples were collected in close distance to the Dikendağı Formation near Gerence Bay in the western part of the Karaburun Peninsula (Figure 2.1b). The sediments are classified as fine- to medium-grained sublitharenites (KAR3) and litharenites (KAR4), respectively. Petrographic features are very similar and their general texture is characterised by poorly-sorted subangular to subrounded grains (Figure 2.5e). Quartz is the dominant phase and altered plagioclase and K-feldspar are present in small amounts. Lithic fragments are comparatively abundant and appear as either volcanic or (meta)sedimentary lithoclasts (Figure 2.6f).

Two samples were collected from the Lower Triassic Gerence Formation at the west coast of the Karaburun Peninsula at Gerence Bay (Figure 2.1b). The first one (KAR1) is a fine- to medium-grained, carbonate-bearing (feldspathic) litharenite with poorly-sorted, subangular grains. Quartz and feldspar (mainly plagioclase) are the dominant phases and few grains show myrmekitic textures (Figure 2.5f). Lithic fragments, mainly derived from felsic volcanic rocks are highly abundant (40%) and sedimentary lithoclasts including chert are present but of subordinate importance (Figure 2.6g). Non-opaque accessory phases include zircon, apatite, tourmaline, pyroxene, garnet and chrome spinel.

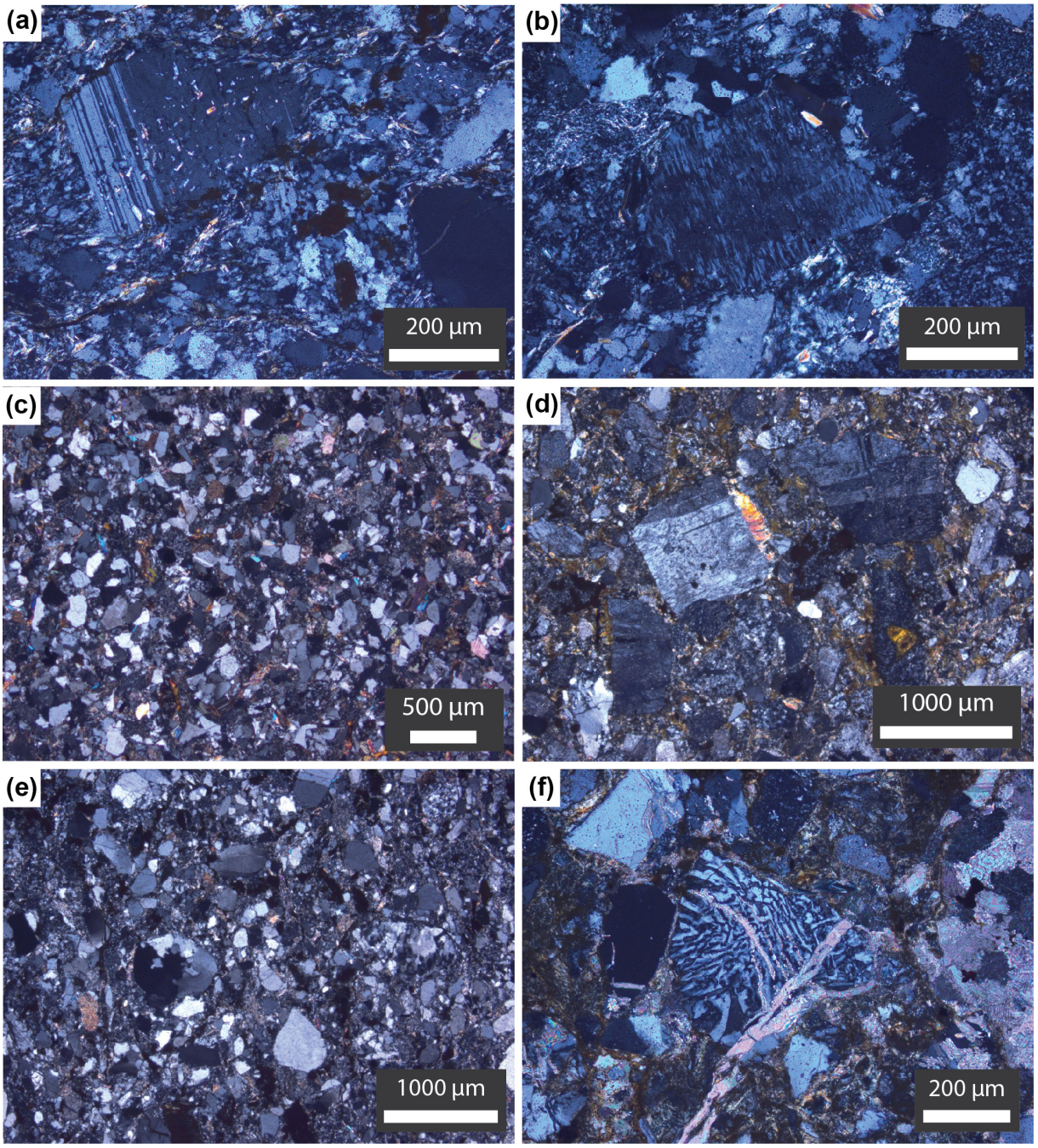

Fig. 2.5: Selection of photomicrographs (cross-polarised light) of studied sediments from the Karaburun Peninsula. **a** Polysynthetic twinning in inclusion-rich plagioclase (Küçükbahçe Formation). **b** Perthitic exsolution lamellae of plagioclase (albite) in K-feldspar (Küçükbahçe Formation). **c** Overview showing the texture of sandstone from the Dikendağı Formation. Main composition is monocrystalline quartz with minor feldspar, mica and calcite. **d** Large, angular plagioclase crystals and lithic fragments in an arkosic sandstone (Dikendağı Formation). **e** Overview photograph of well-rounded and poorly-sorted grains with predominantly quartzitic composition (İdecik unit). **f** Myrmekitic intergrowth of quartz in plagioclase cut by calcite veins (Gerence Formation).

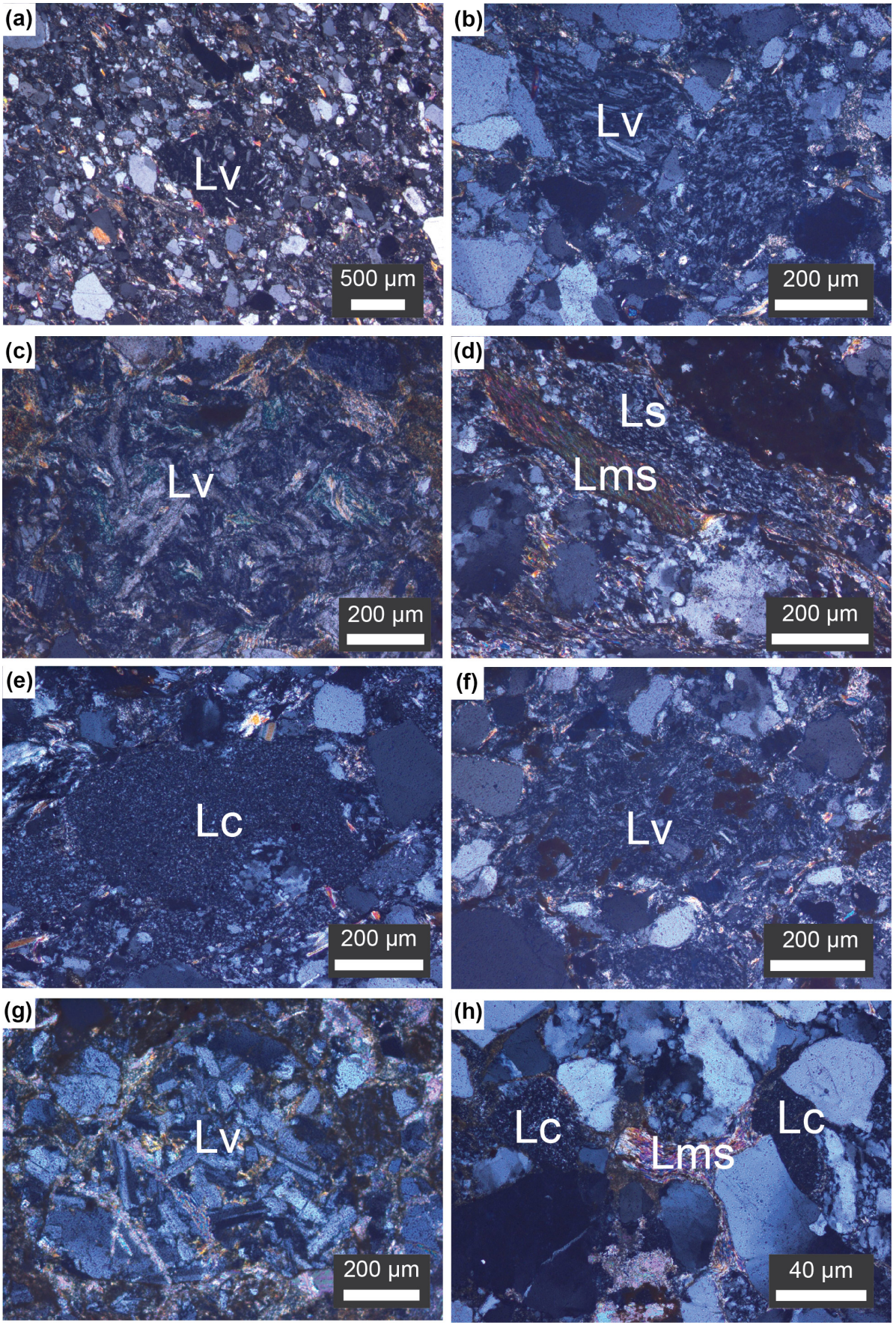
(a)
Lv
500 µm
(b)
Lv
200 µm
(c)
Lv
200 µm
(d)
Ls
Lms
200 µm
(e)
Lc
200 µm
(f)
Lv
200 µm
(g)
Lv
200 µm
(h)
Lc
Lms
Lc
40 µm

Fig. 2.6: Compilation of photomicrographs showing the main lithic fragments of studied sediments from the Karaburun Peninsula (cross-polarised light). **a** Mafic volcanic fragment (Lv) with plagioclase laths and needles (Alandere Formation). **b** Lithic volcanic fragment mainly composed of plagioclase (Dikendağı Formation). **c** Coarse-grained, altered fragment derived from a mafic volcanic rock (Dikendağı Formation). **d** Low-grade metasedimentary (mica-schist; Lms) and quartzitic fragments (Ls) (Küçükbahçe Formation). **e** Chert fragment (Lc) (Küçükbahçe Formation) **f** Fine-grained volcanic fragment with plagioclase laths and needles (İdecik unit). **g** Coarse-grained volcanic lithic fragment including plagioclase laths (Gerence Formation). **h** Fragments of mica-schist squeezed in intergranular spaces and chert (Güvercinlik Formation).

In contrast, sample KAR2 is a very fine-grained, mica-rich lithic subarkose with comparatively high textural maturity (Figure 2.3a). Its quartz content is considerably higher, whereas lithic fragments are less common. Accessory phases include zircon, amphibole, chloritoid and rutile.

Two samples (KAR20A and KAR20B) of the Güvercinlik Formation were collected from an outcrop at the eastern coast of the Karaburun Peninsula, ca. 4 km north of Balıklıova (Figure 2.1b). Both sediments are (highly) mature, medium-grained sublitharenitic rocks. Quartz is by far the most abundant phase and rock fragments are scarce and of sedimentary origin. These are often altered, highly deformed and occupy intergranular spaces (Figure 2.6h). Moreover, sample KAR20A contains small amounts of sparitic to micritic carbonate lithoclasts. Non-opaque accessory phases include zircon, garnet, tourmaline, rutile, amphibole (only KAR20A) and orthopyroxene (only KAR20A).

4.2 Whole-rock geochemistry

Whole-rock geochemical data of samples from the Karaburun Peninsula are shown in Figure 2.7. Geochemical composition of sediments from the Küçükbahçe and Alandere formations is very homogeneous with respect to major elements. Samples are characterised by moderate SiO_2 (74–77 wt.%) and Al_2O_3 contents (10–12 wt.%), low CaO (<0.75 wt.%), Na_2O (1.9–2.5 wt.%), K_2O (1.3–1.9 wt.%) and Fe_2O_3 contents (3.8–4.9 wt.%). In contrast, samples from the Dikendağı Formation are highly variable in major element compositions with low to high SiO_2 (64–83 wt.%), moderate to high Al_2O_3 (8–17 wt.%) and Na_2O contents (0.7–5.5 wt.%). Combination of high Al_2O_3 and Na_2O concentrations document abundant albite components for sample KAR7, as confirmed by petrographic observations. Geochemistry of samples from the İdecik unit is comparable with the Küçükbahçe Formation with the exception of slightly lower Fe_2O_3 (2.9–3.9

wt.%) and comparatively high TiO_2 contents (0.8 wt.%). Two sediments of the Gerence Formation have the lowest overall SiO_2 content (62–69 wt.%; except of KAR7), moderate to high Al_2O_3 content (10–15 wt.%) and high Fe_2O_3 content ($\sim$5 wt.%). Samples from the Güvercinlik Formation are highly mature and characterised by very high SiO_2 contents (>90 wt.%) and only traces of Na_2O (<0.02 wt.%). Low values of CaO and LOI for all sandstones – except of sample KAR1 (CaO $\sim$8 wt.%) – indicate an almost complete absence of carbonate-bearing phases.

Chondrite-normalised rare earth element (REE) patterns of selected sandstone samples from the Karaburun Peninsula (this study) and reference data from time equivalent deposits of the neighboring islands of Chios and Inousses (Meinhold et al., 2007) are shown in Figure 2.8. Triassic samples can be easily discriminated on the basis of their REE composition. Sample KAR1 from the Gerence Formation has a unique REE composition with almost no fractionation between LREE and HREE. In contrast, all other samples, including the samples of Chios and Inousses, have comparable REE patterns with only little variation. They show notably strong enrichment of LREE, followed by a decrease towards Sm, a negative Eu anomaly and flattening out towards the HREE. Due to its high amount of plagioclase sample KAR7 (Dikendağı Formation) has a positive Eu anomaly. Although these samples show similar behavior, the ratios of La_N/Yb_N as a measure for the degree of fractionation between LREE and HREE turned out to be a good indicator for discrimination of the different sedimentary successions. For the Upper Palaeozoic sandstones from the Karaburun Peninsula the fractionation is more pronounced (La_N/Yb_N = 8.00–14.79) compared to samples from Chios (5.82–9.23) and Inousses (7.40–9.95). Sample KAR20B from the Upper Triassic Güvercinlik Formation has a comparable pattern, but the REE concentrations are considerably lower.

Selected trace element concentrations for samples from the Karaburun Peninsula have been normalised to upper continental crust (UCC) and are shown in multielement diagrams (Figure 2.9). These include the large-ion lithophile elements (LILE; e.g., Rb, Ba, Sr) and high-field-strength elements (HFSE; e.g., Zr, Hf, Nb, Ta). Concentration of incompatible and easily mobilised LILE is generally controlled by the presence/absence of feldspar, and LILE are generally enriched in UCC compared to the mantle. The (highly) incompatible HFSE, however, are considered to be relatively immobile and therefore can provide additional information on sedimentary provenance (Taylor and McLennan 1985). During magmatic differentiation processes the HFSE

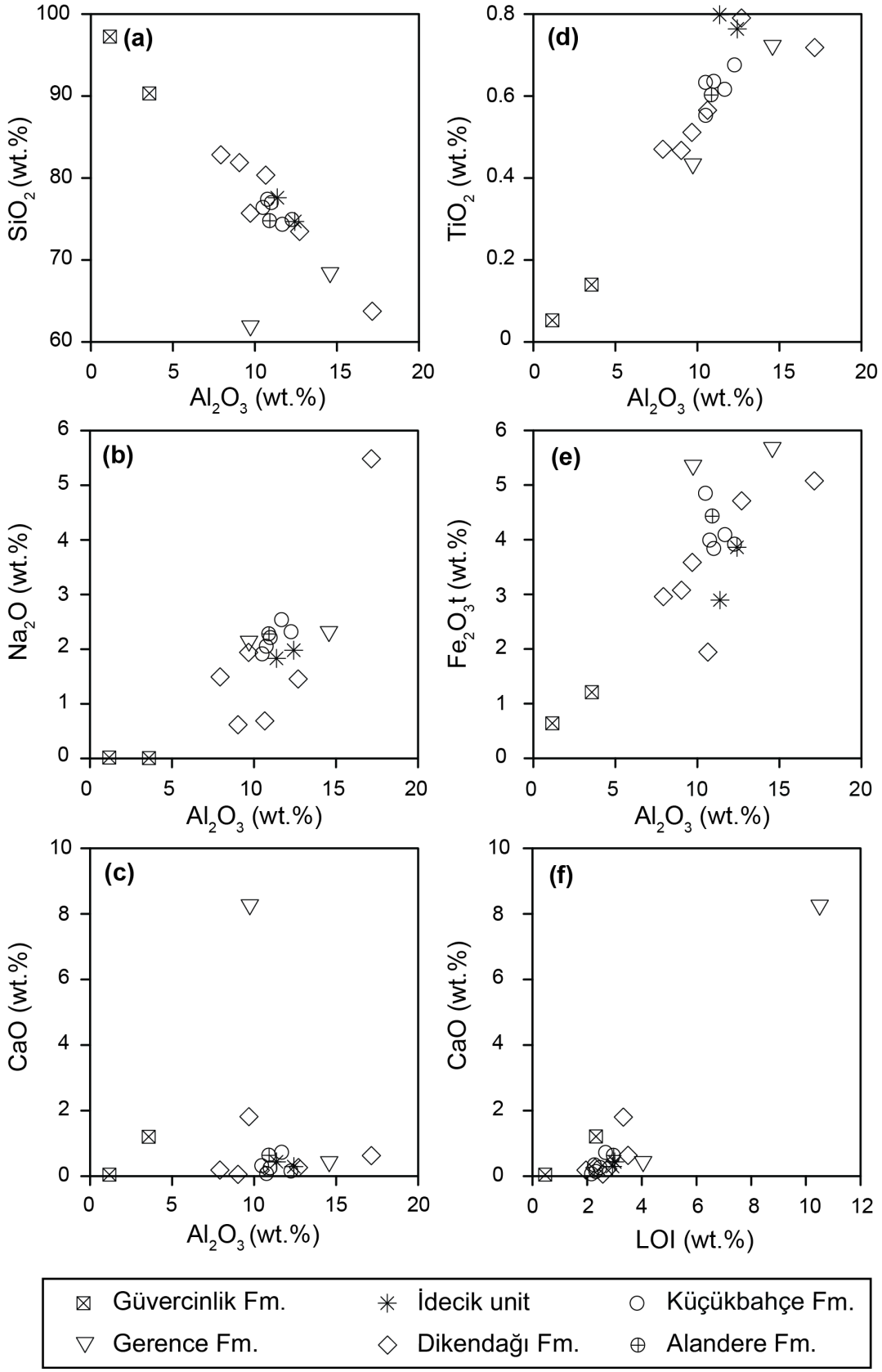

Fig. 2.7: Correlation diagrams of SiO_2, TiO_2, Na_2O, Fe_3O_3t and CaO versus Al_2O_3 and CaO versus LOI.

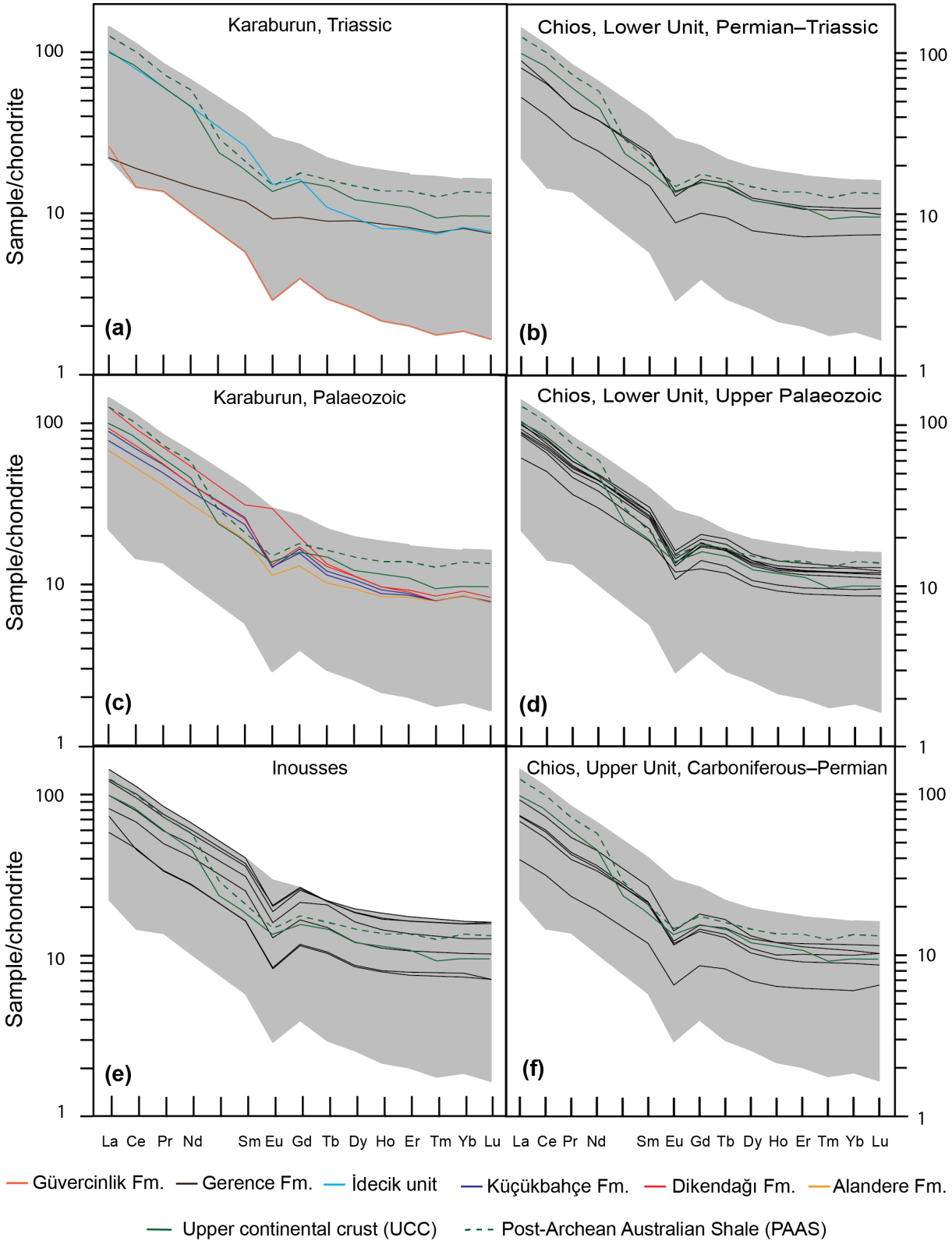

Fig. 2.8: Chondrite-normalised REE diagrams for samples from the Karaburun Peninsula and the islands of Chios and Inousses. Grey shaded areas indicate total range of data from the Karaburun Peninsula. Normalising values from Boynton (1984). UCC and PAAS data from Rudnick and Gao (2003) and McLennan (1989), respectively.

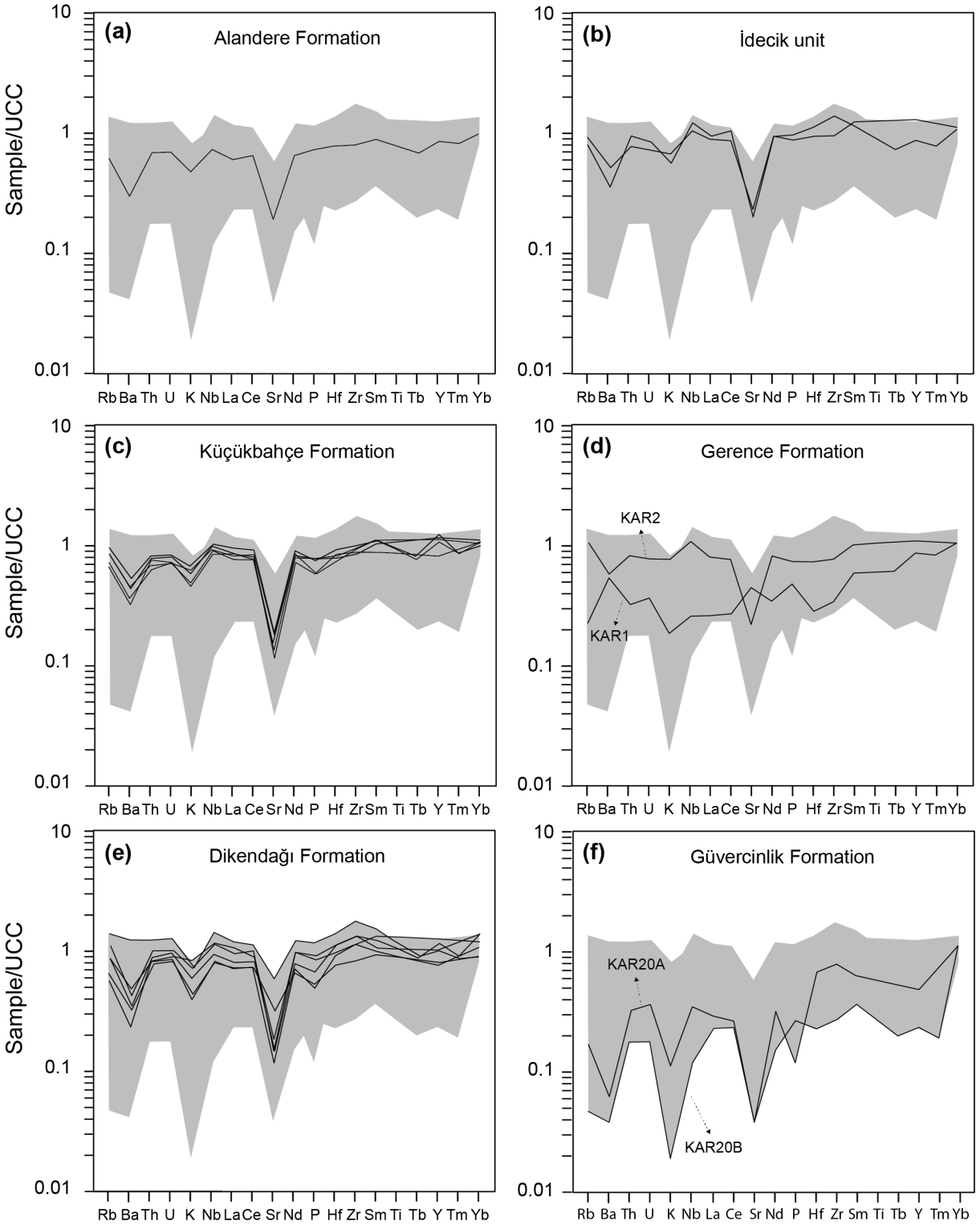

Fig. 2.9: UCC-normalised multielement diagrams for samples from the Karaburun Peninsula. Grey shaded areas indicate total range of data. Normalising values from Rudnick and Gao (2003).

are preferentially partitioned into the melt phase resulting in enrichment in felsic rather than mafic rocks (Bauluz et al. 2000). The similar behavior of Zr and Hf in our samples, revealed by a strong positive linear correlation (r = 0.96) indicates their concentrations are coupled to the mineral zircon, whereas rutile and monazite are major carriers of HFSE as well (Deer et al. 1992). Patterns of UCC-normalised trace element concentrations from the Upper Palaeozoic Küçükbahçe, Dikendağı and Alandere formations and the Ladinian–Carnian İdecik unit are similar with only little variation (Figure 2.9a, b, c, e). Their trace element concentrations are slightly below or at UCC level, with few exceptions. Pronounced negative anomalies exist especially for Sr, but also for Ba and K, probably attributed to the general low occurrence of feldspar. HFSE usually exhibit slight positive anomalies suggesting rather prevailing felsic than mafic source rocks. Sediments from the Güvercinlik Formation are highly depleted in all trace elements (except Yb) and define the lower limit of the overall pattern (Figure 2.9f). Elevated values of Hf, Zr, Sm, and Yb in one of those samples (KAR20A) are indicative for an enrichment of heavy minerals, especially garnet. Mineralogical compositions of samples from the Gerence Formation are significantly different which is well reflected in their multielement patterns (Figure 2.9d). One sample (KAR2) is similar in trace element composition to the above-mentioned samples whereas sample KAR1 is characterised by lower concentrations throughout the whole pattern, positive anomalies of Ba, Sr and P and slight depletion of HFSE.

A compilation of diagrams for the discrimination between felsic and mafic sources and identification of mafic components is shown in Figure 2.10. Elemental ratios of Cr/V and Y/Ni were used as proxies for (ultra)mafic components, i.e., in particular chrome spinel which is a key mineral in mafic and ultramafic rocks. The Y/Ni ratio is a monitor for the concentration of ferromagnesian elements (Ni) in relation to a proxy for the HREE (Y), generally enriched in zircon or garnet (McLennan et al. 1993). Thus, ultramafic (ophiolitic) sources tend to have high Cr/V but low Y/Ni ratios. Samples from the Karaburun Peninsula (black symbols) primarily plot in the lower left area of the diagram, except of two samples with high (>3) Y/Ni ratios (Figure 2.10a). Although high Cr/V ratios (1.6–2.2) and low Y/Ni ratios (0.3–0.5) indicate ultramafic components in five samples from the Gerence (KAR1), Alandere (KAR22), Küçükbahçe (KAR27) and Dikendağı (KAR6, KAR15) formations, chrome spinel was only spotted in thin sections and heavy mineral concentrates of sample KAR1, KAR22 and KAR27.

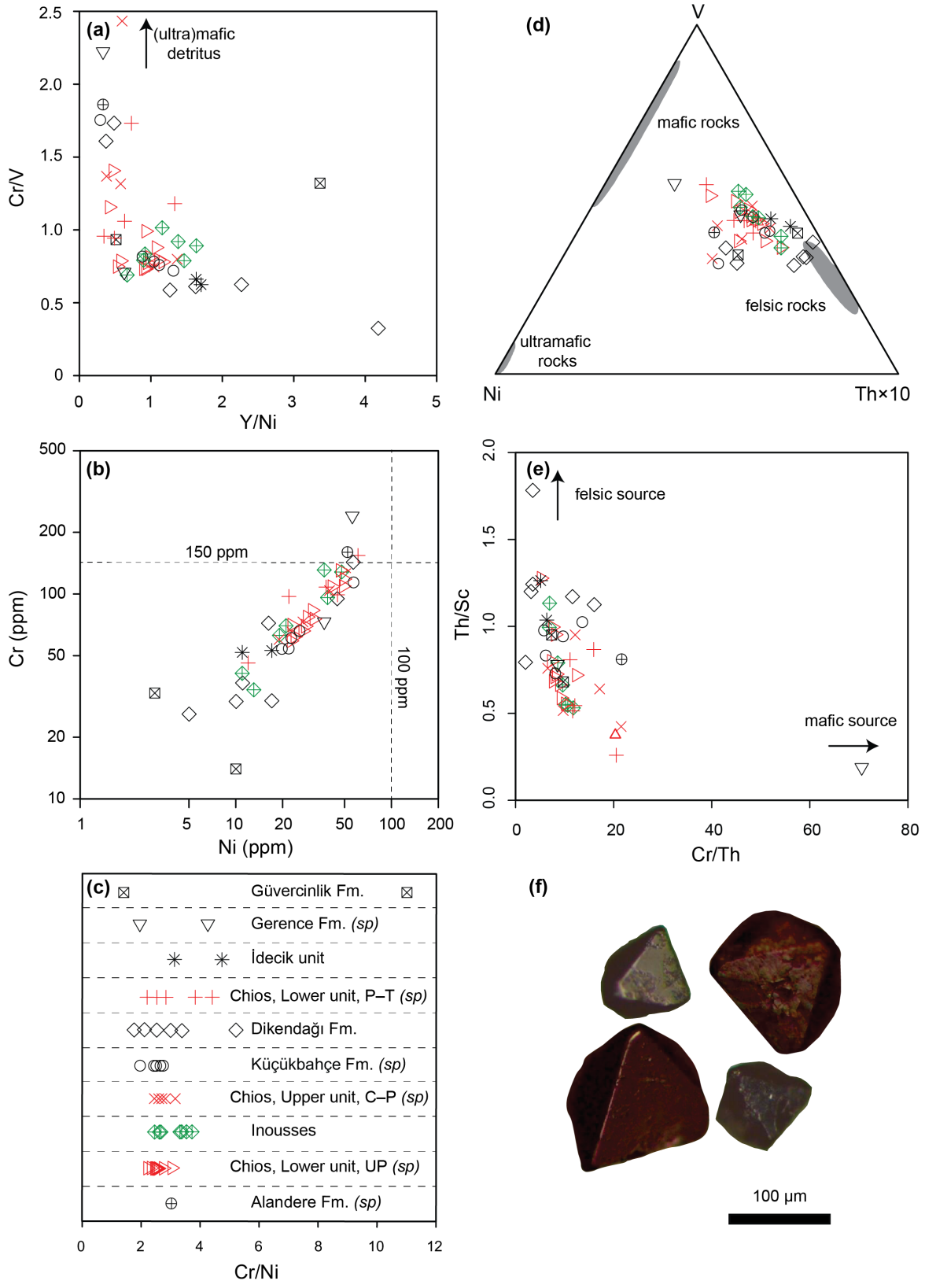
(a)
(ultra)mafic detritus
Cr/V
Y/Ni
(b)
150 ppm
100 ppm
Cr (ppm)
Ni (ppm)
(c)
Güvercinlik Fm.
Gerence Fm. (sp)
İdecik unit
Chios, Lower unit, P–T (sp)
Dikendağı Fm.
Küçükbahçe Fm. (sp)
Chios, Upper unit, C–P (sp)
Inousses
Chios, Lower unit, UP (sp)
Alandere Fm. (sp)
Cr/Ni
(d)
V
mafic rocks
felsic rocks
ultramafic rocks
Ni
Th×10
(e)
felsic source
mafic source
Th/Sc
Cr/Th
(f)
100 µm

Fig. 2.10: Discrimination diagrams for identifying an (ultra)mafic provenance. **a** Cr/V versus Y/Ni diagram after McLennan et al. (1993). **b** Cr versus Ni diagram and **c** Cr/Ni ratios. High concentrations of Cr (>150 ppm) and Ni (>100 ppm) combined with Cr/Ni ratios ranging from 1.3 to 1.5 are indicative of an ultramafic provenance; Cr/Ni ratios of 2 and greater typify an input of mafic volcanic rocks (Garver et al. 1996). Abbreviations: sp = presence of Cr-spinel, observed in thin section and/or heavy mineral concentrate; P–T = Permian–Triassic; C–P = Carboniferous–Permian; UP = Upper Palaeozoic. **d** Ternary V–Ni–Th×10 diagram for source rock discrimination after Bracciali et al. (2007). Grey shaded areas represent source rock endmembers. **e** Th/Sc versus Cr/Th diagram. Felsic sources tend towards enrichment of incompatible elements (Th) and mafic rocks have higher concentrations of compatible elements (Cr, Sc). **f** Photomicrographs of idiomorphic chrome spinel grains from sample KAR1 (Lower Triassic Gerence Formation).

Additionally, Garver et al. (1996) showed that high concentrations of Cr (>150 ppm) and Ni (>100 ppm) combined with Cr/Ni ratios of 1.3–1.5 in sandstones are indicative of ultramafic rocks in the source region as well. Although, total concentrations of Ni and Cr in our samples are low for Ni (3–57 ppm) and variable for Cr (14–240 ppm) and neither samples from the Karaburun Peninsula nor reference samples from the islands of Inousses and Chios meet both criteria, there is evidence of chrome spinel in several of these sediments (Figure 2.10b, c, f). The ternary V–Ni–Th×10 and bivariate Th/Sc vs. Cr/Th plots use elements and/or elemental ratios that are sensitive to (ultra)mafic and felsic components, respectively (Figure 2.10d, e). High Cr/Th values typify input of mafic character, whereas high Th/Sc values are indicative for detritus derived from felsic rocks (e.g., Hofmann et al. 2003). The signature of our samples in both diagrams suggests rocks of felsic lithology as primary source with variable but minor contribution of mafic detritus. Samples from the Dikendağı Formation are seemingly closer to the felsic composition and a set of samples including KAR1, KAR22 and KAR27 (Gerence, Alandere and Küçükbahçe formations) received notably amounts of mafic components.

4.3 Geochemistry and tectonic settings

Whole-rock geochemical data of sedimentary rocks can provide information for the interpretation of the tectonic setting of depositional basins. Conventional diagrams of Bhatia (1983), Roser and Korsch (1986) or Bhatia and Crook (1986) have been used for a long time to discriminate active and passive continental margin settings, but recent re-evaluations by Verma and Armstrong-Altrin (2013, 2016) contested the efficiency of the existing plots. Verma and Armstrong-Altrin (2013, 2016) used statistical tools and proposed new multidimensional diagrams based on loge-ratio transformation of major and combined major and trace elements and linear discriminant analysis. These new

plots were used in this study in combination with the conventional approach of Roser and Korsch (1986) to decipher the tectonic setting from sedimentary rock geochemistry (Figure 2.11). Discriminant functions were calculated using revised equations published in the corrigendum to Verma and Armstrong-Altrin (2016) (Figure 2.11c, d). At first sight the diagrams predict consistent tectonic settings for a small number of samples only, but yield contradictory results for many samples as well. The geochemical signal of the Güvercinlik Formation unambiguously indicates a passive margin setting. Even though samples from the İdecik unit are not equally well defined, a passive margin setting seems most likely as well. Data of the Gerence Formation are of ambiguous character with slight affinities to an active margin setting. However, there are limitations for the discrimination of active and passive tectonic settings, relying solely based on geochemical data. This becomes obvious with respect to the Upper Palaeozoic sediments of the Küçükbahçe and Dikendağı formations. On the one hand, multidimensional diagrams based on major elements clearly indicate an active margin setting (Figure 2.11c) and, considering trace elements as well, a passive margin setting on the other hand (Figure 2.11d) whereas mixed signals are inferred from additional diagrams (Figure 2.11a, b).

4.4 Mineral chemistry

Geochemical single-grain analysis of detrital heavy minerals is a complementary technique and frequently conducted in sedimentary provenance studies (Mange and Morton 2007, and references therein). Garnet, rutile and chrome spinel, amongst others, are very useful accessory minerals for deciphering source rock lithologies.

Garnet is a very common heavy mineral that occurs in a wide range of metamorphic and also igneous rocks and is relatively stable during sedimentary transport and burial diagenetic conditions (e.g., Wright 1938; Morton 1985; Deer et al. 1992). Its comparatively wide range of major and trace element composition is primarily controlled by host rock composition and reflects changes in pressure and temperature conditions during mineral growth as well. Therefore, mineral chemistry of detrital garnet is widely used as a provenance indicator in studies of sedimentary rocks (e.g., Mange and Morton 2007; Krippner et al. 2014, 2015, 2016, and references therein).

Rutile is the most common TiO_2 polymorph, mainly formed during medium- to high-grade metamorphic processes; thus eclogites, granulites and high-grade metasedi-

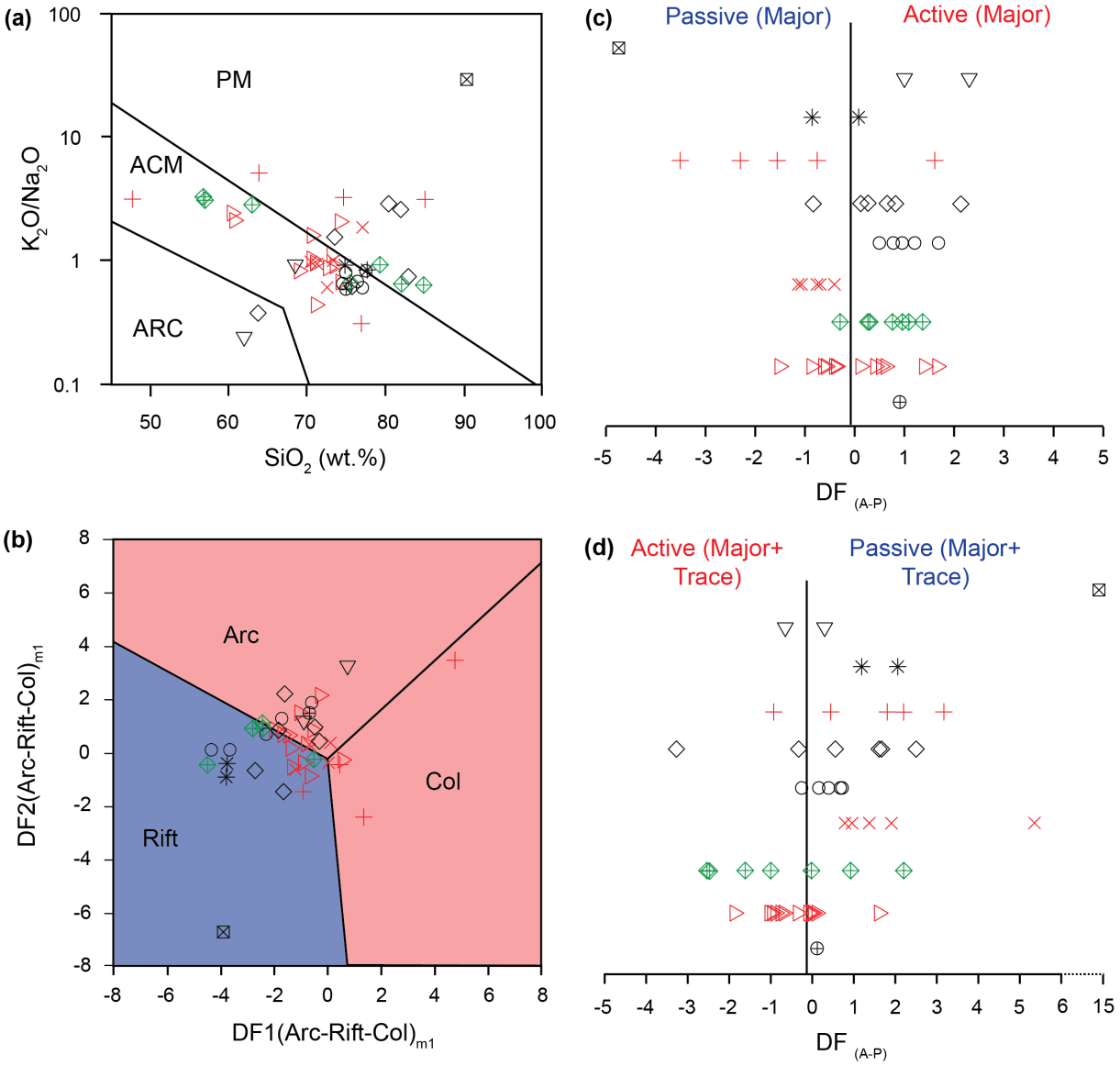

Fig. 2.11: Tectonic discrimination for samples from the Karaburun Peninsula and the islands of Chios and Inousses. **a** Diagram after Roser and Korsch (1986). PM – passive margin; ACM – active continental margin; ARC – oceanic island arc margin. **b** Multidimensional diagram after Verma and Armstrong-Altrin (2013) for discrimination of tectonic settings (63%<SiO_2<95%). Arc – island or continental arc; Rift – continental rift; Col – collision. **c, d** Multidimensional discriminant function diagrams for the discrimination of active and passive margin settings after Verma and Armstrong-Altrin (2016). See Figure 2.10 for explanation of symbols.

ments are the primary host rocks (e.g., Meinhold et al. 2010, and references therein). Due to its high chemical and physical resistance during sedimentary processes rutile is widespread in modern and ancient sedimentary rocks, preserving information on source rock lithology. For discrimination of mafic and felsic sources, based on the Cr–Nb system, the most recent criterion proposed by Triebold et al. (2012) was used:

$$x = 5 \times (Nb_{ppm} - 500) - Cr_{ppm}$$

with negative values representing rutiles from mafic rocks and positive values representing rutiles from felsic rocks. Grains with Nb and Cr concentrations below the detection limit were excluded from the calculation. If possible (i.e., Zr concentration>detection limit) formation temperatures were calculated using the Zr-in-rutile thermometer of Tomkins et al. (2007):

$$T(^{\circ}\mathrm{C}) = \frac{83.9 + 0.410 \times P}{0.1428 - R \times lnZr_{ppm}} - 273$$

in which R is the gas constant (0.0083144 kJ/K) and P = 10 kbar (default setting, as no pressure information is available for the detrital rutile grains).

Chrome spinel is a very stable, accessory mineral associated with mafic and ultramafic igneous rocks and is widely used as provenance indicator in studies of sedimentary rocks (e.g., Pober and Faupl 1988; Cookenboo et al. 1997; Lužar-Oberiter et al. 2009; Caracciolo et al. 2015). Its chemical composition is controlled by several factors, as the behavior of the main components Cr, Mg and Al is different during fractional crystallisation or partial melting. Thus, their ratios expressed as Cr-number (Cr#) = Cr / (Al + Cr) and Mg-number (Mg#) = Mg / (Mg + Fe^{2+}) are sensitive to different physicochemical conditions and reveal petrogenetic signatures. Furthermore, the geodynamic setting of source rocks can be deduced from concentrations of Al_2O_3 and TiO_2 in chrome spinel as these elements are linked to magma type and composition (e.g., Cookenboo et al. 1997; Kamenetsky et al. 2001).

4.4.1 Garnet

A total of 156 single grains of detrital garnet were analysed from three samples of the Serpukhovian–Bashkirian Alandere Formation, the Lower Triassic Gerence Formation, and the Upper Triassic Güvercinlik Formation. Compositional data are presented using the triangular diagram for garnet discrimination after Mange and Morton (2007) (Figure 2.12). Garnets from the three formations predominantly scatter in the lower left corner of the diagram but, nonetheless, show distinct characteristics. The most diverse garnet population is present in the Güvercinlik Formation with dominant input of type Bi (intermediate to felsic igneous rocks – 48%) and Bii (amphibolite-facies metased-

iments – 29%) garnet, but small amounts of type Ci (high-grade meta mafic rocks – 14%) and A (granulite-facies metasediments – 9%) grains as well (Figure 2.12a). In contrast, the Gerence Formation exhibits considerably higher amounts of Bii (56%) but lower percentage of Bi type (30%) grains with negligible amounts of garnet from high-grade metamafic igneous and granulite-facies metasedimentary rocks (Figure 2.12b). Compositional data of garnets from the Alandere Formation are very homogenous and suggest mainly intermediate to felsic igneous rocks (74%) as host lithologies with only minor input of Bii and A type garnets (Figure 2.12c).

4.4.2 Rutile

Results for source rock classification from 358 single EMPA measurements of rutiles from eight sandstone samples are shown in Figure 2.13. For most of our samples the data indicate a mixture of mafic and felsic sources with a majority of rutiles being derived from felsic rocks (44–78%) (Figure 2.13a). However, rutiles from the Küçükbahçe Formation and Idecik unit (KAR4) indicate significant supply from mafic source rocks (49–56%).

Results of Zr-in-rutile thermometry are shown in Figure 2.13c. Although the application of this thermometer works best for rutiles derived from rocks with rutile–quartz–zircon assemblages, it has been shown that calculations of rutiles from mafic rocks can provide complementary temperature information (Zack and Luvizotto 2006; Triebold et al. 2007). Calculated formation temperatures for rutiles of the Karaburun samples range from 500 to 950 °C. The major population in all samples, except KAR7, occurs in the range from 600 to 700 °C (42–61%). High- temperature rutiles (>700 °C) are of minor importance in samples KAR20A (Güvercinlik Formartion), KAR4 (Idecik unit) and the Küçükbahçe Formation but dominate in sample KAR7 (Dikendağı Formation) and are present in great numbers in KAR3 (İdecik unit) and KAR22 (Alandere Formation).

4.4.3 Chrome spinel

Compositional data of detrital chrome spinel were obtained from 122 single grains of the Upper Palaeozoic Küçükbahçe and Alandere formations and the Lower Triassic Gerence Formation. Analysed grains have TiO_2 concentrations <0.8 wt.% with variable Al_2O_3 contents of 2–37 wt.% (Figure 2.14a). Cr-spinel from the Upper Palaeozoic

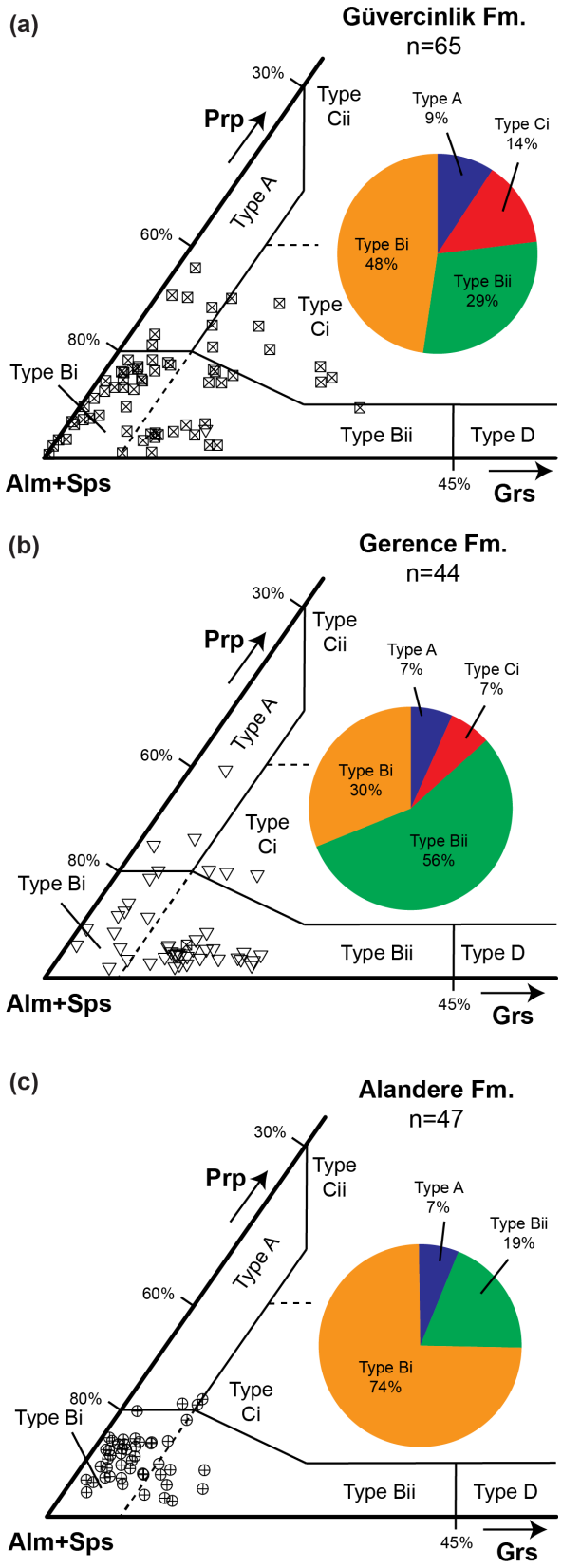

Fig. 2.12: Composition of garnets in the ternary classification scheme of Mange and Morton (2007) with idealised almandine+spessartine (Alm+Sps), pyrope (Prp) and grossular (Grs) compositions as poles. Pie charts give percentage distribution of garnet types.Garnet types: A – sourced from granulite facies metasediments, charnockites or intermediate to felsic deeper crust rocks; Bi – from intermediate to felsic igneous rocks; Bii – from amphibolite-facies metasediments; Ci – from high-grade metamafic rocks; Cii – from ultramafic rocks with high Mg; D – from Ca-rich metamorphites like metasomatic rocks (skarns), very low-grade metabasic rocks or ultra-high temperature calc-silicate granulites.

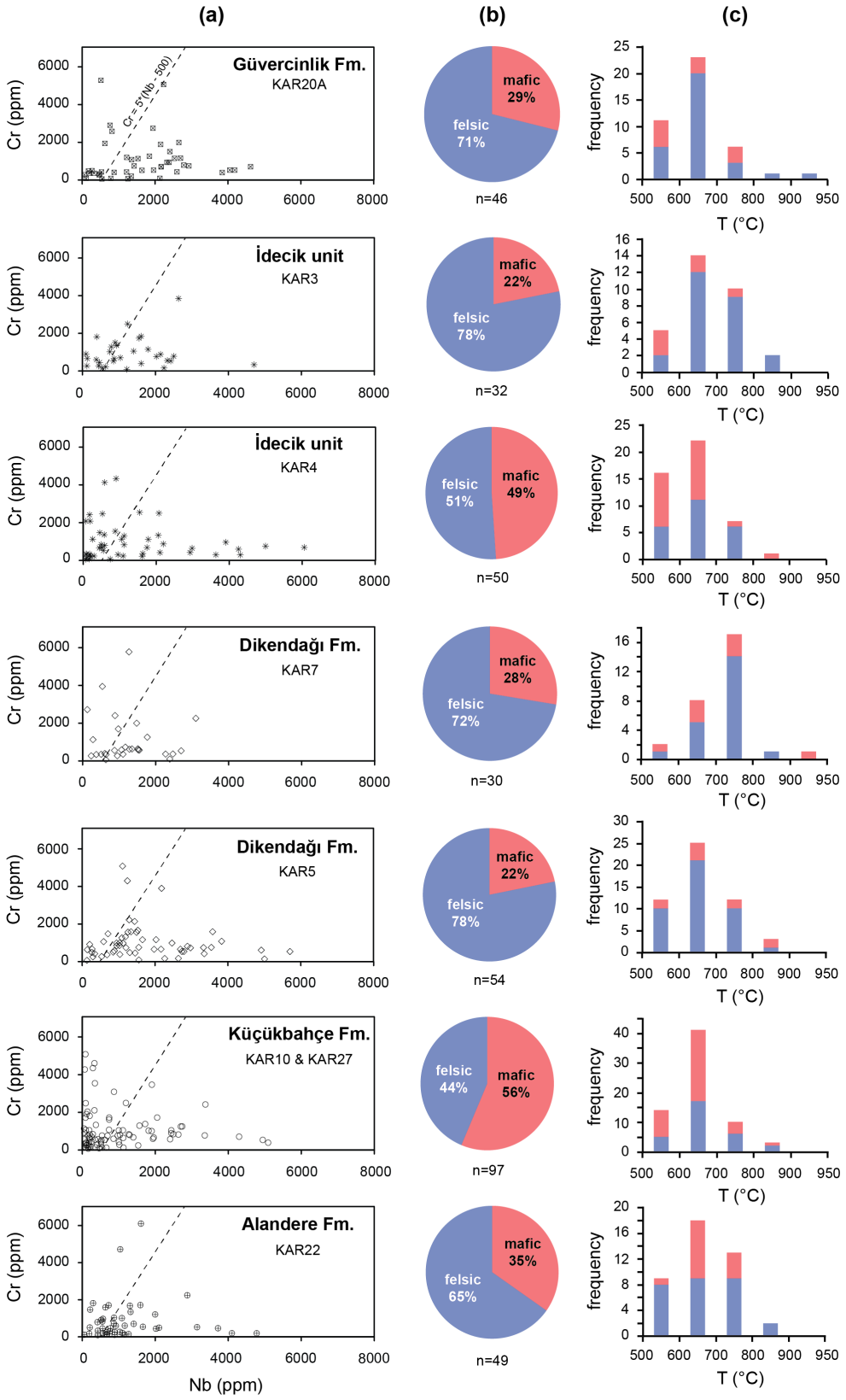

Fig. 2.13: **a** Plot of Nb versus Cr contents of detrital rutiles with discrimination line from Triebold et al. (2007). **b** Percentage distribution of rutile derived from felsic and mafic rocks. **c** Histograms of calculated formation temperatures for metamafic and metapelitic rutiles.

formations mostly scatter in the lower area of the diagram (<0.1 wt.% TiO_2). Many grains from the Alandere Formation reveal MORB peridotite affinity and preferably more chrome spinels of the Küçükbahçe Formation plot in the field of supra-subduction zone (SSZ) peridotites. Grains from the Lower Triassic Gerence Formation form a distinct group, characterised by generally higher TiO_2 and lower Al_2O_3 concentrations. This signature is preferably indicative of island-arc basalts but also mid-ocean ridge basalts to a lesser extent. Calculated Cr# and Mg# values vary between 0.33 and 0.83 (with one very Cr-rich spinel at 0.94) and 0.25–0.75, respectively (Figure 2.14b). Chrome spinel grains from the Upper Palaeozoic samples of the Karaburun Peninsula overlap with reference data of chrome spinels from Upper Palaeozoic and Lower Mesozoic siliciclastic sediments of Chios Island and suggest a mixed (ultra)mafic source of dominant harzburgite and minor lherzolite composition. The chrome spinel composition in the Gerence Formation is more variable in Mg# and a proportion of grains has considerably high Cr# and Mg#, and for the most part they overlap with the field of podiform chromitites. At this point it should be mentioned that chrome spinel grains of this Lower Triassic sample (KAR1) are often euhedral (Figure 2.10f), which was not observed in any other population.

5 Discussions

5.1 Tectonic setting

The new dataset from the Karaburun Peninsula provides some important parameters that allow a refined interpretation of the tectonic settings of these sediments. Besides the petrographic and chemical composition of sediments also the zircon population and corresponding age spectra help deciphering the tectonic setting of a basin. Depending on the nature of a sedimentary basin, the magmatic and tectonic activity and the extent of erosion are of variable intensity. These processes are the main factors controlling the supply and preservation potential of zircon in sedimentary rocks. Cawood et al. (2012) used the difference between crystallisation ages of detrital zircon and depositional age of sediments to infer information on the tectonic setting of a basin. Following their approach, it allows to discriminate three settings: i) Convergent settings, including basins within supra-subduction zone (SSZ) settings, extending from trench to back-arc that exhibit high quantities of zircons with ages close to the depositional age. ii) In con-

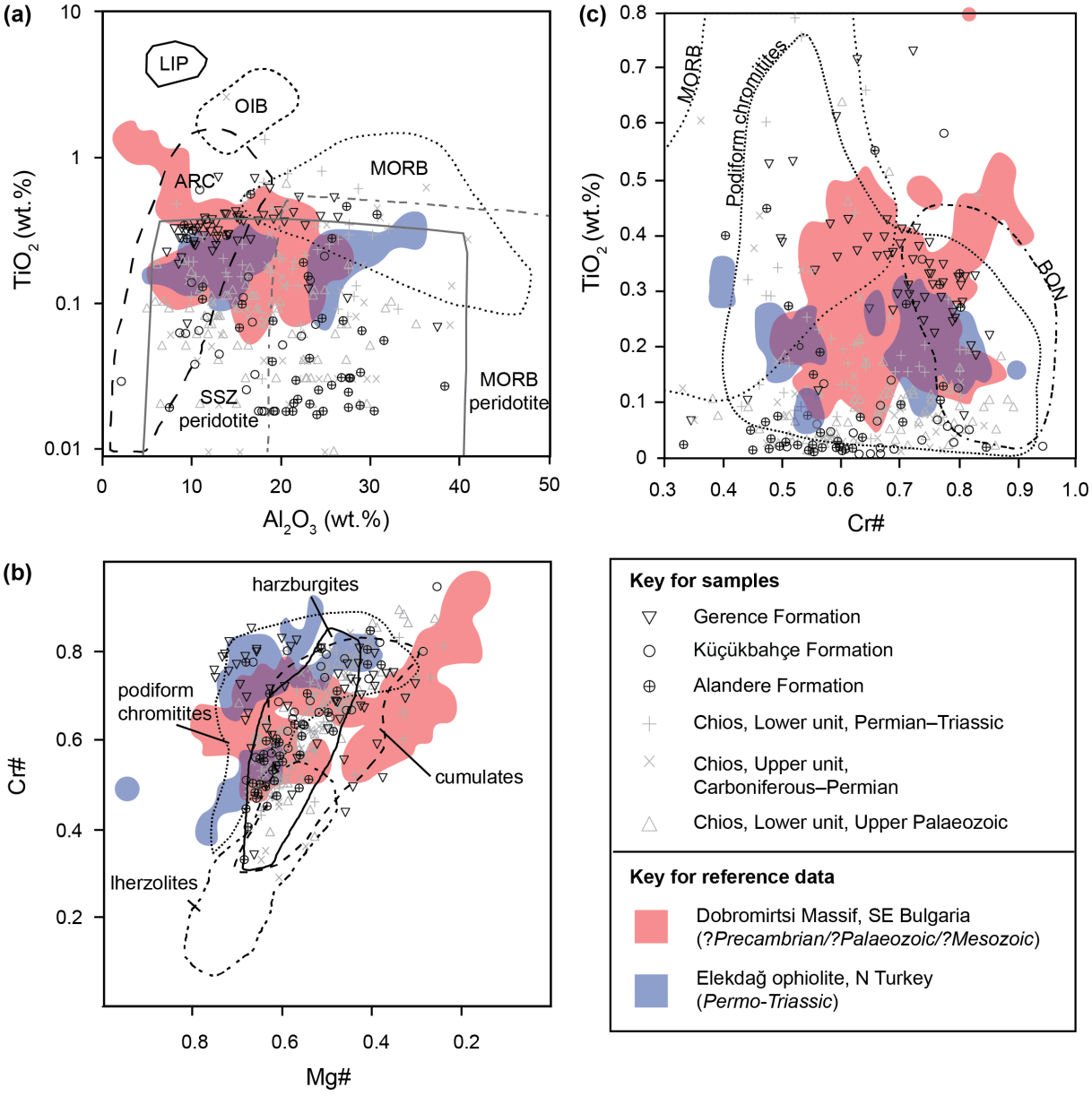

Fig. 2.14: Compositional data for detrital chrome spinel from the Lower Triassic Gerence Formation and Upper Palaeozoic Alandere and Küçükbahçe formations. Grey symbols represent data from Upper Palaeozoic and Lower Mesozoic sediments of Chios (taken from Meinhold et al. 2007). Coloured fields refer to compositions of chrome spinel from the Dobromirtsi Ultramafic Massif in Bulgaria (González-Jiménez et al. 2015) and the Elekdağ ophiolite in northern Turkey (Dönmez et al. 2014). The age of the Dobromirtsi ophiolite is unknown – its protoliths have been considered to be Precambrian, Palaeozoic or Mesozoic. A Palaeozoic age is supported by a prominent Os model-age peak at 0.4 Ga from platinum-group minerals in chromite (González-Jiménez et al. 2015). **a** TiO_2 versus Al_2O_3 diagram with Cr-spinel discrimination fields (after Kamenetsky et al. 2001). LIP–large igneous province, OIB–ocean-islandbasalts, ARC–island-arc basalts; MORB–mid-ocean ridge basalts, SSZ–supra-subduction zone. **b** Cr- and Mg-numbers with discrimination fields for harzburgites and lherzolites (after Pober and Faupl 1988). **c** TiO_2 versus Cr# diagram for tectonic discrimination (after Pagé and Barnes 2009).

trast, zircon age spectra with large differences between crystallisation and depositional age and negligible amount of grains with ages close to the depositional age (<150 Ma) are indicative of extensional settings. iii) Basins resulting from continental collision are identified by intermediate zircon spectra with low proportion of grains with ages approximating the depositional age, but moderate amount of zircons having ages within 150 Ma of the sedimentation age. Zircon data of sedimentary rocks from the Karaburun Peninsula and the islands of Inousses and Chios are shown in Figure 2.15, following the approach of Cawood et al. (2012). Samples from the Güvercinlik Formation have a high amount of zircon (48%) with ages within 150 Ma of the host sediment, suggesting deposition in convergent or more probably a collisional setting. A similar pattern is revealed by sediments of the Gerence Formation with a very high proportion of grains (>90%) with ages within 200 Ma of the age of the sediment, indicative of collisional or convergent settings. It should be mentioned that the number of detrital zircons is comparatively low (n = 51) – a higher number of zircons would potentially yield a clearer result. In contrast, the Ladinian–Carnian İdecik unit shows highest deviation of the youngest zircon population and depositional age – only 7% of all grains are within a 150 Ma difference – and (almost) match the criteria for extensional settings. Samples from the Küçükbahçe, Dikendağı and Alandere formations have variable amounts of zircons with ages within 150 Ma of the depositional age (24%, 12% and 28%, respectively) and plot in the field of collisional settings. Sample KAR7 from the Dikendağı Formation is illustrated in a separate graph because its petrographic and geochemical features, and unimodal detrital zircon spectrum (400–450 Ma) are of special character. A similar unimodal spectrum (350–400 Ma) is revealed by zircons of the Gerence Formation, suggesting a collisional or convergent setting. Data from sedimentary rocks of Chios are plotted for comparison, but they are of limited validity due to the very low number of data points (n = 27 and n = 23). However, their patterns suggest deposition in a collisional setting. The zircon population of Inousses is comparable to the Küçükbahçe and Alandere formations of Karaburun, thus suggesting a collisional setting. One should keep in mind that this approach can be very sensitive to the accuracy to which the depositional ages are known. This is of special importance for the interpretation of basins with extensive syndepositional magmatic activity (Cawood et al. 2012).

Deciphering the tectonic settings of depositional basins has proven to be a chal-

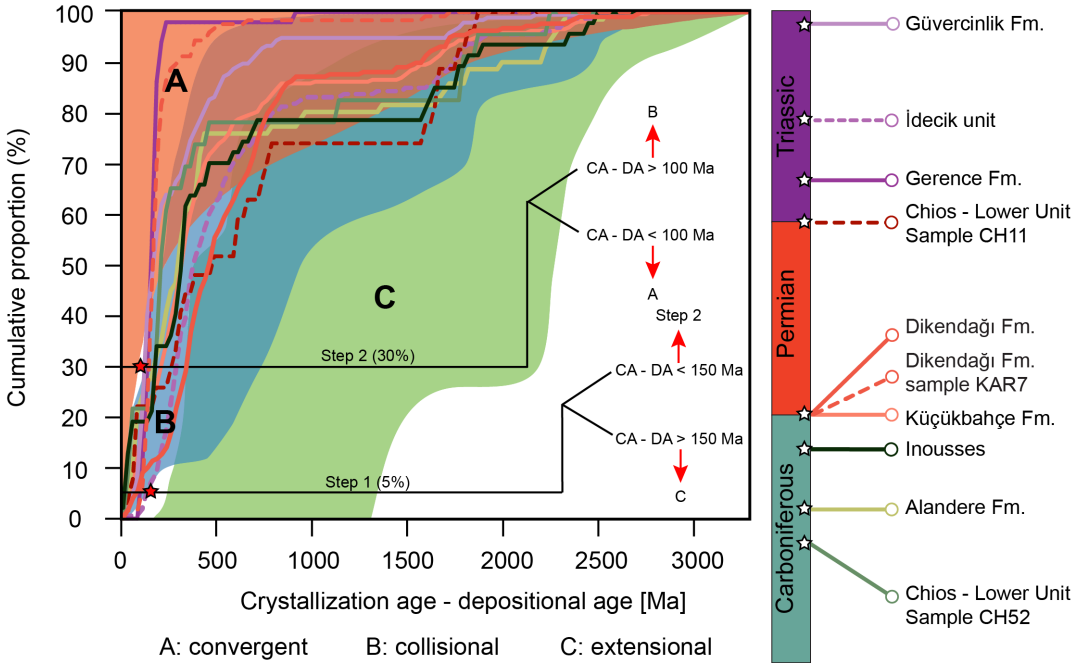

Fig. 2.15: Crystallisation age minus depositional age versus cumulative proportion of detrital zircon ages (after Cawood et al. 2012). Data for samples from the Karaburun Peninsula are from Löwen et al. (2017) and for the islands of Chios and Inousses are from Meinhold et al. (2008b) and Meinhold and Frei (2008), respectively.

lenging task, and the use of complementary techniques (e.g., petrography, geochemistry, geochronology) is essential for well-founded interpretations. For instance, Armstrong-Altrin and Verma (2005) highlighted significant problems with conventional well-established tectonic discrimination diagrams. Proposed plots of Bhatia (1983) were evaluated using Miocene to Recent sandstones from known tectonic settings and turned out to yield unsatisfactory results with low rates of success, varying from 0 to 62%. A more recent study by Verma and Armstrong-Altrin (2016) tested the performance of the Roser and Korsch (1986) diagram with respect to grain-size dependency. For fine-grained samples from active margins a success rate of nearly 72% was yielded whereas only 14% of coarse-grained sandstones were successfully classified. Performance of the diagram was even worse for passive margin environments with rates of success between 17% and 39%, respectively. The authors suggest the chosen database for establishment of the diagram was not representative of a worldwide average and might be a major source of error. New discrimination function-based diagrams proposed by Verma and Armstrong-Altrin (2013, 2016) (Figure 2.10b–d) were tested on a large number of Neogene and Quaternary siliciclastic sediments from known tectonic

settings and yielded very high success rates of 85 to 94% and 87 to 97%, respectively. A compilation of discrimination diagrams used for the present study is given in Figure 2.16 and points out remarkably different results. In spite of the great performance of the Verma and Armstrong-Altrin's plots, discrimination of samples from Karaburun Peninsula and Chios Island, especially the Upper Palaeozoic sandstones of the Küçükbahçe and Dikendağı formations is problematic and to some extent contradictory. Verma and Armstrong-Altrin (2013, 2016) state that their approach has shown to be robust against weathering and diagenetic processes but potential uncertainty might arise from other factors. For instance, the diagram published in 2013 (Figure 2.16c) was successfully tested on old, Precambrian rocks, but the effect of grain size is not discussed. In contrast, the database for plots published in 2016 (Figure 2.16d–e) includes a wide range of mud-, clay-, silt- and sandstones, thus considering grain size but performance was not yet tested on pre-Quaternary rocks.

Within the framework of previous studies on the Karaburun Peninsula the sedimentary units have been interpreted in different ways and the formation and tectonic setting of the mélange unit has been discussed controversially. Kozur (1995, 1998) favour a sedimentary olistostromal origin of the mélange as an accretionary complex with periodic emplacement of olistoliths. Robertson and Pickett (2000) agree with this model but suggest a tectonic rather than a sedimentary formation process. In this model, mélange blocks were produced by shearing of limestones, cherts and a siliciclastic matrix during collisional processes. In another scenario the Palaeozoic successions are interpreted as remnants of an accretionary complex that was exhumed and reworked as olistostromes into a fore-arc basin during Late Carboniferous time (Stampfli et al. 2003). According to Erdoğan et al. (1990, 2000), the Palaeozoic and Triassic successions including Upper Palaeozoic blocks of limestone and chert were related to Triassic rifting and continuous synsedimentary tectonic activities.

Most of the discussed models consider the Palaeozoic silciclastic rocks of the Karaburun and Chios mélange as remnants of an accretionary complex that represents the (first) passive, then active margin of the Palaeotethyan Ocean. Incipient subduction beneath the either Gondwana or Eurasian margin in Carboniferous times led to the formation of a magmatic-arc and development of a fore-arc basin (Moix et al. 2013). Also the polarity of subduction and palaeoposition of the Chios– Karaburun units during this time period is still a matter of discussion. Some workers favour a position along the

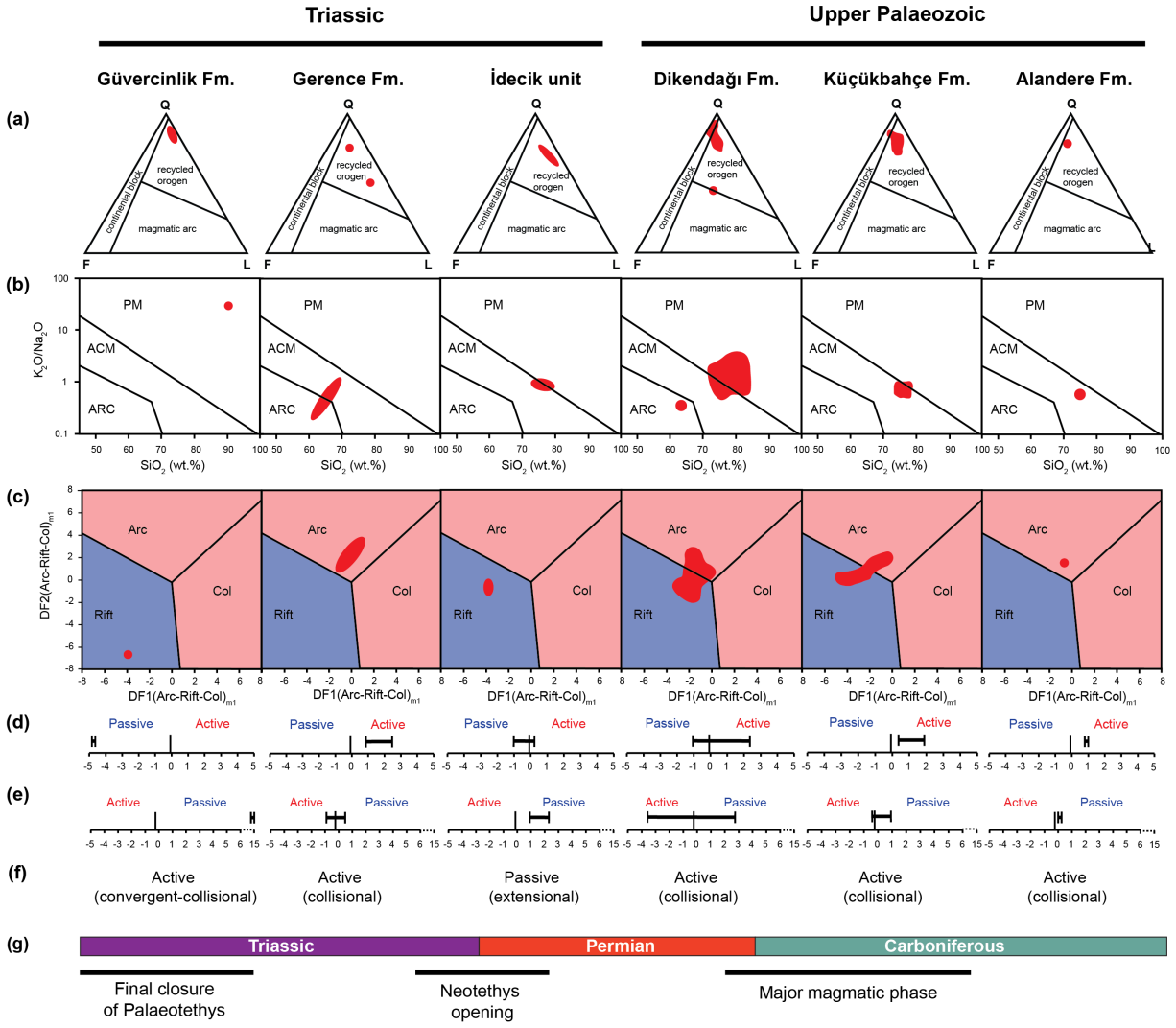

Fig. 2.16: Compilation of information on tectonic settings based on petrographical, geochemical and geochronological data from the Karaburun Peninsula. **a** Diagrams after Dickinson et al. (1983). **b** Diagrams after Roser and Korsch (1986). **c** Diagrams after Verma and Armstrong-Altrin (2013). **d, e** Diagrams after Verma and Armstrong-Altrin (2016). **f** Determination of tectonic setting after Cawood et al. (2012).

northern margin of Gondwana in combination with southward subduction (e.g., Robertson and Pickett 2000; Robertson and Ustaömer 2009b; Akal et al. 2011). Comparable units have also been described from the Konya area (south-central Turkey) and are interpreted to have been deposited either along the northern margin of Palaeotethys, i.e. southern margin of Eurasia (Eren et al. 2004), or along the southern margin of Palaeotethys, i.e. northern margin of Gondwana (Göncüoğlu et al. 2007; Robertson and Ustaömer 2009a). Carboniferous arc-type magmatic rocks have been reported from the Simav area (NW Afyon Zone) and were interpreted as evidence for short-lived southward subduction of Palaeotethys beneath the northern Gondwana margin (Candan et al. 2016). In contrast, models proposing a position along the southern Eurasian margin are discussed as well (e.g., Stampfli 2000; Stampfli et al. 2003; Zanchi et al. 2003; Moix et al. 2008) (Figure 2.17) and are supported by this study based on the sedimentary provenance data from Chios Island and the Karaburun Peninsula. Detrital zircons from the Chios–Karaburun units and Inousses Island have shown that they share similar provenance and were sourced from basement units located at the southern Eurasian margin during Late Palaeozoic time (Meinhold and Frei 2008; Meinhold et al. 2008b; Löwen et al. 2017), the exception being two samples from the heterogeneous Dikendağı Formation (see Löwen et al. 2017). Carboniferous foraminiferal fauna with distinct bio- geographical affinities to the southern Laurasian shelf support this interpretation (Kalvoda 2003).

As discussed above, information on the nature of this margin inferred from geochemical data of the Upper Carboniferous–Lower Permian sediments from Karaburun (i.e., Dikendağı and Küçükbahçe formations) is ambiguous. Some of these samples, in particular KAR7 of the Dikendağı Formation, indicate deposition in close proximity to a magmatic-arc source. This is further supported by its petrographic composition (i.e., high amount of lithic volcanic fragments and large, sub-/euhedral plagioclase crystals) as well as the observed detrital zircon spectra (Figure 2.15). Deposition close to a magmatic-arc is also indicated by petrographic analysis of sample KAR27 that has been tentatively assigned to the Küçükbahçe Formation and exhibits high amounts of mafic volcanic fragments. The presence of such fragments is not common and has not been observed in other parts of this formation. This observation in combination with its sample location close to the boundary of the Dikendağı Formation (Figure 2.1b), and slightly different zircon spectra (Löwen et al. 2017) make a correct stratigraphic assign-

ment difficult. Geochemical signatures of some Upper Palaeozoic samples are indicative of a passive margin setting (Figure 2.16). However, deposition most likely took place spatially separated from each other at an active margin, probably in a continental island-arc environment related to subduction of the Palaeotethys. These successions, forming the present-day stack of units have been tectonically juxtaposed by supposed post-Cretaceous thrusting. Fossil-rich limestones in the upper part of the Alandere Formation mark a shallowing upward trend to reefal conditions in Late Mississippian time.

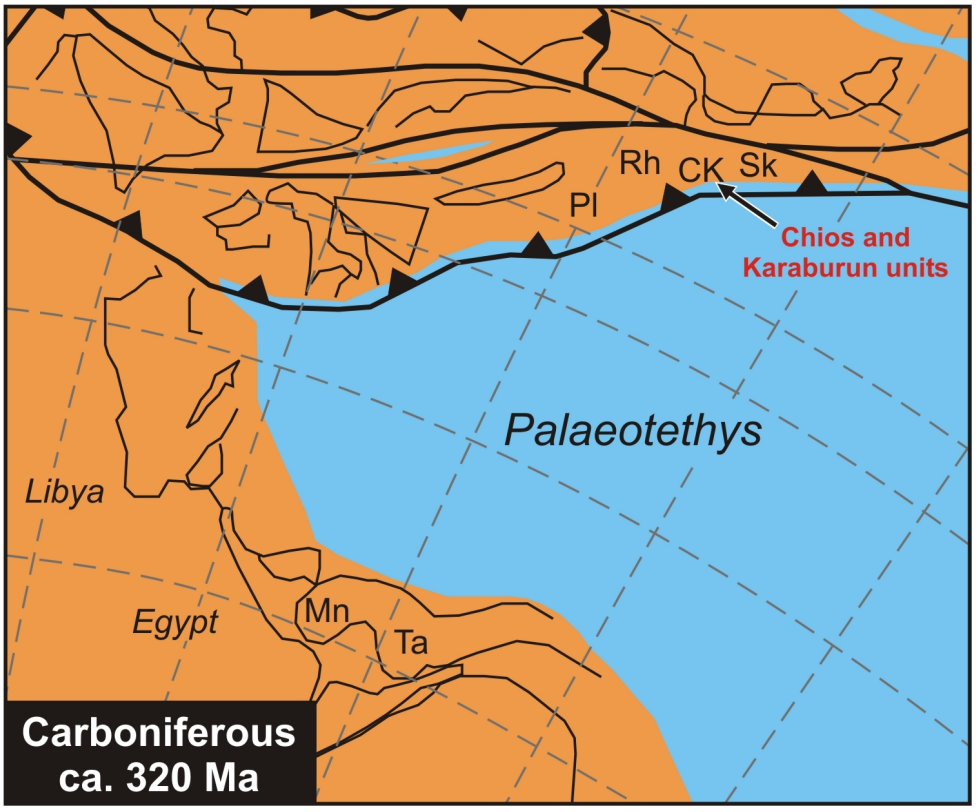

Fig. 2.17: Palaeogeographic reconstruction indicating the supposed position of some of the Chios–Karaburun units in Carboniferous time (after Stampfli and Borel 2002). CK: Chios–Karaburun units, Sk: Sakarya, Rh: Rhodope, Pl: Pelagonia, Mn: Menderes, Ta: Taurides.

Transgressive conglomerates at the basal part of the Gerence Formation that is interpreted as synrift sequence (Robertson and Pickett 2000) unconformably overlie the Palaeozoic successions and mark the end of a period of intensified erosion. Geochemical data of siliciclastic sediments and their petrographic composition with highly abundant fragments of felsic volcanic rocks (Figure 2.1) support this interpretation. Shallow water conditions, indicated by shallow macrofauna in Triassic limestones were followed

by rapid tectonic subsidence and accompanied volcanic activity (Stampfli et al. 2003). This is documented by Early Triassic I-type granitoid bodies within the Dikendağı Formation that intruded in a subduction influenced setting related to a continental-arc environment (Erkül et al. 2008; Akal et al. 2011). Indication for enhanced volcanic activity during that period can be found elsewhere in the larger study area, e.g., the Serbo-Macedonian Massif, the Pelagonian Zone, the External Hellenides, the Attic-Cycladic zone and the Menderes Massif (e.g., Tomaschek et al. 2001; Koralay et al. 2001; Bröcker and Pidgeon 2007; Anders et al. 2007; Himmerkus et al. 2009b; Zulauf et al. 2015). The presence of a Ladinian–Carnian carbonate platform (i.e., Camiboğazı Formation) documents a return to shallow water conditions that evolved into a siliciclastic dominated system in Late Triassic time. Lithological features of sediments from the Late Triassic Güvercinlik Formation indicate a tidal flat and reefal environment accompanied by sporadic occurrence of evaporitic deposits (Erdoğan et al. 1990). High geochemical and compositional maturity and inferred information from tectonic discrimination diagrams suggest deposition in a passive margin setting.

5.2 Provenance

Unraveling the provenance of Palaeozoic to Early Mesozoic Palaeotethys-related sedimentary rocks of the Karaburun Peninsula is essential for a better understanding of the geodynamic evolution during that period. The analyses of petrographic and bulk-rock chemical com- positions and complementary single-grain analyses provide valuable information in this regard. A short summary of the main observations is given in Table 2.3.

Detrital chrome spinel of sandstones from the Alandere, Küçükbahçe and Gerence formations is attributed to the (former) presence of (ultra)mafic rocks in the surrounding area. At the present time, outcrops of Palaeotethyan ophiolites are rare in the Eastern Mediterranean as they are either not preserved or not exposed, and chemical data from associated chrome spinel are only available from a few occurrences. These include the Elekdağ ophiolite of the Central Pontides in northern Turkey and the Dobromirtsi Ultramafic Massif in south-eastern Bulgaria (Figure 2.1a). The compositions of analysed chrome spinel from the Alandere and Küçükbahçe formations are similar to those reported from Upper Palaeozoic and Lower Mesozoic sediments of Chios and do not overlap with chrome spinel derived from the above-mentioned ophiolites (Figure

Table 2.3: Main observations from petrography, geochemistry and composition of heavy minerals.

	Lithic fragments	Bulk-rock geochemistry	Single-grain geochemistry
Güvercinlik Formation	Rare; mainly (meta)-sedimentary (Figure 2.6h)	REE and trace element depletion relative to UCC (Figures 2.8a, 2.9f)	Diverse garnet population; dominant input from intermediate to acidic igneous rocks and amphibolite-facies metasediments; rutiles were mainly derived from amphibolite- to eclogite-facies rocks High
Gerence Formation	Abudant; primarily volcanic (Figure 2.6g)	Indicative for (ultra)mafic material (Figure 2.10; *KAR1*: HFSE depletion (Figure 2.9d)	High amount of garnets derived from amphibolite-facies metasediments (∼60%) and intermediate to felsic igneous rocks (∼30%); chrome spinels with high Cr- and Mg-numbers are indicative of spinels from podiform chromitites
İdecik unit	Abundant; volcanic and meta-sedimentary (Figure 2.6f)	Indicative of felsic rather than mafic sources (Figure 2.10)	Variable rutile composition suggests mainly felsic source rocks; geothermometry data indicate amphibolite- to eclogite-facies source rocks; considerable amount of higher temperature (>700 °C) rutiles (*KAR3*)
Dikendağı Formation	Rare; mainly (meta)sedimentary and minor volcanic (Figure 2.6b); *KAR7*: abundant volcanic fragments (Figures 2.10)	Heterogenous; Indicative of predominant felsic sources (Figure 2.10)	Rutile compositional data indicate mainly metapelitic sources; geothermometry data reveal variable formation temperatures mainly between 600 and 700 °C (*KAR5*) and 700–800 °C (*KAR7*)
Küçükbahçe Formation	Low to moderate amount; mainly (meta)sedimentary (Figure 2.6d, e) *KAR27*: abundant volcanic fragments	Homogeneous; dominant felsic sources; variable contribution from (ultra)mafic rocks (Figure 2.10)	Rutile data reveal a mixed but dominant metamafic source of amphibolite- to eclogite-facies rocks; compositional data of chrome spinel show SSZ to MORB peridotite affinity and suggest a mixed source of dominant harzburgite and minor lherzolite composition
Alandere Formation	Rare; primarily volcanic (Figure 2.6a)	Indicative of (ultra)mafic detritus (Figure 2.10)	Homogeneous garnet compositions suggest mainly intermediate to felsic igneous source rocks; rutiles were derived from dominant felsic sources (∼65%) of amphibolite- to granulite-facies rocks; chrome spinel compositions reveal MORB peridotite affinity and suggest a mixed source of dominant harzburgite and minor lherzolite composition

2.14). It is rather likely that these grains were either recycled from older sediments or derived from Late Neoproterozoic ophiolitic bodies of NW Turkey and/or the Balkans as suggested by Meinhold et al. (2007) for detrital chrome spinels from Chios. In contrast, compositional data of chrome spinel from the Lower Triassic Gerence Formation pinpoint a remarkably different source. Additionally, the euhedral shape of these grains indicates short sedimentary transport implying a very proximal provenance and also excludes recycling of older sedimentary rocks, i.e., underlying formations. Chrome spinel chemistry shows great overlap with grains from the Dobromirtsi Ultramafic Massif of south-eastern Bulgaria and the Elekdağ ophiolite of northern Turkey, but there is no perfect match for one of them (Figure 2.14). The observed signatures on the one hand typify grains derived from boninitic rocks related to fore-arc settings during subduction initiation, which is the favoured interpretation for the Elekdağ ophiolite (Ustaömer and Robertson 1997, 1999; Dönmez et al. 2014). But then they could also be indicative for chrome spinel derived from podiform chromitites that were formed in an intra-oceanic back-arc setting above a supra-subduction zone – a model suggested for chromitites of the Dobromirtsi Ultramafic Massif (González-Jiménez et al. 2012). The lack of a suitable number of reference data and generally low occurrence of Palaeotethys-related ophiolites complicate the approach to unravel the provenance of detrital chrome spinel in Karaburun sediments. Nevertheless, on the basis of the available information we consider Palaeozoic ophiolites of northern Turkey and south-eastern Bulgaria or equivalent occurrences in the SE Europe that are not exposed or not preserved as most likely sources for chrome spinel in the Gerence Formation. This assumption is consistent with a unimodal age spectra of analysed detrital zircons ($\sim$80% of all zircons have ages between 350 and 450 Ma) indicating sediment supply from a localised source of mainly Silurian and Devonian age (Löwen et al. 2017). These findings document the existence of an (intra-oceanic) SSZ setting within the Palaeotethys. Ophiolite obduction must have occurred before deposition of the Gerence Formation, and due to the euhedral shaped chrome spinels the ophiolite was likely in very close distance to the depositional site of the Gerence Formation in Early Triassic time. Zr-in-rutile thermometry has shown that a majority of rutile grains were derived from amphibolite- to eclogite-facies rocks and input from granulite-facies lithologies is only documented in a few samples (KAR3, KAR7, KAR22). Additionally, the Cr–Nb composition generally indicates prominent input from felsic lithologies to the siliciclastic rocks of the study

area, the exception being analysed sediments of the Küçükbahçe Formation and one sample (KAR4) of the İdecik unit that exhibit a higher proportion of rutiles from mafic source rocks. This is consistent with the similar detrital zircon spectra of these sediments, further suggesting recycling of Palaeozoic rocks into the İdecik unit or sediment supply by the same source (Löwen et al. 2017). Nonetheless, one should keep in mind the doubtful assignment of sample KAR27. By comparison, observed formation temperatures of detrital rutile from Chios are similar, but grains of the Carboniferous succession were mainly derived from mafic rocks whereas Permian–Carboniferous and Permian–Triassic units record major input from felsic lithologies (Meinhold et al. 2008a). Possible sources of amphibolite- to eclogite-facies rocks were located in the metamorphic basement of the Balkan region including the Sredna Gora Zone and Strandja, Rhodope and Serbo-Macedonian massifs (e.g., Okay et al. 2001; Carrigan et al. 2006). Furthermore, high-grade, granulite-facies metamorphic rocks are documented in the Pelagonian Zone, the Variscan basement of the Sakarya Zone and the eclogite-facies basement of the Menderes Massif (e.g., Candan et al. 2001; Mposkos et al. 2001).

Analyses of garnet from the Alandere Formation has shown that most grains exhibit an intermediate to felsic volcanic provenance and were not supplied by the same source with chrome spinel. Geochemical signatures and abundant mafic volcanic fragments document the importance of (ultra)mafic lithologies in the source area. Garnets of the Triassic formations were predominantly derived from felsic igneous rocks and amphibolite-facies metasediments. The classification scheme does not provide any indication for an ultramafic provenance, implying that garnet and chrome spinel of the Gerence Formation were likely not supplied by a common source. In case of high mature sandstones from the Güvercinlik Formation, material was probably supplied by mainly quartzose, amphibolite-facies metasediments and volcanic rocks of a more distal region.

6 Conclusions

The petrographic and geochemical data presented in our study provide new constraints on the provenance and depositional tectonic setting of sediments from the Karaburun Peninsula that can be summarised as followed:

- Provenance sensitive elements (Cr, Ni, Th, Sc, V) document a predominant felsic

character of source lithologies but also indicate considerable amount of mafic components in selected samples.

- Tectonic discrimination diagrams utilizing bulk-rock geochemical data can provide good indication on the tectonic setting of depositional basins, but should be treated with caution. The choice of a representative and extensive database is a key prerequisite for testing these diagrams as their performance can be hampered by insufficient review of age and grain-size effects of analysed samples. Additionally, complementary techniques and the regional geological context should not be disregarded for conclusive interpretation of these results.
- Mineral chemical analysis of rutile and abundant sedimentary lithic fragments revealed the major importance of amphibolte- to eclogite- facies sources for sediments throughout the whole stratigraphic sequence of the Karaburun Peninsula. Material was predominantly derived from felsic lithologies, but detritus of mafic provenance was supplied to some extent.
- Euhedral chrome spinels from the Lower Triassic Gerence Formation document the existence of an (intra-oceanic) SSZ setting within the Palaeotethys. Related ophiolites were present in proximity to the depositional site of the Gerence Formation and supplied detritus. We assume that these Palaeozoic ophiolites were probably located in northern Turkey or the Balkans but are not exposed or preserved anymore. Deciphering a more accurate provenance of this material is hindered by the lack of reference data (i.e., mineral chemical data of chrome spinel) from other Palaeozoic (ultra)mafic bodies.
- We assume that most of the Upper Palaeozoic successions of the Karaburun Peninsula were (contemporaneously) deposited along the southern active Eurasian margin. Low textural and compositional maturity indicate relatively proximal provenance and the presence of a nearby volcanic-arc, probably related to northward subduction of Palaeotethys.

7 Acknowledgements

We gratefully acknowledge financial support by the German Research Foundation (DFG grant ME 3882/3-1) and the Göttingen University start-up funding for young aca-

demics (grant to GM). We thank Gerald Hartmann for XRF analysis, Klaus Simon for ICP-MS analysis, and Andreas Kronz for providing access to the EMPA. Günay Kurtuluş kindly provided chrome spinel reference data of the Elekdağ ophiolite. Constructive reviews were provided by Shane Tyrrell and Mehmet Cemal Göncüoğlu and are greatly appreciated.

Chapter 3

Manuscript II: Palaeotethys-related sediments of the Karaburun Peninsula, western Turkey: constraints on provenance and stratigraphy from detrital zircon geochronology

Kersten Löwen[1,*], Guido Meinhold[1], Talip Güngör[2], Jasper Berndt[3]

[1]Abteilung Sedimentologie/Umweltgeologie, Geowissenschaftliches Zentrum Göttingen, Universität Göttingen, Göttingen, Germany

[2]Department of Geological Engineering, Dokuz Eylül University, Izmir, Turkey

[3]Institut für Mineralogie, Westfälische Wilhelms-Universität Münster, Münster, Germany

[*]Corresponding author

Published in: International Journal of Earth Sciences 8 (2017): 2771–2796

Abstract

Detrital zircon U–Pb geochronology of 15 Late Palaeozoic to Early Mesozoic siliciclastic sandstones from the Karaburun Peninsula in western Turkey determines maximum sedimentation ages, identifies possible source areas, and anchors the study area within the Palaeotethyan realm. Siliciclastic sandstones yielded ages from Triassic to Archean with major input from Palaeozoic to Neoproterozoic sources and very few Mesoproterozoic zircons. The youngest age groups set the new limit of the maximum depositional ages to Late Carboniferous–Early Permian for the Küçükbahçe and Dikendağı formations. Detrital zircons from Triassic sandstones are mainly Neoproterozoic and Palaeozoic in age. Zircons from the Scythian–Anisian Gerence Formation are predominantly Devonian and Carboniferous in age, while also Permian and Triassic zircon grains occur in the Carnian–Rhaetian Güvercinlik Formation. According to the zircon age populations and the data available from possible source regions, the Karaburun siliciclastic sediments, with the exception of two samples from the Dikendağı Formation, record sediment supply from units located at the southern margin of Eurasia during Late Palaeozoic and Early Mesozoic times. This interpretation is in agreement with palaeotectonic reconstructions for the closely related Greek islands of Chios and Inousses. The presence of Devonian accompanied by Carboniferous zircons in some of the Karaburun samples reveals similarities with Karakaya Complex sandstones of the Sakarya Zone in NW Turkey.

Keywords: U–Pb geochronology; Detrital zircon; Sediment provenance; Palaeotethys; Karaburun Peninsula; Turkey

1 Introduction

The Eastern Mediterranean region is made up of several continental fragments which document a highly geodynamic history. Turkey finds itself in a unique position as it represents a geographical junction point between the Asian and European continents

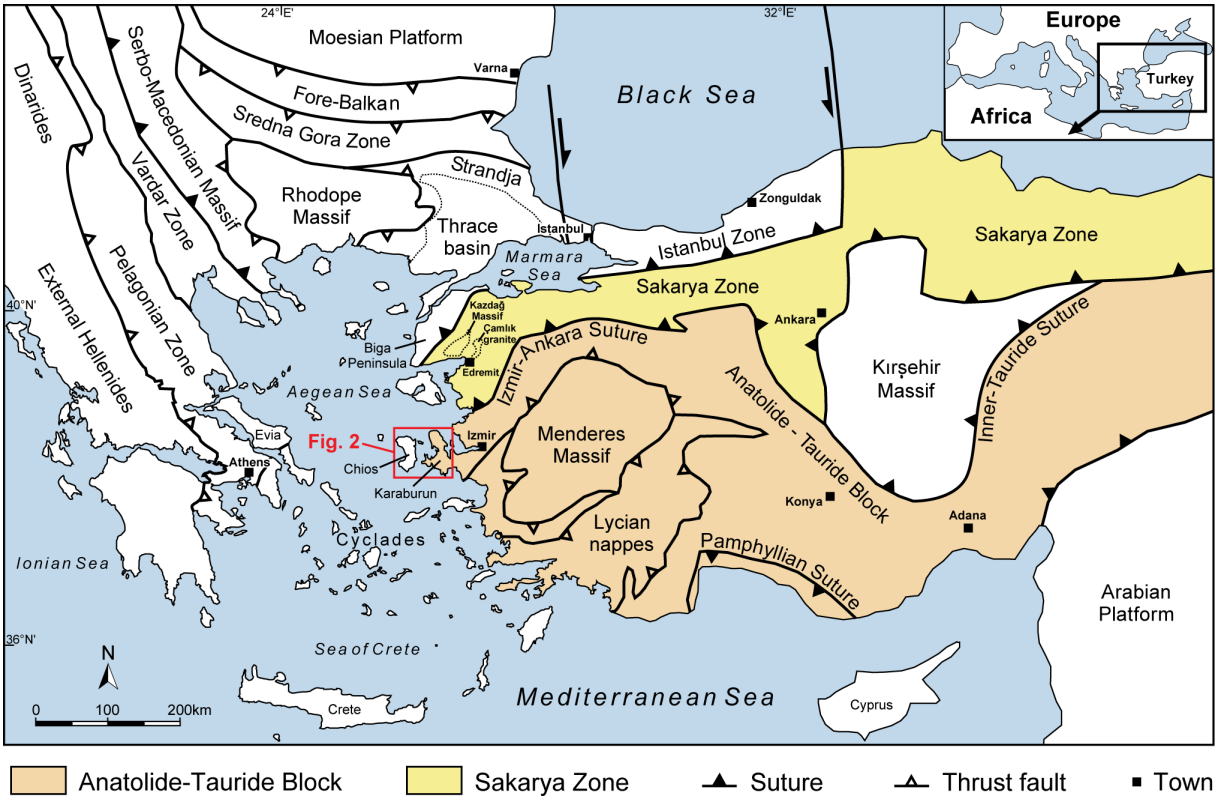

Fig. 3.1: Simplified geotectonic map of the Eastern Mediterranean region (after Jacobshagen 1986; Okay and Tüysüz 1999; Okay et al. 2006).

as well as a geological link between Gondwana to the south and Eurasia to the north. From north to south, the major geotectonic units and suture zones in western Turkey are: the İstanbul Zone, Sakarya Zone, İzmir–Ankara Zone, Menderes Massif, Lycian nappes, and the Taurides (Figure 3.1).

Remnants of oceanic basins record the existence of two major oceanic realms, the Palaeozoic to Early Mesozoic Palaeotethys and (mainly) Mesozoic Neotethys (e.g., Şengör et al. 1984; Stampfli 2000, and references therein). It is a general consensus that Palaeotethys closed in response to northward drift of the Cimmerian terranes (e.g., Taurides) and the opening of Neotethys to the south (e.g., Stampfli and Borel 2002). The exact timing and polarity of subduction of Palaeotethys, however, remain controversial. Different models have been published during the last decades, proposing either northward subduction under Eurasia (e.g., Stampfli 2000; Stampfli and Borel 2002; Robertson et al. 2004; Okay et al. 2006; Moix et al. 2008), southward subduction beneath Gondwana (e.g., Şengör et al. 1984; Okay et al. 1996; Xypolias et al. 2006, 2008; Akal et al. 2011), or a combination of both (e.g., Robertson and Ustaömer 2009b).

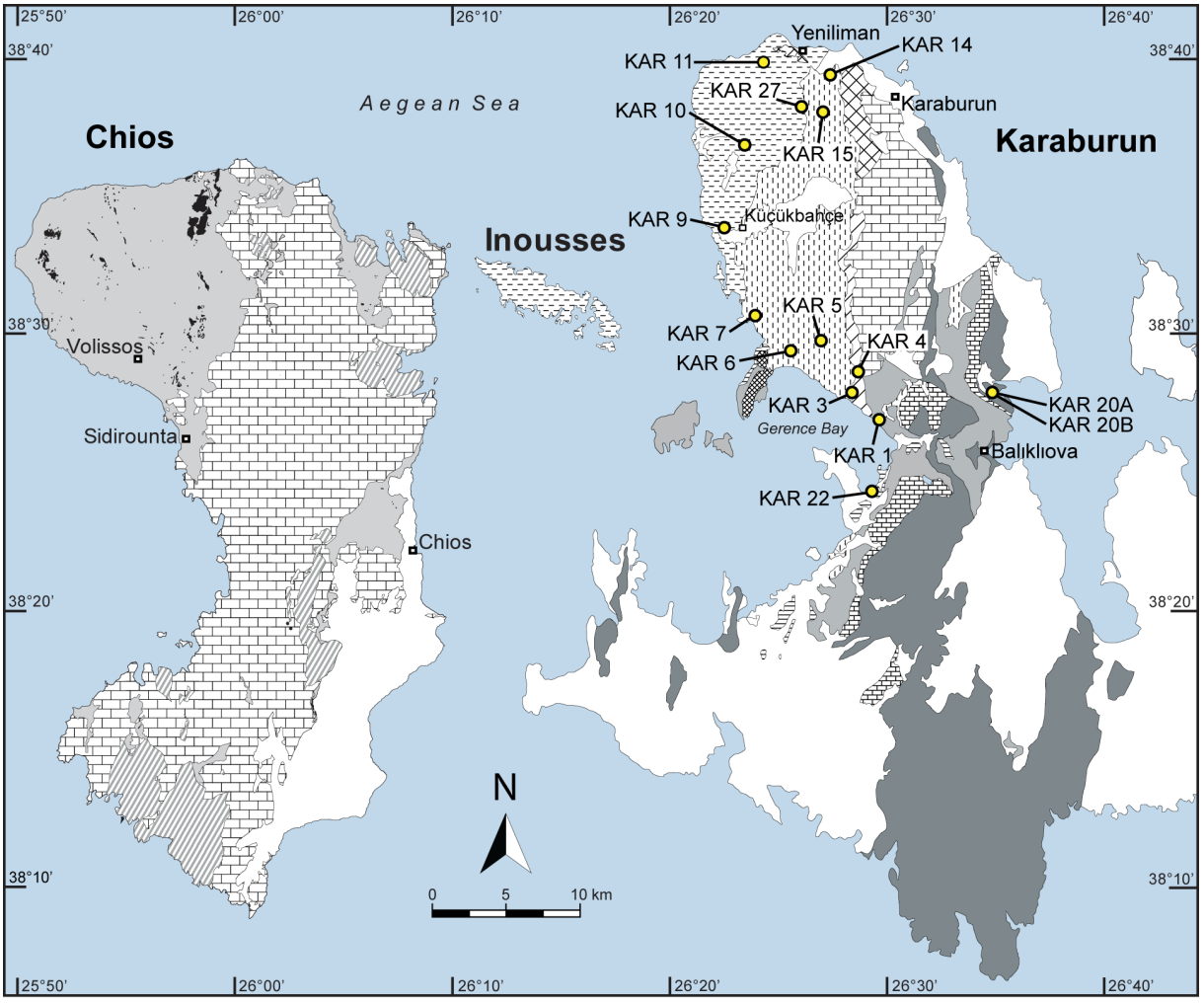

Karaburun

- Sample locality
- Cenozoic - Recent
- Late Cretaceous mélange Izmir flysch

Late Palaeozoic

- Tekedağı Fm.
- Dikendağı Fm.
- Küçükbahçe Fm.
- Alandere Fm.

Triassic and Jurassic

- Nohutalan & Güvercinlik fms.
- Camiboğazı Fm.
- İdecik unit
- Gerence Fm.

Chios

- Cenozoic - Recent

Upper Unit

- Late Carboniferous to Jurassic rocks

Lower Unit

- Mesozoic rocks
- Late Palaeozoic with Silurian to Carboniferous olistoliths

Inousses

- Late Palaeozoic metasediments (equivalent of Küçükbahçe Fm.)

Fig. 3.2: Simplified geological map of the study area with sample locations. The Karaburun map is modified after Çakmakoğlu and Bilgin (2006) and the Chios and Inousses maps are modified after Meinhold et al. (2007).The sedimentary succession of Inousses Island is correlated with the Küçükbahçe Formation of Karaburun Peninsula, based on field observations and data of this study.

Uncertainty concerning the Palaeotethyan evolution is mainly because of lack of hard data (e.g., provenance data) for testing the various palaeotectonic models. Chios Island (Greece) and the Karaburun Peninsula (W Turkey) are regarded as key areas for understanding the closure history of Palaeotethys. Unlike the high-grade metamorphic units in the surrounding area (e.g., Sakarya Zone, Menderes Massif, Cyclades, Pelagonian Zone, and Serbo-Macedonian and Rhodope massifs), the Chios and Karaburun localities exhibit virtually unmetamorphosed Palaeozoic and Mesozoic sedimentary rocks (e.g., Besenecker et al. 1968; Erdoğan et al. 1990; Kozur 1998; Robertson and Pickett 2000; Zanchi et al. 2003; Meinhold et al. 2007, 2008a,b; Robertson and Ustaömer 2009b). For the Late Palaeozoic, some workers place the Chios–Karaburun units along the northern margin of Palaeotethys (e.g., Stampfli 2000; Meinhold et al. 2008b; Moix et al. 2008), while others favor a position along the southern margin of Palaeotethys, i.e., along the northern margin of Gondwana (e.g., Robertson and Pickett 2000; Robertson and Ustaömer 2009b; Akal et al. 2011).

Provenance data including detrital zircon U–Pb ages were already published for the islands of Chios and Inousses (Meinhold et al. 2008b; Meinhold and Frei 2008) (Figure 3.2). Such data are unavailable for the Karaburun Peninsula, except of a few detrital zircon ages from the Karareis and Küçükbahçe formations mentioned in abstract form only (Rosselet and Stampfli 2003). This study provides detrital zircon U–Pb ages for a provenance study of the siliciclastic successions from the Karaburun Peninsula to constrain their origin and the palaeoposition within the Palaeotethyan realm. Besides that, the detrital zircon ages are also crucial for estimating the maximum age of the (Palaeozoic) sedimentary successions, which has long been a matter of debate.

2 Geological setting

The Karaburun Peninsula is located in the central, westernmost part of Turkey adjacent to the Aegean Sea (Figure 3.1). It is part of the İzmir–Ankara Zone, a suture zone separating continental fragments of Eurasian affinity (e.g., Sakarya Zone to the north) from fragments of Gondwana affinity (e.g., Menderes Massif to the south) (e.g., Okay and Tüysüz 1999; Stampfli 2000; Moix et al. 2008). The Karaburun area has been studied for more than 100 years and was first mapped by Philippson (1911), followed by Kalafatçıoğlu (1961) and more recently by other workers (Erdoğan et al. 1990;

Robertson and Pickett 2000; Stampfli et al. 2003; Çakmakoğlu and Bilgin 2006).

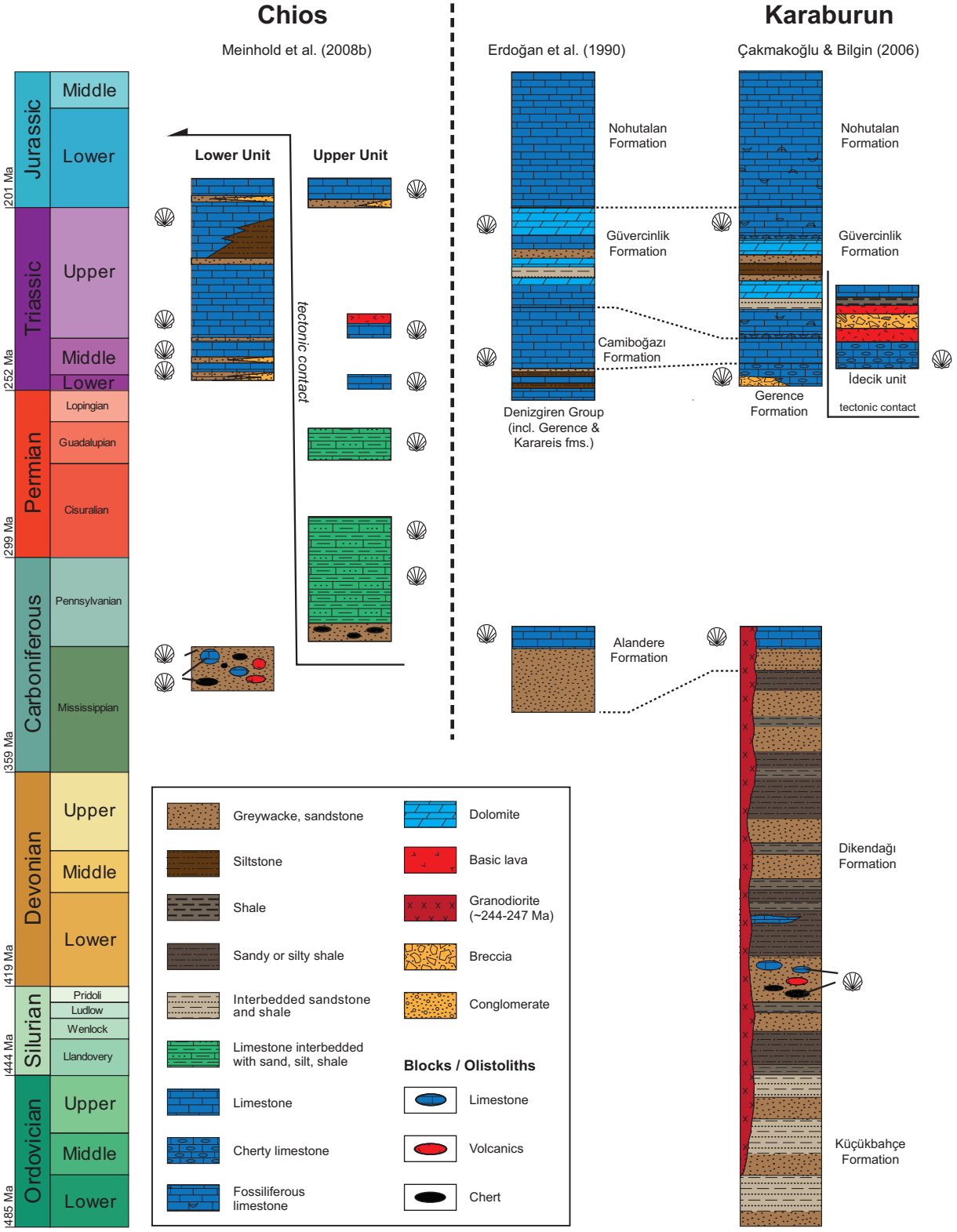

Fig. 3.3: Stratigraphic sections of Chios and Karaburun. For simplification, the ?Late Permian Tekedağı Formation, consisting of bioclastic limestone, dolomitic limestone, partly oolitic/pisolitic, and limestone with sandstone, siltstone, and marl interfingers (Çakmakoğlu and Bilgin 2006), is not shown here. The Tekedağı Formation is only present in a small area to the NW of Gerence Bay. This formation probably correlates with the stratigraphically younger part of the Permian limestones from the Upper Unit of Chios Island. Biostratigraphic data from Brinkmann et al. (1972); Çakmakoğlu and Bilgin (2006); Erdoğan et al. (1990, 2000); Kozur (1997, 1998)). Blocks/olistoliths in the Palaeozoic succession of Karaburun Peninsula have been described by Kozur (1998); Robertson and Ustaömer (2009b).

Based on the current knowledge, the Karaburun units comprise a mélange zone of blocks of black chert and pelagic limestones, ranging in age from Silurian to Carboniferous and poorly dated volcanic rocks embedded in a highly deformed siliciclastic matrix of Early Carboniferous age. Thick, autochthonous Mesozoic carbonate platform units unconformably overlie this mélange zone. However, the interpretation of the Karaburun units and the mélange zone is ambiguous; different models have been proposed for their formation. Kozur (1995, 1998) favors a sedimentary olistostromal origin, whereas Robertson and Pickett (2000) suggest an origin as tectonic mélange and interpret the rocks as an accretionary complex related to Late Palaeozoic subduction including a collisional setting. Yet, another model proposed an origin as a Triassic rift-related succession including Palaeozoic and Triassic rocks (Erdoğan et al. 1990, 2000), and in a fourth scenario, the mélange is considered as an accretionary complex, which was exhumed and reworked as olistostromes into a fore-arc basin during Late Carboniferous time (Stampfli et al. 2003).

The structurally lowest unit was first defined by Kozur (1998) as Küçükbahçe Formation and crops out in the western part of the Karaburun Peninsula (Figures 3.2 and 3.3). It is composed of a relatively monotonous alternation of low-grade metamorphosed (turbiditic) sandstones and shales, with intercalations of conglomerates, silt- and mudstones, without any blocks (Figure 3.4c, d). These sediments have experienced intense folding and shearing and have pronounced schistosity. The Küçükbahçe Formation was long supposed to be of Ordovician (or Cambro–Ordovician) age (Kozur 1998), but based on a detrital zircon study by Rosselet and Stampfli (2003), this age has been revised to Early Carboniferous. The upper clastic part of the mélange was first identified as Dikendağı Formation by Çakmakoğlu and Bilgin (2006) and has been assigned to a Silurian–Carboniferous (Visean) age (Kozur 1995, 1998). In the northern part, the formation is dominated by alternations of shales and coarse- to fine-grained sandstones with very low occurrence of olistoliths (black chert). A more pronounced bedding and

large blocks of limestone and folded chert that are enclosed in the matrix rocks characterise the succession in the southwestern part of this formation (Figure 3.4e, f). Blocks of black chert contain radiolarians, ranging in age from Silurian to Carboniferous, and limestone blocks have been dated as Silurian to Early Devonian (Kozur 1997, 1998). The existence of chert and limestone blocks, and very slight schistosity, which suggest a decrease in metamorphic degree are the most distinctive features compared to the lower clastic unit (Küçükbahçe Formation). Within the Dikendağı Formation, two small granitoid bodies crop out in the northern part of the Karaburun Peninsula and the contacts were interpreted as intrusive (Erkül et al. 2008; Akal et al. 2011). The age of these bodies was constrained to Early Triassic by a biotite Rb–Sr isochron age of 239.9 $\pm$ 2.4 Ma (Ercan et al. 2000) and zircon U–Pb ages of 244.4 $\pm$ 1.5 Ma (Ustaömer et al. 2016a) and 247.1 $\pm$ 2.0 Ma, respectively (Akal et al. 2011). The uppermost part of the mélange, only exposed locally (i.e., at the southern coast area of Gerence Bay, Figure 3.2), is named Alandere Formation and is interpreted to be gradational with the Dikendağı Formation (Çakmakoğlu and Bilgin 2006). Robertson and Pickett (2000) consider the Alandere Formation as structurally highest block within the mélange. Erdoğan et al. (1990, 2000) consider this formation as fundament on which a Triassic rift-related succession (Karaburun mélange sensu lato) was deposited. The Alandere Formation is mainly composed of fossil-rich, shallow-water limestones, and contains sandstones, conglomerates, shales, and chert. The age is well constrained by biostratigraphic data to Carboniferous (Serpukhovian–Bashkirian) (Erdoğan et al. 1990, 2000).

According to Robertson and Pickett (2000) and Çakmakoğlu and Bilgin (2006), the Palaeozoic rocks are unconformably overlain by a thick sequence dominated by Mesozoic platform carbonates, which make up large parts of the eastern and southern area of Karaburun Peninsula. This succession is of Early Triassic to Late Cretaceous (Campanian–Maastrichtian) age and is subdivided into several units, amongst others, the Gerence Formation, İdecik unit, Camiboğazı Formation, and Güvercinlik Formation. The Gerence Formation unconformably overlies the Karaburun mélange. At its base, it consists of conglomerates with reworked material of the underlying formations and passes upwards into more carbonate-rich conglomerates (Figure 3.4b). Besides, this unit comprises mainly siliciclastic material and carbonates with tectonically stressed and intensely folded cherts. The age of these rocks has been determined by fossils (ammonites, conodonts, foraminifera) to be Early Triassic. The Camiboğazı Formation

on top of this unit is made up of thick bedded and massive limestones (Figure 3.4a). Based on fossils, the age of this unit has been determined to be Middle–Late Triassic (Ladinian–Carnian) in several studies (e.g., Brinkmann et al. 1972; Erdoğan et al. 1990, 2000). In the upper part of the Mesozoic sequence, these carbonates are gradationally overlain by the Güvercinlik Formation. This is a detritic succession that contains highly mature, red sandstones, and conglomerates as well as oolitic and dolomitic limestones (Stampfli et al. 2003; Çakmakoğlu and Bilgin 2006) with abundant megalodon fossils, algae, and gastropods of Late Triassic age (Çakmakoğlu and Bilgin 2006). The İdecik unit is thrust between the Karaburun mélange and the Gerence Formation and is only exposed in a small strip in the central part of northern Karaburun Peninsula. It mainly consists of volcanoclastic rocks, basic lavas, tuffaceous material, limestone, and radiolarites. According to the red radiolarites from the lower part a Ladinian–Carnian age has been assigned for this unit (Çakmakoğlu and Bilgin 2006).

3 Methods

Rock samples were collected from outcrop and processed at the Geoscience Center of Göttingen University. Lithology, stratigraphy, and geographic coordinates of studied samples are given in Table 3.1. For U–Pb geochronology, zircons were separated from bulk-rock samples by standard routines: jaw crusher, disc mill, Wilfley table, Frantz magnetic separator, and heavy liquid (sodium polytungstate). Final selection of zircon grains was done by handpicking under a stereomicroscope. The zircons were fixed in epoxy resin mounts and polished to expose the interior of the grains. Prior to the analyses, cathodoluminescence (CL) imaging was applied to reveal their internal structures (e.g., growth zones) and to guide spot placement. The U–Pb age determination was performed on a sector-field ICP-MS (Element2, ThermoFisher) coupled to a 193-nm Analyte G2 Excimer Laser Ablation System. Laser spot size was commonly 35 µm, but was reduced to 25 µm in some cases to analyse thin overgrowths. Isotope data were acquired on masses 202, 204, 206, 207, and 238. The mass 202 was used to quantify interference of ^{204}Hg on ^{204}Pb. Common Pb correction was only applied to an analysis if the fraction of common ^{206}Pb to total ^{206}Pb exceeded 1%. Mass discrimination and elemental fractionation during laser ablation were corrected by bracketing 10 unknown samples by three measurements of the GJ-1 reference zircon (Jackson et al. 2004). To

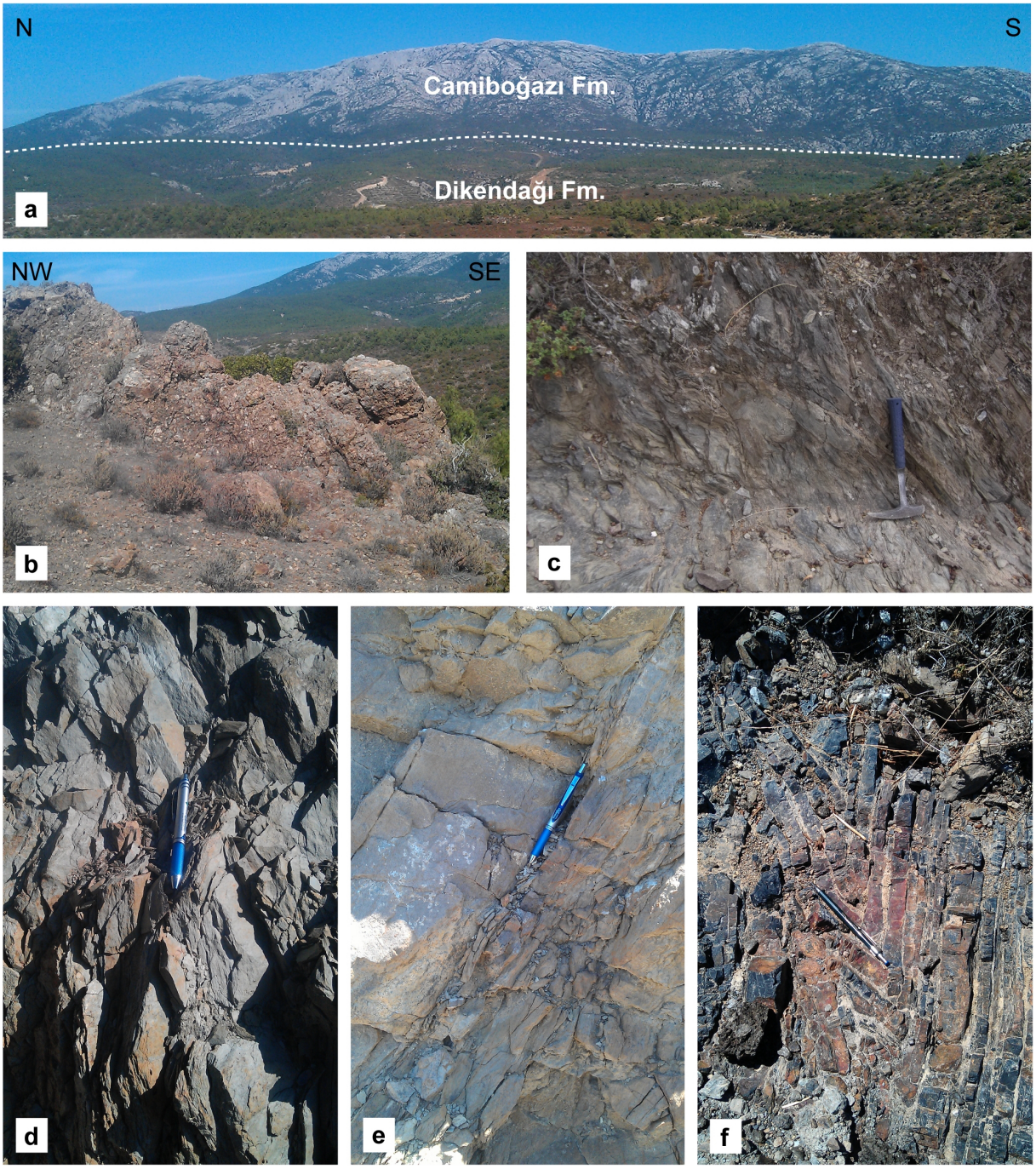

Fig. 3.4: Field photographs from the Karaburun Peninsula. **a** View to the Mesozoic platform carbonates of the Camiboğazı Formation. **b** Outcrop of conglomerates from the basal part of the Gerence Formation (north of Gerence Bay). **c–d** Low-grade metamorphosed mudrocks of the Küçükbahçe Formation (NW part of Karaburun Peninsula) (pen for scale: 15 cm; hammer for scale: 30 cm). **e** Section from silt-/sandstone succession of the Dikendağı Formation (north of Gerence Bay). **f** Chevron folds in black chert in the Dikendağı Formation (north of Gerence Bay). In **c**-**f**, hammer (30 cm long) and pen (15 cm long) for scale, respectively.

keep track of precision and reproducibility of U–Pb ages, the 91,500 reference zircon ($^{206}Pb/^{238}U$ = 1062.4 $\pm$ 0.8 Ma; $^{207}Pb/^{206}Pb$ = 1065.4 $\pm$ 0.6 Ma; Wiedenbeck et al. 1995) was analysed in the course of this study. Measured isotopic ratios matched the published values of Wiedenbeck et al. (1995) within error.

Data reduction was done following the procedure described by Kooijman et al. (2012). Given the natural break in U–Pb ages between ca. 800 and 1200 Ma, the data were filtered based on two criteria: accepted were all zircon ages (a) within 90–110% concordance [100 $\times$ ($^{206}Pb/^{238}U$ /$^{207}Pb/^{206}Pb$)] for grains older than 1200 Ma and (b) grains showing a difference of the U–Pb ages in the range of 10% for ages younger than 1200 Ma (see also Allen and Barnes 2006; Spencer et al. 2014). By this means, we want to account for low precision of $^{207}Pb/^{206}Pb$ values for younger (<1200 Ma) ages. $^{206}Pb/^{238}U$ ages were quoted for zircons younger than 1200 Ma, and $^{207}Pb/^{206}Pb$ ages to depict zircons older than 1200 Ma (Gehrels et al. 2008). This age was chosen, because there is a natural gap in the ages of zircons in the analysed samples. Concordia plots (Figures 3.5, 3.7, 3.9) were produced with Isoplot version 3.75 (Ludwig 2003) and kernel density estimates and histograms (Figures 3.6, 3.8, 3.10, 3.11) were produced using the DensityPlotter software by Vermeesch (2012). The analytical data are given as electronic supplementary material (see Table B.1). The geological time scale GTS of Gradstein et al. (2012) was used as stratigraphic reference for data interpretation.

4 Results

We present the detrital zircon U–Pb ages for each of the studied formations in upward order in the tectonostratigraphy, first for the Triassic, followed by the Palaeozoic, because the stratigraphic ages of the youngest formations are well constrained by biostratigraphic data (Figure 3.3), while the ages of the older formations are a matter of debate.

4.1 Gerence Formation

From the Gerence Formation, one sample (KAR1) was collected near the west coast of Karaburun at Gerence Bay (Figure 3.2). The sample is a coarse-grained feldspar-rich litharenite which consists of mainly quartz and abundant chert, plagioclase, and lithic fragments of volcanic and sedimentary origin. Many grains are cut by carbonate veins.

Table 3.1: Sample list with GPS coordinates and comparison of stratigraphic ages from fossils and depositional ages derived from detrital zircon.

Sample	Lithology	Latitude	Longitude	Stratigraphic age according to fossils	Maximum depositional age according to zircon ages	Accepted in this study
Güvercinlik Formation				*Late Triassic*		*Late Triassic*
KAR20A	Sublitharenite	38°27'51.56"	26°35'23.41"		Late Triassic	
KAR20B	Sublitharenite	38°27'51.56"	26°35'23.41"		Late Triassic	
Gerence Formation				*Early Triassic*		*Early Triassic*
KAR1	(Feldspatic) Litharenite	38°26'41.44"	26°30'08.24"		Late Carboniferous	
İdecik unit				*Ladinian–Carnian*		*Ladinian–Carnian*
KAR3	Sublitharenite	38°27'39.21"	26°28'37.59"		Late Ordovician	
KAR4	Litharenite	38°28'24.21"	26°28'23.18"		Late Carboniferous	
Dikendağı Formation				*No record*		*Pennsylvanian–Cisuralian*
KAR5	Sublitharenite	38°29'39.03"	26°27'16.20"		Early Cambrian	
KAR6	Lithic subarkose	38°29'14.58"	26°25'57.37"		Pennsylvanian–Cisuralian	
KAR7	Lithic arenite	38°30'31.44"	26°24'17.82"		Late Devonian	
KAR14	Subarkose	38°39'25.02"	26°27'32.04"		Ediacaran	
KAR15	Subarkose	38°38'00.70"	26°27'21.10"		Early Carboniferous	
Küçükbahçe Formation				*No record*		*Pennsylvanian–Cisuralian*
KAR9	Sublitharenite	38°33'48.12"	26°22'51.24"		Late Carboniferous	
KAR10	Subarkose	38°36'44.64"	26°23'40.18"		Pennsylvanian–Cisuralian	
KAR11	Lithic arkose	38°39'43.73"	26°24'27.59"		Mid–Carboniferous	
KAR27	Sublitharenite	38°38'07.78"	26°26'34.40"		Late Carboniferous	
Alandere Formation				*Serpukhovian–Bashkirian*		*Serpukhovian–Bashkirian*
KAR22	Subarkose	38°24'05.34"	26°29'43.62"		Mississippian	

The detrital zircons are commonly subhedral and have oscillatory zoning patterns. A total of 59 spots on 56 zircon grains were analysed and filtered data (n = 51; Figure 3.6a) show a unimodal age distribution with a well-defined population at 350–400 Ma (n = 24). More than 50% of the zircons are of Devonian age and only a single analysis yielded a Mesoproterozoic age (ca. 1140 Ma), which marks the upper end of the spectrum. The youngest age group [n = 3, analyse numbers (#): 23, 39, 45] occurs at 330–345 Ma including the youngest grain (#: 39) of 334 $\pm$ 7 Ma that indicates a late Early Carboniferous maximum depositional age.

4.2 İdecik unit

From the İdecik unit, two samples were collected in close distance to the Dikendağı Formation near the Gerence Bay in western Karaburun (Figure 3.2). Sample KAR3 is a coarse-grained sublitharenite dominated by monocrystalline quartz with minor amounts of feldspar, muscovite, and lithic fragments of mainly volcanic and (meta)sedimentary origin. In general, the zircon grains are well rounded, but some euhedral grains are also present. Most of them have oscillatory zoning and a small number exhibits xenocrystic cores. U–Pb ages were obtained from 104 spots on the same number of grains, resulting in 81 accepted zircon ages (Figure 3.6b). The age spectrum ranges from $\sim$230 Ma to 2.75 Ga and is dominated by Proterozoic zircons (ca. 70%). Two major age groups occur at ca. 500–550 Ma (n = 8), and 650–750 Ma (n = 15). Minor populations exist at 900–1000, 1950, and 2500 Ma. The youngest apparent age is 234 $\pm$ 5 Ma, but belongs to a high U- (1072 ppm) and common Pb-bearing (3.25%) crystal and is, therefore, not considered as reliable indicator for the maximum age (#: 89). Another single grain yielded an age of 313 $\pm$ 5 Ma (#: 126); however, the youngest coherent age group (n = 4, #: 69, 92, 106, 117) occurs at 450–470 Ma.

Sample KAR4 is a fine-grained litharenite that predominantly consists of mono- and polycrystalline quartz and volcanic and (meta)sedimentary lithoclasts. Small amounts of feldspar, muscovite, chlorite, and carbonate are also present. The data set comprises 96 analyses from 94 zircon grains. These are generally well rounded or short prismatic, and CL images revealed oscillatory zoning and irregular patterns. Filtered data (n = 80) indicate a bimodal age spectrum from ca. 330 Ma to 2.7 Ga (Figure 3.6c). A major Cambrian age group occurs at ca. 510 Ma and a second group exists at ca. 2.0 Ga. The input of Palaeozoic zircons (ca. 55%) is much higher compared to sample

KAR3. The maximum age of deposition is indicated by the youngest group (n = 4, #: 145, 183, 186, 206) of coherent zircons between 330 and 345 Ma.

4.3 Güvercinlik Formation

Two samples (KAR20A and KAR20B) of the Güvercinlik Formation were collected from an outcrop at the eastern coast of Karaburun, ca. 4 km north of Balıklıova (Figure 3.2). KAR20A is a highly mature coarse-grained litharenite and KAR20B is a (detrital garnet-bearing) sublitharenite. Both samples almost purely consist of quartz. The zircon population of both samples consists of mainly colorless to pinkish, euhedral grains with oscillatory zoning patterns. For sample KAR20A, 110 spots on 85 grains were analysed of which 103 U–Pb ages were accepted. The total spectrum ranges from 200 Ma to 2.6 Ga with a distinct Mesoproterozoic age gap and a major input of Palaeozoic, especially Carboniferous zircons (Figure 3.6d). Three distinct groups occur at ca. 320 Ma, ca. 510 Ma and ca. 1.9 Ga, respectively. The youngest grain occurs at 202 $\pm$ 4 Ma (#: 291), whereas the youngest age group is defined by three zircons (#: 271, 274, 308) at ca. 235–245 Ma. The data set of sample KAR20B comprises 104 spots on 87 zircon grains. Filtered data (n = 94) vary between 200 Ma and 1.0 Ga, with a single spot age at 2.0 Ga (Figure 3.6e). Of the Palaeozoic zircons, Carboniferous ages (n = 35) are most common and define a prominent group at 330 Ma. The youngest coherent group (n = 3, #: 386, 391, 395) is of latest Triassic age (ca. 202 Ma). It is worth mentioning that these grains exhibit large amounts of common ^{206}Pb (2–10%).

4.4 Küçükbahçe Formation

The Küçükbahçe Formation is one of the main siliciclastic units and was, therefore, studied in detail. Four samples were collected from different locations of the formation to obtain a representative overview. Sample KAR9 is a fine-grained sublitharenite made up of monocrystalline quartz and small amounts of feldspar and muscovite from a location ca. 1 km west of Küçükbahçe village (Figure 3.2). From this sample, 79 spots on 70 grains were analysed, of which 64 U–Pb ages were accepted. The grains are subhedral and smaller grains are well-rounded with mainly oscillatory zoning and occasional homogenous CL patterns. The data define a polymodal age spectrum between 250 Ma to 3.0 Ga with an age gap between 1.2 and 1.8 Ga and prominent peaks

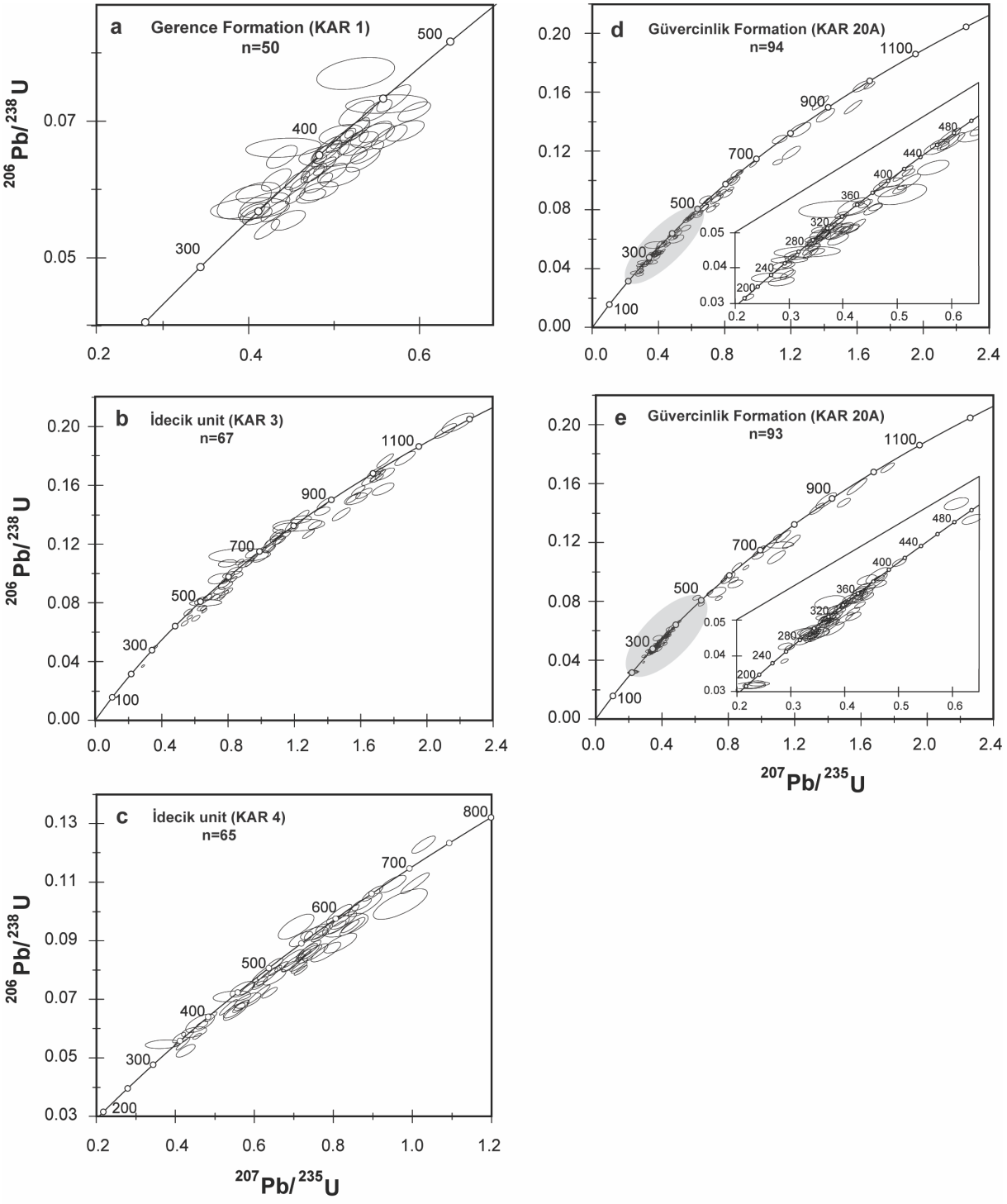

Fig. 3.5: U–Pb concordia plots showing LA-ICP-MS data of samples from the Triassic successions. Data *point error ellipses* indicate 2σ uncertainties. *Shaded grey ellipses* outline areas that are shown as close-up.

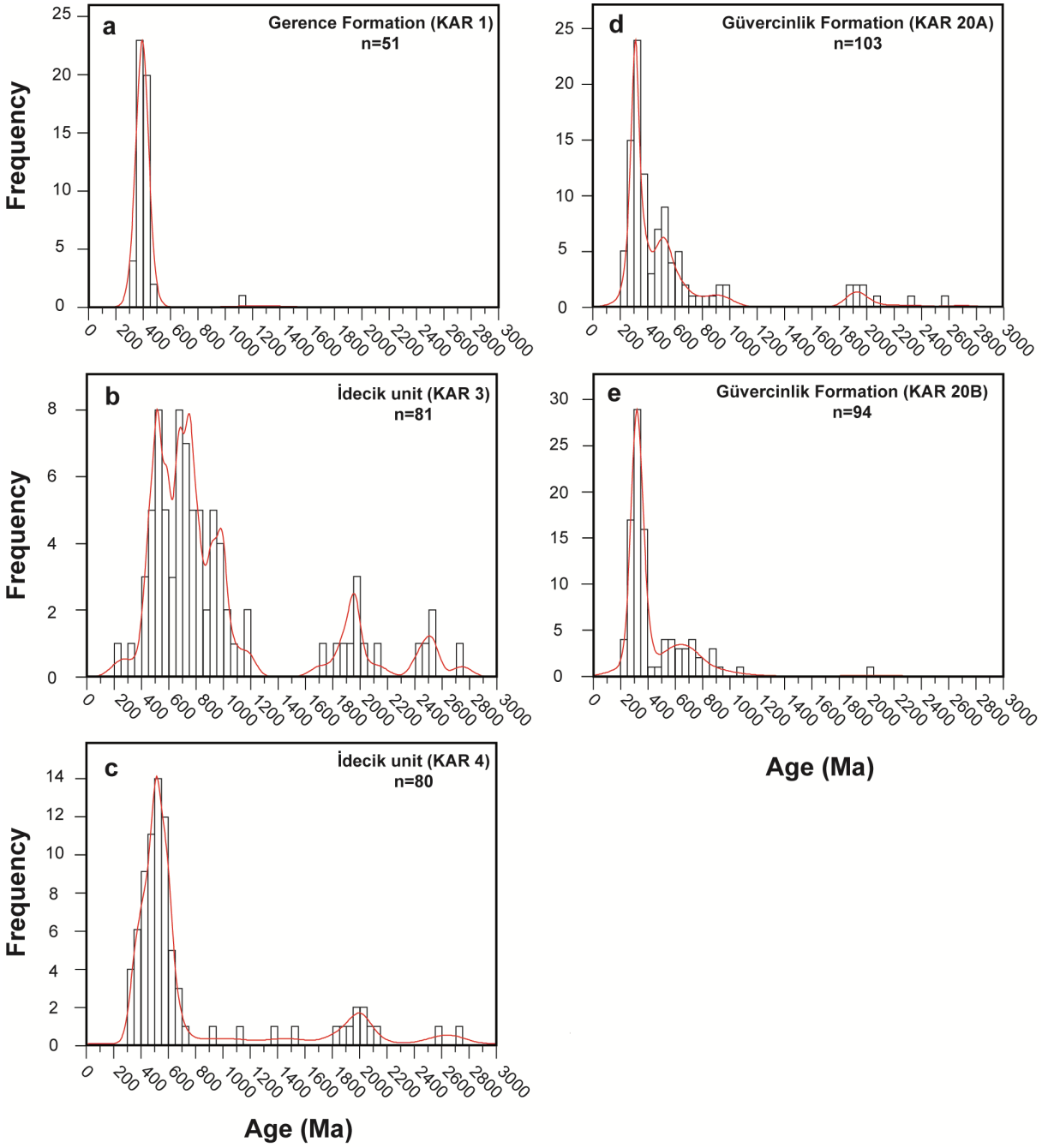

Fig. 3.6: Histograms and kernel density estimates of detrital U–Pb zircon ages from the Triassic successions.

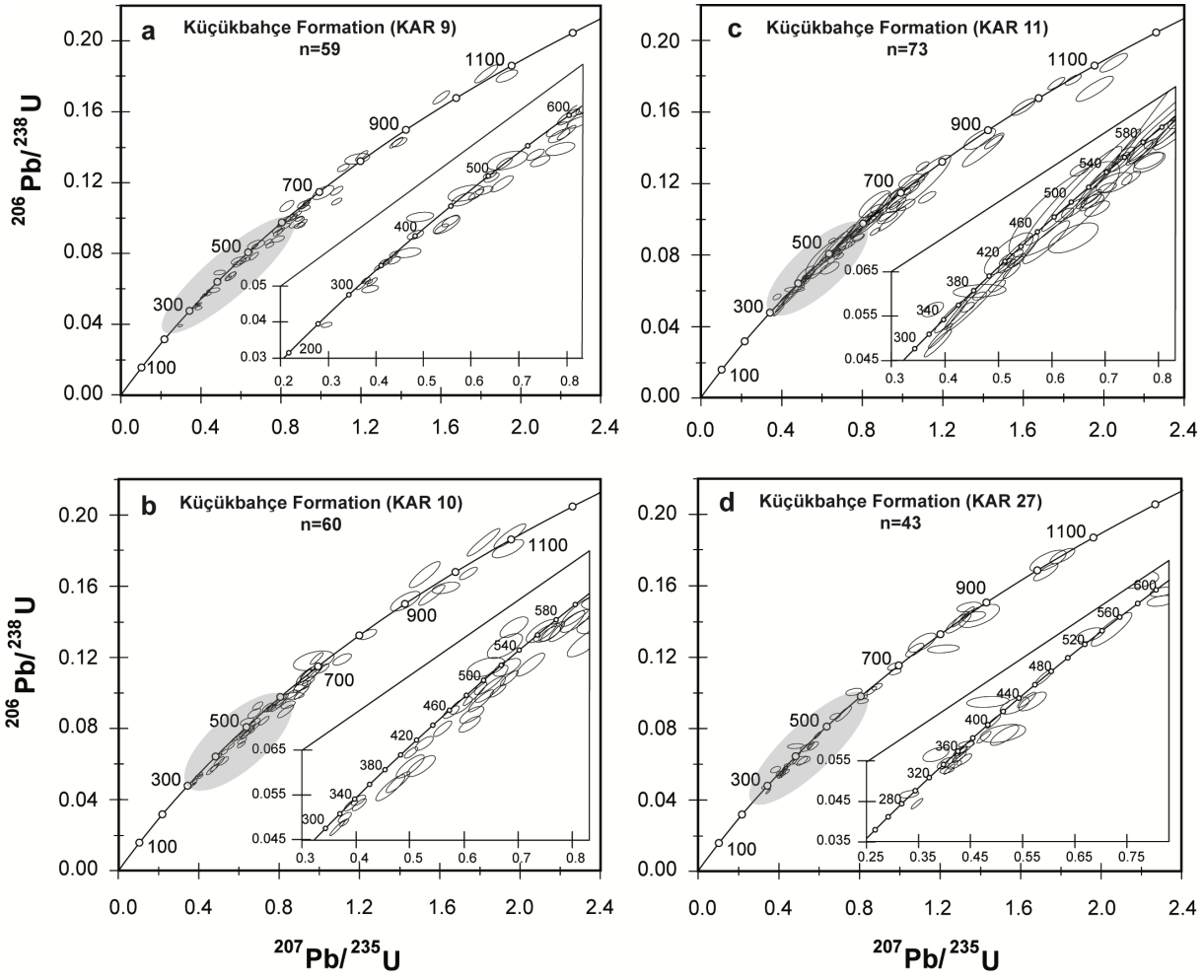

Fig. 3.7: U–Pb concordia plots showing LA-ICP-MS data of samples from the Küçükbahçe Formation. Data *point error ellipses* indicate 2σ uncertainties. *Shaded grey ellipses* outline areas that are shown as close-up.

at ca. 320 Ma and ca. 630 Ma (Figure 3.8a). Minor peaks occur at ca. 840 Ma and 1.95 Ga. The lower end of the spectrum is defined by a single spot age of 248 $\pm$ 4 Ma from an U-rich (2496 ppm) and common Pb- bearing (2.76%) grain that is not considered as geologically meaningful. A group (n = 5, #: 427, 447, 448, 460, 470) of zircons at 310–325 Ma indicates the maximum age of deposition.

The second sample (KAR10), a fine-grained subarkosic rock, is from the central part of the unit and is texturally similar to the previous one. Well-rounded grains with diverse, often chaotic or homogenous CL patterns, characterise the zircon population. The zircon data comprise 83 spots on 75 grains and the filtered data (n = 65) are dominated by Neoproterozoic U–Pb ages (ca. 50%) (Figure 3.8b). The spectrum is comparable to sample KAR9 and ranges from ca. 300 Ma to 3.0 Ga with an age gap

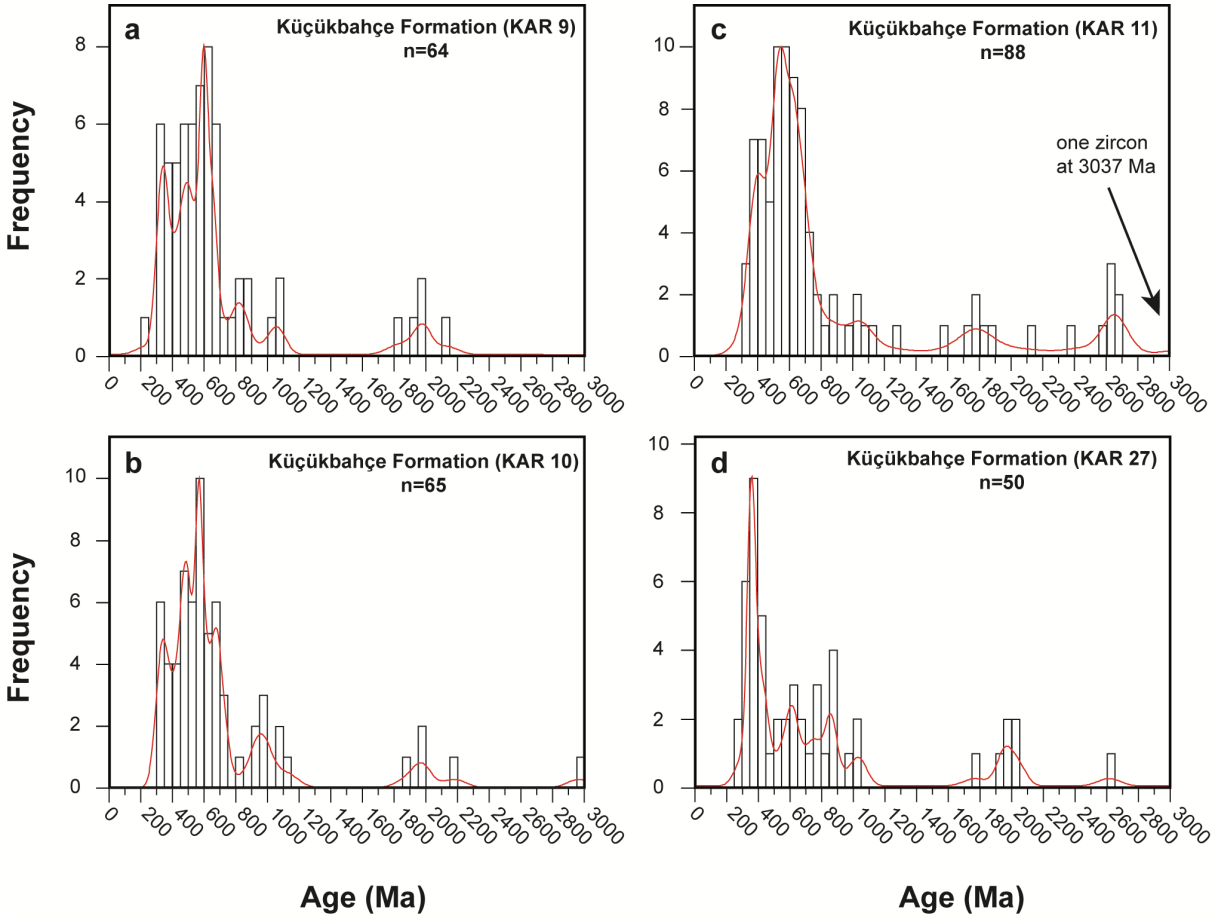

Fig. 3.8: Histograms and kernel density estimates of detrital U–Pb zircon ages from the Küçükbahçe Formation.

between 1.2 and 1.8 Ga. Several age groups are present at ca. 300–350 Ma, ca. 550–600 Ma and ca. 975 Ma of which the youngest group (n = 3, #: 481, 503, 535) indicates a maximum age of deposition of Pennsylvanian–Cisuralian.

Sample KAR11 is a lithic arkose that was collected from the northern part of the study area, ca. 4 km SW of Yeniliman village (Figure 3.2). This sample mainly consists of quartz, plagioclase, K-feldspar, muscovite, and predominantly metasedimentary fragments in a very fine-grained matrix. Although some zircon grains are euhedral to subhedral, most of them are rounded. CL images revealed that xenocrystic cores are common and many grains have disturbed patterns. Filtered data comprise 88 zircon ages from 109 spots measured on 103 grains. Zircon ages range from 300 Ma to 3.0 Ga and define two major groups at 350–450 and 500–650 Ma (Figure 3.8c). Two smaller groups occur at ca. 1.8 and ca. 2.6 Ga. The youngest single spot ages (#: 588, 612) are 307 $\pm$ 15 and 318 $\pm$ 14 Ma, but the maximum depositional age is constrained

by a group (n = 3, #: 559, 598, 626) of coherent U–Pb ages at ca. 345–360 Ma.

A fourth sample (KAR27), classified as sublitharenite, was collected from the eastern central part of the unit, close to the Dikendağı Formation (Figure 3.2). It predominantly consists of monocrystalline quartz and lithic fragments with some feldspar and mica. The majority of the zircon grains are subhedral or well-rounded and CL images show oscillatory zoning and xenocrystic cores surrounded by younger rims. Filtered zircon ages (n = 50) result from analyses of 57 spots on the same number of grains and show a polymodal age distribution with a major group (n = 9) at 350–400 Ma (Figure 3.8d). Minor populations exist at ca. 625 Ma, ca. 875 Ma, ca. 1.0 Ga, and ca. 2.0 Ga. Proterozoic zircons make up 50% of the data and Devonian to Carboniferous grains dominate the Palaeozoic age group. Two single grains (#: 657, 663) yielded Cisuralian ages and the youngest group of coherent zircon ages (n = 4, #: 651, 659, 662, 675) occurs at 330–340 Ma, defining the upper limit for deposition.

4.5 Dikendağı Formation

The second main clastic unit of inferred Palaeozoic age is the Dikendağı Formation from which five samples were analysed. Samples KAR5 and KAR6 were collected from the southern part of this formation within a close distance (ca. 2 km). The sediments are fine-grained sublitharenitic and lithic subarkosic rocks with similar mineral assemblages of quartz, feldspar, muscovite, and chlorite. Their zircon populations are dominated by well-rounded, colorless to pinkish grains with various, oscillatory zoning, homogenous, or chaotic CL patterns. The data set of sample KAR5 comprises 109 spots on 106 grains of which 90 U–Pb ages between ca. 330 Ma and 2.9 Ga were accepted. A prominent group occurs at 550–650 Ma (Figure 3.10a) and several smaller groups exist between 850 Ma and 1.1 Ga and 1.7–2.1 Ga, respectively. One single spot age (#: 688) at 334 $\pm$ 7 Ma defines the lower limit of the spectrum, but the maximum age of sedimentation is indicated by a group of zircons (n=3, #: 740, 757, 761) at 550–565 Ma. For sample KAR6, 62 spots on 52 grains were analysed. Filtered zircon ages (n=47) show a polymodal age distribution ranging from 200 Ma to 2.0 Ga. Major groups occur at 300–400 and 550–600 Ma (Figure 3.10b) and additional age groups appear at ca. 750–800 and 850–900 Ma. The youngest three single spot ages are Permian and Triassic (#: 778, 785, 797) including a high common Pb-bearing (4.56%) Late Triassic grain which is not considered to be geologically meaningful. A group (n=8,

#: 774, 775, 783, 787, 789, 790, 804, 810) of grains within the range of 300–350 Ma defines the maximum age of sediment deposition. Mesoproterozoic zircons are except of two grains at ca. 1.0 Ga completely absent, but a small amount of Paleoproterozoic grains exists.

A third sample (KAR7) from the southern area was classified as a lithic arenite and is characterised by highly abundant and large feldspar crystals and lithic fragments. The U–Pb zircon data consist of 134 spots on 127 grains, of which 126 ages were accepted. These grains are colorless to light orange and of subhedral to euhedral shape with predominantly oscillatory zoning patterns. Most of the zircons (ca. 90%) are of Palaeozoic age and define a single, Early Palaeozoic peak at 400–450 Ma (Figure 3.10c). Although the youngest single spot ages occur at 294 and 308 Ma (#: 833, 841), the maximum age of deposition is constrained by a group (n=5, #: 836, 852, 857, 906, 938) of zircons between 370 and 385 Ma.

Sample KAR14 was collected ca. 2 km southeast of Yeniliman village (Figure 3.2). It is a subarkosic sediment dominated by monocrystalline quartz and to some extend feldspar within a muscovite-bearing matrix. In most cases, the zircon grains are light pinkish and well-rounded with oscillatory growth zoning. In total, 72 spots were analysed on 65 grains and filtered data contain 61 U–Pb ages. Except of two, they are all Proterozoic or older in age and show a distribution pattern characterised by two broad groups at 550–700 and 900–1100 Ma (Figure 3.10d) and a smaller peak at 1.85–1.9 Ga. A group of Ediacaran-aged zircons (n = 6) between ca. 550 and 570 Ma marks the maximum age of sedimentation for this sample.

One last sample (KAR15) was taken from a location close to the contact to the Early Triassic granitoid intrusions in northern Karaburun. The sediment is classified as subarkose and thus predominantly consists of quartz with only small amounts of feldspar, muscovite, and chlorite. Lithic fragments are virtually absent. From this sample, 22 grains were analysed on 27 spots, of which 23 were accepted. Zircon grains are well-rounded and of euhedral shape, in similar abundance, and have oscillatory zoning patterns and rare xenocrystic cores. The ages range from ca. 340 Ma to 2.7 Ga with main groups at 350–400 and 500–550 Ma (Figure 3.10e).

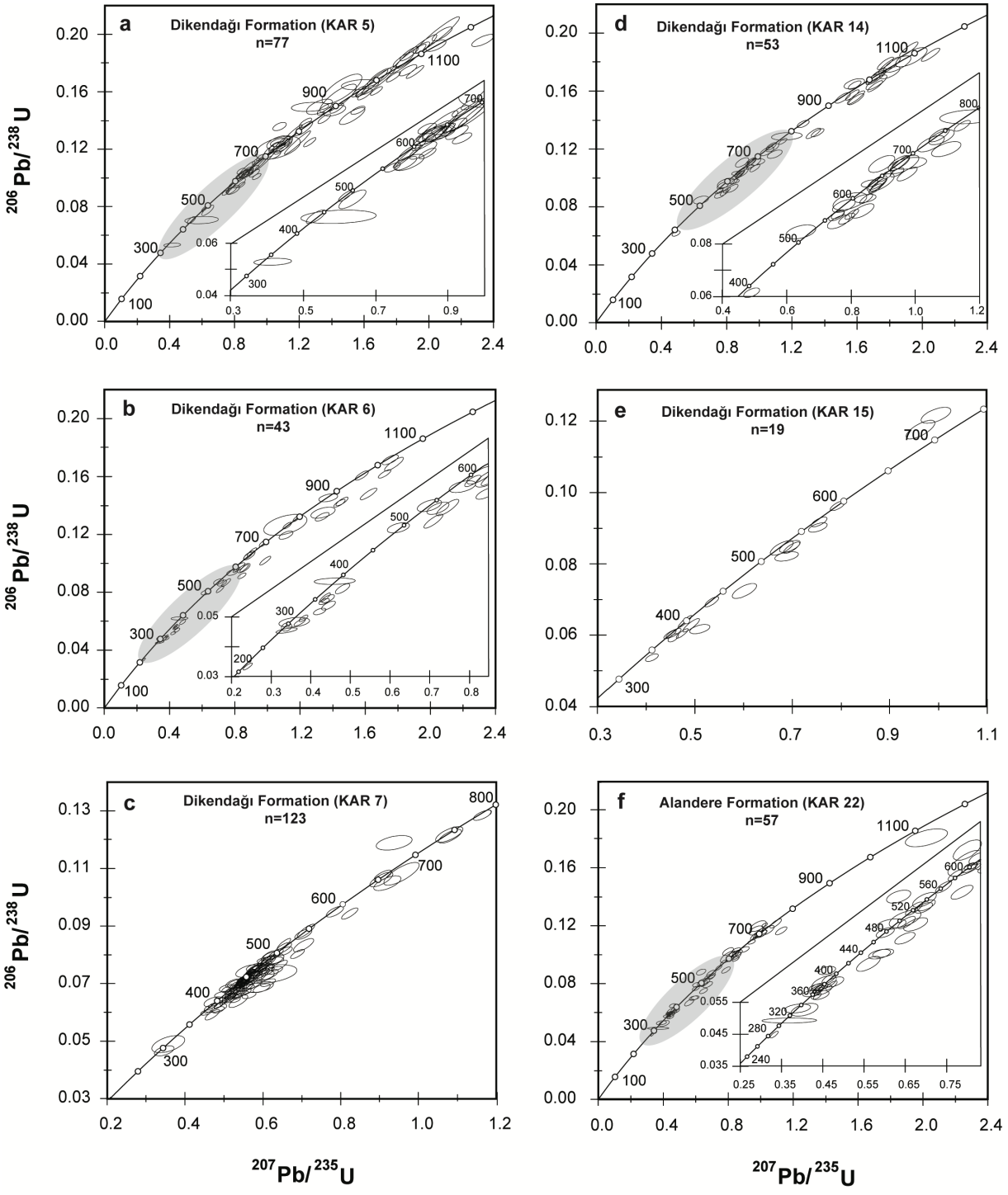

Fig. 3.9: U–Pb concordia plots showing LA-ICP-MS data of samples from the Dikendağı and Alandere formations. Data *point error ellipses* indicate 2σ uncertainties. *Shaded grey ellipses* outline areas that are shown as close-up.

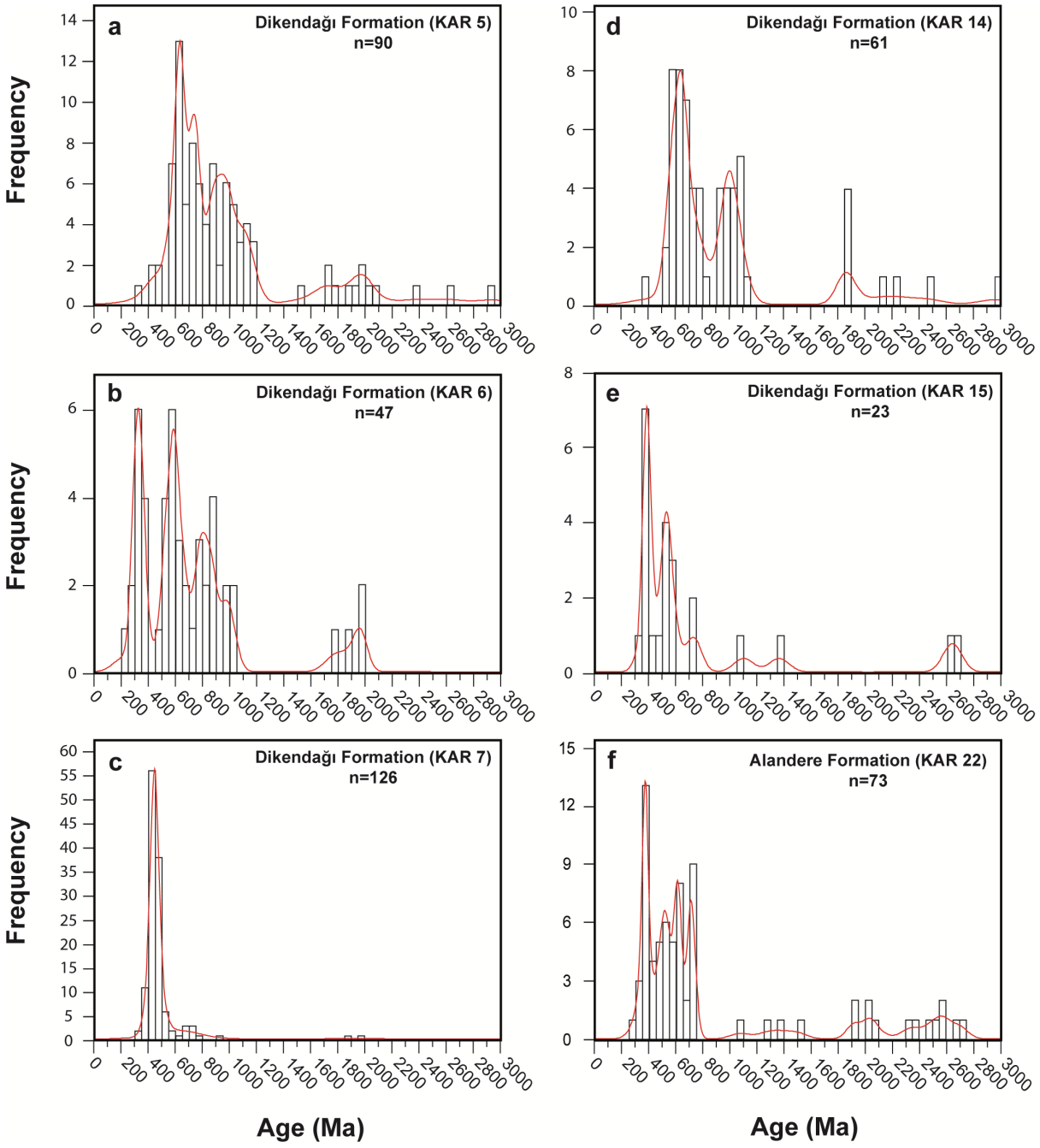

Fig. 3.10: Histograms and kernel density estimates of detrital zircon U–Pb ages from the Dikendağı and Alandere formations.

4.6 Alandere Formation

For the Alandere Formation, one sample (KAR22) was collected from a location at the southern coast of Gerence Bay (Figure 3.2). The sediment is a coarse-grained, garnet-chromite-bearing subarkosic rock consisting of primarily quartz and feldspar with lithic

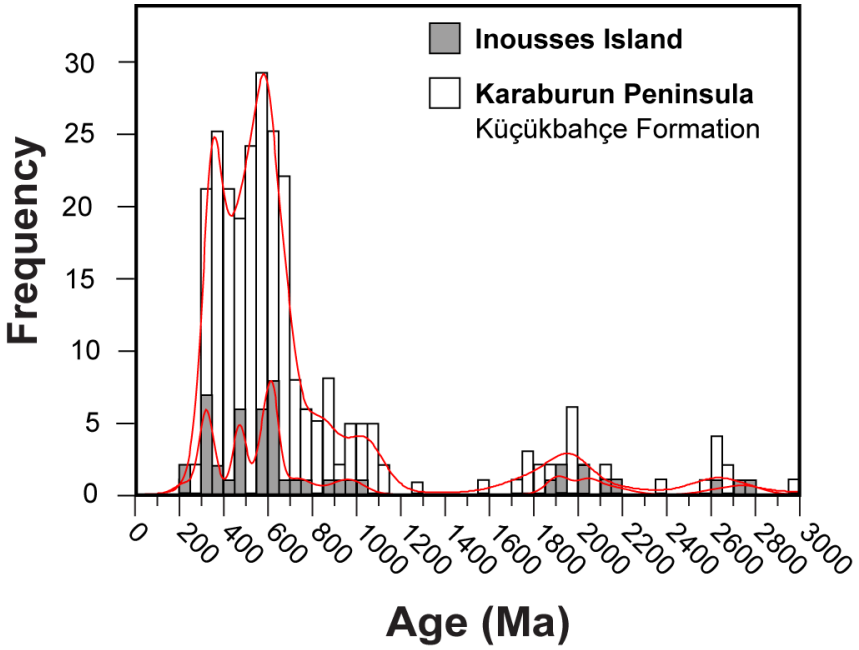

Fig. 3.11: Histograms and kernel density estimates of detrital zircon U–Pb ages from the Küçükbahçe Formation of Karaburun Peninsula (n = 267, this study) and Inousses Island (n = 49, Meinhold and Frei 2008) for comparison.

fragments of mostly volcanic origin. The most zircon grains are colorless to light pinkish and have a subhedral shape with oscillatory zoning patterns. For this sample, 88 spots on 73 grains were analysed. Of these, 73 zircons met the filtering criteria and yielded U–Pb ages between 280 Ma and 2.7 Ga with very few zircons from 800 Ma to 1.8 Ga (Figure 3.10f). One major age group (n = 13) exists at 350–400 Ma and three smaller peaks occur at ca. 520, ca. 620, and ca. 720 Ma. The youngest small group (n = 2, #: 1034, 1047) of zircons occurs at ca. 330 Ma, but a larger coherent group (n = 6, #: 1029, 1031, 1045, 1051, 1071, 1097) exists at 357–370 Ma and is considered to indicate a Carboniferous (Mississippian) maximum depositional age. The Permian and Late Carboniferous single spot ages (#: 1033, 1076) at ca. 280 and 310 Ma are due to their high U and common Pb content not considered for further interpretation.

5 Discussion

5.1 Maximum depositional ages and revised stratigraphy

Age spectra of detrital zircons from sedimentary rocks provide provenance information as well as constraints for the timing of sediment deposition (e.g., Fedo et al. 2003). In

case of the Karaburun Peninsula, the depositional ages of the Mesozoic sequences were already well defined by biostratigraphic data. However, the age of the underlying Palaeozoic clastic rocks was only loosely constrained and stratigraphic correlations were interpreted in different ways (e.g., Erdoğan et al. 1990, 2000; Çakmakoğlu and Bilgin 2006). Based on our results, we present new evidence for the timing of sediment deposition and review previously published stratigraphic models (Figure 3.3). Compiled information on the stratigraphic age of the different formations of Karaburun Peninsula inferred from fossils and the depositional age according to new U–Pb detrital zircon data are given in Table 3.1.

The Güvercinlik Formation represents the highest structural and stratigraphic level of the investigated sediments. Two samples (KAR20A and KAR20B) yielded consistently similar distribution of zircon ages (Figure 3.12), including one grain of ca. 202 Ma in the first sample, but three more latest Triassic zircons in the latter. As the sample locations are in close proximity and their chemical and petrographic characteristics are matching, the youngest group extracted from the combined data set, probably indicates the maximum age of sediment deposition, thus confirming the data of Erdoğan et al. (1990, 2000) and Çakmakoğlu and Bilgin (2006). An Early Triassic age has been assigned to the Gerence Formation based on biostratigraphic data: the youngest group of zircons from this study is Visean, which provides the maximum age of deposition for this succession based on U–Pb geochronology. This could be a result of a low zircon count (n = 51), which might be insufficient to detect every population that was present in the sample. Another more likely explanation implies that rocks of Early Triassic age were either never present or not yet exposed in the source area at the time of deposition. A similar scenario could explain the situation for the İdecik unit. Çakmakoğlu and Bilgin (2006) assigned a Ladinian–Carnian age to this unit, whereas results from U–Pb dating indicate an Early Carboniferous depositional age. The age distribution pattern of one of the samples (KAR4) shows striking similarities to the late Palaeozoic Küçükbahçe Formation (Figure 3.12). This suggests that recycling of these rocks could have provided large amounts of detritus for the İdecik unit or both were supplied by the same source.

Information on the siliciclastic rocks that make up large parts of the northern and western area of Karaburun Peninsula is scarce. Erdoğan et al. (1990) introduced the term Karareis Formation to describe the clastic sequences in northwestern Karaburun

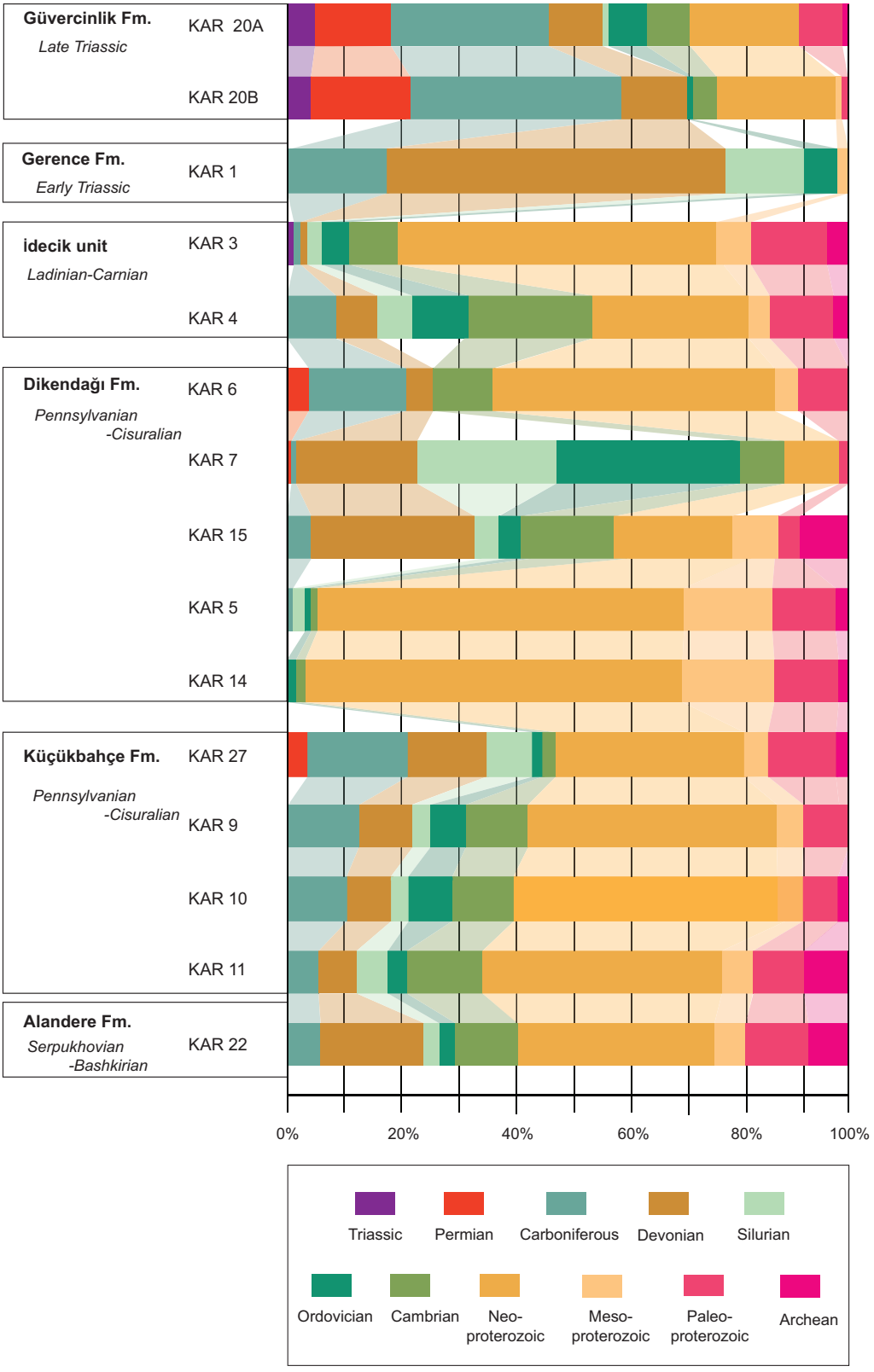

Fig. 3.12: Percentages of detrital zircon U–Pb ages for studied samples.

and interpreted the carbonate-rich Gerence Formation in the southwestern and eastern part as a lateral equivalent of the Karareis Formation. Both were assigned to the so-called Denizgiren Group of assumed Scythian–Anisian age (Figure 3.3). Later, these detrital sequences to the west were considered as separate units: (1) the Küçükbahçe Formation for which an Ordovician (or Cambro–Ordovician) deposition was suggested and (2) the Dikendağı Formation of assumed Silurian–Carboniferous age (Visean) (Kozur 1998; Çakmakoğlu and Bilgin 2006) (Figure 3.3). Some Visean zircons have been mentioned for the Küçükbahçe Formation in an abstract by Rosselet and Stampfli (2003), but here, we present the first extensive U–Pb data set of detrital zircons from the siliciclastic units. Our results comprise more than 600 single zircons and clearly indicate a considerably younger depositional age for both formations, which is in marked difference to previously published data (Figure 3.3). The maximum age of deposition for the Küçükbahçe Formation is constrained by a group (n = 11) of Pennsylvanian–Cisuralian zircons extracted from the combined dataset of all samples. Filtered data from the Dikendağı Formation contain less (n = 7) grains of Late Carboniferous–Early Permian age, almost exclusively from samples (KAR5, KAR6, and KAR7) collected from the southern part of the formation. According to the zircon spectra alone, samples from the northern region could have a slightly older, probably Lower Devonian–Early Carboniferous maximum depositional age. This could also be an effect of the smaller database for the northern part (n = 84) or refer to one of the reasons given below. Nevertheless, we consider this as sufficient indication for time equivalent deposition of both formations. Regarding the Dikendağı Formation, the minimum age of sedimentation is defined by an Early Triassic (247 $\pm$ 2.0 Ma, Akal et al. 2011; 244.4 $\pm$ 1.5 Ma; Ustaömer et al. 2016a) granitoid intrusion in the northern part of the peninsula. During fieldwork, an unknown mafic intrusion was discovered in the northwestern part of the Küçükbahçe Formation that may also provide a lower limit of sediment deposition (Figure 3.13). With respect to the zircon spectra, the Küçükbahçe Formation is characterised by notably consistent age distribution with only little variation (Figure 3.12). On the contrary, the supposed time equivalent Dikendağı Formation shows distinct heterogeneity with respect to, not only zircon distribution, but also petrography and chemical composition (Löwen et al. 2018). This may have several reasons: (1) it is the result of provenance change through time; (2) field observations reveal that the lithology of the northern and southern part of this unit is variable; large chert and limestone blocks are

restricted to the south only. Nonetheless, the entire area is mapped as a single formation but possibly needs further subdivision; (3) above-listed differences correspond to distal and/or proximal extensions of turbidity currents; (4) some of the analysed samples could have been part of larger blocks (probably olistolithes) that are enclosed in the matrix rocks and do not represent the matrix itself. Future studies might solve the issue of heterogeneity within the Dikendağı Formation.

For the Alandere Formation, our zircon results are in good agreement with the previously assigned Serpukhovian–Bashkirian age. These findings allow refinement of the current stratigraphy and regional correlations of the Palaeozoic units (Figures 3.3, 3.13). New data indicate that sediment accumulation of the Küçükbahçe and Dikendağı formations did not start in Ordovician (or Cambro-Ordovician) time, but most probably began in the mid-Carboniferous and continued to at least Pennsylvanian–Cisuralian. This implies that the Alandere Formation, until now interpreted as youngest section of the mélange (Robertson and Pickett 2000), represents the oldest and, therefore, lowermost part of the mélange (see also Erdoğan et al. 1990). In the light of these findings, a supposed gradational contact with the Dikendağı Formation and its stratigraphic position seems questionable. Besides, the Küçükbahçe Formation and overlying Dikendağı Formation were also thought to be separated by a gradational contact. However, as both units, to some extent, exhibit very similar lithologies but have different provenance and show different metamorphic overprint, we favor a tectonic contact in agreement with Robertson and Ustaömer (2009b). Thus, the previously construed Ordovician–Carboniferous sedimentary sequence is rather a pile of units deposited in Carboniferous–Early Permian times. Combined new data and indications from field work suggest that the present-day stratigraphic order was established by westward thrusting, not before Cretaceous times.

Similar Palaeozoic rocks that are comparable to the mélange zone of Karaburun occur on the neighboring islands of Chios and Inousses in the eastern Aegean Sea (Figure 3.2). Chios is tectonostratigraphically subdivided into an ‘autochthonous’ Lower Unit including a Carboniferous mélange and Mesozoic carbonates and a tectonically overlying ‘allochthonous’ Upper Unit of Late Carboniferous to Jurassic age (Besenecker et al. 1968; Meinhold et al. 2007, 2008b) (Figure 3.3). The Lower Unit consists of Late Palaeozoic siliciclastic rocks including blocks of limestone, radiolarites, and volcanic rocks of Silurian to Carboniferous age, and shows striking similarities to the block-

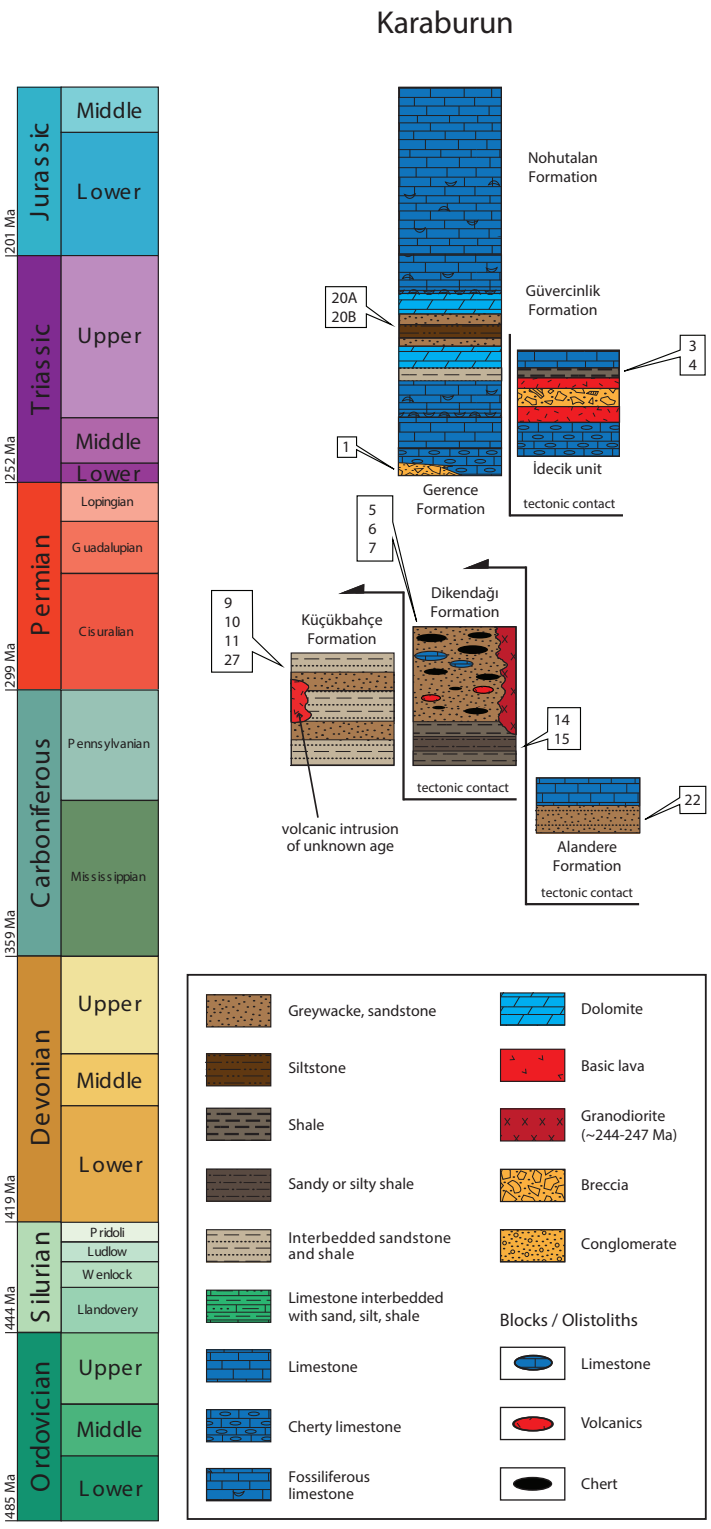

Fig. 3.13: Revised stratigraphic section of Karaburun Peninsula. Sediment accumulation of the Küçükbahçe and Dikendağı formations most probably began in the mid-Carboniferous and continued to at least Pennsylvanian–Cisuralian. The Alandere Formation represents the oldest part of the mélange. Contacts between the Alandere, Dikendağı and Küçükbahçe formations are supposed to be rather tectonic than gradational. Blocks/olistoliths in the Palaeozoic succession of Karaburun Peninsula have been described by Kozur (1998) and Robertson and Ustaömer (2009b).

bearing Dikendağı Formation of Karaburun (e.g., Robertson and Ustaömer 2009b). This (supposed) relation is further underlined by the refined stratigraphic section and indicates that this succession may represent a Late Carboniferous–Early Permian equivalent of the Chios mélange.

On Inousses Island, low-grade metasedimentary rocks are subdivided into two lithostratigraphic units (Besenecker et al. 1971; Kilias 1987; Meinhold et al. 2007). The Lower unit mainly crops out as small patches in the southern part of the island and consists of psammitic rocks with conglomeratic layers. The Upper Unit is made up of pelitic to psammitic rocks and covers the northern part including a small area on the NE tip of Chios that is interpreted as part of Inousses (Kauffmann 1965; Besenecker et al. 1968, 1971). The whole sequence is of a monotonous character and does not contain fossils or specific marker horizons for certain stratigraphic correlations. Some workers assigned the metasedimentary succession of Inousses to Permian–Triassic rocks of the Pelagonian Zone of continental Greece and the Sporades Islands (Mountrakis et al. 1983; Kilias 1987). In contrast, Kozur (1998) correlated the Inousses clastic rocks with the Küçükbahçe Formation of the Karaburun Peninsula to the east, for which he suggested an Ordovician (or Cambro–Ordovician) age. Meinhold and Frei (2008) constrained the maximum age of deposition to be Late Carboniferous by dating of detrital zircons. Based on field observations and provenance data, the metasedimentary rocks of Inousses are correlated with the Küçükbahçe Formation; a Pennsylvanian–Cisuralian depositional age is suggested (this study). A comparison of age spectra from both successions reveals congruent distribution patterns, characterised by a predominance of 300–700 Ma-old zircons and minor groups between 1.7 and 2.2 and 2.45–2.8 Ga as well as a lack of 1.1–1.7 Ga-old zircon grains (Figure 3.11). In addition to the zircon data, petrographic observations and geochemical analysis of the sediments of Küçükbahçe Formation reveal great similarities to those from Inousses (Löwen et al. 2018).

6 Provenance

Our samples derive from different stratigraphic levels and cover a time slice from Late Palaeozoic to latest Triassic. The zircon age distribution of these rocks reflects the entirety of zircon from exposed rocks at the time of sediment deposition and, therefore,

is a powerful tool to identify possible source region(s).

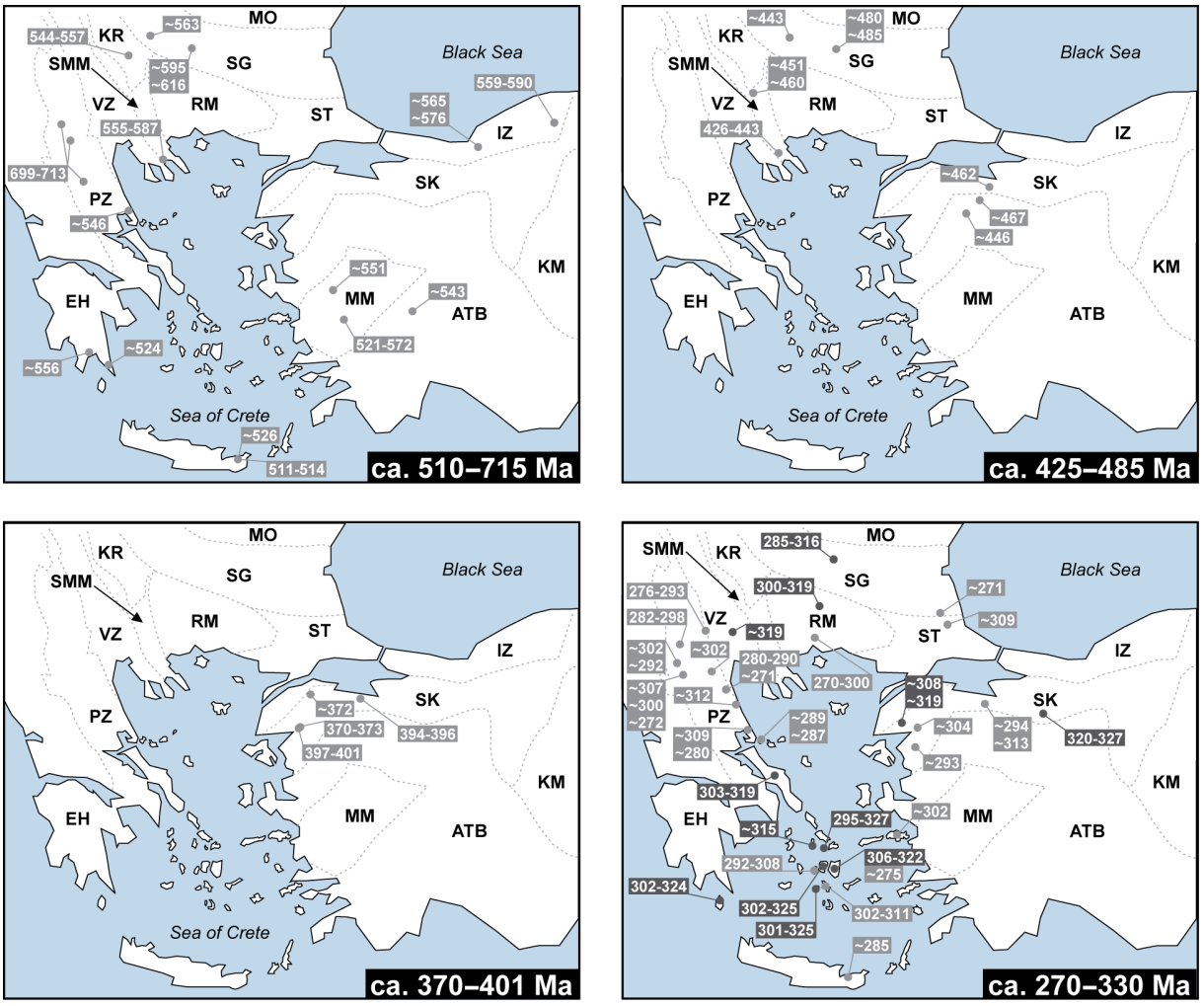

Fig. 3.14: Compilation of Late Neoproterozoic and Palaeozoic zircon age distribution data of potential igneous source rocks from Greece and the surrounding region after Meinhold et al. (2008b, and reference therein), with additional data from Okay et al. (2008); Himmerkus et al. (2009a); Aysal et al. (2012); Sunal (2012); Ustaömer et al. (2012); Özbey et al. (2013); Dörr et al. (2015) and Zulauf et al. (2015). For better visualisation, the dark grey fillings in the map lower right mark localities with Early to earliest Late Carboniferous ages (≥315–330 Ma) reported. Triassic igneous rocks are widespread in the Serbo-Macedonian Massif, the Pelagonian Zone, the Cycladic Islands, and the Menderes Massif (e.g., Tomaschek et al. 2001; Koralay et al. 2001; Bröcker and Pidgeon 2007; Anders et al. 2007; Himmerkus et al. 2009b) and for simplification are not shown in the maps. ATB Anatolide–Tauride block, EH external Hellenides, İstanbul zone, KM Kırşehir Massif, KR Kraište, MM Menderes Massif, MO Moesia, PZ Pelagonian Zone, RM Rhodope Massif, SG Sredna Gora zone, SK Sakarya, SMM Serbo-Macedonian Massif, ST Strandja, VZ Vardar zone.

In recent times, several studies have been performed on detrital zircons of Palaeozoic siliciclastic rocks from the larger study area that provide important references for the provenance of the Karaburun sediments. In the Menderes Massif of the western

Taurides, Neoproterozoic basement rocks are covered by lower Palaeozoic platform sediments. Zircon age spectra from the lower part of this cover are dominated by Neoproterozoic zircons with generally negative εHf values and reveal striking similarities to Cambrian–Ordovician sandstones from Israel and Jordan. The patterns were interpreted to tie the Menderes Massif to the Afro-Arabian margin of northern Gondwana in lower Palaeozoic time (Zlatkin et al. 2013). Similar Palaeozoic to Triassic sedimentary cover rocks crop out in the Karacahisar dome of the Taurides (south-central Turkey). U–Pb zircon data reveal a predominant Neoproterozoic zircon population in Cambrian–Ordovician sandstones and were linked to sediments from Afro–Arabia of the same age as well (Abbo et al. 2015). Furthermore, zircon spectra of the Triassic sequence lack evidence for any post-Cambrian or Variscan sources and suggest that the Tauride domain remained in close proximity to northern Gondwana and did not detach until Middle–Upper Triassic time (Abbo et al. 2015). A study on the Palaeozoic evolution of the northern Gondwana continent was carried out by Meinhold et al. (2011) in the eastern Murzuq Basin of southern Libya. Analysed Palaeozoic and Mesozoic sandstones of this basin cover the Archean to Proterozoic rocks of the Saharan Metacraton. Detrital zircons from the Palaeozoic and Mesozoic sandstones revealed similar age spectra with four main populations of early Proterozoic–Neoarchean, Paleoproterozoic, Stenian–Tonian, and Cryogenian–Ediacaran age with variable abundance. Zircons of the pre-Paleoproterozoic age groups were assigned to basement rocks of the underlying Saharan Metacraton, whereas the younger Cryogenian–Ediacaran grains were related to orogenic events affecting northern Gondwana. The provenance of the Stenian–Tonian population is not yet clarified, but zircons could have been derived either from igneous rocks from areas south(east) of Libya or represent recycled detritus from Neoproterozoic sediments (Meinhold et al. 2011). An extensive dataset has also been established for late Palaeozoic siliciclastic rocks of the External Hellenides. Detrital zircon spectra obtained from rocks of the Phyllite-Quartzite Unit from Crete, Kythera and the Peloponnesus (Marsellos et al. 2012; Chatzaras et al. 2016; Zulauf et al. 2016) are characterised by a prominent Neoproterozoic population with significant input of Ediacaran and Stenian/Tonian proportions. Based on these similarities and the lack of Ordovician to Triassic zircons, combined with a Mesoproterozoic age gap, these rocks were interpreted as time and facies equivalent sequences, deposited along the northern margin of Gondwana, isolated from Variscan sources (Chatzaras et al. 2016). In

contrast, Early Permian quartzites from the pre-Alpine basement and cover rocks of the lower Tyros Unit on Crete record distinct influx of Variscan detritus (50–70% Carboniferous/Permian detrital zircons) suggesting deposition in close proximity to the southern active margin of Eurasia (Zulauf et al. 2015).

In case of the Karaburun samples, the overall zircon data comprise a wide range of ages from 202 Ma to 3.0 Ga, thus reflecting various stages of crustal growth and/or recycling. Common features of the population are several groups of Palaeozoic to Neoproterozoic zircons, a very low number or even lack of zircons from 1.2 to 1.7 Ga and the presence of smaller populations at ca. 1.7–2.2 Ga and/ or ca. 2.5 Ga, respectively. These attributes clearly exclude Amazonian (west Gondwana) or Baltican provenance as Mesoproterozoic zircons are widespread in these regions and would have been recorded in their erosional products. For the purpose of our study—identifying possible source regions—the Early Neoproterozoic and older zircons are not necessarily useful to pinpoint a certain area as those ages come up in nearly all samples and may have a variety of sources. A more promising approach focuses on the distribution of Late Neoproterozoic (ca. 540–650 Ma, i.e., 'Pan-African/Cadomian') and Palaeozoic (ca. 280–330 Ma, ca. 370–400 Ma, ca. 430–460 Ma, ca. 480 Ma) potential igneous source rocks, since they are important time-markers for palaeotectonic reconstructions in the Eastern Mediterranean (e.g., Meinhold et al. 2008b) (Figure 3.14).

The large input of zircons from 650 to 540 Ma is most probably related to the Pan-African and Cadomian orogenies. Both events were linked to the formation of the Gondwana supercontinent in Late Neoproterozoic time, whereas the term 'Pan-African' orogeny generally refers to the cratonic domains (continent–continent collision) and the Cadomian domain (Avalonian–Cadomian belt) is interpreted as peripheral or accretionary orogenic belt that assembled at the northern margin of Gondwana and was accompanied by subduction-related magmatism (Nance and Murphy 1994; Windley 1995). Detrital and magmatic zircons of Late Neoproterozoic age (Pb–Pb, U–Pb) have been published for several terranes in the Eastern Mediterranean region: Menderes Massif (e.g., Sandıklı, Çine, and Ödemiş submassifs) in western Turkey (Kröner and Şengör 1990; Hetzel and Reischmann 1996; Hetzel et al. 1998; Loos and Reischmann 1999; Gessner et al. 2004); İstanbul Zone in northern Turkey (Chen et al. 2002; Ustaömer et al. 2005); Kraište region in Bulgaria (von Quadt et al. 2000; Graf 2001; Kounov 2002); Serbo-Macedonian Massif in northern Greece (Himmerkus et al. 2006,

2007) (Figure 3.14).

A group of two samples from the Gerence Formation (KAR1) and Dikendağı Formation (KAR7) reveals unimodal age spectra in the range of 350–450 and 400–500 Ma, respectively (Figures 3.6a, 3.10c). These patterns clearly indicate sediment supply from localised sources of Ordovician to Devonian age. In case of the Ordovician zircons, these rocks are restricted to very few regions only. Possible source rocks are located in the Sakarya Zone from which Özmen and Reischmann (1999) reported Middle Ordovician (462 $\pm$ 6 Ma) ages for basement rocks of the Biga Peninsula; smaller metagranitic bodies occur in the Tavşanlı Zone (467 $\pm$ 5 Ma, Okay et al. 2008; 446 $\pm$ 8 Ma; Özbey et al. 2013) (Figure 3.14). Similar ages are also known from granites and gneisses of different parts of the Balkan region, such as the Sredna Gora Zone and Serbo-Macedonian Massif (Titorenkova et al. 2003; Peytcheva and von Quadt 2004; Carrigan et al. 2005) (Figure 3.14). Large volumes of possible Silurian orthogneisses make up the basement of the Vertiskos Unit of the NW Serbo-Macedonian Massif (Himmerkus et al. 2006, 2007, 2009a; Meinhold et al. 2010). The above-mentioned areas exhibit suitable source rocks and may have provided large volumes of detritus for the siliciclastic rocks of Karaburun.

Early Devonian igneous rocks are well documented from different parts of the Sakarya Zone (Figure 3.14). Zircon U–Pb ages of ca. 395 Ma have been reported for the Karacabey Pluton (Sunal 2012) and similar Pb–Pb ages were obtained from metagranodiorite and gneisses of the Biga Peninsula (Okay et al. 1996, 2006). Magmatic rocks of Carboniferous to Early Permian age ('Variscan') are very common and widespread in the Eastern Mediterranean region and have been reported from the External Hellenides, the Cycladic Islands, the Kazdağ Massif of the Sakarya Zone and several parts of the Rhodope Zone (e.g., Engel and Reischmann 1998; Reischmann 1998; Özmen and Reischmann 1999; Keay et al. 2001; Xypolias et al. 2006; Anders et al. 2007; Turpaud and Reischmann 2010; Zulauf et al. 2015). They record a major magmatic phase during that period which was related to subduction and closure of Palaeotethys (Pe-Piper and Piper 2002).

Studied rocks from the Mesozoic part of the Karaburun Peninsula are of Early to Late Triassic stratigraphic age, but only samples of the Güvercinlik Formation document sediment supply from (Permian)–Triassic sources. These ages are not common for domains of the N-African continent, but Triassic magmatic activity has been recognised

in many places of the Eastern Mediterranean region. Such zircons are most likely related to the Serbo-Macedonian Massif, the Pelagonian Zone, the Cycladic Islands, the External Hellenides, and/or the Menderes Massif from which U–Pb and Pb–Pb data have been reported (e.g., Tomaschek et al. 2001; Koralay et al. 2001; Bröcker and Pidgeon 2007; Anders et al. 2007; Himmerkus et al. 2009b; Zulauf et al. 2015).

As aforementioned detrital zircons of Palaeozoic to Triassic sediments from parts of the Taurides (Menderes Massif, Karacahisar) and External Hellenides (Crete and Peloponnesus) revealed significant differences between terranes that were placed either at the southern Eurasian or northern Gondwana margin (Zlatkin et al. 2013; Chatzaras et al. 2016; Abbo et al. 2015; Zulauf et al. 2015, 2016). The latter were generally characterised by large Cambrian and Neoproterozoic populations with low amount of Palaeozoic zircons (e.g., Karacahisar dome and Menderes Massif), whereas widespread occurrence of Carboniferous to Permian zircons (e.g. pre-Alpine basement on Crete) was attributed to Variscan sources. Even though our samples exhibit prominent Neoproterozoic populations as well, the available information and indicative Palaeozoic age groups—Ordovician–Devonian in particular—clearly support terranes north of the present location of our study area as most likely sources for the Karaburun, Chios, and Inousses sediments. In terms of palaeogeography, we propose a location in close proximity to the Sakarya, Pelagonian and/or Rhodope zones, or equivalent rock units not present anymore due to erosion and/or subduction, definitely at the southern margin of Eurasia in Late Palaeozoic time (see also Meinhold and Frei 2008; Meinhold et al. 2008b) (Figure 3.15). Carboniferous foraminiferal fauna of the Chios–Karaburun units, which show distinct biogeographical affinities to the southern Laurasian shelf (Kalvoda 2003), support this. However, the above-mentioned statements do not seem to be valid for two samples from the Dikendağı Formation (KAR5 and KAR14), which have detrital zircon age populations very similar to those seen in Palaeozoic and Mesozoic siliciclastic sediments of the central North Gondwana margin (e.g., Meinhold et al. 2011, 2013; Dörr et al. 2015). Future studies may shed light on their palaeotectonic history. Moreover, Devonian-aged zircon populations characterise some of the Late Triassic Karakaya Complex sandstones exposed in the Sakarya Zone of NW Turkey (Ustaömer et al. 2016a). Some of the studied Karaburun sediments (e.g., Dikendağı and Gerence formations) also have zircon grains with such ages. Based on their zircon age populations (with the exception of the occurrence of Late Triassic zircons ages), some of the

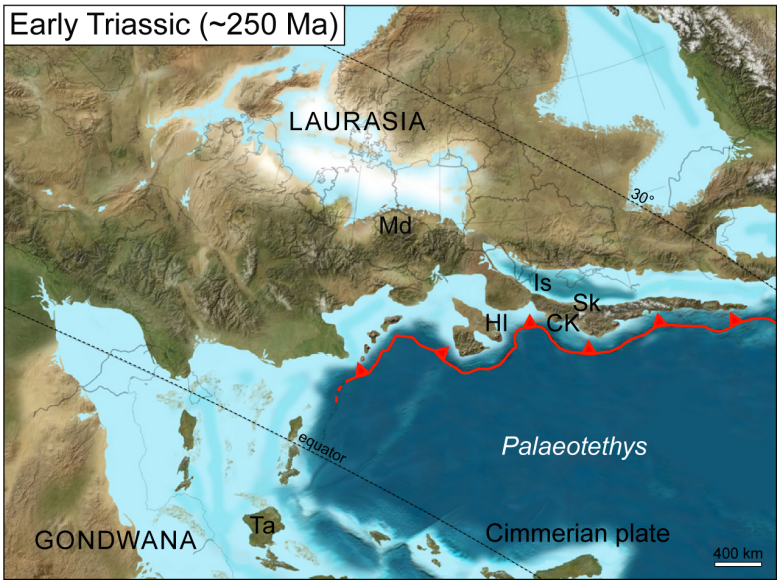

Fig. 3.15: Palaeotectonic reconstruction for the Early Triassic indicating the presumed position of the Chios–Karaburun units at the southern margin of Eurasia. The exception being some rocks of the heterogeneous Dikendağı Formation, which have similar detrital zircon age populations as sediments from the northern margin of Gondwana. Base map adapted from ©Ron Blakey, Colorado Plateau Geosystems, Arizona, USA (http://cpgeosystems.com/), used with permission. CK Chios–Karaburun units, İstanbul zone, HI internal Hellenides, Md Moldanubian zone, Sk Sakarya zone, Ta Taurides.

Karaburun sediments share similarities with the Karakaya Complex sandstones of the Sakarya Zone.

7 Conclusions

Our study provides the first comprehensive U–Pb database of Palaeozoic and Mesozoic siliciclastic sedimentary rocks from the Karaburun Peninsula of western Turkey. These data give new constraints for the timing of sediment deposition and stratigraphy of the study area as well as information on provenance. The most important findings of this study are as follows:

- Küçükbahçe and Dikendağı formations are not of Ordovician or Early Carboniferous age: sediment accumulation probably began in mid-Carboniferous times and continued to at least Pennsylvanian–Cisuralian.
- Zircons from the Küçükbahçe Formation yielded consistent and homogenous results throughout all samples. In contrast, the Dikendağı Formation is charac-

terised by large heterogeneity.

- The Alandere Formation (Serpukhovian–Bashkirian) is the oldest formation of Karaburun Peninsula.
- The Palaeozoic sequence composed of the Küçükbahçe, Dikendağı, and Alandere formations is, in fact, a stack of units formed by supposed post-Cretaceous thrusting.
- Karaburun, Chios, and Inousses sediments are closely related and share similar provenance. They were located along the southern margin of Eurasia during Late Palaeozoic time, the exception being two samples from the Dikendağı Formation.
- Some of the Late Palaeozoic and Triassic sediments of Karaburun Peninsula share similarities in respect of detrital zircon ages with the Karakaya Complex sandstones of the Sakarya Zone in NW Turkey.

Chapter 4

Manuscript III: Evolution of the Palaeotethys in the Eastern Mediterranean: A multi-method approach to unravel the age, provenance and tectonic setting of the Upper Palaeozoic Konya Complex and its Mesozoic cover sequence (south-central Turkey)

Kersten Löwen[a,*], Guido Meinhold[a,b], Arzu Arslan[b] Talip Güngör[c] Jasper Berndt[d]

[a] Abteilung Sedimentologie/Umweltgeologie, Geowissenschaftliches Zentrum Göttingen, Universität Göttingen, Goldschmidtstraße 3, 37077 Göttingen, Germany

[b] School of Geography, Geology and the Environment, Keele University, Staffordshire,

ST5 5BG, UK

[c] Department of Geological Engineering, Dokuz Eylül University, Tınaztepe Campus, 35160 Buca-İzmir, Turkey

[d] Institute of Mineralogy, Westfälische Wilhelms-University Münster, Corrensstraße 24, 48149 Münster, Germany

[*]e-mail: kersten.loewen@geo.uni-goettingen.de
Tel.: +49 551 399818

Published in: International Geology Review (2019): https://doi.org/10.1080/00206814.2019.1616619

Abstract

Siliciclastic sediments from the Upper Palaeozoic Konya Complex and its Mesozoic cover were studied by a multi-method approach combining thin-section petrography, bulk-rock geochemistry, mineral chemistry of rutile, and U–Pb geochronology of detrital zircons. Provenance sensitive data of samples from the Upper Palaeozoic Halıcı Formation indicate sediment supply from mainly low- to medium-grade metamorphosed sedimentary rocks of felsic character, while the contribution from volcanic rocks was rare. The detrital zircon record of sediments from the Halıcı Formation documents sediment supply from different sources and excludes a similar provenance. Some samples show great similarities with Palaeozoic sandstones from the cover sequence of the Saharan Metacraton and the Arabian–Nubian Shield, while the other samples indicate a provenance that must be sought in units with a southern Eurasian affinity. The upper limit for sediment deposition in the Halıcı Formation is mostly constrained by Early Palaeozoic zircon populations; however, sediment accumulation in Pennsylvanian–Cisuralian time is more likely, contemporaneously with the Upper Palaeozoic succession on the Karaburun Peninsula (western Turkey). The provenance of sediments from the Upper Triassic Ardıçlı Formation remains enigmatic, but the source should be sought nonetheless in units close to the depositional site. In any case, detrital zircon age spectra and compositional data exclude recycling of underlying rock units (i.e. Halıcı Formation). Overall, our new provenance data reveal great

similarities between the Konya Complex and comparable units (Chios, Karaburun) but also highlight distinct differences in terms of sediment composition and provenance.

Keywords: Palaeotethys; Turkey; Konya Complex; sediment provenance; U–Pb geochronology; whole-rock geochemistry; rutile chemistry

1 Introduction

The Eastern Mediterranean region experienced intense geodynamic reorganization during the Palaeozoic and Mesozoic era due to the opening and closure of the Palaeo- and Neotethyan oceans (e.g. Şengör and Yilmaz 1981; Şengör et al. 1984; Okay and Tüysüz 1999; Stampfli and Borel 2002). As a result, the geology of Turkey was shaped by the accretion of several oceanic and continental fragments (Figure 4.1a).

The study area, located ca. 30 km NW of Konya city in south-central Turkey, is part of the Afyon Zone on the northern margin of the Anatolide–Tauride Block (Figure 4.1a). The Anatolide–Tauride Block is subdivided into an unmetamorphosed Gondwana-derived southern part referred to as Taurides and the northerly Anatolides representing the northern margin of the Palaeotethys in Palaeozoic time. Northward subduction of the Palaeotethys during the Carboniferous led to the formation of magmatic arc/fore-arc complexes and to the amalgamation of both blocks in latest Triassic time when the Palaeotethys (supposedly) finally closed (e.g. Stampfli et al. 2001a,b; Stampfli and Borel 2002; Moix et al. 2008). In an alternative view, the Anatolide–Tauride Block is interpreted as part of the passive northern margin of Gondwana that switched to an active margin with induced back-arc rifting during the Carboniferous (e.g. Göncüoğlu et al. 2007; Robertson and Ustaömer 2009a,b). Some of the models that advocate southward subduction beneath the northern margin of Gondwana do not necessarily exclude northward subduction beneath Eurasia (Robertson and Ustaömer 2009b).

Different palaeotectonic models and implications for the evolution of the Palaeotethys are strongly debated in the literature. In this regard, the investigation of Palaeozoic and Mesozoic ocean-related sedimentary successions is of special importance. Such occurrences are sparse in the Eastern Mediterranean since they are either overlain by younger Mesozoic units or primary structures and information are obscured by meta-

morphism and/or deformation due to Alpine overprint. However, Upper Palaeozoic and Lower Mesozoic Palaeotethys-related successions have been identified on the Aegean island of Chios (Greece), the Karaburun Peninsula (western Turkey) and in our study area, the Konya Complex (name adopted from Robertson and Ustaömer 2009a) in south-central Turkey. Even though these areas have been the subject of several studies, their role within the Palaeotethyan realm is controversial. Provenance data have been published for the islands of Chios and Inousses (Meinhold et al. 2007, 2008a,b; Meinhold and Frei 2008) and recently for the Karaburun Peninsula (Löwen et al. 2017, 2018). This kind of data is crucial for the understanding of the evolution of the Palaeotethys but is not yet available for the Konya Complex.

In our study, we present results from thin-section petrography, whole-rock geochemistry, single-grain geochemistry of detrital rutile and U–Pb dating of detrital zircons from Upper Palaeozoic–Lower Mesozoic sediments from the Konya Complex. The new data provide insight into their age, composition and provenance and contribute to a better understanding of the origin of the sedimentary successions and the closure history of the Palaeotethys.

2 Geological setting

The Konya Complex comprises a complex mixture of Upper Silurian to Upper Cretaceous rocks including a Palaeozoic carbonate platform, an Upper Palaeozoic mélange unit, and Permian–Triassic cover units. Basic palaeontological studies have provided a good biostratigraphic framework (Eren 1993a; Kurt 1994; Göncüoğlu et al. 2000) and other studies addressed the nature of the metasedimentary matrix and embedded blocks of the Palaeozoic mélange (e.g. Eren et al. 2004; Robertson and Ustaömer 2009a, 2011). During the last decades, several geological maps of the area have been presented and alternative tectonostratigraphic schemes using nonuniform nomenclature of formations were discussed in the literature (Figure 4.2). The main dissension centres around the question whether the Konya Complex is largely interpreted as a mélange (Robertson and Ustaömer 2009a), existed as a single overall stratigraphic succession (Özcan et al. 1988, 1990) or is subdivided into a lower autochthon and upper allochthon related to Alpine deformation (Eren 1993a; Eren et al. 2004). For a better understanding, a stratigraphic panel illustrating the various stratigraphic schemes and

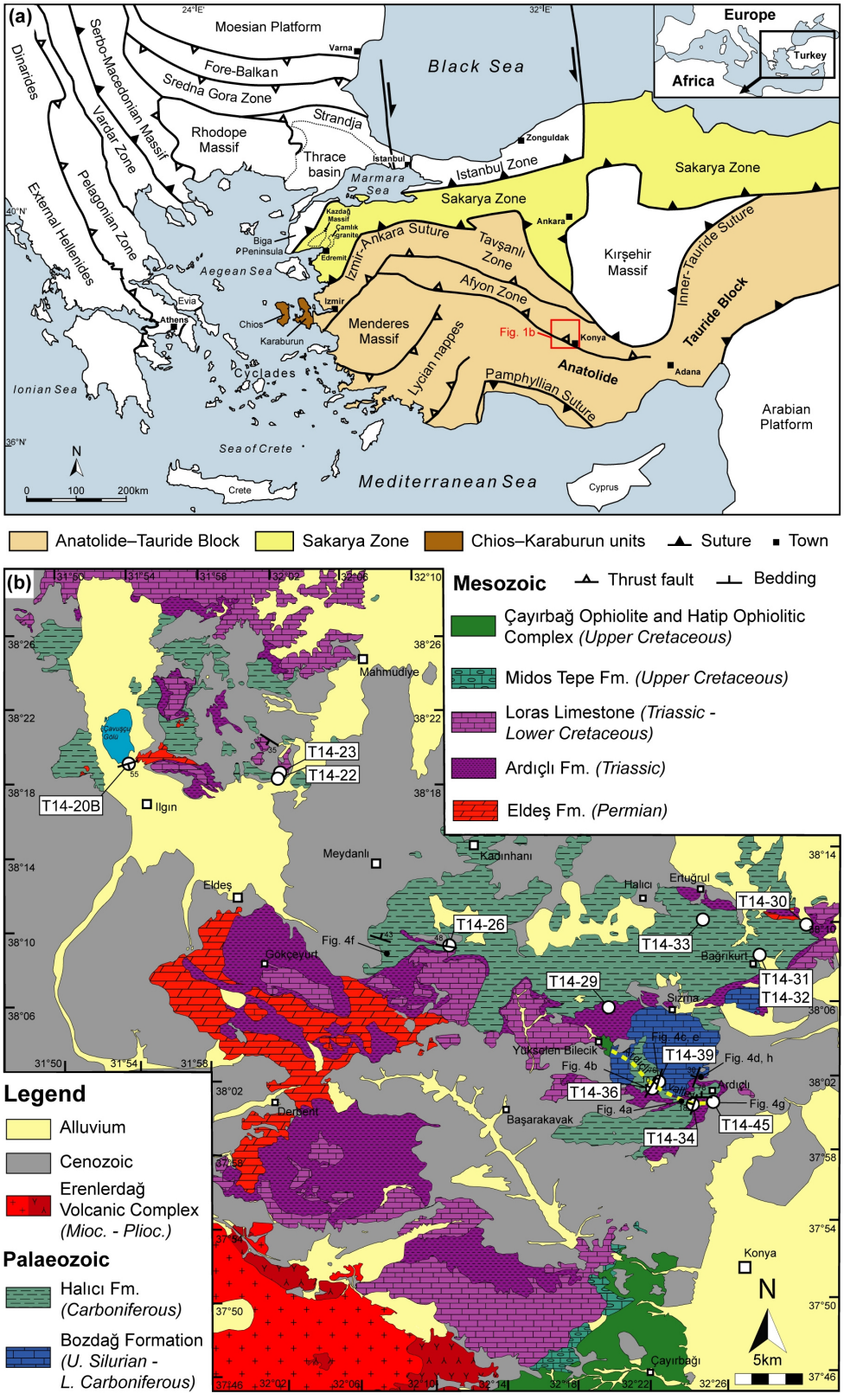

Fig. 4.1: **a** Simplified geotectonic map of the Eastern Mediterranean region (after Jacobshagen 1986; Okay and Tüysüz 1999; Okay et al. 2006). **b** Simplified geological map of the study area NW of Konya (modified after Özcan et al. 1990) with sample locations indicated with the pre-fix T14.

nomenclature used by different authors is provided (Figure 4.2).

The oldest rocks in the study area belong to the Bozdağ Formation that mainly crops out NW of Ardıçlı village. It is interpreted as a massive, reefal carbonate platform containing abundant micro- and macrofossils (e.g. fusulinids, crinoids, corals, and trilobites) of Late Silurian–Early Devonian (Göncüoğlu et al. 2000), Middle–Late Devonian and Early Carboniferous age (Eren 1993a; Kurt 1994). It passes upwards into a mélange unit that comprises a variety of rock types and is widely exposed in the central and NW part of the study area (Figure 4.1b). The mélange is largely equivalent to the Bağrıkurt Formation of the Sızma Group described by Eren et al. (2004) and the Halıcı Formation of Özcan et al. (1988, 1990), respectively. It comprises an (often) strongly folded and foliated metasedimentary matrix made up of alternations of phyllites, mudstones, (turbiditic) sandstones, quartzites, conglomerates, limestones, and black chert with exotic blocks/olistoliths. The main types are carbonates (limestones and dolomites) – mostly derived from the underlying Bozdağ Formation – black chert and minor basic igneous rocks.

Corals and fusulinids from limestone blocks yielded Late Silurian–Devonian and Early Carboniferous ages and blocks of black chert have been dated as Late Silurian–Early Devonian using microfossils and conodonts (Özcan et al. 1990; Eren 1993a; Göncüoğlu and Kozur 1998; Kozur 1999; Eren and Kurt 2000; Göncüoğlu et al. 2000, 2007). The depositional age of the siliciclastic matrix is only poorly constrained. Locally, Early Carboniferous (Visean) fossils from limestones that either represent detached blocks within the matrix or belong to the matrix itself have been reported by Özcan et al. (1990) and Göncüoğlu et al. (2007). Even a Permian age was discussed based on fossils from metacarbonate intercalations indicative of that period (Eren 1996). Furthermore, meta-igneous rocks of basaltic to rhyolitic composition (Özcan et al. 1990) are widely exposed in an area SW of Bağrıkurt village and N to NE of Sızma town (Figure 4.1b) and are referred to as Kadınhanı metamagmatics by Eren et al. (2004). The age of these rocks is only poorly constrained to Early Permian by preliminary radiometric data (Candan et al. 2009), but an Early Triassic age has also been reported for trachyandesitic metavolcanics (Akal et al. 2012). The stratigraphic position and relationship to the adjacent sedimentary rocks have not yet been completely clarified. They were interpreted as dikes and sills crosscutting the Bozdağ Formation and alternatively, as lava flows or blocks within the siliciclastic rocks of the Halıcı Formation

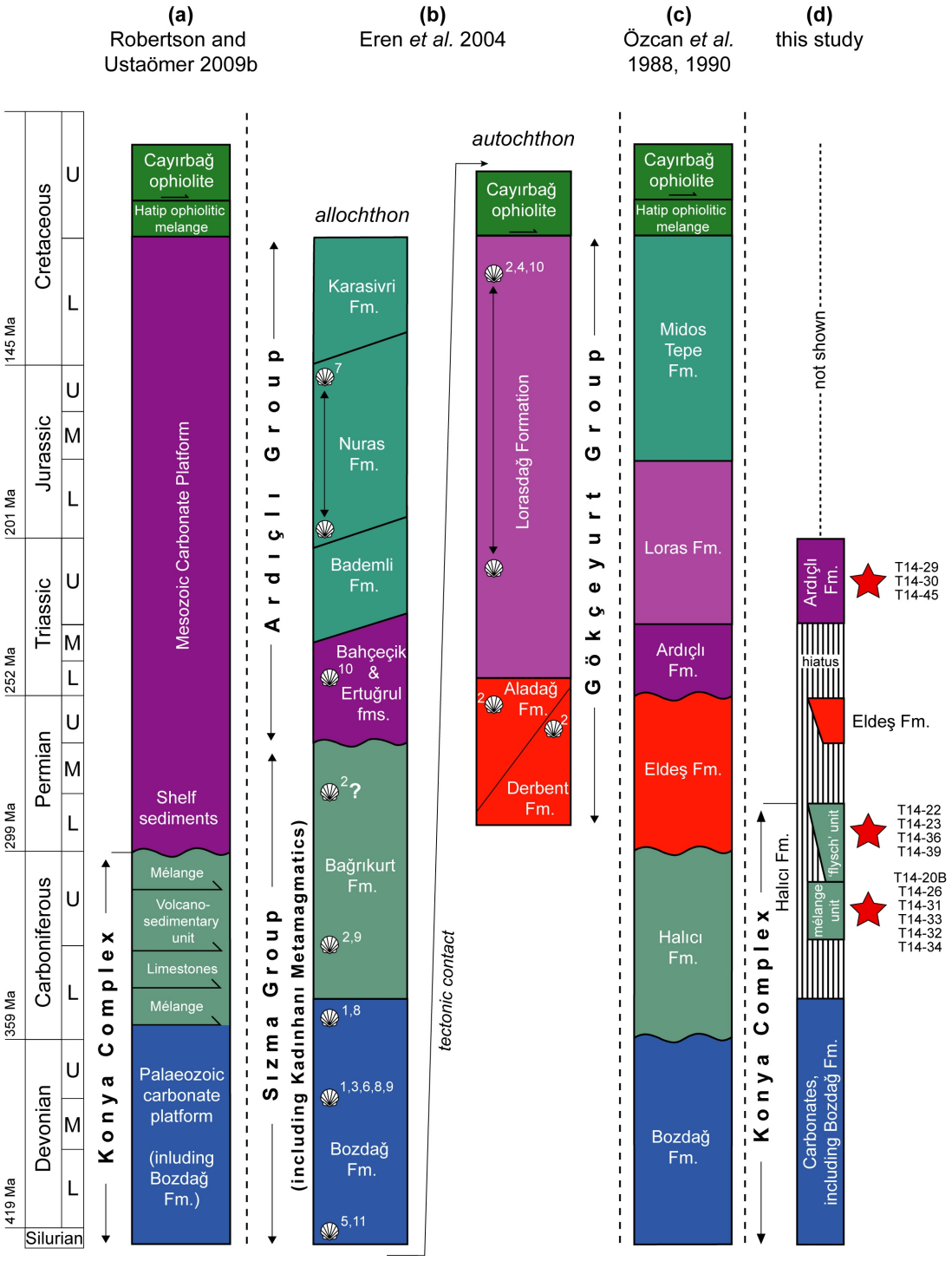

Fig. 4.2: Correlation panel showing different stratigraphic schemes and nomenclatures of the Palaeozoic and Mesozoic units exposed in the Konya area. The colour code labels equivalent formations described by different authors. **a** Informal stratigraphy by Robertson and Ustaömer (2009a) on a local scale where the Eldeş and Ardıçlı formations are not exposed. **b** Tectonostratigraphic subdivision into a lower autochthonous and an upper allochthonous unit (Eren et al. 2004). **c** Continuous stratigraphic succession (Özcan et al. 1988, 1990). **d** Revised stratigraphic column for the Palaeozoic and Lower Mesozoic succession west of Ardıçlı village (this study). The Halıcı Group is subdivided into the mélange and 'flysch' units based on our field observations. Biostratigraphic data from: [1]Eren 1993b, [2]Eren 1993a, [3]Eren 1996, [4]Göğer and Kıral 1969, [5]Göncüoğlu et al. 2000, [6]Göncüoğlu et al. 2007, [7]Karaman 1986, [8]Kurt 1994, [9]Özcan et al. 1988, [10]Özcan et al. 1990, [11]Wiesner 1938.

(Özcan et al. 1990; Eren 2001; Eren et al. 2004). However, contact relations are often obscure and the existence of a separate, mappable volcano-sedimentary unit including the Kadınhanı metamagmatics and siliciclastic sequences was proposed by Robertson and Ustaömer (2009a).

The Halıcı Formation is unconformably overlain by the Eldeş Formation which comprises a thick sedimentary succession and mainly crops out in the western part of the study area, south of Eldeş (Figure 4.1b). It corresponds to the Lower (Derbent Formation) and Middle (Aladağ Formation) unit of the Gökçeyurt Group described by Eren (1993b) and Eren et al. (2004) and was interpreted as (para)autochthonous and structurally lowermost sequence. On the contrary, according to Robertson and Ustaömer (2009a), these sediments unconformably overlay the mélange unit although the original contact was not observed due to the presence of a Cenozoic sedimentary cover. The Eldeş Formation is dominantly composed of alternations of dark grey fossiliferous limestones, marbles, phyllites, and quartzites containing a rich faunal assemblage of Late Permian age (Eren 1993a). Separated by an angular unconformity, these rocks are overlain by a transgressive sequence of violet coloured siliciclastic sediments of the Ardıçlı Formation interfingering with metacarbonates that contain Early Triassic foraminifera and conodonts (Özcan et al. 1988, 1990). It is conformably covered by thick, Upper Triassic–Jurassic limestone and dolomite of the Loras Formation and Jurassic–Cretaceous cherty limestone and mudstone of the Midos Tepe Formation (also known as Midos Formation), which are equivalent to the Upper unit of the Gökçeyurt Group autochthon (Göğer and Kıral 1969; Özcan et al. 1990; Eren 1993a). These carbonates are tectonically overlain by Neotethyan-related magmatic and metamorphic units that are exposed in an area SW of Konya city (Figure 4.1b). They comprise the Hatip ophiolitic mélange including harzburgite blocks (locally with high-grade metamorphic sole rocks) and the Çayırbağ ophiolite of Late Cretaceous age. Recently obtained $^{40}Ar/^{39}Ar$ data from amphibolites of the metamorphic sole yielded ages ranging from 87.04 $\pm$ 0.36 to 84.66 $\pm$ 0.30 Ma and were interpreted to date the timing of metamorphism (Daşçı et al. 2015). Overall, the autochthonous and allochthonous rocks in the study area were overprinted by multi-phase Alpine deformation (e.g. Eren 2001; Eren et al. 2004; Robertson and Ustaömer 2009a).

3 Methods

Thirteen sandstone samples were collected from outcrops NW of Konya town, ten from the Upper Palaeozoic Halıcı Formation and three from the Lower Mesozoic Ardıçlı Formation and were prepared for petrographic, bulk-rock geochemical and single-grain chemical (rutile) and geochronological (zircon) analyses (Table 4.1). These formations were targeted as they show great similarities in terms of lithology and age with comparable successions on Chios Island and the Karaburun Peninsula further to the west (Figure 4.1b). The Chios–Karaburun units have recently been studied in detail and provenance data have become available.

Samples were processed at the Geoscience Center of Göttingen University and disintegrated by standard routines (jaw crusher, disc mill) in a first step. Part of the material was cut off for bulk-rock geochemical analysis and grinded to $<$63 µm using an agate ball mill. The remaining material was separated to different grains-size fractions by wet-sieving in a mechanical shaker. Prior to heavy mineral extraction from the 63–250 µm fraction the material was decarbonated with acetic acid (5%). Gravitational separation was done in separation funnels using sodium polytungstate ($Na_6[H_2W_{12}O_{40}]$, r = 2.85 g/cm^3). Unless stated otherwise, all analyses were carried out at the Geoscience Center Göttingen (Department of Sedimentology and Environmental Geology and Department of Geochemistry).

Thin sections were prepared from all samples and were analysed using a petrographic microscope. Mineralogical composition was determined by point counting of at least 300 grains of mono- and polycrystalline quartz (Q_m, Q_p), plagioclase feldspar (P), alkali feldspar (Kfs) and lithic fragments (L_v, L_s) following the Gazzi-Dickinson method. Matrix and cement were not counted but estimated using standard comparison charts for visual estimation.

Whole-rock geochemical major and trace element analyses were conducted using a PANalytical AXIOS Advanced sequential X-ray spectrometer. Fused glass discs were produced by adding Spectromelt® and LiF to the sample powder and melting in platinum crucibles. Loss on ignition (LOI) was determined gravimetrically by stepwise heating to 1000°C.

Solution inductively coupled plasma mass spectrometry (ICP–MS) was applied for rare element geochemistry. Sample powder ($\sim$100 mg per sample) was dissolved by

Table 4.1: Geographic location of samples and summary of applied analyses.

Sample information		Geographic position			Applied methods				
Sample ID	**Lithology**	**Location**	**Latitude**	**Longitude**	**QFL**	**XRF**	**ICP-MS**	**EMPA**	**U–Pb**
Halıcı Formation - mélange unit									
T14-20B	Subarkose	SE end of lake Çavuşçu	38° 19' 30.53"	31° 53' 36.38"	X	X	X	X	X
T14-26	Lithic wacke	3 km S of Söğütözü village	38° 09' 06.06"	32° 10' 58.63"	X	X	X		
T14-31	Subarkose	1 km N of Bağrıkurt	38° 08' 26.63"	32° 28' 43.91"	X	X	X	X	X
T14-32	Arkosic wacke	1 km N of Bağrıkurt	38° 08' 34.84"	32° 28' 43.96"	X	X	X		
T14-33	Lithic wacke	3 km S of Ertuğrul	38° 10' 15.48"	32° 25' 37.41"	X	X			
T14-34	Lithic wacke	Ardıçlı valley (block in mélange)	38° 00' 42.85"	32° 24' 55.30"	X	X	X		X
Halıcı Formation - 'flysch' unit									
T14-22	Subarkose	3 km SW of Karaköy village	38° 18' 27.36"	32° 02' 21.72"	X	X	X	X	X
T14-23 (not in-place)	Quartz arenite	3 km SW of Karaköy village	38° 18' 19.72"	32° 02' 16.83"	X	X	X		
T14-36	Arkosic wacke	Ardıçlı valley	38° 01' 19.02"	32° 22' 35.25"	X	X	X	X	X
T14-39	Lithic/Arkosic wacke	Ardıçlı valley	38° 01' 32.09"	32° 23' 03.45"	X	X	X	X	X
Ardıçlı Formation									
T14-29	Sublitharenite	W of Sızma	38° 05' 42.71"	32° 20' 29.69"	X	X	X	X	X
T14-30	Conglomerate	NE of Bağrıkurt	38° 09' 50.55"	32° 31' 13.21"	X	X	X		X
T14-45	Sublitharenite	S of Ardıçlı	38° 00' 28.49"	32° 25' 47.50"	X	X	X		

PicoTrace® acid digestion system. Analytical procedures were started by overnight pre-reaction with 2 ml HNO_3 at 50℃. The first pressure phase (heating to 150℃ for 8 h) including treatment with 3 ml HF and 3 ml $HClO_4$ was launched after cooling to room temperature. For evaporation the digestion vessels were heated to 180℃ for 16 h. After cooling 10 ml H_2O (double de-ionised), 2 ml HNO_3 and 0.5 ml HCl were added to the samples for the final pressure phase and the solution was re-heated to 150 ℃ for 4 h. Samples were transferred into 100 ml volumetric flasks after final cooling and an internal standard (200 µl) was added to the solution. Trace element analysis was performed on a ThermoElectron VG PlasmaQuad 2 quadrupole ICP–MS. All analytical data for main and trace element geochemistry are available as Supplementary data (Table C.1)

Zircon and rutile grains for mineral chemical and geochronological analyses were randomly selected by handpicking from the 63–250 µm fraction. Mineral grains were mounted in epoxy discs composed of Araldite® and hardener (mixed 5:1) and polished to expose the grain interior. Prior to U–Pb zircon dating, cathodoluminescence (CL) imaging was applied to reveal internal structures and to guide spot placement. The age determination was carried out on a sector-field ICP–MS (Element2, ThermoFisher) coupled to a 193-nm Analyte G2 Excimer Laser Ablation System at the Institute of Mineralogy of the University Münster. For U–Pb analysis, the laser spot size was set to 35 µm and isotope data were acquired on masses 202, 204, 206, 207 and 238. Isotope ^{202}Hg was used to quantify the isobaric interference of ^{204}Hg on ^{204}Pb. Common Pb correction was exclusively applied to an analysis when the contribution of common ^{206}Pb to total ^{206}Pb exceeded 1%. Mass discrimination and elemental fractionation during laser ablation were corrected by bracketing 10 unknown samples by three measurements of the GJ-1 reference zircon (Jackson et al. 2004). Precision and reproducibility of U–Pb ages was monitored by multiple measurements of the 91500 reference zircon (^{206}Pb/^{238}U = 1062.4 $\pm$ 0.8 Ma; ^{207}Pb/^{206}Pb = 1065.4 $\pm$ 0.6 Ma; Wiedenbeck et al. 1995). Measured isotopic ratios matched the published values of Wiedenbeck et al. (1995) within error.

Data reduction was done following the procedure described by Kooijman et al. (2012) and data were filtered based on two criteria: accepted were all zircons ages (a) within 90–110% concordance [100 $\times$ (^{206}Pb/^{238}U /^{207}Pb/^{206}Pb)] for grains older than 1200 Ma and (b) grains showing a difference of the U–Pb ages in the range of 10% for ages

younger than 1200 Ma (see also Allen and Barnes 2006 and Spencer et al. 2014). Following this procedure we want to account for the low precision of $^{207}Pb/^{206}Pb$ values for younger (<1200 Ma) zircons. For the interpretation of zircons we quoted the $^{206}Pb/^{238}U$ ages for grains younger than 1200 Ma and used $^{207}Pb/^{206}Pb$ ages of grains older than 1200 Ma (Gehrels et al. 2008). Concordia plots (Figure 4.10) were compiled with Isoplot version 3.75 (Ludwig 2003) and histograms (Figure 4.11) were produced using the DensityPlotter (v. 7.3) software by Vermeesch (2012). The analytical data are given as Supplementary material (see Table C.2). The geological time scale GTS of Gradstein et al. (2012) was used as a stratigraphic reference for data interpretation.

Prior to geochemical analysis of rutile the polished grain mounts were carbon-coated to ensure conductivity. Measurements were carried out with a JEOL JXA 8900 RL electron microprobe analyzer (EMPA) equipped with five wavelength dispersive spectrometers. The analytical data, measurement parameters and spectrometer configurations are available as Supplementary Material (see Tables C.3 and C.4).

4 Results

Here we present a compilation of new petrographic (Figure 4.4), radiometric and geochemical data from sedimentary sequences of the Konya area. Emphasis was placed on the Upper Palaeozoic Halıcı Formation that is widely exposed in the central and eastern part of the study area (Figure 4.1b) and the Lower Triassic Ardıçlı Formation from the Mesozoic cover sequence.

4.1 Field Observations

We divide the Halıcı Formation into two subunits based on our field observations. Part of the formation is characterized by alternations of low-grade phyllitic rocks (Figure 4.3a) with intercalations of limestones, fine- to medium-grained sandstones, conglomerates and cherts, and includes isolated blocks/olistoliths of different lithologies (e.g. cherts, limestones, igneous rocks). In the following, we are referring to it as a mélange unit, which represents the actual mélange as described above. Although we consider the mélange unit as a single and differentiable complex, we recognize that it could be made up of several subunits. The phyllitic rocks of the mélange unit often contain large Fe-oxide pseudomorphs after pyrite, indicative of anoxic, probably deep-water condi-

tions. Additionally, we are introducing the term ‘flysch‘ unit to describe a low-grade metamorphosed part of the Halıcı Formation that is free of any blocks/olistoliths and was deposited on top of the mélange unit. It mainly comprises mudstones, siltstones, well-bedded sandstones (Figure 4.3b, c), locally also containing plant fossils and Fe-oxide pseudomorphs. We prefer using inverted commas for the term ‘flysch‘ as we use it as a descriptive lithofacies term, following Sestini (1970)and Mitchell and Reading (1986).

Even though the Konya Complex has been studied for decades, its internal tectonostratigraphy is not yet fully understood since the study area experienced Alpine deformation and large-scale folding and contacts are often covered by younger sediments. In this respect, the valley extending over a distance of ca. 10 km from the villages of Ardıçlı to Yükselen Bilecik (in NW direction) has turned out to be one of the key areas for illustrating its complex internal structure (Figure 4.1b). Close to Ardıçlı, a thick succession of Palaeozoic sediments and the Mesozoic cover sequence are well exposed on the slopes of the valley over several tens to hundreds of meters. From bottom to top the sequence starts with limestone of the Bozdağ Formation (Figure 4.2d). This limestone is in parts conglomeratic and contains pebbles and slightly deformed corals (Figure 4.3d). The Bozdağ Formation is unconformably overlain by the mélange unit, but in some areas, the mélange unit is likely missing and the ‘flysch‘ unit is unconformably above the Bozdağ Formation (Figure 4.2d). The supposed unconformable contact between the ‘flysch‘ unit and Bozdağ limestone is exposed in an old quarry, located ca. 4 km to the west of Ardıçlı. At this place, the massive limestones are conformably covered by sedimentary rocks of the ‘flysch‘ unit (Figure 4.3e). These include conglomerates with phyllitic pebbles, probably from a reworked material of the mélange unit, which is situated in deeper levels. The contact between these rocks and the Bozdağ limestone can be observed elsewhere in the study area and is (probably) of tectonic nature. In these cases, the sediments are intensely folded and deformed close to the contact with the Bozdağ Formation (Figure 4.3f). From the Permian–Triassic cover units, the Eldeş Formation of Eren (1993a) is not present in the study area around Ardıçlı. However, the Triassic Ardıçlı Formation is present and consists of a characteristic purple-coloured siliciclastic material with carbonate intercalations (Figure 4.3g). The succession ends with a thick sequence of massive, well-bedded Mesozoic limestones of the Loras Formation at the top (Figure 4.3h).

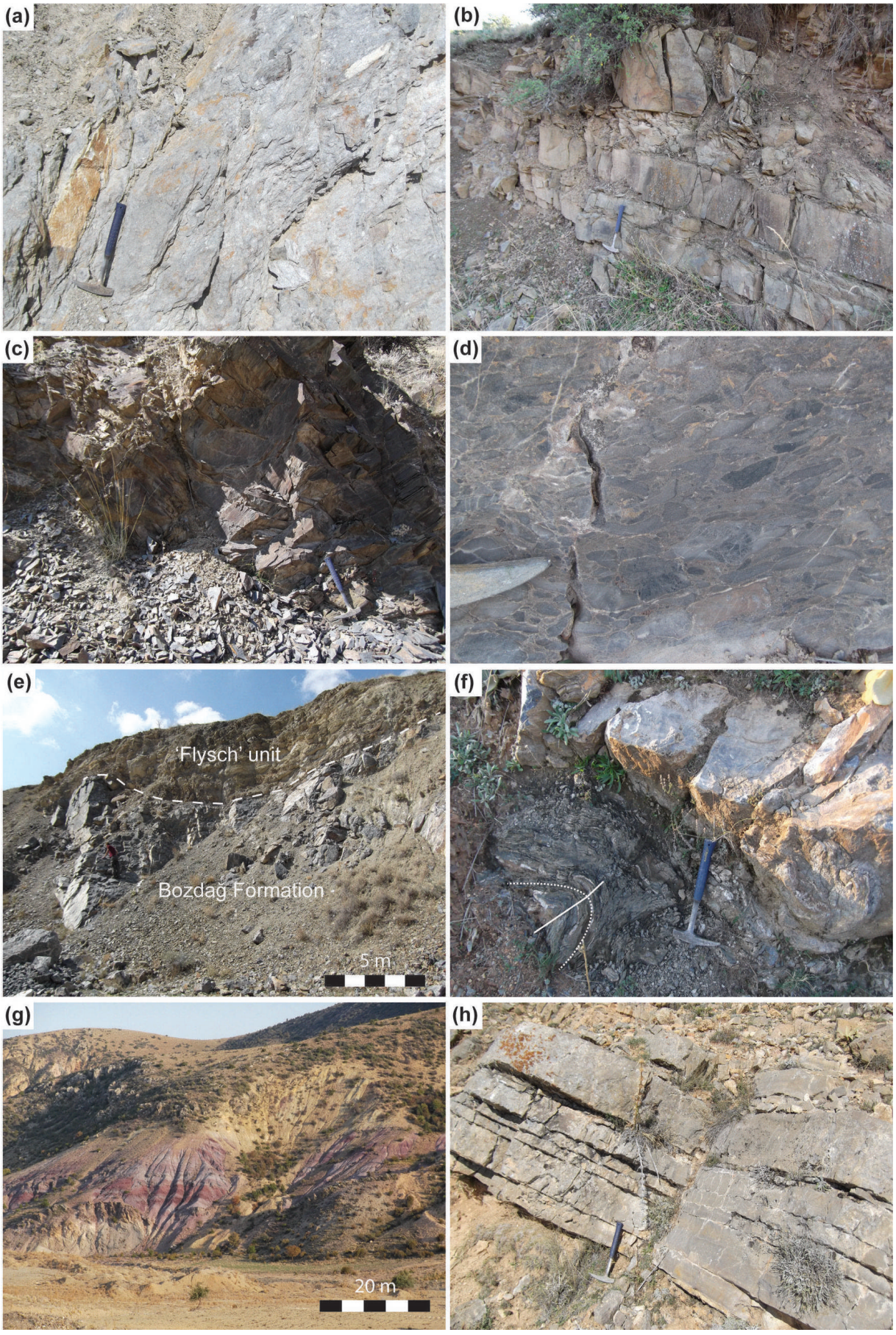
(a)
(b)
(c)
(d)
(e)
'Flysch' unit
Bozdag Formation
5 m
(f)
(g)
20 m
(h)

Fig. 4.3: Field photographs from the Konya area. **a** Low-grade metamorphosed, fine-grained sediments of the mélange unit. **b** Well-bedded sandstones of the 'flysch' unit (at the location of sample T14-36). **c** Mudrock, locally with silt laminae from the 'flysch' unit. **d** Brecciated limestone of the Bozdağ Formation (west of Ardıçlı). **e** Outcrop showing massive limestones of the Bozdağ Formation, depositionally overlain by sedimentary rocks of the 'flysch' unit (Ardıçlı valley). **f** Refolded fold in sediments of the mélange unit at the contact with a limestone block of the Bozdağ Formation(south of Meydanlı). Dotted and solid white lines show relatively older and younger traces of axial surfaces. **g** View to the Southeast (Southeast of Ardıçlı Dam), the characteristic purple-coloured sediments of the Triassic Ardıçlı Formation. **h** Massive, well-bedded Mesozoic limestone (partly dolomitic) (west of Ardıçlı). Hammer for scale in a–c, f, and h is about 30 cm long.

4.2 Sediment petrography

Important parameters that were considered during petrographic analysis to describe sediment properties are given in Table S2. These include results from point counting for QFL classification, observed accessory minerals and textural information (grain-size, sorting, roundness). For classification of sandstones, we used the scheme proposed by Dott (1964) to account for variable proportions of matrix material in our samples.

The analysis has shown that samples from the Halıcı Formation have high percentages of quartz (average 87%) and only contain low amounts of feldspars ($\leq$14%) and lithic fragments ($\leq$12%) (Figure 4.4). Rocks from the mélange unit are classified as subarkoses (Figure 4.5a, 4.6a, d) and lithic/arkosic wackes (Figure 4.5a–d, 4.6b, c, e) with a low textural maturity and highly variable matrix contents of 5–50%. Some samples show evidence for strong chemical alteration (Figure 4.5a) and also foliation and shearing (Figure 4.6b, d). The above-mentioned sandstones represent the sedimentary matrix, the exception being a lithic wacke (T14-34) (Figure 4.5c, 4.6e) that was identified as a larger block/ olistolith (several meters) embedded in the siliciclastic rocks. Samples from the 'flysch' unit comprise one pair of subarkose and quartzarenite rocks and one pair of more immature lithic/arkosic wackes (Figure 4.4, Table S2). The former are highly mature (Q: 91–98%) and contain a very low amount of matrix material ($<$5%), negligible amounts of lithic fragments and rare feldspars (Figure 4.5b). In contrast, the latter are characterized by higher amounts of feldspars (8–14%) and lithic fragments (6–12%) in a fine-grained matrix (Figure 4.5e, 4.6f, g). The most common accessory phases in these samples are tourmaline, rutile, zircon, titanite and Fe-oxides. The majority of lithic fragments ($>$90%) was derived from (meta)sediments (quartzites, mica-schists, and rare chert), whereas volcanic fragments are rare and were primarily observed in wackes of the 'flysch' unit (Figure 4.6a–g). Observed petrographic features

Table 4.2: Mineralogical composition and point counting results of sediments from the study area.

Sample ID	Lithology	Q_m		Q_p		C		P		Kfs		L_v		L_s		Total	Matrix	Accessory minerals	Grain size	Sorting	Roundness
		#	%	#	%	#	%	#	%	#	%	#	%	#	%						
Halıcı Formation - mélange unit																					
T14-20B	Subarkose	160	50	121	38	0	0	31	10	7	2	0	0	2	1	321	<5	Amp, Chl, Tur, Zrn, Rt, Ttn	vfS	poor	angular
T14-26	Lithic wacke	179	59	77	26	5	2	0	0	5	2	0	0	35	12	301	20	Chl, Cld, Zrn, Ttn	cS	poor	subangular- subrounded
T14-31	Subarkose	225	75	35	12	0	0	22	7	2	1	2	1	16	5	302	5	Chl, Tour, Rt, Ttn, Zrn	mS	moderate	subrounded
T14-32	Arkosic wacke	180	59	90	30	0	0	11	4	7	2	0	0	15	5	303	30	Chl, Rt, Ttn, Zrn	cS	very poor	angular
T14-33	Lithic wacke	68	22	171	55	0	0	5	2	0	0	5	2	60	19	309	50	Rt, Zrn	cS	very poor	subangular-subrounded
T14-34	Lithic wacke	195	57	103	30	1	0	12	3	6	2	6	2	20	6	343	50	Chl, Ep, Zrn	cS	very poor	subangular
Halıcı Formation - 'flysch' unit																					
T14-22	Subarkose	208	65	83	26	0	0	12	4	5	2	0	0	12	4	320	<5	Bt, Tur, Zrn, Rt, Ttn	fS	moderate	subrounded
T14-23	Quartz arenite	292	85	46	13	0	0	0	0	0	0	0	0	4	1	342	0	Bt, Tur, Zrn,Rt	mS	moderate	subangular
T14-36	Arkosic wacke	206	64	32	10	0	0	35	11	9	3	14	4	25	8	321	15	Chl, Zrn, Ms, Rt, Tur	mS	poor	subangular- subrounded
T14-39	Lithic/arkosic wacke	173	57	85	28	4	1	5	2	19	6	0	0	19	6	305	40	Ms, Tur, Zrn, Rt	mS	moderate	subrounded
Ardıçlı Formation																					
T14-29	Sublitharenite	134	42	140	44	0	0	2	1	0	0	3	1	42	13	321	10	Amph, Chl, Rt, Ttn, Tur, Zrn	cS	very poor	angular
T14-30	Conglomerate	-	-	-	-	-	-	-	-	-	-	-	-	-	-	-	-	Chl, Musc, Ttn, Zrn	cS	very poor	
T14-45	Sublitharenite	20	6	82	25	206	62	0	0	0	0	0	0	22	7	330	<5	Musc, Rt, Zrn	cS	poor	subrounded

Abbreviations: vfS = very fine sand; fS = fine sand; mS = medium sand; cS = coarse sand; Qm = monocrystalline quartz (in %); Qp = polycrystalline quartz (in %); P = plagioclase (in %);
C = chert (in %); Kfs = K-feldspar (in %); Lv = volcanic lithic fragments (in %); Ls = (meta)sedimentary lithic fragments (in %); Bt = biotite; Ms = muscovite; Chl = chlorite;
Cld = chloritoid; Ep = epidote; Tur = tourmaline; Zrn = zircon; Amp = amphibole; Rt = rutile; Ttn = titanite

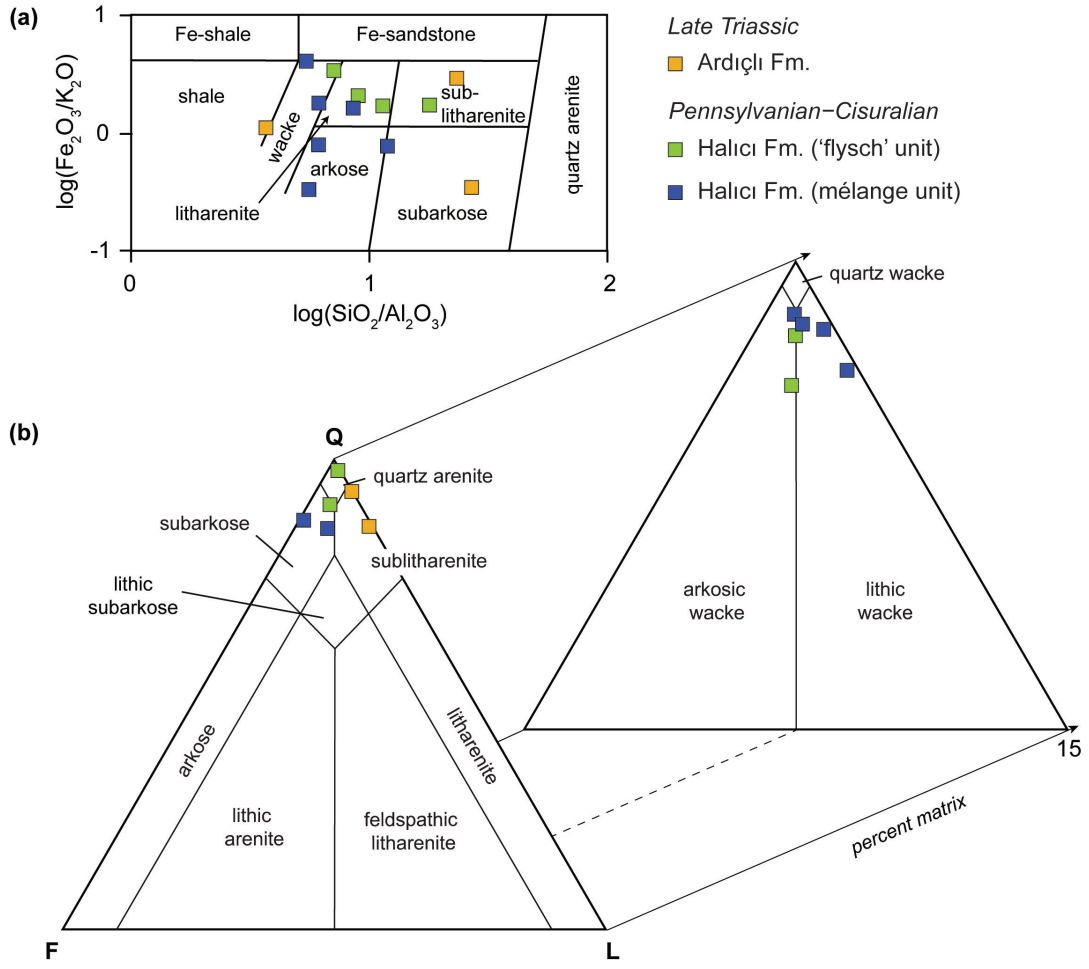

Fig. 4.4: **a** Chemical classification scheme for siliciclastic sediments (after Herron 1988). **b** QFL diagram for lithological classification of sandstones (after Dott 1964). Sample T14-30 (conglomerate) is not shown.

of these sandstones are in good agreement with previous descriptions of the Halıcı Formation (e.g. Kurt 1997; Robertson and Ustaömer 2011).

Studied sediments from the Ardıçlı Formation are of different composition and texture (Figure 4.5f–h). One quartzitic litharenite (T14-29) is characterized by a fine-grained quartzitic matrix with poorly sorted, large (up to 1400 µm) grains of mono- and polycrystalline quartz and rare sedimentary fragments (Figure 4.5g). Textural features are shear bands that are associated with muscovite and abundant fine particles of Fe-oxides. In contrast, sample T14-30 is a metaconglomerate composed of a mica-dominated matrix with deformed large (up to 1.4 cm) sedimentary and volcanic fragments (chert, quartzite, schists, felsic plutonic rocks) (Figure 4.5f, 4.6h).

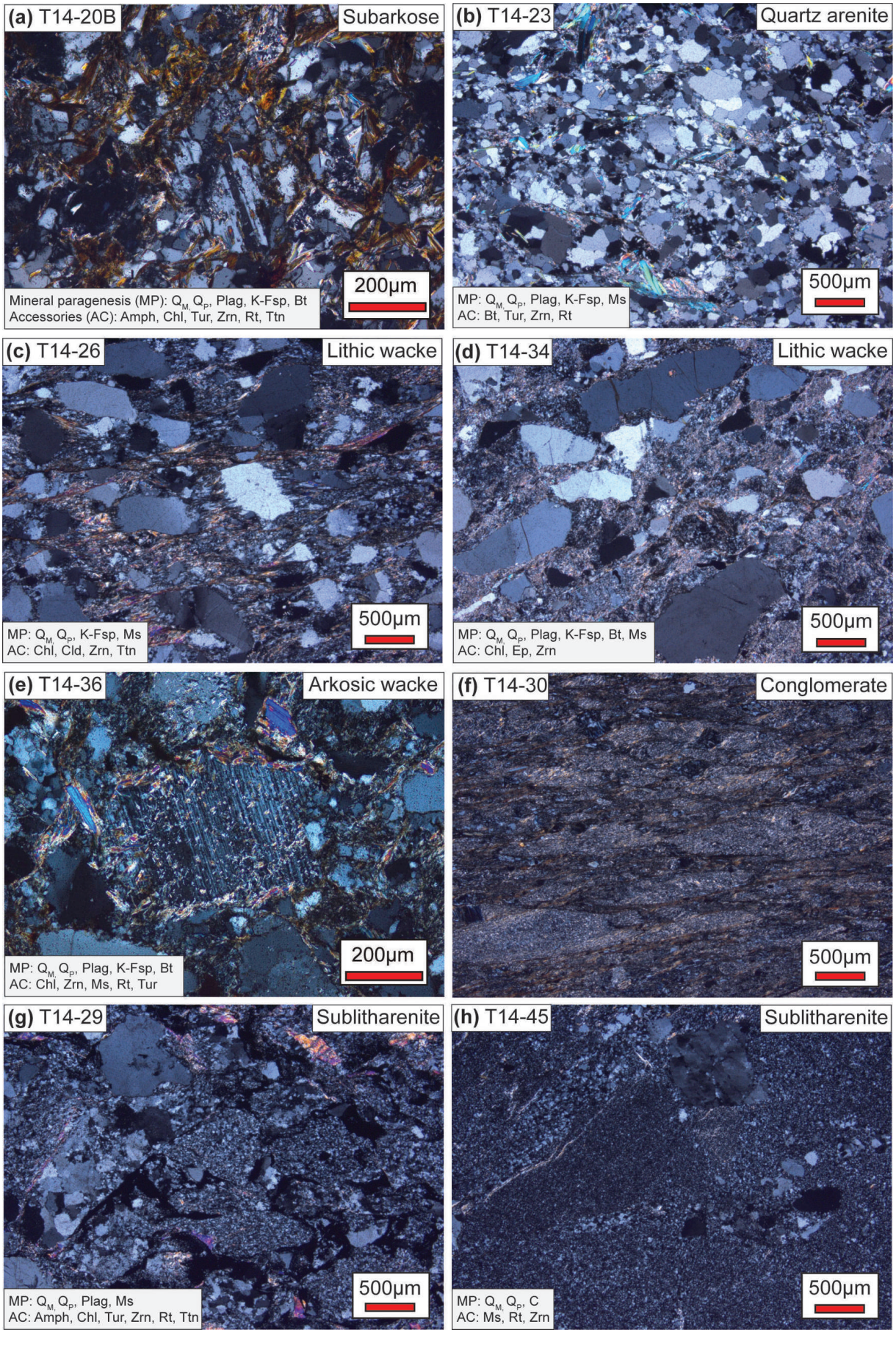
(a) T14-20B
Subarkose
Mineral paragenesis (MP): Q_M, Q_P, Plag, K-Fsp, Bt
Accessories (AC): Amph, Chl, Tur, Zrn, Rt, Ttn
200µm
(b) T14-23
Quartz arenite
MP: Q_M, Q_P, Plag, K-Fsp, Ms
AC: Bt, Tur, Zrn, Rt
500µm
(c) T14-26
Lithic wacke
MP: Q_M, Q_P, K-Fsp, Ms
AC: Chl, Cld, Zrn, Ttn
500µm
(d) T14-34
Lithic wacke
MP: Q_M, Q_P, Plag, K-Fsp, Bt, Ms
AC: Chl, Ep, Zrn
500µm
(e) T14-36
Arkosic wacke
MP: Q_M, Q_P, Plag, K-Fsp, Bt
AC: Chl, Zrn, Ms, Rt, Tur
200µm
(f) T14-30
Conglomerate
500µm
(g) T14-29
Sublitharenite
MP: Q_M, Q_P, Plag, Ms
AC: Amph, Chl, Tur, Zrn, Rt, Ttn
500µm
(h) T14-45
Sublitharenite
MP: Q_M, Q_P, C
AC: Ms, Rt, Zrn
500µm

Fig. 4.5: Photomicrographs (cross-polarized light) of sediments from the Halıcı and Ardıçlı formations. **a** Strongly altered subarkose (mélange unit). **b** Mature quartz arenite ('flysch' unit). **c** Low-grade metamorphosed lithic wacke with mica beards (mélange unit). **d** Poorly sorted lithic wacke (block within mélange unit). **e** Initial sericitization of plagioclase ('flysch' unit). **f** Metaconglomerate with deformed sedimentary fragments (Ardıçlı Formation). **g, h** Sandstone samples from the Ardıçlı Formation.

4.3 Whole-rock geochemistry

Major and trace element compositions of samples from the Konya Complex are shown in Figure 4.7, 4.8, 4.9. Siliciclastic rocks from the mélange unit of the Halıcı Formation have moderate to high SiO_2 (70–88 wt.%) and moderate Al_2O_3 (7–14 wt.%) concentrations and low Na_2O (0.4–3.2 wt.%) contents. The concentration of K_2O is generally low (1.4–2.8 wt.%), but the highest measured concentration is at almost 5%, caused by high amounts of phyllosilicates as indicated by high Rb contents. Sandstones from the 'flysch' unit are characterized by on average slightly higher SiO_2 (76–90 wt.%) but lower Al_2O_3 (5–11 wt.%), K_2O ($<$2 wt.%) and Na_2O ($<$2 wt.%) concentrations. Two samples from the Ardıçlı Formation are very similar in their major element composition with high SiO_2 (90–95 wt.%) and very low K_2O ($\leq$1.1 wt.%) concentrations and a lack of Na_2O. In contrast, the conglomeratic sample (T14-30) from this formation has highest Al_2O_3 (16.5%) and K_2O (4.4%) and Rb (192 ppm) due to the dominance of mica in its fine-grained matrix.

Selected trace elements for samples of the Konya area and data of Upper Palaeozoic and Triassic sandstones from the Karaburun Peninsula in western Turkey (Löwen et al. 2018) have been normalized to the upper continental crust (UCC) and are shown in multi-element diagrams (Figure 4.8a–c). Most trace elements are slight to moderately depleted compared to UCC for all but one sample from the Ardıçlı Formation (T14-30) and exhibit pronounced negative anomalies for Sr, Y, Cr, and Ni. Heaviest depletion in both, trace elements and rare earth elements (REE) is revealed by a highly mature quartz arenite (T14-23) from the 'flysch' unit due to dilution effects from high quartz contents. Chondrite-normalized REE patterns of the studied sediments and UCC and Post-Archaean Australian Average Shale (PAAS) reference values are shown in Figure 4.8d–f. In general, the REE geochemistry of most samples is characterized by lower total REE concentrations compared to UCC and PAAS, a (heavy) fractionation between light rare earth elements (LREE) and heavy rare earth elements (HREE) and a slightly negative Eu anomaly (calculated from $Eu/Eu^* = Eu_N/(Sm_N \times Gd_N)^{0.5}$ = 0.47–0.87),

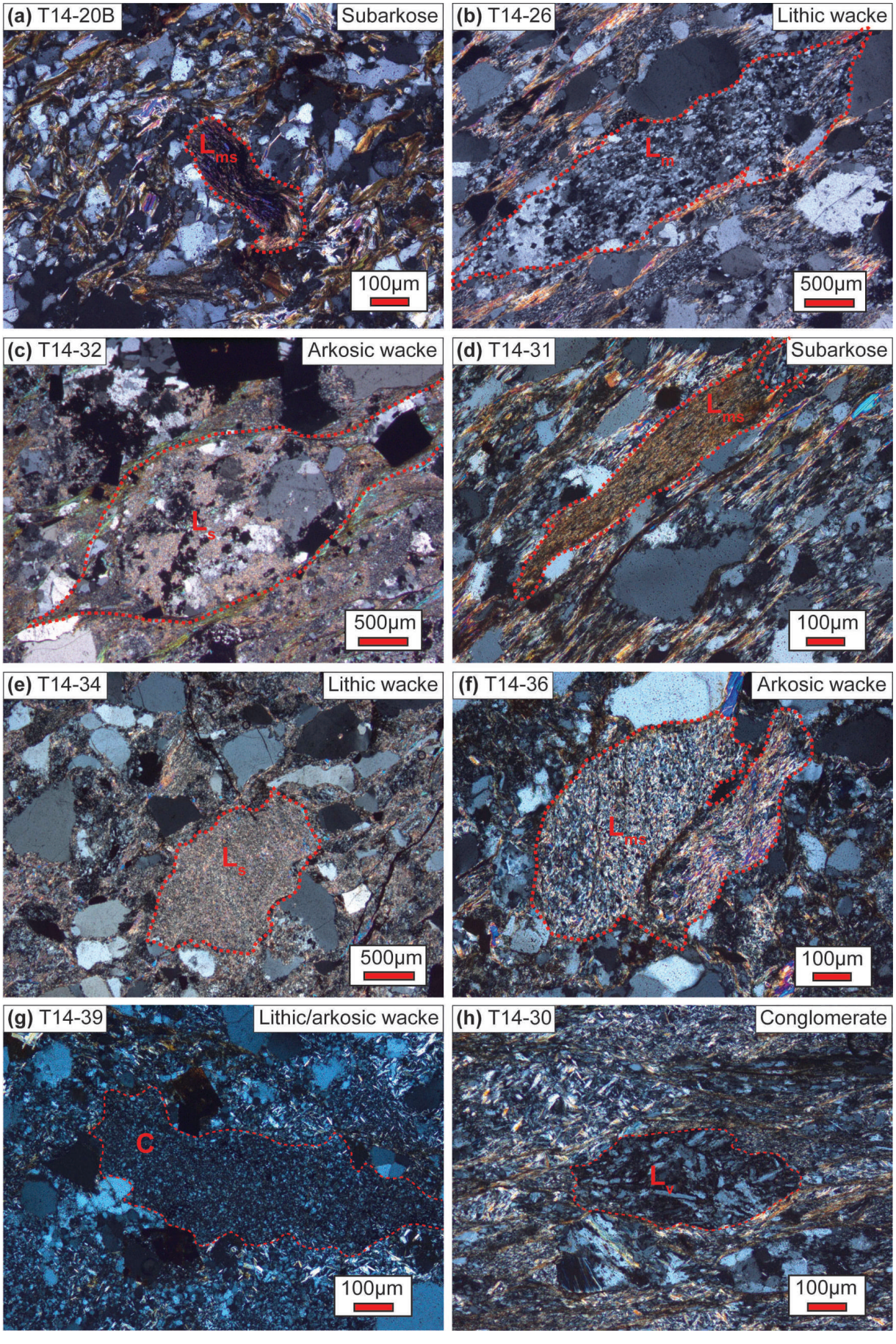
(a) T14-20B
Subarkose
L_{ms}
100µm
(b) T14-26
Lithic wacke
L_m
500µm
(c) T14-32
Arkosic wacke
L_s
500µm
(d) T14-31
Subarkose
L_{ms}
100µm
(e) T14-34
Lithic wacke
L_s
500µm
(f) T14-36
Arkosic wacke
L_{ms}
100µm
(g) T14-39
Lithic/arkosic wacke
C
100µm
(h) T14-30
Conglomerate
L_v
100µm

Fig. 4.6: Photomicrographs (cross-polarized light) showing the main types of lithic fragments in sediments from the study area. **a** Low-grade metasedimentary fragment (Lms: mica schist) in the mélange unit. **b** Large elongate (c. 4 mm) quartzitic fragment in the mélange unit. **c** Strongly altered sedimentary fragment (Ls) in the mélange unit). **d** Low-grade metasedimentary (Lms: mica-schist) fragment in the mélange unit. **e** Fine-grained sedimentary fragment in a block of the mélange unit. **f** Low-grade metasedimentary fragments (mica-schists) in the 'flysch' unit. **g** Chert fragment ('flysch' unit). **h** Volcanic fragment with plagioclase laths and needles in the Ardıçlı Formation. Abbreviations: L_s = sedimentary lithoslcast; L_{ms} = metasedimentary lithoclast; L_m = metamorphic lithoclast; L_v = volcanic lithoclast.

with the exception of sample T14-34 ($Eu/Eu^* = 1.07$). The average total amount of REE concentrations is lower in the 'flysch' unit ($\sum$ REE = 80.77 ppm) compared to the mélange unit ($\sum$ REE = 124.61 ppm). Highest total REE concentrations ($\sum$ REE = 373.61 ppm) and very strong fractionation of LREE and HREE ($La_N/Yb_N = 39.97$) can be observed in the Ardıçlı Formation (T14-30). The degree of fractionation is highly variable in the mélange unit ($La_N/Yb_N = 5.74–30.24$) and is lower in the 'flysch' unit ($La_N/Yb_N = 4.84–10.18$).

The different behaviour (e.g. mobility, compatibility) of specific trace elements in sediments allows using their concentrations and/or elemental ratios as proxies to identify input from either felsic or (ultra)mafic sources. In a compilation of discrimination diagrams utilizing these characteristics, the signature of our samples suggests the supply of detritus from predominantly felsic source rocks (Figure 4.9). However, one sample from the Ardıçlı Formation (T14-30) is characterized by high Ni and Cr concentrations as well as high Cr/V (2.65) and low Y/Ni (0.15) ratios, which is indicative for the presence of (ultra)mafic components. In contrast, rocks from the 'flysch' unit have generally low concentrations of Cr (13–170 ppm) and Ni (6–37 ppm) that are even lower in samples from the mélange unit (4–58 and 1–34 ppm, respectively) (Figure 4.9b). Slight indication for (ultra)mafic detritus in these samples is given by relatively high Cr, Cr/V, and Cr/Th values in combination with low Y/Ni and Th/ Sc ratios as observed in an arkosic wacke from the 'flysch' unit (T14-36) (Figure 4.9b–d).

4.4 Detrital zircon geochronology

4.4.1 Halıcı Formation – mélange unit

Detrital zircons from sample T14-20B are of comparatively small size (<100 µm) and have a pinkish colour. The grains are generally well rounded and often show oscillatory zoning patterns. U–Pb ages were obtained from 99 grains of which 73 were accepted

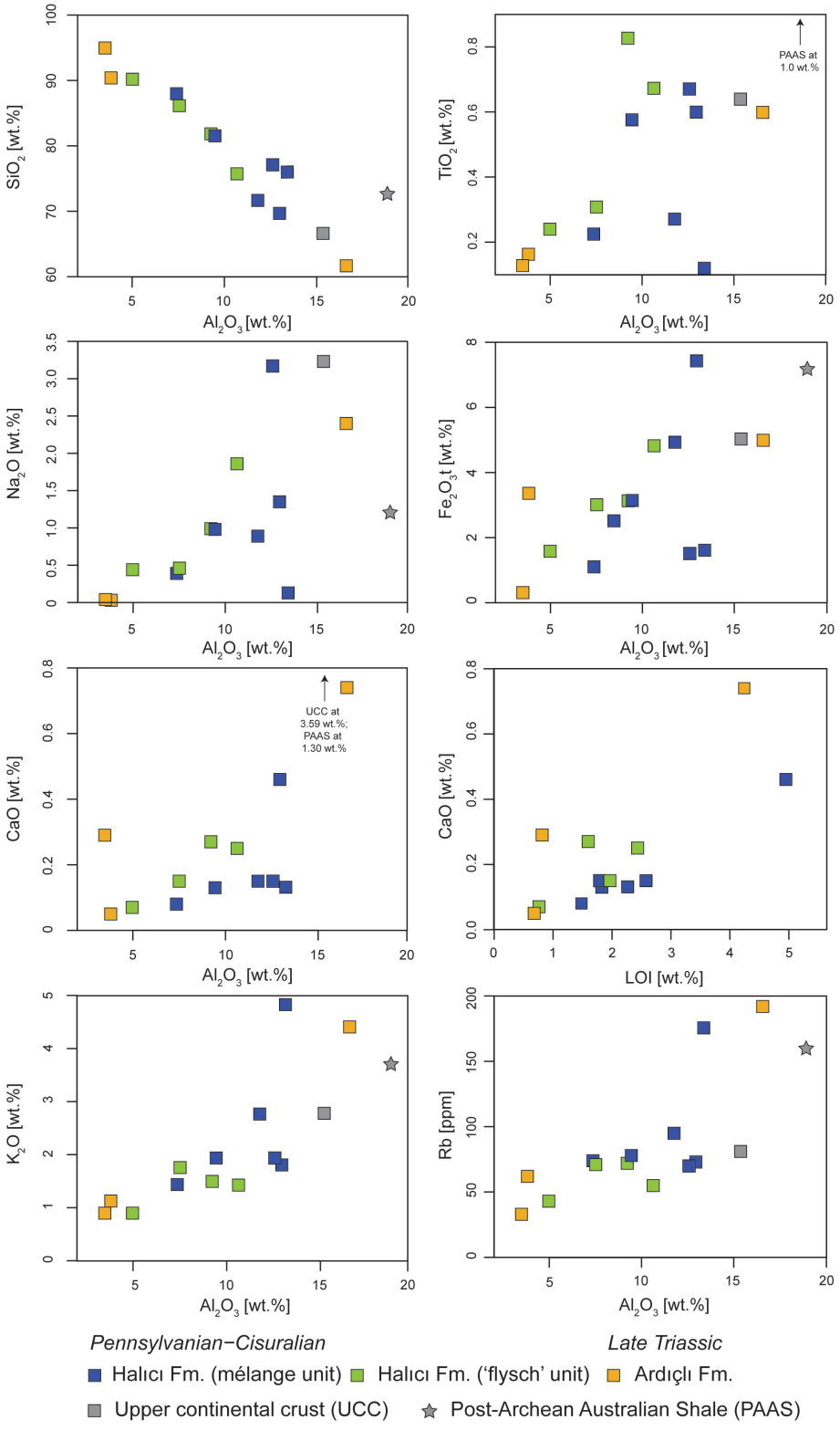

Fig. 4.7: Correlation diagrams of SiO_2, TiO_2, Na_2O, Fe_2O_3, CaO, K_2O and Rb versus Al_2O_3 and CaO versus LOI (loss on ignition). Data for UCC and PAAS from Rudnick and Gao (2003) and Taylor and McLennan (1985), respectively.

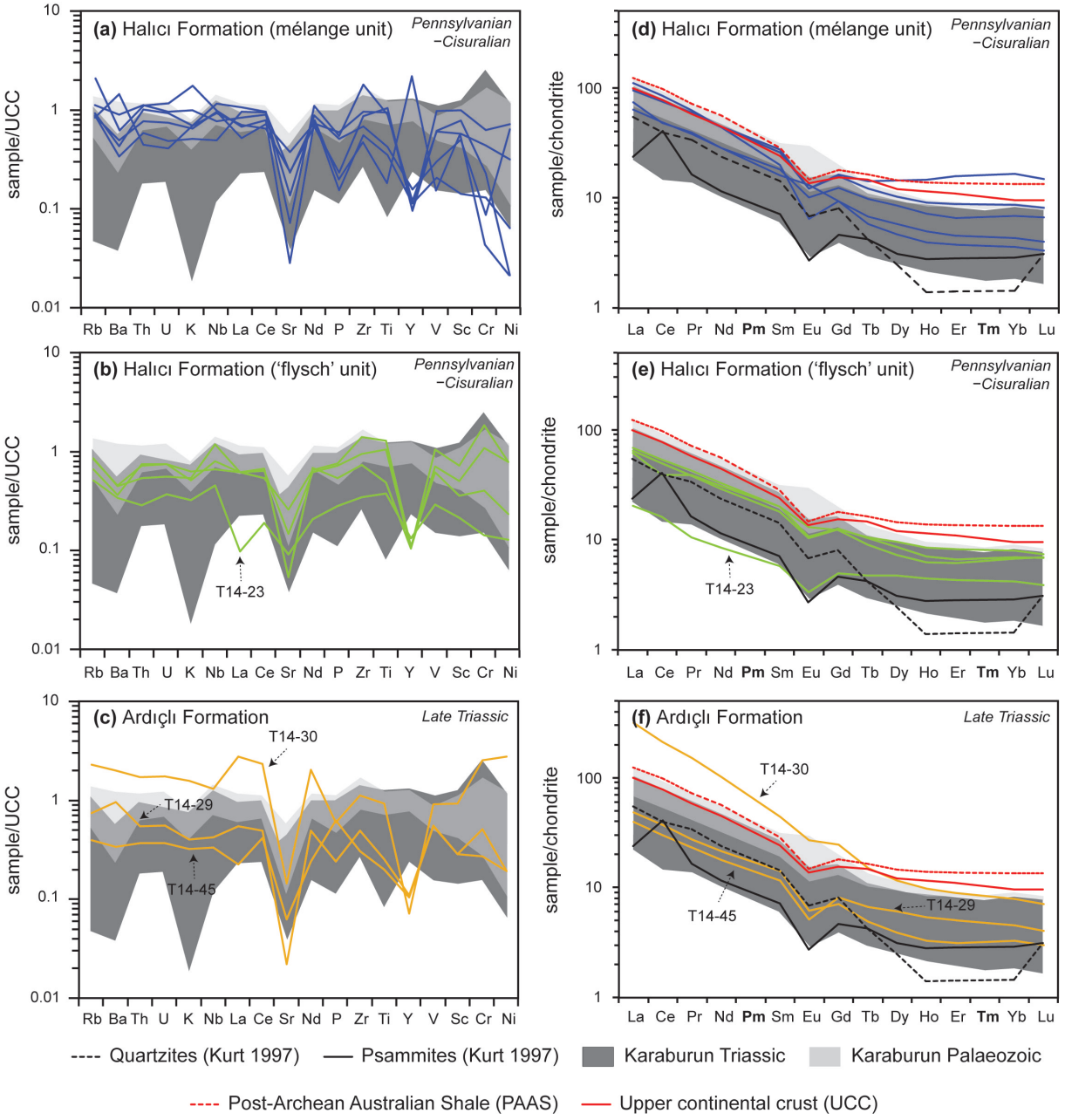

Fig. 4.8: **a–c** UCC-normalized multielement diagrams for samples from the Halıcı and Ardıçlı formations. Normalizing values from Rudnick and Gao (2003). **d–f** Chondrite- normalized REE diagrams for samples from the Halıcı and Ardıçlı formations. Normalizing values from Boynton (1984). Grey shaded areas indicate data from Triassic and Pennsylvanian–Cisuralian sediments from the Karaburun Peninsula(Löwen et al. 2018). Pm and Tm (bold) were not measured.

(based on the criteria outlined in the methods section). The data define a polymodal age spectrum from 423 Ma to 2.6 Ga with a gap of ages from 1.2 to 1.8 Ga (Figure 4.11). Almost 25% of the zircons are of a Palaeozoic age with a major Cambrian–Ordovician population, but the dominant group (49%) occurs in the Neoproterozoic. The youngest

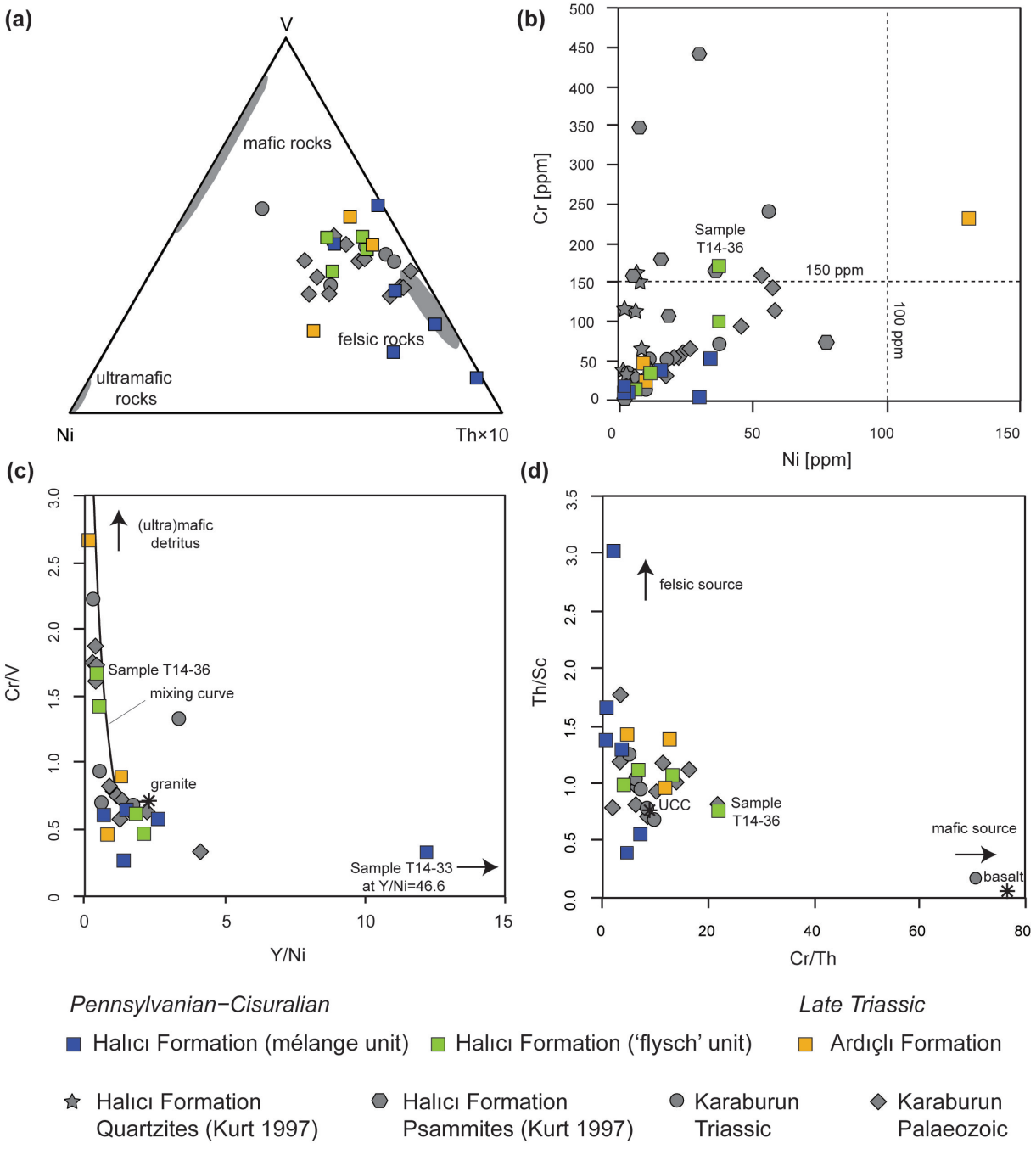

Fig. 4.9: Discrimination diagrams for identifying (ultra)mafic provenance. **a** Ternary Ni–V–Th×10 plot for source rock discrimination after Bracciali et al. (2007) with source rock endmembers highlighted in grey. **b** Correlation diagram of Cr and Ni. High concentrations of Cr (>150 ppm) and Ni (>100 ppm) combined with Cr/Ni ratios ranging from 1.3 to 1.5 are indicative of an ultramafic provenance. **c** Cr/V versus Y/Ni diagram after McLennan et al. (1993). (Ultra)mafic sources are enriched in compatible elements (Cr, Ni) and tend towards high Cr/V and low Y/Ni ratios. **d** Th/Sc versus Cr/Th diagram. Felsic rocks are characterised by enrichment of incompatible elements (Th) and mafic sources have higher concentrations of compatible elements (Cr, Sc).

coherent age group (n = 3) occurs at ∼450–460 Ma and the youngest single grain yielded an age of 423.4 ± 13.5 Ma.

Zircon grains from sample T14-31 are colourless to pinkish and often well rounded (<50%) while euhedral grains are rare. CL imaging revealed mainly oscillatory and rare sector zoning as well as some thin metamorphic overgrowths. The dataset includes 100 spots of which 89 yielded concordant ages. The total spectrum of filtered ages ranges from 478 Ma to 3.0 Ga, comprising a minor number of zircons from 1.2 to 1.9 Ga (Figure 4.11). A large Proterozoic population (87%) with a dominating Neoproterozoic age group exists and Palaeozoic grains are virtually absent. The youngest single spot ages are 478 ± 11 Ma and 495 ± 7 Ma, but the youngest group (n = 4) of coherent U–Pb ages occurs at ∼530–545 Ma.

The analysed grains of sample T14-34 often have elongated, euhedral shapes and are characterized by a comparatively dark pinkish colour and show either oscillatory or banded CL patterns (Figure 4.11). In total, 99 spots were analysed and filtered data contain 94 U–Pb ages, ranging from 413 Ma to 2.0 Ga (Figure 4.11e). Most of the grains (∼85%) are of Palaeozoic age and define a unimodal, Ordovician–Silurian population. The youngest group of coherent zircon ages (n = 21) occurs at ∼440–450 Ma but two younger, post-Silurian grains exist as well.

4.4.2 Halıcı Formation – 'flysch' unit

The majority of zircon grains from sample T14-22 are light pinkish in colour and well-rounded or subhedral. Oscillatory zoning is a common feature, and some grains show thin metamorphic overgrowths. U–Pb ages were obtained from 94 spots and filtered data (n = 84) show an age spectrum from 407 Ma to 2.7 Ga (Figure 4.11b). Palaeozoic zircons are present in small amounts only, and the bulk population is dominated by a large number of Proterozoic – mainly Neoproterozoic (59%) – grains while zircons with ages of 1.2–1.9 Ga are lacking. The youngest single grains yielded ages of 407.8 ± 13.8 and 420.5 ± 13.7 Ma, but a group (n = 5) of coherent U–Pb ages occurs at ∼430–440 Ma.

The dataset of sample T14-36 comprises 100 spots with 94 accepted U–Pb ages. The grains are mostly rounded or subhedral, have a pinkish or occasionally darker colour and often reveal oscillatory zoning. The age spectrum ranges from 326 Ma to 3.1 Ga and is dominated by a Palaeozoic (primarily Devonian) population (64%) and an

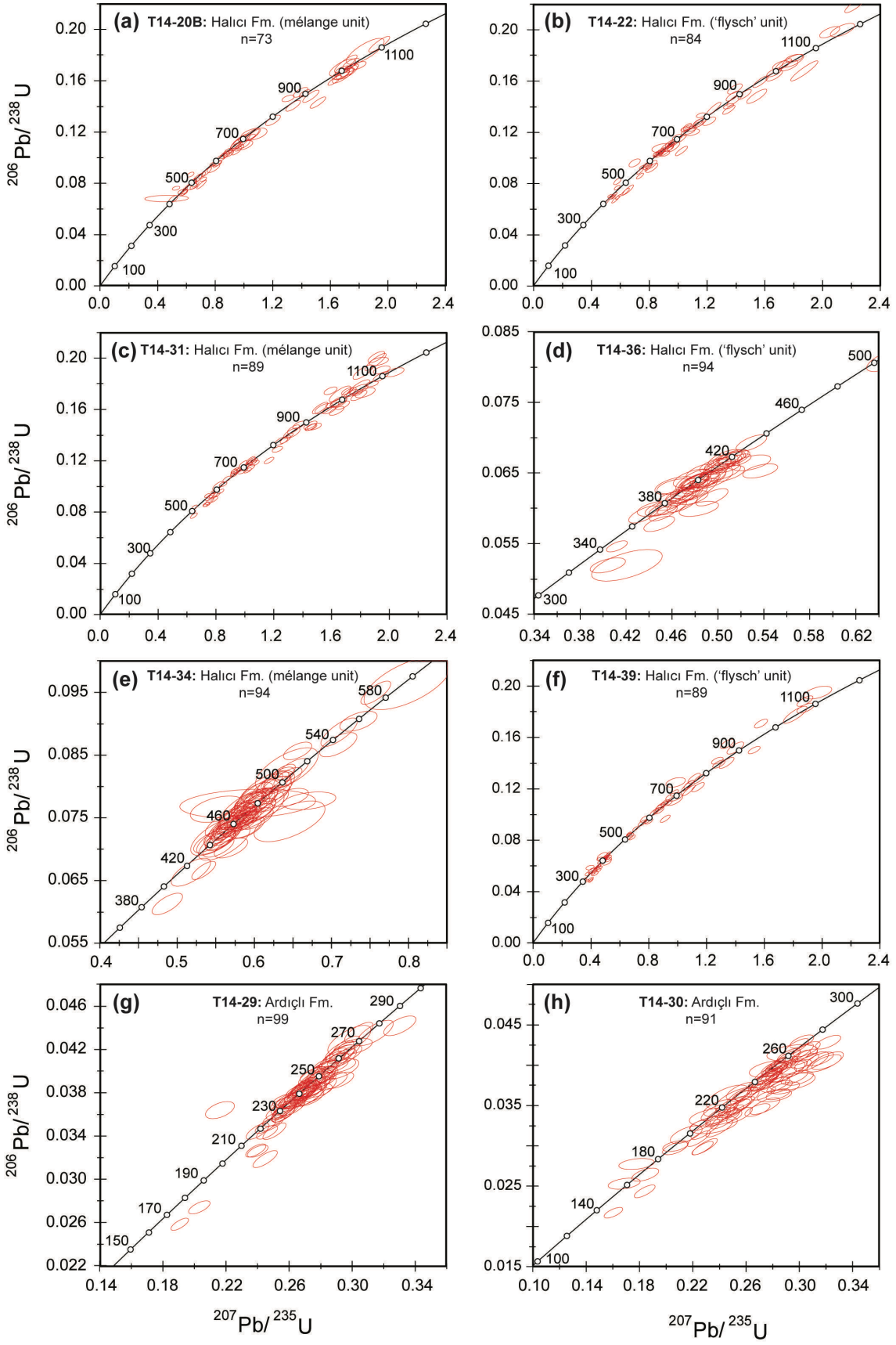

Fig. 4.10: U–Pb concordia plots showing LA-ICP-MS data of samples from the Halıcı and Ardıçlı formations.

additional Neoproterozoic age group (10%) (Figure 4.11d). Two single spot ages occur at 326.3 $\pm$ 5.3 and 328.3 $\pm$ 3.8 Ma followed by a group (n = 14) of coherent grains at $\sim$360–380 Ma.

For sample T14-39, data were obtained from 100 single grains that yielded 89 concordant U–Pb ages. The majority of zircons are pinkish in colour, have rounded or subhedral shapes and reveal oscillatory zoning or homogeneous CL patterns. The data show a polymodal age distribution ranging from 305 Ma to 3.3 Ga with a dominant Palaeozoic (43%), mainly Carboniferous–Devonian and minor Neoproterozoic population (Figure 4.11f). The youngest group (n = 8) of zircons occurs at $\sim$340–350 Ma but three Late Carboniferous single spot ages define the lower limit of the spectrum.

4.4.3 Ardıçlı Formation

Detrital zircons from sample T14-29 are pinkish in colour and characterized by a high amount of subhedral to euhedral grains, almost exclusively with oscillatory zoning. A total of 100 grains were analysed and yielded 99 concordant U–Pb ages. The spectrum shows a unimodal age distribution with dominant Triassic (64%) and Permian (20%) populations and isolated single grains with a maximum age of 1.4 Ga (Figure 4.11g). Two single grains at 165 and 175 Ma define the lower limit of the spectrum while the youngest coherent group (n = 5) occurs at $\sim$220 Ma. It is worth mentioning that the youngest eight grains are characterized by high (>1000 ppm, up to 3600 ppm) U concentrations.

Zircons separated from sample T14-30 comprise the biggest population of euhedral grains (35%), are comparatively large (>150 µm) and reveal a characteristic dark pinkish to brownish colour. A total of 102 spots were analysed and filtered data (n = 91) show unimodal age spectra with a well-defined Triassic population (84%) (Figure 4.11h). The age spectrum ranges from 138 Ma to 900 Ma but only three grains are of pre-Mesozoic age. A special feature of most grains is their very weak CL luminescence and notably high U concentrations of up to 3600 ppm ($\sim$2274 ppm average).

4.5 Rutile geochemistry

Rutile is mainly formed in medium- to high-grade metamorphic rocks (i.e. eclogites, granulites, high-grade metasediments), which are considered as the primary source

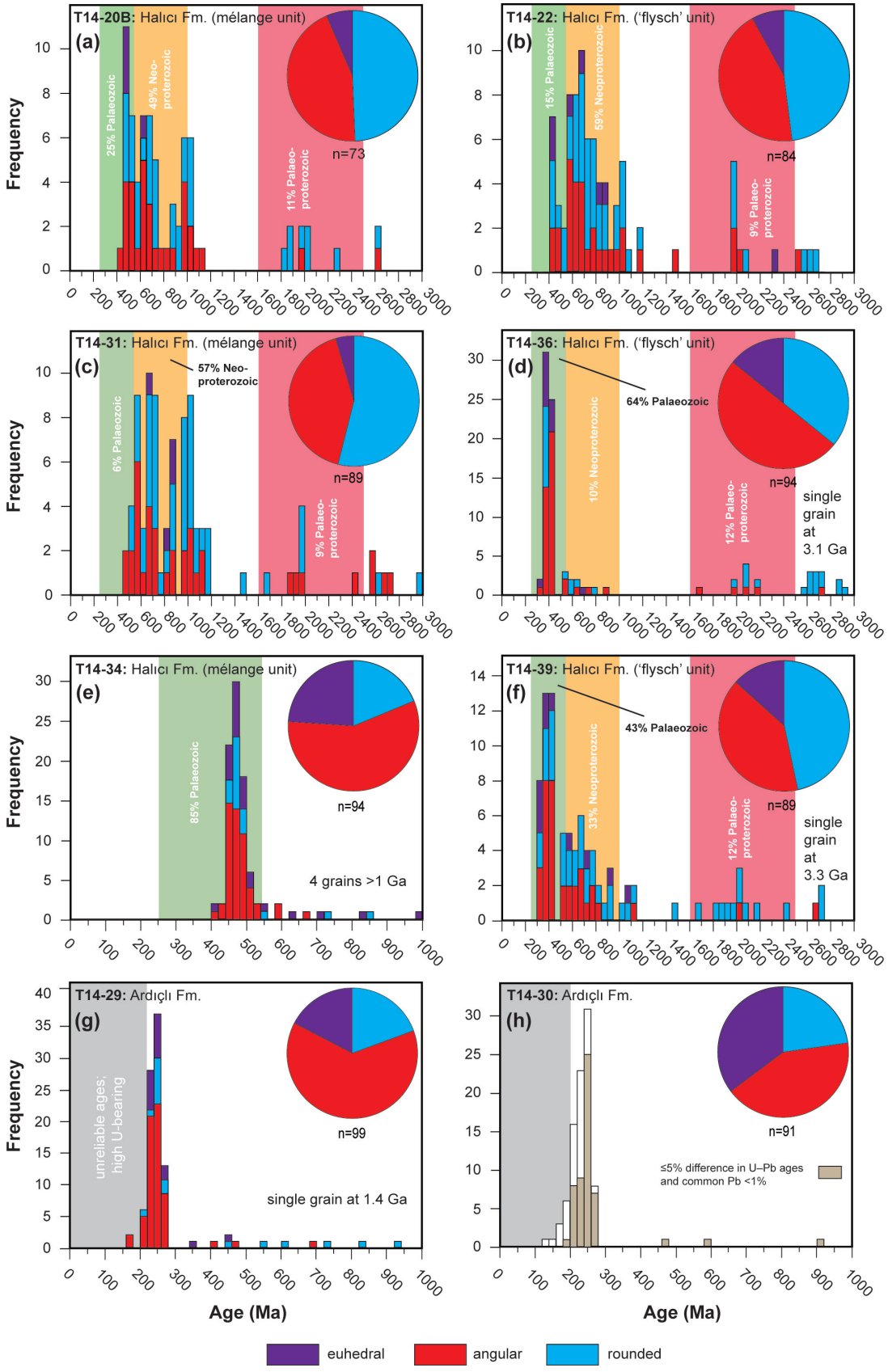

Fig. 4.11: Histograms showing the age spectra for LA-ICP-MS zircon data of samples from the Halıcı and Ardıçlı formations. Sample T14-34 **e** represents a block within the mélange unit.

Fig. 4.12: Cathodoluminescence images of representative Devonian-aged detrital zircon grains from sample T14-34 of the mélange unit.

for detrital rutile (e.g. Meinhold 2010, and references therein). Its high chemical and physical resistance and widespread appearance in sedimentary rocks make rutile a valuable mineral for provenance studies. Information on source rock lithology can be inferred from trace element composition, in particular the Cr–Nb system. For discrimination of rutiles from metamafic and metafelsic sources, the most recent criterion proposed by Triebold et al. (2012) was used:

$$x = 5 \times (Nb_{ppm} - 500) - Cr_{ppm}$$

where metamafic rutiles have negative values and metafelsic rutiles have positive values. Grains with Nb and Cr concentration below the detection limit were not considered for calculation.

Additionally, it has been demonstrated that Zr incorporation in rutile is strongly temperature dependent in quartz and zircon-bearing systems (e.g., Zack et al. 2004a; Tomkins et al. 2007). In this study, formation temperatures of rutile were calculated using the thermometer equation of Tomkins et al. (2007):

$$T(^{\circ}\mathrm{C}) = \frac{83.9 + 0.410 \times P}{0.1428 - R \times lnZr_{ppm}} - 273$$

with the gas constant R (0.0083144 kJ/K) and P = 10 kbar (default setting, as no pressure information is available for the detrital rutile grains).

For source rock classification and temperature calculations, a total of 178 single rutile grains from six sandstone samples of the Halıcı and Ardıçlı formations were analysed by EMPA. Results for source rock classification and calculated formation temperatures are shown in Figure 4.13. The data are indicative of prevailing metafelsic sources for all but one sample. Results from both samples of the mélange unit are congruent and suggest that ca. 75% of rutile grains were derived from metafelsic lithologies. In contrast, sandstones from the ‘flysch‘ unit contain rutiles with more variable Cr–Nb compositions. Results for a mature subarkose (T14-22) clearly indicate supply of rutile from almost exclusively felsic source rocks (94%), but the influence of mafic sources is increasing and even dominating (59%) in the arkosic wackes (Figure 4.13a). Calculated formation temperatures for rutiles from the studied samples range from 500 °C to 850 °C with a major population in the range of amphibolite- to eclogite-facies conditions (Figure 4.13b). Temperatures from grains of the mélange unit are mainly between 550 °C and

650 °C (T14-20B) and 600–700 °C (T14-31), respectively. Sandstones of the 'flysch' unit seem to contain a higher proportion of rutiles formed under slightly lower temperature conditions (550–600 °C). It should be mentioned that calculation of formation temperatures was not possible for a large number (70%) of rutile grains from sample T14-22 due to very low Zr concentrations (below detection limit). Results for the Ardıçlı Formation also indicate a dominant metafelsic source for detrital rutiles. Calculated formation temperatures range from 500 °C to 850 °C with a dominant population between 550 °C and 700 °C.

5 Discussion

The palaeogeographic affinity (i.e. Eurasia- or Gondwana-related) and geodynamic evolution of the Konya Complex and comparable units in western Turkey and the Aegean Sea (i.e. Chios and Karaburun units) (Figure 4.1a) in Late Palaeozoic–Early Mesozoic times is strongly debated in the scientific community. In this study, the terms 'Eurasia-related' or 'Eurasian affinity' refer to terranes, which were once located along the periphery of Gondwana but rifted off during the early Palaeozoic and were accreted to Eurasia at different times. The terms 'Gondwana-related' or 'Gondwanan affinity' refer to units that were part of Gondwana throughout most of the Palaeozoic.

The new petrographical, geochemical, and chronological data from the Upper Palaeozoic Halıcı Formation and its Mesozoic cover sequence are used here to determine their maximum depositional ages and constrain their provenance. These parameters are important prerequisites for understanding the depositional history of the Konya basin and to test current tectonic and palaeogeographic reconstructions. To this day several alternative interpretations have been proposed: (i) A Eurasian setting is inferred by Eren et al. (2004) in which the Bozdağ limestone is interpreted as a deposit at the northern passive margin of the Palaeotethys. Early Carboniferous northward subduction induced the formation of a magmatic arc and fore-arc basin and olistostrome deposition. (ii) An earlier model suggests the formation of the Konya Complex along the northern passive margin of Gondwana. Incipient southward subduction in Carboniferous times led to the construction of a continental arc, which supplied detritus for the olistostromal unit (Eren and Kurt 2000). (iii) In contrast, Özcan et al. (1988, 1990) interpreted the Konya Complex as a failed back-arc rift at the northern margin of Gondwana

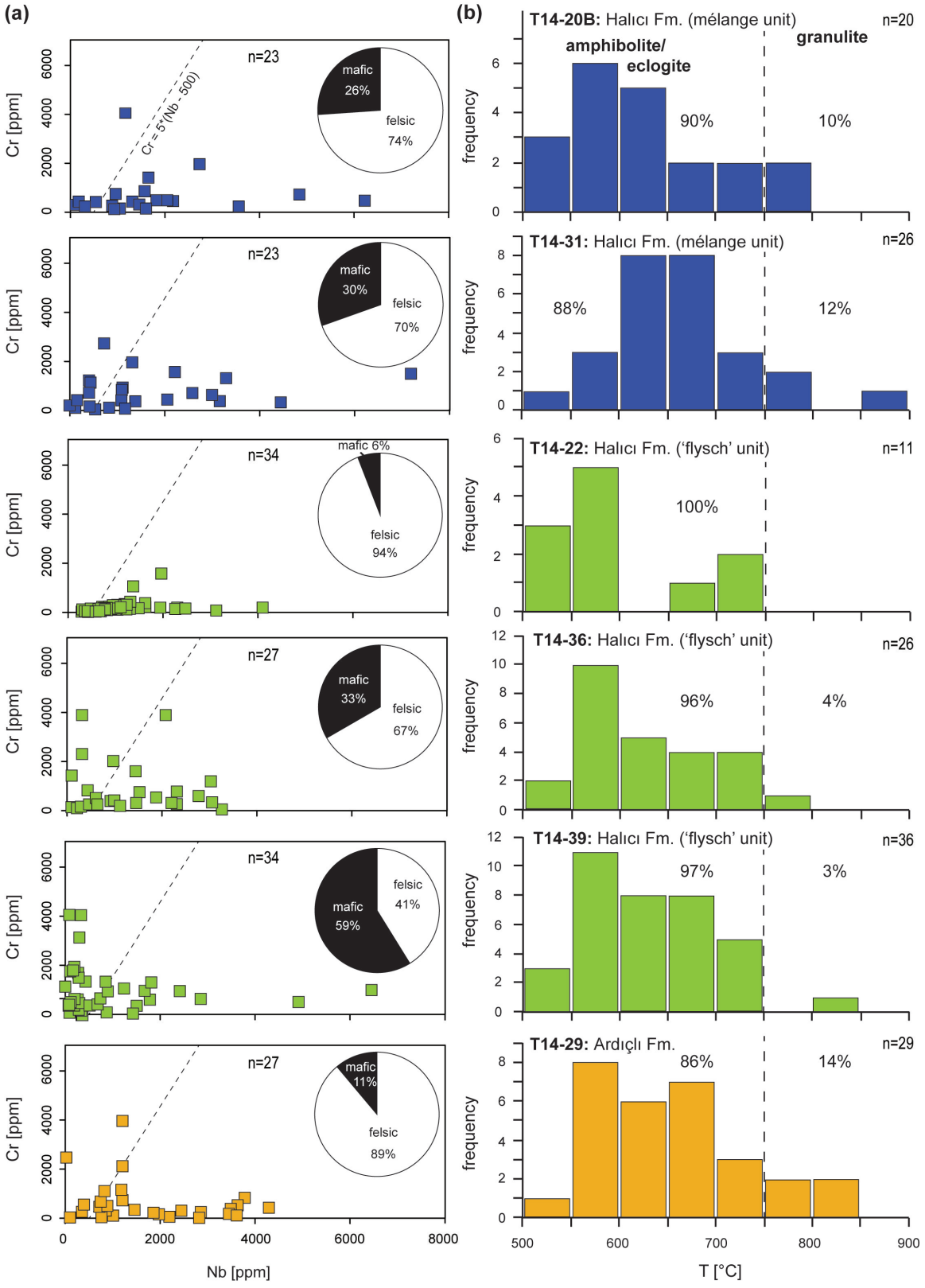

Fig. 4.13: **a** Plot of Nb versus Cr contents of detrital rutiles for discrimination between metamafic and metapelitic grains (linear slope after Triebold et al. (2012)). **b** Histograms of calculated formation temperatures for analysed rutiles from the Halıcı and Ardıçlı formations. Number of measurements (n) in both types of diagrams varies depending on the number of grains with Nb, Cr or Zr below the detection limit.

related to southward subduction. The Palaeozoic Bozdağ limestone rifted and subsided in Carboniferous time while olistostrome deposition occurred in an intracontinental basin. (iv) Another alternative includes pre-Silurian rifting of a continental fragment including the future Upper Palaeozoic carbonate platform away from the Gondwana margin. Incipient southward subduction in mid-Carboniferous time led to re-accretion to the continent and formation of the mélange (Robertson and Ustaömer 2009a). This model also includes northward subduction beneath Eurasia accompanied by arc magmatism (e.g. Sakarya arc). To sum up, the basic dissent in the discussion is related to the palaeoposition of the Konya Complex during the Late Palaeozoic and the nature of the northern Gondwana margin.

5.1 Maximum depositional ages

Previous workers have already provided good age constraints from biostratigraphic data, especially for the fossiliferous Bozdağ limestone and parts of the Permian–Cretaceous cover units of the Konya area (Özcan et al. 1988, 1990; Eren 1993a; Kozur 1999; Göncüoğlu et al. 2000; Eren et al. 2004). Biostratigraphic information is sparse in the Halıcı Formation, and until now, radiometric data from detrital zircons of metasedimentary matrix rocks have not been available. Data from limestone intercalations indicate an Early Carboniferous age (Özcan et al. 1990) but also Early Permian fossils (fusulinids, corals, trilobites, crinoids) were reported from the upper part of the Formation (Eren 1996). First U–Pb detrital zircon data obtained from six sandstones of the Halıcı Formation presented in this study give insight into the depositional history of these sediments. In the case of the block-bearing mélange unit, the youngest zircon populations occur at ∼450–460 Ma (T14-20B) and ∼530–545 Ma (T14-31). Slightly younger grains (∼400–440 Ma) were identified in a lithic wacke (T14-34) that represents a block in the mélange. Since sediment accumulation must have occurred contemporaneously or after the emplacement of the youngest, Mississippian to Serpukhovian–Bashkirian limestone blocks within the mélange (Göncüoğlu et al. 2007), the actual depositional age of the matrix has to be younger than indicated by detrital zircons. In contrast to the mélange unit, considerably younger Mississippian-aged zircons occur in two arkosic wackes of the ‘flysch‘ unit (Figure 4.11d, f), even though the youngest grains in a third sample are of Silurian–Devonian age (Figure 4.11b). Given the age of the blocks, the youngest detrital zircon populations in the sediments and re-

ported biostratigraphic data we assume a Pennsylvanian–Cisuralian depositional age for matrix rocks of the Halıcı Formation.

An Early Triassic age was assigned to the Ardıçlı Formation based on foraminifera and conodonts described from metacarbonates interfingering with the siliciclastic sediments (Özcan et al. 1988). However, Eren et al. (2004) assigned a ?Late Permian–Triassic age to this formation solely based on stratigraphic correlation, i.e. their Ertuğrul and Bahçecik formations which they further correlated to part of the autochthonous Gökçeyurt Group. Detrital zircons from two samples revealed considerably younger Jurassic and even Cretaceous ages. In any case, these results should be treated with caution due to the fact that especially the youngest grains are suffering from high (>1000 ppm) U concentrations and/or short signal intervals. We consider these ages as not reliable and rejected them for further interpretations (Figure 4.11g). The youngest group within the remaining population yielded Late Triassic (Norian) ages and is slightly younger than the previously inferred age. The issue of significantly U-rich grains that are affected by radiation damage (i.e. metamictization) is even more evident for zircons from sample T14-30. For this reason, the filtering criteria were tightened for this sample and only grains showing a difference of the U–Pb ages in the range of 5% and low (<1%) common Pb were considered. The residual population indicates a slightly younger latest Triassic–earliest Jurassic depositional age (Figure 4.11h).

5.2 Provenance

5.2.1 Upper Palaeozoic sediments

In terms of provenance, the obtained age spectra exclude a common palaeogeographic origin for the Upper Palaeozoic sediments of the Halıcı Formation. The analysed samples reveal three different types of age spectra that rather suggest derivation of detritus from different source areas.

A first distinct group comprises two subarkoses from the mélange unit (T14-20B and T14-31) and a single one from the ‘flysch‘ unit (T14-22). It is characterized by a variable (6–25%) Early Palaeozoic (mainly Cambrian–Ordovician) population, a high proportion (48–59%) of Neoproterozoic grains and a significant Tonian–Stenian age group (27–37%) (Figure 4.11a–c). Similar age spectra have lately been reported from Carboniferous sandstones of the Aladağ Nappe (eastern Taurides) and the Konya

mélange (Ustaömer et al. 2016b, 2018) and were attributed to source regions on the northern Gondwana continent. The lack of Devonian and post-Devonian grains indicates a source region isolated from Variscan influence. The Neoproterozoic population is dominated by Cryogenian–Ediacaran zircons, which can be related to several orogenic cycles in conjunction with the assembly of northern Gondwana (Cadomian–Pan-African orogeny), whereas the abundant Tonian–Stenian grains are attributed to Grenvillian orogenic events. The latter are rather sparse in siliciclastic rocks of western North Africa (Avigad et al. 2012), but have been recorded in sediments from central North Gondwana and the Afro-Arabian margin (i.e. Saharan Metacraton and Arabian–Nubian Shield) (Avigad et al. 2003; Kolodner et al. 2006; Be'eri-Shlevin et al. 2009; Meinhold et al. 2011). Apart from the additional Early Palaeozoic population, our samples show great similarities with Lower to Middle Ordovician sandstones in southern Jordan (Kolodner et al. 2006) and Middle to Upper Ordovician sandstones from the Murzuq and Kufra basins in Libya (Meinhold et al. 2011, 2013). In the Taurides, comparable signatures were observed in Cambrian–Triassic metasedimentary cover rocks of the Karacahisar dome in south-central Turkey. They were used to establish a close link between the Tauride Block and the Afro-Arabian margin, from Cambrian to at least Triassic time (Abbo et al. 2015). Further studies carried out on Upper Palaeozoic–Lower Mesozoic sediments of Crete (Zulauf et al. 2016), Kythera (Marsellos et al. 2012) and the Peloponnesus (Chatzaras et al. 2016) also revealed zircon populations suggesting a northern Gondwana provenance. In contrast, cover rocks of the lower Tyros Unit on eastern Crete dominantly contain Variscan detritus and indicate deposition along the southern active margin of Eurasia (Zulauf et al. 2015; Chatzaras et al. 2016).

Furthermore, rutile chemistry and thermometry revealed the importance of amphibolite- to eclogite- facies rocks of predominantly acidic character in the source area. A small proportion ($\leq$12%) of rutiles derived from high-T rocks has also been observed which requires the presence of a high-grade metamorphic source. Such rocks are rare in the Arabian–Nubian Shield and small occurrences of granulites and granulite-facies orthogneisses are only locally exposed in the Afif Terrane of Saudi Arabia and the Barka Terrane in Sudan, respectively (Johnson and Woldehaimanot 2003). A more proximal source is represented by upper Neoproterozoic granulites from the Pan-African basement in the Menderes Massif (Candan et al. 2001, and references therein).

A completely different age spectrum comprising a largely unimodal late Cambrian–Ordovician zircon population is obtained from a lithic wacke (T14-34) of the mélange unit (Figure 4.11e). Igneous source rocks of corresponding age are well known from the larger study area and have been ascribed to rifting processes related to the opening of the Rheic Ocean along the northern margin of Gondwana (von Raumer et al. 2002). Cambrian U–Pb zircon ages of 511 $\pm$ 16 Ma and 514 $\pm$ 14 Ma are documented from the pre-Alpine basement of eastern Crete (Romano et al. 2004). Evidence for Middle to Late Ordovician magmatism is present from metagranite occurrences in the Tavşanlı Zone (467 $\pm$ 5 Ma, Okay et al. 2008; 446 $\pm$ 8 Ma, Özbey et al. 2013) of the Anatolide–Tauride Block. They are interpreted to represent regional rifting events at the northern Gondwana margin. Other examples of Early and Middle Ordovician magmatism are documented from basement rocks of the Biga Peninsula of the Sakarya Zone (462 $\pm$ 6 Ma, Özmen and Reischmann 1999), gneisses of the Sredna Gora Zone (480 $\pm$ 30 Ma, 485 $\pm$ 50 Ma, Peytcheva and von Quadt 2004) and granites of the Serbo-Macedonian Massif (460 $\pm$ 8 Ma, Titorenkova et al. 2003) in the Balkan region. In contrast, Ordovician magmatic activity has not been reported from terranes of the Arabian plate. Considering the low textural maturity of the sediment and high proportion of euhedral and angular zircon grains, a proximal provenance is likely. Furthermore, the abundance of volcanic quartz grains and lack of rutile suggest a significant contribution from igneous rocks in the source region. Thus, we assume the lithic wacke (T14-34) was originally deposited at the northern margin of Gondwana, in proximity to Cambrian–Ordovician felsic igneous rocks related to the opening of the Rheic Ocean.

A third group of detrital zircon spectra has been detected in two lithic/arkosic wackes from the ‘flysch‘ unit (T14-36 and T14-39). They contain dominantly Devonian–Carboniferous (34–57%), small Neoproterozoic (10–33%) but only minor Tonian–Stenian populations (1–10%) (Figure 4.11d, f). With respect to provenance, a large number of Devonian-aged grains is of special importance as it allows narrowing down possible source areas that are restricted to very few localities only. The closest known exposures of igneous bodies are the Çamlık granodiorite (398 $\pm$ 1 Ma, Okay et al. 1996, 2006) and the Karacabey Pluton (394 $\pm$ 3 Ma and 396 $\pm$ 4 Ma, Sunal 2012) located in the Sakarya Zone in NW Turkey that are suggested to have an arc magmatic origin. The presence of a magmatic arc in close proximity to the depositional site of the Halıcı Formation has previously been proposed by Eren (1993b) and Kurt (1994). The

presence of high amounts of feldspars (14%) and lithic sedimentary and volcanic (12%) fragments in both samples is in accordance with this assumption (Table S2). Internal structures of Devonian zircons from both samples revealed by cathodoluminescence imaging share similarities with grains from the Karacabey Pluton (Sunal 2012) in terms of pronounced oscillatory zoning and inherited cores and can be considered as a possible source (see Figure 4.12).

5.2.2 Lower Mesozoic sediments

The youngest analysed sediments from the Upper Triassic Ardıçlı Formation stand out with largely unimodal age distribution spectra that record contribution from almost exclusively Triassic and Upper Permian source rocks. In previous studies, rock fragments identified in sediments of this formation were interpreted as being derived from both, the underlying Sızma Group (including Kadınhanı metamagmatics) plus an unknown, more metamorphosed source (Eren et al. 2004). In the light of our findings, we can exclude recycling of the underlying rock units since their signature should be visible in the age spectra of the Ardıçlı Formation. Triassic-aged zircons can have various origins, as evidence for Triassic igneous activity is widespread in the Eastern Mediterranean region such as the Serbo-Macedonian Massif (Himmerkus et al. 2009a), the Pelagonian Zone (Anders et al. 2007), the Cyclades (Tomaschek et al. 2001; Bröcker and Pidgeon 2007) or the Menderes Massif (Koralay et al. 2001). However, a very proximal provenance is likely and can be deduced from the high proportion of (>75%) euhedral and angular zircon grains (Figure 4.11g, h). The closest possible rocks that could have provided detritus to the Ardıçlı Formation are the Kadınhanı metamagmatics of the Konya Complex itself. Recent U–Pb dating of zircon from metatrachyandesites north of Konya yielded a Triassic age of 220.2 $\pm$ 0.7 Ma (Ustaömer et al. 2016a) and confirmed the previously published age of 221.6 $\pm$ 1.7 Ma (Güven et al. 2012). Compositional data of zircons from sample T14-30, however, revealed remarkably high U concentrations (average of 2300 ppm) and show that sediment cannot have been derived from any of the above-mentioned occurrences. Unfortunately, no other rocks containing zircons of corresponding age and composition could be identified in the larger study area. Nonetheless, it has been demonstrated by Belousova et al. (2002) that the trace element composition of zircon is sensitive to the type of source rock. Their study reveals a positive correlation of U with incompatible elements like Y and other REE that conse-

quently are enriched in zircons from evolved granitoid rocks. Even though the second sample (T14-29) reveals a very similar age spectrum, the zircons exhibit considerably lower amounts of U, thus providing evidence that both samples do not share the same provenance. Thus, we assume that the sediment was supplied from a nearby source of evolved igneous rocks that are not existent anymore or presently not exposed. Due to the very small difference between crystallization ages of zircons and the depositional age of these sediments we suggest volcanic rather than plutonic rocks as most likely sources. Even though granitic rocks may have been exposed by rapid exhumation in an active tectonic setting.

5.3 Tectonic setting

The chemical composition of sedimentary rocks is mainly controlled by the nature of their source rocks but can subsequently be modified by secondary processes such as diagenesis, weathering, sorting and/or recycling (McLennan et al. 1993). Even though the emphasis of many geological studies is placed on the provenance of sedimentary rocks, it has become common practice to utilize geochemical data for inferring tectonic settings of sedimentary basins (e.g. Bhatia 1983; Bhatia and Crook 1986; Roser and Korsch 1986). However, geochemical signatures cannot necessarily be assigned to a specific tectonic setting and it has been shown that these approaches often do not provide satisfactory results or are inconsistent with the regional geological framework or plate tectonic reconstructions (e.g. McLennan 1990; Armstrong-Altrin and Verma 2005).

In this study, we used the conventional discrimination diagrams of Roser and Korsch (1986) and recently published discriminant function-based diagrams of Verma and Armstrong-Altrin (2013, 2016) to decipher the tectonic setting of the Konya basin (Figure 4.14, Table 4.3). Their new statistical approach was successfully tested on Neogene to Quarternary sediments from known tectonic settings and utilizes $\log_e$-ratio transformation of major (SiO_2, TiO_2, Al_2O_3, Fe_2O_3, MnO, MgO, CaO, Na_2O, K_2O and P_2O_5) and trace elements (Cr, Nb, Ni, V, Y and Zr). In addition to the geochemical data, we also used detrital zircon spectra of the studied samples (Figure 4.15). Following Cawood et al. (2012), the detrital zircon record of sedimentary rocks, in particular the difference between crystallization ages of zircon and the depositional age of the sediment reflects the nature of the depositional basin they were deposited in and allows for

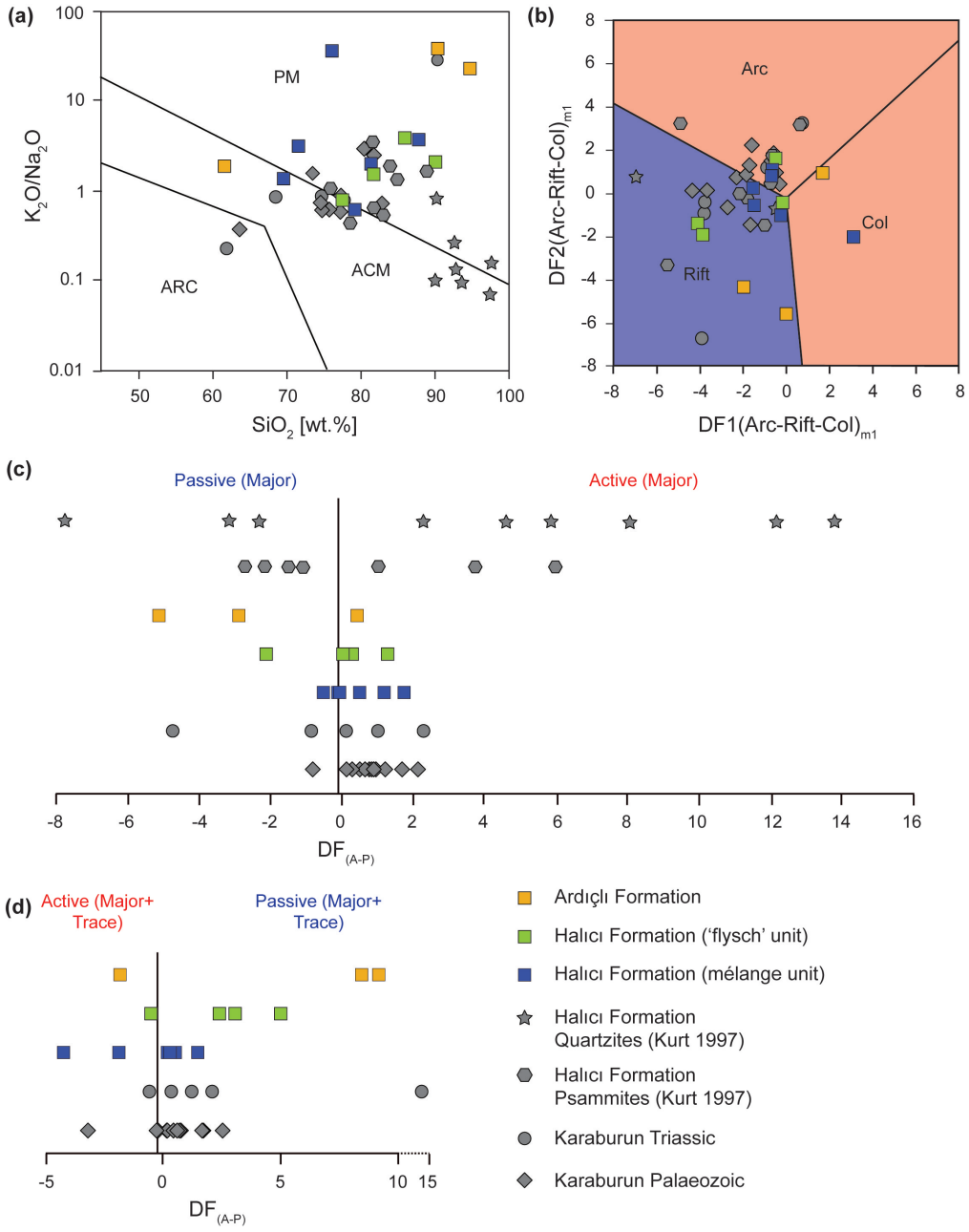

Fig. 4.14: Tectonic discrimination diagrams for samples from the Halıcı and Ardıçlı formations (this study). For comparison, data from a previous study of the Halıcı Formation (Kurt 1997) and from the Karaburun Peninsula (Löwen et al. 2018) are plotted as well. **a** K_2O/Na_2O versus SiO_2 diagram after Roser and Korsch (1986). PM – passive margin; ACM – active continental margin; ARC – oceanic island arc. **b** Multidimensional diagram after Verma and Armstrong-Altrin (2013). Discriminant functions (DF) based on major element oxides. Arc – island or continental arc; Rift – continental rift; Col – collision. **c** and **d** Multidimensional discriminant function diagrams based on major and selected trace elements after Verma and Armstrong-Altrin (2016). Discriminant functions were calculated using revised equations published in the corrigendum to Verma and Armstrong-Altrin (2016). In cases where samples show 0% concentrations of a specific element, the concentrations were set to 0.0001% in order to allow calculation of K_2O/Na_2O and $\log_e$-ratios for discriminant diagrams.

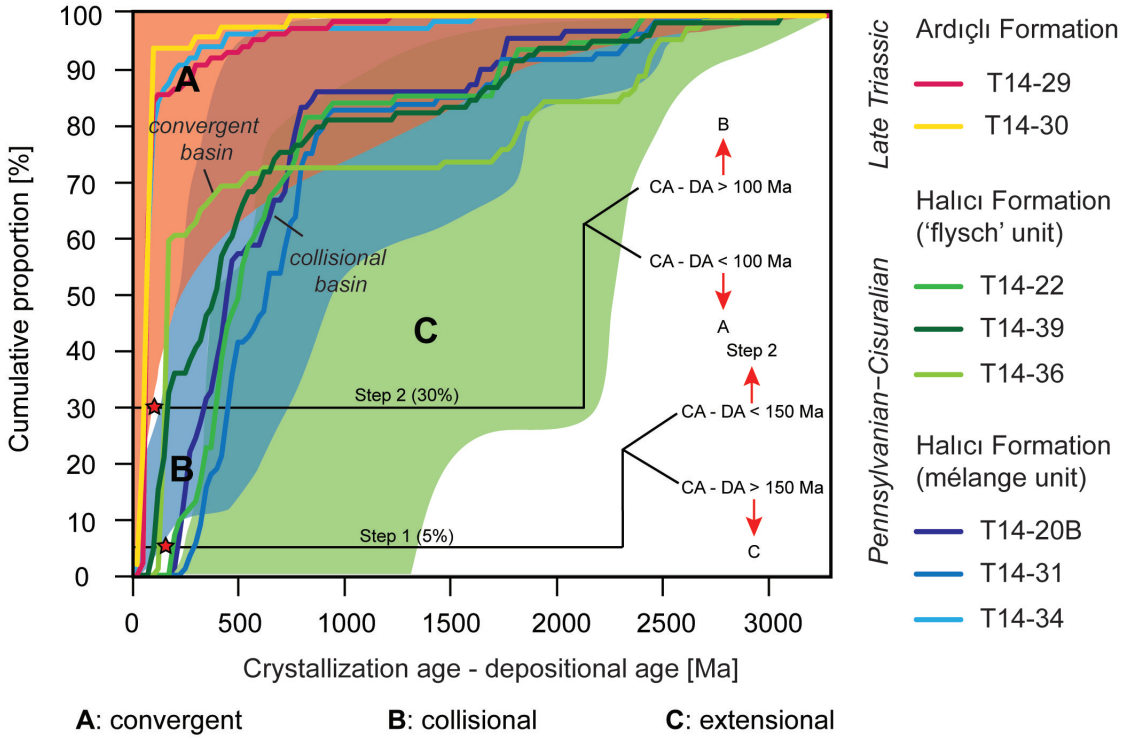

Fig. 4.15: Diagram showing the difference between measured crystallization ages for detrital zircon grains and the depositional age of the sediment versus cumulative proportion of detrital zircon ages from samples of the Halıcı Formation (after Cawood et al. 2012).

discrimination of convergent, collisional and extensional settings.

In the conventional diagram of Roser and Korsch (1986), the majority of our samples, as well as quartzites and psammites from the Halıcı Formation (analysed by Kurt 1996, 1997), are characterized by SiO_2, K_2O and Na_2O abundances typical for passive margin settings (Figure 4.14a, Table 4.3). With respect to the discriminant function-based diagrams, the sample population shows a larger spread (Figure 4.14b–d, Table 4.3). Samples from the mélange unit show a tendency towards a passive margin setting, the exception being the sedimentary block from the mélange (T14-34) that has a continental and oceanic island arc affinity. This is in accordance with detrital zircon data, suggesting an extensional setting for sedimentary matrix rocks (T14-20B and T14-31), but a convergent margin setting for the mélange block (Figure 4.15). In the 'flysch' unit, geochemical signatures of two highly mature samples (T14-22 and T14-23) point towards a passive margin setting, whereas data from two wackes (T14-36 and T14-39) are more ambiguous, slightly tending to an active setting (Figure 4.14). This is also inferred from the detrital zircon record, reflecting a passive margin setting (extensional)

for the former and an active margin setting (collisional) for the latter samples (Figure 4.15). Two out of three samples from the Ardıçlı Formation plot in the 'Rift' and passive margin fields in every single diagram whereas the conglomeratic sample (T14-30) shows active margin characteristics (Figure 4.14). The detrital zircon record of both dated samples (T14-29 and T14-30) indicates a convergent setting and documents high syndepositional igneous activity (Figure 4.15). However, a passive margin setting is most likely and fits very well with previous considerations, in which the Ardıçlı Formation was interpreted as synrift sequence related to the opening of several back-arc oceans (e.g. Küre, Meliata, Pindos) during Triassic time in response to Palaeotethyan slab roll-back (Eren et al. 2004).

With respect to the previous (palaeo)tectonic interpretations of the basin, an unambiguous affinity to either northern Gondwana or southern Eurasia of the complex as a whole cannot be established based on the available data. In fact, the Halıcı Formation has turned out as a complex mixture of heterogeneous (mainly) sedimentary rocks that do not have a common origin and reflect different depositional tectonic settings. The suite of samples that strongly resembles Lower Palaeozoic sandstones of northern Gondwana reflects passive margin signatures and does not document any input from an arc-derived material. Thus, certain models proposing an active northern Gondwana margin (e.g. Özcan et al. 1988, 1990; Eren and Kurt 2000; Robertson and Ustaömer 2009a) are not supported by our data. A possible scenario, however, could involve short-lived or shallow-dipping southward subduction beneath Gondwana without the formation of a major magmatic arc, as evidence for arc-related magmatism on the Tauride domain is scarce (Figure 4.16a). Nonetheless, Carboniferous arc-type magmatic rocks have been reported, for instance from the Simav area of the north-western Afyon Zone and the Cyclades and were interpreted as evidence for southward subduction in Late Carboniferous–Early Permian time (e.g. Xypolias et al. 2006; Candan et al. 2016). In contrast, samples documenting sediment supply (supposedly) from units with a southern Eurasian affinity (i.e. T14-34, T14-36, T14-39) tend to have compositional and geochemical features pointing to an active margin setting and contain some arc-derived material (Figure 4.14). The high abundance of Devonian-aged zircons led to suggest a magmatic arc could have developed during that time and was subsequently uplifted and eroded in the Late Carboniferous–Early Permian. Results from the Ardıçlı Formation indicate that subduction along a continental block with Eurasian

Table 4.3: Inferred tectonic settings from geochemical and geochronological data, based on various discrimination diagrams that are published in the literature. Please note the excellent agreement between the different methods for some of the samples. The possible source areas for the Palaeozoic sediments, North Gondwana-related (NG) *versus* Eurasia-related (EU), based on U-Pb zircon ages is indicated in the last column. The Triassic sandstones of the Ardıçlı Formation have likely a local igneous source (LIS) of so far unknown origin.

Formation		Sample	Geochemistry				Geochronology	Method agreement	Source based on U-Pb data
			Roser and Korsch (1986)	Verma and Armstrong-Altrin (2013, 2016)			Cawood *et al.* (2012)		
			Figure 12 (a)	Figure 12 (b)	Figure 12 (c)	Figure 12 (d)	Figure 13		
Ardıçlı Formation		T14-45	Passive margin	Rift	Passive margin	Passive margin	*no data*		
		T14-30	Active continental margin	Collisional/Arc	Active margin	Active margin	Convergent setting	Yes	LIS
		T14-29	Passive margin	Rift	Passive margin	Passive margin	Convergent setting		LIS
Halıcı Formation	'flysch' unit	T14-39	Passive margin	*undetermined*	Active margin	Passive margin	Collisional setting		EU
		T14-36	Active continental margin/Passive margin	Arc	Active margin	Active margin	Collisional setting	Yes	EU
		T14-23	Passive margin	Rift	*undetermined*	Passive margin	*no data*		
		T14-22	Passive margin	Rift	Passive margin	Passive margin	Extensional setting	Yes	NG
	mélange unit	T14-34 (block)	Active continental margin/Passive margin	Arc	Active margin	Active margin	Convergent setting	Yes	EU
		T14-33	Passive margin	Collisional	Active margin	Active margin	*no data*		
		T14-32	Passive margin	Rift	Active margin	Passive margin	*no data*		
		T14-31	Passive margin	Rift	Passive margin	Passive margin	Extensional setting	Yes	NG
		T14-26	Passive margin	Rift	Passive margin	Passive margin	*no data*		
		T14-20B	Active continental margin	Arc	Active margin	Passive margin	Extensional setting		NG

affinity ceased before Late Triassic time and a passive rift margin developed (Figure 4.16b).

In addition to the sedimentary sequences that were the focus of most studies, a large number of igneous rocks from the Kadınhanı metamagmatics or volcano-sedimentary unit, respectively, have been studied in the past decade as well (Eren et al. 2004; Göncüoğlu et al. 2007; Robertson and Ustaömer 2009a). Studied metavolcanic rocks and dykes exhibit arc- and MORB-type characteristics and consistently show variable degrees of enrichment in MORB-normalized trace element patterns in combination with (slightly) negative Nb anomalies. These signatures were interpreted to document the initiation of a subduction event in Carboniferous time, accompanied by the development of magmatic arc/ fore-arc sequences on the northern margin of Palaeotethys (Eren et al. 2004) or induced back-arc rifting at the northern Gondwana margin, respectively (e.g. Göncüoğlu et al. 2007; Robertson and Ustaömer 2009a). It should be noted that metatrachyandesites from the Kadınhanı and Sızma areas, analysed by Göncüoğlu et al. (2007), have later been dated as Early Triassic by Akal et al. (2012) and thus were probably related to rifting processes of a Neotethyan ocean. In contrast, radiometric dating of metavolcanic rocks from the volcano-sedimentary unit yielded Early Permian ages (Candan et al. 2009).

It remains to state that the complex structure and formation of the Upper Palaeozoic sedimentary sequence (NW of Konya) is not yet fully understood. Impressions from the field campaign already arose the question, whether the Halıcı Formation can be adequately described as a single unit or, in fact, is composed of two or more subunits. Our initially introduced subdivision into a mélange unit and a ‘flysch‘ unit is primarily based on observed differences in lithology, deformation and metamorphic degree. More specifically, studied rocks from the mélange unit (in contrast to the ‘flysch‘ unit) show phyllitic textures and contain sigma-shaped quartz crystals witnessing relatively higher metamorphic conditions that allow ductile deformation. Also, the presented data have shown considerable differences in terms of composition and provenance within a supposedly single formation. In any case, we conclude that the final assembly of the formation must have been completed until Late Triassic time, as it is unconformably overlain by the Upper Triassic Ardıçlı Formation.

5.4 Comparable units

The studied area has often been compared to Palaeotethys-related units on the Karaburun Peninsula in western Turkey and on the Aegean island of Chios (e.g. Eren et al. 2004; Robertson and Ustaömer 2011) (Figure 4.1a). On the Karaburun Peninsula, the Palaeozoic succession is mainly composed of siliciclastic sedimentary rocks of Pennsylvanian–Cisuralian age (Löwen et al. 2017). It comprises low-grade metamorphosed sandstones and shales (Küçükbahçe Formation) and a mélange unit with Silurian–Carboniferous blocks of black chert, pelagic limestones and poorly dated volcanic rocks that are embedded in a highly deformed siliciclastic matrix (Dikendağı Formation) (Kozur 1997, 1998; Çakmakoğlu and Bilgin 2006). The Dikendağı Formation is intruded by two Early Triassic granitoid bodies that yielded a biotite Rb–Sr isochron age of 239.9 $\pm$ 2.4 Ma (Erkül et al. 2008) and zircon U–Pb ages of 244.4 $\pm$ 1.5 Ma (Ustaömer et al. 2016b) and 247.1 $\pm$ 2.0 Ma, respectively (Akal et al. 2011). Previous studies revealed an arc-related geochemical signature for these rocks and document ongoing subduction during that period. The Palaeozoic sequence is unconformably overlain by a thick, carbonate-dominated sequence of Early Triassic to Late Cretaceous age (Çakmakoğlu and Bilgin 2006). On Chios, the mélange is part of the 'autochthonous' Lower Unit and comprises a mid-Carboniferous siliciclastic matrix with blocks of limestone, radiolarites and volcanic rocks of Silurian to Carboniferous age (Meinhold et al. 2008b). The Lower Unit is tectonically overlain by an 'allochthonous' Upper Unit of Late Carboniferous to Jurassic age (Besenecker et al. 1968; Meinhold et al. 2007, 2008b). In contrast to the Konya Complex, a Silurian–Devonian carbonate platform is absent in both localities and Palaeozoic limestones exclusively occur as blocks in the mélange units. All these areas play an important role in geodynamic reconstructions in a period of time when the Palaeotethys diminished in size and finally vanished. Previously, the tectonostratigraphic similarities of the Chios, Karaburun and Konya units were used as strong arguments to correlate these units and interpret them as different parts of the same active continental margin (Robertson and Ustaömer 2009a). Essential provenance data to test if this correlation is viable were scarce but were provided over the last years for both, Chios and Karaburun (Meinhold et al. 2007, 2008a,b; Löwen et al. 2017, 2018). These studies have identified low-grade metamorphosed sedimentary rocks as major sources but locally also recognized high proportions of (sub)angular grains derived from a felsic volcanic source that was interpreted as an indication for the

presence of a relatively proximal continental-arc. Similar to Konya, compositional data of detrital rutile are indicative of amphibolite- to eclogite-facies rocks. Nevertheless, a considerable amount (up to 25%) of high-temperature rutiles in the Dikendağı Formation implies the existence of high-grade (granulite-facies) rocks in the source area. In terms of source rock composition, detrital rutiles from the Upper Palaeozoic rocks of Karaburun were (with few exceptions) dominantly derived from felsic lithologies, which is also recorded by grains from the Permian–Carboniferous and Permian–Triassic units of Chios (Meinhold et al. 2008a; Löwen et al. 2018). Despite the many similarities, detrital garnet and Cr-spinel do only occur in the Chios–Karaburun units, while they are virtually absent in studied rocks from the Konya Complex. In the Upper Palaeozoic units, the compositions of Cr-spinel indicate a mixed (ultra)mafic source of predominantly harzburgite and minor lherzolite composition. In contrast, euhedral Cr-spinel extracted from Lower Triassic siliciclastic rocks of the Karaburun Peninsula (Gerence Formation) exhibit significantly higher Cr- and Mg- numbers and were interpreted as being derived from podiform chromitites related to an intra-oceanic back-arc setting above a supra-subduction zone within the Palaeotethys (Löwen et al. 2018). Furthermore, the detrital zircon record of sandstones from Chios and Karaburun provided a substantial piece of information for palaeogeographic considerations. Their age spectra were dominated by Palaeozoic to Neoproterozoic zircons, but locally contained large Ordovician–Devonian populations. It was concluded that most of the Carboniferous–Triassic successions were deposited along the southern active margin of a continental block with Eurasian affinity in a continental-arc environment, and their source areas should probably be sought in basement rocks of units located along this margin (e.g. Sakarya Zone, present-day Balkan region) (Meinhold et al. 2008b; Löwen et al. 2017). Nevertheless, detrital zircon spectra of a few samples from the Karaburun mélange closely resemble Palaeozoic and Mesozoic siliciclastic rocks from the northern Gondwana margin (Meinhold et al. 2011, 2013; Dörr et al. 2015) and show great similarities with samples from the Palaeozoic Konya Complex as well (T14-20B, T14-22 and T14-31).

In summary, the discussed units do not only have comparable tectonostratigraphic structures but, partially, do also share a similar provenance. Available data from the Chios–Karaburun units on the one hand mainly favour an assignment to an active margin of Eurasian affinity in Late Palaeozoic time. Data from time-equivalent deposits

of the Konya Complex on the other hand record sediment supply from units of both, Eurasia-related and Gondwana-related. Future tectonometamorphic and structural studies are necessary to fully understand the formation of the Konya Complex and adjust the palaeoposition of these rocks within the Tethyan realm.

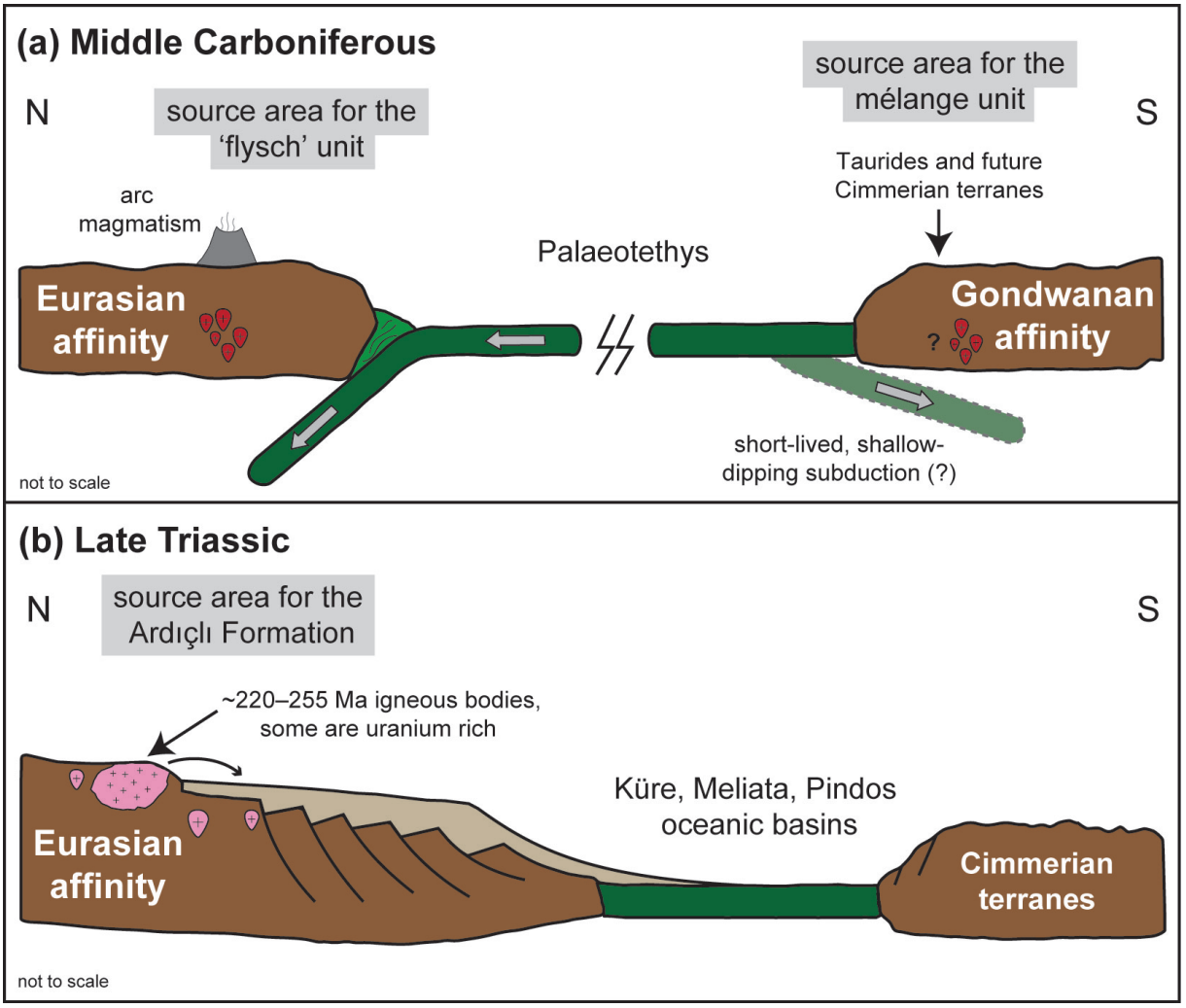

Fig. 4.16: Schematic reconstructions of the palaeomargins with Eurasian and Gondwanan affinities for the **a** Middle Carboniferous and **b** Late Triassic time as inferred from geochemical and geochronological data. The terms 'Eurasian affinity' and 'Gondwanan affinity' are defined in Section 5. The new data of this study show that previous palaeotectonic models presented in the literature have to be treated with caution as it is difficult to explain the provenance signals. Further work is required to develop a ceomprehensive revised palaeotectonic model.

6 Conclusions

The new data from siliciclastic rocks of the Upper Palaeozoic Konya Complex and its Mesozoic cover sequence give insight on the depositional history of the Konya basin and shed light on their age, composition and origin. The most important findings can be summarized as followed:

- The Halıcı Formation is not considered as a single overall unit but can be divided into (several) subunits, such as a low-grade 'flysch' unit (e.g. mudstones, siltstones, sandstones) and a slightly more metamorphosed, block-bearing mélange unit (e.g. sandstones, conglomerates, cherts), representing the actual mélange.
- Provenance sensitive elements and mineral chemical data of rutile from the Ardıçlı and Halıcı formations document sediment supply from predominantly amphibolite- to eclogite-facies rocks of felsic character. Evidence for input from metamafic source rocks is rare.
- The youngest populations of detrital zircons indicate an Early Palaeozoic depositional age for the Halıcı Formation. But given the available biostratigraphic data from the matrix rocks and embedded limestone blocks, we assume that sediment accumulation in Pennsylvanian–Cisuralian time, contemporaneously to the Karaburun mélange is most likely.
- Sandstones of this formation revealed significantly different detrital zircon age spectra and document sediment supply from units of both, southern Eurasian affinity (i.e. Sakarya Zone, Sredna Gora Zone, Serbo-Maedonian Massif) and northern Gondwanan affinity (i.e. Saharan Metacraton, Arabian–Nubian Shield).
- Samples with a (supposed) Eurasian affinity are characterized by prominent Silurian–Devonian and Ordovician–Silurian populations. We assume that large volumes of detritus were derived from felsic igneous bodies related to arc magmatic activity due to ongoing subduction beneath Eurasia-related continental blocks.
- The provenance of Upper Triassic sandstones from the Ardıçlı Formation remains enigmatic. Our data clearly indicate a very proximal source and exclude recycling of material from the underlying formations of the Sızma Group.

7 Acknowledgements

We gratefully acknowledge financial support from the German Research Foundation (DFG, grant number ME 3882/3-1) and the Göttingen University start-up funding for young academics (grant to GM). We thank Gerald Hartmann for XRF analysis, Klaus Simon for ICP-MS analysis, and Andreas Kronz for providing access to the EMPA. Finally, we are grateful to Vasileios Chatzaras, Alastair H. F. Robertson and an anonymous reviewer for their constructive comments which helped to improve the original manuscript, and to Robert J. Stern for his careful editorial handling.

Chapter 5

Summary

In this PhD thesis a detailed provenance analysis was conducted on 28 siliciclastic sediments from the Karaburun Peninsula and the Konya Complex to provide data for a better understanding and improvement of current palaeotectonic models for Turkey during the Late Palaeozoic to Early Mesozoic. As presented in the introduction of this thesis, basically three alternative concepts are discussed in the literature but previous attempts to embed the study areas into the evolution of the Tethyan realm during that period were hampered, mainly by the lack of provenance data. In the course of this thesis, a fundamental geological basis was established by constraining the maximum depositional age of siliciclastic units and by reviewing their supposed stratigraphic relationships. For testing the proposed palaeotectonic models, it was crucial to identify possible source areas for the studied sediments and to characterise the source area geology, but also decipher the tectonic setting of the basin they were deposited in.

On the Karaburun Peninsula, the Late Palaeozoic succession was previously interpreted as a continuous Ordovician–Carboniferous sequence composed of three separate formations. The new detrital zircon U–Pb ages presented here, allowed to set the maximum depositional age of the lowermost Küçükbahçe Formation and overlying Dikendağı formations to Pennsylvanian–Cisuralian. Considering the distinct differences in composition, provenance and metamorphic overprint, this stack of units is most probably separated by tectonic rather than gradational contacts. Provenance information derived from detrital zircons suggest that these formations were deposited spatially separated from each other along the same margin of the Palaeotethys ocean. The observed age spectra in Late Palaeozoic sediments, especially the occurrence

of large Ordovician–Devonian populations strongly suggest sediment supply from terranes north of the present location of the study area. Most likely sources should be sought in basement rocks of units located in the present-day Balkan region and the Sakarya Zone or equivalent successions. These findings are also in accordance with interpretations for time-equivalent units of the closely related Greek islands of Chios and Inousses. Therefore, it is proposed that the Chios and Karaburun units were deposited along the southern margin of Eurasia in Late Carboniferous–Early Permian time. Even though the information on the nature of this margin inferred from geochemical data are ambiguous, some sediments clearly record input of volcanic material, probably derived from a nearby magmatic arc related to the northward subduction of Palaeotethys lithosphere.

In the second study area, siliciclastic rocks of the Halıcı Formation from the Upper Palaeozoic Konya Complex and the Ardıçlı Formation of its Mesozoic cover sequences were targeted. Detrital zircon ages from sediments of the Halıcı Formation in conjunction with available biostratigraphic data from olistoliths suggests sediment accumulation in Pennsylvanian–Cisuralian times, contemporaneously with the comparable Upper Palaeozoic units on Chios and Karaburun. Detrital zircon age spectra of individual samples of this Formation differ significantly and document sediment supply not only from units of the southern Eurasian margin but also from North Gondwana and the Afro–Arabian margin. Geochemical and compositional features of sediments with northern Gondwana affinity reveal passive margin signatures and lack evidence of contribution from arc-related magmatic sources. In contrast, chemical and compositional data of samples assigned to the Eurasian margin tend towards active margin signatures. In terms of source rock composition, the available data from Chios, Karaburun and the Konya Complex suggest felsic, amphibolite- to eclogite-facies lithologies as major host rocks. In places, however, material was also derived from (ultra)mafic bodies as documented by provenance sensitive data (bulk geochemistry, single-grain geochemistry) and the presence Cr-spinel in Upper Palaeozoic and Lower Mesozoic rocks of the Chios–Karaburun units.

Overall, the presented data constrain some important parameters in Palaeotethyan evolution and add another piece to the puzzle of palaeotectonic reconstructions. The conclusions drawn from this study contradict palaeogeographic models that place the study areas along an active northern Gondwana margin in Late Palaeozoic time. In

fact, the current findings support a concept combining elements of different palaeotectonic reconstructions. Sediment accumulation for most of the Upper Palaeozoic successions of Chios and Karaburun probably started in mid-Carboniferous times and continued to at least Pennsylvanian–Cisuralian along the southern Eurasian margin, while Palaeotethys lithosphere was subducting. Low textural and compositional maturity of the studied sediments indicate relatively proximal provenance, suggesting detritus was derived from basement rocks of units located along this margin (Sakarya Zone, Sredna Gora Zone, Serbo-Macedonian Massif). Parts of the time-equivalent Halıcı Formation of the Konya Complex, which is probably composed of two or more subunits were deposited along the same active margin. Abundant volcanic fragments and notable Devonian zircon populations led to suggest a magmatic arc could have developed close to the depositional site during that time and provided material for the examined Late Carboniferous–Early Permian units. Furthermore, compositional data of euhedral Cr-spinel from the Lower Triassic Gerence Formation of the Karaburun Peninsula indicate the existence of an intra-oceanic back-arc setting within the Palaeotethys in Palaeozoic time. On the opposite side, the nature of the northern Gondwana margin during that period is controversial. Late Palaeozoic arc-type magmatic rocks have been reported from very few localities only (e.g., Simav area of the northwestern Afyon Zone, Cyclades) and examined samples with northern Gondwana affinity do not record any input of arc-derived material either. Nonetheless, southward subduction beneath Gondwana, as proposed by Xypolias et al. (2006) or Robertson and Ustaömer (2009b) could have been restricted to a short time period or took place at a shallow angle, leaving behind no evidence for arc-related magmatism. In Triassic time, the Eurasian margin was characterised by the opening of several back-arc oceans (e.g., Küre, Meliata, Pindos) in response to Palaeotethyan slab roll-back, separating Eurasia from the Gondwana-derived Cimmerian terranes. This period was also accompanied by the formation of synrift sequences (i.e., Ardıçlı Formation in the Konya area or Gerence Formation on the Karaburun Peninsula) and strong volcanic activity in the larger study area, producing igneous (partially uranium rich) bodies along the Eurasian margin. Palaeotethys subduction probably ceased until Late Triassic time when the final assembly of the Halıcı Formation was completed and a passive margin established along Eurasia.

Bibliography

Abbo A, Avigad D, Gerdes A, Güngör T (2015) Cadomian basement and Paleozoic to Triassic siliciclastics of the Taurides (Karacahisar dome, south-central Turkey): Paleogeographic constraints from U-Pb-Hf in zircons. Lithos, 227:122–139

Akal C, Candan O, Koralay O, Oberhänsli R, Chen F, Prelević D (2012) Early Triassic potassic volcanism in the Afyon Zone of the Anatolides/Turkey: implications for the rifting of the Neo-Tethys. International Journal of Earth Sciences, 101:177–194

Akal C, Koralay O, Candan O, Oberhänsli R, Chen F (2011) Geodynamic significance of the Early Triassic Karaburun granitoid (Western Turkey) for the opening history of Neo-Tethys. Turkish Journal of Earth Sciences, 20:255–271

Allen CM, Barnes CG (2006) Ages and some cryptic sources of Mesozoic plutonic rocks in the Klamath Mountains, California and Oregon. In: AW Snoke, GG Barnes (eds.) Geological studies in the Klamath Mountains Province, California and Oregon: a volume in honor of William P. Irwin. Geological Society of America, Special Papers 410, 223–245

Anders B, Reischmann T, Kostopoulos D (2007) Zircon geochronology of basement rocks from the Pelagonian Zone, Greece: constraints on the pre-Alpine evolution of the westernmost Internal Hellenides. International Journal of Earth Sciences, 96:639–661

Armstrong-Altrin JS, Verma SP (2005) Critical evaluation of six tectonic setting discrimination diagrams using geochemical data of Neogene sediments from known tectonic settings. Sedimentary Geology, 177:115–129

Avigad D, Gerdes A, Morag N, Bechstädt T (2012) Coupled U–Pb–Hf of detrital zircons of Cambrian sandstones from Morocco and Sardinia: implications for provenance and Precambrian crustal evolution of North Africa. Gondwana Research, 21:690–703

Avigad D, Kolodner K, McWilliams M, Persing H, Weissbrod T (2003) Origin of northern Gondwana Cambrian sandstone revealed by detrital zircon SHRIMP dating. Geology, 331:227–230

Aysal N, Ustaömer T, Öngen S, Keskin M, Köksal S, Peytcheva I, Fanning M (2012) Origin of the Early-Middle Devonian magmatism in the Sakarya Zone, NW Turkey: Geochronology, geochemistry and isotope systematics. Journal of Asian Earth Sciences, 45:201–222

Bauluz B, Mayayo MJ, Fernandez-Nieto C, Lopez JMG (2000) Geochemistry of Precambrian and Paleozoic siliciclastic rocks from the Iberian Range (NE Spain): implications for source-area weathering, sorting, provenance, and tectonic setting. Chemical Geology, 168:135–150

Be'eri-Shlevin Y, Katzir Y, Whitehouse MJ, Kleinhanns IC (2009) Contribution of pre Pan-African crust to formation of the Arabian Nubian Shield: new secondary ionization mass spectrometry U–Pb and O studies of zircon. Geology, 37:899–902

Belousova E, Griffin W, O'Reilly SY, Fischer N (2002) Igneous zircon: trace element composition as an indicator of source rock type. Contribution to Mineralogy and Petrology, 143:602–622

Besenecker H, Dürr S, Herget G, Jacobshagen V, Kauffmann GL, Lüdtke G, Roth W, Tietze KW (1968) Geologie von Chios (Ägäis). Geologica et Palaeontologica, 2:121–150

Besenecker H, Dürr S, Herget G, Kauffmann G, Lüdtke G, Roth W, Tietze KW (1971) Geological Map of Greece, Chios sheet, 1:50 000 (two sheets: Northern and Southern). Institute for Geology and Subsurface Research, Athens

Bhatia MR (1983) Plate tectonics and geochemical composition of sandstones. Journal of Geology, 91:611–627

Bhatia MR, Crook AW (1986) Trace element characteristics of graywackes and tectonic setting discrimination of sedimentary basins. Contributions to Mineralogy and Petrology, 92:181–193

Boynton WV (1984) Geochemistry of the rare earth elements: Meteorite studies. In: P Henderson (ed.) Geochemistry of the Rare Earth Elements. Elsevier, 63–114

Bracciali L, Marroni M, Pandolfi L, Rocchi S (2007) Geochemistry and petrography of Western Tethys Cretaceous sedimentary covers (Corsica and Northern Apennines): From source areas to configuration of margins. In: J Arribas, S Critelli, MJ Johnsson (eds.) Sedimentary Provenance and Petrogenesis: Perspectives from Petrography and Geochemistry. Geological Society of American, Special Papers 420, 73–93

Brinkmann R, Flügel E, Jacobshagen V, Lechner H, Rendel B, Trick P (1972) Trias, Jura und Unterkreide der Halbinsel Karaburun (West Anatolien). Geologica et Palaeontologica, 6:139–150

Bröcker M, Pidgeon RT (2007) Protolith ages of meta-igneous and metatuffaceous rocks from the Cycladic Blueschist unit, Greece: results of a reconnaissance U–Pb zircon study. Journal of Geology, 115:83–98

Çakmakoğlu A, Bilgin Z (2006) Pre-Neogene stratigraphy of the Karaburun Peninsula (W of İzmir Turkey). Bulletin Of The Mineral Research and Exploration, 132:33–61

Candan O, Aral C, Koralay OE, Okay AI, Oberhänsli R, Prelević D, Mertz-Kraus R (2016) Carboniferous granites on the northern margin of Gondwana, Anatolide-Tauride Block, Turkey – Evidence for southward subduction of Paleotethys. Tectonophysics, 683:349–366

Candan O, Dora O, Oberhänsli R, Çetinkaplan M, Partzsch J, Warkus F, Dü S (2001) Pan-African high-pressure metamorphism in the Precambrian basement of the Menderes Massif, western Anatolia, Turkey. International Journal of Earth Sciences, 89:793–811

Candan O, Oberhänsli R, Akal C, Koralay OE, Pourteau A, Çetinkaplan M (2009) Stratigraphy and Alpine metamorphism of the Afyon Zone. 62nd Geological Kurultai of Turkey, 13(17):32–33

Caracciolo L, Critelli S, Cavazza W, Meinhold G, von Eynatten H, Manetti P (2015) The Rhodope Zone as a primary sediment source of the southern Thrace basin (NE Greece and NW Turkey): evidence from detrital heavy minerals and implications for central-eastern Mediterranean palaeogeography. International Journal of Earth Sciences, 104:815–832

Carrigan CW, Mukasa SB, Haydoutov I, Kolcheva K (2005) Age of Variscan magmatism from the Balkan sector of the orogen, central Bulgaria. Lithos, 82:125–147

Carrigan CW, Mukasa SB, Haydoutov I, Kolcheva K (2006) Neoproterozoic magmatism and Carboniferous high-grade metamorphism in the Sredna Gora Zone, Bulgaria: An extension of the Gondwana-derived Avalonian-Cadomian belt? Precambrian Research, 147:404–416

Cawood PA, Hawkesworth CJ, Dhuime B (2012) Detrital zircon record and tectonic setting. Geology, 40:875–878

Chatzaras V, Dörr W, Gerdes A, Krahl J, Xypolias P, Zulauf G (2016) Tracking the late Paleozoic to early Mesozoic margin of northern Gondwana in the Hellenides: paleotectonic constraints from U–Pb detrital zircon ages. International Journal of Earth Sciences, 105:1881–1899

Chen F, Siebel W, Satir M, Terzioğlu M, Saka K (2002) Geochronology of the Karadere basement (NW Turkey) and implications for the geological evolution of the İstanbul zone. International Journal of Earth Sciences, 91:469–481

Cookenboo HO, Bustin RM, Wilks KR (1997) Detrital chromian spinel compositions used to reconstruct the tectonic setting of provenance: implications for orogeny in the Canadian Cordillera. Journal of Sedimentary Research, 67:116–123

Daşçı HT, Parlak O, Nurlu N, Bilor Z (2015) Geochemical characteristics and age of metamorphic sole rocks within a Neotethyan ophiolitic mélange from Konya region (central southern Turkey). Geodinamica Acta, 27:223–243

Deer WA, Howie RA, Zussman J (1992) An Introduction to the Rock-Forming Minerals. Longman Group Ltd. Harlow, UK, 712 pp

Dickinson WR, Beard LS, Brakenridge GR, Erjavec JL, Ferguson RC, Inman KF, Knepp RA, Lindberg FA, Ryberg PT (1983) Provenance of North American Phanerozoic sandstones in relation to tectonic setting. Geological Society of America Bulletin, 94:222–235

Dönmez C, Keskin S, Günay K, Çolakoğlu AO, Çiftçi Y, Uysal I, Türkel A, Yıldırım N (2014) Chromite and PGE geochemistry of the Elekdağ Ophiolite (Kastamonu, Northern Turkey): Implications for deep magmatic processes in a supra-subduction zone setting. Ore Geology Reviews, 57:216–228

Dörr W, Zulauf G, Gerdes A, Lahaye Y, Kowalczyk G (2015) A hidden Tonian basement in the eastern Mediterranean: Age constraints from U–Pb data of magmatic and detrital zircons of the External Hellenides (Crete and Peloponnesus). Precambrian Research, 258:83–108

Dott RH (1964) Wacke, graywacke and matrix; what approach to immature sandstone classification? Journal of Sedimentary Petrology, 34:625–632

Engel M, Reischmann T (1998) Single zircon geochronology of orthogneisses from Paros, Greece. Bulletin of the Geological Society of Greece, 32:91–99

Ercan T, Türkecan A, Satır M (2000) Karaburun Yaramadasının Neojen volkanizması [Neogene volcanism of Karaburun Peninsula]. Cumhuriyetin 75. Yıldönümü Yerbilimleri ve Madencilik Kongresi Bildiriler Kitabı, Mineral Research Exploration Institute of Turkey. Ankara, pp. 1–18

Erdoğan B, Altıner D, Güngör T, Özer S (1990) Stratigraphy of Karaburun peninsula. Bulletin of the Mineral Research and Exploration Institute of Turkey, 111:1–23

Erdoğan B, Güngör T, Özer S (2000) Stratigraphy of Karaburun peninsula excursion guide. International Earth Science Colloqium on the Aegean Region (IESCA) 2000, İzmir, pp. 1-32

Eren Y (1993a) Stratigraphy of autochthonous and cover units of the Bozdağlar massif NW Konya. Geological Bulletin of Turkey, 36:7–23

Eren Y (1993b) The geology of the Eldeğ-Derbent-Tepeköy-Söğütözü (Konya) region. Phd thesis (unpublished), Selçuk University Konya, p 224

Eren Y (1996) Stratigraphy and geological evolution of the Bozdağlar Massif in the south of Ilgın and Sarayönü (Konya). In: S Kormaz, M Akçay (eds.) Karadeniz Technical University Department of Geology 30th Year Symposium, Proceedings, II. 694–707

Eren Y (2001) Polyphase alpine deformation at the northern edge of the Menderes-Taurus block, North Konya, central Turkey. Journal of Asian Earth Sciences, 19:737–749

Eren Y, Kurt H (2000) The stratigraphical, geochemical and geodynamical modelling of the northeast margin of Menderes-Taurus Block. Journal of the Faculty of Engineering and Architecture, Selçuk University, Konya, 15:25–41

Eren Y, Kurt H, Rosselet F, Stampfli GM (2004) Palaeozoic deformation and magmatism in the northern area of the Anatolide block (Konya), witness of the Palaeotethys active margin. Eclogae Geologicae Helvetiae, 97:293–306

Erkül ST, Sözbilir H, Erkül F, Helvacı C, Ersoy EY, Sümer Ö (2008) Geochemistry of I-type granitoids in the Karaburun Peninsula, West Turkey: evidence for Triassic continental arc magmatism following closure of the Palaeotethys. Island Arc, 17:394–418

Fedo CM, Sircombe KN, Rainbird RH (2003) Detrital zircon analysis of the sedimentary record. In: JM Hanchar, PO Hoskin (eds.) Zircon, vol 53. Reviews in Mineralogy and Geochemistry, 277–303

Garver JI, Royce PR, Smick TA (1996) Chromium and nickel in shale of the Taconic foreland: a case study for the provenance of fine-grained sediments with an ultramafic source. Journal of Sedimentary Research, 66:100–106

Gehrels GE, Valencia VA, Ruiz J (2008) Enhanced precision, accuracy, efficiency, and spatial resolution of U-Pb ages by laser ablation-multicollector-inductively coupled plasma-mass spectrometry. Geochemistry, Geophysics, Geosystems, 9(3):Q03017

Gessner K, Collins AS, Ring U, Güngör T (2004) Structural and thermal history of poly-orogenic basement: U-Pb geochronology of granitoid rocks in the southern Menderes Massif, Western Turkey. Journal of the Geological Society London, 161:93–101

Göncüoğlu MC, Çapkınoğlu Ş, Gürsu S, Noble P, Turhan N, Tekin UK, Okuyucu C, Göncüoğlu C (2007) The Mississippian in the Central and Eastern Taurides (Turkey): constraints on the tectonic setting of the Tauride–Anatolide Platform. Geologica Carpathica, 58:427–442

Göncüoğlu MC, Kozur HW (1998) Remarks to the pre-Variscan development in Turkey. In: U Linnemann, T Heuse, O Fatka, P Kraft, R Brocke, B Erdtmann (eds.) Pre-Variscan terrane analysis of "Gondwanan Europe". Staatliche Naturhistorische Sammlungen Dresden, Museum für Mineralogie und Geologie, Dresden, 137–138

Göncüoğlu MC, Kozur HW, Turhan N, Göncüoğlu Y (2000) Stratigraphy of the Silurian–Lower Carboniferous rock units in Konya area. In: VIII International Meeting of IGCP 421 in 1st Congresso Iberico de Paleontologia, Evora. 227–228

González-Jiménez JM, Colás V, Sergeeva I, Griffin WL, O'Reilly SY, Gervilla F, Kerestedjian T, Fanlo I, Locmelis M, Pearson N, Belousova E (2012) Back-Arc Origin for Chromitites of the Dobromirtsi Ultramafic Massif. Revista de la Sociedad Española de Mineralogía, 16:240–241

González-Jiménez JM, Locmelis M, Belousova E, Griffin WL, Gervilla F, Kerestedjian T, O'Reilly SY, Pearson NJ, Sergeeva I (2015) Genesis and tectonic implications of podiform chromitites in the metamorphosed ultramafic massif of Dobromirtsi (Bulgaria). Gondwana Research, 27:555–574

Göğer E, Kıral K (1969) Geology of the Kızılören region: Mineral Research and Exploration Institute of Turkey (MTA) 5204

Gradstein FM, Ogg G, Schmitz M (2012) The geologic time scale, 2-volume set. Elsevier, Amsterdam, p 1176

Graf J (2001) Alpine tectonics in western Bulgaria: Cretaceous compression of the Kraište region and Cenozoic exhumation of the crystalline Osogovo-Lisec Complex. Phd thesis, ETH Zürich, Switzerland, p 182

Güven A, Ustaömer T, Peytcheva I (2012) Late Triassic crustal extension in NW Konya (Afyon Zone): new findings from LA-ICP-MS U–Pb zircon dating of the Ladik Dyke Swarm and the Kadınhanı meta-volcanics. In: Proceedings of the 5th Geochemistry Symposium, 23–25 May 2012, Pamukkale University, Denizli-Turkey. pp. 122–123

Herron MM (1988) Geochemical classification of terrigenous sands and shales from core or log data. Journal of Sedimentary Petrology, 58:820–829

Hetzel R, Reischmann T (1996) Intrusion age of Pan-African augen gneisses in the southern Menderes Massif and the age of cooling after Alpine ductile extensional deformation. Geological Magazine, 133:565–572

Hetzel R, Romer RL, Candan O, Passchier CW (1998) Geology of the Bozdag area, central Menderes massif, SW Turkey: Pan-African basement and Alpine deformation. Geologische Rundschau, 87:394–406

Himmerkus F, Reischmann T, Kostopoulos D (2006) Late Proterozoic and Silurian basement units within the Serbo-Macedonian Massif, northern Greece: the significance of terrane accretion in the Hellenides. In: AHF Robertson, D Mountrakis (eds.) Tectonic development of the Eastern Mediterranean Region, volume 260. Geological Society, London, Special Publications, 260, 33–50

Himmerkus F, Reischmann T, Kostopoulos D (2007) Gondwana-derived terranes in the northern Hellenides. In: RD Hatcher, MP Carlson, JH McBride, JR Martínez Catalán (eds.) 4-D Framework of continental crust, vol 200. Geological Society of America, Memoirs, 379–39

Himmerkus F, Reischmann T, Kostopoulos D (2009a) Serbo-Macedonian revisited: a Silurian basement terrane from northern Gondwana in the Internal Hellenides, Greece. Tectonophysics, 473:20–35

Himmerkus F, Reischmann T, Kostopoulos D (2009b) Triassic rift-related meta-granites in the Internal Hellenides, Greece. Geological Magazine, 146:252–265

Hofmann A, Bolhar R, Dirks P, Jelsma H (2003) The geochemistry of Archean shales derived from a Mafic volcanic sequence, Belingwe greenstone belt, Zimbabwe: provenance, source area unroofing and submarine versus subaerial weathering. Geochimica et Cosmochimica Acta, 67:421–440

Ibbeken H, Schleyer R (1991) Source and Sediment: A Case Study of Provenance and Mass Balance at an Active Plate Margin (Calabria, Southern Italy). Springer, Berlin, 286 pp

Ingersoll RV, Bullard TF, Ford RL, Grimm JP, Pickle JD, Sares SW (1984) The effect of grain size on detrital modes: a test of the Gazzi-Dickinson point-counting method. Journal of Sedimentary Petrology, 54:103–116

Jackson SE, Pearson NJ, Griffin WL, Belousova EA (2004) The application of laser ablation-inductively coupled plasma-mass spectrometry to in situ U–Pb zircon geochronology. Chemical Geology, 211:47–69

Jacobshagen V (1986) Geologie von Griechenland. Gebrüder Borntraeger, Berlin, pp 1-363

Johnson PR, Woldehaimanot B (2003) Development of the Arabian–Nubian Shield: perspectives on accretion and deformation in the northern East African Orogen and the assembly of Gondwana. In: M Yoshida, BF Windley (eds.) Proterozoic East Gondwana: Supercontinent Assembly and Breakup. Geological Society, London, Special Publications, 206, 289–325

Johnsson MJ (1993) The system controlling the composition of clastic sediments. In: MJ Johnsson, A Basu (eds.) Processes Controlling the Composition of Clastic Sediments. Geological Society of America, Special Papers 284, 1–19

Kalafatçıoğlu (1961) A geological study in the Karaburun Peninsula. Bulletin of the Mineral Research and Exploration Institute of Turkey, 56:40–49

Kalvoda J (2003) Carboniferous foraminiferal paleobiogeography in Turkey and its implications for plate tectonic reconstructions. Rivista Italiana di Paleontologia e Stratigrafia, 109:255–266

Kamenetsky VS, Crawford AJ, Meffre S (2001) Factors controlling chemistry of magmatic spinel: an empirical study of associated olivine, Cr-spinel and melt inclusions from primitive rocks. Journal of Petrology, 42:655–671

Karaman ME (1986) The geology and tectonic evolution of the Altınekin (Konya) region. Geological Bulletin of Turkey, 29(1):157–171

Kauffmann G (1965) Fossil-belegtes Altpaläozoikum im Nordost-Teil der Insel Chios (Ägäis). Neues Jahrbuch fü Geologie and Paläontologie Monatshefte, 1965:647–659

Keay S, Lister G, Buick I (2001) The timing of partial melting, Barrovian metamorphism and granite intrusion in the Naxos metamorphic core complex, Cyclades, Aegean Sea, Greece. Tectonophysics, 342:275–312

Kilias A (1987) Die Phyllit-Schiefer-Serie der Insel Oinousai: Mikrostrukturen, Kinematik und tektonische Stellung im Helleniden Orogen (Griechenland). Geologica Balcanica, 17:83–90

Kolodner K, Avigad D, McWilliams M, Wooden JL, Weissbrod T, Feinstein S (2006) Provenance of north Gondwana Cambrian–Ordovician sandstone: U–Pb SHRIMP dating of detrital zircons from Israel and Jordan. Geological Magazine, 143:367–391

Kooijman E, Berndt J, Mezger K (2012) U-Pb dating of zircon by laser ablation ICP-MS: recent improvements and new insights. European Journal of Mineralogy, 24:5–21

Koralay OE, Satir M, Dora OÖ (2001) Geochemical and geochronological evidence for Early Triassic calc-alkaline magmatism in the Menderes Massif, western Turkey. International Journal of Earth Sciences, 89:822–835

Kounov A (2002) Thermotectonic evolution of Kraishte, western Bulgaria. Ph.D. thesis. ETH Zürich, Switzerland, p 219

Kozur HW (1995) New stratigraphic results on the Palaeozoic of the Western parts of the Karaburun Peninsula, Western Turkey. In: O PiÅŸkin, M Ergün, MY SavaÅŸçin, G Tarcan (eds.) Proceedings of International Earth Sciences. Colloquium on the Aegean Region, İzmir, 289–308

Kozur HW (1997) First discovery of Muellerisphaerida (inc. sedis) and Eoalbaillella (Radiolaria) in Turkey and the age of the siliciclastic sequence (clastic series) in Karaburun peninsula. Freiberger Forschungshefte C, Geowissenschaften Geologie C, 46:33–59

Kozur HW (1998) The age of the siliciclastic series ("Karareis formation") of the western Karaburun peninsula, western Turkey. In: H Szaniawski (ed.) Proceedings of the Sixth European Conodont Symposium (ECOS VI), vol 58. Palaeontologia Polonica, 171–189

Kozur HW (1999) A review of the systematic position and stratigraphic value of Muellerisphaerida. In: M Tongiorgi, G Palyford (eds.) Studies in Palaeozoic palynology. Selected papers from the CIMP Symposium at Pisa, 1998. Bolletino della Societa Paleontologia Italiano 38, 197–206

Krippner A, Meinhold G, Morton AC, Russell E, von Eynatten H (2015) Grain-size dependence of garnet composition revealed by provenance signatures of modern stream sediments from the western Hohe Tauern (Austria). Sedimentary Geology, 321:25–38

Krippner A, Meinhold G, Morton AC, Schöning J, von Eynatten H (2016) Heavy minerals and garnet geochemistry of stream sediments and bedrocks from the Almklovdalen area, Western Gneiss Region, SW Norway: implications for provenance analysis. Sedimentary Geology, 336:96–105

Krippner A, Meinhold G, Morton AC, von Eynatten H (2014) Evaluation of garnet discrimination diagrams using geochemical data of garnets derived from various host rocks. Sedimentary Geology, 306:36–52

Kröner A, Şengör AMC (1990) Archean and Proterozoic ancestry in late Precambrian to early Paleozoic crustal elements of southern Turkey as revealed by single-zircon dating. Geology, 18:1186–1190

Kurt H (1994) Petrography and Geochemistry of Kadınhanı (Konya) area, Central Turkey. Phd thesis (unpublished), Glasgow University, U.K., p 191

Kurt H (1996) Geochemical characteristics of the meta-igneous rocks near Kadınhanı (Konya), Turkey. Geosound, 28:1–22

Kurt H (1997) Geochemistry of metasedimentary rocks of the Kadınhanı (Konya) area, Turkey. Geosound, 31:1–21

Loos S, Reischmann T (1999) The evolution of the southern Menderes Massif in SW Turkey as revealed by zircon dating. Journal of the Geological Society London, 156:1021–1030

Löwen K, Meinhold G, Güngör T (2018) Provenance and tectonic setting of Carboniferous–Triassic sandstones from the Karaburun Peninsula, western Turkey: A multi-method approach with implications for the Palaeotethys evolution. Sedimentary Geology, 375:232–255

Löwen K, Meinhold G, Güngör T, Berndt J (2017) Palaeotethys-related sediments of the Karaburun Peninsula, western Turkey: constraints on provenance and stratigraphy from detrital zircon geochronology. International Journal of Earth Sciences, 8:2771–2796

Ludwig K (2003) Isoplot/Ex 3.00. A geochronological toolkit for Microsoft Excel. Berkeley Geochronology Center Special Publications:1–70

Lužar-Oberiter B, Mikes T, von Eynatten H, Babić L (2009) Ophiolitic detritus in Cretaceous clastic formations of the Dinarides (NW Croatia): evidence from Cr-spinel chemistry. International Journal of Earth Sciences, 98:1097–1108

Mange MA, Morton AC (2007) Geochemistry of heavy minerals. In: MA Mange, DT Wright (eds.) Heavy Minerals in Use. Developments in Sedimentology 58. Elsevier, Amsterdam, pp 345–391

Marsellos A, Foster DA, Kamenov GD, Kyriakopoulos K (2012) Detrital zircon U-Pb data from the Hellenic south Aegean belts: constraints on the age and source of the South Aegean basement. Journal of the Virtual Explorer:doi:10.3809/jvirtex.2011.00284

Mcbride EF (1963) A classification of common sandstones. Journal of Sedimentary Research, 33:664–669

McLennan SM (1989) Rare earth elements in sedimentary rocks: influence of provenance and sedimentary processes. In: BR Lipin, GA McKay (eds.) Geochemistry and Mineralogy of Rare Earth Elements. Reviews in Mineralogy 21, 169–200

McLennan SM (1990) Geochemical and Nd–Sr isotopic composition of deep-sea turbidites: crustal evolution and plate tectonic associations. Geochimica et Cosmochimica Acta, 54:2015–2050

McLennan SM, Hemming S, McDaniel DK, Hanson GN (1993) Geochemical approaches to sedimentation, provenance, and tectonics. In: MJ Johnsson, A Basu (eds.) Processes Controlling the Composition of Clastic Sediments. Geological Society of America, Special Papers 284, 21–40

Meinhold G (2010) Rutile and its applications in earth sciences. Earth-Science Reviews, 102:1–28

Meinhold G, Anders B, Kostopoulos D, Reischmann T (2008a) Rutile chemistry and thermometry as provenance indicator: An example from Chios Island, Greece. Sedimentary Geology, 203:98–111

Meinhold G, Frei D (2008) Detrital zircon ages from the islands of Inousses and Psara, Aegean Sea, Greece: constraints on depositional age and provenance. Geological Magazine, 145:886–891

Meinhold G, Kostopoulos D, Frei D, Himmerkus F, Reischmann T (2010) U–Pb LA-SF-ICP-MS zircon geochronology of the Serbo-Macedonian Massif, Greece: palaeotectonic constraints for Gondwana-derived terranes in the Eastern Mediterranean. International Journal of Earth Sciences, 99:813–832

Meinhold G, Kostopoulos D, Reischmann T (2007) Geochemical constraints on the provenance and depositional setting of sedimentary rocks from the islands of Chios, Inousses and Psara, Aegean Sea, Greece: implications for the evolution of Palaeotethys. Journal of the Geological Society London, 164:1145–1163

Meinhold G, Morton AC, Avigad D (2013) New insights into peri-Gondwana paleogeography and the Gondwana super-fan system from detrital zircon U–Pb ages. Gondwana Research, 23:661–665

Meinhold G, Morton AC, Fanning CM, Frei D, Howard JP, Phillips RJ, Strogen D, Whitham AG (2011) Evidence from detrital zircons for recycling of Mesoproterozoic and Neoproterozoic crust recorded in Paleozoic and Mesozoic sandstones of southern Libya. Earth and Planetary Science Letters, 312:164–175

Meinhold G, Reischmann T, Kostopoulos D, Lehnert O, Matukov D, Sergeev S (2008b) Provenance of sediments during subduction of Palaeotethys: detrital zircon ages and olistolith analysis in Palaeozoic sediments from Chios Island, Greece. Palaeogeography, Palaeoclimatology, Palaeoecology, 263:71–91

Mitchell AHG, Reading HG (1986) Sedimentation and tectonics. In: HG Reading (ed.) Sedimentary environments and facies, 2nd edition. Oxford, Blackwell, 471–519

Moix P, Beccaletto L, Kozur HW, Hochard C, Rosselet F, Stampfli GM (2008) A new classification of the Turkish terranes and sutures and its implication for the paleotectonic history of the region. Tectonophysics, 451:7–39

Moix P, Vachard D, Allibon J, Martini R, Wernli R, Kozur HW, Stampfli GM (2013) Palaeotethyan, Neotethyan and Huglu-Pindos series in the Lycian Nappes (SW Turkey): geodynamical implications. In: LH Tanner, SJ A, SG Lucas (eds.) The Triassic System. New Mexico Museum of Natural History and Science, New Mexico, 401–444

Morton AC (1985) A new approach to provenance studies: electron microprobe analysis of detrital garnets from Middle Jurassic sandstones of the northern North Sea. Sedimentology, 32:553–566

Morton AC (1991) Geochemical studies of detrital heavy minerals and their application to provenance research. In: A Morton, S Todd, P Haughton (eds.) Developments in Sedimentary Provenance Studies. Geological Society, London, Special Publications, 57, 31–45

Mountrakis D, Sapountzis E, Kilias A, Eleftheriadis G, Christofides G (1983) Paleogeographic conditions in the western Pelagonian margin in Greece during the initial rifting of the continental area. Canadian Journal of Earth Sciences, 20:1673–1681

Mposkos E, Kostopoulos DK, Krohe A (2001) Low-P/high-T pre-Alpine metamorphism and medium-P Alpine overprint of the Pelagonian Zone documented in high-alumina metapelites from the Vernon Massif, western Macedonia, northern Greece. Bulletin of the Geological Society of Greece, 34:949–958

Nance RD, Murphy JB (1994) Contrasting basement isotopic signatures and the palinspastic restoration of peripheral orogens: example from the Neoproterozoic Avalonian-Cadomian belt. Geology, 22:617–620

Okay AI, Satir M, Maluski M, Siyako M, Monie P, Metzger R, Akyüz S (1996) Palaeo- and Neo-Tethyan events in northwestern Turkey: geologic and geochronologic constraints. In: A Yin, T Harrison (eds.) The tectonic evolution of Asia. Cambridge University Press, pp 420–441

Okay AI, Satir M, Shang CK (2008) Ordovician metagranitoid from the Anatolide-Tauride block, northwest Turkey: geodynamic implications. Terra Nova, 20:280–288

Okay AI, Satir M, Siebel W (2006) Pre-Alpide Palaeozoic and Mesozoic orogenic events in the Eastern Mediterranean region. In: D Gee, R Stephenson (eds.) European Lithosphere Dynamics. Geological Society Memoirs 32, 389–405

Okay AI, Satir M, Tüysüz O, Akyüz S, Chen F (2001) The tectonics of the Strandja Massif: late-Variscan and mid-Mesozoic deformation and metamorphism in the Northern Aegean. International Journal of Earth Sciences, 90:217–233

Okay AI, Tüysüz O (1999) Tethyan sutures of northern Turkey. In: B Durand, L Jolivet, F Horivath, M Séranne (eds.) The Mediterranean Basin: tertiary extension within the Alpine Orogen. Geological Society, London, Special Publications, 156, 475–515

Özbey Z, Ustaömer T, Robertson AHF, Ustaömer PA (2013) Tectonic significance of Late Ordovician granitic magmatism and clastic sedimentation on the northern margin of Gondwana (Tavsanli Zone, NW Turkey). Journal of the Geological Society London, 170:159–173

Özcan A, Göncüoğlu MC, Turhan N, Uysal S, Şentürk K, Işık A (1988) Late Palaeozoic evolution of the Kütahaya-Bolkardağ Belt). METU Journal of Pure and Applied Science, 21:211–220

Özcan A, Göncüoğlu MC, Turhan N, Uysal S, Işık A, Şentürk K (1990) Basic Geology of the Konya-Kadınhanı-Ilgın and adjacent areas. Technical Report 9535, MTA

Özmen F, Reischmann T (1999) The age of the Sakarya continent in W Anatolia: implications for the evolution of the Aegean region. Journal of Conference Abstracts, 4:805

Pagé P, Barnes SJ (2009) Using trace elements in chromites to constrain the origin of podiform chromitites in the Thetford Mines Ophiolite, Québec, Canada. Economic Geology, 104:997–1018

Pe-Piper G, Piper DJW (2002) The igneous rocks of Greece: the anatomy of an orogen. Gebrüder Borntraeger, Stuttgart, 573 pp

Peytcheva I, von Quadt A (2004) The Palaeozoic protoliths of the Central Srednogorie, Bulgaria: records in zircons from basement rocks and Cretaceous magmatites. 5th ISEMG Conference Proceedings, 1:392–395

Philippson A (1911) Reisen und Forschungen im westlichen Kleinasien, 2. Heft: Ionien und das westliche Lydien. Peterm Mitt Erg H, 172:1–100

Pober E, Faupl P (1988) The chemistry of detrital chromian spinels and its implications for the geodynamic evolution of the Eastern Alps. Geologische Rundschau, 77:641–670

Potter PE (1978) Petrology and chemistry of modern big river sands. Journal of Geology, 86:423–449

Reischmann T (1998) Pre-alpine origin of tectonic units from the metamorphic complex of Naxos, Greece, identified by single Pb/Pb dating. Bulletin of the Geological Society of Greece, 32:101–111

Robertson AHF, Clift PD, Degnan P, Jones G (1991) Palaeogeographic and palaeotectonic evolution of the Eastern Mediterranean Neotethys. Palaeogeography, Palaeoclimatology, Palaeoecology, 87:289–344

Robertson AHF, Pickett EA (2000) Palaeozoic–Early Tertiary Tethyan evolution of mélanges, rift and passive margin units in the Karaburun Peninsula (western Turkey) and Chios Island (Greece). In: E Bozkurt, JA Winchester, JDA Piper (eds.) Tectonic and magmatism in Turkey and the surrounding area. Geological Society, London, Special Publications, 173, 43–82

Robertson AHF, Ustaömer T (2009a) Formation of the Late Palaeozoic Konya Complex and comparable units in southern Turkey by subduction–accretion processes: Implications for the tectonic development of Tethys in the Eastern Mediterranean region. Tectonophysics, 473:113–148

Robertson AHF, Ustaömer T (2009b) Upper Palaeozoic subduction/accretion processes in the closure of Palaeotethys: Evidence from the Chios Melange (E Greece), the Karaburun Melange (W Turkey) and the Teke Dere Unit (SW Turkey). Sedimentary Geology, 220:29–59

Robertson AHF, Ustaömer T (2011) Role of tectonic-sedimentary melange and Permian–Triassic cover units, central southern Turkey in Tethyan continental margin evolution. Journal of Asian Earth Sciences, 40:98–120

Robertson AHF, Ustaömer T, Pickett EA, Collins AS, Andrew T, Dixon JE (2004) Testing models of Late Palaeozoic-Early Mesozoic orogeny in Western Turkey: support for an evolving open-Tethys model. Journal of the Geological Society London, 161:501–511

Romano SS, Dörr W, Zulauf G (2004) Significant Pb loss of Cadomian zircons due to Alpine subduction of pre-Alpine basement of eastern Crete (Greece). International Journal of Earth Sciences, 93:844–859

Roser BP, Korsch RJ (1986) Determination of tectonic setting of sandstone–mudstone suites using SiO_2 content and K_2O/Na_2O ratio. Journal of Geology, 94:635–650

Rosselet F, Stampfli G (2003) The Paleozoic siliclastic sequences in Karaburun, a remnant of the Paleotethys fore-arc basin in Western Turkey. Geophysical Research Abstracts, 5:09770

Rudnick RL, Gao S (2003) Composition of the continental crust. Treatise on Geochemistry, 3:1–64

Şengör AMC, Yilmaz Y (1981) Tethyan evolution of Turkey: a plate tectonic approach. Tectonophysics, 75:181–241

Şengör AMC, Yilmaz Y, Sungurlu O (1984) Tectonics of the Mediterranean Cimmerides: nature and evolution of the western termination of Palaeo-Tethys. In: JE Dixon, AHF Robertson (eds.) The geological evolution of the eastern Mediterranean. Geological Society, London, Special Publications, 17, 77–112

Sestini G (1970) Flysch facies and turbidite sedimentology. Sedimentary Geology, 4:559–597

Spencer CJ, Prave AR, Cawood PA, Roberts NMW (2014) Detrital zircon geochronology of the Grenville/Llano foreland and basal Sauk Sequence in west Texas, USA. Bulletin of the Geological Society of America, 126:1117–1128

Stampfli GM (2000) Tethyan oceans. In: E Bozkurt, JA Winchester, JDA Piper (eds.) Tectonics and magmatism in Turkey and the surrounding area, vol 173. Geological Society, London, Special Publications, 173, 1–23

Stampfli GM, Borel G (2002) A plate tectonic model for the Paleozoic and Mesozoic constrained by dynamic plate boundaries and restored synthetic oceanic isochrons. Earth and Planetary Science Letters, 196:17–33

Stampfli GM, Borel G, Cavazza W, Mosar J, Ziegler PA (2001a) The Palaeotectonic atlas of the Peritethyan domain. CD ROM. European Geophysical Society

Stampfli GM, Hochard C, Vérard C, Wilhem C, von Raumer J (2013) The formation of Pangea. Tectonophysics, 593:1–19

Stampfli GM, Mosar J, Favre P, Pillevuit A, Vannay JC (2001b) Permo-Mesozoic evolution of the western Tethyan realm: the Neotethys/East-Mediterranean connection. In: PA Ziegler, W Cavazza, AHF Robertson, S Crasquin-Soleau (eds.) PeriTethys memoir 6: Peritethyan rift/wrench basins and passive margins, IGCP 369. Mémoires du Muséum National d'Histoire Naturelle 186, 51–108

Stampfli GM, Vavassis I, De Bono A, Rosselet F, Matti B, Bellini M (2003) Remnants of the Paleotethys oceanic suture-zone in the western Tethyn area. In: G Cassinis (ed.) Stratigraphic and structural Evolution on the Late Carboniferous to Triassic Continental and marine successions in Tuscany (Italy): Regional Reports and General Correlation. Bolletino della Società Geologica Italiana vol. speciale 2, 1–23

Stampfli GM, von Raumer J, Borel GD (2002) Palaeozoic evolution of pre-Variscan terranes: From Gondwana to the Variscan collision. In: JR Martínez-Catalán, RD Hatcher, F Díaz García (eds.) Variscan-Appalachian dynamics: the building of the late Paleozoic basement, vol. 364. Geological Society of American, Special Papers 364, 263–280

Sunal G (2012) Devonian magmatism in the western Sakarya Zone, Karacabey region, NW Turkey. Geodinamica Acta, 25:183–201

Taylor SR, McLennan SM (1985) The continental crust: its composition and evolution. Blackwell Scientific Publications, Oxford, pp 312

Titorenkova R, Macheva L, Zidarov N, von Quadt A, Peytcheva I (2003) Metagranites from SW Bulgaria as a part of the Neoproterozoic to early Paleozoic system in Europe: new insight from zircon typology, U-Pb isotope data and Hf-tracing. Geophysical Research Abstracts, 5:08963

Tomaschek F, Kennedy A, Keay S, Ballhaus C (2001) Geochronological constraints on Carboniferous and Triassic magmatism in the cyclades: SHRIMP U–Pb ages of zircons from Syros, Greece. Journal of Conference Abstracts, 6:315

Tomkins HS, Powell R, Ellis DJ (2007) The pressure dependence of the zirconium-in-rutile thermometer. Journal of Metamorphic Geology, 25:703–713

Triebold S, von Eynatten H, Luvizotto GL, Zack T (2007) Deducing source rock lithology from detrital rutile geochemistry: an example from the Erzgebirge, Germany. Chemical Geology, 244:421–436

Triebold S, von Eynatten H, Zack T (2012) A recipe for the use of rutile in sedimentary provenance analysis. Sedimentary Geology, 282:268–275

Turpaud P, Reischmann T (2010) Characterisation of igneous terranes by zircon dating: implications for UHP occurrences and suture identification in the Central Rhodope, northern Greece. International Journal of Earth Sciences, 99:567–591

Ustaömer PA, Mundil R, Renne PR (2005) U/Pb and Pb/Pb zircon ages for arc-related intrusions of the Bolu Massif (W Pontides, NW Turkey): evidence for Late Precambrian (Cadomian) age. Terra Nova, 17:215–223

Ustaömer PA, Ustaömer T, Robertson AHF (2012) Ion probe U–Pb dating of the central Sakarya basement: a peri-Gondwana terrane intruded by Late Lower Carboniferous subduction/collision-related granitic rocks. Turkish Journal of Earth Sciences, 21:905–932

Ustaömer T, Robertson AHF (1997) Tectonic-sedimentary evolution of the north Tethyan margin in the Central Pontides of northern Turkey. In: AG Robinson (ed.) Regional and Petroleum Geology of the Black Sea and Surrounding Region. American Association of Petroleum Geologists Memoirs 68, 255–290

Ustaömer T, Robertson AHF (1999) Geochemical evidence used to test alternative plate tectonic models for pre-Upper Jurassic (Paleo-Tethyan) units in the Central Pontides, N. Turkey. Geological Journal, 34:25–54

Ustaömer T, Ustaömer PA, Robertson AHF, Gerdes A (2016a) Implications of U–Pb and Lu–Hf isotopic analysis of detrital zircons for the depositional age, provenance and tectonic setting of the Permian–Triassic Palaeotethyan Karakaya Complex, NW Turkey. International Journal of Earth Sciences, 105:7–38

Ustaömer T, Ustaömer PA, Robertson AHF, Gerdes A (2016b) Testing alternative tectonic models of Palaeotethys in the E Mediterranean region: New U-Pb and Lu-Hf isotopic analyses of detrital zircons from Late Carboniferous and Late Triassic sandstones associated with the Anatolide and Tauride blocks (S Turkey): EGU General Assembly 2016. Geophysical Research Abstracts, 18:EGU2016–15469–1

Ustaömer T, Ustaömer PA, Robertson AHF, Gerdes A (2018) U-Pb and Lu-Hf isotopic data from detrital zircons in Late Carboniferous and Late Triassic sandstones used to determine provenance and test alternative tectonic models of the tectonic setting of the Anatolide and Taurides, S Turkey: Abstracts, GeoBonn 2018, 2–6th 2018, Bonn, Germany:65

Verma SP, Armstrong-Altrin JS (2013) New multi-dimensional diagrams for tectonic discrimination of siliciclastic sediments and their application to Precambrian basins. Chemical Geology, 355:117–133

Verma SP, Armstrong-Altrin JS (2016) Geochemical discrimination of siliciclastic sediments from active and passive margin settings. Sedimentary Geology, 332:1–12

Vermeesch P (2012) On the visualisation of detrital age distributions. Chemical Geology, 312–313:190–194

von Quadt A, Graf J, Bernoulli D (2000) Pre-Variscan and Tertiary magmatism in western Bulgaria (Kraiste) based on U–Pb single zircon analyses, trace and REE element distribution and Sm/Nd – Rb/Sr investigation. Terra Nostra:1(2000):87

von Raumer J, Stampfli GM, Borel G, Bussy F (2002) Organizationn of pre-Variscan basement areas at the North-Gondwanan margin. International Journal of Earth Sciences:35–52

Wiedenbeck M, Allé P, Corfu F, Griffin WL, Meier M, Oberli F, von Quadt A, Roddick JC, Spiegel W (1995) Three natural zircon standards for U–Th–Pb, Lu–Hf, trace element and REE analyses. Geostandards Newsletter, 19:1–23

Wiesner K (1938) Konya mercury deposits and studies on them. Mineral Research and Exploration Bulletin, 70:178–213

Windley BF (1995) The evolving continents, 3rd edn. Wiley, Chichester, pp 544

Wright WI (1938) The composition and occurrence of garnets. American Mineralogist, 23:436–449

Xypolias P, Dörr W, Zulauf G (2006) Late Carboniferous plutonism within the pre-Alpine basement of the External Hellenides (Kithira, Greece): evidence from U-Pb zircon dating. Journal of the Geological Society London, 163:539–547

Xypolias P, Koukouvelas I, Zulauf G (2008) Cenozoic tectonic evolution of northeastern Apulia: insights from a key study area in the Hellenides (Kythira, Greece). Zeitschrift der Deutschen Gesellschaft für Geowissenschaften, 159:439–455

Zack T, Luvizotto GL (2006) Application of rutile thermometry to eclogites. Mineralogy and Petrology, 88:69–85

Zack T, Moraes R, Kronz A (2004a) Temperature dependence of Zr in rutile: empirical calibration of a rutile thermometer. Contributions to Mineralogy and Petrology, 148:471–488

Zack T, von Eynatten H, Kronz A (2004b) Rutile geochemistry and its potential use in quantitative provenance studies. Sedimentary Geology, 171:37–58

Zanchi A, Garzanti E, Larghi C, Angiolini L, Gaetani M (2003) The Variscan orogeny in Chios (Greece): Carboniferous accretion along a Palaeotethyan active margin. Terra Nova, 15:213–223

Ziegler PA, Stampfli GM (2001) Late Paleozoic Early Mesozoic plate boundary reorganisation: collapse of the Variscan orogen and opening of Neotethys. In: R Cassinis (ed.) The continental Permian of the Southern Alps and Sardinia (Italy) regional reports and general correlations. Annali Museo Civico Science Naturali, Brescia, 25, 17–34

Zlatkin O, Avigad D, Gerdes A (2013) Evolution and provenance of Neoproterozoic basement and Lower Paleozoic siliciclastic cover of the Menderes Massif (western Taurides): coupled U-Pb-Hf zircon isotope geochemistry. Gondwana Research, 23:682–700

Zulauf G, Dörr W, Fisher-Spurlock SC, Gerdes A, Chatzaras V, Xypolias P (2015) Closure of the Paleotethys in the external Hellenides: Constraints from U–Pb ages of magmatic and detrital zircons (Crete). Gondwana Research, 28:642–667

Zulauf G, Dörr W, Krahl J, Lahaye Y, Chatzaras V, Xypolias P (2016) U–Pb zircon and biostratigraphic data of high-pressure/low-temperature metamorphic rocks of the Talea Ori: tracking the Paleotethys suture in central Crete, Greece. International Journal of Earth Sciences, 105:1901–1922

Appendix

Manuscript I: Supplementary data

- **Table A.1: Main and trace element data from XRF and ICP-MS analysis**
- **Table A.2: Operating conditions for EMPA**
- **Table A.3: Composition of detrital chrome spinels from the Karaburun Peninsula**
- **Table A.4: Composition of detrital rutiles from the Karaburun Peninsula**
- **Table A.5: Composition of detrital garnets from the Karaburun Peninsula**

Table A.1: Main and trace element data from XRF and ICP-MS analysis

	Güvercinlik Formation		Gerence Formation		İdecik unit				Dikendağı Formation					Küçükbahçe Formation				Alandere Fm.
Sample	KAR 20A	KAR 20B	KAR 1	KAR 2	KAR 3	KAR 4	KAR 5	KAR 6	KAR 7	KAR 14	KAR 15	KAR 23	KAR 9	KAR 10	KAR 11	KAR 25A	KAR 27	KAR 22
Major elements in wt.%																		
SiO_2	90.31	97.25	61.94	68.44	77.65	74.72	82.86	75.75	63.77	80.36	73.52	81.9	74.9	74.38	77.03	77.39	76.34	74.81
TiO_2	0.139	0.053	0.434	0.724	0.8	0.764	0.471	0.512	0.719	0.565	0.79	0.467	0.676	0.616	0.635	0.634	0.553	0.602
Al_2O_3	3.57	1.16	9.73	14.58	11.37	12.42	7.91	9.68	17.16	10.65	12.7	9.02	12.34	11.75	11.06	10.83	10.57	10.97
MnO	0.005	0.015	0.231	0.054	0.027	0.048	0.03	0.057	0.098	0.075	0.057	0.101	0.02	0.087	0.051	0.026	0.069	0.046
MgO	0.01	0.01	1.97	1.85	0.36	0.39	0.76	1.31	1.72	0.29	1.75	0.23	0.59	0.71	1.05	0.39	1.64	1.82
CaO	1.21	0.06	8.28	0.43	0.44	0.3	0.18	1.81	0.63	0.18	0.24	0.07	0.17	0.73	0.25	0.08	0.32	0.65
Na_2O	0.01	0	2.13	2.32	1.84	1.98	1.5	1.95	5.49	0.69	1.46	0.62	2.32	2.54	2.22	2.05	1.91	2.27
K_2O	0.3	0.05	0.51	2.14	1.58	1.89	1.11	1.21	2.09	2.01	2.29	1.62	1.9	1.67	1.36	1.8	1.3	1.34
P_2O_5	0.017	0.041	0.071	0.109	0.149	0.134	0.071	0.077	0.175	0.136	0.124	0.098	0.114	0.118	0.12	0.088	0.087	0.11
$Fe_2O_{3(tot)}$	1.21	0.64	5.36	5.69	2.9	3.86	2.96	3.59	5.09	1.95	4.71	3.07	3.92	4.09	3.84	3.99	4.85	4.43
LOI	2.33	0.46	10.49	4.05	3.01	2.93	1.96	3.32	3.5	2.73	2.3	2.58	2.36	2.72	2.5	2.19	2.32	3.01
Total	99.11	99.74	101.15	100.39	100.13	99.44	99.81	99.27	100.44	99.64	99.94	99.78	99.31	99.41	100.12	99.47	99.96	100.06
Trace elements in ppm																		
Ba	36	23	340	353	220	324	145	195	779	245	299	214	339	268	224	290	201	183
Ce	17	15	17	48	63	57	47	45	72	63	56	53	59	51	49	54	53	42
Co	2	4	14	13	9	9	6	8	8	8	14	9	8	7	9	7	14	11
Cr	33	14	240	73	52	53	30	95	26	37	144	30	54	54	66	61	114	160
Cu	1	1	19	18	30	8	8	1	9	12	7	16	10	10	8	15	9	12
Ga	4	1	8	19	13	15	9	11	21	14	16	12	15	14	14	13	12	13
Hf	3.6	1.2	1.5	3.9	6.3	5.2	5	4.1	7.5	5.9	5.2	5.9	5	4.2	4.4	4	4.5	4.2
La	9	7	8	25	30	28	22	22	37	30	33	25	30	27	24	26	27	19
Mo	1.7	0.9	2.1	1.3	1.2	1.5	1	1.3	1.6	0.9	0.9	1.1	1	1	0.7	0.7	1.2	0.7
Nb	4	1	3	13	15	13	10	10	17	13	14	11	13	12	11	11	10	9
Nd	9	4	9	22	26	27	20	18	33	26	27	22	25	22	22	24	21	18
Ni	3	10	56	37	11	17	10	45	5	11	57	17	20	22	26	23	58	53
Pb	9	9	8	13	13	10	11	13	22	67	9	24	15	12	14	9	13	12
Rb	14	4	19	89	67	76	46	52	116	90	72	73	80	72	62	73	58	53
S	6	20	80	9	12	24	9	49	6	10	19	23	14	1	10	35	52	42
Sc	5	2	18	11	8	8	7	7	16	6	8	8	9	10	7	10	8	9
Sm	3	1.7	2.8	4.8	5.6	6	4.8	4.4	6.9	5.7	6.2	4.9	5.1	5	5.4	5.3	4.3	4.2
Sr	12	13	142	67	65	73	37	99	187	47	51	45	59	51	40	54	36	59
Th	3.4	1.9	3.4	8.6	10.1	8.3	8.7	8.2	12.7	10.7	9	9.6	8.8	8.3	6.6	7.3	8.2	7.3
U	1	0.5	1	2.1	2.3	2	2.3	2.2	3.4	2.7	2.4	2.6	2.3	2.2	2	1.9	2	1.9
V	25	15	108	103	82	80	49	59	80	59	83	51	75	71	81	78	65	86
Y	10	5	18	23	19	28	16	17	21	25	27	22	27	25	23	24	18	18
Yb	2.3	2.3	2.1	2.1	2.3	2.4	2.2	1.8	1.8	2.8	2.4	2.8	2.2	2.3	2.2	2.1	2.2	2
Zn	8	5	47	79	51	62	39	41	77	35	62	41	63	55	54	48	59	56
Zr	154	52	65	147	274	188	216	158	337	258	222	259	191	168	187	179	173	156
Rare earth elements in ppm																		
La		8.1	6.9		31.6				39.0	28.9			27.6		24.2			21.0
Ce		11.8	15.3		63.4				74.5	58.5			56.1		49.9			42.7
Pr		1.7	2.0		7.4				8.6	6.8			6.7		6.0			5.0
Nd		6.1	8.8		27.6				32.5	25.1			25.2		22.7			19.0
Sm		1.1	2.3		5.1				6.1	4.9			5.1		4.6			3.7
Eu		0.2	0.7		1.1				2.2	1.0			0.9		0.9			0.8
Gd		1.0	2.4		4.2				5.1	4.4			4.3		4.0			3.4
Tb		0.1	0.4		0.5				0.6	0.6			0.6		0.5			0.5
Dy		0.8	2.9		3.0				3.6	3.6			3.4		3.3			3.0
Ho		0.2	0.6		0.6				0.7	0.7			0.7		0.6			0.6
Er		0.4	1.7		1.7				1.9	1.9			1.8		1.8			1.7
Tm		0.1	0.2		0.2				0.3	0.3			0.3		0.3			0.3
Yb		0.4	1.7		1.7				1.8	1.9			1.8		1.8			1.8
Lu		0.1	0.2		0.2				0.2	0.3			0.2		0.3			0.2

Major and trace elements were analysed by XRF
Rare earth elements were measured by ICP-MS

Table A.2: Operating conditions for EMPA

Garnet	***Acc. voltage: 15 kV***	***Beam Diameter: 5 µm***	***Beam current: 20 nA***
Spectrometer	***Element (line)***	***Count time***	***Backgr.***	***Standard***
1 TAP	Si (Kα)	15	5	Garnet, nat.
1 TAP	Al (Kα)	15	5	Garnet, nat.
2 TAP	Mg (Kα)	15	5	MgO, synth.
3 PETJ	Ca (Kα)	15	5	$CaSiO_3$, nat.
4 PETJ	Ti (Kα)	30	15	TiO_2, synth.
4 PETJ	Cr (Kα)	30	15	Cr_2O_3
5 LIFH	Mn (Kα)	30	15	Rhodonite
5 LIFH	Fe (Kα)	15	5	Fe_2O_3
4 LIF	Ti (Kα)	15	5	TiO_2Rt
5 LIFH	W (Lα)	100	50	W_metallic

Rutile	***Acc. voltage: 25 kV***	***Beam Diameter: 10 µm***	***Beam current: 80 nA***
Spectrometer	**Element (line)**	**Count time**	**Backgr.**	**Standard**
1 PETJ	Nb (Lα)	200	100	Nb_metallic
2 TAP	Si (Kα)	100	50	$ZrSiO_4$
5 PETH	Zr (Lα)	200	100	$ZrSiO_4$
1 PETJ	Sn (Lα)	100	50	Cassiterite
2 TAP	Al (Kα)	200	100	Al_2O_3
4 LIF	V (Kα)	200	100	V_metallic
3 LIF	Cr (Kα)	200	100	Cr_2O_3
3 LIF	Fe (Kα)	100	50	Hematite

Cr-spinel	***Acc. voltage: 20 kV***	***Beam Diameter: 5 µm***	***Beam current: 20 nA***
Spectrometer	**Element (line)**	**Count time**	**Backgr.**	**Standard**
1 TAP	Mg (Kα)	15	5	MgO
2 TAP	Al (Kα)	15	5	Al_2O_3
2 TAP	Si (Kα)	15	5	Wollastonite
3 PETJ	Cr (Kα)	30	15	Cr_2O_3
3 PETJ	Ti (Kα)	30	15	TiO_2
4 LIF	Fe (Kα)	15	5	Hematite
4 LIF	Mn (Kα)	30	15	Rhodonite
5 LIFH	V (Kα)	30	15	V_metallic
5 LIFH	Ni (Kα)	30	15	NiO
5 LIFH	Zn (Kα)	30	15	Ghanite

Table A.3: Composition of detrital chrome spinels from the Karaburun Peninsula

No.	Sample	MgO	Al2O3	Cr2O3	FeO	V2O3	SiO2	TiO2	MnO	NiO	ZnO	Total
1	KAR1	6.47	14.07	47.80	29.64	0.18	<0.022	0.30	0.49	0.04	0.37	99.37
2	KAR1	12.50	15.72	49.18	21.93	0.11	0.05	0.37	0.21	0.07	0.09	100.24
3	KAR1	15.49	10.36	57.31	16.04	0.07	0.08	0.25	0.17	0.18	<0.033	99.96
4	KAR1	10.35	9.46	59.45	20.22	0.15	0.02	0.07	0.30	0.04	0.15	100.20
5	KAR1	9.13	10.30	52.08	26.93	0.16	<0.022	0.31	0.35	0.04	0.18	99.52
6	KAR1	7.94	11.40	50.08	28.94	0.25	0.02	0.38	0.42	0.06	0.22	99.72
7	KAR1	9.97	27.32	31.87	29.97	0.16	<0.022	0.11	0.32	0.12	0.24	100.07
8	KAR1	12.27	22.98	43.60	20.42	0.19	0.02	0.13	0.24	0.11	0.27	100.22
9	KAR1	14.67	17.36	50.55	16.81	0.10	0.11	0.37	0.21	0.17	0.06	100.40
10	KAR1	6.00	12.72	50.60	29.06	0.17	<0.023	0.28	0.39	0.09	0.41	99.71
11	KAR1	11.55	8.03	56.64	22.66	0.22	0.03	0.33	0.25	0.06	0.07	99.84
12	KAR1	14.78	17.95	48.71	17.16	0.16	0.05	0.40	0.19	0.10	0.06	99.55
13	KAR1	14.82	13.63	53.85	16.70	0.17	<0.022	0.41	0.22	0.11	<0.033	99.95
14	KAR1	14.38	10.23	56.98	18.24	0.10	0.17	0.27	0.18	0.13	0.07	100.74
15	KAR1	8.82	12.23	49.62	28.25	0.21	<0.022	0.38	0.39	0.05	0.17	100.12
16	KAR1	13.24	13.99	52.64	19.41	0.18	0.03	0.30	0.26	0.07	0.07	100.17
17	KAR1	16.08	12.27	57.31	13.92	0.08	0.09	0.23	0.20	0.21	0.04	100.43
18	KAR1	6.96	10.71	48.55	32.07	0.19	<0.023	0.33	0.40	0.07	0.18	99.47
19	KAR1	9.88	15.32	49.98	23.65	0.14	0.06	0.37	0.33	0.08	0.10	99.90
20	KAR1	9.07	12.65	53.25	24.07	0.14	<0.023	0.25	0.34	0.05	0.22	100.05
21	KAR1	9.82	22.60	42.28	23.89	0.16	<0.022	0.34	0.38	0.07	0.37	99.91
22	KAR1	9.46	24.31	35.65	28.75	0.24	<0.022	0.40	0.31	0.10	0.29	99.49
23	KAR1	14.71	21.29	44.16	18.50	0.11	0.08	0.42	0.18	0.15	0.04	99.64
24	KAR1	9.39	12.91	48.35	27.84	0.14	<0.023	0.32	0.34	0.03	0.20	99.51
25	KAR1	7.91	12.66	49.02	28.69	0.22	0.03	0.36	0.39	0.05	0.20	99.52
26	KAR1	8.53	8.58	53.59	28.23	0.21	0.04	0.28	0.32	0.04	0.10	99.91
27	KAR1	12.54	12.92	49.89	22.99	0.19	0.07	0.73	0.23	0.11	0.04	99.72
28	KAR1	13.73	7.18	61.73	16.59	0.14	0.03	0.22	0.26	0.04	0.03	99.94
29	KAR1	8.60	10.25	52.09	27.50	0.16	<0.023	0.35	0.37	0.06	0.15	99.54
30	KAR1	8.71	14.87	46.62	28.28	0.19	<0.022	0.43	0.36	0.07	0.22	99.76
31	KAR1	7.90	21.91	34.92	33.22	0.19	<0.022	0.53	0.35	0.11	0.26	99.39
32	KAR1	15.25	12.05	55.61	15.95	0.13	0.04	0.31	0.19	0.13	0.04	99.71
33	KAR1	12.27	8.50	61.69	16.89	0.10	<0.022	0.19	0.24	0.06	0.05	99.99
34	KAR1	15.36	10.15	58.39	15.52	0.11	0.06	0.26	0.20	0.13	<0.033	100.18
35	KAR1	9.75	16.52	45.28	26.86	0.14	0.07	0.27	0.35	0.13	0.25	99.62
36	KAR1	11.13	20.28	43.91	23.30	0.19	<0.021	0.36	0.27	0.07	0.19	99.71
37	KAR1	12.79	25.84	35.20	24.47	0.13	0.06	0.53	0.24	0.15	0.08	99.49
38	KAR1	13.65	9.61	57.05	18.68	0.15	0.02	0.33	0.26	0.07	0.05	99.86
39	KAR1	7.75	8.83	51.40	30.13	0.18	<0.023	0.28	0.41	0.08	0.15	99.22
40	KAR1	13.55	19.66	46.15	19.71	0.12	0.03	0.43	0.21	0.17	0.07	100.12
41	KAR1	13.69	9.33	57.34	19.00	0.13	0.06	0.31	0.20	0.05	0.05	100.17
42	KAR1	14.85	11.36	57.08	16.21	0.13	0.04	0.29	0.23	0.10	0.03	100.34
43	KAR1	7.28	10.97	49.20	30.33	0.20	<0.023	0.35	0.42	0.06	0.16	98.97
44	KAR1	8.53	15.19	46.71	27.90	0.23	0.03	0.40	0.36	0.04	0.23	99.63
45	KAR1	16.08	12.88	55.01	15.34	0.09	0.25	0.29	0.17	0.21	0.05	100.36
46	KAR1	10.49	16.98	42.42	27.96	0.27	<0.023	0.72	0.30	0.10	0.10	99.34
47	KAR1	9.90	15.06	49.61	23.94	0.19	<0.023	0.27	0.29	0.08	0.20	99.54
48	KAR1	15.41	37.34	29.13	16.92	0.09	<0.021	0.07	0.18	0.17	0.30	99.61
49	KAR1	8.62	13.84	48.72	27.20	0.20	<0.023	0.41	0.34	0.08	0.20	99.59
50	KAR1	11.89	8.86	56.76	21.56	0.17	0.05	0.33	0.28	0.08	0.08	100.06
51	KAR1	13.69	19.08	47.95	17.84	0.11	0.05	0.38	0.23	0.13	0.08	99.53
52	KAR1	14.20	26.25	39.04	19.37	0.15	0.09	0.39	0.20	0.14	0.08	99.90
53	KAR1	14.57	15.01	51.67	17.76	0.13	0.07	0.39	0.19	0.15	0.05	99.98
54	KAR1	9.67	11.66	51.96	25.56	0.16	<0.023	0.34	0.36	0.06	0.14	99.90
55	KAR1	8.09	18.65	40.35	31.03	0.34	<0.022	0.61	0.34	0.08	0.23	99.73
56	KAR1	15.02	8.80	60.61	15.11	0.10	<0.023	0.21	0.21	0.10	0.05	100.23
57	KAR22	8.03	9.26	55.88	25.10	0.18	<0.023	0.33	0.37	0.03	0.12	99.30
58	KAR22	14.31	24.76	44.48	15.47	0.22	<0.021	0.02	0.22	0.09	0.12	99.70
59	KAR22	10.35	16.70	48.09	23.02	0.21	<0.023	0.55	0.37	0.04	0.16	99.50
60	KAR22	14.20	24.07	44.52	16.30	0.20	0.03	<0.017	0.18	0.08	0.11	99.72
61	KAR22	14.73	29.07	38.54	16.93	0.19	<0.020	0.06	0.19	0.11	0.16	100.01
62	KAR22	14.72	28.91	39.71	15.49	0.20	<0.020	0.03	0.17	0.11	0.21	99.57

Table A.3 Continued

No.	Sample	MgO	Al2O3	Cr2O3	FeO	V2O3	SiO2	TiO2	MnO	NiO	ZnO	Total
63	KAR22	12.05	19.06	49.37	18.32	0.22	0.03	0.04	0.25	0.04	0.19	99.56
64	KAR22	14.54	28.91	39.26	15.81	0.22	<0.021	0.02	0.18	0.11	0.17	99.23
65	KAR22	9.76	14.07	50.84	24.17	0.11	<0.022	0.29	0.32	0.06	0.19	99.81
66	KAR22	13.95	23.28	45.34	16.51	0.20	0.05	0.04	0.20	0.12	0.16	99.85
67	KAR22	13.63	26.83	41.18	17.44	0.24	<0.021	0.03	0.22	0.08	0.29	99.95
68	KAR22	13.22	15.69	55.22	15.30	0.20	<0.023	0.10	0.25	0.06	0.12	100.15
69	KAR22	14.10	30.45	37.07	16.78	0.20	<0.020	0.02	0.19	0.09	0.22	99.12
70	KAR22	14.18	11.17	57.08	16.80	0.25	0.08	0.13	0.18	0.10	0.04	100.00
71	KAR22	13.04	23.28	45.02	17.68	0.26	<0.021	0.02	0.22	0.07	0.14	99.74
72	KAR22	15.95	38.33	28.15	16.40	0.19	<0.020	0.03	0.16	0.14	0.20	99.55
73	KAR22	11.72	19.19	49.03	19.55	0.17	<0.022	0.07	0.26	0.06	0.18	100.24
74	KAR22	14.33	27.64	41.25	15.43	0.21	<0.021	0.02	0.17	0.08	0.17	99.31
75	KAR22	13.43	24.60	43.07	18.22	0.23	<0.022	0.08	0.22	0.08	0.15	100.07
76	KAR22	13.36	25.71	42.52	17.78	0.26	<0.021	0.03	0.24	0.08	0.20	100.19
77	KAR22	7.83	7.60	61.70	21.96	0.26	<0.023	<0.019	0.34	<0.020	0.24	99.97
78	KAR22	10.30	9.52	58.49	20.41	0.13	<0.023	0.27	0.27	0.07	0.15	99.61
79	KAR22	12.30	27.06	38.93	20.96	0.21	<0.021	0.07	0.22	0.07	0.22	100.06
80	KAR22	13.74	21.50	47.51	16.68	0.23	<0.022	0.02	0.19	0.09	0.14	100.10
81	KAR22	13.08	21.73	47.24	16.66	0.24	<0.022	0.03	0.19	0.07	0.18	99.42
82	KAR22	11.79	20.66	47.71	18.99	0.26	0.02	<0.018	0.24	0.06	0.22	99.95
83	KAR22	10.13	19.26	46.66	23.07	0.22	0.04	<0.018	0.30	0.10	0.37	100.14
84	KAR22	15.52	31.59	37.75	14.31	0.17	0.02	0.05	0.16	0.10	0.15	99.80
85	KAR22	12.04	22.51	43.41	20.93	0.26	<0.021	0.19	0.27	0.12	0.21	99.94
86	KAR22	13.20	21.36	48.21	16.53	0.28	<0.021	<0.018	0.21	0.07	0.15	100.04
87	KAR22	7.45	10.12	49.73	30.79	0.17	<0.023	0.31	0.41	0.05	0.18	99.20
88	KAR22	11.78	25.76	39.93	21.66	0.17	<0.021	0.27	0.25	0.10	0.21	100.14
89	KAR22	13.93	23.07	42.73	19.11	0.16	0.04	0.15	0.19	0.12	0.16	99.66
90	KAR22	14.77	27.69	41.44	14.97	0.18	0.03	0.03	0.20	0.10	0.16	99.56
91	KAR22	13.00	24.27	44.34	17.66	0.27	<0.021	0.03	0.21	0.08	0.23	100.07
92	KAR22	14.04	27.65	40.32	16.79	0.22	<0.021	0.02	0.22	0.09	0.13	99.50
93	KAR22	11.23	15.23	53.74	18.87	0.23	<0.022	0.07	0.26	0.04	0.17	99.86
94	KAR22	15.35	30.73	30.87	21.07	0.18	0.04	0.40	0.19	0.08	0.07	98.97
95	KAR22	13.20	21.94	47.15	16.95	0.23	0.03	0.02	0.21	0.08	0.11	99.92
96	KAR22	8.12	11.12	55.20	24.57	0.19	<0.023	0.11	0.33	0.08	0.21	99.95
97	KAR22	13.64	27.41	36.78	20.95	0.25	<0.021	0.45	0.24	0.13	0.21	100.04
98	KAR27	12.00	17.66	51.54	17.84	0.23	<0.022	<0.018	0.24	0.06	0.16	99.74
99	KAR27	10.62	16.85	48.97	21.48	0.24	0.04	0.07	0.27	0.08	0.22	98.85
100	KAR27	10.02	10.43	58.97	19.51	0.20	<0.022	0.04	0.29	0.03	0.18	99.67
101	KAR27	14.48	23.89	45.09	16.00	0.16	<0.022	0.07	0.18	0.11	0.08	100.06
102	KAR27	13.50	24.87	41.74	18.53	0.20	<0.022	0.21	0.22	0.07	0.14	99.48
103	KAR27	12.10	18.32	50.06	18.57	0.29	<0.022	<0.018	0.26	0.04	0.19	99.86
104	KAR27	10.21	18.12	49.95	20.77	0.27	<0.021	<0.018	0.30	0.02	0.31	99.97
105	KAR27	7.45	8.72	58.20	24.74	0.27	<0.023	0.06	0.37	0.02	0.26	100.10
106	KAR27	9.10	17.13	50.85	21.77	0.35	<0.022	0.03	0.33	<0.019	0.39	99.97
107	KAR27	13.92	10.99	55.98	17.63	0.19	0.05	0.59	0.24	0.11	<0.033	99.73
108	KAR27	12.55	20.22	49.04	18.04	0.20	<0.022	0.05	0.24	0.08	0.13	100.55
109	KAR27	9.30	15.87	46.91	26.38	0.22	<0.023	0.11	0.33	0.09	0.27	99.49
110	KAR27	11.70	19.40	49.41	18.43	0.27	<0.021	<0.018	0.27	0.06	0.17	99.73
111	KAR27	10.26	13.15	55.33	20.34	0.25	<0.023	0.04	0.27	0.06	0.18	99.89
112	KAR27	12.61	22.29	45.97	18.20	0.24	<0.022	0.06	0.22	0.07	0.20	99.87
113	KAR27	8.13	11.66	48.51	30.18	0.21	<0.022	0.37	0.34	0.07	0.20	99.69
114	KAR27	10.41	11.82	57.01	20.11	0.18	<0.022	0.08	0.29	0.04	0.12	100.07
115	KAR27	11.11	16.19	53.22	18.53	0.25	<0.022	0.03	0.25	0.07	0.17	99.82
116	KAR27	15.14	27.56	42.37	13.96	0.20	<0.021	0.03	0.15	0.12	0.10	99.64
117	KAR27	12.81	16.38	52.82	17.23	0.12	0.02	0.15	0.22	0.09	0.05	99.89
118	KAR27	13.57	23.32	46.07	16.24	0.16	<0.021	0.14	0.26	0.07	0.17	100.01
119	KAR27	9.15	10.91	58.26	20.55	0.17	<0.023	0.06	0.34	0.04	0.22	99.72
120	KAR27	4.66	2.27	55.34	35.49	0.15	<0.024	0.03	0.49	0.06	0.30	98.79
121	KAR27	5.47	9.42	55.51	28.45	0.18	<0.023	0.06	0.51	<0.020	0.32	99.93
122	KAR27	12.02	10.09	59.73	17.64	0.07	<0.023	0.14	0.27	0.05	0.05	100.06

Table A.4: Composition of detrital rutiles from the Karaburun Peninsula

No.	Sample	Nb2O5	Al2O3	Cr2O3	TiO2	ZrO2	SnO2	SiO2	FeO	V2O3	WO3	Total
1	KAR20A	0.07	0.02	0.05	99.80	0.01	<0.007	0.03	0.17	0.08	<0.010	100.23
2	KAR20A	0.17	0.04	0.18	99.19	0.07	0.01	0.04	0.10	0.10	<0.010	99.92
3	KAR20A	0.58	0.05	0.08	98.36	0.03	0.03	0.02	0.59	0.11	0.02	99.87
4	KAR20A	0.42	0.02	0.11	98.26	0.06	0.03	0.02	0.34	0.31	0.05	99.62
5	KAR20A	0.05	0.01	0.05	99.11	0.05	<0.007	0.03	0.58	0.22	<0.010	100.11
6	KAR20A	0.20	0.02	0.11	99.64	0.01	0.01	0.03	0.25	0.13	0.01	100.41
7	KAR20A	0.07	0.04	0.77	98.47	0.18	0.01	0.02	0.23	0.15	<0.010	99.94
8	KAR20A	0.37	0.03	0.06	98.36	<0.005	0.01	0.03	0.49	0.18	0.02	99.55
9	KAR20A	0.08	0.06	<0.003	99.14	0.10	0.01	0.12	0.61	0.09	<0.010	100.22
10	KAR20A	0.60	0.02	0.08	98.76	0.02	0.02	0.03	0.39	0.24	<0.010	100.16
11	KAR20A	0.13	0.02	0.06	99.55	0.03	0.01	0.03	0.28	0.16	<0.010	100.26
12	KAR20A	0.08	0.02	0.01	100.09	0.05	<0.007	0.03	0.47	0.12	0.01	100.87
13	KAR20A	0.39	0.07	0.17	99.39	0.02	0.02	0.02	0.38	0.18	0.03	100.67
14	KAR20A	0.33	0.03	0.14	99.44	0.01	0.01	0.03	0.40	0.35	0.27	101.01
15	KAR20A	0.36	0.02	0.17	99.38	0.03	0.02	0.03	0.22	0.30	0.02	100.55
16	KAR20A	0.08	0.04	0.06	99.08	0.01	<0.007	0.04	0.22	0.41	<0.010	99.96
17	KAR20A	0.34	0.04	0.14	98.91	0.03	0.03	0.02	0.34	0.23	0.07	100.15
18	KAR20A	0.03	0.02	0.05	99.64	<0.005	<0.007	0.02	0.21	0.22	<0.010	100.21
19	KAR20A	0.28	0.06	0.08	99.65	0.01	0.01	0.02	0.32	0.18	0.05	100.66
20	KAR20A	0.26	0.01	0.18	99.86	0.52	<0.007	0.03	0.11	0.49	<0.010	101.48
21	KAR20A	0.09	0.01	0.28	99.72	0.01	0.01	0.03	0.18	0.31	<0.010	100.65
22	KAR20A	0.31	0.01	0.10	100.06	0.02	0.01	0.02	0.35	0.15	0.02	101.04
23	KAR20A	0.18	0.02	0.01	100.18	0.11	0.03	0.03	0.30	0.38	0.08	101.32
24	KAR20A	0.66	0.02	0.10	98.65	0.03	0.02	0.03	0.53	0.18	0.03	100.25
25	KAR20A	0.40	0.01	0.12	99.34	0.06	0.01	0.02	0.31	0.21	0.01	100.50
26	KAR20A	0.31	0.02	0.10	98.23	0.01	0.02	0.03	0.39	0.20	0.02	99.33
27	KAR20A	0.22	0.03	0.17	100.16	0.07	0.02	0.02	0.16	0.31	0.06	101.21
28	KAR20A	0.02	0.01	0.07	100.10	0.01	<0.007	0.04	0.60	0.18	<0.010	101.03
29	KAR20A	0.19	0.05	0.16	99.22	0.04	0.01	0.05	0.37	0.13	<0.010	100.23
30	KAR20A	0.11	0.02	0.01	99.58	0.03	0.02	0.03	0.21	0.25	0.04	100.30
31	KAR20A	0.31	0.08	0.01	98.20	0.04	0.03	0.10	0.56	0.17	0.07	99.58
32	KAR20A	0.28	0.01	0.40	99.40	0.11	0.01	0.03	0.09	0.42	0.03	100.77
33	KAR20A	0.17	0.04	0.06	98.98	0.29	0.01	0.02	0.15	0.37	0.01	100.11
34	KAR20A	0.38	0.13	0.29	97.67	0.03	<0.007	0.25	0.31	0.12	<0.010	99.19
35	KAR20A	0.11	0.01	0.42	99.49	<0.005	0.03	0.02	0.05	0.24	<0.010	100.38
36	KAR20A	0.23	0.08	0.08	99.82	0.01	0.01	0.05	0.28	0.16	<0.010	100.72
37	KAR20A	0.19	0.02	0.03	99.96	0.02	0.01	0.02	0.45	0.13	0.01	100.85
38	KAR20A	0.55	0.03	0.06	98.87	0.06	0.03	0.03	0.59	0.19	0.04	100.44
39	KAR20A	0.04	0.04	0.07	100.04	0.12	<0.007	0.03	0.47	0.31	<0.010	101.14
40	KAR20A	0.02	0.03	0.01	100.27	0.01	<0.007	0.03	0.43	0.11	<0.010	100.92
41	KAR20A	0.31	0.10	0.28	98.97	0.11	<0.007	0.33	0.09	0.03	<0.010	100.22
42	KAR20A	0.12	0.01	0.38	100.33	0.19	<0.007	0.04	0.12	0.64	<0.010	101.82
43	KAR20A	0.01	0.06	0.04	99.84	0.05	<0.007	0.04	0.16	0.30	<0.010	100.52
44	KAR20A	0.32	0.16	0.74	98.60	0.04	<0.007	0.28	0.56	0.21	0.02	100.93
45	KAR20A	0.07	0.02	0.04	99.34	0.05	<0.007	0.07	0.53	0.19	<0.010	100.31
46	KAR20A	0.34	0.04	0.22	98.94	0.04	0.02	0.03	0.23	0.30	0.04	100.20
47	KAR3	0.08	1.40	0.02	96.34	0.02	<0.007	1.00	0.26	0.20	<0.010	99.33
48	KAR3	0.06	0.02	0.04	99.41	0.01	<0.007	0.03	0.15	0.21	<0.010	99.93
49	KAR3	0.09	0.01	0.03	98.71	0.04	<0.008	0.03	0.54	0.15	0.03	99.63
50	KAR3	0.15	0.03	0.10	98.46	0.11	0.01	0.02	0.09	0.49	0.03	99.51
51	KAR3	0.13	0.01	0.20	98.06	0.05	0.02	0.02	0.04	0.66	0.03	99.23
52	KAR3	0.38	0.01	0.56	98.68	0.12	0.02	0.02	0.04	0.33	0.06	100.22
53	KAR3	0.32	0.01	0.02	97.86	0.03	0.03	0.05	0.48	0.26	<0.010	99.05
54	KAR3	0.23	<0.002	0.27	98.71	0.13	0.02	0.03	0.06	0.37	0.06	99.87
55	KAR3	2.00	0.03	1.25	95.32	0.09	0.01	0.01	0.15	0.32	<0.010	99.18
56	KAR3	0.02	0.01	0.10	98.62	<0.005	0.01	0.03	0.06	0.42	0.03	99.29
57	KAR3	0.67	0.03	0.05	96.72	0.07	0.01	0.04	0.98	0.11	0.56	99.24
58	KAR3	0.33	0.02	0.08	98.27	0.02	0.02	0.02	0.23	0.20	0.02	99.21
59	KAR3	0.06	0.01	0.26	99.06	0.02	<0.008	0.02	0.25	0.19	<0.010	99.87
60	KAR3	0.05	0.03	0.09	99.26	0.15	<0.007	0.02	0.13	0.29	<0.010	100.02
61	KAR3	0.11	0.01	0.15	98.78	0.05	0.02	0.02	0.18	0.23	<0.010	99.55
62	KAR3	0.01	0.03	0.13	98.56	0.03	<0.008	0.03	0.21	0.43	<0.010	99.45

Table A.4 Continued

No.	Sample	Nb2O5	Al2O3	Cr2O3	TiO2	ZrO2	SnO2	SiO2	FeO	V2O3	WO3	Total
63	KAR3	0.36	0.02	0.11	98.51	0.11	0.02	0.03	0.20	0.21	0.02	99.58
64	KAR3	0.07	0.01	0.07	98.02	0.01	0.04	0.05	0.23	0.28	<0.010	98.79
65	KAR3	0.23	0.27	0.06	98.10	0.11	0.02	0.32	0.19	0.12	0.02	99.43
66	KAR3	0.22	0.01	0.25	98.15	0.15	0.01	0.03	0.05	0.44	0.04	99.36
67	KAR3	0.17	0.05	0.01	97.94	0.01	0.01	0.15	0.45	0.20	<0.010	99.00
68	KAR3	0.11	0.01	0.19	98.16	0.02	0.01	0.05	0.06	0.39	<0.010	99.00
69	KAR3	0.29	0.03	0.11	97.65	0.03	0.01	0.02	0.15	0.31	0.09	98.70
70	KAR3	0.26	0.02	0.17	97.65	0.09	0.01	0.02	0.15	0.56	<0.010	98.92
71	KAR3	0.20	0.04	0.15	97.37	0.02	0.01	0.02	1.13	0.09	0.04	99.09
72	KAR3	0.12	0.01	0.08	98.84	0.03	0.01	0.02	0.11	0.21	0.02	99.45
73	KAR3	0.35	0.04	0.08	98.15	0.02	0.02	0.03	0.28	0.33	0.02	99.31
74	KAR3	0.12	0.02	0.10	97.99	0.03	0.02	0.02	0.13	0.40	0.02	98.85
75	KAR3	0.02	0.01	0.04	97.91	0.01	0.01	0.03	0.34	0.48	<0.010	98.85
76	KAR3	0.18	0.07	0.36	98.15	0.04	<0.007	0.04	0.17	0.16	<0.010	99.19
77	KAR3	0.13	0.02	0.22	98.49	0.28	<0.007	0.02	0.04	0.65	0.01	99.86
78	KAR3	0.31	0.01	0.13	96.83	0.45	0.03	0.04	0.25	0.40	0.15	98.58
79	KAR4	0.11	0.02	0.01	99.60	0.07	0.01	0.04	0.15	0.06	0.04	100.09
80	KAR4	0.07	0.01	0.10	99.23	0.01	<0.008	0.03	0.11	0.25	<0.010	99.82
81	KAR4	0.22	0.01	0.37	98.52	0.03	<0.008	0.03	0.13	0.36	0.02	99.71
82	KAR4	0.16	<0.002	0.19	99.23	0.02	<0.008	0.03	0.15	0.25	0.02	100.05
83	KAR4	0.02	0.02	0.35	99.10	0.01	0.01	0.03	0.07	0.16	<0.010	99.78
84	KAR4	0.01	0.01	0.01	99.57	0.02	<0.008	0.03	0.27	0.11	<0.010	100.03
85	KAR4	0.30	0.10	0.37	99.03	<0.006	0.01	0.06	0.13	0.12	<0.011	100.11
86	KAR4	0.29	0.01	0.19	98.71	0.08	<0.008	0.07	0.24	0.03	<0.011	99.64
87	KAR4	0.06	0.03	0.21	100.07	0.02	<0.008	0.02	0.17	0.19	<0.010	100.78
88	KAR4	0.71	<0.002	0.11	98.77	0.12	0.01	0.04	0.58	0.17	<0.011	100.54
89	KAR4	0.15	0.01	0.16	99.98	0.01	0.01	0.04	0.15	0.12	0.03	100.67
90	KAR4	0.62	0.05	0.04	99.19	0.06	0.02	0.03	0.40	0.18	<0.011	100.59
91	KAR4	0.61	0.07	0.09	98.26	0.05	0.04	0.03	0.42	0.22	0.03	99.81
92	KAR4	0.14	0.06	0.05	100.58	0.06	<0.008	0.03	0.28	0.11	<0.011	101.31
93	KAR4	<0.008	0.01	0.01	99.79	0.02	<0.008	0.05	0.31	0.14	<0.011	100.33
94	KAR4	0.16	0.04	0.03	100.65	0.02	0.01	0.02	0.37	0.12	<0.010	101.42
95	KAR4	0.02	0.01	0.01	99.91	0.04	<0.008	0.02	0.43	0.24	<0.011	100.69
96	KAR4	0.42	0.02	0.06	99.98	0.02	0.04	0.03	0.41	0.10	0.03	101.11
97	KAR4	0.31	0.01	0.13	100.10	0.12	0.01	0.04	0.46	0.09	0.03	101.30
98	KAR4	0.08	0.01	0.20	99.30	0.06	<0.008	0.03	0.38	0.19	<0.010	100.25
99	KAR4	0.08	0.12	0.36	95.74	0.20	<0.008	2.01	0.25	0.30	<0.010	99.08
100	KAR4	0.03	0.01	0.04	100.96	0.04	0.01	0.03	0.43	0.13	<0.010	101.68
101	KAR4	0.03	0.01	0.30	99.27	0.02	<0.008	0.02	0.19	0.12	<0.010	99.97
102	KAR4	0.01	0.02	0.02	99.64	0.03	0.01	0.03	0.19	0.20	<0.010	100.15
103	KAR4	<0.008	0.01	0.06	98.87	0.02	<0.008	0.03	0.31	0.34	<0.010	99.64
104	KAR4	0.08	<0.002	0.60	98.58	0.01	<0.008	0.02	0.08	0.23	<0.010	99.60
105	KAR4	0.16	0.08	0.12	97.66	0.04	<0.008	0.08	0.12	0.35	<0.010	98.60
106	KAR4	0.04	0.02	0.16	98.75	0.05	<0.008	0.02	0.33	0.08	<0.010	99.44
107	KAR4	0.06	0.02	0.10	98.72	0.01	0.01	0.03	0.23	0.28	<0.010	99.45
108	KAR4	0.52	0.07	0.04	98.80	0.06	<0.008	0.04	0.36	0.15	<0.010	100.04
109	KAR4	<0.008	0.02	0.12	99.07	0.03	<0.008	0.03	0.18	0.21	<0.010	99.66
110	KAR4	0.25	0.02	0.10	99.07	0.08	0.02	0.02	0.35	0.22	0.03	100.15
111	KAR4	0.04	0.02	0.03	99.29	0.02	<0.008	0.05	0.27	0.14	0.02	99.89
112	KAR4	0.13	<0.002	0.63	98.46	0.31	<0.008	0.02	0.05	0.09	<0.011	99.71
113	KAR4	0.01	<0.002	0.05	97.18	0.05	0.01	0.03	1.33	0.26	<0.010	98.90
114	KAR4	0.25	0.02	0.16	98.39	0.04	0.01	0.02	0.21	0.19	<0.010	99.30
115	KAR4	0.01	0.11	0.05	98.05	0.01	<0.008	0.20	0.13	0.28	<0.010	98.85
116	KAR4	0.07	0.01	0.12	99.01	0.04	<0.008	0.07	0.11	0.33	<0.010	99.77
117	KAR4	0.02	<0.002	0.05	99.82	0.06	0.01	0.03	0.21	0.12	<0.010	100.33
118	KAR4	0.30	0.01	0.06	99.10	0.01	0.01	0.03	0.33	0.15	<0.010	100.01
119	KAR4	0.08	0.01	0.12	99.12	0.06	<0.008	0.03	0.28	0.37	<0.010	100.07
120	KAR4	0.08	0.02	0.08	99.40	0.01	0.01	0.03	0.36	0.08	<0.010	100.06
121	KAR4	0.13	0.02	0.23	98.54	0.02	0.02	0.02	0.16	0.16	<0.010	99.28
122	KAR4	0.87	0.05	0.10	98.03	0.08	0.02	0.03	0.62	0.17	0.11	100.09
123	KAR4	0.03	0.01	0.03	100.46	0.03	<0.008	0.02	0.24	0.17	<0.010	101.00
124	KAR4	0.56	0.03	0.14	98.37	0.03	0.02	0.03	0.30	0.24	0.07	99.79

Table A.4 Continued

No.	Sample	Nb2O5	Al2O3	Cr2O3	TiO2	ZrO2	SnO2	SiO2	FeO	V2O3	WO3	Total
125	KAR4	0.43	0.06	0.09	98.17	0.06	<0.008	0.02	0.45	0.27	0.02	99.58
126	KAR4	0.01	0.01	0.30	99.16	0.04	<0.008	0.03	0.18	0.12	<0.010	99.85
127	KAR4	0.23	0.06	0.05	98.11	0.14	0.02	0.04	0.22	0.17	<0.010	99.04
128	KAR4	0.23	0.03	0.03	98.44	0.01	<0.008	0.02	0.43	0.19	0.10	99.50
129	KAR7	0.08	0.01	0.58	97.52	0.58	<0.008	0.02	0.06	0.38	0.01	99.24
130	KAR7	0.02	0.01	0.40	99.45	0.13	<0.008	0.02	0.01	0.36	<0.010	100.40
131	KAR7	0.04	0.02	<0.004	99.46	0.02	<0.008	0.04	0.45	0.08	<0.010	100.13
132	KAR7	0.07	0.02	0.05	99.28	0.01	<0.007	0.03	0.18	0.12	<0.010	99.77
133	KAR7	0.14	0.18	0.04	97.62	0.18	<0.008	0.37	0.49	0.40	0.09	99.51
134	KAR7	0.39	0.06	0.08	98.37	0.08	0.02	0.03	0.77	0.38	0.02	100.20
135	KAR7	0.34	0.04	0.01	98.93	0.06	0.02	0.02	0.47	0.10	0.15	100.14
136	KAR7	0.14	0.02	0.25	99.88	0.15	0.01	0.05	0.06	0.01	0.02	100.59
137	KAR7	0.09	0.03	0.01	99.18	0.04	<0.007	0.03	0.56	0.25	0.01	100.20
138	KAR7	0.35	0.03	0.05	97.53	0.03	0.01	0.04	0.34	0.16	0.01	98.57
139	KAR7	0.05	<0.002	0.05	97.37	0.08	<0.008	0.06	0.04	0.01	<0.010	97.66
140	KAR7	0.22	0.05	0.09	97.60	0.09	<0.008	0.09	0.15	0.43	0.01	98.74
141	KAR7	0.09	0.04	0.05	95.82	0.24	0.01	0.14	0.22	0.06	<0.010	96.68
142	KAR7	0.33	0.01	0.05	97.29	0.10	0.01	0.02	0.12	0.27	<0.010	98.21
143	KAR7	0.03	0.02	0.04	96.94	0.03	<0.008	0.04	0.40	0.10	<0.010	97.60
144	KAR7	0.16	0.28	0.05	96.26	0.05	<0.008	0.27	0.58	0.05	0.03	97.73
145	KAR7	0.22	0.13	0.08	96.60	0.09	<0.008	0.42	0.08	0.02	<0.010	97.65
146	KAR7	0.09	<0.002	0.06	98.35	0.12	<0.008	0.04	0.08	0.02	0.02	98.78
147	KAR7	0.13	0.01	0.08	98.51	0.15	<0.008	0.06	0.05	< 0.00	<0.010	98.98
148	KAR7	0.15	0.01	0.09	98.39	0.16	<0.008	0.08	0.04	0.04	0.01	98.97
149	KAR7	0.19	0.11	0.09	96.88	0.09	<0.008	0.42	0.09	0.01	<0.010	97.89
150	KAR7	0.25	0.03	0.18	98.08	0.08	0.01	0.06	0.03	0.07	<0.010	98.80
151	KAR7	0.22	0.15	0.09	96.30	0.12	<0.008	0.55	0.09	0.02	<0.010	97.55
152	KAR7	0.21	0.05	0.29	96.70	0.09	<0.008	0.08	0.06	0.07	<0.010	97.56
153	KAR7	0.18	<0.002	0.84	96.93	0.14	<0.008	0.01	0.09	0.47	0.01	98.68
154	KAR7	0.44	0.01	0.33	97.51	0.05	<0.008	0.04	0.35	0.05	<0.010	98.77
155	KAR7	0.13	<0.002	0.35	97.49	0.03	0.01	0.02	0.15	0.12	<0.010	98.31
156	KAR7	0.18	0.09	0.09	95.74	0.02	0.01	0.19	0.48	0.10	0.07	96.98
157	KAR7	0.04	<0.002	0.17	97.24	0.06	<0.008	0.03	0.04	0.31	<0.010	97.89
158	KAR7	0.17	0.01	0.11	97.44	0.10	<0.008	0.02	0.05	0.62	<0.010	98.52
159	KAR5	0.39	0.02	0.08	99.66	0.01	0.01	0.02	0.21	0.27	<0.010	100.67
160	KAR5	0.39	0.03	0.10	99.50	0.03	0.01	0.03	0.17	0.34	<0.010	100.61
161	KAR5	0.04	0.03	0.04	100.06	0.06	<0.008	0.03	0.13	0.22	<0.010	100.60
162	KAR5	0.29	0.01	0.17	98.67	0.07	0.03	0.03	0.03	0.91	<0.010	100.20
163	KAR5	0.02	0.01	0.09	99.47	0.03	0.01	0.03	0.06	0.51	<0.010	100.24
164	KAR5	0.41	0.01	0.12	98.44	0.04	0.01	0.03	0.80	0.07	0.02	99.96
165	KAR5	0.03	0.01	0.13	99.47	0.04	0.01	0.02	0.02	0.83	<0.010	100.57
166	KAR5	0.22	0.01	0.11	100.90	0.07	<0.008	0.02	0.04	0.42	<0.010	101.80
167	KAR5	0.12	0.01	0.07	99.55	0.14	<0.008	0.04	0.07	0.48	<0.010	100.49
168	KAR5	0.16	0.02	0.18	100.21	0.14	0.03	0.03	0.12	0.59	<0.010	101.48
169	KAR5	0.18	0.03	0.33	99.67	0.02	<0.008	0.07	0.02	0.07	<0.010	100.39
170	KAR5	0.43	0.04	0.11	99.04	0.10	0.03	0.03	0.24	0.28	0.04	100.33
171	KAR5	0.16	0.02	0.74	98.19	0.44	<0.008	0.02	0.06	0.58	<0.010	100.22
172	KAR5	0.08	0.01	0.16	99.11	0.44	0.01	0.03	0.11	0.19	<0.010	100.14
173	KAR5	0.10	0.01	0.22	99.23	0.10	0.01	0.03	0.06	0.45	0.02	100.22
174	KAR5	0.10	0.02	0.05	99.09	0.01	<0.008	0.03	0.43	0.17	<0.010	99.90
175	KAR5	0.55	0.01	0.16	99.11	0.02	0.04	0.05	0.61	0.08	0.05	100.68
176	KAR5	0.32	0.02	0.02	99.03	0.06	0.01	0.02	0.34	0.19	0.05	100.06
177	KAR5	0.18	0.07	0.63	98.19	<0.005	0.01	0.17	0.10	0.19	<0.010	99.55
178	KAR5	0.51	0.02	0.11	98.62	0.05	0.01	0.03	0.23	0.30	<0.010	99.88
179	KAR5	0.31	0.08	0.57	97.24	0.01	0.02	0.11	0.58	0.19	0.85	99.97
180	KAR5	0.40	0.03	0.08	98.59	0.09	<0.008	0.03	0.16	0.36	0.02	99.76
181	KAR5	0.24	0.02	0.17	98.84	0.09	0.01	0.02	0.05	0.47	0.03	99.94
182	KAR5	0.17	<0.002	0.19	98.06	0.08	0.05	0.02	0.01	0.55	0.03	99.16
183	KAR5	0.14	0.01	0.15	98.21	0.01	<0.008	0.03	0.53	0.12	<0.010	99.19
184	KAR5	0.04	0.01	0.07	98.20	0.08	<0.008	0.03	0.16	0.17	<0.010	98.76
185	KAR5	0.35	0.01	0.14	97.89	0.01	<0.008	0.03	0.59	0.08	<0.010	99.11
186	KAR5	0.48	0.01	0.06	98.07	0.06	0.02	0.03	0.28	0.25	0.01	99.27

Table A.4 Continued

No.	Sample	Nb2O5	Al2O3	Cr2O3	TiO2	ZrO2	SnO2	SiO2	FeO	V2O3	WO3	Total
187	KAR5	0.04	0.02	0.10	99.65	0.02	0.02	0.03	0.09	0.19	<0.010	100.15
188	KAR5	0.22	0.03	0.24	97.30	0.04	<0.008	0.01	0.12	0.21	0.02	98.20
189	KAR5	0.70	0.08	0.09	96.82	0.06	0.02	0.03	0.53	0.20	0.15	98.67
190	KAR5	0.28	0.03	0.10	97.97	0.07	0.01	0.04	0.16	0.21	0.01	98.89
191	KAR5	0.02	0.02	0.01	98.85	0.07	<0.008	0.03	0.51	0.16	<0.010	99.67
192	KAR5	0.15	0.02	0.06	98.99	<0.005	0.06	0.03	0.12	0.37	<0.010	99.80
193	KAR5	0.15	<0.002	0.15	98.33	0.07	0.01	0.02	0.09	0.83	<0.010	99.66
194	KAR5	0.31	0.03	0.10	98.50	0.02	0.02	0.02	0.23	0.18	0.04	99.46
195	KAR5	0.82	0.03	0.08	97.20	0.01	0.02	0.03	0.56	0.25	0.02	99.02
196	KAR5	0.17	0.01	0.11	98.47	0.01	0.02	0.03	0.13	0.33	0.02	99.29
197	KAR5	0.19	0.02	0.07	97.98	0.04	0.03	0.02	0.21	0.27	<0.010	98.84
198	KAR5	0.14	0.01	0.12	98.40	0.03	<0.007	0.02	0.44	0.12	<0.010	99.28
199	KAR5	0.15	0.01	0.13	97.74	0.02	0.02	0.03	0.08	0.38	0.05	98.60
200	KAR5	0.08	0.03	0.04	100.40	0.01	<0.007	0.03	0.21	0.19	<0.010	100.99
201	KAR5	0.51	0.02	0.23	97.43	0.02	0.01	0.03	0.22	0.45	<0.010	98.92
202	KAR5	0.21	0.02	0.07	99.00	0.05	<0.007	0.02	0.11	0.27	<0.010	99.75
203	KAR5	0.22	0.02	0.01	97.92	0.05	0.02	0.03	0.16	0.24	0.04	98.71
204	KAR5	0.72	0.08	0.02	97.67	0.10	0.01	0.03	0.46	0.18	<0.010	99.27
205	KAR5	0.19	0.02	0.23	98.57	0.15	<0.007	0.05	0.05	0.05	<0.010	99.32
206	KAR5	0.13	0.02	0.09	98.51	0.26	<0.007	0.02	0.10	0.27	<0.010	99.38
207	KAR5	0.38	<0.002	0.03	97.95	0.01	<0.007	0.03	0.62	0.13	<0.010	99.14
208	KAR5	0.16	0.01	0.14	98.25	0.04	0.01	0.02	0.04	0.49	0.04	99.19
209	KAR5	0.21	0.07	0.23	98.24	0.07	<0.007	0.18	0.08	0.07	<0.010	99.15
210	KAR5	0.48	0.01	0.11	98.03	0.12	<0.008	0.03	0.27	0.27	0.08	99.40
211	KAR5	0.05	0.01	0.06	99.36	<0.005	0.01	0.03	0.10	0.25	<0.010	99.86
212	KAR5	0.18	0.02	0.23	98.29	0.04	<0.008	0.03	0.36	0.14	<0.010	99.30
213	KAR10	0.11	0.02	0.25	99.15	0.03	<0.008	0.22	0.15	0.12	<0.010	100.05
214	KAR10	0.13	0.03	0.45	98.16	0.05	<0.007	0.03	0.11	0.18	<0.010	99.15
215	KAR10	<0.008	0.02	0.12	98.50	0.01	<0.007	0.04	0.07	0.34	<0.010	99.10
216	KAR10	0.05	0.02	0.12	100.04	0.08	<0.008	0.02	0.18	0.11	<0.010	100.63
217	KAR10	0.10	0.03	0.11	99.43	0.06	<0.007	0.04	0.23	0.18	<0.010	100.18
218	KAR10	0.02	0.01	0.36	98.67	0.08	<0.008	0.02	0.07	0.14	<0.010	99.39
219	KAR10	0.05	0.02	<0.003	98.71	0.03	0.01	0.04	0.15	0.19	0.03	99.23
220	KAR10	0.73	0.09	0.06	97.45	0.04	0.01	0.03	0.52	0.15	0.02	99.08
221	KAR10	0.01	0.02	0.05	98.96	0.04	<0.007	0.03	0.16	0.29	<0.010	99.57
222	KAR10	0.06	0.02	0.04	99.29	0.03	<0.007	0.04	0.20	0.13	<0.010	99.81
223	KAR10	0.02	0.02	0.28	98.65	0.06	<0.008	0.03	0.13	0.24	0.01	99.44
224	KAR10	0.02	0.01	0.74	98.56	0.08	<0.007	0.03	0.05	0.37	<0.010	99.87
225	KAR10	0.05	0.01	0.52	97.61	0.21	<0.007	0.02	0.03	1.52	<0.010	99.96
226	KAR10	0.11	0.01	0.24	99.13	0.01	<0.007	0.03	0.08	0.32	<0.010	99.92
227	KAR10	0.08	0.16	0.01	98.62	0.03	0.01	0.03	0.21	0.26	0.02	99.43
228	KAR10	0.02	0.06	0.15	98.44	0.02	<0.007	0.05	0.13	0.13	<0.010	99.02
229	KAR10	0.25	0.01	0.20	99.07	0.03	0.02	0.04	0.10	0.46	0.03	100.21
230	KAR10	0.35	0.05	0.13	98.79	0.02	0.02	0.04	0.33	0.10	0.03	99.88
231	KAR10	0.02	0.05	0.25	99.51	0.02	<0.007	0.17	0.08	0.16	<0.010	100.27
232	KAR10	0.35	0.02	0.15	98.73	0.03	0.02	0.04	0.26	0.23	0.04	99.87
233	KAR10	0.01	0.02	0.02	98.45	0.04	0.01	0.04	0.23	0.13	<0.010	98.96
234	KAR10	0.13	0.01	0.09	99.32	0.04	0.01	0.13	0.22	0.13	<0.010	100.09
235	KAR10	0.39	0.02	0.18	98.63	0.03	0.02	0.12	0.18	0.19	0.02	99.80
236	KAR10	0.03	0.02	0.09	99.13	<0.005	<0.008	0.05	0.16	0.09	<0.010	99.58
237	KAR10	0.17	0.04	<0.004	98.62	0.06	0.03	0.04	0.37	0.17	0.13	99.62
238	KAR10	0.04	0.01	0.10	99.50	0.07	<0.007	0.04	0.06	0.56	<0.010	100.39
239	KAR10	0.71	0.08	0.08	97.50	0.04	0.03	0.03	0.57	0.11	0.10	99.24
240	KAR10	0.05	0.01	0.31	97.72	0.03	<0.007	0.03	0.08	0.25	<0.010	98.48
241	KAR10	0.03	0.01	0.15	99.49	0.03	<0.007	0.03	0.18	0.12	<0.010	100.05
242	KAR10	0.14	0.02	0.11	97.39	0.08	<0.007	0.33	0.12	0.28	0.01	98.49
243	KAR10	0.07	0.01	0.01	96.48	0.02	<0.008	0.07	0.21	0.08	<0.010	96.95
244	KAR10	0.30	0.01	0.25	96.83	0.03	0.02	0.07	0.13	0.24	0.07	97.94
245	KAR10	0.38	0.01	0.12	97.24	0.03	0.02	0.04	0.27	0.16	0.02	98.29
246	KAR10	0.35	0.16	0.09	95.12	0.08	0.20	0.72	0.27	0.09	0.02	97.10
247	KAR10	0.62	0.03	0.10	97.14	0.03	0.01	0.03	0.39	0.18	0.02	98.55
248	KAR10	0.03	0.01	0.12	97.90	0.03	<0.008	0.06	0.13	0.16	<0.010	98.45

Table A.4 Continued

No.	Sample	Nb2O5	Al2O3	Cr2O3	TiO2	ZrO2	SnO2	SiO2	FeO	V2O3	WO3	Total
249	KAR10	0.05	0.01	0.08	97.38	0.06	<0.008	0.04	0.12	0.21	0.03	97.99
250	KAR10	0.03	0.20	0.10	97.28	0.06	<0.008	0.04	0.20	0.17	<0.010	98.09
251	KAR10	0.36	0.02	0.12	97.50	0.03	0.02	0.03	0.26	0.19	0.02	98.56
252	KAR10	0.06	0.01	0.19	99.52	0.05	<0.008	0.02	0.15	0.17	<0.010	100.18
253	KAR10	<0.008	0.01	0.02	96.85	0.04	<0.008	0.05	0.13	0.20	<0.010	97.31
254	KAR10	0.08	0.01	0.06	97.46	0.06	<0.008	0.05	0.25	0.21	<0.010	98.19
255	KAR10	0.23	< 0.00	0.19	98.49	0.09	0.01	0.03	0.06	0.55	<0.010	99.65
256	KAR10	0.02	0.01	0.30	99.06	0.03	<0.008	0.08	0.13	0.06	<0.010	99.70
257	KAR10	<0.008	0.01	0.03	98.36	0.04	<0.008	0.03	0.21	0.41	<0.010	99.08
258	KAR10	0.22	0.01	0.03	99.18	0.01	<0.008	0.07	0.17	0.14	<0.010	99.86
259	KAR10	0.48	0.02	0.11	97.96	0.03	0.02	0.04	0.34	0.13	0.05	99.19
260	KAR10	0.01	0.01	0.01	99.37	0.08	0.01	0.05	0.14	0.18	<0.010	99.86
261	KAR10	0.01	0.06	0.03	98.88	0.03	<0.008	0.04	0.23	0.14	<0.010	99.42
262	KAR27	0.01	0.01	0.17	98.39	0.01	<0.008	0.03	0.13	0.11	<0.010	98.85
263	KAR27	0.03	0.01	0.03	98.39	0.02	<0.008	0.03	0.13	0.20	<0.010	98.83
264	KAR27	0.03	0.02	0.04	99.15	0.03	<0.008	0.04	0.15	0.12	<0.010	99.58
265	KAR27	0.05	0.05	0.02	97.61	0.03	<0.008	0.02	0.22	0.12	<0.010	98.12
266	KAR27	0.01	0.01	0.04	97.55	0.02	0.01	0.03	0.08	0.33	<0.010	98.08
267	KAR27	0.05	<0.002	0.67	95.78	0.02	0.01	0.02	0.02	0.55	<0.010	97.13
268	KAR27	0.28	0.02	0.09	96.44	0.10	0.01	0.02	0.30	0.28	0.04	97.59
269	KAR27	0.08	0.02	0.08	97.39	0.02	<0.008	0.03	0.11	0.26	<0.011	97.99
270	KAR27	0.04	0.01	0.03	97.29	<0.005	0.01	0.03	0.13	0.22	<0.010	97.76
271	KAR27	0.16	0.03	0.15	97.67	0.04	<0.008	0.02	0.17	0.25	<0.010	98.50
272	KAR27	0.15	<0.002	0.06	97.06	0.41	0.01	0.03	0.04	0.50	<0.010	98.24
273	KAR27	0.03	0.05	0.04	97.48	0.03	0.01	0.13	0.14	0.12	0.04	98.06
274	KAR27	0.19	0.01	0.12	97.71	0.14	0.04	0.03	0.20	0.08	<0.010	98.51
275	KAR27	0.02	0.01	0.03	98.35	0.02	<0.008	0.03	0.19	0.09	<0.010	98.73
276	KAR27	<0.008	0.02	0.06	97.17	0.01	<0.008	0.02	0.19	0.13	<0.010	97.60
277	KAR27	0.10	0.01	0.01	98.47	0.01	<0.008	0.03	0.11	0.06	<0.010	98.79
278	KAR27	0.05	<0.002	0.64	97.09	0.05	<0.008	0.02	0.03	0.50	<0.010	98.37
279	KAR27	0.03	0.01	0.27	98.33	0.01	<0.008	0.04	0.07	0.11	<0.010	98.86
280	KAR27	0.09	0.15	0.08	98.23	0.02	<0.008	0.03	0.19	0.06	<0.010	98.86
281	KAR27	0.15	0.01	0.12	96.73	0.02	<0.008	0.02	0.11	0.38	<0.010	97.54
282	KAR27	0.28	0.01	0.51	96.15	0.06	0.01	0.05	0.03	0.63	<0.011	97.74
283	KAR27	0.39	0.01	0.18	98.10	0.08	<0.008	0.03	0.06	0.34	<0.011	99.19
284	KAR27	0.28	0.01	0.10	97.28	0.14	<0.008	0.03	0.16	0.30	<0.010	98.32
285	KAR27	0.04	0.01	0.06	97.27	0.02	<0.008	0.07	0.15	0.10	<0.010	97.71
286	KAR27	0.17	0.01	0.01	97.49	0.01	0.01	0.02	0.28	0.13	<0.010	98.12
287	KAR27	0.15	0.01	0.15	97.19	0.27	<0.008	0.02	0.10	0.38	<0.010	98.27
288	KAR27	0.28	0.03	0.15	96.51	0.15	0.02	0.03	0.08	0.33	<0.010	97.56
289	KAR27	0.03	0.09	0.01	96.28	0.08	0.01	0.03	0.20	0.21	<0.010	96.94
290	KAR27	0.03	0.02	0.03	97.04	0.03	0.01	0.07	0.23	0.12	<0.010	97.59
291	KAR27	0.11	0.23	0.16	96.16	0.03	<0.008	0.04	0.18	0.10	<0.010	97.01
292	KAR27	0.01	0.12	0.03	95.92	0.02	<0.008	0.04	0.20	0.19	<0.010	96.54
293	KAR27	0.02	0.02	0.11	98.10	0.02	0.01	0.07	0.13	0.11	<0.010	98.57
294	KAR27	0.16	0.01	0.09	96.13	0.04	<0.008	0.03	0.16	0.41	<0.010	97.03
295	KAR27	0.19	0.02	0.12	97.04	0.02	<0.008	0.03	0.23	0.11	<0.010	97.77
296	KAR27	0.01	0.01	0.13	97.82	0.02	<0.008	0.03	0.09	0.08	<0.010	98.19
297	KAR27	0.06	0.10	0.08	98.13	0.05	<0.008	0.04	0.24	0.20	<0.010	98.91
298	KAR27	<0.008	0.02	0.14	99.74	0.01	<0.008	0.03	0.11	0.14	<0.010	100.20
299	KAR27	0.17	< 0.00	0.36	97.31	0.05	0.03	0.03	0.04	0.26	<0.010	98.27
300	KAR27	0.49	0.01	0.35	98.28	0.07	0.06	0.03	0.32	0.15	0.01	99.76
301	KAR27	0.08	0.01	0.05	99.28	0.03	<0.008	0.02	0.29	0.09	<0.010	99.85
302	KAR27	0.15	0.04	0.04	99.02	0.04	0.02	0.03	0.17	0.24	<0.010	99.74
303	KAR27	0.26	0.07	0.15	91.20	0.02	0.02	1.85	0.17	0.19	<0.010	93.93
304	KAR27	0.20	0.07	0.10	97.34	0.07	0.01	0.15	0.21	0.07	<0.010	98.21
305	KAR27	0.08	0.20	0.11	98.75	0.02	<0.008	0.04	0.18	0.12	<0.010	99.52
306	KAR27	0.01	0.39	<0.003	97.35	0.02	<0.008	0.03	0.18	0.19	<0.010	98.18
307	KAR27	0.01	0.02	0.08	98.68	0.03	<0.008	0.02	0.15	0.16	<0.010	99.15
308	KAR27	0.01	0.08	0.62	96.25	0.02	<0.008	0.15	0.03	0.24	<0.010	97.43
309	KAR27	<0.008	0.02	0.06	97.19	0.02	<0.008	0.04	0.11	0.09	<0.010	97.53
310	KAR22	0.17	0.02	0.09	98.06	0.10	<0.008	0.04	0.66	0.24	<0.011	99.37

Table A.4 Continued

No.	Sample	Nb2O5	Al2O3	Cr2O3	TiO2	ZrO2	SnO2	SiO2	FeO	V2O3	WO3	Total
311	KAR22	0.19	0.08	0.20	98.55	0.20	<0.008	0.01	0.13	0.63	<0.010	99.99
312	KAR22	0.29	0.02	0.17	98.27	0.10	<0.008	0.03	0.15	0.18	<0.010	99.22
313	KAR22	0.08	0.02	0.07	99.20	0.06	<0.008	0.03	0.29	0.13	<0.010	99.88
314	KAR22	0.01	0.01	0.01	99.03	0.13	0.01	0.03	0.29	0.28	<0.010	99.80
315	KAR22	0.45	0.25	0.08	97.49	0.06	0.01	0.05	0.50	0.20	0.02	99.11
316	KAR22	0.54	0.02	0.07	98.52	0.25	0.01	0.02	0.28	0.26	<0.010	99.96
317	KAR22	0.06	0.08	0.04	99.82	0.01	<0.008	0.02	0.21	0.16	<0.011	100.41
318	KAR22	0.14	0.01	0.09	98.47	0.07	0.01	0.02	0.50	0.33	<0.010	99.64
319	KAR22	0.10	0.01	0.03	99.23	<0.005	<0.008	0.03	0.17	0.07	<0.010	99.65
320	KAR22	0.11	0.02	0.04	97.58	0.28	<0.007	0.19	0.31	0.16	<0.010	98.70
321	KAR22	0.08	0.03	0.13	98.01	0.06	<0.008	0.10	0.75	0.19	<0.011	99.37
322	KAR22	0.06	<0.002	0.12	98.39	<0.005	<0.008	0.03	0.59	0.10	0.01	99.30
323	KAR22	0.10	0.08	0.02	98.55	0.01	0.03	0.04	0.20	0.15	<0.010	99.18
324	KAR22	0.08	0.08	0.14	97.81	0.07	0.01	0.29	0.14	0.18	<0.010	98.80
325	KAR22	0.13	0.08	0.01	98.24	0.01	0.02	0.16	0.59	0.08	<0.010	99.33
326	KAR22	0.11	0.16	0.25	97.10	<0.005	<0.008	0.42	0.32	0.12	0.01	98.49
327	KAR22	0.73	0.02	<0.004	97.33	0.11	<0.008	0.04	0.88	0.11	<0.011	99.21
328	KAR22	0.30	0.01	0.07	98.74	0.02	<0.008	0.03	0.29	0.09	0.03	99.59
329	KAR22	0.10	3.07	0.23	89.72	0.06	0.02	4.13	0.41	0.16	0.02	97.89
330	KAR22	0.09	0.04	0.01	98.55	0.01	0.02	0.05	0.32	0.09	<0.010	99.18
331	KAR22	0.24	0.04	0.08	98.35	0.09	0.01	0.03	0.53	0.28	<0.010	99.67
332	KAR22	0.42	0.04	0.33	97.75	0.02	0.01	0.06	0.52	0.07	0.19	99.40
333	KAR22	0.29	0.04	0.06	99.04	0.02	0.01	0.03	0.29	0.14	0.02	99.94
334	KAR22	0.23	0.02	0.89	95.36	0.05	0.23	0.01	0.34	0.53	1.93	99.59
335	KAR22	0.13	0.76	0.04	93.67	0.15	0.01	1.50	0.47	0.09	<0.010	96.81
336	KAR22	0.08	0.01	0.12	97.19	0.03	<0.008	0.02	0.31	0.16	<0.010	97.93
337	KAR22	0.16	< 0.00	0.15	97.45	0.05	<0.008	0.10	0.11	0.23	<0.010	98.26
338	KAR22	0.06	0.01	0.01	97.82	0.16	<0.008	0.04	0.18	0.18	<0.010	98.45
339	KAR22	<0.008	0.01	0.09	96.62	0.03	<0.008	0.02	0.30	0.27	<0.010	97.34
340	KAR22	0.17	0.01	0.02	97.67	<0.005	<0.008	0.03	0.45	0.03	<0.010	98.39
341	KAR22	0.09	0.01	0.03	96.76	0.02	<0.008	0.04	0.31	0.12	<0.010	97.38
342	KAR22	0.13	1.67	0.15	90.91	0.13	0.02	2.43	0.57	0.17	<0.010	96.19
343	KAR22	0.59	0.01	0.01	95.18	0.04	0.06	0.04	0.80	0.13	0.06	96.91
344	KAR22	0.11	0.03	0.07	96.45	0.13	<0.008	0.03	0.22	0.24	<0.010	97.28
345	KAR22	0.04	0.03	0.21	96.82	0.18	<0.008	0.03	0.12	0.24	<0.010	97.67
346	KAR22	0.19	0.02	0.02	96.88	0.01	<0.008	0.02	0.37	0.08	<0.010	97.59
347	KAR22	0.03	0.01	0.02	97.02	0.02	<0.008	0.03	0.25	0.18	<0.010	97.56
348	KAR22	0.05	0.08	0.26	96.02	0.05	<0.008	0.02	0.08	0.20	<0.011	96.76
349	KAR22	0.13	0.01	0.10	97.14	0.05	<0.008	0.03	0.22	0.11	<0.010	97.79
350	KAR22	0.21	0.02	0.10	96.71	0.06	<0.008	0.07	0.20	0.18	<0.010	97.55
351	KAR22	0.16	<0.002	0.03	95.33	0.01	<0.008	0.03	1.73	0.12	<0.010	97.42
352	KAR22	0.23	0.01	0.25	97.34	0.10	<0.008	0.02	0.60	0.26	<0.010	98.81
353	KAR22	0.69	0.02	0.01	96.09	0.13	0.01	0.03	0.58	0.13	<0.010	97.69
354	KAR22	<0.008	0.01	0.01	99.07	0.01	<0.008	0.02	0.18	0.19	<0.010	99.50
355	KAR22	0.03	0.07	0.07	97.46	0.06	<0.008	0.07	0.09	0.22	0.01	98.10
356	KAR22	0.19	0.01	0.24	97.71	0.04	<0.008	0.03	0.55	0.36	<0.010	99.13
357	KAR22	0.15	0.01	0.04	98.07	0.01	0.01	0.03	0.27	0.09	<0.010	98.67
358	KAR22	0.15	<0.002	0.69	98.33	0.09	<0.008	0.02	0.15	0.10	0.09	99.62

Table A.5: Composition of detrital garnets from the Karaburun Peninsula

No.	Sample	SiO2	MgO	CaO	TiO2	FeO	Al2O3	Cr2O3	MnO	Total
1	KAR20A	38.14	3.58	11.14	0.30	24.55	21.26	<0.026	0.60	99.59
2	KAR20A	37.21	3.21	2.23	<0.024	34.32	21.13	<0.028	2.19	100.31
3	KAR20A	36.29	1.75	0.75	0.04	30.73	20.86	<0.028	9.05	99.47
4	KAR20A	37.50	4.09	2.65	0.04	34.35	21.27	<0.028	0.35	100.24
5	KAR20A	35.64	0.84	0.24	0.04	28.71	20.70	<0.028	12.05	98.23
6	KAR20A	37.87	5.26	4.57	0.04	29.66	21.60	<0.028	1.10	100.12
7	KAR20A	38.24	4.37	10.49	0.08	24.47	21.46	0.07	0.24	99.43
8	KAR20A	36.97	3.93	1.19	0.07	31.47	21.07	0.03	4.66	99.39
9	KAR20A	37.51	4.30	1.58	<0.024	30.27	21.29	0.03	5.05	100.02
10	KAR20A	37.46	4.50	2.81	<0.024	33.23	21.54	<0.027	0.45	100.01
11	KAR20A	37.00	3.59	0.64	0.04	37.21	21.02	<0.028	0.33	99.85
12	KAR20A	38.11	3.80	11.55	0.03	24.58	21.49	<0.027	0.65	100.20
13	KAR20A	37.59	4.58	2.39	<0.024	28.89	21.21	<0.028	5.63	100.34
14	KAR20A	36.03	0.22	3.64	0.18	11.09	20.76	<0.028	26.32	98.24
15	KAR20A	37.47	3.70	1.34	<0.024	32.53	21.16	<0.028	4.03	100.23
16	KAR20A	37.84	4.11	5.37	0.03	29.95	21.32	<0.027	1.01	99.65
17	KAR20A	37.88	4.19	5.40	0.04	30.51	21.51	<0.028	1.00	100.53
18	KAR20A	36.62	2.35	2.38	<0.024	31.06	20.93	<0.028	6.21	99.56
19	KAR20A	36.62	2.74	0.77	0.03	33.62	20.88	<0.028	5.17	99.86
20	KAR20A	37.27	3.56	3.17	0.13	29.79	20.64	<0.028	5.59	100.16
21	KAR20A	36.95	0.95	5.23	0.10	29.13	20.54	<0.028	7.21	100.12
22	KAR20A	38.36	7.72	3.84	<0.023	22.10	22.12	0.13	5.76	100.04
23	KAR20A	38.06	2.39	13.55	0.08	23.65	21.70	<0.027	0.58	100.03
24	KAR20A	36.22	0.58	0.54	0.08	27.51	20.52	<0.028	15.10	100.55
25	KAR20A	37.77	6.90	4.81	1.67	22.95	21.28	<0.027	4.62	100.00
26	KAR20A	37.08	1.04	6.71	0.16	33.83	20.99	<0.028	0.65	100.47
27	KAR20A	36.58	1.81	1.01	0.04	39.20	20.96	<0.028	0.37	99.98
28	KAR20A	38.12	6.22	6.54	0.05	26.19	21.45	<0.026	1.23	99.82
29	KAR20A	37.07	3.05	1.16	<0.024	26.03	21.05	<0.028	12.23	100.61
30	KAR20A	36.86	0.58	7.43	0.06	28.58	21.19	<0.028	5.78	100.48
31	KAR20A	35.01	0.11	0.15	0.13	23.53	20.82	<0.028	19.32	99.07
32	KAR20A	37.14	3.31	1.14	<0.024	30.94	21.28	0.03	6.36	100.21
33	KAR20A	37.34	3.55	5.36	<0.024	30.90	21.50	<0.028	1.26	99.91
34	KAR20A	37.23	3.27	1.94	<0.024	33.64	20.99	<0.028	3.36	100.45
35	KAR20A	36.63	0.24	5.18	0.21	15.90	20.77	<0.028	20.89	99.83
36	KAR20A	36.76	1.24	3.09	0.08	34.89	20.84	<0.028	2.75	99.64
37	KAR20A	37.10	0.56	8.08	0.12	30.14	20.98	<0.027	3.52	100.51
38	KAR20A	37.00	3.56	2.41	<0.024	34.14	21.09	<0.028	1.57	99.78
39	KAR20A	37.35	3.45	6.70	0.15	27.71	20.91	<0.027	3.32	99.59
40	KAR20A	38.03	5.19	7.34	<0.023	26.68	21.68	<0.028	0.76	99.71
41	KAR20A	37.09	4.57	0.95	<0.024	33.98	21.40	<0.028	2.20	100.22
42	KAR20A	37.84	7.70	0.97	0.02	30.69	21.84	0.05	0.93	100.04
43	KAR20A	38.40	7.29	7.03	0.09	24.40	21.40	0.05	0.75	99.41
44	KAR20A	37.02	4.15	1.60	<0.023	32.17	21.50	0.03	3.20	99.70
45	KAR20A	37.21	4.07	2.10	0.09	25.18	20.83	<0.028	10.24	99.73
46	KAR20A	36.52	1.95	1.44	<0.024	30.57	20.85	<0.028	8.44	99.81
47	KAR20A	36.82	1.21	5.48	0.07	34.87	20.82	0.03	0.44	99.74
48	KAR20A	37.08	4.31	3.36	0.09	30.59	20.98	<0.028	2.54	98.95
49	KAR20A	38.48	9.18	1.05	0.02	28.36	22.10	<0.027	0.72	99.94
50	KAR20A	35.67	0.83	0.58	0.03	29.06	20.76	<0.028	11.57	98.50
51	KAR20A	36.53	2.36	0.51	0.07	32.71	20.88	0.04	6.87	99.97
52	KAR20A	37.15	1.59	6.49	0.10	32.68	21.05	<0.028	0.49	99.56
53	KAR20A	36.78	1.07	4.66	0.10	31.01	20.82	<0.028	5.02	99.48
54	KAR20A	36.81	1.12	4.65	0.09	31.06	20.85	0.04	5.32	99.94
55	KAR20A	37.33	3.94	2.07	0.17	28.95	20.65	<0.028	7.11	100.24
56	KAR20A	38.25	7.71	1.65	<0.024	29.57	21.88	<0.027	0.71	99.81
57	KAR20A	36.81	1.51	5.66	0.05	32.89	21.10	<0.029	1.84	99.86
58	KAR20A	36.68	1.10	4.44	0.07	31.65	20.97	0.04	5.29	100.23
59	KAR20A	36.57	0.76	4.38	0.03	18.11	20.64	<0.028	18.92	99.42
60	KAR20A	38.08	6.28	4.17	<0.023	27.36	21.31	<0.027	2.25	99.47
61	KAR20A	37.46	5.84	1.32	<0.024	32.66	21.44	<0.028	0.79	99.52
62	KAR20A	36.17	1.53	0.48	0.03	35.66	20.75	<0.028	4.84	99.47

Table A.5 Continued

No.	Sample	SiO2	MgO	CaO	TiO2	FeO	Al2O3	Cr2O3	MnO	Total
63	KAR20A	37.62	3.88	6.48	0.06	29.90	21.44	<0.027	0.63	100.00
64	KAR20A	36.01	1.74	0.38	0.05	23.18	20.22	<0.028	17.59	99.19
65	KAR20A	37.61	5.29	1.76	<0.023	28.86	21.27	0.05	4.92	99.78
66	KAR1	36.83	0.86	3.68	0.13	24.01	20.63	<0.028	13.82	99.98
67	KAR1	37.33	2.75	3.81	0.09	32.15	20.71	<0.028	3.59	100.46
68	KAR1	38.25	5.17	4.54	<0.024	28.80	21.60	0.03	2.27	100.67
69	KAR1	37.37	2.08	6.85	0.05	27.61	20.68	<0.027	5.21	99.85
70	KAR1	38.02	6.24	1.37	0.04	25.94	21.41	<0.027	7.25	100.27
71	KAR1	36.96	1.39	5.00	0.05	31.32	20.91	<0.028	4.19	99.82
72	KAR1	36.84	2.11	1.97	0.07	31.10	20.83	<0.028	6.69	99.63
73	KAR1	38.26	4.88	7.29	0.08	25.99	21.31	<0.028	2.14	99.95
74	KAR1	37.17	1.19	8.68	0.08	30.38	21.04	<0.028	1.15	99.71
75	KAR1	37.07	1.77	6.21	0.06	31.31	20.98	0.03	2.68	100.10
76	KAR1	36.74	2.24	1.05	<0.025	31.16	20.57	<0.029	8.18	99.95
77	KAR1	37.12	0.93	8.76	0.14	26.12	20.82	<0.027	5.63	99.52
78	KAR1	36.88	1.36	2.66	0.10	26.46	20.69	0.04	11.37	99.56
79	KAR1	37.09	0.59	6.47	0.11	22.66	20.63	<0.028	12.65	100.20
80	KAR1	38.14	6.63	2.80	<0.023	28.98	21.80	0.03	2.08	100.49
81	KAR1	37.12	1.06	6.14	0.08	22.07	20.55	<0.029	13.01	100.03
82	KAR1	37.12	1.22	5.26	0.07	30.44	21.12	<0.028	4.90	100.13
83	KAR1	36.68	1.55	0.55	0.05	27.15	20.99	<0.028	13.45	100.44
84	KAR1	37.00	0.89	8.67	0.10	29.95	21.12	<0.028	2.13	99.87
85	KAR1	37.05	1.03	5.74	0.05	30.11	20.97	<0.027	5.09	100.05
86	KAR1	37.24	3.48	1.96	0.06	28.87	21.07	<0.028	7.59	100.31
87	KAR1	37.03	1.32	7.42	0.09	31.13	20.73	<0.028	1.83	99.58
88	KAR1	36.99	0.86	7.59	0.11	27.41	20.82	<0.028	5.41	99.20
89	KAR1	36.53	0.93	6.18	1.08	20.98	20.58	<0.028	13.78	100.07
90	KAR1	36.87	1.32	6.15	0.10	33.02	21.17	0.03	1.05	99.70
91	KAR1	36.68	0.45	2.75	0.11	14.99	20.74	<0.028	23.92	99.63
92	KAR1	37.03	0.59	9.71	0.17	23.46	20.82	<0.028	7.82	99.60
93	KAR1	38.73	10.10	1.91	0.07	25.32	22.30	<0.027	1.43	99.89
94	KAR1	37.76	4.97	5.32	<0.023	26.73	21.50	0.05	3.27	99.62
95	KAR1	37.73	5.07	1.98	<0.024	30.48	21.39	<0.027	3.12	99.79
96	KAR1	36.77	0.65	5.10	0.07	23.06	20.54	<0.028	13.79	99.99
97	KAR1	37.07	1.14	5.63	0.12	30.49	20.77	<0.028	4.38	99.58
98	KAR1	37.46	0.79	9.65	0.11	27.28	20.98	<0.028	3.97	100.25
99	KAR1	36.83	0.51	6.35	0.11	22.12	20.43	<0.028	13.23	99.57
100	KAR1	36.73	0.63	6.21	0.05	32.20	20.87	<0.028	2.55	99.25
101	KAR1	36.95	3.14	1.91	0.09	30.95	20.70	0.03	5.25	99.03
102	KAR1	36.94	1.07	6.10	0.14	21.09	20.40	<0.028	13.85	99.59
103	KAR1	37.52	4.68	1.84	<0.024	33.34	21.36	<0.027	1.02	99.77
104	KAR1	37.29	1.09	9.67	0.13	26.58	21.07	0.05	4.05	99.93
105	KAR1	36.89	1.43	6.81	0.04	29.56	20.57	0.03	3.42	98.75
106	KAR1	36.84	2.90	1.53	<0.024	35.57	21.13	<0.028	1.31	99.31
107	KAR1	37.04	0.91	7.17	0.07	24.96	20.57	0.04	8.88	99.64
108	KAR1	36.82	0.99	5.83	0.05	23.36	20.59	<0.028	10.26	97.91
109	KAR1	37.27	1.47	4.86	0.06	31.66	21.01	0.03	3.74	100.09
110	KAR22	37.02	0.87	5.15	0.11	27.00	21.07	<0.029	9.55	100.78
111	KAR22	37.07	1.80	2.37	0.04	34.50	21.12	<0.028	3.58	100.48
112	KAR22	36.99	2.67	1.45	0.03	33.93	20.92	0.04	4.42	100.46
113	KAR22	37.32	3.17	1.48	<0.024	31.65	21.22	0.03	5.56	100.45
114	KAR22	37.29	2.20	4.40	0.04	33.51	21.14	<0.028	1.50	100.08
115	KAR22	37.08	3.58	1.28	<0.024	33.67	21.23	<0.028	3.38	100.24
116	KAR22	36.96	1.88	1.73	<0.024	37.06	21.11	<0.028	1.47	100.23
117	KAR22	36.71	1.60	1.48	0.08	32.51	20.70	0.03	7.05	100.15
118	KAR22	36.82	3.35	1.16	<0.024	24.29	21.11	<0.027	12.60	99.35
119	KAR22	36.63	2.27	1.48	0.09	32.66	20.64	<0.028	5.85	99.63
120	KAR22	36.76	2.78	1.93	0.11	32.40	20.55	<0.028	5.27	99.79
121	KAR22	37.10	0.74	5.41	0.13	24.06	20.91	<0.028	11.77	100.12
122	KAR22	37.06	2.79	2.48	<0.024	33.72	21.01	<0.028	3.05	100.14
123	KAR22	36.91	2.23	1.89	0.06	26.90	20.52	<0.028	11.13	99.66
124	KAR22	36.70	3.48	0.87	<0.024	28.48	20.98	<0.027	8.85	99.38

Table A.5 Continued

No.	Sample	SiO2	MgO	CaO	TiO2	FeO	Al2O3	Cr2O3	MnO	Total
125	KAR22	37.06	3.11	1.23	<0.024	33.80	20.59	<0.028	3.76	99.57
126	KAR22	36.27	1.68	0.82	<0.024	34.98	21.02	0.06	5.16	100.02
127	KAR22	36.42	4.81	1.05	<0.024	31.85	20.87	0.06	2.74	97.79
128	KAR22	36.99	2.94	1.56	<0.024	34.60	21.09	<0.028	2.68	99.87
129	KAR22	37.21	2.47	3.67	0.05	33.21	21.35	<0.028	2.41	100.39
130	KAR22	37.88	5.54	3.90	0.04	30.02	21.40	<0.027	1.01	99.77
131	KAR22	37.00	1.95	4.21	0.04	30.12	20.85	<0.028	5.42	99.57
132	KAR22	36.51	1.10	1.76	0.12	34.15	20.44	<0.029	5.83	99.91
133	KAR22	37.12	3.40	1.40	<0.024	32.23	21.15	<0.028	4.54	99.86
134	KAR22	37.27	3.66	1.76	0.03	30.56	21.19	<0.027	5.32	99.82
135	KAR22	36.82	1.28	6.47	0.04	33.43	21.13	<0.029	0.81	99.98
136	KAR22	36.53	3.01	1.34	0.79	34.49	20.86	<0.028	2.24	99.28
137	KAR22	37.70	5.31	3.17	<0.024	26.15	21.29	0.04	6.14	99.80
138	KAR22	37.01	2.61	2.49	0.05	34.03	20.88	<0.028	2.70	99.80
139	KAR22	37.07	2.24	2.69	0.06	34.19	20.78	<0.028	2.85	99.88
140	KAR22	37.20	3.48	2.73	0.04	33.66	21.14	<0.028	1.66	99.92
141	KAR22	37.28	3.38	3.24	0.07	30.60	20.68	<0.028	4.33	99.60
142	KAR22	37.86	5.30	3.68	<0.024	30.18	21.38	<0.028	1.15	99.57
143	KAR22	36.75	2.38	1.96	0.04	34.32	20.95	<0.029	3.16	99.56
144	KAR22	36.59	0.99	4.10	0.07	32.51	20.69	<0.028	4.51	99.48
145	KAR22	37.20	3.44	2.49	<0.024	32.25	20.99	<0.028	3.87	100.26
146	KAR22	37.04	3.10	1.95	0.03	32.99	20.77	<0.028	3.58	99.48
147	KAR22	36.82	1.45	5.04	0.10	31.43	20.66	<0.028	3.97	99.46
148	KAR22	37.10	2.00	3.18	0.04	33.19	20.98	<0.028	3.40	99.89
149	KAR22	36.81	3.25	2.04	<0.025	33.83	20.88	<0.028	2.08	98.90
150	KAR22	36.81	1.94	3.53	0.04	29.73	20.90	0.05	7.08	100.08
151	KAR22	36.95	2.14	6.14	0.07	32.65	21.03	<0.028	0.65	99.65
152	KAR22	37.40	4.51	3.93	0.21	30.57	21.11	<0.027	1.51	99.24
153	KAR22	37.27	3.53	3.49	0.03	30.83	21.00	<0.028	3.13	99.28
154	KAR22	36.60	1.49	2.56	0.06	28.40	20.79	<0.028	9.11	99.03
155	KAR22	36.73	3.60	1.02	<0.024	30.08	20.77	<0.028	7.27	99.49
156	KAR22	36.52	1.80	1.69	0.03	38.40	20.78	<0.028	0.49	99.72

Manuscript II: Supplementary data

- **Table B.1: U–Pb LA-ICP-MS data of detrital zircons from the Karaburun Peninsula**

Table B.1: U–Pb LA-ICP-MS data of detrital zircons from the Karaburun Peninsula

KAR1: Gerence Formation

#	U [ppm]	f206%	Isotope ratios						Ages (Ma)						Data filter A*	Data filter B#
			$^{206}Pb/^{238}U$	±2σ	$^{207}Pb/^{235}U$	±2σ	$^{207}Pb/^{206}Pb$	±2σ	$^{206}Pb/^{238}U$	±2σ	$^{207}Pb/^{235}U$	±2σ	$^{207}Pb/^{206}Pb$	±2σ		
1	356	0.32	0.0665	0.0012	0.5109	0.0120	0.0558	0.0008	415	7	419	8	443	32	99	94
2	258	0.05	0.0588	0.0011	0.4823	0.0185	0.0595	0.0020	368	7	400	13	586	72	92	63
3	189	0.08	0.0706	0.0013	0.5506	0.0144	0.0566	0.0011	440	8	445	9	475	42	99	93
4	369	0.47	0.0624	0.0011	0.4893	0.0109	0.0568	0.0008	390	7	404	7	486	30	97	80
5	167	0.00	0.0603	0.0011	0.4570	0.0118	0.0549	0.0010	378	7	382	8	410	41	99	92
6	342	0.29	0.0612	0.0011	0.4750	0.0113	0.0562	0.0009	383	6	395	8	462	36	97	83
7	255	0.25	0.0614	0.0011	0.4780	0.0113	0.0565	0.0009	384	7	397	8	470	34	97	82
8	55	0.06	0.0669	0.0015	0.5450	0.0210	0.0591	0.0019	417	9	442	14	570	69	95	73
9	390	0.07	0.0680	0.0012	0.5271	0.0118	0.0562	0.0008	424	7	430	8	461	30	99	92
10	309	0.84	0.0633	0.0014	0.5342	0.0163	0.0612	0.0013	396	9	435	11	647	45	91	61
11	290	3.52	0.0760	0.0019	0.5254	0.0373	0.0502	0.0033	472	12	429	25	202	154	110	234
12	492	0.03	0.0623	0.0015	0.4765	0.0125	0.0555	0.0006	389	9	396	9	433	25	98	90
13	210	0.17	0.0723	0.0016	0.5700	0.0165	0.0572	0.0010	450	10	458	11	497	40	98	90
14	297	0.17	0.0649	0.0015	0.4903	0.0140	0.0548	0.0009	405	9	405	10	405	36	100	100
15	264	1.28	0.0567	0.0015	0.4191	0.0239	0.0536	0.0027	355	9	355	17	355	113	100	100
16	361	0.07	0.0659	0.0015	0.5224	0.0148	0.0575	0.0010	411	9	427	10	511	39	96	80
17	212		0.0558	0.0012	0.4305	0.0129	0.0560	0.0011	350	8	364	9	451	45	96	78
18	137	1.78	0.0585	0.0012	0.4113	0.0211	0.0510	0.0024	367	8	350	15	239	108	105	153
19	135	0.48	0.0657	0.0014	0.5295	0.0185	0.0585	0.0016	410	9	431	12	547	60	95	75
20	295	0.20	0.0600	0.0012	0.4817	0.0137	0.0583	0.0012	375	7	399	9	540	44	94	70
21	182	1.49	0.0640	0.0013	0.4989	0.0328	0.0566	0.0035	400	8	411	22	475	138	97	84
22	232	0.78	0.0674	0.0013	0.5485	0.0155	0.0590	0.0012	421	8	444	10	567	46	95	74
23	330	1.22	0.0551	0.0011	0.4102	0.0143	0.0540	0.0016	346	7	349	10	369	65	99	94
24	136	1.50	0.0638	0.0014	0.4390	0.0149	0.0499	0.0013	399	8	370	11	191	61	108	208
25	114	1.23	0.0702	0.0015	0.5264	0.0169	0.0544	0.0013	437	9	429	11	388	53	102	113
26	203	0.80	0.0608	0.0012	0.5067	0.0191	0.0604	0.0020	381	7	416	13	618	70	91	62
27	191	0.35	0.0614	0.0012	0.4977	0.0138	0.0588	0.0012	384	7	410	9	560	43	94	69
28	538	1.90	0.0572	0.0020	0.3950	0.0260	0.0501	0.0028	359	12	338	19	199	129	106	180
29	238	1.13	0.0604	0.0013	0.4325	0.0143	0.0519	0.0013	378	8	365	10	282	56	104	134
30	245	0.25	0.0660	0.0013	0.5068	0.0130	0.0557	0.0009	412	8	416	9	440	35	99	94
31	109		0.1934	0.0042	2.1886	0.0658	0.0821	0.0017	1140	22	1177	21	1247	42	97	91
32	136	0.05	0.0645	0.0014	0.4923	0.0136	0.0553	0.0010	403	8	406	9	426	39	99	95
33	128	0.83	0.0644	0.0014	0.4961	0.0176	0.0558	0.0016	403	9	409	12	446	62	98	90
34	218	0.80	0.0667	0.0014	0.5647	0.0172	0.0614	0.0013	416	9	455	11	653	46	92	64
35	161	2.39	0.0558	0.0011	0.4065	0.0152	0.0528	0.0017	350	6	346	11	321	73	101	109
36	420		0.0582	0.0010	0.4390	0.0101	0.0547	0.0009	365	6	370	7	401	36	99	91
37	125	2.68	0.0671	0.0012	0.5080	0.0208	0.0549	0.0020	419	7	417	14	409	83	100	102
38	250	0.87	0.0633	0.0011	0.4902	0.0131	0.0561	0.0011	396	7	405	9	458	45	98	86
39	127	0.00	0.0532	0.0012	0.4217	0.0122	0.0575	0.0011	334	7	357	9	511	41	93	65
40	468	0.76	0.0580	0.0009	0.4547	0.0095	0.0568	0.0007	364	6	381	7	485	29	96	75
41	256	0.92	0.0704	0.0012	0.5940	0.0157	0.0612	0.0012	439	7	473	10	646	44	93	68
42	212	0.84	0.0645	0.0014	0.5388	0.0158	0.0606	0.0012	403	8	438	10	626	43	92	64
43	334	1.96	0.0651	0.0012	0.4409	0.0362	0.0491	0.0039	407	7	371	26	153	165	110	266
44	275	1.42	0.0562	0.0013	0.4017	0.0379	0.0518	0.0047	352	8	343	27	279	210	103	126
45	71		0.0545	0.0012	0.4464	0.0165	0.0594	0.0018	342	7	375	12	583	65	91	59
46	299	0.92	0.0580	0.0009	0.4731	0.0142	0.0591	0.0015	364	5	393	10	572	57	92	64
47	315		0.0598	0.0009	0.4590	0.0087	0.0557	0.0007	374	5	384	6	439	26	98	85
48	383	1.84	0.0715	0.0011	0.5615	0.0392	0.0570	0.0039	445	7	453	26	490	151	98	91
49	306	0.04	0.0675	0.0013	0.5245	0.0143	0.0563	0.0010	421	8	428	10	465	41	98	91
50	492	2.14	0.0555	0.0011	0.4042	0.0119	0.0528	0.0012	348	7	345	9	319	50	101	109
51	89	0.83	0.0676	0.0012	0.5831	0.0184	0.0626	0.0016	421	7	466	12	694	55	90	61

KAR3: Idecik unit

#	U [ppm]	f206%	Isotope ratios						Ages (Ma)						Data filter A*	Data filter B#
			$^{206}Pb/^{238}U$	±2σ	$^{207}Pb/^{235}U$	±2σ	$^{207}Pb/^{206}Pb$	±2σ	$^{206}Pb/^{238}U$	±2σ	$^{207}Pb/^{235}U$	±2σ	$^{207}Pb/^{206}Pb$	±2σ		
52	558	0.17	0.1073	0.0025	0.9342	0.0235	0.0631	0.0007	657	14	670	12	713	22	98	92
53	238	0.08	0.3719	0.0081	6.1618	0.1476	0.1202	0.0012	2038	38	1999	21	1959	17	102	104
54	161		0.1214	0.0035	1.0612	0.0347	0.0634	0.0010	738	20	734	17	723	34	101	102
55	1134	1.47	0.0838	0.0021	0.6919	0.0248	0.0599	0.0015	519	13	534	15	598	55	97	87
56	259	0.01	0.3414	0.0075	5.3147	0.1276	0.1129	0.0011	1894	36	1871	21	1847	17	101	103
57	211	1.05	0.1065	0.0022	0.9033	0.0335	0.0615	0.0019	652	13	654	18	658	66	100	99
58	594	0.68	0.1967	0.0041	2.1155	0.0536	0.0780	0.0011	1157	22	1154	17	1147	28	100	101
59	325	0.70	0.1644	0.0039	1.6664	0.0470	0.0735	0.0011	981	21	996	18	1029	31	98	95
60	94	3.69	0.0919	0.0023	0.7869	0.0359	0.0621	0.0024	567	14	589	20	679	81	96	83
61	270	0.11	0.1108	0.0022	0.9579	0.0215	0.0627	0.0007	677	13	682	11	698	24	99	97
62	292		0.1665	0.0033	1.7075	0.0377	0.0744	0.0007	993	18	1011	14	1052	19	98	94
63	269	0.69	0.2735	0.0075	3.9403	0.1336	0.1045	0.0021	1559	38	1622	27	1705	37	96	91
64	856	0.07	0.3156	0.0062	5.0844	0.1082	0.1168	0.0009	1768	30	1834	18	1908	14	96	93
65	426	0.65	0.1512	0.0031	1.5592	0.0366	0.0748	0.0009	908	17	954	15	1063	23	95	85
66	384	1.34	0.0660	0.0015	0.5410	0.0175	0.0595	0.0013	412	9	439	12	584	49	94	70
67	129	1.48	0.0926	0.0020	0.7768	0.0275	0.0609	0.0017	571	12	584	16	634	61	98	90
68	320	0.16	0.1766	0.0037	1.7506	0.0416	0.0719	0.0008	1048	20	1027	15	983	22	102	107
69	466	3.81	0.0763	0.0015	0.6447	0.0228	0.0613	0.0018	474	9	505	14	649	63	94	73
70	161	0.38	0.1261	0.0026	1.1431	0.0320	0.0657	0.0012	766	15	774	15	798	39	99	96
71	728	0.16	0.1155	0.0021	1.0043	0.0228	0.0631	0.0009	704	12	706	12	711	30	100	99
72	139	0.45	0.3233	0.0059	5.5027	0.1145	0.1235	0.0012	1806	29	1901	18	2007	18	95	90
73	171		0.1264	0.0030	1.0960	0.0324	0.0629	0.0011	767	17	751	16	705	39	102	109
74	426	0.01	0.0975	0.0022	0.8163	0.0208	0.0607	0.0007	600	13	606	12	629	25	99	95
75	733	2.04	0.0834	0.0018	0.6775	0.0223	0.0589	0.0015	516	11	525	14	564	54	98	92

Table B.1 Continued

#	U [ppm]	f206%	Isotope ratios						Ages (Ma)						Data filter A*	Data filter B#
			$^{206}Pb/^{238}U$	±2σ	$^{207}Pb/^{235}U$	±2σ	$^{207}Pb/^{206}Pb$	±2σ	$^{206}Pb/^{238}U$	±2σ	$^{207}Pb/^{235}U$	±2σ	$^{207}Pb/^{206}Pb$	±2σ		
76	1610	2.55	0.0701	0.0011	0.5718	0.0133	0.0592	0.0010	437	7	459	9	573	37	95	76
77	184	0.26	0.0879	0.0017	0.8058	0.0205	0.0665	0.0011	543	10	600	12	821	36	91	66
78	82	0.05	0.4095	0.0075	8.8878	0.2036	0.1574	0.0021	2213	34	2327	21	2428	23	95	91
79	74		0.1542	0.0029	1.6221	0.0401	0.0763	0.0012	924	16	979	16	1103	32	94	84
80	307	0.98	0.1780	0.0039	1.8706	0.0505	0.0762	0.0012	1056	22	1071	18	1101	31	99	96
81	402		0.0958	0.0017	0.8344	0.0185	0.0632	0.0008	590	10	616	10	714	28	96	83
82	400	0.08	0.4769	0.0087	12.5061	0.2582	0.1902	0.0019	2513	38	2643	19	2744	16	95	92
83	184	0.46	0.1674	0.0034	1.7486	0.0479	0.0758	0.0014	998	19	1027	18	1089	37	97	92
84	177	0.28	0.4656	0.0069	10.6940	0.1956	0.1666	0.0018	2464	30	2497	17	2524	18	99	98
85	275		0.1400	0.0036	1.4859	0.0450	0.0770	0.0012	845	20	925	18	1121	32	91	75
86	237	0.29	0.0947	0.0015	0.7836	0.0189	0.0600	0.0011	583	9	588	11	605	40	99	96
87	119	0.27	0.1421	0.0023	1.3710	0.0389	0.0700	0.0016	857	13	877	17	927	48	98	92
88	110	1.73	0.1364	0.0021	1.2434	0.0516	0.0661	0.0025	824	12	820	23	810	81	100	102
89	1072	3.25	0.0369	0.0007	0.2887	0.0081	0.0567	0.0011	234	5	258	6	480	44	91	49
90	72	1.25	0.1014	0.0023	0.8441	0.0355	0.0604	0.0021	622	14	621	20	618	76	100	101
91	193	0.01	0.4190	0.0084	7.6717	0.1783	0.1328	0.0015	2256	38	2193	21	2135	20	103	106
92	321	0.66	0.0760	0.0014	0.6538	0.0163	0.0624	0.0011	472	8	511	10	687	37	92	69
93	247	1.84	0.0987	0.0022	0.8312	0.0500	0.0611	0.0034	607	13	614	28	642	121	99	95
94	410	0.45	0.4550	0.0150	10.5274	0.3708	0.1678	0.0021	2417	66	2482	33	2536	21	97	95
95	274	0.72	0.0880	0.0018	0.7501	0.0284	0.0618	0.0020	544	11	568	16	667	68	96	82
96	164	0.04	0.1561	0.0027	1.5891	0.0335	0.0738	0.0009	935	15	966	13	1037	25	97	90
97	275	0.54	0.0834	0.0016	0.7600	0.0186	0.0661	0.0010	517	10	574	11	809	32	90	64
98	462	0.77	0.1170	0.0025	1.0528	0.0282	0.0653	0.0010	713	14	730	14	784	34	98	91
99	308		0.0837	0.0015	0.7257	0.0218	0.0629	0.0015	518	9	554	13	704	52	94	74
100	88	3.84	0.1122	0.0038	0.8727	0.1524	0.0564	0.0097	685	22	637	83	470	386	108	146
101	60	2.99	0.1067	0.0020	0.7985	0.0450	0.0543	0.0029	653	12	596	25	383	119	110	171
102	72	5.71	0.1327	0.0034	1.2294	0.1280	0.0672	0.0068	803	19	814	58	844	211	99	95
103	205	0.15	0.4331	0.0093	9.5941	0.2246	0.1607	0.0015	2320	42	2397	22	2463	16	97	94
104	605	0.07	0.3208	0.0066	5.3260	0.1190	0.1204	0.0011	1793	32	1873	19	1963	16	96	91
105	381	0.14	0.1571	0.0034	1.7389	0.0539	0.0803	0.0018	941	19	1023	20	1204	44	92	78
106	289	1.70	0.0734	0.0018	0.5614	0.0210	0.0554	0.0016	457	11	452	14	430	63	101	106
107	305	0.18	0.1222	0.0026	1.1072	0.0284	0.0657	0.0009	743	15	757	14	797	30	98	93
108	268	0.79	0.0694	0.0017	0.6078	0.0208	0.0636	0.0015	432	10	482	13	727	51	90	59
109	545	0.90	0.0857	0.0022	0.7773	0.0230	0.0658	0.0010	530	13	584	13	800	32	91	66
110	171	0.65	0.1246	0.0028	1.0964	0.0321	0.0638	0.0012	757	16	752	16	736	40	101	103
111	131	0.71	0.2022	0.0054	2.1889	0.0790	0.0785	0.0019	1187	29	1178	25	1160	48	101	102
112	99	2.37	0.0812	0.0022	0.6388	0.0316	0.0571	0.0024	503	13	502	20	495	92	100	102
113	112	0.57	0.1356	0.0059	1.2190	0.0592	0.0652	0.0014	820	34	809	27	781	44	101	105
114	167		0.3834	0.0056	6.3601	0.1128	0.1203	0.0012	2092	26	2027	16	1961	18	103	107
115	97	1.54	0.1135	0.0025	0.9484	0.0332	0.0606	0.0016	693	15	677	17	626	58	102	111
116	111	1.29	0.1075	0.0016	0.8727	0.0200	0.0589	0.0010	658	9	637	11	563	37	103	117
117	1750	0.41	0.0744	0.0013	0.6594	0.0133	0.0643	0.0007	463	8	514	8	751	22	90	62
118	93	2.80	0.0962	0.0029	0.7454	0.0516	0.0562	0.0035	592	17	566	30	460	139	105	129
119	137		0.1224	0.0022	1.1178	0.0261	0.0663	0.0010	744	13	762	13	815	31	98	91
120	143		0.1645	0.0024	1.6994	0.0334	0.0749	0.0010	982	13	1008	13	1067	27	97	92
121	133	0.12	0.1208	0.0017	1.0482	0.0193	0.0629	0.0008	735	10	728	10	705	26	101	104
122	760	0.18	0.1162	0.0021	1.0630	0.0216	0.0663	0.0006	709	12	735	11	817	19	96	87
123	274	0.44	0.1266	0.0025	1.2883	0.0296	0.0738	0.0009	768	14	841	13	1037	25	91	74
124	124	0.92	0.1474	0.0030	1.3794	0.0323	0.0679	0.0008	886	17	880	14	865	25	101	102
125	816	2.84	0.1327	0.0024	1.3282	0.0332	0.0726	0.0013	803	14	858	14	1002	35	94	80
126	431	1.62	0.0498	0.0009	0.3627	0.0109	0.0528	0.0013	313	5	314	8	321	56	100	98
127	59	5.09	0.0798	0.0018	0.6669	0.0799	0.0606	0.0071	495	10	519	49	625	256	95	79
128	242	3.13	0.1306	0.0029	1.1495	0.0627	0.0638	0.0032	791	17	777	30	736	106	102	108
129	450	0.66	0.1110	0.0029	0.9999	0.0392	0.0654	0.0019	678	17	704	20	786	62	96	86
130	102	0.26	0.1680	0.0029	1.6894	0.0383	0.0729	0.0011	1001	16	1005	14	1012	29	100	99
131	200	0.08	0.3293	0.0063	5.2392	0.1182	0.1154	0.0014	1835	30	1859	19	1886	22	99	97
132	433	0.86	0.1505	0.0033	1.5736	0.0563	0.0758	0.0022	904	18	960	22	1090	57	94	83

KAR4: Idecik unit

#	U [ppm]	f206%	Isotope ratios						Ages (Ma)						Data filter A*	Data filter B#
			$^{206}Pb/^{238}U$	±2σ	$^{207}Pb/^{235}U$	±2σ	$^{207}Pb/^{206}Pb$	±2σ	$^{206}Pb/^{238}U$	±2σ	$^{207}Pb/^{235}U$	±2σ	$^{207}Pb/^{206}Pb$	±2σ		
133	669	0.02	0.0572	0.0016	0.4304	0.0133	0.0546	0.0006	358	10	363	9	396	25	99	90
134	224	0.33	0.0784	0.0022	0.6171	0.0192	0.0571	0.0008	487	13	488	12	494	29	100	98
135	197	0.37	0.0991	0.0027	0.8144	0.0263	0.0596	0.0010	609	16	605	15	588	37	101	104
136	132	0.04	0.5851	0.0157	14.9812	0.4199	0.1857	0.0015	2969	64	2814	27	2705	13	106	110
137	108	0.23	0.3693	0.0101	6.3658	0.1895	0.1250	0.0015	2026	47	2028	26	2029	21	100	100
138	93	1.34	0.0588	0.0015	0.4473	0.0261	0.0552	0.0029	368	9	375	18	419	117	98	88
139	164		0.0612	0.0011	0.4670	0.0125	0.0553	0.0011	383	7	389	9	425	44	98	90
140	418	0.50	0.0851	0.0017	0.7237	0.0162	0.0617	0.0006	527	10	553	10	663	21	95	79
141	180		0.0679	0.0014	0.5678	0.0154	0.0606	0.0010	424	9	457	10	626	36	93	68
142	45		0.3009	0.0062	4.6385	0.1091	0.1118	0.0013	1696	31	1756	20	1829	21	97	93
143	124	1.26	0.0925	0.0019	0.7515	0.0285	0.0589	0.0019	570	11	569	17	565	70	100	101
144	139	0.22	0.1229	0.0024	1.0280	0.0245	0.0607	0.0008	747	14	718	12	628	29	104	119
145	358		0.0550	0.0010	0.4068	0.0086	0.0536	0.0006	345	6	347	6	356	26	100	97
146	214		0.0861	0.0024	0.7543	0.0261	0.0636	0.0013	532	14	571	15	727	42	93	73
147	178	0.11	0.1094	0.0024	0.9503	0.0274	0.0630	0.0012	669	14	678	14	707	40	99	95
148	26	0.93	0.1025	0.0043	0.9692	0.0559	0.0685	0.0027	629	25	688	29	885	82	91	71
149	417	0.01	0.0640	0.0014	0.4903	0.0122	0.0556	0.0007	400	8	405	8	435	29	99	92
150	78	0.02	0.0906	0.0021	0.7178	0.0243	0.0575	0.0014	559	12	549	14	509	54	102	110
151	570	0.62	0.0818	0.0018	0.7121	0.0186	0.0631	0.0009	507	11	546	11	713	30	93	71
152	988	1.49	0.0710	0.0015	0.5431	0.0390	0.0555	0.0038	442	9	440	26	431	153	100	103

Table B.1 Continued

#	U [ppm]	ƒ206%	Isotope ratios $^{206}Pb/^{238}U$	±2σ	$^{207}Pb/^{235}U$	±2σ	$^{207}Pb/^{206}Pb$	±2σ	Ages (Ma) $^{206}Pb/^{238}U$	±2σ	$^{207}Pb/^{235}U$	±2σ	$^{207}Pb/^{206}Pb$	±2σ	Data filter A*	Data filter B#
153	474	0.52	0.0735	0.0016	0.5815	0.0147	0.0574	0.0007	457	10	465	9	506	26	98	90
154	612	0.16	0.0798	0.0014	0.6522	0.0138	0.0592	0.0007	495	8	510	8	576	25	97	86
155	231	0.46	0.0760	0.0014	0.6152	0.0150	0.0587	0.0009	472	9	487	9	557	33	97	85
156	397		0.0813	0.0015	0.6886	0.0164	0.0615	0.0009	504	9	532	10	655	31	95	77
157	898		0.0825	0.0024	0.6975	0.0233	0.0613	0.0010	511	14	537	14	650	34	95	79
158	401	0.53	0.0950	0.0018	0.8423	0.0187	0.0643	0.0007	585	11	620	10	752	24	94	78
159	2006	0.83	0.0799	0.0014	0.7173	0.0139	0.0651	0.0006	496	8	549	8	778	19	90	64
160	168		0.0864	0.0022	0.7328	0.0219	0.0615	0.0009	534	13	558	13	656	33	96	81
161	414	0.20	0.0946	0.0018	0.8094	0.0187	0.0621	0.0008	583	11	602	10	676	27	97	86
162	374	0.50	0.0808	0.0016	0.7131	0.0167	0.0640	0.0008	501	9	547	10	741	28	92	68
163	364	0.27	0.0812	0.0014	0.6683	0.0137	0.0597	0.0007	503	8	520	8	592	25	97	85
164	511	0.15	0.0784	0.0013	0.6217	0.0123	0.0575	0.0006	486	8	491	8	513	23	99	95
165	373		0.0917	0.0017	0.7651	0.0172	0.0605	0.0008	566	10	577	10	622	27	98	91
166	331	0.03	0.4456	0.0092	10.4110	0.2343	0.1694	0.0015	2376	41	2472	21	2552	15	96	93
167	154		0.1574	0.0026	1.6307	0.0327	0.0751	0.0009	942	14	982	13	1072	23	96	88
168	195	0.10	0.0970	0.0025	0.8253	0.0274	0.0617	0.0013	597	15	611	15	665	45	98	90
169	289	0.23	0.1025	0.0017	0.8712	0.0203	0.0616	0.0010	629	10	636	11	662	34	99	95
170	125		0.0838	0.0026	0.6939	0.0256	0.0600	0.0012	519	16	535	15	605	43	97	86
171	389	0.04	0.0673	0.0022	0.5341	0.0187	0.0576	0.0007	420	13	435	12	514	28	97	82
172	153	0.04	0.0777	0.0024	0.6323	0.0219	0.0590	0.0009	483	14	498	14	567	34	97	85
173	754	0.30	0.2458	0.0071	3.2403	0.1096	0.0956	0.0017	1417	37	1467	26	1540	33	97	92
174	343		0.3410	0.0100	5.7741	0.1796	0.1228	0.0013	1892	48	1943	27	1997	19	97	95
175	1161		0.0717	0.0027	0.6106	0.0238	0.0618	0.0008	446	16	484	15	666	26	92	67
176	428	0.01	0.2586	0.0078	3.1429	0.1454	0.0881	0.0031	1483	40	1443	36	1386	67	103	107
177	245		0.0662	0.0021	0.5488	0.0224	0.0602	0.0015	413	13	444	15	610	56	93	68
178	436	0.10	0.0854	0.0026	0.7407	0.0245	0.0629	0.0008	528	15	563	14	706	28	94	75
179	96	0.63	0.0892	0.0028	0.8171	0.0340	0.0664	0.0018	551	16	606	19	820	57	91	67
180	899		0.3077	0.0182	4.8325	0.2919	0.1139	0.0014	1729	90	1791	51	1863	21	97	93
181	247	2.22	0.0948	0.0035	0.7055	0.0370	0.0540	0.0020	584	21	542	22	369	84	108	158
182	565		0.0986	0.0030	0.8310	0.0279	0.0611	0.0008	606	18	614	15	643	28	99	94
183	469		0.0547	0.0017	0.4191	0.0143	0.0555	0.0008	344	10	355	10	434	31	97	79
184	164	1.20	0.0953	0.0033	0.8302	0.0471	0.0632	0.0028	587	19	614	26	714	95	96	82
185	174	0.37	0.1022	0.0033	0.8803	0.0349	0.0624	0.0014	628	19	641	19	690	49	98	91
186	1094	2.81	0.0546	0.0012	0.3686	0.0368	0.0489	0.0048	343	7	319	27	145	179	108	237
187	148	0.29	0.0822	0.0015	0.6524	0.0162	0.0576	0.0010	509	9	510	10	513	37	100	99
188	311	0.04	0.1062	0.0021	0.8989	0.0214	0.0614	0.0008	650	12	651	11	654	27	100	100
189	355		0.3169	0.0050	5.2546	0.0947	0.1203	0.0011	1774	24	1862	15	1960	16	95	91
190	576	0.51	0.3606	0.0055	6.3341	0.1107	0.1274	0.0011	1985	26	2023	15	2062	15	98	96
191	958	0.52	0.0722	0.0015	0.6381	0.0161	0.0641	0.0009	450	9	501	10	744	29	90	60
192	425	0.03	0.0574	0.0009	0.4551	0.0089	0.0575	0.0007	360	5	381	6	512	27	94	70
193	376	0.19	0.0748	0.0012	0.6099	0.0127	0.0591	0.0008	465	7	483	8	572	28	96	81
194	353	1.79	0.0569	0.0014	0.4094	0.0135	0.0522	0.0011	357	9	348	10	294	49	102	122
195	50	0.92	0.0930	0.0023	0.7580	0.0259	0.0591	0.0014	573	13	573	15	572	52	100	100
196	119		0.0953	0.0028	0.7975	0.0350	0.0607	0.0020	587	16	595	20	628	70	99	93
197	128	2.32	0.0618	0.0026	0.4623	0.0298	0.0542	0.0027	387	16	386	21	381	110	100	101
198	193	0.22	0.0696	0.0022	0.5830	0.0274	0.0608	0.0021	434	13	466	18	631	76	93	69
199	187		0.3102	0.0073	5.0719	0.1328	0.1186	0.0014	1742	36	1831	22	1935	21	95	90
200	89		0.3464	0.0078	5.9089	0.1507	0.1237	0.0014	1917	38	1963	22	2011	21	98	95
201	99		0.0862	0.0028	0.7809	0.0309	0.0657	0.0015	533	16	586	18	798	49	91	67
202	447	0.12	0.1873	0.0050	2.0778	0.1630	0.0804	0.0059	1107	27	1142	54	1208	146	97	92
203	150	0.53	0.0859	0.0021	0.7366	0.0220	0.0622	0.0011	531	12	560	13	680	38	95	78
204	758		0.0872	0.0024	0.7398	0.0234	0.0615	0.0009	539	14	562	14	658	32	96	82
205	168		0.0775	0.0021	0.6507	0.0238	0.0609	0.0015	481	13	509	15	636	52	95	76
206	250	0.36	0.0524	0.0018	0.4259	0.0198	0.0589	0.0019	329	11	360	14	565	69	91	58
207	296		0.0676	0.0018	0.5658	0.0172	0.0607	0.0010	422	11	455	11	628	34	93	67
208	321		0.3626	0.0092	6.5146	0.1748	0.1303	0.0011	1994	43	2048	24	2102	15	97	95
209	443	0.53	0.0949	0.0025	0.8480	0.0261	0.0648	0.0010	584	15	624	14	769	32	94	76
210	638	0.32	0.0659	0.0025	0.5526	0.0254	0.0608	0.0016	412	15	447	17	632	55	92	65
211	192	1.71	0.0735	0.0022	0.5699	0.0259	0.0563	0.0019	457	13	458	17	462	76	100	99
212	514	0.05	0.1096	0.0029	1.0063	0.0297	0.0666	0.0008	671	17	707	15	825	26	95	81

KAR20A: Güvercinlik Formation

#	U [ppm]	ƒ206%	*Isotope ratios* $^{206}Pb/^{238}U$	±2σ	$^{207}Pb/^{235}U$	±2σ	$^{207}Pb/^{206}Pb$	±2σ	Ages (Ma) $^{206}Pb/^{238}U$	±2σ	$^{207}Pb/^{235}U$	±2σ	$^{207}Pb/^{206}Pb$	±2σ	Data filter A*	Data filter B#
213	171		0.0509	0.0008	0.3704	0.0094	0.0528	0.0010	320	5	320	7	319	44	100	101
214	355	0.13	0.0743	0.0011	0.5782	0.0145	0.0565	0.0011	462	7	463	9	471	44	100	98
215	343	0.31	0.0625	0.0010	0.4691	0.0110	0.0545	0.0009	391	6	391	8	390	39	100	100
216	249	0.30	0.0577	0.0010	0.4409	0.0104	0.0554	0.0009	362	6	371	7	429	37	98	84
217	345	0.09	0.0494	0.0006	0.3647	0.0066	0.0536	0.0007	311	4	316	5	353	29	98	88
218	571	3.34	0.0504	0.0007	0.3523	0.0091	0.0507	0.0011	317	4	306	7	226	52	103	140
219	222	3.19	0.0569	0.0020	0.4195	0.0246	0.0535	0.0025	357	12	356	18	349	107	100	102
220	132	0.27	0.1280	0.0023	1.1331	0.0369	0.0642	0.0017	776	13	769	18	749	57	101	104
221	1173	3.32	0.0765	0.0014	0.6379	0.0219	0.0605	0.0017	475	9	501	14	620	62	95	77
222	130	0.54	0.0996	0.0015	0.8303	0.0177	0.0605	0.0009	612	9	614	10	620	33	100	99
223	482	0.20	0.0915	0.0010	0.7625	0.0113	0.0604	0.0006	565	6	575	7	619	22	98	91
224	552	1.46	0.0577	0.0007	0.4280	0.0089	0.0538	0.0009	362	4	362	6	362	39	100	100
225	235		0.0528	0.0006	0.3918	0.0071	0.0538	0.0007	332	4	336	5	361	31	99	92
226	407	0.22	0.0567	0.0008	0.4597	0.0104	0.0588	0.0011	355	5	384	7	560	39	93	64
227	74	0.93	0.0507	0.0009	0.4119	0.0135	0.0589	0.0017	319	5	350	10	564	61	91	57
228	103		0.0510	0.0009	0.3990	0.0144	0.0567	0.0018	321	6	341	10	481	69	94	67
229	181	0.96	0.1125	0.0015	1.1207	0.0242	0.0722	0.0012	687	9	763	12	993	34	90	69

Table B.1 Continued

#	U [ppm]	f206%	Isotope ratios						Ages (Ma)						Data filter A*	Data filter B♯
			$^{206}Pb/^{238}U$	±2σ	$^{207}Pb/^{235}U$	±2σ	$^{207}Pb/^{206}Pb$	±2σ	$^{206}Pb/^{238}U$	±2σ	$^{207}Pb/^{235}U$	±2σ	$^{207}Pb/^{206}Pb$	±2σ		
230	416	0.02	0.1648	0.0021	1.6754	0.0275	0.0737	0.0008	983	11	999	10	1034	21	98	95
231	504	0.27	0.0617	0.0010	0.5040	0.0106	0.0593	0.0008	386	6	414	7	577	30	93	67
232	228		0.0813	0.0022	0.6776	0.0212	0.0604	0.0010	504	13	525	13	620	35	96	81
233	171		0.0545	0.0008	0.3969	0.0103	0.0528	0.0011	342	5	339	7	320	49	101	107
234	265	0.50	0.0504	0.0008	0.3963	0.0108	0.0570	0.0012	317	5	339	8	494	47	93	64
235	264	1.63	0.0478	0.0007	0.3451	0.0136	0.0523	0.0019	301	4	301	10	301	83	100	100
236	807	3.99	0.0458	0.0005	0.3382	0.0067	0.0536	0.0009	289	3	296	5	353	36	98	82
237	416	0.62	0.0505	0.0008	0.4023	0.0085	0.0577	0.0008	318	5	343	6	520	32	93	61
238	272	0.33	0.0747	0.0018	0.5938	0.0168	0.0577	0.0009	464	11	473	11	518	32	98	90
239	187	0.11	0.0496	0.0014	0.3844	0.0136	0.0562	0.0011	312	9	330	10	460	45	95	68
240	530	0.42	0.3287	0.0101	5.3480	0.1764	0.1180	0.0014	1832	49	1877	28	1926	21	98	95
241	213	0.30	0.3461	0.0093	5.5303	0.1659	0.1159	0.0016	1916	44	1905	26	1894	24	101	101
242	230	0.53	0.0996	0.0024	0.8628	0.0253	0.0628	0.0010	612	14	632	14	702	34	97	87
243	91	0.31	0.1444	0.0038	1.4097	0.0456	0.0708	0.0014	869	21	893	19	952	39	97	91
244	65		0.1346	0.0041	1.2535	0.0556	0.0676	0.0022	814	23	825	25	855	67	99	95
245	104	0.59	0.0870	0.0024	0.7451	0.0260	0.0621	0.0013	537	14	565	15	679	46	95	79
246	369	0.33	0.0487	0.0012	0.3622	0.0103	0.0540	0.0009	306	7	314	8	370	36	98	83
247	229	0.07	0.0637	0.0018	0.5210	0.0177	0.0593	0.0011	398	11	426	12	578	41	94	69
248	72	0.99	0.1004	0.0020	0.8421	0.0273	0.0609	0.0016	616	12	620	15	635	55	99	97
249	214	0.18	0.0941	0.0013	0.8368	0.0156	0.0645	0.0008	580	7	617	9	758	27	94	77
250	475	0.82	0.0833	0.0010	0.7500	0.0137	0.0653	0.0009	516	6	568	8	784	29	91	66
251	251	0.24	0.0918	0.0019	0.7836	0.0222	0.0619	0.0012	566	11	588	13	672	41	96	84
252	33	0.09	0.3194	0.0062	5.0859	0.1310	0.1155	0.0019	1787	30	1834	22	1887	30	97	95
253	348	2.04	0.0408	0.0006	0.2962	0.0074	0.0527	0.0010	258	4	263	6	314	45	98	82
254	262		0.0431	0.0007	0.3081	0.0082	0.0518	0.0011	272	4	273	6	277	49	100	98
255	211		0.0444	0.0007	0.3515	0.0115	0.0574	0.0016	280	4	306	9	507	63	92	55
256	329		0.0663	0.0008	0.5202	0.0096	0.0569	0.0008	414	5	425	6	487	30	97	85
257	204		0.0562	0.0013	0.4547	0.0139	0.0586	0.0011	353	8	381	10	553	41	93	64
258	180	0.05	0.5196	0.0117	12.4912	0.3024	0.1743	0.0016	2698	50	2642	23	2600	15	102	104
259	161	0.22	0.0814	0.0018	0.6786	0.0207	0.0605	0.0012	505	11	526	13	620	45	96	81
260	274	0.35	0.0507	0.0011	0.4133	0.0132	0.0591	0.0014	319	7	351	9	571	50	91	56
261	305	0.35	0.0489	0.0011	0.3619	0.0100	0.0537	0.0008	308	7	314	7	359	35	98	86
262	143		0.0854	0.0021	0.6899	0.0203	0.0586	0.0010	528	12	533	12	551	36	99	96
263	108	0.20	0.0910	0.0022	0.8104	0.0299	0.0646	0.0018	562	13	603	17	760	59	93	74
264	399	0.26	0.0509	0.0011	0.3863	0.0098	0.0550	0.0007	320	7	332	7	412	29	97	78
265	227		0.0750	0.0020	0.6019	0.0184	0.0582	0.0009	466	12	478	12	537	35	97	87
266	611	11.82	0.0444	0.0012	0.3332	0.0501	0.0545	0.0080	280	8	292	38	391	336	96	72
267	324	0.76	0.0516	0.0015	0.4234	0.0144	0.0595	0.0010	324	9	358	10	586	36	90	55
268	394		0.0439	0.0012	0.3397	0.0111	0.0561	0.0010	277	7	297	8	457	40	93	61
269	466	0.32	0.0451	0.0014	0.3405	0.0127	0.0547	0.0012	285	9	298	10	400	48	96	71
270	893	4.59	0.0362	0.0010	0.2855	0.0195	0.0572	0.0036	229	6	255	15	500	137	90	46
271	1015	8.49	0.0373	0.0010	0.2632	0.0271	0.0512	0.0051	236	6	237	22	250	230	99	94
272	331	0.42	0.1500	0.0039	1.5765	0.0441	0.0762	0.0008	901	22	961	17	1101	22	94	82
273	268		0.0660	0.0018	0.5101	0.0151	0.0560	0.0007	412	11	419	10	453	28	99	91
274	599	4.09	0.0385	0.0011	0.2882	0.0160	0.0543	0.0025	243	7	257	13	385	105	95	63
275	64	0.90	0.0881	0.0023	0.7552	0.0292	0.0622	0.0018	544	14	571	17	681	60	95	80
276	50	0.21	0.1190	0.0036	1.2041	0.0445	0.0734	0.0016	725	21	802	21	1025	43	90	71
277	132		0.0612	0.0012	0.4869	0.0239	0.0578	0.0026	383	7	403	16	521	98	95	74
278	224	1.16	0.0731	0.0015	0.5722	0.0190	0.0568	0.0015	455	9	459	12	482	58	99	94
279	202		0.0473	0.0010	0.3447	0.0098	0.0529	0.0010	298	6	301	7	324	45	99	92
280	806	4.62	0.0435	0.0010	0.3162	0.0205	0.0527	0.0032	275	6	279	16	316	138	98	87
281	91		0.3438	0.0070	6.1359	0.1510	0.1294	0.0018	1905	34	1995	21	2091	24	95	91
282	83		0.0808	0.0019	0.7195	0.0238	0.0646	0.0015	501	11	550	14	762	50	91	66
283	302	4.69	0.0406	0.0009	0.2901	0.0166	0.0518	0.0027	257	6	259	13	277	121	99	93
284	642	3.11	0.0421	0.0007	0.3001	0.0277	0.0517	0.0047	266	4	266	22	270	209	100	98
285	50		0.0677	0.0017	0.5659	0.0239	0.0606	0.0021	422	10	455	15	627	74	93	67
286	71		0.3212	0.0073	5.3544	0.1579	0.1209	0.0023	1795	36	1878	25	1970	33	96	91
287	87		0.3192	0.0049	5.3274	0.1294	0.1211	0.0023	1786	24	1873	21	1972	33	95	91
288	196	0.44	0.0487	0.0008	0.3629	0.0114	0.0541	0.0015	306	5	314	8	374	61	97	82
289	549	2.63	0.0426	0.0007	0.3029	0.0086	0.0515	0.0012	269	4	269	7	265	54	100	101
290	164	1.33	0.0493	0.0011	0.3571	0.0157	0.0526	0.0020	310	7	310	12	310	85	100	100
291	601	3.97	0.0318	0.0007	0.2250	0.0079	0.0514	0.0014	202	4	206	7	257	65	98	78
292	143	0.06	0.3882	0.0064	7.9435	0.1471	0.1484	0.0013	2115	30	2225	17	2328	15	95	91
293	71	1.26	0.0870	0.0021	0.6847	0.0306	0.0571	0.0021	538	13	530	18	495	82	102	109
294	629	0.63	0.0491	0.0008	0.3872	0.0087	0.0572	0.0009	309	5	332	6	498	33	93	62
295	403		0.0514	0.0009	0.3767	0.0094	0.0532	0.0010	323	5	325	7	335	41	100	96
296	174		0.0865	0.0018	0.6995	0.0183	0.0587	0.0010	535	11	538	11	555	36	99	96
297	425	0.08	0.0456	0.0008	0.3461	0.0096	0.0551	0.0012	287	5	302	7	416	47	95	69
298	121	0.05	0.1047	0.0022	0.8721	0.0274	0.0604	0.0014	642	13	637	15	619	51	101	104
299	562	1.36	0.0636	0.0011	0.4879	0.0183	0.0557	0.0019	397	6	403	13	439	75	98	91
300	249	0.16	0.3112	0.0048	5.0529	0.0890	0.1178	0.0010	1746	24	1828	15	1923	15	96	91
301	164		0.1641	0.0031	1.6280	0.0423	0.0719	0.0013	980	17	981	16	984	36	100	100
302	269	0.11	0.0475	0.0008	0.3538	0.0077	0.0540	0.0008	299	5	308	6	373	33	97	80
303	446	0.10	0.1110	0.0016	0.9730	0.0173	0.0635	0.0007	679	9	690	9	727	22	98	93
304	274		0.1053	0.0015	0.8915	0.0174	0.0614	0.0008	645	9	647	9	654	28	100	99
305	171	0.25	0.0782	0.0014	0.6525	0.0154	0.0606	0.0010	485	8	510	9	623	35	95	78
306	309	0.05	0.0472	0.0009	0.3399	0.0082	0.0522	0.0008	297	5	297	6	294	35	100	101
307	291		0.0494	0.0008	0.3597	0.0073	0.0528	0.0007	311	5	312	5	319	29	100	98
308	730	4.25	0.0380	0.0011	0.2973	0.0115	0.0567	0.0015	240	7	264	9	482	58	91	50
309	406	4.26	0.0602	0.0023	0.5087	0.0368	0.0612	0.0038	377	14	418	25	648	132	90	58
310	77	0.03	0.0501	0.0019	0.3931	0.0209	0.0569	0.0021	315	12	337	15	487	82	94	65
311	58	1.25	0.0562	0.0019	0.3816	0.0524	0.0493	0.0066	352	12	328	39	161	223	107	218
312	126		0.1529	0.0040	1.3790	0.0410	0.0654	0.0010	917	22	880	18	788	31	104	116

Table B.1 Continued

#	U [ppm]	f206%	Isotope ratios						Ages (Ma)						Data filter A*	Data filter B#
			$^{206}Pb/^{238}U$	±2σ	$^{207}Pb/^{235}U$	±2σ	$^{207}Pb/^{206}Pb$	±2σ	$^{206}Pb/^{238}U$	±2σ	$^{207}Pb/^{235}U$	±2σ	$^{207}Pb/^{206}Pb$	±2σ		
313	528		0.0531	0.0014	0.3910	0.0125	0.0534	0.0010	334	9	335	9	345	41	100	97
314	210	0.51	0.0762	0.0020	0.5948	0.0178	0.0566	0.0008	473	12	474	11	477	32	100	99
315	165	0.02	0.0478	0.0013	0.3902	0.0158	0.0592	0.0018	301	8	335	12	576	66	90	52

KAR20B: Güvercinlik Formation

#	U [ppm]	f206%	Isotope ratios						Ages (Ma)						Data filter A*	Data filter B#
			$^{206}Pb/^{238}U$	±2σ	$^{207}Pb/^{235}U$	±2σ	$^{207}Pb/^{206}Pb$	±2σ	$^{206}Pb/^{238}U$	±2σ	$^{207}Pb/^{235}U$	±2σ	$^{207}Pb/^{206}Pb$	±2σ		
316	121	1.71	0.0624	0.0018	0.4610	0.0172	0.0535	0.0013	390	11	385	12	352	54	101	111
317	250	0.09	0.1176	0.0036	1.0490	0.0353	0.0647	0.0009	716	21	728	17	765	28	98	94
318	92	0.66	0.1204	0.0038	1.1805	0.0436	0.0711	0.0013	733	22	792	20	961	38	93	76
319	237	0.02	0.0505	0.0015	0.3721	0.0131	0.0534	0.0010	318	9	321	10	346	42	99	92
320	260	1.03	0.1579	0.0045	1.5765	0.0495	0.0724	0.0009	945	25	961	19	998	25	98	95
321	168	0.51	0.0564	0.0017	0.4200	0.0145	0.0540	0.0010	354	10	356	10	371	41	99	95
322	244		0.0542	0.0016	0.3977	0.0139	0.0533	0.0010	340	10	340	10	340	44	100	100
323	329	1.85	0.0608	0.0018	0.4610	0.0155	0.0550	0.0009	380	11	385	11	413	36	99	92
324	484	3.03	0.0469	0.0014	0.3358	0.0158	0.0520	0.0019	295	9	294	12	284	83	100	104
325	1242	4.03	0.0464	0.0013	0.3365	0.0297	0.0526	0.0044	292	8	295	23	313	192	99	93
326	391		0.0509	0.0014	0.3833	0.0117	0.0546	0.0008	320	8	329	9	398	34	97	80
327	521	0.30	0.0453	0.0013	0.3408	0.0112	0.0545	0.0010	286	8	298	9	394	40	96	73
328	127		0.1240	0.0035	1.1315	0.0365	0.0662	0.0011	753	20	768	17	813	34	98	93
329	264	0.63	0.0568	0.0016	0.4344	0.0153	0.0554	0.0012	356	10	366	11	430	46	97	83
330	74	0.17	0.1485	0.0043	1.3905	0.0504	0.0679	0.0015	892	24	885	21	867	45	101	103
331	278	0.60	0.0475	0.0015	0.3809	0.0155	0.0581	0.0015	299	9	328	11	534	57	91	56
332	449	0.43	0.0454	0.0012	0.3467	0.0113	0.0554	0.0010	286	8	302	9	427	40	95	67
333	392	0.30	0.0459	0.0012	0.3441	0.0105	0.0543	0.0008	290	7	300	8	384	35	96	75
334	274	0.07	0.3454	0.0100	5.9688	0.1834	0.1253	0.0013	1912	48	1971	27	2034	18	97	94
335	241	2.30	0.0462	0.0015	0.3444	0.0225	0.0541	0.0031	291	9	301	17	375	128	97	78
336	46		0.0958	0.0031	0.7994	0.0342	0.0605	0.0017	590	18	596	19	623	60	99	95
337	365	2.30	0.0447	0.0013	0.3261	0.0152	0.0530	0.0019	282	8	287	12	328	82	98	86
338	107		0.1099	0.0036	1.0905	0.0440	0.0720	0.0017	672	21	749	21	985	48	90	68
339	754	0.10	0.0484	0.0014	0.3756	0.0128	0.0562	0.0009	305	9	324	9	462	36	94	66
340	439	0.35	0.0458	0.0013	0.3386	0.0113	0.0537	0.0009	288	8	296	9	357	37	97	81
341	572	0.38	0.0504	0.0015	0.4004	0.0135	0.0577	0.0010	317	9	342	10	517	36	93	61
342	161	0.24	0.0556	0.0009	0.4218	0.0110	0.0550	0.0011	349	5	357	8	413	45	98	85
343	705	0.15	0.0541	0.0006	0.3993	0.0065	0.0535	0.0006	340	4	341	5	351	26	100	97
344	218		0.0601	0.0008	0.4615	0.0138	0.0557	0.0015	376	5	385	10	442	59	98	85
345	477	1.44	0.0550	0.0015	0.3733	0.0231	0.0492	0.0027	345	9	322	17	158	131	107	218
346	219	0.21	0.0526	0.0007	0.3906	0.0096	0.0539	0.0011	330	4	335	7	367	47	99	90
347	466	0.01	0.0547	0.0006	0.4019	0.0073	0.0533	0.0007	343	4	343	5	342	32	100	100
348	209	0.04	0.1032	0.0024	0.8506	0.0242	0.0598	0.0009	633	14	625	13	595	34	101	106
349	98	0.26	0.0918	0.0022	0.8422	0.0369	0.0666	0.0025	566	13	620	20	825	77	91	69
350	63	0.48	0.0560	0.0011	0.4153	0.0153	0.0538	0.0016	351	7	353	11	362	69	100	97
351	292	0.05	0.0614	0.0009	0.4632	0.0091	0.0547	0.0008	384	5	386	6	400	31	99	96
352	308		0.0943	0.0014	0.7719	0.0150	0.0594	0.0007	581	8	581	9	580	27	100	100
353	340		0.1157	0.0017	0.9991	0.0184	0.0627	0.0007	705	10	703	9	697	24	100	101
354	591	0.23	0.1028	0.0013	0.9061	0.0150	0.0639	0.0007	631	8	655	8	738	22	96	85
355	489	0.24	0.0489	0.0007	0.3716	0.0069	0.0551	0.0007	308	4	321	5	418	26	96	74
356	348	0.22	0.0543	0.0009	0.4034	0.0093	0.0539	0.0008	341	6	344	7	368	35	99	93
357	320	0.11	0.0578	0.0009	0.4275	0.0105	0.0536	0.0011	362	5	361	7	355	44	100	102
358	230	0.62	0.0524	0.0009	0.4169	0.0098	0.0577	0.0009	329	6	354	7	519	34	93	63
359	948	1.95	0.0506	0.0007	0.3707	0.0113	0.0532	0.0015	318	4	320	8	335	62	99	95
360	321	0.02	0.0457	0.0008	0.3304	0.0089	0.0524	0.0010	288	5	290	7	303	45	99	95
361	99		0.0944	0.0016	0.8323	0.0227	0.0639	0.0013	582	10	615	13	739	44	95	79
362	233		0.0495	0.0009	0.3657	0.0093	0.0536	0.0009	311	6	316	7	355	40	98	88
363	279	2.81	0.0427	0.0007	0.2903	0.0107	0.0493	0.0016	269	5	259	8	164	76	104	164
364	206		0.0526	0.0008	0.3829	0.0095	0.0527	0.0011	331	5	329	7	318	46	100	104
365	252	0.39	0.0590	0.0010	0.4344	0.0108	0.0534	0.0009	369	6	366	8	347	40	101	107
366	232	0.41	0.0543	0.0010	0.3976	0.0093	0.0531	0.0008	341	6	340	7	332	34	100	103
367	56	0.22	0.1182	0.0017	1.1147	0.0659	0.0684	0.0039	720	10	760	32	880	119	95	82
368	388	0.30	0.1707	0.0027	1.7616	0.0338	0.0748	0.0008	1016	15	1031	12	1064	22	99	95
369	317	0.40	0.0504	0.0007	0.3629	0.0079	0.0522	0.0009	317	4	314	6	294	38	101	108
370	845	0.60	0.0542	0.0008	0.4290	0.0082	0.0574	0.0007	340	5	362	6	509	28	94	67
371	149	0.02	0.1108	0.0018	0.9776	0.0284	0.0640	0.0015	677	11	692	15	741	50	98	91
372	447	0.83	0.0820	0.0012	0.7425	0.0169	0.0657	0.0011	508	7	564	10	796	37	90	64
373	669	0.42	0.0576	0.0007	0.4322	0.0079	0.0544	0.0007	361	4	365	6	388	30	99	93
374	419	0.62	0.0565	0.0009	0.4420	0.0102	0.0567	0.0010	355	5	372	7	480	39	95	74
375	506	1.81	0.0423	0.0007	0.2988	0.0073	0.0512	0.0010	267	4	265	6	250	44	101	107
376	117	0.10	0.0612	0.0011	0.4418	0.0147	0.0524	0.0014	383	7	372	10	301	63	103	127
377	343	0.17	0.0455	0.0006	0.3418	0.0075	0.0544	0.0009	287	4	298	6	389	39	96	74
378	253		0.0569	0.0009	0.4234	0.0105	0.0540	0.0010	357	5	358	7	370	43	100	97
379	258	0.14	0.0583	0.0009	0.4287	0.0092	0.0533	0.0008	365	5	362	7	341	35	101	107
380	149		0.0530	0.0010	0.3836	0.0125	0.0525	0.0014	333	6	330	9	308	60	101	108
381	218	0.22	0.0976	0.0013	0.7952	0.0151	0.0591	0.0008	600	7	594	9	571	30	101	105
382	416	0.40	0.0497	0.0006	0.3724	0.0071	0.0543	0.0008	313	4	321	5	384	32	97	82
383	409	0.06	0.0661	0.0009	0.5022	0.0105	0.0551	0.0009	412	6	413	7	417	35	100	99
384	469		0.0567	0.0009	0.4319	0.0099	0.0552	0.0009	356	5	365	7	421	38	98	84
385	163	1.94	0.0466	0.0009	0.3349	0.0177	0.0521	0.0026	294	5	293	13	289	113	100	102
386	1231	9.20	0.0321	0.0004	0.2421	0.0156	0.0547	0.0034	204	3	220	13	398	142	93	51
387	355	5.39	0.0508	0.0008	0.3700	0.0186	0.0528	0.0025	319	5	320	14	321	109	100	100
388	299		0.0515	0.0007	0.3761	0.0078	0.0529	0.0008	324	4	324	6	325	36	100	100
389	1195	6.36	0.0386	0.0005	0.2889	0.0058	0.0543	0.0008	244	3	258	5	385	34	95	63

Table B.1 Continued

#	U [ppm]	f206%	Isotope ratios						Ages (Ma)						Data filter A*	Data filter B#
			$^{206}Pb/^{238}U$	±2σ	$^{207}Pb/^{235}U$	±2σ	$^{207}Pb/^{206}Pb$	±2σ	$^{206}Pb/^{238}U$	±2σ	$^{207}Pb/^{235}U$	±2σ	$^{207}Pb/^{206}Pb$	±2σ		
390	368	0.70	0.0510	0.0009	0.4168	0.0116	0.0593	0.0012	321	6	354	8	577	45	91	56
391	158	2.36	0.0320	0.0009	0.2322	0.0168	0.0527	0.0035	203	5	212	14	315	154	96	64
392	308		0.0472	0.0006	0.3442	0.0071	0.0529	0.0008	297	4	300	5	326	36	99	91
393	312	0.27	0.1237	0.0016	1.0975	0.0202	0.0643	0.0008	752	9	752	10	753	28	100	100
394	284	0.39	0.0781	0.0011	0.6369	0.0150	0.0592	0.0011	485	7	500	9	573	40	97	85
395	582	3.59	0.0316	0.0007	0.2231	0.0252	0.0512	0.0057	201	4	205	21	248	242	98	81
396	292		0.0496	0.0007	0.3645	0.0074	0.0533	0.0008	312	4	316	6	342	34	99	91
397	275	0.78	0.0466	0.0007	0.3526	0.0076	0.0549	0.0009	294	4	307	6	407	36	96	72
398	777	0.29	0.0461	0.0007	0.3402	0.0064	0.0535	0.0006	290	4	297	5	351	27	98	83
399	380	0.19	0.0588	0.0008	0.4467	0.0091	0.0551	0.0008	368	5	375	6	417	33	98	88
400	86	0.93	0.0862	0.0027	0.7297	0.0458	0.0614	0.0033	533	16	556	27	653	116	96	82
401	193		0.0857	0.0015	0.6875	0.0157	0.0582	0.0009	530	9	531	9	538	32	100	98
402	83	2.53	0.0824	0.0014	0.6080	0.0185	0.0535	0.0014	511	8	482	12	349	58	106	146
403	425		0.1125	0.0019	0.9690	0.0184	0.0624	0.0006	687	11	688	10	689	20	100	100
404	436		0.0505	0.0009	0.3686	0.0088	0.0530	0.0009	317	5	319	7	328	37	100	97
405	182	0.73	0.1469	0.0025	1.4970	0.0327	0.0739	0.0010	884	14	929	13	1039	28	95	85
406	129	0.17	0.1428	0.0031	1.3351	0.0362	0.0678	0.0011	861	18	861	16	863	33	100	100
407	299		0.0500	0.0008	0.3608	0.0079	0.0523	0.0007	315	5	313	6	300	32	101	105
408	309	0.46	0.0495	0.0009	0.3766	0.0095	0.0552	0.0010	312	5	325	7	419	39	96	74
409	410		0.0483	0.0008	0.3510	0.0075	0.0527	0.0007	304	5	306	6	317	30	99	96

KAR9: Küçükbahçe Formation

#	U [ppm]	f206%	Isotope ratios						Ages (Ma)						Data filter A*	Data filter B#
			$^{206}Pb/^{238}U$	±2σ	$^{207}Pb/^{235}U$	±2σ	$^{207}Pb/^{206}Pb$	±2σ	$^{206}Pb/^{238}U$	±2σ	$^{207}Pb/^{235}U$	±2σ	$^{207}Pb/^{206}Pb$	±2σ		
410	647	0.05	0.3661	0.0054	6.1833	0.1071	0.1225	0.0011	2011	26	2002	15	1993	16	100	101
411	321	0.40	0.0661	0.0011	0.5381	0.0117	0.0591	0.0008	412	7	437	8	570	31	94	72
412	354	0.85	0.1004	0.0017	0.8546	0.0227	0.0617	0.0013	617	10	627	12	665	43	98	93
413	105	0.02	0.2984	0.0045	4.5816	0.0866	0.1113	0.0013	1684	22	1746	16	1821	21	96	92
414	118	0.11	0.1815	0.0042	1.8272	0.0474	0.0730	0.0009	1075	23	1055	17	1015	25	102	106
415	45	0.06	0.4061	0.0062	7.4430	0.1494	0.1329	0.0017	2197	29	2166	18	2137	23	101	103
416	242	0.32	0.1094	0.0016	1.0797	0.0213	0.0716	0.0010	669	9	743	10	974	28	90	69
417	243	0.52	0.0959	0.0013	0.8935	0.0226	0.0675	0.0014	591	8	648	12	855	44	91	69
418	296	0.35	0.0866	0.0013	0.7351	0.0152	0.0616	0.0009	535	8	560	9	659	31	96	81
419	242	0.52	0.0997	0.0012	0.8913	0.0158	0.0649	0.0008	612	7	647	8	770	27	95	80
420	172	0.05	0.0766	0.0010	0.6280	0.0148	0.0594	0.0012	476	6	495	9	583	43	96	82
421	137	0.78	0.0593	0.0011	0.4683	0.0219	0.0573	0.0025	371	7	390	15	502	95	95	74
422	639	0.05	0.0590	0.0006	0.4379	0.0074	0.0539	0.0007	369	4	369	5	365	29	100	101
423	655	0.34	0.0956	0.0013	0.8231	0.0181	0.0625	0.0011	588	8	610	10	690	36	96	85
424	157	1.11	0.1068	0.0026	0.8303	0.0290	0.0564	0.0014	654	15	614	16	467	56	107	140
425	320	0.03	0.0567	0.0006	0.4176	0.0078	0.0534	0.0008	356	4	354	6	346	34	100	103
426	208	0.73	0.0742	0.0015	0.5836	0.0200	0.0571	0.0016	461	9	467	13	495	61	99	93
427	504	0.22	0.0512	0.0005	0.3859	0.0059	0.0546	0.0007	322	3	331	4	397	27	97	81
428	634	0.53	0.1284	0.0018	1.1122	0.0243	0.0628	0.0011	779	10	759	12	702	36	103	111
429	186	0.04	0.0842	0.0013	0.6701	0.0134	0.0577	0.0007	521	8	521	8	520	28	100	100
430	155	1.13	0.0643	0.0010	0.4835	0.0141	0.0545	0.0013	402	6	400	10	393	54	100	102
431	688		0.0553	0.0007	0.4055	0.0068	0.0532	0.0006	347	4	346	5	339	26	100	102
432	1794	0.11	0.1024	0.0012	0.8848	0.0144	0.0626	0.0007	629	7	644	8	696	23	98	90
433	111	0.89	0.0971	0.0018	0.8040	0.0186	0.0601	0.0008	597	11	599	10	606	30	100	99
434	304	0.63	0.1004	0.0011	0.8631	0.0131	0.0623	0.0006	617	7	632	7	685	22	98	90
435	2496	2.76	0.0393	0.0006	0.2972	0.0093	0.0549	0.0015	248	4	264	7	407	61	94	61
436	469		0.1426	0.0025	1.3781	0.0278	0.0701	0.0007	859	14	880	12	931	21	98	92
437	422	0.07	0.1682	0.0031	1.6022	0.0346	0.0691	0.0008	1002	17	971	14	902	23	103	111
438	168	0.03	0.0918	0.0016	0.7848	0.0185	0.0620	0.0010	566	9	588	11	673	35	96	84
439	137	1.16	0.0759	0.0018	0.5893	0.0308	0.0563	0.0026	472	11	470	20	465	103	100	101
440	621		0.1803	0.0028	1.9309	0.0443	0.0777	0.0013	1068	15	1092	15	1139	33	98	94
441	613	0.17	0.0755	0.0012	0.6102	0.0126	0.0586	0.0008	469	7	484	8	554	28	97	85
442	805	0.02	0.1074	0.0019	0.9207	0.0193	0.0622	0.0007	658	11	663	10	680	23	99	97
443	402	0.88	0.0972	0.0018	0.9075	0.0202	0.0677	0.0009	598	10	656	11	860	26	91	69
444	380	0.34	0.1154	0.0021	1.0800	0.0256	0.0679	0.0010	704	12	744	13	864	32	95	81
445	175	0.61	0.0976	0.0026	0.8795	0.0304	0.0653	0.0014	600	15	641	16	785	46	94	76
446	127	0.16	0.3458	0.0068	5.6544	0.1274	0.1186	0.0013	1914	32	1924	19	1935	20	99	99
447	688	0.05	0.0502	0.0009	0.3696	0.0080	0.0534	0.0006	315	6	319	6	348	26	99	91
448	493		0.0513	0.0009	0.3926	0.0088	0.0555	0.0007	322	6	336	6	434	30	96	74
449	251		0.0998	0.0018	0.8419	0.0181	0.0612	0.0008	613	10	620	10	645	27	99	95
450	669	0.14	0.0927	0.0016	0.8003	0.0160	0.0626	0.0006	572	10	597	9	694	20	96	82
451	301		0.0785	0.0018	0.6650	0.0192	0.0614	0.0010	487	11	518	12	655	36	94	74
452	396	0.35	0.1428	0.0021	1.3934	0.0308	0.0708	0.0012	861	12	886	13	951	34	97	91
453	139		0.1077	0.0019	0.9137	0.0248	0.0615	0.0013	660	11	659	13	657	45	100	100
454	616	0.88	0.0848	0.0012	0.7451	0.0168	0.0637	0.0011	525	7	565	10	733	36	93	72
455	616	0.18	0.1352	0.0024	1.2043	0.0255	0.0646	0.0007	818	14	803	12	761	24	102	107
456	157		0.0992	0.0016	0.8256	0.0188	0.0604	0.0010	610	9	611	10	617	35	100	99
457	144		0.1055	0.0013	0.9186	0.0231	0.0631	0.0014	647	8	662	12	713	46	98	91
458	282	0.29	0.0810	0.0009	0.6397	0.0114	0.0573	0.0008	502	5	502	7	502	30	100	100
459	158	1.23	0.0693	0.0011	0.4931	0.0233	0.0516	0.0023	432	6	407	16	268	103	106	161
460	415	0.24	0.0516	0.0007	0.3792	0.0073	0.0533	0.0007	325	4	326	5	340	32	99	95
461	206	0.42	0.0802	0.0011	0.6435	0.0128	0.0582	0.0009	497	6	504	8	536	32	99	93
462	67	0.94	0.0882	0.0015	0.7870	0.0251	0.0647	0.0018	545	9	589	14	765	57	92	71
463	22	0.04	0.1335	0.0025	1.1820	0.0513	0.0642	0.0025	808	14	792	24	749	83	102	108
464	584	0.18	0.0568	0.0009	0.4240	0.0087	0.0541	0.0007	356	5	359	6	375	30	99	95
465	315	0.20	0.0671	0.0021	0.5486	0.0230	0.0593	0.0017	419	12	444	15	578	62	94	72
466	169		0.0572	0.0009	0.4391	0.0105	0.0557	0.0010	359	5	370	7	439	42	97	82

Table B.1 Continued

#	U [ppm]	ƒ206%	Isotope ratios						Ages (Ma)						Data filter A*	Data filter B#
			$^{206}Pb/^{238}U$	±2σ	$^{207}Pb/^{235}U$	±2σ	$^{207}Pb/^{206}Pb$	±2σ	$^{206}Pb/^{238}U$	±2σ	$^{207}Pb/^{235}U$	±2σ	$^{207}Pb/^{206}Pb$	±2σ		
467	61		0.3761	0.0057	6.3356	0.1182	0.1222	0.0013	2058	27	2023	16	1988	19	102	103
468	291	0.51	0.0936	0.0017	0.7809	0.0188	0.0605	0.0010	577	10	586	11	621	34	98	93
469	226	2.44	0.0850	0.0022	0.6762	0.0348	0.0577	0.0026	526	13	524	21	519	98	100	101
470	325	0.23	0.0492	0.0008	0.3883	0.0145	0.0572	0.0019	310	5	333	11	499	74	93	62
471	231	0.90	0.0682	0.0013	0.5566	0.0147	0.0592	0.0011	425	8	449	10	575	39	95	74
472	189	0.28	0.1144	0.0032	1.0118	0.0433	0.0641	0.0021	698	19	710	22	746	68	98	94
473	626	0.04	0.1091	0.0017	0.9300	0.0170	0.0618	0.0006	668	10	668	9	668	20	100	100

KAR10: Küçükbahçe Formation

#	U [ppm]	ƒ206%	Isotope ratios						Ages (Ma)						Data filter A*	Data filter B#
			$^{206}Pb/^{238}U$	±2σ	$^{207}Pb/^{235}U$	±2σ	$^{207}Pb/^{206}Pb$	±2σ	$^{206}Pb/^{238}U$	±2σ	$^{207}Pb/^{235}U$	±2σ	$^{207}Pb/^{206}Pb$	±2σ		
474	245		0.0699	0.0014	0.5605	0.0138	0.0582	0.0008	435	9	452	9	537	30	96	81
475	58	0.01	0.1187	0.0026	1.1135	0.0377	0.0680	0.0017	723	15	760	18	870	53	95	83
476	1980	0.32	0.0811	0.0014	0.6837	0.0137	0.0611	0.0006	503	8	529	8	644	22	95	78
477	243		0.0835	0.0016	0.6796	0.0205	0.0590	0.0014	517	10	527	12	567	50	98	91
478	688		0.0529	0.0011	0.4064	0.0107	0.0557	0.0009	332	7	346	8	440	36	96	75
479	646	0.36	0.0915	0.0018	0.7643	0.0179	0.0606	0.0008	565	11	576	10	624	28	98	91
480	341		0.0539	0.0010	0.4049	0.0106	0.0545	0.0011	338	6	345	8	391	43	98	87
481	328	0.23	0.0501	0.0009	0.3794	0.0100	0.0550	0.0010	315	6	327	7	411	42	96	77
482	414		0.1192	0.0028	0.9860	0.0263	0.0600	0.0008	726	16	697	13	604	28	104	120
483	206		0.1135	0.0022	1.0152	0.0264	0.0648	0.0012	693	12	711	13	770	38	97	90
484	1095	0.20	0.0528	0.0010	0.3907	0.0100	0.0537	0.0009	332	6	335	7	357	37	99	93
485	492		0.1105	0.0023	0.9330	0.0225	0.0612	0.0007	676	13	669	12	647	26	101	104
486	212	0.04	0.0730	0.0015	0.6144	0.0182	0.0611	0.0013	454	9	486	11	642	45	93	71
487	90	0.55	0.1327	0.0023	1.2415	0.0354	0.0678	0.0015	803	13	820	16	864	47	98	93
488	242	0.12	0.0910	0.0014	0.7584	0.0162	0.0604	0.0009	562	8	573	9	619	31	98	91
489	133	0.57	0.1063	0.0021	0.9445	0.0251	0.0644	0.0012	651	12	675	13	755	38	96	86
490	487		0.0645	0.0010	0.5021	0.0101	0.0564	0.0007	403	6	413	7	469	28	98	86
491	205	0.95	0.0895	0.0030	0.8311	0.0329	0.0674	0.0015	552	17	614	18	849	46	90	65
492	245	0.23	0.1514	0.0045	1.4272	0.0603	0.0684	0.0020	909	25	900	25	880	62	101	103
493	168	0.47	0.1881	0.0056	1.9483	0.0650	0.0751	0.0012	1111	30	1098	22	1072	31	101	104
494	56		0.0932	0.0017	0.8437	0.0287	0.0657	0.0019	574	10	621	16	796	60	92	72
495	117	1.03	0.1809	0.0042	1.9390	0.0642	0.0777	0.0018	1072	23	1095	22	1140	47	98	94
496	1129	0.60	0.0783	0.0012	0.6628	0.0121	0.0614	0.0006	486	7	516	7	652	22	94	75
497	253	0.42	0.0750	0.0016	0.5946	0.0171	0.0575	0.0011	466	9	474	11	510	43	98	91
498	448		0.0736	0.0011	0.5763	0.0122	0.0568	0.0008	458	7	462	8	484	32	99	94
499	315	0.37	0.0912	0.0017	0.7543	0.0209	0.0600	0.0012	563	10	571	12	602	45	99	93
500	809	1.23	0.0836	0.0018	0.6407	0.0285	0.0556	0.0022	517	10	503	18	436	87	103	119
501	276	0.03	0.0999	0.0031	0.9103	0.0306	0.0661	0.0009	614	18	657	16	809	28	93	76
502	126	0.59	0.1589	0.0027	1.6299	0.0562	0.0744	0.0022	951	15	982	22	1052	61	97	90
503	853	0.20	0.0489	0.0007	0.3784	0.0068	0.0561	0.0007	308	4	326	5	456	26	94	67
504	191	0.64	0.1670	0.0028	1.7417	0.0367	0.0756	0.0009	996	16	1024	14	1085	25	97	92
505	116	0.52	0.0916	0.0021	0.7437	0.0235	0.0589	0.0013	565	12	565	14	562	47	100	101
506	101	0.19	0.3201	0.0092	5.3173	0.1654	0.1205	0.0015	1790	45	1872	27	1963	22	96	91
507	143	0.22	0.1664	0.0060	1.5241	0.0629	0.0664	0.0013	992	33	940	25	821	42	106	121
508	387	0.70	0.0567	0.0024	0.4641	0.0223	0.0594	0.0014	356	15	387	15	581	51	92	61
509	308	0.07	0.0927	0.0028	0.7901	0.0269	0.0618	0.0010	572	17	591	15	668	34	97	86
510	76	0.06	0.5241	0.0175	15.7046	0.5738	0.2173	0.0032	2716	74	2859	35	2961	24	95	92
511	241	0.13	0.1549	0.0047	1.5595	0.0534	0.0730	0.0011	928	26	954	21	1015	31	97	91
512	198	0.18	0.1845	0.0064	1.8173	0.0671	0.0714	0.0009	1091	35	1052	24	970	26	104	113
513	230	0.01	0.0961	0.0028	0.8129	0.0271	0.0614	0.0010	591	16	604	15	652	35	98	91
514	140	1.40	0.1179	0.0045	0.9714	0.0826	0.0597	0.0045	719	26	689	43	594	166	104	121
515	58		0.1097	0.0045	0.9433	0.0485	0.0624	0.0020	671	26	675	25	687	68	99	98
516	95	0.15	0.1035	0.0028	0.9061	0.0305	0.0635	0.0013	635	16	655	16	724	43	97	88
517	410	0.09	0.1107	0.0039	0.9470	0.0368	0.0620	0.0010	677	23	677	19	675	35	100	100
518	232		0.1122	0.0031	0.9803	0.0314	0.0634	0.0011	685	18	694	16	721	36	99	95
519	572	0.31	0.0842	0.0021	0.7231	0.0214	0.0623	0.0010	521	12	552	13	685	34	94	76
520	340	0.00	0.3443	0.0079	5.7968	0.1400	0.1221	0.0009	1907	38	1946	21	1987	13	98	96
521	125	1.42	0.0925	0.0019	0.6925	0.0212	0.0543	0.0012	570	11	534	13	384	51	107	149
522	299		0.0939	0.0021	0.8060	0.0228	0.0623	0.0011	578	12	600	13	683	38	96	85
523	181	0.48	0.0991	0.0019	0.8604	0.0240	0.0630	0.0013	609	11	630	13	708	43	97	86
524	286		0.0666	0.0013	0.5264	0.0137	0.0573	0.0010	416	8	429	9	504	39	97	82
525	69	0.10	0.3968	0.0084	7.4449	0.2019	0.1361	0.0023	2154	39	2166	24	2178	30	99	99
526	58		0.1039	0.0024	0.9157	0.0337	0.0639	0.0019	637	14	660	18	738	61	97	86
527	244	0.10	0.3105	0.0056	4.9258	0.1032	0.1150	0.0012	1743	28	1807	18	1881	19	96	93
528	384	0.31	0.0981	0.0016	0.8701	0.0432	0.0643	0.0030	604	9	636	23	752	99	95	80
529	337	0.70	0.0761	0.0020	0.6313	0.0188	0.0602	0.0008	473	12	497	12	610	29	95	77
530	325	0.29	0.0579	0.0019	0.4780	0.0181	0.0598	0.0011	363	12	397	12	598	40	92	61
531	304	0.97	0.0786	0.0024	0.6486	0.0230	0.0598	0.0011	488	14	508	14	597	40	96	82
532	1053	0.05	0.0776	0.0021	0.6204	0.0180	0.0580	0.0006	482	13	490	11	529	22	98	91
533	274		0.0614	0.0021	0.5004	0.0212	0.0591	0.0015	384	13	412	14	570	54	93	67
534	542	0.10	0.0807	0.0027	0.6503	0.0252	0.0584	0.0012	500	16	509	16	546	45	98	92
535	1279	0.81	0.0477	0.0014	0.3659	0.0116	0.0556	0.0006	301	9	317	9	436	22	95	69
536	467	0.44	0.0708	0.0014	0.6105	0.0162	0.0625	0.0011	441	9	484	10	691	36	91	64
537	311	0.61	0.0615	0.0019	0.5208	0.0213	0.0614	0.0016	385	12	426	14	653	57	90	59
538	653	1.17	0.0883	0.0023	0.6756	0.0266	0.0555	0.0017	545	13	524	16	432	67	104	126

Table B.1 Continued

KAR11: Küçükbahçe Formation

#	U [ppm]	ƒ206%	Isotope ratios						Ages (Ma)						Data filter A*	Data filter B#
			$^{206}Pb/^{238}U$	±2σ	$^{207}Pb/^{235}U$	±2σ	$^{207}Pb/^{206}Pb$	±2σ	$^{206}Pb/^{238}U$	±2σ	$^{207}Pb/^{235}U$	±2σ	$^{207}Pb/^{206}Pb$	±2σ		
539	262	0.22	0.0808	0.0017	0.6725	0.0169	0.0604	0.0008	501	10	522	10	618	30	96	81
540	603	0.01	0.4604	0.0077	11.2183	0.2203	0.1767	0.0018	2441	34	2541	18	2623	17	96	93
541	504	1.18	0.2260	0.0080	2.6087	0.1591	0.0837	0.0042	1314	42	1303	45	1286	97	101	102
542	345		0.0922	0.0023	0.7707	0.0217	0.0606	0.0008	568	13	580	12	627	29	98	91
543	434	0.88	0.0651	0.0014	0.5247	0.0130	0.0585	0.0007	407	8	428	9	547	28	95	74
544	537		0.0682	0.0014	0.5298	0.0136	0.0564	0.0008	425	9	432	9	466	33	99	91
545	220	0.35	0.1122	0.0027	1.1236	0.0351	0.0726	0.0015	686	16	765	17	1003	41	90	68
546	329	0.29	0.1433	0.0032	1.4528	0.0367	0.0735	0.0009	863	18	911	15	1029	24	95	84
547	823	0.02	0.0859	0.0019	0.6890	0.0172	0.0582	0.0006	531	12	532	10	536	23	100	99
548	110	0.08	0.4478	0.0110	9.5344	0.2797	0.1544	0.0025	2385	49	2391	27	2396	27	100	100
549	417	0.05	0.5446	0.0140	13.4520	0.3714	0.1791	0.0018	2803	59	2712	26	2645	17	103	106
550	153	0.12	0.1080	0.0026	1.0182	0.0370	0.0684	0.0018	661	15	713	19	880	55	93	75
551	110	1.76	0.1213	0.0033	1.0471	0.0529	0.0626	0.0027	738	19	727	26	694	91	101	106
552	118	0.03	0.2837	0.0075	4.2689	0.1258	0.1091	0.0014	1610	37	1687	24	1785	24	95	90
553	146	0.95	0.1171	0.0030	1.0480	0.0322	0.0649	0.0011	714	17	728	16	771	37	98	93
554	708	0.19	0.0895	0.0020	0.7237	0.0175	0.0586	0.0006	553	12	553	10	553	23	100	100
555	266		0.0793	0.0018	0.6417	0.0192	0.0587	0.0011	492	11	503	12	555	42	98	89
556	367	0.60	0.1076	0.0018	0.9621	0.0207	0.0649	0.0008	659	11	684	11	770	28	96	86
557	228	0.08	0.3509	0.0053	5.6227	0.1029	0.1162	0.0012	1939	25	1920	16	1899	19	101	102
558	261		0.0618	0.0011	0.4977	0.0128	0.0584	0.0011	386	7	410	9	546	40	94	71
559	488	0.19	0.0570	0.0009	0.4424	0.0106	0.0563	0.0010	357	5	372	7	464	40	96	77
560	218	0.06	0.0851	0.0019	0.7166	0.0273	0.0611	0.0019	526	11	549	16	643	67	96	82
561	145	0.66	0.1295	0.0022	1.1003	0.0262	0.0616	0.0010	785	12	754	13	660	36	104	119
562	105	1.17	0.1061	0.0018	0.8736	0.0258	0.0597	0.0014	650	10	638	14	594	52	102	109
563	30	0.89	0.3584	0.0062	5.5545	0.1369	0.1124	0.0020	1974	30	1909	21	1839	32	103	107
564	399	0.04	0.0856	0.0094	0.6739	0.0756	0.0571	0.0012	530	56	523	46	495	45	101	107
565	203	1.83	0.1011	0.0111	0.8227	0.0925	0.0590	0.0014	621	65	610	52	568	53	102	109
566	366	0.29	0.0597	0.0066	0.4680	0.0528	0.0568	0.0014	374	40	390	37	485	55	96	77
567	303		0.0600	0.0066	0.4621	0.0516	0.0559	0.0012	376	40	386	36	447	48	97	84
568	448	0.31	0.0915	0.0100	0.7485	0.0840	0.0593	0.0014	564	59	567	49	579	52	99	97
569	145	1.62	0.0791	0.0088	0.6232	0.0844	0.0572	0.0044	491	52	492	53	498	172	100	99
570	427	1.40	0.0821	0.0091	0.6406	0.0741	0.0566	0.0019	509	54	503	46	475	75	101	107
571	42		0.1198	0.0132	1.0800	0.1311	0.0654	0.0033	729	76	744	64	787	107	98	93
572	83	0.19	0.1141	0.0020	0.9684	0.0220	0.0616	0.0009	696	12	688	11	659	31	101	106
573	113	0.11	0.1760	0.0028	1.7646	0.0341	0.0727	0.0008	1045	15	1033	13	1006	22	101	104
574	248	0.27	0.0819	0.0014	0.6761	0.0133	0.0599	0.0006	507	8	524	8	600	23	97	85
575	125		0.4730	0.0087	12.0184	0.2559	0.1843	0.0019	2497	38	2606	20	2692	17	96	93
576	160	0.08	0.0792	0.0014	0.6845	0.0192	0.0627	0.0013	491	8	530	12	698	46	93	70
577	226	0.10	0.4835	0.0095	12.3193	0.2666	0.1848	0.0017	2542	41	2629	20	2697	15	97	94
578	413	0.86	0.0931	0.0018	0.8655	0.0206	0.0674	0.0010	574	10	633	11	850	30	91	68
579	634	0.14	0.0918	0.0023	0.7640	0.0206	0.0604	0.0006	566	13	576	12	617	23	98	92
580	138	0.12	0.4296	0.0084	10.0855	0.2298	0.1703	0.0020	2304	38	2443	21	2560	20	94	90
581	37	0.50	0.0901	0.0016	0.7812	0.0224	0.0629	0.0014	556	9	586	13	706	49	95	79
582	486	0.39	0.1236	0.0022	1.1015	0.0226	0.0646	0.0006	751	13	754	11	762	21	100	99
583	841	0.38	0.3047	0.0085	4.0979	0.2236	0.0975	0.0046	1714	42	1654	45	1578	88	104	109
584	103		0.0994	0.0019	0.8443	0.0230	0.0616	0.0012	611	11	621	13	659	43	98	93
585	135	0.53	0.1019	0.0019	0.8699	0.0200	0.0619	0.0008	626	11	636	11	671	29	98	93
586	51		0.1629	0.0039	1.6010	0.0482	0.0713	0.0013	973	21	971	19	965	38	100	101
587	388	0.34	0.0674	0.0013	0.5347	0.0127	0.0575	0.0008	421	8	435	8	511	31	97	82
588	616	0.59	0.0488	0.0025	0.3871	0.0209	0.0575	0.0010	307	15	332	15	511	39	92	60
589	308	0.05	0.0958	0.0049	0.7940	0.0430	0.0601	0.0011	590	29	593	24	607	40	99	97
590	496	0.44	0.1056	0.0056	0.9521	0.0548	0.0654	0.0015	647	32	679	29	787	49	95	82
591	307	0.03	0.0997	0.0051	0.8476	0.0441	0.0616	0.0007	613	30	623	24	662	25	98	93
592	219	0.83	0.1002	0.0055	0.9506	0.0557	0.0688	0.0014	615	32	678	29	894	42	91	69
593	178		0.0690	0.0035	0.5376	0.0308	0.0565	0.0014	430	21	437	20	471	56	99	91
594	69		0.0987	0.0051	0.8476	0.0469	0.0623	0.0012	607	30	623	26	684	41	97	89
595	110	1.14	0.1084	0.0061	0.8636	0.0643	0.0578	0.0028	664	35	632	35	521	108	105	127
596	273	1.51	0.0690	0.0039	0.5194	0.0374	0.0546	0.0025	430	23	425	25	395	101	101	109
597	255	0.01	0.1105	0.0061	0.9341	0.0547	0.0613	0.0012	676	36	670	29	650	41	101	104
598	361	0.13	0.0549	0.0030	0.4109	0.0245	0.0543	0.0012	345	19	350	18	382	50	99	90
599	74		0.5459	0.0305	13.4056	0.7934	0.1781	0.0035	2808	127	2709	56	2635	32	104	107
600	141	0.11	0.1142	0.0067	1.0033	0.0638	0.0637	0.0015	697	39	705	32	732	50	99	95
601	333	1.08	0.1388	0.0077	1.4013	0.0846	0.0732	0.0017	838	44	890	36	1020	48	94	82
602	205	0.65	0.0717	0.0040	0.5894	0.0357	0.0597	0.0015	446	24	471	23	591	54	95	75
603	209	0.93	0.0726	0.0028	0.6399	0.0381	0.0639	0.0029	452	17	502	24	739	97	90	61
604	147	0.44	0.1730	0.0058	1.9551	0.0759	0.0819	0.0016	1029	32	1100	26	1244	39	94	83
605	385	1.69	0.0960	0.0027	0.8058	0.0270	0.0609	0.0011	591	16	600	15	636	39	98	93
606	167	0.10	0.2938	0.0089	4.2678	0.1648	0.1054	0.0025	1660	45	1687	32	1721	44	98	96
607	287	0.25	0.4104	0.0121	7.4153	0.3221	0.1310	0.0042	2217	56	2163	39	2112	56	102	105
608	272	0.20	0.2921	0.0086	4.3284	0.1479	0.1075	0.0019	1652	43	1699	28	1757	32	97	94
609	233	0.74	0.1449	0.0049	1.3846	0.0640	0.0693	0.0022	872	27	882	27	908	65	99	96
610	275	0.02	0.6328	0.0253	19.8821	0.8823	0.2279	0.0044	3160	100	3086	43	3037	31	102	104
611	293	0.51	0.1154	0.0013	1.0224	0.0159	0.0643	0.0007	704	8	715	8	750	22	98	94
612	536	0.25	0.0505	0.0023	0.3917	0.0186	0.0562	0.0008	318	14	336	14	462	30	95	69
613	251	1.04	0.0879	0.0012	0.6522	0.0147	0.0538	0.0010	543	7	510	9	362	42	107	150
614	274	0.37	0.0917	0.0011	0.7391	0.0131	0.0585	0.0007	565	7	562	8	547	28	101	103
615	107	0.13	0.1027	0.0018	0.8525	0.0206	0.0602	0.0010	630	10	626	11	610	37	101	103
616	368	0.21	0.0677	0.0011	0.5157	0.0114	0.0552	0.0008	423	7	422	8	421	34	100	100
617	139	0.52	0.0839	0.0009	0.7041	0.0137	0.0608	0.0010	519	5	541	8	634	35	96	82
618	620	0.65	0.0809	0.0013	0.6758	0.0176	0.0606	0.0013	501	8	524	11	626	45	96	80
619	141	4.36	0.0607	0.0012	0.4650	0.0403	0.0556	0.0047	380	7	388	28	437	189	98	87

Table B.1 Continued

#	U [ppm]	ƒ206%	Isotope ratios						Ages (Ma)						Data filter A*	Data filter B#
			$^{206}Pb/^{238}U$	±2σ	$^{207}Pb/^{235}U$	±2σ	$^{207}Pb/^{206}Pb$	±2σ	$^{206}Pb/^{238}U$	±2σ	$^{207}Pb/^{235}U$	±2σ	$^{207}Pb/^{206}Pb$	±2σ		
620	368	0.29	0.0896	0.0019	0.7821	0.0242	0.0633	0.0015	553	11	587	14	719	49	94	77
621	226	0.87	0.1876	0.0043	2.0497	0.0562	0.0792	0.0012	1108	23	1132	19	1178	30	98	94
622	158	0.06	0.1781	0.0024	1.8490	0.0330	0.0753	0.0009	1057	13	1063	12	1076	23	99	98
623	454	0.41	0.0861	0.0013	0.7484	0.0144	0.0630	0.0007	533	8	567	8	709	25	94	75
624	2892	2.16	0.0595	0.0007	0.4649	0.0107	0.0567	0.0011	373	4	388	7	478	43	96	78
625	132	0.19	0.1010	0.0029	0.9260	0.0410	0.0665	0.0022	620	17	666	22	822	70	93	76
626	314	1.72	0.0565	0.0014	0.3777	0.0163	0.0485	0.0017	354	8	325	12	124	84	109	286
627	501	0.31	0.0778	0.0012	0.6235	0.0144	0.0581	0.0010	483	7	492	9	535	36	98	90

KAR27: Küçükbahçe Formation

#	U [ppm]	ƒ206%	Isotope ratios						Ages (Ma)						Data filter A*	Data filter B#
			$^{206}Pb/^{238}U$	±2σ	$^{207}Pb/^{235}U$	±2σ	$^{207}Pb/^{206}Pb$	±2σ	$^{206}Pb/^{238}U$	±2σ	$^{207}Pb/^{235}U$	±2σ	$^{207}Pb/^{206}Pb$	±2σ		
628	132	0.85	0.0877	0.0034	0.7200	0.0319	0.0595	0.0013	542	20	551	19	587	46	98	92
629	286	0.09	0.4876	0.0157	11.8010	0.4005	0.1755	0.0019	2560	68	2589	32	2611	18	99	98
630	718	0.18	0.1419	0.0046	1.3103	0.0456	0.0670	0.0008	855	26	850	20	837	26	101	102
631	79	0.92	0.1384	0.0046	1.2874	0.0512	0.0675	0.0015	836	26	840	23	852	46	99	98
632	134	0.73	0.1275	0.0044	1.1079	0.0558	0.0630	0.0023	774	25	757	27	709	78	102	109
633	256	0.30	0.3584	0.0115	5.9504	0.2035	0.1204	0.0014	1975	55	1969	30	1962	21	100	101
634	181	0.11	0.0614	0.0020	0.5149	0.0222	0.0608	0.0017	384	12	422	15	633	60	91	61
635	52		0.1424	0.0053	1.3907	0.0814	0.0708	0.0032	858	30	885	35	953	93	97	90
636	95	0.10	0.3152	0.0105	5.1418	0.1829	0.1183	0.0015	1766	51	1843	30	1931	23	96	91
637	449	0.20	0.0576	0.0011	0.4298	0.0105	0.0542	0.0008	361	7	363	7	378	35	99	95
638	175	0.04	0.2989	0.0059	4.4511	0.1048	0.1080	0.0014	1686	29	1722	20	1766	23	98	95
639	184	0.10	0.1668	0.0039	1.7193	0.0494	0.0748	0.0012	994	22	1016	18	1062	33	98	94
640	40		0.1731	0.0049	1.7303	0.0731	0.0725	0.0023	1029	27	1020	27	1000	64	101	103
641	66	0.50	0.1758	0.0035	1.8015	0.0504	0.0743	0.0015	1044	19	1046	18	1050	40	100	99
642	517	0.31	0.1007	0.0019	0.8583	0.0199	0.0618	0.0008	618	11	629	11	668	29	98	93
643	406	1.19	0.0592	0.0006	0.4419	0.0126	0.0542	0.0014	371	4	372	9	378	60	100	98
644	400	0.16	0.0971	0.0010	0.8163	0.0182	0.0610	0.0012	597	6	606	10	639	43	99	93
645	173	0.84	0.0948	0.0011	0.8153	0.0223	0.0624	0.0015	584	7	605	12	687	53	96	85
646	311	0.24	0.1142	0.0017	0.9661	0.0237	0.0614	0.0012	697	10	686	12	652	42	102	107
647	126	1.95	0.1240	0.0018	1.2128	0.0641	0.0709	0.0036	754	10	806	29	956	104	93	79
648	75	1.18	0.1000	0.0016	0.7707	0.0329	0.0559	0.0022	614	10	580	19	449	88	106	137
649	78	0.18	0.3876	0.0046	6.7044	0.1727	0.1254	0.0029	2112	21	2073	23	2035	40	102	104
650	314	0.56	0.1112	0.0013	0.9749	0.0243	0.0636	0.0014	680	8	691	13	728	46	98	93
651	685	0.36	0.0527	0.0006	0.4044	0.0110	0.0556	0.0014	331	4	345	8	437	54	96	76
652	245		0.1028	0.0015	0.8855	0.0209	0.0625	0.0011	631	9	644	11	690	39	98	91
653	314	2.03	0.0864	0.0014	0.6783	0.0217	0.0570	0.0016	534	8	526	13	490	61	102	109
654	272	2.27	0.0697	0.0011	0.4827	0.0331	0.0502	0.0033	434	7	400	23	205	155	109	212
655	473	1.79	0.1473	0.0022	1.3402	0.0496	0.0660	0.0022	886	12	863	22	805	71	103	110
656	415	1.30	0.0566	0.0015	0.3830	0.0203	0.0491	0.0023	355	9	329	15	151	109	108	236
657	1270	1.14	0.0468	0.0008	0.3320	0.0149	0.0515	0.0021	295	5	291	11	263	96	101	112
658	103	0.63	0.1420	0.0023	1.3635	0.0472	0.0696	0.0021	856	13	873	20	918	63	98	93
659	585	0.39	0.0541	0.0009	0.4191	0.0109	0.0562	0.0012	340	5	355	8	460	46	96	74
660	603	0.19	0.0698	0.0019	0.5685	0.0217	0.0591	0.0016	435	11	457	14	569	58	95	76
661	483	0.09	0.0557	0.0012	0.4178	0.0104	0.0544	0.0007	349	7	354	7	387	30	99	90
662	285	1.06	0.0545	0.0011	0.4008	0.0123	0.0533	0.0012	342	7	342	9	343	51	100	100
663	872	0.63	0.0444	0.0011	0.3469	0.0093	0.0566	0.0007	280	7	302	7	477	26	93	59
664	546	0.90	0.0554	0.0012	0.4378	0.0116	0.0573	0.0009	348	7	369	8	504	36	94	69
665	783		0.0648	0.0014	0.4933	0.0114	0.0552	0.0005	405	8	407	8	422	22	99	96
666	429	0.41	0.0560	0.0012	0.4286	0.0105	0.0555	0.0007	351	7	362	7	432	30	97	81
667	835	0.39	0.0609	0.0012	0.4754	0.0111	0.0566	0.0007	381	7	395	8	476	26	97	80
668	142	2.36	0.0619	0.0018	0.5118	0.0356	0.0600	0.0038	387	11	420	24	603	137	92	64
669	466	0.04	0.0758	0.0016	0.5900	0.0144	0.0565	0.0006	471	10	471	9	471	25	100	100
670	315	0.07	0.3640	0.0072	6.3055	0.1405	0.1256	0.0013	2001	34	2019	20	2038	18	99	98
671	445	0.07	0.0571	0.0012	0.4311	0.0103	0.0548	0.0007	358	7	364	7	402	27	98	89
672	60	0.06	0.1233	0.0031	1.0715	0.0363	0.0630	0.0014	750	18	739	18	708	49	101	106
673	146	1.55	0.0688	0.0017	0.5341	0.0229	0.0563	0.0019	429	10	435	15	464	77	99	92
674	253		0.0702	0.0016	0.5571	0.0144	0.0576	0.0008	437	9	450	9	513	29	97	85
675	1001	0.36	0.0530	0.0010	0.4092	0.0090	0.0560	0.0005	333	6	348	6	452	21	96	74
676	530	0.07	0.0584	0.0012	0.4420	0.0111	0.0548	0.0008	366	7	372	8	406	31	99	90
677	794	0.02	0.3700	0.0075	6.1088	0.1352	0.1198	0.0010	2029	35	1992	19	1953	15	102	104

KAR5: Dikendağı Formation

#	U [ppm]	ƒ206%	Isotope ratios						Ages (Ma)						Data filter A*	Data filter B#
			$^{206}Pb/^{238}U$	±2σ	$^{207}Pb/^{235}U$	±2σ	$^{207}Pb/^{206}Pb$	±2σ	$^{206}Pb/^{238}U$	±2σ	$^{207}Pb/^{235}U$	±2σ	$^{207}Pb/^{206}Pb$	±2σ		
678	212	0.33	0.1010	0.0014	0.8369	0.0204	0.0601	0.0012	620	8	617	11	607	43	100	102
679	129	1.99	0.1245	0.0024	1.0826	0.0495	0.0631	0.0026	756	14	745	24	710	88	102	106
680	70	0.60	0.3380	0.0081	5.6290	0.1624	0.1208	0.0019	1877	39	1921	25	1968	28	98	95
681	114	0.51	0.2000	0.0040	2.0829	0.0508	0.0755	0.0011	1175	21	1143	17	1083	29	103	109
682	170	0.21	0.1409	0.0027	1.3545	0.0318	0.0697	0.0010	849	15	870	14	921	29	98	92
683	379	3.11	0.0705	0.0021	0.5972	0.0848	0.0615	0.0085	439	13	475	54	655	301	92	67
684	301	0.22	0.1059	0.0022	0.9212	0.0244	0.0631	0.0011	649	13	663	13	711	36	98	91
685	99		0.1030	0.0022	0.9235	0.0255	0.0650	0.0011	632	13	664	13	775	37	95	82
686	365	0.50	0.0950	0.0017	0.8424	0.0193	0.0643	0.0009	585	10	620	11	753	31	94	78
687	177	1.20	0.1483	0.0029	1.4327	0.0344	0.0701	0.0010	891	16	903	14	930	29	99	96
688	1341	2.99	0.0531	0.0011	0.4158	0.0425	0.0568	0.0057	334	7	353	30	482	222	95	69
689	181	0.21	0.3164	0.0091	4.7821	0.1532	0.1096	0.0016	1772	44	1782	27	1793	26	99	99

Table B.1 Continued

#	U [ppm]	f206%	Isotope ratios						Ages (Ma)						Data filter A*	Data filter B#
			$^{206}Pb/^{238}U$	±2σ	$^{207}Pb/^{235}U$	±2σ	$^{207}Pb/^{206}Pb$	±2σ	$^{206}Pb/^{238}U$	±2σ	$^{207}Pb/^{235}U$	±2σ	$^{207}Pb/^{206}Pb$	±2σ		
690	188	0.08	0.1598	0.0031	1.5677	0.0360	0.0711	0.0009	956	17	958	14	961	25	100	99
691	224	0.48	0.1579	0.0031	1.6066	0.0378	0.0738	0.0009	945	17	973	15	1036	26	97	91
692	51	0.31	0.3697	0.0076	6.5359	0.1582	0.1282	0.0016	2028	36	2051	21	2074	22	99	98
693	114	0.29	0.1381	0.0027	1.2381	0.0318	0.0650	0.0011	834	15	818	14	776	35	102	108
694	90		0.1877	0.0097	1.9227	0.1044	0.0743	0.0013	1109	52	1089	36	1049	35	102	106
695	216	3.67	0.1207	0.0065	1.0677	0.1140	0.0641	0.0059	735	38	738	56	746	196	100	98
696	83	1.26	0.1551	0.0082	1.4404	0.0924	0.0674	0.0025	929	45	906	38	849	76	103	109
697	59	1.74	0.1617	0.0084	1.4642	0.1005	0.0657	0.0029	966	47	916	41	796	94	106	121
698	55	0.30	0.2994	0.0172	4.3158	0.2636	0.1046	0.0021	1688	86	1696	50	1707	37	100	99
699	87		0.1993	0.0103	2.0541	0.1115	0.0747	0.0013	1172	55	1134	37	1061	34	103	110
700	304	0.39	0.1243	0.0067	1.1894	0.0664	0.0694	0.0010	755	38	796	31	910	30	95	83
701	143	0.65	0.1083	0.0055	0.9424	0.0499	0.0631	0.0010	663	32	674	26	712	33	98	93
702	367		0.0947	0.0043	0.7930	0.0374	0.0607	0.0007	583	26	593	21	630	24	98	93
703	75	0.39	0.1054	0.0049	0.8720	0.0445	0.0600	0.0012	646	29	637	24	604	44	101	107
704	277	0.10	0.1113	0.0051	0.9845	0.0468	0.0642	0.0008	680	30	696	24	748	27	98	91
705	76		0.1826	0.0084	1.8723	0.0912	0.0744	0.0012	1081	46	1071	32	1051	32	101	103
706	69		0.1678	0.0082	1.6948	0.0878	0.0732	0.0013	1000	45	1007	33	1020	35	99	98
707	60		0.1655	0.0078	1.6486	0.0810	0.0723	0.0010	987	43	989	31	993	29	100	99
708	135	0.46	0.1095	0.0053	0.9450	0.0503	0.0626	0.0014	670	31	675	26	695	47	99	96
709	320	1.86	0.1018	0.0047	0.8532	0.0444	0.0608	0.0014	625	28	626	24	631	51	100	99
710	297		0.1296	0.0059	1.1524	0.0554	0.0645	0.0009	785	34	778	26	758	30	101	104
711	135	1.04	0.1954	0.0034	2.3345	0.0563	0.0866	0.0014	1151	19	1223	17	1353	32	94	85
712	270	1.37	0.1046	0.0017	0.8412	0.0208	0.0583	0.0011	641	10	620	11	543	41	103	118
713	192		0.1023	0.0023	0.8659	0.0236	0.0614	0.0010	628	13	633	13	652	34	99	96
714	169		0.3495	0.0056	5.5062	0.1025	0.1143	0.0011	1932	27	1902	16	1869	17	102	103
715	520	0.82	0.1469	0.0023	1.5630	0.0359	0.0772	0.0013	883	13	956	14	1126	33	92	78
716	210	1.17	0.1025	0.0024	0.8688	0.0330	0.0615	0.0019	629	14	635	18	656	65	99	96
717	104		0.1861	0.0041	1.8791	0.0474	0.0732	0.0009	1100	22	1074	17	1020	26	102	108
718	87	0.77	0.1747	0.0032	1.8719	0.0449	0.0777	0.0012	1038	17	1071	16	1140	31	97	91
719	72	0.87	0.1466	0.0030	1.4181	0.0567	0.0701	0.0024	882	17	897	24	933	70	98	95
720	88	0.07	0.1218	0.0025	1.0485	0.0280	0.0624	0.0011	741	14	728	14	688	37	102	108
721	73		0.1476	0.0032	1.3591	0.0393	0.0668	0.0013	887	18	871	17	831	39	102	107
722	67	1.53	0.1356	0.0023	1.0791	0.0341	0.0577	0.0015	819	13	743	17	520	58	110	158
723	136	0.06	0.2731	0.0047	3.5989	0.0749	0.0956	0.0011	1556	24	1549	17	1540	22	100	101
724	105	0.17	0.1903	0.0033	1.9548	0.0422	0.0745	0.0010	1123	18	1100	14	1055	26	102	106
725	94	0.93	0.1493	0.0044	1.3253	0.0657	0.0644	0.0026	897	25	857	29	755	84	105	119
726	142	0.89	0.1158	0.0025	1.0405	0.0378	0.0652	0.0019	707	14	724	19	779	62	98	91
727	117		0.4218	0.0089	8.8876	0.2308	0.1528	0.0023	2269	40	2327	24	2378	26	98	95
728	88		0.1822	0.0043	1.8439	0.0523	0.0734	0.0012	1079	23	1061	19	1025	32	102	105
729	75	0.80	0.1213	0.0031	1.0637	0.0424	0.0636	0.0020	738	18	736	21	729	65	100	101
730	120	0.98	0.1248	0.0030	1.1019	0.0334	0.0640	0.0012	758	17	754	16	743	38	101	102
731	391		0.1190	0.0026	1.0140	0.0252	0.0618	0.0008	725	15	711	13	667	27	102	109
732	159	0.02	0.1140	0.0018	0.9595	0.0200	0.0610	0.0008	696	10	683	10	641	29	102	109
733	138		0.1113	0.0018	0.9332	0.0192	0.0608	0.0008	680	10	669	10	632	28	102	108
734	189	1.56	0.1647	0.0029	1.5758	0.0940	0.0694	0.0040	983	16	961	37	911	118	102	108
735	170	0.40	0.1008	0.0017	0.9376	0.0220	0.0675	0.0011	619	10	672	12	852	33	92	73
736	97	1.55	0.1492	0.0026	1.2670	0.0944	0.0616	0.0045	897	15	831	42	659	156	108	136
737	56	0.65	0.1597	0.0027	1.5899	0.0344	0.0722	0.0010	955	15	966	13	992	27	99	96
738	48		0.1044	0.0018	0.8848	0.0257	0.0615	0.0014	640	10	644	14	656	50	99	98
739	256	0.97	0.1701	0.0029	1.7818	0.0358	0.0760	0.0008	1013	16	1039	13	1095	21	97	92
740	231	1.17	0.0896	0.0015	0.7458	0.0181	0.0604	0.0011	553	9	566	11	618	38	98	89
741	206	2.30	0.0961	0.0028	0.8301	0.0310	0.0626	0.0015	592	16	614	17	696	50	96	85
742	67	0.36	0.1017	0.0031	0.8470	0.0343	0.0604	0.0016	624	18	623	19	618	59	100	101
743	75	1.85	0.1428	0.0048	1.5274	0.0644	0.0776	0.0020	861	27	941	26	1135	51	91	76
744	320	4.29	0.0705	0.0021	0.5344	0.0213	0.0550	0.0014	439	13	435	14	411	59	101	107
745	185	0.52	0.1223	0.0038	1.0983	0.0470	0.0651	0.0019	744	22	753	23	779	62	99	96
746	423	0.25	0.0954	0.0026	0.7919	0.0255	0.0602	0.0010	587	15	592	14	611	36	99	96
747	56		0.0773	0.0030	0.6354	0.0306	0.0597	0.0017	480	18	499	19	591	63	96	81
748	167	1.00	0.1699	0.0051	1.6946	0.0599	0.0724	0.0014	1011	28	1006	23	996	38	100	102
749	78	1.07	0.1244	0.0040	1.0792	0.0654	0.0629	0.0032	756	23	743	32	705	110	102	107
750	177	0.18	0.1603	0.0025	1.6767	0.0308	0.0758	0.0008	959	14	1000	12	1091	20	96	88
751	229	0.14	0.1247	0.0026	1.2651	0.0314	0.0736	0.0010	757	15	830	14	1031	26	91	73
752	144	0.13	0.3658	0.0059	6.2015	0.1287	0.1230	0.0016	2009	28	2005	18	2000	23	100	100
753	215	0.34	0.1918	0.0032	2.0452	0.0504	0.0774	0.0014	1131	17	1131	17	1130	36	100	100
754	27		0.3343	0.0165	5.6160	0.4796	0.1218	0.0085	1859	80	1919	74	1983	124	97	94
755	338	0.02	0.1158	0.0014	1.0213	0.0172	0.0640	0.0008	706	8	715	9	741	26	99	95
756	457		0.0786	0.0017	0.6164	0.0161	0.0569	0.0008	488	10	488	10	488	31	100	100
757	102		0.0912	0.0021	0.7835	0.0243	0.0623	0.0013	563	13	587	14	685	43	96	82
758	339	0.14	0.5531	0.0128	16.4383	0.4253	0.2156	0.0025	2838	53	2903	25	2948	19	98	96
759	1125	0.00	0.1038	0.0023	0.8912	0.0227	0.0623	0.0008	637	14	647	12	683	26	98	93
760	145	2.94	0.2722	0.0063	3.9130	0.1311	0.1043	0.0025	1552	32	1616	27	1702	45	96	91
761	29		0.0915	0.0026	0.7916	0.0339	0.0628	0.0020	564	15	592	19	700	69	95	81
762	554	0.83	0.1735	0.0037	1.9152	0.0445	0.0801	0.0008	1031	20	1086	16	1199	19	95	86
763	101	0.40	0.3143	0.0080	5.1097	0.1516	0.1179	0.0018	1762	39	1838	25	1925	28	96	92
764	136	4.77	0.1030	0.0022	0.8735	0.0372	0.0615	0.0023	632	13	637	20	656	79	99	96
765	194	1.00	0.1342	0.0041	1.2275	0.0459	0.0664	0.0014	812	23	813	21	818	45	100	99
766	111	0.15	0.4430	0.0124	10.8235	0.3192	0.1772	0.0016	2364	55	2508	27	2627	15	94	90
767	186	0.37	0.1206	0.0036	1.0939	0.0378	0.0658	0.0012	734	21	750	18	799	37	98	92

Table B.1 Continued

KAR6: Dikendağı Formation

#	U [ppm]	ƒ206%	Isotope ratios						Ages (Ma)						Data filter A*	Data filter B′
			$^{206}Pb/^{238}U$	±2σ	$^{207}Pb/^{235}U$	±2σ	$^{207}Pb/^{206}Pb$	±2σ	$^{206}Pb/^{238}U$	±2σ	$^{207}Pb/^{235}U$	±2σ	$^{207}Pb/^{206}Pb$	±2σ		
768	404		0.3019	0.0047	4.5045	0.0953	0.1082	0.0016	1701	23	1732	18	1769	26	98	96
769	399	0.12	0.1618	0.0024	1.7195	0.0315	0.0771	0.0008	966	13	1016	12	1124	22	95	86
770	258	0.41	0.1715	0.0028	1.7541	0.0408	0.0742	0.0012	1021	15	1029	15	1046	34	99	98
771	416		0.1607	0.0027	1.5798	0.0332	0.0713	0.0009	960	15	962	13	967	27	100	99
772	377	0.16	0.0955	0.0016	0.8100	0.0167	0.0615	0.0008	588	9	602	9	657	27	98	90
773	136	2.00	0.0936	0.0016	0.7838	0.0276	0.0607	0.0019	577	10	588	16	630	66	98	92
774	514	0.78	0.0518	0.0009	0.4227	0.0128	0.0592	0.0015	325	5	358	9	576	54	91	56
775	219	0.64	0.0560	0.0011	0.4439	0.0133	0.0574	0.0013	352	7	373	9	509	49	94	69
776	818	1.28	0.0798	0.0014	0.6219	0.0229	0.0565	0.0018	495	8	491	14	473	72	101	105
777	873	5.55	0.0619	0.0009	0.4609	0.0425	0.0540	0.0049	387	5	385	30	371	206	101	104
778	594	4.56	0.0333	0.0010	0.2408	0.0096	0.0524	0.0015	211	6	219	8	305	63	96	69
779	123	0.17	0.1427	0.0024	1.4582	0.0308	0.0741	0.0009	860	14	913	13	1045	25	94	82
780	147	1.41	0.1321	0.0024	1.3365	0.0351	0.0734	0.0014	800	14	862	15	1024	38	93	78
781	346	0.20	0.3314	0.0041	5.5272	0.0840	0.1209	0.0011	1845	20	1905	13	1970	16	97	94
782	312	0.00	0.3449	0.0043	5.7438	0.0908	0.1208	0.0012	1910	20	1938	14	1968	17	99	97
783	513	4.32	0.0481	0.0010	0.3724	0.0118	0.0561	0.0013	303	6	321	9	458	53	94	66
784	1104	0.04	0.1314	0.0021	1.1838	0.0219	0.0653	0.0006	796	12	793	10	786	21	100	101
785	1478	7.01	0.0453	0.0007	0.3391	0.0221	0.0542	0.0034	286	5	296	17	381	142	96	75
786	270	0.58	0.0913	0.0016	0.8438	0.0210	0.0670	0.0012	563	9	621	12	838	37	91	67
787	599	0.38	0.0495	0.0009	0.3819	0.0092	0.0560	0.0009	311	6	328	7	452	35	95	69
788	782	0.19	0.1054	0.0026	0.8895	0.0294	0.0612	0.0014	646	15	646	16	646	48	100	100
789	819	0.12	0.0565	0.0012	0.4364	0.0111	0.0561	0.0007	354	7	368	8	455	29	96	78
790	619	0.27	0.0537	0.0012	0.4451	0.0144	0.0601	0.0014	337	7	374	10	606	50	90	56
791	119	2.55	0.1350	0.0032	1.3417	0.0609	0.0721	0.0028	816	18	864	26	989	79	94	83
792	324	0.51	0.0820	0.0019	0.7104	0.0196	0.0628	0.0009	508	11	545	12	702	31	93	72
793	715	0.53	0.0966	0.0022	0.8582	0.0220	0.0644	0.0008	595	13	629	12	756	26	94	79
794	308	0.54	0.1685	0.0039	1.7773	0.0476	0.0765	0.0011	1004	21	1037	17	1108	27	97	91
795	581	0.47	0.2998	0.0068	4.7492	0.1203	0.1149	0.0013	1690	34	1776	21	1878	21	95	90
796	117	0.33	0.0967	0.0026	0.8556	0.0320	0.0642	0.0016	595	15	628	17	748	54	95	80
797	818	1.81	0.0466	0.0011	0.3390	0.0107	0.0528	0.0010	293	7	296	8	321	44	99	92
798	14	2.00	0.1265	0.0059	1.1105	0.1084	0.0637	0.0055	768	34	758	52	730	182	101	105
799	189	0.75	0.1479	0.0033	1.6212	0.0418	0.0795	0.0010	889	18	978	16	1184	26	91	75
800	431	1.33	0.0866	0.0022	0.7464	0.0231	0.0625	0.0010	535	13	566	13	692	36	95	77
801	828	0.50	0.0594	0.0014	0.4806	0.0150	0.0587	0.0012	372	8	399	10	556	46	93	67
802	324	0.60	0.1018	0.0025	0.9871	0.0279	0.0703	0.0010	625	15	697	14	938	28	90	67
803	199	0.14	0.1078	0.0024	0.9055	0.0234	0.0609	0.0008	660	14	655	12	636	28	101	104
804	567	0.32	0.0551	0.0008	0.4340	0.0109	0.0571	0.0012	346	5	366	8	497	45	94	70
805	98	0.28	0.1052	0.0020	0.8811	0.0210	0.0607	0.0009	645	11	642	11	630	32	101	102
806	802	1.00	0.1415	0.0022	1.4427	0.0285	0.0739	0.0009	853	12	907	12	1040	25	94	82
807	524	1.78	0.1452	0.0023	1.3739	0.0473	0.0686	0.0021	874	13	878	20	887	64	100	99
808	177		0.1140	0.0020	0.9778	0.0224	0.0622	0.0009	696	12	692	12	681	31	101	102
809	214	0.93	0.1194	0.0023	1.1145	0.0350	0.0677	0.0017	727	14	760	17	859	51	96	85
810	704	2.40	0.0540	0.0016	0.4006	0.0325	0.0538	0.0041	339	10	342	24	364	171	99	93
811	157	1.95	0.0873	0.0016	0.7003	0.0251	0.0582	0.0018	539	10	539	15	538	67	100	100
812	224	2.41	0.0863	0.0017	0.7220	0.0228	0.0606	0.0015	534	10	552	13	627	54	97	85
813	47		0.0974	0.0024	0.8289	0.0276	0.0617	0.0014	599	14	613	15	664	47	98	90
814	215	0.55	0.1261	0.0019	1.1223	0.0213	0.0646	0.0008	765	11	764	10	760	25	100	101

KAR7: Dikendağı Formation

#	U [ppm]	ƒ206%	Isotope ratios						Ages (Ma)						Data filter A*	Data filter B′
			$^{206}Pb/^{238}U$	±2σ	$^{207}Pb/^{235}U$	±2σ	$^{207}Pb/^{206}Pb$	±2σ	$^{206}Pb/^{238}U$	±2σ	$^{207}Pb/^{235}U$	±2σ	$^{207}Pb/^{206}Pb$	±2σ		
815	206	0.39	0.1218	0.0022	1.0792	0.0287	0.0642	0.0012	741	13	743	14	750	41	100	99
816	241	1.16	0.0872	0.0015	0.7043	0.0181	0.0586	0.0011	539	9	541	11	552	42	100	98
817	107	0.94	0.1082	0.0032	0.9565	0.0372	0.0641	0.0016	662	19	681	19	746	53	97	89
818	436	1.46	0.0681	0.0010	0.5113	0.0136	0.0545	0.0012	425	6	419	9	391	50	101	109
819	312	0.23	0.0698	0.0009	0.5448	0.0101	0.0566	0.0007	435	6	442	7	476	28	98	91
820	211	0.79	0.0720	0.0013	0.5614	0.0139	0.0565	0.0010	448	8	452	9	474	39	99	95
821	269	0.37	0.0660	0.0009	0.5647	0.0147	0.0621	0.0014	412	6	455	10	678	47	91	61
822	439		0.0646	0.0009	0.5068	0.0090	0.0569	0.0006	404	5	416	6	487	25	97	83
823	394	0.09	0.0688	0.0009	0.5432	0.0092	0.0573	0.0006	429	5	441	6	502	25	97	85
824	357	0.67	0.0730	0.0010	0.5839	0.0122	0.0580	0.0009	454	6	467	8	530	33	97	86
825	310	0.32	0.0672	0.0009	0.5414	0.0106	0.0584	0.0008	419	5	439	7	545	32	95	77
826	396	0.40	0.0813	0.0012	0.6568	0.0156	0.0586	0.0011	504	7	513	10	553	40	98	91
827	282	0.37	0.0703	0.0008	0.5439	0.0095	0.0561	0.0007	438	5	441	6	456	30	99	96
828	231	0.70	0.0755	0.0009	0.5962	0.0126	0.0573	0.0010	469	6	475	8	502	37	99	93
829	626	1.19	0.0700	0.0012	0.5342	0.0204	0.0553	0.0019	436	7	435	14	426	76	100	102
830	151	0.04	0.0685	0.0012	0.5972	0.0182	0.0633	0.0015	427	7	475	12	718	52	90	59
831	371	1.52	0.0659	0.0007	0.5148	0.0091	0.0566	0.0008	412	4	422	6	478	31	98	86
832	303	0.04	0.0705	0.0008	0.5478	0.0107	0.0563	0.0009	439	5	444	7	465	35	99	94
833	187	3.13	0.0497	0.0014	0.3631	0.0184	0.0530	0.0022	313	9	315	14	328	95	99	95
834	309	1.79	0.0657	0.0008	0.5151	0.0114	0.0569	0.0010	410	5	422	8	486	40	97	84
835	438	1.72	0.0711	0.0008	0.5576	0.0151	0.0569	0.0014	443	5	450	10	487	55	98	91
836	478	1.10	0.0607	0.0007	0.4598	0.0084	0.0550	0.0008	380	4	384	6	411	33	99	92
837	322	0.17	0.0654	0.0007	0.5343	0.0099	0.0592	0.0009	409	4	435	7	575	33	94	71
838	337	0.06	0.0675	0.0009	0.5144	0.0099	0.0553	0.0008	421	5	421	7	424	32	100	99
839	178	1.58	0.0744	0.0017	0.5609	0.0247	0.0547	0.0020	463	10	452	16	399	84	102	116
840	498	0.54	0.0644	0.0008	0.5291	0.0109	0.0596	0.0010	402	5	431	7	590	37	93	68
841	62	1.46	0.0490	0.0024	0.3571	0.0347	0.0528	0.0044	308	15	310	26	322	191	99	96
842	115		0.1285	0.0014	1.1642	0.0189	0.0657	0.0008	779	8	784	9	797	25	99	98

Table B.1 Continued

#	U [ppm]	ƒ206%	Isotope ratios						Ages (Ma)						Data filter A*	Data filter B#
			$^{206}Pb/^{238}U$	±2σ	$^{207}Pb/^{235}U$	±2σ	$^{207}Pb/^{206}Pb$	±2σ	$^{206}Pb/^{238}U$	±2σ	$^{207}Pb/^{235}U$	±2σ	$^{207}Pb/^{206}Pb$	±2σ		
843	468	0.37	0.0634	0.0007	0.4988	0.0075	0.0570	0.0005	396	4	411	5	493	21	96	80
844	349	1.46	0.0756	0.0013	0.5919	0.0280	0.0568	0.0025	470	8	472	18	483	97	100	97
845	542	1.98	0.0624	0.0008	0.4717	0.0095	0.0548	0.0009	390	5	392	7	405	35	99	96
846	188	4.91	0.0687	0.0010	0.5507	0.0227	0.0581	0.0023	428	6	445	15	534	85	96	80
847	491		0.0657	0.0009	0.5213	0.0105	0.0575	0.0008	410	6	426	7	513	31	96	80
848	265	0.00	0.0698	0.0010	0.5486	0.0125	0.0570	0.0010	435	6	444	8	491	40	98	89
849	70		0.1049	0.0021	0.9200	0.0286	0.0636	0.0015	643	12	662	15	729	51	97	88
850	235	0.14	0.0672	0.0009	0.5161	0.0113	0.0557	0.0010	419	5	423	8	441	38	99	95
851	364		0.0704	0.0010	0.5516	0.0115	0.0569	0.0009	438	6	446	8	486	33	98	90
852	330		0.0609	0.0009	0.4856	0.0129	0.0578	0.0013	381	5	402	9	523	48	95	73
853	454	0.05	0.0713	0.0010	0.5549	0.0113	0.0565	0.0008	444	6	448	7	471	33	99	94
854	273	6.23	0.0685	0.0011	0.5095	0.0176	0.0540	0.0017	427	6	418	12	370	70	102	115
855	354	0.29	0.0717	0.0009	0.5530	0.0102	0.0559	0.0008	447	5	447	7	449	30	100	100
856	356	0.13	0.0747	0.0012	0.5777	0.0128	0.0561	0.0008	465	7	463	8	455	33	100	102
857	726	1.06	0.0600	0.0008	0.4540	0.0113	0.0549	0.0012	375	5	380	8	408	48	99	92
858	294	0.72	0.0671	0.0010	0.5516	0.0151	0.0596	0.0014	418	6	446	10	591	49	94	71
859	230	0.05	0.0778	0.0015	0.6128	0.0167	0.0571	0.0011	483	9	485	10	496	42	100	97
860	356	0.18	0.0706	0.0012	0.5441	0.0115	0.0559	0.0007	440	7	441	8	448	27	100	98
861	211		0.0764	0.0013	0.6054	0.0139	0.0575	0.0009	475	8	481	9	510	34	99	93
862	251		0.0838	0.0015	0.6545	0.0141	0.0566	0.0006	519	9	511	9	477	25	101	109
863	439	1.89	0.0783	0.0017	0.6251	0.0240	0.0579	0.0018	486	10	493	15	525	70	99	93
864	219	1.28	0.0679	0.0012	0.5311	0.0160	0.0567	0.0014	423	7	433	11	482	55	98	88
865	307	0.22	0.0796	0.0015	0.6138	0.0147	0.0559	0.0009	494	9	486	9	449	34	102	110
866	278		0.0708	0.0012	0.5705	0.0137	0.0584	0.0010	441	7	458	9	545	37	96	81
867	216	3.17	0.0701	0.0013	0.5259	0.0174	0.0544	0.0015	437	8	429	12	389	62	102	112
868	140	0.32	0.0824	0.0016	0.6531	0.0172	0.0575	0.0010	510	9	510	11	511	40	100	100
869	275		0.0802	0.0015	0.6328	0.0161	0.0572	0.0010	497	9	498	10	501	37	100	99
870	199		0.1189	0.0021	0.9376	0.0378	0.0572	0.0021	724	12	672	20	499	80	108	145
871	278	0.25	0.0735	0.0014	0.5966	0.0169	0.0588	0.0013	457	8	475	11	561	47	96	82
872	287	0.22	0.0734	0.0014	0.5629	0.0122	0.0556	0.0006	457	8	453	8	437	25	101	105
873	267	0.08	0.0727	0.0013	0.5612	0.0124	0.0560	0.0008	452	8	452	8	453	30	100	100
874	300		0.0735	0.0013	0.5668	0.0124	0.0560	0.0008	457	8	456	8	451	30	100	101
875	233	6.93	0.0719	0.0020	0.5636	0.0240	0.0569	0.0018	447	12	454	16	487	71	99	92
876	241	3.35	0.0727	0.0016	0.5919	0.0310	0.0590	0.0028	452	10	472	20	569	104	96	80
877	178	0.49	0.3339	0.0061	5.5981	0.1183	0.1216	0.0013	1857	29	1916	18	1980	19	97	94
878	294	0.40	0.0883	0.0019	0.7109	0.0185	0.0584	0.0008	545	11	545	11	545	31	100	100
879	292		0.0753	0.0014	0.5830	0.0129	0.0561	0.0007	468	8	466	8	458	27	100	102
880	220	0.93	0.0750	0.0014	0.6082	0.0174	0.0588	0.0013	466	8	482	11	559	47	97	83
881	286	0.48	0.0742	0.0013	0.6124	0.0139	0.0599	0.0009	461	8	485	9	599	33	95	77
882	232	0.09	0.0699	0.0014	0.5772	0.0165	0.0599	0.0013	436	8	463	11	599	45	94	73
883	357		0.0725	0.0013	0.5624	0.0118	0.0563	0.0006	451	8	453	8	464	25	100	97
884	103		0.0834	0.0019	0.7049	0.0213	0.0613	0.0012	516	11	542	13	651	43	95	79
885	367	0.16	0.0652	0.0014	0.5142	0.0143	0.0572	0.0010	407	9	421	10	501	38	97	81
886	251	1.47	0.3087	0.0055	4.8456	0.1126	0.1139	0.0017	1734	27	1793	20	1862	27	97	93
887	194		0.1212	0.0020	1.0814	0.0240	0.0647	0.0010	737	11	744	12	765	32	99	96
888	448	0.82	0.0722	0.0011	0.5915	0.0128	0.0594	0.0009	449	7	472	8	584	33	95	77
889	406	0.16	0.0725	0.0012	0.5756	0.0141	0.0576	0.0010	451	7	462	9	513	39	98	88
890	270	0.84	0.0729	0.0013	0.5733	0.0137	0.0571	0.0009	453	8	460	9	494	36	99	92
891	311	0.08	0.0777	0.0012	0.6034	0.0140	0.0563	0.0009	482	7	479	9	465	37	101	104
892	407	0.10	0.0749	0.0014	0.5784	0.0144	0.0560	0.0010	465	8	463	9	454	38	100	103
893	461	0.32	0.0803	0.0013	0.6891	0.0146	0.0622	0.0008	498	8	532	9	682	29	94	73
894	358		0.0688	0.0013	0.5579	0.0145	0.0588	0.0011	429	8	450	9	560	39	95	77
895	533	0.10	0.0693	0.0009	0.5440	0.0101	0.0570	0.0007	432	6	441	7	490	28	98	88
896	189	0.67	0.0746	0.0011	0.6303	0.0169	0.0612	0.0014	464	7	496	11	648	48	93	72
897	224		0.1075	0.0016	0.9084	0.0187	0.0613	0.0009	658	9	656	10	649	31	100	101
898	244	0.75	0.0711	0.0011	0.5482	0.0127	0.0559	0.0009	443	7	444	8	449	37	100	99
899	672	0.04	0.0655	0.0009	0.5173	0.0104	0.0573	0.0008	409	6	423	7	504	32	97	81
900	285	0.16	0.0715	0.0011	0.5482	0.0117	0.0556	0.0009	445	6	444	8	437	35	100	102
901	314	0.43	0.0761	0.0011	0.6002	0.0132	0.0572	0.0010	473	6	477	8	498	37	99	95
902	374	0.29	0.0729	0.0011	0.5622	0.0116	0.0559	0.0008	454	7	453	8	449	30	100	101
903	264	0.37	0.0639	0.0018	0.5371	0.0199	0.0610	0.0015	399	11	437	13	639	52	91	63
904	218	0.02	0.0781	0.0016	0.6131	0.0153	0.0569	0.0008	485	10	486	10	489	30	100	99
905	224	0.15	0.0697	0.0013	0.5434	0.0135	0.0566	0.0009	434	8	441	9	475	36	99	91
906	312	6.75	0.0616	0.0013	0.4785	0.0236	0.0563	0.0025	385	8	397	16	466	99	97	83
907	282	0.28	0.0731	0.0015	0.5764	0.0142	0.0572	0.0008	455	9	462	9	499	30	98	91
908	214		0.0743	0.0014	0.6006	0.0135	0.0586	0.0008	462	8	478	9	552	29	97	84
909	531	0.40	0.0763	0.0015	0.6432	0.0164	0.0611	0.0010	474	9	504	10	645	35	94	74
910	206	1.70	0.0713	0.0013	0.5590	0.0153	0.0569	0.0012	444	8	451	10	487	46	98	91
911	88		0.0748	0.0020	0.5847	0.0232	0.0567	0.0017	465	12	468	15	479	66	100	97
912	336	0.63	0.0732	0.0014	0.6182	0.0177	0.0613	0.0013	455	9	489	11	649	44	93	70
913	359	3.42	0.0781	0.0011	0.6195	0.0281	0.0575	0.0025	485	6	490	18	512	95	99	95
914	654	0.28	0.0625	0.0008	0.4854	0.0092	0.0564	0.0008	391	5	402	6	466	30	97	84
915	398	0.18	0.0665	0.0010	0.5392	0.0123	0.0589	0.0010	415	6	438	8	562	38	95	74
916	414	0.12	0.0695	0.0011	0.5312	0.0127	0.0554	0.0010	433	7	433	8	430	40	100	101
917	230	2.80	0.0662	0.0009	0.4981	0.0182	0.0546	0.0018	413	6	410	12	395	75	101	105
918	160		0.0950	0.0015	0.7852	0.0182	0.0600	0.0010	585	9	588	10	602	36	99	97
919	136		0.1061	0.0021	0.9047	0.0243	0.0618	0.0011	650	12	654	13	668	39	99	97
920	39	0.54	0.1542	0.0026	1.5498	0.0483	0.0729	0.0019	924	15	950	19	1011	53	97	91
921	431	0.38	0.0644	0.0009	0.5156	0.0107	0.0580	0.0009	403	5	422	7	531	35	95	76
922	287	0.91	0.0713	0.0011	0.5524	0.0121	0.0562	0.0009	444	6	447	8	461	36	99	96
923	283	0.36	0.0674	0.0009	0.5470	0.0120	0.0589	0.0010	420	6	443	8	562	37	95	75
924	426	0.90	0.0688	0.0016	0.5922	0.0287	0.0624	0.0027	429	9	472	18	688	91	91	62
925	351		0.0691	0.0015	0.5338	0.0143	0.0560	0.0009	431	9	434	9	454	36	99	95

Table B.1 Continued

#	U [ppm]	ƒ206%	Isotope ratios						Ages (Ma)						Data filter A*	Data filter B#
			$^{206}Pb/^{238}U$	±2σ	$^{207}Pb/^{235}U$	±2σ	$^{207}Pb/^{206}Pb$	±2σ	$^{206}Pb/^{238}U$	±2σ	$^{207}Pb/^{235}U$	±2σ	$^{207}Pb/^{206}Pb$	±2σ		
926	299		0.0661	0.0010	0.5107	0.0113	0.0560	0.0009	413	6	419	8	453	35	99	91
927	308		0.0742	0.0011	0.5842	0.0134	0.0571	0.0010	461	7	467	9	496	39	99	93
928	329	0.23	0.0695	0.0011	0.5426	0.0116	0.0566	0.0008	433	6	440	8	478	33	98	91
929	243	0.70	0.0704	0.0013	0.5460	0.0149	0.0563	0.0011	438	8	442	10	463	43	99	95
930	277		0.0695	0.0011	0.5573	0.0125	0.0581	0.0010	433	6	450	8	535	36	96	81
931	82	4.26	0.0734	0.0026	0.6196	0.0556	0.0613	0.0050	456	16	490	35	648	177	93	70
932	336	0.07	0.0717	0.0011	0.5587	0.0110	0.0565	0.0007	446	6	451	7	474	29	99	94
933	305	0.13	0.0943	0.0016	0.8234	0.0172	0.0633	0.0008	581	9	610	10	719	26	95	81
934	264	0.17	0.0676	0.0012	0.5376	0.0133	0.0577	0.0010	421	7	437	9	519	38	96	81
935	382	2.81	0.0797	0.0011	0.6210	0.0161	0.0565	0.0012	494	7	490	10	472	48	101	105
936	333		0.0629	0.0014	0.4906	0.0128	0.0565	0.0008	393	8	405	9	474	31	97	83
937	440	0.09	0.0781	0.0012	0.6134	0.0130	0.0570	0.0008	485	7	486	8	491	31	100	99
938	261		0.0592	0.0015	0.4703	0.0152	0.0576	0.0012	371	9	391	11	516	45	95	72
939	268	1.54	0.0637	0.0014	0.4728	0.0198	0.0538	0.0019	398	8	393	14	363	80	101	110
940	288	0.98	0.0704	0.0011	0.6132	0.0159	0.0632	0.0013	438	7	486	10	715	44	90	61

KAR14: Dikendağı Formation

#	U [ppm]	ƒ206%	Isotope ratios						Ages (Ma)						Data filter A*	Data filter B#
			$^{206}Pb/^{238}U$	±2σ	$^{207}Pb/^{235}U$	±2σ	$^{207}Pb/^{206}Pb$	±2σ	$^{206}Pb/^{238}U$	±2σ	$^{207}Pb/^{235}U$	±2σ	$^{207}Pb/^{206}Pb$	±2σ		
941	23	0.13	0.5271	0.0084	15.8587	0.3589	0.2182	0.0035	2729	35	2868	22	2968	26	95	92
942	51		0.1373	0.0021	1.2703	0.0303	0.0671	0.0012	829	12	833	14	842	38	100	99
943	300	0.00	0.1252	0.0017	1.1459	0.0203	0.0664	0.0008	761	10	775	10	818	24	98	93
944	418	0.08	0.0913	0.0013	0.7586	0.0166	0.0602	0.0010	563	8	573	10	612	35	98	92
945	401	0.23	0.1307	0.0030	1.3332	0.0368	0.0740	0.0012	792	17	860	16	1040	32	92	76
946	334	0.04	0.1109	0.0024	0.9535	0.0236	0.0623	0.0007	678	14	680	12	686	25	100	99
947	480	2.38	0.0615	0.0015	0.4905	0.0204	0.0579	0.0020	384	9	405	14	526	74	95	73
948	113	0.95	0.1163	0.0024	1.0960	0.0374	0.0683	0.0019	709	14	751	18	878	57	94	81
949	354	0.49	0.1068	0.0022	0.9745	0.0255	0.0662	0.0011	654	13	691	13	811	34	95	81
950	378	0.27	0.0897	0.0017	0.7863	0.0206	0.0636	0.0011	554	10	589	12	727	38	94	76
951	122	0.63	0.3400	0.0111	5.4475	0.2018	0.1162	0.0021	1887	53	1892	32	1898	32	100	99
952	594	1.31	0.0964	0.0027	0.7962	0.0430	0.0599	0.0028	593	16	595	24	600	100	100	99
953	151		0.1791	0.0035	1.7752	0.0407	0.0719	0.0009	1062	19	1036	15	983	25	102	108
954	77	1.38	0.1650	0.0029	1.5843	0.0515	0.0696	0.0019	985	16	964	20	917	56	102	107
955	851	0.45	0.0973	0.0015	0.8471	0.0166	0.0631	0.0008	599	9	623	9	713	25	96	84
956	154	0.98	0.1105	0.0029	0.9659	0.0367	0.0634	0.0018	676	17	686	19	721	59	98	94
957	83	0.00	0.1312	0.0023	1.3593	0.0322	0.0752	0.0012	794	13	872	14	1073	32	91	74
958	348		0.1059	0.0017	0.9051	0.0189	0.0620	0.0008	649	10	654	10	673	28	99	96
959	42	0.20	0.1036	0.0028	0.8917	0.0346	0.0624	0.0018	635	16	647	19	689	60	98	92
960	645	0.27	0.1012	0.0015	0.8753	0.0165	0.0627	0.0007	622	9	638	9	699	24	97	89
961	294	0.67	0.1633	0.0032	1.7119	0.0379	0.0760	0.0008	975	18	1013	14	1096	21	96	89
962	595	0.05	0.4837	0.0100	10.7058	0.2543	0.1605	0.0019	2543	44	2498	22	2461	20	102	103
963	426	0.30	0.2983	0.0060	4.6697	0.1083	0.1135	0.0013	1683	30	1762	19	1857	20	96	91
964	147		0.1544	0.0032	1.5950	0.0389	0.0749	0.0010	925	18	968	15	1067	26	96	87
965	127	0.76	0.1786	0.0047	1.8487	0.0681	0.0751	0.0019	1059	26	1063	24	1071	52	100	99
966	79		0.0927	0.0023	0.8360	0.0288	0.0654	0.0016	572	13	617	16	787	51	93	73
967	136		0.1713	0.0036	1.7300	0.0423	0.0733	0.0009	1019	20	1020	16	1021	26	100	100
968	217		0.1572	0.0030	1.5719	0.0343	0.0725	0.0008	941	17	959	14	1000	22	98	94
969	518	0.04	0.1850	0.0037	2.0527	0.0466	0.0805	0.0009	1094	20	1133	15	1208	21	97	91
970	163	1.19	0.1184	0.0025	1.0482	0.0343	0.0642	0.0016	721	15	728	17	749	52	99	96
971	416	0.03	0.1024	0.0023	0.8829	0.0220	0.0625	0.0007	629	13	643	12	692	23	98	91
972	103		0.1208	0.0023	1.0813	0.0325	0.0649	0.0015	735	13	744	16	771	49	99	95
973	87	1.00	0.0946	0.0020	0.7774	0.0290	0.0596	0.0018	583	12	584	17	589	66	100	99
974	121		0.1217	0.0021	1.0741	0.0258	0.0640	0.0011	740	12	741	13	742	35	100	100
975	308	0.46	0.0914	0.0016	0.8024	0.0174	0.0637	0.0008	564	9	598	10	730	28	94	77
976	111		0.1110	0.0023	0.9489	0.0273	0.0620	0.0012	679	14	678	14	674	42	100	101
977	92	0.78	0.1553	0.0030	1.5134	0.0383	0.0707	0.0011	930	17	936	15	949	33	99	98
978	121		0.0885	0.0021	0.7614	0.0288	0.0624	0.0018	547	13	575	17	687	62	95	80
979	531	2.00	0.1287	0.0022	1.1702	0.0769	0.0659	0.0042	781	13	787	36	804	133	99	97
980	63		0.0908	0.0015	0.7545	0.0200	0.0603	0.0012	560	9	571	12	613	45	98	91
981	126	0.06	0.1727	0.0034	1.8027	0.0510	0.0757	0.0015	1027	19	1046	18	1088	40	98	94
982	126	0.10	0.1683	0.0026	1.6968	0.0347	0.0731	0.0010	1003	14	1007	13	1017	28	100	99
983	144	0.73	0.1035	0.0021	0.8823	0.0242	0.0618	0.0011	635	13	642	13	668	38	99	95
984	717		0.1889	0.0041	1.9189	0.0465	0.0737	0.0008	1115	22	1088	16	1033	22	103	108
985	136	0.16	0.3158	0.0053	4.9485	0.1064	0.1137	0.0015	1769	26	1811	18	1859	24	98	95
986	158	0.01	0.1641	0.0024	1.5863	0.0324	0.0701	0.0010	979	13	965	13	932	29	102	105
987	481	0.47	0.3132	0.0076	4.9118	0.1269	0.1137	0.0010	1756	37	1804	22	1860	16	97	94
988	244	0.44	0.4158	0.0099	7.4653	0.1985	0.1302	0.0015	2241	45	2169	24	2101	20	103	107
989	128	0.23	0.1660	0.0042	1.7203	0.0528	0.0752	0.0013	990	23	1016	20	1073	35	97	92
990	150	0.14	0.1555	0.0038	1.5944	0.0438	0.0744	0.0009	932	21	968	17	1052	25	96	89
991	301	1.26	0.1107	0.0027	0.8954	0.0333	0.0587	0.0017	677	15	649	18	555	62	104	122
992	26		0.1834	0.0054	1.9343	0.0795	0.0765	0.0022	1085	30	1093	28	1108	57	99	98
993	72	0.48	0.1777	0.0046	1.8013	0.0548	0.0735	0.0011	1055	25	1046	20	1028	32	101	103
994	191	2.69	0.0847	0.0022	0.6436	0.0380	0.0551	0.0029	524	13	505	24	417	119	104	126
995	300	0.36	0.1693	0.0041	1.7170	0.0490	0.0735	0.0011	1008	23	1015	18	1029	30	99	98
996	103	0.09	0.3840	0.0045	7.4898	0.1058	0.1415	0.0011	2095	21	2172	13	2245	14	96	93
997	66	4.32	0.1109	0.0019	0.9819	0.0434	0.0642	0.0026	678	11	695	22	749	87	98	91
998	219	1.24	0.1032	0.0011	0.8580	0.0217	0.0603	0.0014	633	7	629	12	614	49	101	103
999	201	0.02	0.1027	0.0020	0.8858	0.0207	0.0625	0.0008	630	12	644	11	693	27	98	91
1000	446	1.55	0.0975	0.0013	0.8443	0.0274	0.0628	0.0019	600	8	622	15	702	63	96	85
1001	221	0.27	0.1074	0.0014	0.9432	0.0174	0.0637	0.0008	658	8	675	9	731	28	98	90

Table B.1 Continued

KAR15: Dikendağı Formation

#	U [ppm]	ƒ206%	Isotope ratios						Ages (Ma)						Data filter A*	Data filter B#
			$^{206}Pb/^{238}U$	±2σ	$^{207}Pb/^{235}U$	±2σ	$^{207}Pb/^{206}Pb$	±2σ	$^{206}Pb/^{238}U$	±2σ	$^{207}Pb/^{235}U$	±2σ	$^{207}Pb/^{206}Pb$	±2σ		
1002	501	0.41	0.0693	0.0012	0.5343	0.0116	0.0559	0.0008	432	7	435	8	448	31	99	97
1003	97	0.18	0.0604	0.0012	0.4537	0.0145	0.0545	0.0014	378	7	380	10	390	57	100	97
1004	702		0.0639	0.0014	0.4795	0.0114	0.0545	0.0005	399	8	398	8	390	23	100	102
1005	213		0.1857	0.0040	2.2869	0.0600	0.0893	0.0013	1098	22	1208	19	1411	29	91	78
1006	455		0.0603	0.0009	0.4507	0.0087	0.0542	0.0006	378	6	378	6	379	25	100	99
1007	748	0.13	0.0845	0.0013	0.6985	0.0137	0.0600	0.0007	523	8	538	8	602	26	97	87
1008	297	0.08	0.1176	0.0021	0.9634	0.0242	0.0594	0.0010	717	12	685	13	581	38	105	123
1009	201	0.28	0.0845	0.0017	0.6782	0.0193	0.0582	0.0012	523	10	526	12	539	45	99	97
1010	513	0.06	0.5130	0.0088	12.7756	0.2440	0.1806	0.0015	2669	37	2663	18	2659	14	100	100
1011	132		0.2254	0.0056	2.7017	0.0800	0.0869	0.0014	1310	29	1329	22	1359	31	99	96
1012	803		0.0605	0.0011	0.4737	0.0101	0.0568	0.0006	378	7	394	7	484	24	96	78
1013	342	0.24	0.0617	0.0011	0.5098	0.0170	0.0599	0.0017	386	6	418	11	601	62	92	64
1014	313		0.5431	0.0092	13.1727	0.2649	0.1759	0.0019	2796	38	2692	19	2615	18	104	107
1015	769	0.05	0.0593	0.0010	0.4554	0.0089	0.0557	0.0006	371	6	381	6	442	24	97	84
1016	331	0.80	0.0724	0.0017	0.6015	0.0205	0.0603	0.0015	451	10	478	13	613	53	94	74
1017	396	0.11	0.0628	0.0015	0.4921	0.0140	0.0569	0.0008	392	9	406	10	486	32	97	81
1018	648	1.44	0.0821	0.0011	0.6882	0.0199	0.0608	0.0016	509	6	532	12	632	55	96	80
1019	425	1.12	0.1217	0.0018	0.9951	0.0250	0.0593	0.0012	740	11	701	13	579	44	106	128
1020	110		0.0849	0.0014	0.6948	0.0175	0.0594	0.0011	525	8	536	10	581	42	98	90
1021	174	0.09	0.0537	0.0009	0.4114	0.0108	0.0556	0.0011	337	5	350	8	436	46	96	77
1022	260	0.04	0.0902	0.0011	0.7524	0.0157	0.0605	0.0010	557	6	570	9	622	37	98	90
1023	276		0.0963	0.0011	0.7932	0.0127	0.0598	0.0007	592	7	593	7	595	24	100	100
1024	227	0.35	0.0917	0.0011	0.7552	0.0132	0.0597	0.0007	566	7	571	8	593	27	99	95

KAR22: Alandere Formation

#	U [ppm]	ƒ206%	Isotope ratios						Ages (Ma)						Data filter A*	Data filter B#
			$^{206}Pb/^{238}U$	±2σ	$^{207}Pb/^{235}U$	±2σ	$^{207}Pb/^{206}Pb$	±2σ	$^{206}Pb/^{238}U$	±2σ	$^{207}Pb/^{235}U$	±2σ	$^{207}Pb/^{206}Pb$	±2σ		
1025	325	2.21	0.0813	0.0022	0.6493	0.0315	0.0580	0.0023	504	13	508	19	528	88	99	95
1026	245	0.20	0.0845	0.0017	0.6712	0.0172	0.0576	0.0009	523	10	521	10	515	34	100	101
1027	267	0.07	0.4736	0.0085	9.9174	0.2239	0.1519	0.0021	2499	37	2427	21	2367	23	103	106
1028	342		0.0603	0.0011	0.4710	0.0114	0.0566	0.0008	378	7	392	8	477	33	96	79
1029	420	2.23	0.0573	0.0011	0.4436	0.0177	0.0562	0.0019	359	7	373	12	459	77	96	78
1030	651	1.02	0.0847	0.0014	0.6948	0.0172	0.0595	0.0011	524	8	536	10	584	41	98	90
1031	272	0.34	0.0584	0.0011	0.4366	0.0113	0.0542	0.0010	366	7	368	8	379	40	100	97
1032	122	0.11	0.0752	0.0015	0.6490	0.0201	0.0626	0.0015	467	9	508	12	695	50	92	67
1033	1333	3.19	0.0449	0.0009	0.3323	0.0080	0.0537	0.0008	283	5	291	6	359	32	97	79
1034	91	2.41	0.0527	0.0017	0.4059	0.0266	0.0559	0.0032	331	10	346	19	447	128	96	74
1035	70		0.0988	0.0034	0.8023	0.0402	0.0589	0.0022	607	20	598	23	563	80	102	108
1036	243	0.49	0.1169	0.0023	1.1276	0.0290	0.0700	0.0012	712	13	767	14	928	35	93	77
1037	87	1.10	0.1025	0.0022	0.7999	0.0273	0.0566	0.0015	629	13	597	15	477	58	105	132
1038	190	1.30	0.0873	0.0019	0.6963	0.0235	0.0579	0.0015	539	11	537	14	525	57	101	103
1039	501	0.14	0.4917	0.0106	11.7280	0.2925	0.1730	0.0022	2578	46	2583	23	2587	21	100	100
1040	182	0.18	0.0992	0.0020	0.8497	0.0248	0.0621	0.0013	610	12	625	14	678	45	98	90
1041	105	0.22	0.1172	0.0028	1.0415	0.0353	0.0644	0.0016	715	16	725	18	756	52	99	94
1042	59	0.29	0.3865	0.0083	6.2755	0.1623	0.1178	0.0017	2106	39	2015	23	1923	25	105	110
1043	255	0.36	0.1220	0.0026	1.0943	0.0291	0.0651	0.0010	742	15	751	14	777	33	99	95
1044	124	1.56	0.1201	0.0030	0.9858	0.0407	0.0595	0.0019	731	17	697	21	586	71	105	125
1045	141	1.43	0.0590	0.0014	0.4452	0.0220	0.0547	0.0023	370	9	374	15	401	96	99	92
1046	117	0.80	0.0897	0.0018	0.7873	0.0218	0.0637	0.0012	553	11	590	12	731	40	94	76
1047	1105	6.91	0.0531	0.0011	0.3889	0.0258	0.0531	0.0033	334	7	334	19	334	143	100	100
1048	372	1.26	0.0612	0.0018	0.4529	0.0245	0.0537	0.0024	383	11	379	17	358	102	101	107
1049	261	0.79	0.0795	0.0017	0.6750	0.0239	0.0615	0.0017	493	10	524	14	658	60	94	75
1050	158	0.17	0.0624	0.0013	0.4650	0.0137	0.0540	0.0011	390	8	388	10	372	48	101	105
1051	200		0.0591	0.0012	0.4395	0.0125	0.0539	0.0011	370	7	370	9	368	45	100	101
1052	145	0.12	0.1813	0.0051	2.0228	0.1061	0.0809	0.0036	1074	28	1123	36	1220	87	96	88
1053	160		0.0801	0.0016	0.6531	0.0173	0.0591	0.0011	497	9	510	11	571	39	97	87
1054	47		0.2918	0.0064	3.7656	0.1049	0.0936	0.0016	1650	32	1585	22	1500	32	104	110
1055	306		0.0592	0.0010	0.4397	0.0100	0.0539	0.0008	371	6	370	7	367	35	100	101
1056	228	0.46	0.1153	0.0030	0.9917	0.0296	0.0624	0.0009	704	18	700	15	687	30	101	102
1057	192		0.1135	0.0026	0.9719	0.0281	0.0621	0.0011	693	15	689	14	679	38	100	102
1058	286	0.01	0.4876	0.0079	11.5069	0.2327	0.1712	0.0021	2560	34	2565	19	2569	20	100	100
1059	222	0.20	0.4253	0.0064	8.6343	0.1908	0.1473	0.0024	2284	29	2300	20	2314	28	99	99
1060	24		0.4742	0.0096	11.9201	0.3022	0.1823	0.0028	2502	42	2598	24	2674	25	96	94
1061	100		0.1005	0.0018	0.8342	0.0247	0.0602	0.0014	617	10	616	14	611	51	100	101
1062	70	1.18	0.0615	0.0013	0.4789	0.0180	0.0565	0.0018	384	8	397	12	473	69	97	81
1063	345	1.74	0.0796	0.0014	0.6165	0.0288	0.0562	0.0024	494	8	488	18	459	96	101	108
1064	200		0.0913	0.0015	0.7426	0.0162	0.0590	0.0008	563	9	564	9	567	31	100	99
1065	48	0.78	0.1171	0.0026	0.9731	0.0360	0.0603	0.0018	714	15	690	19	613	64	103	116
1066	602	1.75	0.0599	0.0010	0.4422	0.0165	0.0536	0.0018	375	6	372	12	353	75	101	106
1067	258	0.14	0.0973	0.0014	0.8472	0.0175	0.0631	0.0010	599	8	623	10	712	32	96	84
1068	30	0.82	0.3563	0.0063	5.7312	0.1252	0.1167	0.0015	1964	30	1936	19	1906	23	101	103
1069	287	0.40	0.2114	0.0033	2.5588	0.0559	0.0878	0.0013	1236	18	1289	16	1378	29	96	90
1070	76		0.1014	0.0019	0.8570	0.0258	0.0613	0.0014	623	11	628	14	649	51	99	96
1071	287	1.26	0.0578	0.0008	0.4222	0.0172	0.0530	0.0020	362	5	358	12	329	87	101	110
1072	331	1.24	0.1034	0.0014	0.8533	0.0225	0.0599	0.0014	634	8	626	12	599	49	101	106
1073	137		0.1147	0.0021	1.0034	0.0290	0.0635	0.0014	700	12	706	15	724	47	99	97
1074	50	0.65	0.3615	0.0057	6.4735	0.1276	0.1299	0.0015	1989	27	2042	17	2096	20	97	95
1075	342		0.1209	0.0011	1.0254	0.0146	0.0615	0.0007	736	7	717	7	657	23	103	112
1076	1024	10.02	0.0493	0.0006	0.3690	0.0543	0.0543	0.0080	310	4	319	40	383	334	97	81

Table B.1 Continued

#	U [ppm]	ƒ206%	Isotope ratios						Ages (Ma)						Data filter A*	Data filter B#
			$^{206}Pb/^{238}U$	±2σ	$^{207}Pb/^{235}U$	±2σ	$^{207}Pb/^{206}Pb$	±2σ	$^{206}Pb/^{238}U$	±2σ	$^{207}Pb/^{235}U$	±2σ	$^{207}Pb/^{206}Pb$	±2σ		
1077	191	0.31	0.4826	0.0050	11.0064	0.1951	0.1654	0.0024	2538	22	2524	17	2512	24	101	101
1078	94	0.13	0.1159	0.0013	1.0140	0.0218	0.0635	0.0012	707	8	711	11	724	39	99	98
1079	373	0.06	0.3872	0.0043	6.6884	0.0893	0.1253	0.0009	2110	20	2071	12	2033	13	102	104
1080	148	0.17	0.3675	0.0050	6.3330	0.1013	0.1250	0.0011	2017	23	2023	14	2029	15	100	99
1081	195	2.04	0.0769	0.0013	0.6013	0.0179	0.0567	0.0014	478	8	478	11	479	54	100	100
1082	253	1.08	0.0597	0.0009	0.4368	0.0161	0.0530	0.0018	374	5	368	11	331	77	102	113
1083	192	0.15	0.0978	0.0009	0.8087	0.0133	0.0600	0.0008	602	5	602	7	602	29	100	100
1084	68	0.40	0.1091	0.0012	0.9446	0.0192	0.0628	0.0011	668	7	675	10	701	36	99	95
1085	159	0.02	0.1039	0.0016	0.9004	0.0250	0.0629	0.0014	637	9	652	13	704	49	98	91
1086	779	6.36	0.0650	0.0011	0.4598	0.0174	0.0513	0.0018	406	6	384	12	253	79	106	160
1087	293		0.0950	0.0014	0.7702	0.0138	0.0588	0.0006	585	8	580	8	560	23	101	104
1088	71		0.0671	0.0019	0.5605	0.0235	0.0605	0.0018	419	12	452	15	623	66	93	67
1089	65	2.51	0.0883	0.0017	0.6338	0.0240	0.0521	0.0017	545	10	498	15	289	75	109	189
1090	519	0.01	0.4959	0.0076	11.0927	0.2097	0.1622	0.0018	2596	33	2531	18	2479	19	103	105
1091	75	0.04	0.5515	0.0089	14.1561	0.2537	0.1862	0.0015	2831	37	2760	17	2709	13	103	105
1092	146	0.33	0.0702	0.0012	0.5874	0.0218	0.0607	0.0020	437	7	469	14	629	70	93	70
1093	167	0.70	0.0705	0.0011	0.5964	0.0208	0.0614	0.0019	439	7	475	13	653	67	92	67
1094	461	1.44	0.0856	0.0014	0.7011	0.0177	0.0594	0.0011	529	8	539	11	583	42	98	91
1095	293	0.06	0.0973	0.0012	0.8056	0.0149	0.0600	0.0008	599	7	600	8	605	29	100	99
1096	110	0.01	0.2155	0.0042	2.4655	0.0552	0.0830	0.0009	1258	22	1262	16	1269	21	100	99
1097	388	0.04	0.0569	0.0007	0.4368	0.0078	0.0556	0.0007	357	5	368	6	438	27	97	81

* Data filter A: Percentages calculated from [100 x ($^{206}Pb/^{238}U$ age / $^{207}Pb/^{235}U$ age)].
# Data filter B: Concordance calculated from [100 x ($^{\Delta 5/6}Pb/^{238}U$ age / $^{\Delta 7/6}Pb/^{206}Pb$ age)].

Manuscript III: Supplementary data

- **Table C.1: Main, trace and rare earth element data from the Upper Palaeozoic Konya Complex, south-central Turkey**
- **Table C.2: U–Pb ages of detrital zircons of the Konya Complex**
- **Table C.3: Composition of detrital rutiles from the Konya Complex**
- **Table C.4: Operating conditions for EMPA**

Table C.1: Main, trace and rare earth element data from the Upper Palaeozoic Konya Complex, south-central Turkey

	Halıcı Formation - mélange unit					Halıcı Formation - 'flysch' unit					Ardıçlı Formation		
Sample	T14-20B	T14-26	T14-31	T14-32	T14-33	T14-34	T14-22	T14-23	T14-36	T14-39	T14-29	T14-30	T14-45
Major elements in wt.%													
SiO_2	69,70	88,00	81,55	71,68	75,90	77,12	81,86	90,22	75,75	86,15	90,41	61,68	94,98
TiO_2	0,600	0,225	0,576	0,271	0,116	0,671	0,827	0,240	0,673	0,308	0,163	0,599	0,128
Al_2O_3	12,94	7,36	9,44	11,76	13,65	12,57	9,22	4,97	10,63	7,51	3,81	16,56	3,49
$Fe_2O_{3(tot)}$	7,43	1,10	3,14	4,93	1,68	1,51	3,13	1,58	4,82	3,01	3,36	4,99	0,31
MnO	0,071	0,013	0,021	0,054	0,014	0,018	0,009	0,022	0,078	0,080	0,003	0,067	0,006
MgO	1,66	0,34	0,79	0,66	0,86	1,11	0,37	0,09	1,73	0,59	0,16	4,47	0,06
CaO	0,46	0,08	0,13	0,15	0,13	0,15	0,27	0,07	0,25	0,15	0,05	0,74	0,29
Na_2O	1,35	0,39	0,98	0,89	0,13	3,17	0,99	0,44	1,86	0,46	0,03	2,40	0,04
K_2O	1,81	1,44	1,94	2,77	4,94	1,94	1,50	0,90	1,43	1,76	1,13	4,41	0,90
P_2O_5	0,090	0,023	0,082	0,077	0,030	0,035	0,113	0,042	0,107	0,081	0,036	0,089	0,094
LOI	4,95	1,48	1,83	2,58	2,26	1,79	1,60	0,76	2,44	1,96	0,68	4,24	0,82
Total	101,06	100,45	100,48	95,82	99,71	100,09	99,89	99,34	99,76	102,06	99,83	100,25	101,11
Trace elements in ppm													
Ba	307	210	267	563	389	899	279	210	226	281	602	1260	212
Cr	58	12	40	8	4	21	37	13	170	99	25	234	47
Nb	12	6	14	9	12	11	14	5	10	8	5	16	4
Ni	34	3	15	30	1	1	11	6	37	37	9	130	9
Rb	73	74	78	95	176	70	72	43	55	71	62	192	33
Sc	14	2	8	7	8	11	5	3	10	7	4	13	4
Sr	121	74	23	44	9	76	83	29	47	17	7	46	20
Th	8,1	6,1	10,6	11,8	11,8	4,7	5,6	3	7,8	7,6	5,7	18,1	3,9
U	2	1,3	2,5	2,6	3,2	1,1	1,5	1	2	2	1,5	4,7	1
V	95	20	59	29	15	60	60	28	102	69	54	88	53
Y	25	8	23	42	47	12	20	13	18	21	7	20	12
Zr	186	108	348	131	92	168	270	67	182	142	95	215	59
Rare earth elements in ppm													
La	19,5	33,7	29,9	29,1		22,5	19,1	6,3	21,4	20,0	15,0	97,3	12,2
Ce	38,8	68,1	60,4	60,4		38,3	31,2	13,0	43,4	40,4	30,2	171,0	24,2
Pr	4,6	7,5	7,1	7,2		4,8	4,8	1,3	5,2	4,7	3,3	18,5	2,8
Nd	16,9	25,9	26,0	26,4		16,9	18,5	5,1	19,6	17,4	12,8	60,8	10,7
Sm	3,5	3,9	5,0	5,3		3,1	3,9	1,1	3,9	3,5	2,7	8,6	2,3
Eu	0,7	0,5	0,9	0,9		1,0	0,8	0,2	1,0	0,8	0,5	2,0	0,4
Gd	3,2	2,4	4,1	4,2		2,4	3,3	1,3	3,2	3,2	1,8	6,3	2,1
Tb	0,5	0,3	0,6	0,7		0,3	0,5	0,2	0,4	0,5	0,2	0,7	0,3
Dy	2,7	1,5	3,3	4,6		1,9	2,8	1,5	2,4	3,1	1,3	3,7	1,9
Ho	0,5	0,3	0,6	1,1		0,4	0,5	0,3	0,4	0,6	0,2	0,7	0,4
Er	1,4	0,8	1,8	3,3		1,0	1,4	0,9	1,3	1,7	0,7	1,9	1,1
Tm	0,2	0,1	0,3	0,5		0,1	0,2	0,1	0,2	0,2	0,1	0,3	0,1
Yb	1,4	0,8	1,8	3,4		0,9	1,5	0,9	1,4	1,7	0,7	1,6	0,9
Lu	0,2	0,1	0,3	0,5		0,1	0,2	0,1	0,2	0,2	0,1	0,2	0,1

Major and trace elements were analysed by XRF
Rare earth elements were measured by ICP-MS

Table C.2: U–Pb ages of detrital zircons of the Konya Complex

T14-20B: Halıcı Formation - mélange unit

#	Spot	U [ppm]	ƒ206%	Isotope ratios						Ages (Ma)						Data filter A*	Data filter B#
				$^{206}Pb/^{238}U$	±2σ	$^{207}Pb/^{235}U$	±2σ	$^{207}Pb/^{206}Pb$	±2σ	$^{206}Pb/^{238}U$	±2σ	$^{207}Pb/^{235}U$	±2σ	$^{207}Pb/^{206}Pb$	±2σ		
1	20B-1	390	0,16	0,07969	0,00120	0,62666	0,01228	0,05703	0,00071	494	7	494	8	493	28	100	100
2	20B-2	222	0,07	0,07358	0,00150	0,57354	0,02729	0,05653	0,00243	458	9	460	18	473	95	99	97
3	20B-3	324	0,13	0,16461	0,00309	1,68002	0,04272	0,07402	0,00127	982	17	1001	16	1042	35	98	94
4	20B-4	1108	0,27	0,15027	0,00243	1,41919	0,03059	0,06850	0,00098	902	14	897	13	884	29	101	102
5	20B-5	286	3,24	0,18313	0,00824	1,84056	0,10740	0,07290	0,00271	1084	45	1060	38	1011	75	102	107
6	20B-6	187		0,17360	0,00333	1,74269	0,04678	0,07280	0,00137	1032	18	1024	17	1009	38	101	102
7	20B-7	204		0,11224	0,00142	0,95135	0,02138	0,06147	0,00114	686	8	679	11	656	40	101	105
8	20B-8	345	0,06	0,17209	0,00252	1,79770	0,04052	0,07577	0,00130	1024	14	1045	15	1089	34	98	94
9	20B-9	146	0,33	0,16663	0,00441	1,71250	0,05993	0,07454	0,00171	993	24	1013	22	1056	46	98	94
10	20B-10	373	0,11	0,16666	0,00273	1,71730	0,03958	0,07473	0,00121	994	15	1015	15	1061	33	98	94
11	20B-11	185	0,14	0,09510	0,00156	0,78676	0,02096	0,06000	0,00126	586	9	589	12	604	45	99	97
12	20B-12	157	0,15	0,16047	0,00322	1,62888	0,03857	0,07362	0,00093	959	18	981	15	1031	25	98	93
13	20B-14	697	0,53	0,07853	0,00237	0,65634	0,02525	0,06062	0,00145	487	14	512	15	626	51	95	78
14	20B-15	371	0,33	0,11229	0,00524	0,97176	0,05586	0,06277	0,00210	686	30	689	29	700	71	100	98
15	20B-16	152	0,21	0,35508	0,00933	5,47790	0,19565	0,11189	0,00271	1959	44	1897	31	1830	44	103	107
16	20B-17	118		0,33751	0,00562	5,60244	0,10979	0,12039	0,00124	1875	27	1916	17	1962	18	98	96
17	20B-18	139	0,31	0,11048	0,00269	0,99923	0,03383	0,06560	0,00154	676	16	703	17	794	49	96	85
18	20B-19	133	0,11	0,08331	0,00138	0,71655	0,01920	0,06238	0,00132	516	8	549	11	687	45	94	75
19	20B-20	191		0,10973	0,00207	0,95287	0,02760	0,06298	0,00138	671	12	680	14	708	47	99	95
20	20B-21	59	0,21	0,32784	0,00833	5,21623	0,17300	0,11540	0,00246	1828	40	1855	28	1886	38	99	97
21	20B-23	499	0,23	0,08062	0,00145	0,64958	0,01878	0,05844	0,00132	500	9	508	12	546	49	98	91
22	20B-24	151		0,09577	0,00177	0,81354	0,02645	0,06161	0,00165	590	10	604	15	661	57	98	89
23	20B-25	392	0,08	0,39925	0,00794	7,97838	0,24133	0,14493	0,00330	2166	37	2229	27	2287	39	97	95
24	20B-26	176		0,10546	0,00187	0,89395	0,02520	0,06148	0,00135	646	11	648	14	656	47	100	98
25	20B-27	294	0,17	0,16511	0,00318	1,67028	0,04833	0,07337	0,00158	985	18	997	18	1024	44	99	96
26	20B-29	64	0,45	0,10319	0,00208	0,89220	0,02881	0,06271	0,00158	633	12	648	15	698	54	98	91
27	20B-30	434	1,08	0,07628	0,00128	0,52835	0,02156	0,05023	0,00187	474	8	431	14	206	86	110	230
28	20B-31	459	1,36	0,08693	0,00156	0,62824	0,01991	0,05241	0,00137	537	9	495	12	304	60	109	177
29	20B-32	517	0,14	0,15109	0,00315	1,39283	0,04180	0,06686	0,00144	907	18	886	18	833	45	102	109
30	20B-35	314		0,16851	0,00268	1,68614	0,04358	0,07257	0,00148	1004	15	1003	16	1002	41	100	100
31	20B-36	354	0,41	0,10204	0,00223	0,86624	0,02713	0,06157	0,00138	626	13	634	15	659	48	99	95
32	20B-37	295		0,14633	0,00210	1,30518	0,03496	0,06469	0,00146	880	12	848	15	764	48	104	115
33	20B-38	583	0,11	0,08659	0,00195	0,70638	0,02191	0,05916	0,00126	535	12	543	13	573	46	99	93
34	20B-40	555	0,52	0,08156	0,00178	0,64803	0,02052	0,05762	0,00132	505	11	507	13	516	50	100	98
35	20B-43	591		0,11535	0,00188	0,98766	0,02396	0,06210	0,00112	704	11	698	12	678	38	101	104
36	20B-44	298	0,48	0,11644	0,00163	1,04969	0,02378	0,06538	0,00117	710	9	729	12	787	37	97	90
37	20B-46	435		0,10335	0,00189	0,86985	0,02155	0,06104	0,00102	634	11	635	12	641	36	100	99
38	20B-47	580	1,06	0,06789	0,00223	0,50880	0,02575	0,05436	0,00209	423	13	418	17	386	86	101	110
39	20B-48	415	0,13	0,10789	0,00212	0,96582	0,02711	0,06493	0,00130	660	12	686	14	772	42	96	86
40	20B-49	160	0,84	0,07767	0,00209	0,63497	0,03476	0,05929	0,00283	482	13	499	22	578	104	97	83
41	20B-53	475	0,43	0,07873	0,00124	0,65578	0,01471	0,06041	0,00096	489	7	512	9	618	34	95	79
42	20B-56	239	0,32	0,16996	0,00261	1,74259	0,04343	0,07436	0,00146	1012	14	1024	16	1051	40	99	96
43	20B-57	845	0,16	0,07553	0,00131	0,58989	0,01432	0,05665	0,00096	469	8	471	9	478	38	100	98
44	20B-58	262		0,18860	0,00506	1,93792	0,05965	0,07452	0,00113	1114	27	1094	21	1056	30	102	105
45	20B-59	244	0,31	0,07283	0,00177	0,58714	0,01883	0,05847	0,00123	453	11	469	12	547	46	97	83
46	20B-61	358	0,22	0,11798	0,00378	1,06580	0,03977	0,06552	0,00126	719	22	737	20	791	40	98	91
47	20B-62	246	0,28	0,10985	0,00295	1,00321	0,04711	0,06624	0,00255	672	17	705	24	814	81	95	83
48	20B-63	497	0,34	0,11141	0,00377	0,94995	0,03676	0,06184	0,00117	681	22	678	19	669	40	100	102
49	20B-64	483	0,10	0,17346	0,00561	1,70560	0,06428	0,07132	0,00138	1031	31	1011	24	967	40	102	107
50	20B-66	527	0,73	0,12924	0,00334	1,20078	0,04225	0,06738	0,00161	784	19	801	19	850	50	98	92
51	20B-67	261	0,12	0,33879	0,00831	5,75544	0,16023	0,12321	0,00162	1881	40	1940	24	2003	23	97	94
52	20B-68	405	0,50	0,08395	0,00306	0,67578	0,03011	0,05838	0,00150	520	18	524	18	544	56	99	95
53	20B-69	212	0,04	0,09531	0,00215	0,81353	0,02272	0,06191	0,00102	587	13	604	13	671	35	97	87
54	20B-70	22	0,72	0,11850	0,00397	1,06832	0,07459	0,06538	0,00400	722	23	738	37	787	129	98	92
55	20B-71	153		0,33492	0,00844	5,35321	0,16370	0,11592	0,00201	1862	41	1877	26	1894	31	99	98
56	20B-73	687	0,16	0,07282	0,00215	0,58037	0,02096	0,05780	0,00121	453	13	465	13	522	46	98	87
57	20B-74	254		0,10338	0,00260	0,88772	0,02587	0,06228	0,00092	634	15	645	14	684	31	98	93
58	20B-75	952	0,73	0,14309	0,00364	1,51247	0,04472	0,07666	0,00116	862	21	935	18	1113	30	92	77
59	20B-76	81		0,32450	0,00856	5,49148	0,20681	0,12274	0,00330	1812	42	1899	32	1996	48	95	91
60	20B-77	173	0,30	0,16430	0,00490	1,68679	0,06112	0,07446	0,00153	981	27	1004	23	1054	41	98	93
61	20B-78	383	0,03	0,14060	0,00347	1,34056	0,04182	0,06915	0,00132	848	20	863	18	903	39	98	94
62	20B-79	1033		0,08189	0,00184	0,64798	0,01924	0,05739	0,00111	507	11	507	12	507	43	100	100
63	20B-82	53	0,45	0,17045	0,00548	1,68282	0,07420	0,07160	0,00216	1015	30	1002	28	975	62	101	104
64	20B-84	179	0,47	0,10040	0,00256	0,84669	0,03002	0,06117	0,00151	617	15	623	17	645	53	99	96
65	20B-85	1272	0,10	0,48209	0,01134	11,90775	0,34806	0,17914	0,00311	2536	49	2597	27	2645	29	98	96
66	20B-86	626	0,47	0,10540	0,00256	0,94802	0,02933	0,06523	0,00125	646	15	677	15	782	40	95	83
67	20B-88	172	0,09	0,35321	0,01174	6,04932	0,23172	0,12421	0,00236	1950	56	1983	33	2018	34	98	97
68	20B-91	81		0,11811	0,00376	1,05149	0,04369	0,06457	0,00172	720	22	730	22	760	56	99	95
69	20B-93	217	0,04	0,54030	0,01568	13,19119	0,45305	0,17707	0,00325	2785	66	2693	32	2626	31	103	106
70	20B-94	330	0,35	0,09216	0,00296	0,78798	0,03627	0,06201	0,00204	568	17	590	21	675	70	96	84
71	20B-97	232	0,66	0,14805	0,00394	1,46353	0,04658	0,07170	0,00125	890	22	915	19	977	36	97	91
72	20B-98	1031	0,13	0,08895	0,00304	0,73910	0,02898	0,06027	0,00116	549	18	562	17	613	42	98	90
73	20B-100	557	0,55	0,07922	0,00283	0,70528	0,02778	0,06457	0,00106	491	17	542	17	761	35	91	65

T14-31: Halıcı Formation - mélange unit

#	Spot	U [ppm]	ƒ206%	Isotope ratios						Ages (Ma)						Data filter A*	Data filter B#
				$^{206}Pb/^{238}U$	±2σ	$^{207}Pb/^{235}U$	±2σ	$^{207}Pb/^{206}Pb$	±2σ	$^{206}Pb/^{238}U$	±2σ	$^{207}Pb/^{235}U$	±2σ	$^{207}Pb/^{206}Pb$	±2σ		
74	31-2	126	0,04	0,14669	0,00220	1,48268	0,04063	0,07331	0,00168	882	12	923	17	1023	46	96	86
75	31-3	1108	0,18	0,12889	0,00186	1,22676	0,02984	0,06903	0,00135	782	11	813	14	900	40	96	87
76	31-4	291	0,22	0,19762	0,00263	1,93066	0,05421	0,07085	0,00175	1163	14	1092	19	953	51	106	122
77	31-8	201	0,02	0,35065	0,00709	5,84920	0,17627	0,12098	0,00270	1938	34	1954	26	1971	40	99	98
78	31-9	368	0,25	0,08582	0,00138	0,73581	0,02067	0,06218	0,00143	531	8	560	12	681	49	95	78
79	31-10	709	0,17	0,19098	0,00259	1,94977	0,04766	0,07405	0,00151	1127	14	1098	16	1043	41	103	108
80	31-11	206		0,11815	0,00177	1,07086	0,02445	0,06573	0,00114	720	10	739	12	798	36	97	90
81	31-13	265	0,45	0,09247	0,00143	0,76673	0,01873	0,06014	0,00114	570	8	578	11	609	41	99	94
82	31-14	303	0,27	0,08976	0,00174	0,78975	0,01991	0,06381	0,00103	554	10	591	11	736	34	94	75
83	31-15	466	0,12	0,14620	0,00204	1,46087	0,03266	0,07247	0,00126	880	11	914	13	999	35	96	88
84	31-16	556	0,10	0,08829	0,00220	0,75740	0,02406	0,06222	0,00123	545	13	573	14	682	42	95	80
85	31-17	378	0,04	0,43966	0,00526	9,50210	0,23306	0,15675	0,00336	2349	24	2388	23	2421	36	98	97
86	31-18	642	0,26	0,11943	0,00195	1,06143	0,02398	0,06446	0,00101	727	11	735	12	757	33	99	96

Table C.2 Continued

#	Spot	U [ppm]	f206%	Isotope ratios						Ages (Ma)						Data filter A*	Data filter B#
				$^{206}Pb/^{238}U$	±2σ	$^{207}Pb/^{235}U$	±2σ	$^{207}Pb/^{206}Pb$	±2σ	$^{206}Pb/^{238}U$	±2σ	$^{207}Pb/^{235}U$	±2σ	$^{207}Pb/^{206}Pb$	±2σ		
87	31-19	752	0,11	0,12025	0,00169	1,04868	0,02142	0,06325	0,00094	732	10	728	11	717	31	101	102
88	31-20	279	0,01	0,10163	0,00149	0,84998	0,02228	0,06066	0,00132	624	9	625	12	627	47	100	99
89	31-21	103	0,60	0,18918	0,00290	2,03863	0,05462	0,07816	0,00172	1117	16	1129	18	1151	44	99	97
90	31-23	541	0,00	0,07702	0,00182	0,64711	0,02005	0,06093	0,00122	478	11	507	12	637	43	94	75
91	31-24	287	0,27	0,17469	0,00243	1,59539	0,03715	0,06624	0,00124	1038	13	968	15	814	39	107	128
92	31-25	185	0,23	0,11021	0,00174	0,92692	0,02183	0,06100	0,00107	674	10	666	12	639	38	101	105
93	31-26	497		0,14622	0,00217	1,45677	0,03107	0,07226	0,00111	880	12	913	13	993	31	96	89
94	31-27	336	0,37	0,11447	0,00210	1,03767	0,02625	0,06575	0,00114	699	12	723	13	798	36	97	87
95	31-28	868	0,30	0,08387	0,00121	0,65370	0,01565	0,05653	0,00108	519	7	511	10	473	42	102	110
96	31-29	643	0,21	0,11243	0,00168	1,02007	0,02139	0,06580	0,00097	687	10	714	11	800	31	96	86
97	31-30	251	0,49	0,14464	0,00276	1,33741	0,03456	0,06706	0,00117	871	16	862	15	840	36	101	104
98	31-31	148	0,07	0,11233	0,00218	0,98495	0,02999	0,06359	0,00149	686	13	696	15	728	50	99	94
99	31-33	296	0,04	0,17577	0,00319	1,79411	0,04987	0,07403	0,00156	1044	17	1043	18	1042	43	100	100
100	31-34	142	0,43	0,17094	0,00330	1,79195	0,04594	0,07603	0,00128	1017	18	1043	17	1096	34	98	93
101	31-35	98	0,11	0,55935	0,01019	14,30897	0,34592	0,18553	0,00295	2864	42	2770	23	2703	26	103	106
102	31-36	265	0,16	0,17314	0,00330	1,72230	0,04153	0,07215	0,00107	1029	18	1017	15	990	30	101	104
103	31-37	342	0,22	0,18925	0,00464	1,82005	0,05647	0,06975	0,00133	1117	25	1053	20	921	39	106	121
104	31-38	114		0,13539	0,00263	1,25413	0,03741	0,06718	0,00152	819	15	825	17	843	47	99	97
105	31-39	85	0,24	0,38224	0,00772	6,32377	0,16777	0,11999	0,00207	2087	36	2022	23	1956	31	103	107
106	31-40	105	0,03	0,54290	0,00978	13,63340	0,33723	0,18213	0,00309	2795	41	2725	23	2672	28	103	105
107	31-41	404	0,10	0,20106	0,00359	1,91308	0,04743	0,06901	0,00119	1181	19	1086	17	899	36	109	131
108	31-42	333	0,03	0,11182	0,00172	0,94801	0,02104	0,06149	0,00099	683	10	677	11	656	34	101	104
109	31-43	358	0,12	0,16334	0,00275	1,67865	0,03952	0,07454	0,00123	975	15	1000	15	1056	33	97	92
110	31-44	218	0,04	0,38945	0,00690	6,54935	0,15192	0,12197	0,00183	2120	32	2053	20	1985	27	103	107
111	31-45	336	0,06	0,33638	0,00556	5,65751	0,12646	0,12198	0,00184	1869	27	1925	19	1985	27	97	94
112	31-46	383		0,14794	0,00243	1,37552	0,03450	0,06743	0,00128	889	14	879	15	851	39	101	104
113	31-47	233	0,36	0,17225	0,00502	1,66092	0,06104	0,06993	0,00157	1024	28	994	23	926	46	103	111
114	31-48	304	0,05	0,33396	0,00558	5,28018	0,12030	0,11467	0,00178	1858	27	1866	19	1875	28	100	99
115	31-49	356	0,06	0,09315	0,00190	0,78370	0,02376	0,06102	0,00137	574	11	588	14	640	48	98	90
116	31-50	596	0,03	0,15898	0,00284	1,63837	0,04215	0,07474	0,00138	951	16	985	16	1062	37	97	90
117	31-51	469		0,16117	0,00367	1,52245	0,04399	0,06851	0,00122	963	20	939	18	884	37	103	109
118	31-52	123	0,26	0,11227	0,00210	0,94237	0,02794	0,06088	0,00140	686	12	674	15	635	50	102	108
119	31-53	363	0,14	0,10569	0,00182	0,87641	0,02249	0,06014	0,00114	648	11	639	12	609	41	101	106
120	31-54	107		0,51478	0,00990	12,48729	0,32245	0,17593	0,00303	2677	42	2642	24	2615	29	101	102
121	31-55	376	0,12	0,10037	0,00283	0,81563	0,03115	0,05894	0,00152	617	17	606	17	565	56	102	109
122	31-56	155		0,55123	0,01011	13,02996	0,32521	0,17144	0,00290	2830	42	2682	24	2572	28	106	110
123	31-57	235	0,14	0,37557	0,00890	6,05670	0,18588	0,11696	0,00228	2055	42	1984	27	1910	35	104	108
124	31-58	76	0,12	0,16082	0,00335	1,54920	0,05111	0,06986	0,00179	961	19	950	20	924	53	101	104
125	31-59	498		0,07983	0,00116	0,64349	0,01369	0,05847	0,00091	495	7	504	8	547	34	98	90
126	31-60	132	0,20	0,19720	0,00548	1,90675	0,06070	0,07013	0,00109	1160	30	1083	21	932	32	107	124
127	31-61	319	0,44	0,11748	0,00213	0,98994	0,02304	0,06112	0,00089	716	12	699	12	643	31	102	111
128	31-62	770	0,09	0,09680	0,00117	0,80260	0,01441	0,06013	0,00080	596	7	598	8	608	29	100	98
129	31-63	230		0,09280	0,00127	0,74051	0,01503	0,05787	0,00087	572	7	563	9	525	33	102	109
130	31-64	338	0,12	0,46931	0,01132	11,01048	0,31023	0,17016	0,00248	2480	50	2524	26	2559	24	98	97
131	31-65	218	0,09	0,58060	0,00781	17,32684	0,35360	0,21644	0,00332	2951	32	2953	20	2954	25	100	100
132	31-66	190	0,23	0,11447	0,00197	0,99907	0,02334	0,06330	0,00100	699	11	703	12	718	34	99	97
133	31-67	308		0,09373	0,00146	0,80606	0,01923	0,06237	0,00113	578	9	600	11	687	39	96	84
134	31-68	37	0,70	0,32891	0,00605	4,66496	0,11598	0,10286	0,00172	1833	29	1761	21	1677	31	104	109
135	31-69	98	0,67	0,11883	0,00173	1,04718	0,02664	0,06391	0,00133	724	10	727	13	739	44	99	98
136	31-71	247		0,15946	0,00230	1,58362	0,03765	0,07203	0,00136	954	13	964	15	987	38	99	97
137	31-72	353		0,17290	0,00227	1,74544	0,03390	0,07322	0,00105	1028	12	1025	13	1020	29	100	101
138	31-73	99		0,14152	0,00339	1,32694	0,04660	0,06800	0,00174	853	19	858	20	869	53	99	98
139	31-75	976	0,02	0,10906	0,00146	0,92548	0,01806	0,06155	0,00087	667	9	665	10	659	30	100	101
140	31-76	82	0,20	0,16532	0,00300	1,64938	0,04706	0,07236	0,00159	986	17	989	18	996	45	100	99
141	31-77	159	0,64	0,17772	0,00460	1,79662	0,05834	0,07332	0,00144	1054	25	1044	21	1023	40	101	103
142	31-79	406		0,13970	0,00146	1,30896	0,02270	0,06795	0,00094	843	8	850	10	867	29	99	97
143	31-80	202	0,55	0,11598	0,00129	1,00781	0,02297	0,06302	0,00125	707	7	708	12	709	42	100	100
144	31-81	1694	0,29	0,09600	0,00149	0,83313	0,01869	0,06294	0,00102	591	9	615	10	706	34	96	84
145	31-82	92	0,06	0,16366	0,00180	1,60730	0,03716	0,07123	0,00145	977	10	973	14	964	42	100	101
146	31-83	218		0,18001	0,00185	1,88214	0,03633	0,07583	0,00124	1067	10	1075	13	1091	33	99	98
147	31-85	555	0,10	0,17309	0,00194	1,78267	0,03044	0,07470	0,00096	1029	11	1039	11	1060	26	99	97
148	31-86	218	0,24	0,27953	0,00351	3,57573	0,06651	0,09278	0,00127	1589	18	1544	15	1483	26	103	107
149	31-87	205		0,18580	0,00323	1,94445	0,04495	0,07590	0,00116	1099	18	1097	16	1093	31	100	101
150	31-88	485	0,21	0,12064	0,00219	1,04258	0,02490	0,06268	0,00097	734	13	725	12	697	33	101	105
151	31-89	313		0,09082	0,00172	0,75298	0,02013	0,06013	0,00113	560	10	570	12	608	41	98	92
152	31-90	308		0,16643	0,00313	1,65399	0,04641	0,07208	0,00150	992	17	991	18	988	42	100	100
153	31-91	497	0,32	0,08592	0,00155	0,73460	0,01703	0,06201	0,00090	531	9	559	10	675	31	95	79
154	31-92	560	0,23	0,13650	0,00245	1,28249	0,03011	0,06814	0,00103	825	14	838	13	873	31	98	94
155	31-93	430	0,48	0,12021	0,00213	1,16927	0,02744	0,07055	0,00108	732	12	786	13	944	31	93	77
156	31-94	229		0,09571	0,00141	0,78654	0,01687	0,05961	0,00093	589	8	589	10	589	34	100	100
157	31-95	55		0,17312	0,00319	1,83532	0,05680	0,07689	0,00191	1029	18	1058	20	1118	50	97	92
158	31-96	71		0,14779	0,00264	1,45520	0,03770	0,07142	0,00134	889	15	912	16	969	38	97	92
159	31-97	426	0,06	0,17440	0,00227	1,71162	0,03283	0,07118	0,00100	1036	12	1013	12	963	29	102	108
160	31-98	634		0,11712	0,00142	1,03079	0,01983	0,06383	0,00095	714	8	719	10	736	32	99	97
161	31-99	220	0,39	0,11356	0,00171	0,97078	0,02270	0,06200	0,00111	693	10	689	12	674	38	101	103
162	31-100	393	0,08	0,11167	0,00153	0,92741	0,01919	0,06023	0,00094	682	9	666	10	612	34	102	112

T13-34: Halıcı Formation - mélange unit

#	Spot	U [ppm]	f206%	Isotope ratios						Ages (Ma)						Data filter A*	Data filter B#
				$^{206}Pb/^{238}U$	±2σ	$^{207}Pb/^{235}U$	±2σ	$^{207}Pb/^{206}Pb$	±2σ	$^{206}Pb/^{238}U$	±2σ	$^{207}Pb/^{235}U$	±2σ	$^{207}Pb/^{206}Pb$	±2σ		
163	34-1	468	3,23	0,07721	0,00190	0,59146	0,07206	0,05556	0,00663	479	11	472	46	435	268	102	110
164	34-2	359		0,08063	0,00134	0,62904	0,01500	0,05658	0,00097	500	8	496	9	475	38	101	105
165	34-3	238	0,24	0,07577	0,00131	0,58523	0,01459	0,05602	0,00100	471	8	468	9	453	40	101	104
166	34-4	271		0,08133	0,00141	0,63220	0,01626	0,05637	0,00107	504	8	497	10	467	42	101	108
167	34-5	447	0,04	0,07736	0,00133	0,59455	0,01363	0,05574	0,00085	480	8	474	9	442	34	101	109
168	34-6	490		0,08142	0,00129	0,64359	0,01498	0,05733	0,00098	505	8	505	9	504	38	100	100
169	34-7	147	0,10	0,07819	0,00132	0,60793	0,01796	0,05639	0,00137	485	8	482	11	468	54	101	104
170	34-8	706		0,08075	0,00106	0,62290	0,01149	0,05595	0,00073	501	6	492	7	450	29	102	111
171	34-9	348		0,07649	0,00105	0,58397	0,01277	0,05537	0,00094	475	6	467	8	427	38	102	111
172	34-10	841		0,08222	0,00106	0,63812	0,01241	0,05629	0,00082	509	6	501	8	464	32	102	110
173	34-11	250	0,13	0,11113	0,00154	0,90586	0,01872	0,05912	0,00091	679	9	655	10	572	33	104	119

Table C.2 Continued

#	Spot	U [ppm]	f206%	Isotope ratios						Ages (Ma)						Data filter A*	Data filter B#
				$^{206}Pb/^{238}U$	±2σ	$^{207}Pb/^{235}U$	±2σ	$^{207}Pb/^{206}Pb$	±2σ	$^{206}Pb/^{238}U$	±2σ	$^{207}Pb/^{235}U$	±2σ	$^{207}Pb/^{206}Pb$	±2σ		
174	34-12	422	0,12	0,09493	0,00152	0,75770	0,01586	0,05789	0,00078	585	9	573	9	526	30	102	111
175	34-13	364	0,03	0,08564	0,00115	0,65621	0,01504	0,05558	0,00103	530	7	512	9	436	41	103	122
176	34-14	324	0,66	0,08019	0,00116	0,62966	0,01495	0,05695	0,00107	497	7	496	9	490	42	100	102
177	34-15	375	0,13	0,07476	0,00107	0,58689	0,01399	0,05694	0,00109	465	6	469	9	489	42	99	95
178	34-17	186	0,04	0,38054	0,00509	6,54412	0,13145	0,12472	0,00187	2079	24	2052	18	2025	27	101	103
179	34-18	225	0,10	0,08663	0,00158	0,70900	0,01978	0,05935	0,00125	536	9	544	12	580	46	98	92
180	34-19	358	0,18	0,07565	0,00098	0,59259	0,01238	0,05681	0,00093	470	6	473	8	484	36	99	97
181	34-20	291	0,08	0,08863	0,00186	0,71005	0,01933	0,05811	0,00101	547	11	545	11	534	38	100	103
182	34-21	466		0,07833	0,00107	0,60835	0,01321	0,05633	0,00095	486	6	483	8	465	37	101	104
183	34-22	160		0,13867	0,00203	1,31156	0,03242	0,06860	0,00137	837	12	851	14	887	41	98	94
184	34-23	464	0,33	0,07471	0,00112	0,58629	0,01300	0,05692	0,00093	464	7	468	8	488	36	99	95
185	34-24	277	0,19	0,07658	0,00093	0,60089	0,01252	0,05691	0,00096	476	6	478	8	488	37	100	97
186	34-25	235	0,89	0,07821	0,00118	0,64584	0,02003	0,05989	0,00162	485	7	506	12	600	59	96	81
187	34-26	310		0,07511	0,00112	0,58305	0,01591	0,05630	0,00129	467	7	466	10	464	51	100	101
188	34-28	227		0,07903	0,00130	0,60370	0,01669	0,05540	0,00123	490	8	480	11	429	50	102	114
189	34-29	493	0,00	0,07896	0,00111	0,62768	0,01462	0,05765	0,00107	490	7	495	9	517	41	99	95
190	34-30	377		0,07960	0,00129	0,61523	0,01506	0,05606	0,00103	494	8	487	9	455	41	101	109
191	34-31	251	0,06	0,16425	0,00245	1,63461	0,04012	0,07218	0,00141	980	14	984	15	991	40	100	99
192	34-32	627	0,29	0,09038	0,00130	0,73520	0,01980	0,05900	0,00134	558	8	560	12	567	50	100	98
193	34-34	338	0,34	0,07499	0,00156	0,57395	0,01747	0,05551	0,00123	466	9	461	11	433	49	101	108
194	34-35	181	0,13	0,07133	0,00179	0,54972	0,02014	0,05590	0,00149	444	11	445	13	448	59	100	99
195	34-36	700	0,18	0,07485	0,00141	0,60288	0,01773	0,05842	0,00132	465	8	479	11	545	49	97	85
196	34-37	476		0,07362	0,00140	0,56357	0,01500	0,05552	0,00103	458	8	454	10	433	41	101	106
197	34-38	214		0,07503	0,00153	0,58727	0,01862	0,05677	0,00138	466	9	469	12	483	54	99	97
198	34-39	355	0,07	0,07110	0,00138	0,54049	0,01580	0,05514	0,00121	443	8	439	10	418	49	101	106
199	34-40	613		0,07504	0,00139	0,57484	0,01585	0,05556	0,00113	466	8	461	10	435	45	101	107
200	34-41	311	0,17	0,07162	0,00146	0,55641	0,01656	0,05635	0,00122	446	9	449	11	466	48	99	96
201	34-42	431	0,37	0,07769	0,00144	0,62233	0,01798	0,05810	0,00129	482	9	491	11	534	49	98	90
202	34-43	453		0,07221	0,00139	0,56104	0,01601	0,05635	0,00118	449	8	452	10	466	47	99	96
203	34-44	298		0,07705	0,00171	0,59245	0,01788	0,05576	0,00114	479	10	472	11	443	46	101	108
204	34-45	304	0,30	0,07228	0,00157	0,55502	0,01625	0,05569	0,00109	450	9	448	11	440	44	100	102
205	34-46	313	0,36	0,07538	0,00163	0,57640	0,01786	0,05546	0,00123	468	10	462	12	431	49	101	109
206	34-47	259	0,70	0,07391	0,00158	0,55684	0,01689	0,05464	0,00118	460	9	449	11	398	48	102	116
207	34-48	450		0,07419	0,00158	0,57509	0,01710	0,05622	0,00117	461	9	461	11	461	46	100	100
208	34-49	305	0,49	0,06628	0,00183	0,51762	0,02088	0,05664	0,00167	414	11	424	14	478	65	98	87
209	34-50	560	0,29	0,07604	0,00164	0,60672	0,01737	0,05787	0,00109	472	10	481	11	525	41	98	90
210	34-51	232	0,50	0,07719	0,00167	0,59230	0,01807	0,05565	0,00120	479	10	472	12	438	48	101	109
211	34-52	206	1,62	0,07634	0,00172	0,55248	0,02908	0,05249	0,00250	474	10	447	19	307	109	106	154
212	34-53	433	0,10	0,07735	0,00163	0,60085	0,01591	0,05634	0,00090	480	10	478	10	466	35	101	103
213	34-54	866	0,11	0,07361	0,00146	0,57670	0,01348	0,05682	0,00070	458	9	462	9	485	27	99	94
214	34-55	421	0,50	0,07341	0,00145	0,55907	0,01481	0,05523	0,00098	457	9	451	10	422	40	101	108
215	34-56	271		0,08040	0,00163	0,62351	0,01736	0,05625	0,00107	498	10	492	11	462	42	101	108
216	34-57	500	0,11	0,07709	0,00158	0,59162	0,01494	0,05566	0,00082	479	9	472	10	439	33	101	109
217	34-58	267	0,38	0,07244	0,00158	0,55483	0,01672	0,05555	0,00116	451	9	448	11	434	46	101	104
218	34-60	413	0,16	0,07311	0,00142	0,56655	0,01468	0,05621	0,00097	455	9	456	10	461	38	100	99
219	34-61	336	0,39	0,07307	0,00145	0,56136	0,01387	0,05572	0,00082	455	9	452	9	441	33	100	103
220	34-62	186	0,04	0,33441	0,00670	5,12862	0,12461	0,11123	0,00153	1860	32	1841	21	1820	25	101	102
221	34-63	513	0,07	0,06656	0,00119	0,53433	0,01273	0,05822	0,00092	415	7	435	8	538	35	96	77
222	34-64	232		0,07432	0,00135	0,58582	0,01588	0,05717	0,00115	462	8	468	10	498	44	99	93
223	34-65	186		0,07031	0,00133	0,55339	0,01652	0,05708	0,00132	438	8	447	11	495	51	98	89
224	34-66	261	0,49	0,07770	0,00162	0,61027	0,01686	0,05696	0,00103	482	10	484	11	490	40	100	98
225	34-67	672	0,05	0,07734	0,00134	0,60029	0,01308	0,05630	0,00074	480	8	477	8	464	29	101	103
226	34-68	338	0,07	0,11631	0,00208	1,00098	0,02314	0,06242	0,00091	709	12	704	12	689	31	101	103
227	34-69	272		0,07139	0,00137	0,55628	0,01562	0,05652	0,00116	444	8	449	10	473	45	99	94
228	34-70	289	0,62	0,07617	0,00159	0,60290	0,02024	0,05740	0,00151	473	9	479	13	507	58	99	93
229	34-71	514		0,07692	0,00135	0,60144	0,01536	0,05671	0,00106	478	8	478	10	480	41	100	99
230	34-72	304	0,26	0,07416	0,00111	0,58074	0,01483	0,05680	0,00117	461	7	465	10	484	46	99	95
231	34-73	434	0,64	0,07015	0,00130	0,56967	0,01775	0,05890	0,00148	437	8	458	11	563	55	95	78
232	34-74	209		0,07636	0,00118	0,58787	0,01475	0,05583	0,00110	474	7	470	9	446	44	101	106
233	34-76	330		0,07298	0,00104	0,56242	0,01305	0,05589	0,00102	454	6	453	8	448	41	100	101
234	34-77	477	0,23	0,07518	0,00117	0,58697	0,01306	0,05663	0,00090	467	7	469	8	477	35	100	98
235	34-79	227	0,24	0,07758	0,00124	0,59294	0,01548	0,05543	0,00114	482	7	473	10	430	46	102	112
236	34-80	121	0,51	0,14129	0,00231	1,35216	0,03519	0,06941	0,00141	852	13	868	15	911	42	98	94
237	34-81	360		0,07579	0,00121	0,60529	0,01544	0,05792	0,00115	471	7	481	10	527	44	98	89
238	34-82	116		0,07250	0,00132	0,56285	0,01678	0,05630	0,00133	451	8	453	11	464	52	100	97
239	34-83	412	0,69	0,07341	0,00138	0,59307	0,01633	0,05860	0,00118	457	8	473	10	552	44	97	83
240	34-84	383	0,01	0,08253	0,00157	0,64886	0,01785	0,05702	0,00113	511	9	508	11	493	44	101	104
241	34-85	429		0,07387	0,00121	0,56783	0,01381	0,05575	0,00100	459	7	457	9	442	40	101	104
242	34-86	381	0,21	0,07385	0,00122	0,56799	0,01417	0,05578	0,00104	459	7	457	9	444	41	101	103
243	34-87	171	0,49	0,07329	0,00126	0,58881	0,01662	0,05827	0,00130	456	8	470	11	540	49	97	84
244	34-88	410		0,07288	0,00111	0,55804	0,01226	0,05553	0,00088	453	7	450	8	434	35	101	105
245	34-89	88		0,10237	0,00176	0,85648	0,02879	0,06068	0,00175	628	10	628	16	628	62	100	100
246	34-90	387		0,07589	0,00129	0,58999	0,01458	0,05638	0,00101	472	8	471	9	467	40	100	101
247	34-91	197	0,44	0,07614	0,00258	0,60185	0,03014	0,05733	0,00211	473	15	478	19	504	81	99	94
248	34-92	260		0,07193	0,00244	0,55117	0,02761	0,05558	0,00205	448	15	446	18	436	82	100	103
249	34-93	344		0,11869	0,00395	1,01793	0,04960	0,06220	0,00221	723	23	713	25	681	76	101	106
250	34-94	363		0,07111	0,00238	0,56095	0,02739	0,05721	0,00203	443	14	452	18	500	78	98	89
251	34-95	323	0,06	0,07839	0,00261	0,61116	0,03031	0,05655	0,00208	486	16	484	19	474	81	100	103
252	34-96	48		0,09649	0,00348	0,79878	0,04610	0,06004	0,00271	594	20	596	26	605	98	100	98
253	34-97	271	0,01	0,07923	0,00268	0,61511	0,03033	0,05631	0,00202	492	16	487	19	465	79	101	106
254	34-98	309		0,07635	0,00268	0,58976	0,02996	0,05602	0,00206	474	16	471	19	453	81	101	105
255	34-99	188	0,07	0,08270	0,00281	0,64212	0,03325	0,05631	0,00220	512	17	504	21	465	87	102	110
256	34-100	251	0,60	0,07440	0,00265	0,64575	0,03765	0,06295	0,00290	463	16	506	23	707	98	91	65

T14-22: Halıcı Formation - 'flysch' unit

#	Spot	U [ppm]	f206%	Isotope ratios						Ages (Ma)						Data filter A*	Data filter B#
				$^{206}Pb/^{238}U$	±2σ	$^{207}Pb/^{235}U$	±2σ	$^{207}Pb/^{206}Pb$	±2σ	$^{206}Pb/^{238}U$	±2σ	$^{207}Pb/^{235}U$	±2σ	$^{207}Pb/^{206}Pb$	±2σ		
257	22-1	1146	0,02	0,10546	0,00305	1,02405	0,03461	0,07043	0,00123	646	18	716	17	941	36	90	69
258	22-2	73	0,96	0,10845	0,00302	0,96903	0,03492	0,06481	0,00148	664	18	688	18	768	48	96	86
259	22-5	311	0,04	0,07340	0,00242	0,63464	0,02373	0,06271	0,00111	457	15	499	15	699	38	92	65
260	22-6	227		0,34932	0,01191	5,88683	0,21041	0,12223	0,00131	1931	57	1959	31	1989	19	99	97

Table C.2 Continued

#	Spot	U [ppm]	f206%	Isotope ratios						Ages (Ma)						Data filter A*	Data filter B#
				$^{206}Pb/^{238}U$	±2σ	$^{207}Pb/^{235}U$	±2σ	$^{207}Pb/^{206}Pb$	±2σ	$^{206}Pb/^{238}U$	±2σ	$^{207}Pb/^{235}U$	±2σ	$^{207}Pb/^{206}Pb$	±2σ		
261	22-7	174		0,34947	0,01211	5,79302	0,21320	0,12022	0,00149	1932	58	1945	32	1960	22	99	99
262	22-8	397		0,06531	0,00228	0,50221	0,01898	0,05577	0,00081	408	14	413	13	443	32	99	92
263	22-9	192	0,05	0,39195	0,01348	6,87736	0,25559	0,12726	0,00179	2132	62	2096	33	2061	25	102	103
264	22-10	235		0,10642	0,00381	0,92709	0,03704	0,06318	0,00112	652	22	666	20	714	38	98	91
265	22-11	408	0,14	0,35416	0,01238	6,16097	0,22755	0,12617	0,00150	1954	59	1999	32	2045	21	98	96
266	22-12	119		0,07496	0,00320	0,65424	0,03142	0,06330	0,00139	466	19	511	19	718	47	91	65
267	22-13	313	0,41	0,06741	0,00227	0,56712	0,02167	0,06101	0,00110	421	14	456	14	640	39	92	66
268	22-14	704	0,04	0,50796	0,02394	12,19483	0,59353	0,17412	0,00211	2648	102	2620	46	2598	20	101	102
269	22-15	675	0,28	0,06950	0,00141	0,55109	0,01379	0,05751	0,00085	433	8	446	9	511	32	97	85
270	22-16	500	0,11	0,11053	0,00218	0,95690	0,02326	0,06279	0,00089	676	13	682	12	701	30	99	96
271	22-17	191	0,43	0,38339	0,00857	6,35905	0,16240	0,12030	0,00148	2092	40	2027	22	1961	22	103	107
272	22-18	444		0,11031	0,00221	0,94769	0,02354	0,06231	0,00092	675	13	677	12	685	31	100	98
273	22-19	199		0,12865	0,00269	1,21626	0,03703	0,06857	0,00152	780	15	808	17	886	46	97	88
274	22-20	186	0,04	0,17326	0,00361	1,73078	0,04572	0,07245	0,00118	1030	20	1020	17	999	33	101	103
275	22-21	141	1,17	0,08161	0,00216	0,58034	0,02152	0,05157	0,00134	506	13	465	14	267	60	109	190
276	22-22	95		0,11138	0,00242	0,94675	0,02721	0,06165	0,00116	681	14	676	14	662	40	101	103
277	22-23	1217	0,17	0,10992	0,00239	0,94538	0,02400	0,06238	0,00082	672	14	676	13	687	28	99	98
278	22-24	229		0,11163	0,00267	0,96645	0,03136	0,06279	0,00138	682	15	687	16	701	47	99	97
279	22-25	183	0,08	0,16808	0,00644	1,87441	0,07745	0,08088	0,00125	1001	36	1072	27	1219	30	93	82
280	22-26	2469	0,26	0,09240	0,00221	0,79568	0,02107	0,06245	0,00071	570	13	594	12	690	24	96	83
281	22-27	306		0,14563	0,00416	1,39409	0,04581	0,06943	0,00113	876	23	886	19	912	33	99	96
282	22-28	319		0,07117	0,00161	0,56076	0,01519	0,05714	0,00085	443	10	452	10	497	33	98	89
283	22-29	1123		0,21952	0,00486	2,22506	0,05765	0,07351	0,00099	1279	26	1189	18	1028	27	108	124
284	22-30	261	0,33	0,10854	0,00246	0,90853	0,02453	0,06071	0,00089	664	14	656	13	629	32	101	106
285	22-31	883	0,11	0,10298	0,00234	0,85725	0,02222	0,06038	0,00075	632	14	629	12	617	27	101	102
286	22-32	565	0,11	0,15957	0,00377	1,57232	0,04382	0,07147	0,00105	954	21	959	17	971	30	99	98
287	22-33	95	1,35	0,09607	0,00261	0,69974	0,03233	0,05283	0,00198	591	15	539	19	321	85	110	184
288	22-34	1293	0,19	0,06954	0,00163	0,58697	0,01609	0,06122	0,00087	433	10	469	10	647	30	92	67
289	22-35	382		0,08957	0,00193	0,73777	0,01897	0,05974	0,00084	553	11	561	11	594	30	99	93
290	22-36	103	2,99	0,10782	0,00288	0,89469	0,06184	0,06018	0,00384	660	17	649	33	610	138	102	108
291	22-37	906	0,14	0,14821	0,00457	1,54532	0,05710	0,07562	0,00154	891	26	949	23	1085	41	94	82
292	22-38	591	0,54	0,10460	0,00220	0,88692	0,02345	0,06150	0,00098	641	13	645	13	657	34	99	98
293	22-39	203		0,07675	0,00154	0,57829	0,01681	0,05465	0,00115	477	9	463	11	398	47	103	120
294	22-40	201	0,10	0,12379	0,00269	1,05860	0,02892	0,06202	0,00103	752	15	733	14	675	35	103	111
295	22-41	79	0,06	0,12753	0,00304	1,14934	0,03846	0,06536	0,00154	774	17	777	18	786	49	100	98
296	22-42	260	0,22	0,13764	0,00291	1,35196	0,03534	0,07124	0,00110	831	16	868	15	964	31	96	86
297	22-44	539	0,05	0,52252	0,01070	12,72653	0,31753	0,17665	0,00252	2710	45	2660	23	2622	24	102	103
298	22-45	470	0,23	0,10307	0,00215	0,87419	0,02400	0,06151	0,00110	632	13	638	13	657	38	99	96
299	22-46	369	0,22	0,16439	0,00345	1,66701	0,04686	0,07355	0,00138	981	19	996	18	1029	38	99	95
300	22-47	95	0,47	0,23946	0,00521	3,05388	0,09088	0,09249	0,00188	1384	27	1421	23	1478	39	97	94
301	22-48	1709	0,10	0,11519	0,00251	1,02583	0,02659	0,06459	0,00090	703	15	717	13	761	30	98	92
302	22-49	225	0,05	0,09377	0,00228	0,78905	0,02541	0,06103	0,00129	578	13	591	14	640	45	98	90
303	22-50	717	0,18	0,14969	0,00312	1,46143	0,03803	0,07081	0,00110	899	17	915	16	952	32	98	94
304	22-51	1652	0,21	0,09464	0,00281	0,81615	0,03230	0,06254	0,00164	583	17	606	18	693	56	96	84
305	22-52	611		0,13849	0,00415	1,24653	0,04175	0,06528	0,00097	836	24	822	19	783	31	102	107
306	22-53	1793	0,12	0,09462	0,00152	0,78156	0,01901	0,05991	0,00109	583	9	586	11	600	40	99	97
307	22-54	1174	0,09	0,08584	0,00192	0,73695	0,02043	0,06227	0,00102	531	11	561	12	683	35	95	78
308	22-56	137	0,26	0,38426	0,00532	6,35252	0,15411	0,11990	0,00239	2096	25	2026	21	1955	36	103	107
309	22-57	440	0,09	0,10724	0,00109	0,90935	0,01754	0,06150	0,00101	657	6	657	9	657	35	100	100
310	22-58	920	0,19	0,09274	0,00125	0,75254	0,01624	0,05885	0,00099	572	7	570	9	562	37	100	102
311	22-59	45		0,12002	0,00226	1,08590	0,05212	0,06562	0,00290	731	13	747	25	794	93	98	92
312	22-60	316		0,07016	0,00113	0,53237	0,01528	0,05503	0,00131	437	7	433	10	414	53	101	106
313	22-61	553	0,18	0,10315	0,00119	0,85067	0,01803	0,05981	0,00106	633	7	625	10	597	39	101	106
314	22-62	384	0,33	0,12784	0,00230	1,14011	0,02856	0,06468	0,00113	775	13	773	14	764	37	100	101
315	22-63	264		0,10486	0,00206	0,87894	0,02540	0,06079	0,00129	643	12	640	14	632	46	100	102
316	22-64	349	0,67	0,15398	0,00326	1,39416	0,04194	0,06567	0,00140	923	18	886	18	796	45	104	116
317	22-65	141		0,17602	0,00417	1,79527	0,06137	0,07397	0,00182	1045	23	1044	22	1041	50	100	100
318	22-66	686	0,24	0,14840	0,00320	1,37936	0,03821	0,06741	0,00117	892	18	880	16	851	36	101	105
319	22-67	246	0,43	0,06936	0,00134	0,54021	0,01526	0,05648	0,00116	432	8	439	10	472	46	99	92
320	22-68	144		0,17220	0,00333	1,76530	0,05369	0,07435	0,00175	1024	18	1033	20	1051	47	99	97
321	22-70	652	0,31	0,16696	0,00284	1,66576	0,04197	0,07236	0,00134	995	16	996	16	996	38	100	100
322	22-71	1034	0,12	0,43984	0,00798	8,85661	0,35749	0,14604	0,00527	2350	36	2323	37	2300	62	101	102
323	22-72	96		0,17796	0,00254	1,80401	0,04953	0,07352	0,00172	1056	14	1047	18	1028	47	101	103
324	22-73	338	0,41	0,13342	0,00155	1,15945	0,02653	0,06303	0,00124	807	9	782	12	709	42	103	114
325	22-74	105	0,97	0,12270	0,00178	1,08737	0,03428	0,06427	0,00180	746	10	747	17	751	59	100	99
326	22-75	182		0,10336	0,00174	0,90768	0,02927	0,06369	0,00175	634	10	656	16	731	58	97	87
327	22-76	188		0,12254	0,00149	1,05007	0,02551	0,06215	0,00131	745	9	729	13	679	45	102	110
328	22-77	271	0,22	0,20003	0,00429	2,13886	0,06893	0,07755	0,00187	1175	23	1161	22	1135	48	101	104
329	22-79	506	0,10	0,14044	0,00169	1,35033	0,02969	0,06973	0,00128	847	10	868	13	921	38	98	92
330	22-80	254	0,79	0,09219	0,00299	0,81910	0,03444	0,06444	0,00173	568	18	608	19	756	57	94	75
331	22-83	110		0,11618	0,00181	0,99543	0,02833	0,06214	0,00148	709	10	701	14	679	51	101	104
332	22-84	146		0,17254	0,00286	1,71175	0,04688	0,07195	0,00157	1026	16	1013	18	985	44	101	104
333	22-85	413	0,05	0,52382	0,00915	12,19393	0,33583	0,16883	0,00360	2715	39	2619	26	2546	36	104	107
334	22-86	531	0,14	0,12355	0,00187	1,06950	0,02681	0,06278	0,00125	751	11	738	13	701	43	102	107
335	22-87	1172	0,24	0,12629	0,00181	1,14063	0,02610	0,06550	0,00117	767	10	773	12	791	37	99	97
336	22-89	251	0,70	0,12108	0,00214	1,08001	0,03268	0,06469	0,00159	737	12	744	16	764	52	99	96
337	22-91	108	0,81	0,19839	0,00361	2,05024	0,05703	0,07495	0,00158	1167	19	1132	19	1067	42	103	109
338	22-92	681	0,00	0,10338	0,00178	0,85293	0,02049	0,05984	0,00100	634	10	626	11	598	36	101	106
339	22-93	101		0,38567	0,00624	6,47074	0,14684	0,12169	0,00194	2103	29	2042	20	1981	28	103	106
340	22-94	258	0,11	0,51030	0,02222	12,64957	0,61854	0,17978	0,00400	2658	95	2654	46	2651	37	100	100

T14-36: Halıcı Formation - 'flysch' unit

#	Spot	U [ppm]	f206%	Isotope ratios						Ages (Ma)						Data filter A*	Data filter B#
				$^{206}Pb/^{238}U$	±2σ	$^{207}Pb/^{235}U$	±2σ	$^{207}Pb/^{206}Pb$	±2σ	$^{206}Pb/^{238}U$	±2σ	$^{207}Pb/^{235}U$	±2σ	$^{207}Pb/^{206}Pb$	±2σ		
341	36-2	489	0,99	0,10468	0,00167	0,94594	0,02449	0,06554	0,00134	642	10	676	13	792	43	95	81
342	36-3	730	0,04	0,06706	0,00095	0,51412	0,01119	0,05561	0,00092	418	6	421	8	437	37	99	96
343	36-4	336		0,06151	0,00081	0,47879	0,01050	0,05645	0,00099	385	5	397	7	470	39	97	82
344	36-5	430	0,40	0,06608	0,00087	0,49775	0,01111	0,05463	0,00098	412	5	410	8	397	40	101	104
345	36-6	589	0,15	0,06055	0,00070	0,45731	0,00935	0,05477	0,00092	379	4	382	7	403	38	99	94
346	36-7	321	0,16	0,55909	0,00620	15,82968	0,25790	0,20535	0,00245	2863	26	2867	16	2869	19	100	100
347	36-8	654	0,19	0,05983	0,00071	0,44980	0,00799	0,05452	0,00072	375	4	377	6	393	30	99	95

Table C.2 Continued

#	Spot	U [ppm]	f206%	Isotope ratios						Ages (Ma)						Data filter A*	Data filter B#
				$^{206}Pb/^{238}U$	±2σ	$^{207}Pb/^{235}U$	±2σ	$^{207}Pb/^{206}Pb$	±2σ	$^{206}Pb/^{238}U$	±2σ	$^{207}Pb/^{235}U$	±2σ	$^{207}Pb/^{206}Pb$	±2σ		
348	36-9	295	0,27	0,06586	0,00069	0,50568	0,01102	0,05569	0,00107	411	4	416	7	440	43	99	93
349	36-10	281	0,25	0,06531	0,00082	0,53697	0,01244	0,05963	0,00116	408	5	436	8	590	42	93	69
350	36-11	183	1,60	0,05994	0,00091	0,44727	0,01417	0,05412	0,00151	375	6	375	10	376	63	100	100
351	36-12	1291	0,18	0,052246	0,000621	0,397473	0,006867	0,055176	0,000692	328	4	340	5	419	28	97	78
352	36-13	188		0,06155	0,00082	0,46352	0,01234	0,05462	0,00126	385	5	387	9	397	52	100	97
353	36-14	486	0,08	0,06389	0,00081	0,48880	0,00977	0,05549	0,00086	399	5	404	7	432	35	99	92
354	36-15	1134	0,21	0,06684	0,00071	0,51793	0,00912	0,05620	0,00079	417	4	424	6	460	31	98	91
355	36-16	204		0,53023	0,00763	12,90131	0,26293	0,17647	0,00255	2742	32	2672	19	2620	24	103	105
356	36-17	120		0,06322	0,00105	0,46357	0,01499	0,05318	0,00148	395	6	387	10	336	63	102	117
357	36-18	452	0,49	0,05992	0,00087	0,48352	0,01400	0,05852	0,00147	375	5	400	10	549	55	94	68
358	36-19	624	0,25	0,06593	0,00087	0,49968	0,01000	0,05497	0,00082	412	5	411	7	411	33	100	100
359	36-21	243	0,15	0,37842	0,00523	6,39469	0,12617	0,12256	0,00173	2069	24	2032	17	1994	25	102	104
360	36-22	163	0,48	0,05999	0,00091	0,45117	0,01183	0,05455	0,00117	376	6	378	8	394	48	99	95
361	36-23	723	0,10	0,06374	0,00091	0,47981	0,00988	0,05459	0,00081	398	6	398	7	396	33	100	101
362	36-24	379	0,14	0,06015	0,00086	0,45996	0,01050	0,05546	0,00098	377	5	384	7	431	40	98	87
363	36-25	261		0,59001	0,01101	19,48322	0,44057	0,23950	0,00306	2989	45	3066	22	3117	20	97	96
364	36-26	104	0,80	0,35730	0,00648	5,90872	0,15190	0,11994	0,00218	1969	31	1963	22	1955	33	100	101
365	36-27	110		0,09055	0,00146	0,74555	0,01970	0,05972	0,00125	559	9	566	11	593	45	99	94
366	36-28	115	0,11	0,42332	0,00597	7,78628	0,15394	0,13340	0,00185	2275	27	2207	18	2143	24	103	106
367	36-30	1253		0,06192	0,00091	0,46691	0,01020	0,05469	0,00088	387	6	389	7	400	36	100	97
368	36-31	888	0,02	0,06925	0,00096	0,52924	0,01097	0,05543	0,00086	432	6	431	7	430	34	100	100
369	36-32	202	0,23	0,06425	0,00117	0,49596	0,01411	0,05598	0,00122	401	7	409	10	452	48	98	89
370	36-33	289	0,09	0,46361	0,00686	11,73523	0,22624	0,18358	0,00227	2455	30	2584	18	2686	20	95	91
371	36-34	513	0,18	0,06368	0,00095	0,47907	0,01091	0,05456	0,00093	398	6	397	7	394	38	100	101
372	36-35	927	0,07	0,06183	0,00093	0,47140	0,01057	0,05529	0,00092	387	6	392	7	424	37	99	91
373	36-36	246	0,02	0,50248	0,00726	14,74895	0,30483	0,21288	0,00315	2624	31	2799	20	2928	24	94	90
374	36-37	240		0,08480	0,00135	0,67561	0,01629	0,05778	0,00104	525	8	524	10	522	40	100	101
375	36-38	140		0,50465	0,00732	12,98108	0,27632	0,18656	0,00291	2634	31	2678	20	2712	26	98	97
376	36-39	357	0,03	0,48446	0,00638	12,22720	0,23314	0,18305	0,00253	2547	28	2622	18	2681	23	97	95
377	36-40	425		0,06142	0,00104	0,46664	0,01178	0,05510	0,00103	384	6	389	8	416	42	99	92
378	36-41	456	0,10	0,06704	0,00107	0,50610	0,01217	0,05475	0,00099	418	6	416	8	402	40	101	104
379	36-42	553	0,16	0,05933	0,00091	0,45254	0,01002	0,05532	0,00088	372	6	379	7	425	35	98	87
380	36-43	599	0,10	0,08111	0,00139	0,64935	0,01618	0,05807	0,00105	503	8	508	10	532	40	99	94
381	36-44	617		0,06404	0,00120	0,47732	0,01149	0,05405	0,00081	400	7	396	8	373	34	101	107
382	36-45	54		0,60391	0,00924	16,91075	0,35877	0,20309	0,00298	3045	37	2930	20	2851	24	104	107
383	36-46	56	0,96	0,40608	0,00767	7,19418	0,20785	0,12849	0,00281	2197	35	2136	26	2077	38	103	106
384	36-47	633	0,25	0,06432	0,00113	0,49231	0,01234	0,05551	0,00100	402	7	406	8	433	40	99	93
385	36-48	80	0,01	0,38287	0,00710	6,72323	0,15796	0,12736	0,00184	2090	33	2076	21	2062	25	101	101
386	36-49	937		0,06614	0,00112	0,50333	0,01175	0,05519	0,00089	413	7	414	8	420	36	100	98
387	36-50	201		0,06377	0,00114	0,48525	0,01369	0,05519	0,00120	398	7	402	9	420	49	99	95
388	36-51	621	0,10	0,06417	0,00100	0,49220	0,01203	0,05563	0,00105	401	6	406	8	438	42	99	92
389	36-52	25		0,42185	0,00773	7,93913	0,22469	0,13649	0,00294	2269	35	2224	26	2183	38	102	104
390	36-53	244	0,12	0,51197	0,00854	13,16427	0,27706	0,18649	0,00239	2665	36	2691	20	2712	21	99	98
391	36-54	596		0,06620	0,00082	0,50180	0,01100	0,05497	0,00100	413	5	413	7	411	41	100	100
392	36-55	206		0,062275	0,001163	0,475557	0,017032	0,055384	0,001692	389	7	395	12	428	68	99	91
393	36-56	484	0,08	0,06705	0,00083	0,51008	0,01156	0,05518	0,00105	418	5	419	8	419	42	100	100
394	36-57	83	0,03	0,38782	0,00628	6,79145	0,16227	0,12701	0,00223	2113	29	2085	21	2057	31	101	103
395	36-58	148	0,89	0,06427	0,00106	0,47788	0,01361	0,05393	0,00125	402	6	397	9	368	52	101	109
396	36-59	936	0,19	0,06651	0,00084	0,50844	0,01009	0,05545	0,00085	415	5	417	7	430	34	99	96
397	36-60	224	0,25	0,09821	0,00146	0,79870	0,02108	0,05898	0,00128	604	9	596	12	567	47	101	107
398	36-61	834	0,09	0,06726	0,00087	0,51339	0,01071	0,05536	0,00090	420	5	421	7	427	36	100	98
399	36-62	297	0,30	0,06645	0,00091	0,52889	0,01404	0,05772	0,00131	415	6	431	9	519	50	96	80
400	36-63	147		0,50079	0,00584	12,59361	0,21734	0,18239	0,00232	2617	25	2650	16	2675	21	99	98
401	36-64	114		0,37406	0,00484	6,49980	0,11552	0,12603	0,00154	2048	23	2046	16	2043	22	100	100
402	36-65	584		0,06711	0,00065	0,51081	0,00974	0,05520	0,00091	419	4	419	7	420	37	100	100
403	36-66	317		0,09548	0,00118	0,77317	0,01788	0,05873	0,00115	588	7	582	10	557	43	101	106
404	36-67	126	0,86	0,08903	0,00149	0,71464	0,01940	0,05821	0,00125	550	9	548	11	538	47	100	102
405	36-68	691	0,32	0,06226	0,00089	0,47664	0,01165	0,05552	0,00110	389	5	396	8	433	44	98	90
406	36-69	585	0,53	0,05913	0,00099	0,43563	0,01080	0,05343	0,00098	370	6	367	8	347	41	101	107
407	36-70	311	0,08	0,06313	0,00085	0,46183	0,01202	0,05306	0,00118	395	5	386	8	331	51	102	119
408	36-72	580	0,23	0,06522	0,00085	0,48384	0,00940	0,05381	0,00077	407	5	401	6	363	32	102	112
409	36-73	476		0,44898	0,00792	10,90934	0,29086	0,17622	0,00352	2391	35	2515	25	2618	33	95	91
410	36-74	1548	0,13	0,06412	0,00095	0,48959	0,00956	0,05538	0,00071	401	6	405	7	427	28	99	94
411	36-75	914	0,07	0,06292	0,00100	0,47795	0,01091	0,05509	0,00090	393	6	397	7	416	37	99	95
412	36-76	689	0,22	0,06391	0,00097	0,48128	0,01045	0,05462	0,00085	399	6	399	7	397	35	100	101
413	36-77	732	0,75	0,06157	0,00100	0,49497	0,01143	0,05831	0,00095	385	6	408	8	541	36	94	71
414	36-78	380		0,27075	0,00488	3,87918	0,08459	0,10391	0,00127	1545	25	1609	18	1695	23	96	91
415	36-79	789	0,05	0,06330	0,00098	0,48156	0,01075	0,05517	0,00089	396	6	399	7	419	36	99	94
416	36-80	93		0,39924	0,00656	7,06535	0,15430	0,12835	0,00185	2165	30	2120	19	2076	25	102	104
417	36-81	314	0,01	0,55193	0,00880	14,26945	0,29598	0,18751	0,00249	2833	37	2768	20	2721	22	102	104
418	36-82	512		0,06492	0,00095	0,50716	0,01324	0,05666	0,00123	405	6	417	9	478	48	97	85
419	36-83	495		0,05192	0,00087	0,40426	0,01258	0,05648	0,00148	326	5	345	9	471	58	95	69
420	36-84	897	0,03	0,10687	0,00138	0,88860	0,01646	0,06030	0,00080	655	8	646	9	615	29	101	107
421	36-85	740	0,12	0,36817	0,00563	6,80545	0,13641	0,13406	0,00174	2021	27	2086	18	2152	23	97	94
422	36-86	881		0,06191	0,00101	0,47312	0,01120	0,05543	0,00095	387	6	393	8	430	38	98	90
423	36-88	812	0,21	0,06519	0,00095	0,49722	0,01011	0,05532	0,00078	407	6	410	7	425	32	99	96
424	36-89	231		0,48420	0,00730	11,92021	0,25289	0,17855	0,00267	2545	32	2598	20	2640	25	98	96
425	36-90	328	1,13	0,12288	0,00221	1,02641	0,03426	0,06058	0,00170	747	13	717	17	625	61	104	120
426	36-91	759	0,47	0,06064	0,00099	0,46916	0,01085	0,05611	0,00092	380	6	391	8	457	36	97	83
427	36-92	217	0,34	0,06517	0,00102	0,50209	0,01451	0,05588	0,00136	407	6	413	10	448	54	99	91
428	36-93	620	0,02	0,05779	0,00089	0,44901	0,01097	0,05635	0,00107	362	5	377	8	466	42	96	78
429	36-94	560	0,19	0,06380	0,00091	0,47888	0,00979	0,05444	0,00080	399	5	397	7	389	33	100	102
430	36-95	170	0,49	0,12765	0,00218	1,11313	0,02947	0,06324	0,00128	774	12	760	14	717	43	102	108
431	36-96	384	0,15	0,14187	0,00298	1,19991	0,03007	0,06134	0,00084	855	17	801	14	651	29	107	131
432	36-97	144	0,12	0,49184	0,00646	11,51567	0,23526	0,16981	0,00266	2579	28	2566	19	2556	26	100	101
433	36-98	440		0,06247	0,00088	0,47119	0,01025	0,05470	0,00090	391	5	392	7	400	37	100	98
434	36-99	889	0,17	0,06266	0,00128	0,48464	0,01235	0,05610	0,00086	392	8	401	8	456	34	98	86

Table C.2 Continued

T14-39: Halıcı Formation - 'flysch' unit

#	Spot	U [ppm]	f206%	Isotope ratios						Ages (Ma)						Data filter A*	Data filter B#
				$^{206}Pb/^{238}U$	±2σ	$^{207}Pb/^{235}U$	±2σ	$^{207}Pb/^{206}Pb$	±2σ	$^{206}Pb/^{238}U$	±2σ	$^{207}Pb/^{235}U$	±2σ	$^{207}Pb/^{206}Pb$	±2σ		
435	39-1	237	2,37	0,06746	0,00242	0,48084	0,03057	0,05169	0,00271	421	15	399	21	272	120	106	155
436	39-2	404		0,05745	0,00101	0,42936	0,01026	0,05421	0,00088	360	6	363	7	380	36	99	95
437	39-3	550	0,05	0,09671	0,00234	0,91567	0,02829	0,06867	0,00132	595	14	660	15	889	40	90	67
438	39-4	141		0,06668	0,00128	0,52200	0,01690	0,05678	0,00148	416	8	426	11	483	58	98	86
439	39-5	721	0,79	0,05665	0,00108	0,45567	0,01267	0,05834	0,00118	355	7	381	9	543	44	93	65
440	39-6	133	0,45	0,06487	0,00144	0,51399	0,02515	0,05747	0,00250	405	9	421	17	510	96	96	79
441	39-7	407	0,41	0,09465	0,00179	0,80237	0,02217	0,06148	0,00124	583	11	598	12	656	43	97	89
442	39-8	331	0,10	0,53306	0,00784	13,24136	0,25556	0,18016	0,00225	2754	33	2697	18	2654	21	102	104
443	39-9	534	0,06	0,06017	0,00102	0,45724	0,01073	0,05511	0,00089	377	6	382	7	417	36	99	90
444	39-10	202	0,29	0,09517	0,00182	0,79023	0,02055	0,06022	0,00106	586	11	591	12	612	38	99	96
445	39-11	266	2,00	0,05865	0,00143	0,39436	0,02330	0,04877	0,00263	367	9	338	17	137	127	109	269
446	39-12	577	0,05	0,05829	0,00083	0,43349	0,00950	0,05394	0,00090	365	5	366	7	369	38	100	99
447	39-15	259	0,44	0,11679	0,00203	0,97796	0,02348	0,06073	0,00101	712	12	693	12	630	36	103	113
448	39-16	382	0,05	0,08206	0,00158	0,68670	0,01776	0,06069	0,00105	508	9	531	11	628	37	96	81
449	39-17	598	0,50	0,05409	0,00075	0,41473	0,00908	0,05561	0,00094	340	5	352	7	437	38	96	78
450	39-18	1695	0,32	0,05866	0,00096	0,46702	0,01058	0,05774	0,00090	367	6	389	7	520	34	94	71
451	39-19	325	0,11	0,17078	0,00281	1,57803	0,03738	0,06701	0,00114	1016	15	962	15	838	36	106	121
452	39-21	888	0,04	0,06533	0,00131	0,49817	0,01303	0,05531	0,00092	408	8	410	9	425	37	99	96
453	39-22	107		0,14022	0,00355	1,33998	0,04262	0,06931	0,00134	846	20	863	18	908	40	98	93
454	39-23	121		0,05379	0,00118	0,37708	0,01413	0,05084	0,00155	338	7	325	10	234	70	104	145
455	39-24	182		0,06307	0,00138	0,46802	0,01731	0,05382	0,00160	394	8	390	12	364	67	101	108
456	39-25	448	1,63	0,05621	0,00165	0,40115	0,01727	0,05176	0,00163	353	10	342	13	275	72	103	128
457	39-26	289		0,12774	0,00288	1,15066	0,03205	0,06533	0,00107	775	16	778	15	785	34	100	99
458	39-28	171		0,09319	0,00192	0,75375	0,02200	0,05866	0,00121	574	11	570	13	555	45	101	104
459	39-29	329	0,04	0,36085	0,00731	6,26387	0,15557	0,12590	0,00181	1986	35	2013	22	2041	25	99	97
460	39-30	209		0,18280	0,00315	1,88714	0,04918	0,07487	0,00147	1082	17	1077	17	1065	39	101	102
461	39-31	122		0,09647	0,00208	0,77231	0,02476	0,05806	0,00138	594	12	581	14	532	52	102	112
462	39-32	94	0,21	0,37189	0,00636	6,27980	0,15682	0,12247	0,00223	2038	30	2016	22	1993	32	101	102
463	39-33	321	0,01	0,13925	0,00260	1,28689	0,03576	0,06703	0,00138	840	15	840	16	839	43	100	100
464	39-34	288		0,10659	0,00193	0,88584	0,02437	0,06028	0,00125	653	11	644	13	614	45	101	106
465	39-35	525	0,24	0,06479	0,00121	0,48374	0,01467	0,05415	0,00129	405	7	401	10	377	54	101	107
466	39-36	42	0,11	0,19494	0,00405	1,97194	0,07905	0,07337	0,00252	1148	22	1106	27	1024	69	104	112
467	39-37	1027		0,10913	0,00202	0,91511	0,02467	0,06082	0,00119	668	12	660	13	633	42	101	105
468	39-38	263	0,02	0,56936	0,01041	14,56892	0,37414	0,18558	0,00335	2905	43	2788	24	2703	30	104	107
469	39-40	586	0,40	0,05407	0,00151	0,42757	0,01968	0,05736	0,00210	339	9	361	14	505	80	94	67
470	39-41	800	0,01	0,12818	0,00323	1,11545	0,03608	0,06311	0,00128	777	18	761	17	712	43	102	109
471	39-43	566	0,27	0,06778	0,00172	0,51307	0,01767	0,05490	0,00128	423	10	421	12	408	52	101	104
472	39-45	554		0,06401	0,00164	0,49040	0,01693	0,05556	0,00128	400	10	405	12	435	51	99	92
473	39-47	365		0,15172	0,00387	1,40097	0,04785	0,06697	0,00152	911	22	889	20	837	47	102	109
474	39-48	73	0,01	0,43457	0,01115	8,02822	0,26954	0,13399	0,00290	2326	50	2234	30	2151	38	104	108
475	39-49	617	0,13	0,37015	0,01071	6,63281	0,21868	0,12996	0,00205	2030	50	2064	29	2098	28	98	97
476	39-50	99	0,06	0,08262	0,00246	0,66374	0,02767	0,05826	0,00170	512	15	517	17	540	64	99	95
477	39-51	1014	0,07	0,06608	0,00201	0,50629	0,01760	0,05557	0,00094	412	12	416	12	435	38	99	95
478	39-52	575	0,11	0,11882	0,00344	1,08008	0,03503	0,06593	0,00096	724	20	744	17	804	30	97	90
479	39-53	95	0,03	0,17763	0,00540	1,81539	0,06715	0,07412	0,00156	1054	30	1051	24	1045	43	100	101
480	39-54	143	0,07	0,33118	0,01020	5,67140	0,19979	0,12420	0,00212	1844	49	1927	30	2018	30	96	91
481	39-55	82		0,37364	0,01092	6,04811	0,20329	0,11740	0,00195	2046	51	1983	29	1917	30	103	107
482	39-56	602		0,12234	0,00349	1,07108	0,03485	0,06350	0,00099	744	20	739	17	725	33	101	103
483	39-57	398		0,06585	0,00190	0,50005	0,01708	0,05507	0,00100	411	12	412	12	415	41	100	99
484	39-58	130	0,17	0,34381	0,00638	5,48089	0,12374	0,11562	0,00149	1905	31	1898	19	1890	23	100	101
485	39-59	226	0,14	0,12340	0,00262	1,07911	0,02874	0,06342	0,00102	750	15	743	14	723	34	101	104
486	39-60	1285		0,05963	0,00098	0,44615	0,00903	0,05427	0,00064	373	6	375	6	382	27	100	98
487	39-61	330	1,29	0,06541	0,00120	0,46796	0,02177	0,05189	0,00222	408	7	390	15	281	98	105	146
488	39-63	1799	0,35	0,04843	0,00092	0,37567	0,00913	0,05626	0,00085	305	6	324	7	463	33	94	66
489	39-65	807		0,05740	0,00100	0,43165	0,00919	0,05454	0,00067	360	6	364	7	393	28	99	91
490	39-66	211	0,73	0,05984	0,00108	0,45618	0,01267	0,05529	0,00117	375	7	382	9	424	47	98	88
491	39-67	704	0,09	0,05655	0,00128	0,42910	0,01279	0,05503	0,00107	355	8	363	9	414	43	98	86
492	39-68	503	0,12	0,25083	0,00455	3,22330	0,07800	0,09320	0,00149	1443	23	1463	19	1492	30	99	97
493	39-69	495		0,08486	0,00131	0,66402	0,01431	0,05675	0,00086	525	8	517	9	482	33	102	109
494	39-70	669	0,13	0,08890	0,00133	0,70895	0,01547	0,05784	0,00092	549	8	544	9	524	35	101	105
495	39-71	407	0,62	0,04962	0,00128	0,40067	0,01440	0,05856	0,00147	312	8	342	10	551	55	91	57
496	39-72	278	1,10	0,11130	0,00348	0,98083	0,04615	0,06392	0,00225	680	20	694	24	739	74	98	92
497	39-73	237	0,08	0,46460	0,00776	11,86403	0,24252	0,18520	0,00219	2460	34	2594	19	2700	19	95	91
498	39-74	138	0,58	0,10317	0,00219	0,87299	0,02713	0,06137	0,00139	633	13	637	15	652	49	99	97
499	39-75	633	0,04	0,06514	0,00159	0,49186	0,01456	0,05477	0,00092	407	10	406	10	403	38	100	101
500	39-76	65	0,30	0,29110	0,00694	4,47048	0,14655	0,11138	0,00251	1647	35	1726	27	1822	41	95	90
501	39-77	129	0,15	0,14191	0,00220	1,27592	0,03341	0,06521	0,00137	855	12	835	15	781	44	102	110
502	39-79	194	0,25	0,08407	0,00139	0,66578	0,01726	0,05744	0,00115	520	8	518	11	508	44	100	102
503	39-80	44		0,11369	0,00283	0,97577	0,04699	0,06225	0,00256	694	16	691	24	683	88	100	102
504	39-81	88		0,39505	0,00610	6,85396	0,13974	0,12583	0,00168	2146	28	2093	18	2041	24	103	105
505	39-82	425	0,28	0,15494	0,00301	1,34407	0,03795	0,06292	0,00129	929	17	865	16	705	44	107	132
506	39-83	553	0,29	0,05474	0,00132	0,42077	0,01402	0,05574	0,00128	344	8	357	10	442	51	96	78
507	39-84	771		0,12124	0,00295	1,14223	0,03624	0,06833	0,00139	738	17	774	17	879	42	95	84
508	39-85	276	0,57	0,05502	0,00116	0,40044	0,01188	0,05279	0,00111	345	7	342	9	320	48	101	108
509	39-86	325		0,10900	0,00189	0,93441	0,02419	0,06217	0,00120	667	11	670	13	680	41	100	98
510	39-87	445	0,17	0,15013	0,00232	1,53066	0,03411	0,07395	0,00119	902	13	943	14	1040	32	96	87
511	39-88	1095	0,13	0,40929	0,00942	8,79476	0,25268	0,15585	0,00268	2212	43	2317	26	2411	29	95	92
512	39-89	269	0,06	0,31747	0,00512	4,55043	0,09880	0,10395	0,00151	1777	25	1740	18	1696	27	102	105
513	39-90	290	0,07	0,71862	0,01607	26,69838	0,76659	0,26946	0,00485	3491	60	3372	28	3303	28	104	106
514	39-91	940	0,22	0,06903	0,00162	0,51974	0,01474	0,05460	0,00086	430	10	425	10	396	35	101	109
515	39-92	985	0,78	0,06293	0,00201	0,51151	0,02511	0,05895	0,00220	393	12	419	17	565	81	94	70
516	39-93	280		0,10831	0,00167	0,90929	0,01990	0,06089	0,00095	663	10	657	11	635	33	101	104
517	39-94	216		0,10187	0,00219	0,84111	0,02487	0,05989	0,00121	625	13	620	14	600	44	101	104
518	39-95	604	0,13	0,18828	0,00336	1,88292	0,04555	0,07253	0,00119	1112	18	1075	16	1001	33	103	111
519	39-96	784	0,07	0,06699	0,00124	0,49956	0,01312	0,05408	0,00101	418	7	411	9	375	42	102	112
520	39-97	109	1,24	0,12499	0,00306	0,98707	0,05519	0,05727	0,00288	759	18	697	28	502	111	109	151
521	39-98	965	1,39	0,04893	0,00152	0,35367	0,01549	0,05243	0,00162	308	9	307	12	304	70	100	101
522	39-99	195	0,02	0,10534	0,00218	0,87808	0,02680	0,06045	0,00136	646	13	640	14	620	48	101	104
523	39-100	881	0,03	0,10328	0,00181	0,85575	0,01943	0,06010	0,00087	634	11	628	11	607	31	101	104

Table C.2 Continued

T14-29: Ardıçlı Formation

#	Spot	U [ppm]	f206%	Isotope ratios						Ages (Ma)						Data filter A*	Data filter B#
				$^{206}Pb/^{238}U$	±2σ	$^{207}Pb/^{235}U$	±2σ	$^{207}Pb/^{206}Pb$	±2σ	$^{206}Pb/^{238}U$	±2σ	$^{207}Pb/^{235}U$	±2σ	$^{207}Pb/^{206}Pb$	±2σ		
524	29-1	524	0,05	0,03870	0,00071	0,27343	0,00796	0,05124	0,00116	245	4	245	6	252	52	100	97
525	29-2	614		0,04186	0,00071	0,29559	0,00782	0,05122	0,00104	264	4	263	6	251	47	101	105
526	29-3	607	0,19	0,04157	0,00070	0,29288	0,00749	0,05110	0,00098	263	4	261	6	245	44	101	107
527	29-4	983	0,02	0,04100	0,00071	0,28766	0,00693	0,05089	0,00085	259	4	257	5	236	39	101	110
528	29-5	574		0,04121	0,00069	0,29375	0,00756	0,05169	0,00101	260	4	262	6	272	45	100	96
529	29-6	350	0,56	0,04019	0,00077	0,29284	0,00951	0,05285	0,00139	254	5	261	7	322	60	97	79
530	29-7	971	0,22	0,03766	0,00066	0,27356	0,00652	0,05269	0,00085	238	4	246	5	315	37	97	76
531	29-8	725		0,04185	0,00079	0,29211	0,00747	0,05062	0,00088	264	5	260	6	224	40	102	118
532	29-9	1184		0,03630	0,00084	0,25827	0,00739	0,05160	0,00087	230	5	233	6	268	39	99	86
533	29-10	769		0,03875	0,00075	0,27492	0,00684	0,05145	0,00080	245	5	247	5	261	36	99	94
534	29-11	995	0,09	0,03951	0,00076	0,28078	0,00773	0,05154	0,00101	250	5	251	6	265	45	99	94
535	29-12	800	0,23	0,03521	0,00061	0,24961	0,00605	0,05141	0,00088	223	4	226	5	259	39	99	86
536	29-13	502	0,37	0,03954	0,00074	0,27479	0,00712	0,05041	0,00091	250	5	247	6	214	42	101	117
537	29-14	248	0,60	0,03819	0,00076	0,26963	0,00821	0,05120	0,00118	242	5	242	7	250	53	100	97
538	29-15	384	0,76	0,03929	0,00068	0,27827	0,00746	0,05137	0,00105	248	4	249	6	257	47	100	96
539	29-16	817	0,37	0,04353	0,00095	0,31483	0,00945	0,05246	0,00108	275	6	278	7	305	47	99	90
540	29-17	729	0,33	0,03825	0,00088	0,28048	0,00798	0,05318	0,00088	242	5	251	6	337	38	96	72
541	29-18	1010	0,26	0,03638	0,00082	0,25688	0,00679	0,05121	0,00071	230	5	232	5	250	32	99	92
542	29-19	560	0,50	0,04286	0,00110	0,29847	0,01124	0,05050	0,00139	271	7	265	9	218	64	102	124
543	29-20	643	0,21	0,03998	0,00088	0,28216	0,00778	0,05119	0,00086	253	5	252	6	250	39	100	101
544	29-21	808	0,39	0,03755	0,00083	0,26484	0,00731	0,05116	0,00084	238	5	239	6	248	38	100	96
545	29-22	832		0,03653	0,00078	0,25763	0,00695	0,05114	0,00084	231	5	233	6	247	38	99	93
546	29-23	267	0,13	0,15367	0,00333	1,58342	0,04081	0,07473	0,00104	921	19	964	16	1061	28	96	87
547	29-24	394		0,04128	0,00092	0,29140	0,00875	0,05119	0,00103	261	6	260	7	250	46	100	104
548	29-25	259	0,13	0,11351	0,00247	0,96682	0,02426	0,06178	0,00077	693	14	687	13	666	27	101	104
549	29-26	560		0,04356	0,00077	0,30447	0,00741	0,05070	0,00085	275	5	270	6	227	39	102	121
550	29-27	1650	0,32	0,03446	0,00063	0,25081	0,00602	0,05279	0,00083	218	4	227	5	320	36	96	68
551	29-28	207	0,73	0,05620	0,00122	0,41503	0,01161	0,05356	0,00094	352	7	352	8	353	40	100	100
552	29-29	911		0,03648	0,00065	0,25736	0,00597	0,05117	0,00076	231	4	233	5	248	34	99	93
553	29-30	232	0,31	0,11932	0,00248	1,00511	0,02724	0,06109	0,00106	727	14	706	14	643	37	103	113
554	29-31	967	0,16	0,03767	0,00066	0,26874	0,00610	0,05174	0,00074	238	4	242	5	274	33	99	87
555	29-32	502		0,04116	0,00079	0,28814	0,00713	0,05077	0,00079	260	5	257	6	230	36	101	113
556	29-33	1222	0,17	0,03802	0,00067	0,27045	0,00638	0,05159	0,00081	241	4	243	5	267	36	99	90
557	29-34	665	0,08	0,04230	0,00076	0,29652	0,00714	0,05084	0,00081	267	5	264	6	234	37	101	114
558	29-35	831		0,03865	0,00061	0,27002	0,00599	0,05067	0,00079	244	4	243	5	226	36	101	108
559	29-36	812		0,03891	0,00056	0,27457	0,00613	0,05118	0,00087	246	3	246	5	249	39	100	99
560	29-37	3622	0,60	0,03189	0,00064	0,24487	0,00635	0,05570	0,00091	202	4	222	5	440	36	91	46
561	29-38	899		0,04085	0,00070	0,28925	0,00732	0,05135	0,00096	258	4	258	6	257	43	100	101
562	29-39	740		0,04155	0,00066	0,29777	0,00710	0,05198	0,00092	262	4	265	6	285	40	99	92
563	29-40	1437	0,41	0,02587	0,00046	0,19053	0,00461	0,05341	0,00088	165	3	177	4	346	37	93	48
564	29-41	1384	0,21	0,03268	0,00050	0,23893	0,00528	0,05302	0,00085	207	3	218	4	330	36	95	63
565	29-42	233	0,25	0,18713	0,00324	1,91796	0,04414	0,07433	0,00113	1106	18	1087	15	1051	31	102	105
566	29-43	764	0,56	0,03915	0,00062	0,29193	0,00760	0,05408	0,00112	248	4	260	6	375	47	95	66
567	29-44	651	0,51	0,03816	0,00063	0,26912	0,00703	0,05114	0,00103	241	4	242	6	247	46	100	98
568	29-45	801	0,42	0,03777	0,00062	0,26743	0,00680	0,05135	0,00100	239	4	241	5	257	45	99	93
569	29-46	916		0,03927	0,00058	0,27803	0,00644	0,05134	0,00091	248	4	249	5	256	41	100	97
570	29-47	864	0,42	0,08758	0,00142	0,77092	0,01953	0,06384	0,00124	541	8	580	11	737	41	93	73
571	29-48	861	0,15	0,03560	0,00056	0,25092	0,00625	0,05112	0,00099	226	3	227	5	246	44	99	92
572	29-49	1053		0,03445	0,00061	0,24012	0,00598	0,05055	0,00089	218	4	219	5	221	41	100	99
573	29-50	428		0,03726	0,00060	0,26262	0,00755	0,05112	0,00122	236	4	237	6	246	55	100	96
574	29-51	865	0,08	0,04006	0,00075	0,28134	0,00770	0,05093	0,00101	253	5	252	6	238	46	101	106
575	29-52	800		0,03734	0,00061	0,25980	0,00657	0,05047	0,00098	236	4	235	5	217	45	101	109
576	29-53	732	0,80	0,03836	0,00064	0,26946	0,00680	0,05095	0,00097	243	4	242	5	239	44	100	102
577	29-54	734	0,74	0,03774	0,00060	0,26496	0,00639	0,05092	0,00093	239	4	239	5	237	42	100	101
578	29-55	878	0,07	0,03831	0,00068	0,27086	0,00675	0,05128	0,00089	242	4	243	5	253	40	100	96
579	29-56	302	0,45	0,07440	0,00125	0,60024	0,01755	0,05851	0,00140	463	7	477	11	549	52	97	84
580	29-57	885	0,20	0,03918	0,00068	0,27461	0,00675	0,05084	0,00089	248	4	246	5	234	40	101	106
581	29-58	232		0,23772	0,00384	2,89526	0,06446	0,08833	0,00136	1375	20	1381	17	1390	29	100	99
582	29-60	446	0,09	0,03738	0,00067	0,26322	0,00697	0,05107	0,00100	237	4	237	6	244	45	100	97
583	29-61	752	0,04	0,03631	0,00063	0,25699	0,00636	0,05133	0,00091	230	4	232	5	256	41	99	90
584	29-62	568	0,71	0,03906	0,00065	0,28786	0,00754	0,05344	0,00108	247	4	257	6	348	46	96	71
585	29-63	846	0,18	0,03601	0,00058	0,25655	0,00581	0,05167	0,00082	228	4	232	5	271	37	98	84
586	29-64	809	0,42	0,03661	0,00058	0,26134	0,00673	0,05177	0,00105	232	4	236	5	275	46	98	84
587	29-65	284		0,03756	0,00067	0,27146	0,00879	0,05242	0,00141	238	4	244	7	304	61	97	78
588	29-66	243	0,60	0,06588	0,00129	0,52463	0,01495	0,05776	0,00119	411	8	428	10	521	45	96	79
589	29-67	336		0,09758	0,00165	0,85481	0,02142	0,06353	0,00118	600	10	627	12	726	39	96	83
590	29-68	368		0,07301	0,00138	0,56138	0,01868	0,05576	0,00153	454	8	452	12	443	61	100	103
591	29-69	910	0,49	0,03852	0,00079	0,27653	0,00772	0,05206	0,00098	244	5	248	6	288	43	98	85
592	29-70	853		0,03799	0,00059	0,27322	0,00623	0,05215	0,00088	240	4	245	5	292	38	98	82
593	29-71	706		0,03845	0,00062	0,27022	0,00733	0,05096	0,00111	243	4	243	6	239	50	100	102
594	29-72	1065	0,05	0,03436	0,00052	0,24611	0,00551	0,05195	0,00086	218	3	223	4	283	38	97	77
595	29-73	684	0,30	0,03917	0,00056	0,28061	0,00764	0,05196	0,00120	248	3	251	6	284	53	99	87
596	29-74	617	0,22	0,04417	0,00074	0,33056	0,00839	0,05428	0,00103	279	5	290	6	383	43	96	73
597	29-75	659		0,04230	0,00059	0,30216	0,00887	0,05181	0,00134	267	4	268	7	277	59	100	96
598	29-76	1156	0,37	0,02743	0,00049	0,20298	0,00559	0,05366	0,00112	174	3	188	5	357	47	93	49
599	29-77	867		0,04019	0,00053	0,28250	0,00648	0,05098	0,00096	254	3	253	5	240	43	101	106
600	29-78	933	0,01	0,03880	0,00054	0,27857	0,00645	0,05207	0,00096	245	3	250	5	289	42	98	85
601	29-79	834		0,03663	0,00052	0,25642	0,00641	0,05077	0,00105	232	3	232	5	231	48	100	101
602	29-80	712		0,03953	0,00071	0,27970	0,00799	0,05131	0,00114	250	4	250	6	255	51	100	98
603	29-81	1585	0,05	0,03262	0,00046	0,24014	0,00539	0,05340	0,00094	207	3	219	4	346	40	95	60
604	29-82	813		0,03784	0,00058	0,26438	0,00612	0,05067	0,00088	239	4	238	5	226	40	101	106
605	29-83	999	0,37	0,03491	0,00054	0,24508	0,00537	0,05092	0,00079	221	3	223	4	237	36	99	93
606	29-84	961		0,03914	0,00063	0,28061	0,00683	0,05199	0,00095	248	4	251	5	285	42	99	87
607	29-85	572	0,92	0,03626	0,00059	0,25297	0,00619	0,05060	0,00093	230	4	229	5	223	42	100	103
608	29-86	977	0,81	0,07258	0,00117	0,60200	0,01763	0,06016	0,00147	452	7	479	11	609	53	94	74
609	29-87	682	0,09	0,03667	0,00063	0,26229	0,00665	0,05188	0,00097	232	4	237	5	280	43	98	83
610	29-88	931	0,64	0,03805	0,00060	0,26972	0,00640	0,05140	0,00091	241	4	242	5	259	41	99	93
611	29-89	900	0,32	0,03733	0,00061	0,26135	0,00630	0,05077	0,00089	236	4	236	5	231	41	100	103
612	29-90	108		0,13642	0,00216	1,22767	0,02944	0,06527	0,00117	824	12	813	13	783	38	101	105
613	29-91	1132	0,62	0,03788	0,00092	0,27347	0,00877	0,05237	0,00109	240	6	245	7	302	48	98	79
614	29-92	447	0,04	0,03822	0,00056	0,27605	0,00941	0,05238	0,00161	242	3	248	7	302	70	98	80

Table C.2 Continued

#	Spot	U [ppm]	f206%	Isotope ratios						Ages (Ma)						Data filter A*	Data filter B#
				$^{206}Pb/^{238}U$	±2σ	$^{207}Pb/^{235}U$	±2σ	$^{207}Pb/^{206}Pb$	±2σ	$^{206}Pb/^{238}U$	±2σ	$^{207}Pb/^{235}U$	±2σ	$^{207}Pb/^{206}Pb$	±2σ		
615	29-93	770	0,01	0,04054	0,00059	0,28678	0,00896	0,05130	0,00142	256	4	256	7	254	64	100	101
616	29-94	774		0,03730	0,00056	0,25939	0,00803	0,05044	0,00137	236	3	234	6	215	63	101	110
617	29-95	952		0,03694	0,00055	0,25853	0,00831	0,05076	0,00145	234	3	233	7	230	66	100	102
618	29-96	489		0,03834	0,00055	0,27230	0,00897	0,05151	0,00153	243	3	245	7	264	68	99	92
619	29-97	473	0,17	0,03963	0,00067	0,27922	0,00984	0,05110	0,00158	251	4	250	8	245	71	100	102
620	29-98	515		0,03813	0,00058	0,26955	0,00911	0,05128	0,00155	241	4	242	7	253	69	100	95
621	29-99	627		0,04052	0,00058	0,29033	0,00992	0,05197	0,00161	256	4	259	8	284	71	99	90
622	29-100	784		0,03713	0,00053	0,26116	0,00805	0,05101	0,00139	235	3	236	6	242	63	100	97

T14-30: Ardıçlı Formation

#	Spot	U [ppm]	f206%	Isotope ratios						Ages (Ma)						Data filter A*	Data filter B#
				$^{206}Pb/^{238}U$	±2σ	$^{207}Pb/^{235}U$	±2σ	$^{207}Pb/^{206}Pb$	±2σ	$^{206}Pb/^{238}U$	±2σ	$^{207}Pb/^{235}U$	±2σ	$^{207}Pb/^{206}Pb$	±2σ		
623	30-2	2494	1,83	0,03409	0,00082	0,23603	0,00797	0,05022	0,00118	216	5	215	7	205	55	100	105
624	30-3	3273	0,16	0,03329	0,00100	0,24448	0,00901	0,05326	0,00113	211	6	222	7	340	48	95	62
625	30-5	2488	0,07	0,03617	0,00057	0,25594	0,00540	0,05131	0,00072	229	4	231	4	255	32	99	90
626	30-6	2631	0,09	0,03845	0,00061	0,27529	0,00586	0,05192	0,00074	243	4	247	5	282	32	99	86
627	30-7	2251	0,16	0,03791	0,00092	0,27360	0,00798	0,05234	0,00085	240	6	246	6	300	37	98	80
628	30-8	2972	1,80	0,02994	0,00055	0,20704	0,00787	0,05016	0,00167	190	3	191	7	202	77	100	94
629	30-9	2307	0,09	0,04025	0,00067	0,28544	0,00646	0,05144	0,00078	254	4	255	5	261	35	100	98
630	30-10	1921	0,23	0,04117	0,00072	0,29203	0,00718	0,05144	0,00089	260	4	260	6	261	40	100	100
631	30-13	2359	0,51	0,02432	0,00065	0,18387	0,00644	0,05483	0,00125	155	4	171	6	405	51	90	38
632	30-14	2618	0,23	0,03597	0,00069	0,25633	0,00651	0,05168	0,00085	228	4	232	5	271	38	98	84
633	30-16	2642	0,44	0,03755	0,00076	0,28217	0,00878	0,05450	0,00129	238	5	252	7	392	53	94	61
634	30-17	497	0,26	0,09738	0,00163	0,80565	0,02420	0,06000	0,00150	599	10	600	14	604	54	100	99
635	30-19	2178	1,15	0,03381	0,00093	0,24082	0,00898	0,05166	0,00130	214	6	219	7	270	58	98	79
636	30-20	2182	0,63	0,03441	0,00064	0,26861	0,00775	0,05662	0,00124	218	4	242	6	477	49	90	46
637	30-21	2491	1,10	0,03253	0,00054	0,22551	0,00639	0,05027	0,00115	206	3	206	5	208	53	100	99
638	30-22	2459	0,03	0,04013	0,00075	0,28968	0,00772	0,05235	0,00100	254	5	258	6	301	44	98	84
639	30-23	2425	0,09	0,03944	0,00066	0,28260	0,00682	0,05197	0,00090	249	4	253	5	284	40	99	88
640	30-25	2652	0,16	0,03445	0,00062	0,24645	0,00583	0,05188	0,00080	218	4	224	5	280	35	98	78
641	30-26	2217	0,41	0,03214	0,00088	0,23998	0,00826	0,05416	0,00113	204	5	218	7	378	47	93	54
642	30-27	2165	1,15	0,02772	0,00056	0,17777	0,01087	0,04652	0,00269	176	3	166	9	24	79	106	720
643	30-28	2633	0,05	0,03876	0,00064	0,27918	0,00630	0,05224	0,00081	245	4	250	5	296	35	98	83
644	30-29	2269	0,06	0,03787	0,00063	0,26835	0,00563	0,05139	0,00065	240	4	241	5	258	29	99	93
645	30-30	1676	0,33	0,04074	0,00070	0,31564	0,00829	0,05618	0,00112	257	4	279	6	460	44	92	56
646	30-31	2915	0,56	0,03831	0,00068	0,30008	0,00865	0,05682	0,00129	242	4	266	7	484	50	91	50
647	30-32	1511	0,23	0,04197	0,00077	0,30578	0,00823	0,05284	0,00104	265	5	271	6	322	45	98	82
648	30-33	1752	0,45	0,04049	0,00077	0,30423	0,00859	0,05449	0,00114	256	5	270	7	391	47	95	65
649	30-34	2029		0,04020	0,00072	0,28667	0,00685	0,05172	0,00082	254	4	256	5	273	36	99	93
650	30-35	2239	1,15	0,03136	0,00090	0,21510	0,00983	0,04975	0,00177	199	6	198	8	183	83	101	109
651	30-36	2907	0,09	0,03882	0,00079	0,27508	0,00724	0,05140	0,00086	245	5	247	6	259	39	99	95
652	30-37	1861	1,25	0,03951	0,00084	0,27830	0,01293	0,05109	0,00211	250	5	249	10	245	95	100	102
653	30-38	2781	0,55	0,03729	0,00065	0,28526	0,00788	0,05549	0,00118	236	4	255	6	432	48	93	55
654	30-39	2645	1,61	0,02528	0,00056	0,16851	0,00984	0,04835	0,00261	161	4	158	9	116	120	102	138
655	30-40	3608	0,32	0,03378	0,00079	0,25514	0,00793	0,05478	0,00112	214	5	231	6	403	46	93	53
656	30-41	3218	0,21	0,03398	0,00062	0,24601	0,00629	0,05250	0,00093	215	4	223	5	307	41	96	70
657	30-42	3339	0,12	0,03709	0,00059	0,26828	0,00565	0,05246	0,00073	235	4	241	5	306	32	97	77
658	30-43	2783	0,11	0,03993	0,00069	0,28196	0,00618	0,05121	0,00069	252	4	252	5	250	31	100	101
659	30-44	2630	0,27	0,03523	0,00068	0,25872	0,00640	0,05326	0,00082	223	4	234	5	340	35	96	66
660	30-45	1314		0,03956	0,00072	0,28365	0,00678	0,05200	0,00081	250	4	254	5	285	36	99	88
661	30-46	1989	0,27	0,04110	0,00062	0,30116	0,00600	0,05314	0,00069	260	4	267	5	335	30	97	78
662	30-47	1757	0,03	0,04080	0,00086	0,29114	0,00803	0,05175	0,00092	258	5	259	6	275	41	99	94
663	30-48	2156	0,34	0,04099	0,00080	0,30373	0,00820	0,05374	0,00100	259	5	269	6	360	42	96	72
664	30-49	1795	0,49	0,03958	0,00090	0,29774	0,00945	0,05456	0,00121	250	6	265	7	394	50	95	63
665	30-50	1912	0,59	0,03649	0,00069	0,27311	0,00755	0,05428	0,00110	231	4	245	6	383	45	94	60
666	30-51	268		0,15006	0,00303	1,37889	0,03863	0,06664	0,00130	901	17	880	16	827	41	102	109
667	30-52	2416	0,15	0,03954	0,00083	0,28118	0,00751	0,05158	0,00086	250	5	252	6	267	38	99	94
668	30-53	1036		0,04226	0,00083	0,29777	0,00769	0,05110	0,00086	267	5	265	6	245	39	101	109
669	30-54	3030	0,11	0,03418	0,00072	0,25018	0,00673	0,05308	0,00090	217	4	227	5	332	38	96	65
670	30-55	1719	1,22	0,03604	0,00120	0,24607	0,01296	0,04952	0,00202	228	7	223	11	173	95	102	132
671	30-57	2488	1,61	0,03258	0,00090	0,23579	0,01454	0,05249	0,00290	207	6	215	12	307	126	96	67
672	30-58	1120	1,75	0,04151	0,00083	0,29478	0,01561	0,05151	0,00253	262	5	262	12	264	113	100	99
673	30-59	2742	0,18	0,04165	0,00079	0,30186	0,00726	0,05257	0,00078	263	5	268	6	310	34	98	85
674	30-60	2033	0,76	0,04035	0,00076	0,32047	0,00910	0,05760	0,00123	255	5	282	7	515	47	90	50
675	30-61	2961	0,26	0,03792	0,00080	0,27902	0,00717	0,05336	0,00079	240	5	250	6	344	33	96	70
676	30-62	2001	1,36	0,03610	0,00082	0,25455	0,00738	0,05115	0,00091	229	5	230	6	247	41	99	92
677	30-63	2176	0,58	0,03792	0,00088	0,29472	0,01409	0,05637	0,00235	240	5	262	11	467	93	91	51
678	30-65	196	0,09	0,07543	0,00183	0,58314	0,02046	0,05607	0,00142	469	11	466	13	455	56	100	103
679	30-66	2944	0,18	0,03087	0,00080	0,22454	0,00708	0,05276	0,00095	196	5	206	6	319	41	95	61
680	30-67	3065	0,22	0,03323	0,00076	0,23813	0,00691	0,05197	0,00092	211	5	217	6	284	41	97	74
681	30-68	2727	0,80	0,02968	0,00069	0,22736	0,00658	0,05556	0,00097	189	4	208	5	435	39	91	43
682	30-69	1740	0,20	0,03866	0,00090	0,27784	0,00828	0,05212	0,00097	245	6	249	7	291	43	98	84
683	30-70	1581	1,80	0,03922	0,00107	0,28971	0,01198	0,05357	0,00167	248	7	258	9	353	70	96	70
684	30-71	2202	0,26	0,03838	0,00103	0,27569	0,00927	0,05210	0,00106	243	6	247	7	290	46	98	84
685	30-72	3077	0,38	0,03480	0,00077	0,25412	0,00732	0,05296	0,00097	221	5	230	6	327	42	96	67
686	30-73	2780	1,59	0,02639	0,00066	0,18437	0,00823	0,05067	0,00188	168	4	172	7	226	86	98	74
687	30-74	1984	0,10	0,03856	0,00087	0,27685	0,00792	0,05207	0,00091	244	5	248	6	288	40	98	85
688	30-75	2001	1,41	0,03676	0,00088	0,25606	0,00892	0,05052	0,00128	233	5	231	7	219	59	101	106
689	30-76	2066	0,09	0,03199	0,00101	0,22955	0,00889	0,05204	0,00116	203	6	210	7	287	51	97	71
690	30-77	2335	0,67	0,04044	0,00099	0,30926	0,01051	0,05546	0,00130	256	6	274	8	431	52	93	59
691	30-79	2576	0,86	0,03491	0,00085	0,27416	0,00928	0,05696	0,00134	221	5	246	7	490	52	90	45
692	30-80	3244	2,22	0,03467	0,00088	0,24132	0,01072	0,05048	0,00184	220	5	219	9	217	85	100	101
693	30-81	2165	0,89	0,04039	0,00102	0,31955	0,01120	0,05738	0,00140	255	6	282	9	506	54	91	50
694	30-82	2558	0,10	0,03572	0,00125	0,25336	0,01350	0,05144	0,00206	226	8	229	11	261	92	99	87
695	30-83	2093	0,25	0,03810	0,00098	0,27408	0,00918	0,05218	0,00112	241	6	246	7	293	49	98	82
696	30-84	2549	0,10	0,03354	0,00082	0,23908	0,00768	0,05169	0,00108	213	5	218	6	272	48	98	78
697	30-85	2235	0,17	0,03746	0,00059	0,27104	0,00661	0,05248	0,00097	237	4	244	5	306	42	97	77
698	30-86	2334	0,06	0,04291	0,00067	0,30197	0,00737	0,05104	0,00096	271	4	268	6	243	43	101	112
699	30-87	3075	0,62	0,03715	0,00061	0,28941	0,00884	0,05650	0,00145	235	4	258	7	472	57	91	50
700	30-88	1958	0,48	0,03973	0,00072	0,29625	0,00800	0,05408	0,00109	251	4	263	6	375	45	95	67
701	30-89	1866	0,35	0,02167	0,00053	0,16041	0,00576	0,05369	0,00140	138	3	151	5	358	59	91	39

Table C.2 Continued

#	Spot	U [ppm]	f206%	Isotope ratios						Ages (Ma)						Data filter A*	Data filter B#
				$^{206}Pb/^{238}U$	±2σ	$^{207}Pb/^{235}U$	±2σ	$^{207}Pb/^{206}Pb$	±2σ	$^{206}Pb/^{238}U$	±2σ	$^{207}Pb/^{235}U$	±2σ	$^{207}Pb/^{206}Pb$	±2σ		
702	30-90	2232		0,03962	0,00057	0,28303	0,00686	0,05182	0,00101	250	4	253	5	277	45	99	90
703	30-91	2968	2,88	0,02967	0,00067	0,20670	0,00769	0,05052	0,00150	189	4	191	6	219	69	99	86
704	30-92	2933	0,12	0,03480	0,00109	0,25018	0,01154	0,05215	0,00176	220	7	227	9	292	77	97	76
705	30-93	2268	0,13	0,03877	0,00079	0,28751	0,00846	0,05378	0,00115	245	5	257	7	362	48	96	68
706	30-95	1509	0,35	0,04283	0,00070	0,32166	0,00783	0,05447	0,00099	270	4	283	6	391	41	95	69
707	30-96	1950	0,02	0,03644	0,00067	0,26031	0,00704	0,05181	0,00103	231	4	235	6	277	45	98	83
708	30-97	2363	0,49	0,03847	0,00072	0,29640	0,00817	0,05588	0,00113	243	4	264	6	448	45	92	54
709	30-98	2053	0,51	0,02987	0,00082	0,22909	0,00771	0,05563	0,00107	190	5	209	6	438	43	91	43
710	30-99	2780	1,48	0,03358	0,00094	0,23722	0,01615	0,05124	0,00318	213	6	216	13	252	143	98	85
711	30-100	2014	0,63	0,03620	0,00063	0,28137	0,01058	0,05638	0,00188	229	4	252	8	467	74	91	49
712	30-101	2110	0,72	0,03637	0,00056	0,28402	0,00735	0,05663	0,00118	230	3	254	6	477	46	91	48
713	30-102	1506		0,03963	0,00068	0,27927	0,00643	0,05111	0,00079	251	4	250	5	246	36	100	102

Table C.3: Composition of detrital rutiles from the Konya Complex

No.	Sample	Nb2O5	Al2O3	Cr2O3	TiO2	ZrO2	SnO2	SiO2	FeO	V2O3	WO3	Total
1	T14-20B	0.01	0.14	0.03	98.51	0.02	0.01	0.21	0.23	0.12	0.02	99.31
2	T14-20B	0.14	0.08	<0.003	97.63	0.01	<0.007	0.57	0.50	0.05	<0.010	98.98
3	T14-20B	0.29	0.04	0.08	99.02	0.07	0.01	0.06	0.22	0.20	0.01	100.00
4	T14-20B	0.22	0.02	0.13	98.91	0.01	0.01	0.03	0.21	0.31	<0.010	99.85
5	T14-20B	0.31	0.02	0.07	97.71	0.08	0.01	0.09	0.22	0.45	0.06	99.03
6	T14-20B	0.12	0.02	0.04	99.26	0.04	0.02	0.06	0.22	0.34	<0.010	100.10
7	T14-20B	0.12	0.87	0.04	96.98	0.02	<0.007	1.08	0.30	0.04	<0.010	99.46
8	T14-20B	0.14	0.13	0.02	98.17	0.02	0.01	0.25	0.66	0.06	0.01	99.47
9	T14-20B	0.23	0.02	0.02	98.85	0.10	<0.007	0.10	0.30	0.16	<0.010	99.76
10	T14-20B	0.08	0.04	0.05	98.58	0.01	0.02	0.04	0.33	0.09	0.01	99.24
11	T14-20B	0.14	0.03	0.11	98.64	0.01	0.02	0.05	0.24	0.12	0.04	99.40
12	T14-20B	0.01	0.02	0.05	99.16	0.15	0.01	0.04	0.20	0.27	<0.010	99.90
13	T14-20B	0.23	0.04	0.20	98.20	0.05	0.01	0.14	0.24	0.09	<0.010	99.21
14	T14-20B	0.89	0.06	0.06	97.32	0.04	0.02	0.07	0.62	0.16	0.02	99.27
15	T14-20B	0.26	0.03	0.07	98.81	0.14	0.01	0.06	0.18	0.32	<0.010	99.88
16	T14-20B	0.04	0.03	0.04	98.68	0.03	<0.007	0.03	0.26	0.09	0.01	99.20
17	T14-20B	0.20	0.16	0.05	98.01	<0.005	<0.007	0.52	0.32	0.11	<0.010	99.37
18	T14-20B	0.69	0.05	0.10	97.01	0.04	<0.007	0.08	0.49	0.12	<0.010	98.58
19	T14-20B	0.39	0.02	0.29	97.69	0.01	0.01	0.03	0.21	0.32	0.02	98.99
20	T14-20B	0.19	0.07	0.06	98.31	0.02	0.01	0.07	0.29	0.15	<0.010	99.17
21	T14-20B	0.07	0.05	0.06	99.13	0.02	<0.007	0.07	0.25	0.04	<0.010	99.70
22	T14-20B	0.51	0.04	0.03	98.48	<0.005	0.04	0.02	0.44	0.11	0.01	99.67
23	T14-20B	0.17	0.50	0.59	95.84	<0.005	0.02	0.69	0.63	0.16	<0.010	98.60
24	T14-31	0.02	0.05	0.02	99.22	0.01	<0.007	0.10	0.20	0.22	<0.010	99.83
25	T14-31	0.16	0.03	0.13	98.87	0.13	0.01	0.07	0.15	0.38	0.06	99.99
26	T14-31	0.06	0.01	0.16	99.56	0.03	<0.007	0.04	0.11	0.37	<0.010	100.34
27	T14-31	0.16	0.08	0.14	97.43	0.10	0.02	0.92	0.12	0.50	0.03	99.50
28	T14-31	0.29	0.05	0.06	99.11	0.05	0.02	0.03	0.43	0.27	<0.010	100.31
29	T14-31	0.47	0.01	0.19	98.48	0.05	0.02	0.06	0.25	0.27	0.09	99.90
30	T14-31	0.32	0.01	0.23	97.73	0.32	<0.007	0.01	0.11	0.62	<0.010	99.35
31	T14-31	0.08	0.01	<0.003	100.90	0.11	0.01	0.02	0.12	0.38	<0.010	101.64
32	T14-31	0.02	0.01	0.06	99.60	0.02	<0.007	0.02	0.24	0.17	<0.010	100.16
33	T14-31	0.12	0.02	0.01	99.29	0.07	0.01	0.03	0.32	0.14	0.01	100.01
34	T14-31	0.43	0.01	0.09	98.57	0.06	0.01	0.05	0.22	0.28	<0.010	99.72
35	T14-31	0.17	0.02	0.01	98.79	0.03	0.04	0.03	0.36	0.11	<0.010	99.57
36	T14-31	0.20	0.02	0.05	98.13	0.10	0.01	0.10	0.15	0.45	<0.010	99.22
37	T14-31	0.06	0.02	0.10	98.91	0.04	<0.007	0.02	0.30	0.10	0.08	99.64
38	T14-31	<0.007	0.01	0.02	97.93	0.01	<0.007	0.09	0.26	0.14	<0.010	98.47
39	T14-31	0.16	0.22	0.12	96.72	0.07	<0.007	0.44	0.39	0.11	0.01	98.23
40	T14-31	0.63	0.02	0.04	98.83	0.03	0.02	0.04	0.43	0.07	<0.010	100.13
41	T14-31	0.06	0.02	0.02	98.27	0.03	0.01	0.03	0.28	0.22	<0.010	98.94
42	T14-31	0.06	0.02	0.17	98.31	0.04	<0.007	0.03	0.22	0.20	<0.010	99.04
43	T14-31	0.10	0.01	0.40	98.39	0.04	<0.007	0.03	0.19	0.08	0.03	99.27
44	T14-31	0.45	0.02	0.06	97.04	0.02	0.02	0.07	0.33	0.21	0.03	98.24
45	T14-31	1.03	0.03	0.21	96.18	0.16	0.01	0.04	0.46	0.15	0.02	98.30
46	T14-31	0.19	0.42	0.28	95.89	0.05	<0.007	0.68	0.89	0.06	0.01	98.48
47	T14-31	0.16	0.02	0.06	98.59	0.02	0.02	0.03	0.21	0.21	0.01	99.32
48	T14-31	0.37	0.01	0.10	98.04	0.04	<0.007	0.02	0.22	0.30	<0.010	99.11
49	T14-22	0.16	0.06	0.02	97.81	<0.005	0.02	0.14	0.73	0.05	<0.010	98.97
50	T14-22	0.17	0.07	0.03	98.35	<0.005	0.02	0.18	0.73	0.04	<0.010	99.59
51	T14-22	0.45	0.14	0.01	97.47	<0.005	<0.007	0.24	0.86	0.06	0.03	99.26
52	T14-22	0.11	0.05	0.01	97.26	<0.005	<0.007	0.14	0.85	0.09	0.01	98.52
53	T14-22	0.20	0.01	0.14	98.06	0.02	0.01	0.08	0.61	0.13	0.02	99.29
54	T14-22	0.33	0.08	0.01	98.01	<0.005	0.01	0.15	0.88	0.05	0.01	99.54
55	T14-22	0.35	0.16	0.02	97.08	<0.005	0.01	0.27	1.31	0.05	0.01	99.26
56	T14-22	0.19	0.07	0.06	98.43	<0.005	0.01	0.14	0.71	0.07	<0.010	99.66
57	T14-22	0.28	0.06	0.02	97.39	0.01	0.01	0.18	0.73	0.08	<0.010	98.74
58	T14-22	0.10	0.07	0.01	98.31	<0.005	0.01	0.15	0.71	0.05	0.01	99.43
59	T14-22	0.15	0.06	0.01	98.11	0.01	<0.007	0.14	0.63	0.07	<0.010	99.19
60	T14-22	0.33	0.06	0.02	97.71	<0.005	0.02	0.15	0.82	0.05	0.01	99.18
61	T14-22	0.11	0.16	0.01	97.11	<0.005	<0.007	0.33	0.91	0.05	0.01	98.70
62	T14-22	0.28	0.01	0.22	98.26	0.09	0.02	0.02	0.66	0.41	0.06	100.04

Table C.3 Continued

No.	Sample	Nb2O5	Al2O3	Cr2O3	TiO2	ZrO2	SnO2	SiO2	FeO	V2O3	WO3	Total
63	T14-22	0.12	0.10	0.01	97.23	<0.005	<0.007	0.25	0.73	0.05	0.04	98.53
64	T14-22	0.17	0.08	0.01	98.21	<0.005	0.01	0.14	0.96	0.04	<0.010	99.63
65	T14-22	0.13	0.24	0.03	98.47	<0.005	<0.007	0.46	0.75	0.06	0.01	100.16
66	T14-22	0.07	0.08	0.01	98.02	<0.005	0.01	0.14	0.69	0.06	0.13	99.21
67	T14-22	0.23	0.01	0.05	98.30	<0.005	0.01	0.01	0.82	0.06	0.02	99.51
68	T14-22	0.59	0.05	0.02	97.43	0.09	0.01	0.14	0.94	0.09	0.01	99.36
69	T14-22	0.13	0.09	0.02	98.15	<0.005	0.01	0.21	0.65	0.07	0.01	99.33
70	T14-22	0.16	0.52	0.03	96.69	<0.005	0.01	0.79	1.27	0.06	0.05	99.59
71	T14-22	0.13	0.06	0.01	98.68	<0.005	<0.007	0.13	0.71	0.04	0.01	99.78
72	T14-22	0.10	0.10	0.01	98.95	0.02	<0.007	0.19	0.78	0.04	<0.010	100.20
73	T14-22	0.15	0.08	0.03	97.29	<0.005	<0.007	0.19	0.70	0.05	0.01	98.50
74	T14-22	0.17	0.21	0.04	96.75	<0.005	<0.007	0.27	1.34	0.09	0.10	98.99
75	T14-22	0.19	0.05	0.02	97.98	0.01	0.01	0.13	0.69	0.07	<0.010	99.13
76	T14-22	0.21	0.06	0.02	98.35	<0.005	<0.007	0.13	0.68	0.05	<0.010	99.51
77	T14-22	0.23	0.09	0.03	98.15	<0.005	0.01	0.21	0.82	0.05	0.01	99.61
78	T14-22	0.04	0.06	<0.003	99.02	0.02	<0.007	0.09	0.64	0.07	<0.010	99.94
79	T14-22	0.10	0.06	0.02	98.41	<0.005	<0.007	0.16	0.63	0.06	0.01	99.46
80	T14-22	0.16	0.08	0.03	97.93	0.01	0.01	0.23	0.85	0.05	0.05	99.39
81	T14-22	0.14	0.05	0.02	97.79	0.01	0.01	0.13	0.74	0.06	<0.010	98.96
82	T14-22	0.05	0.05	0.01	98.65	<0.005	<0.007	0.13	0.66	0.05	<0.010	99.60
83	T14-22	0.10	0.05	0.02	98.03	0.05	0.01	0.12	0.66	0.07	<0.010	99.11
84	T14-36	0.22	0.02	0.11	99.62	0.12	0.01	0.02	0.25	0.14	<0.010	100.50
85	T14-36	0.01	0.02	0.01	98.72	0.04	<0.007	0.11	0.17	0.17	0.06	99.31
86	T14-36	0.40	0.04	0.09	96.95	0.01	0.01	0.12	0.25	0.14	0.04	98.05
87	T14-36	0.33	0.02	0.11	97.89	0.04	0.01	0.04	0.23	0.19	<0.010	98.86
88	T14-36	0.01	0.01	0.21	97.47	0.01	<0.007	0.03	0.06	0.52	<0.010	98.35
89	T14-36	0.14	0.10	0.29	97.64	0.04	<0.007	0.03	0.12	0.19	0.02	98.57
90	T14-36	0.14	0.01	0.06	97.89	0.02	0.01	0.02	0.21	0.14	<0.010	98.50
91	T14-36	0.27	0.01	0.08	98.32	0.01	0.03	0.03	0.29	0.10	0.03	99.17
92	T14-36	0.16	0.02	0.02	97.91	0.01	<0.007	0.06	0.25	0.04	<0.010	98.48
93	T14-36	0.44	0.02	0.05	96.51	0.01	<0.007	0.56	0.32	0.08	0.03	98.03
94	T14-36	0.13	0.01	0.04	98.19	0.13	<0.007	0.07	0.19	0.19	<0.010	98.96
95	T14-36	0.05	0.01	0.56	98.52	0.01	0.02	0.07	0.07	0.12	<0.010	99.43
96	T14-36	0.43	0.01	0.17	97.02	0.01	0.02	0.04	0.20	0.25	0.01	98.16
97	T14-36	0.30	0.03	0.57	97.54	0.07	0.01	0.06	0.13	0.07	0.03	98.80
98	T14-36	0.03	0.02	0.01	99.58	0.12	<0.007	0.02	0.20	0.14	0.01	100.13
99	T14-36	0.07	0.01	0.03	98.94	0.08	<0.007	0.02	0.16	0.23	<0.010	99.55
100	T14-36	0.06	0.17	0.12	96.94	0.01	<0.007	0.81	0.23	0.11	<0.010	98.47
101	T14-36	0.09	0.01	0.02	99.44	0.03	0.01	0.02	0.18	0.11	<0.010	99.92
102	T14-36	0.21	0.01	0.23	99.26	0.12	<0.007	0.22	0.07	0.43	<0.010	100.55
103	T14-36	0.09	0.02	0.03	98.19	0.01	<0.007	0.02	0.21	0.08	<0.010	98.65
104	T14-36	0.05	0.01	0.34	98.77	0.06	0.01	0.03	0.11	0.33	0.05	99.77
105	T14-36	0.21	0.03	0.05	97.43	0.05	0.01	0.09	0.26	0.19	<0.010	98.31
106	T14-36	0.33	0.02	0.04	97.61	0.02	<0.007	0.04	0.31	0.07	<0.010	98.43
107	T14-36	0.32	0.02	0.05	97.65	0.02	<0.007	0.03	0.30	0.14	0.02	98.55
108	T14-36	0.08	0.05	0.06	97.77	<0.005	<0.007	0.12	0.22	0.10	<0.010	98.41
109	T14-36	0.04	0.01	0.01	97.88	0.01	<0.007	0.04	0.23	0.14	<0.010	98.37
110	T14-36	0.47	0.03	0.01	97.01	0.02	<0.007	0.10	0.38	0.03	<0.010	98.04
111	T14-39	0.03	0.01	0.09	99.26	0.01	<0.007	0.03	0.17	0.12	<0.010	99.71
112	T14-39	0.06	0.03	0.20	98.62	0.07	<0.007	0.14	0.17	0.12	0.02	99.43
113	T14-39	0.70	0.02	0.07	98.46	0.07	0.02	0.02	0.45	0.15	0.06	100.03
114	T14-39	0.05	0.01	<0.003	99.80	0.07	0.01	0.06	0.17	0.11	<0.010	100.29
115	T14-39	0.01	0.02	0.05	99.38	0.03	<0.007	0.08	0.17	0.15	<0.010	99.90
116	T14-39	0.02	0.04	0.07	99.26	0.02	<0.007	0.09	0.31	0.19	0.01	100.01
117	T14-39	0.02	0.01	0.26	98.86	0.02	0.01	0.04	0.12	0.10	<0.010	99.45
118	T14-39	0.05	0.02	<0.003	98.58	0.01	<0.007	0.03	0.35	0.16	0.52	99.73
119	T14-39	0.24	0.01	0.14	99.14	0.08	0.02	0.02	0.13	0.54	0.10	100.41
120	T14-39	0.01	0.01	0.05	99.38	0.02	<0.007	0.04	0.19	0.12	<0.010	99.82
121	T14-39	0.04	0.01	0.22	98.60	0.21	0.01	0.04	0.14	0.26	0.02	99.55
122	T14-39	0.13	0.04	0.14	97.92	0.02	<0.007	0.14	0.32	0.09	0.04	98.85
123	T14-39	0.41	0.02	0.09	99.13	0.08	0.01	0.04	0.29	0.18	0.06	100.30
124	T14-39	0.21	0.01	0.04	98.78	0.03	<0.007	0.07	0.20	0.26	<0.010	99.61

Table C.3 Continued

No.	Sample	Nb2O5	Al2O3	Cr2O3	TiO2	ZrO2	SnO2	SiO2	FeO	V2O3	WO3	Total
125	T14-39	0.10	0.02	0.06	98.38	0.12	<0.007	0.04	0.19	0.16	<0.010	99.06
126	T14-39	0.05	0.03	0.02	97.17	<0.005	<0.007	0.60	0.17	0.11	<0.010	98.14
127	T14-39	0.12	0.01	0.20	98.53	0.06	0.03	0.04	0.12	0.58	0.09	99.78
128	T14-39	0.04	0.01	0.03	100.15	0.09	0.03	0.03	0.15	0.31	<0.010	100.85
129	T14-39	0.35	0.02	0.14	97.95	0.01	0.02	0.43	0.24	0.20	0.08	99.42
130	T14-39	0.01	0.01	0.01	99.66	0.02	<0.007	0.04	0.20	0.12	<0.010	100.08
131	T14-39	0.11	0.03	0.10	98.26	0.01	<0.007	0.26	0.17	0.09	0.04	99.08
132	T14-39	0.18	0.01	0.15	96.67	0.02	<0.007	0.68	0.13	0.17	<0.010	98.03
133	T14-39	0.13	0.01	0.01	97.46	0.04	<0.007	0.02	0.23	0.14	<0.010	98.05
134	T14-39	0.04	0.01	0.58	98.05	0.07	<0.007	0.03	0.07	0.15	<0.010	99.01
135	T14-39	0.20	0.01	<0.003	98.27	0.08	<0.007	0.05	0.21	0.14	<0.010	98.98
136	T14-39	0.08	0.02	0.05	98.91	0.06	<0.007	0.02	0.17	0.11	<0.010	99.42
137	T14-39	<0.007	0.02	0.17	99.13	0.03	<0.007	0.10	0.15	0.09	<0.010	99.69
138	T14-39	0.26	0.01	0.09	99.34	<0.005	<0.007	0.02	0.21	0.24	0.01	100.19
139	T14-39	0.01	0.01	0.25	99.12	0.02	<0.007	0.05	0.12	0.12	<0.010	99.71
140	T14-39	0.04	0.01	0.46	98.40	0.01	0.01	0.01	0.10	0.14	<0.010	99.19
141	T14-39	0.03	0.03	0.28	98.79	0.02	<0.007	0.10	0.12	0.09	0.02	99.47
142	T14-39	0.04	0.01	0.07	98.85	0.01	0.01	0.02	0.12	0.25	<0.010	99.39
143	T14-39	0.26	0.24	0.19	97.26	0.05	0.01	0.57	0.20	0.14	0.03	98.94
144	T14-39	0.01	0.01	0.59	99.05	0.03	<0.007	0.01	0.08	0.12	<0.010	99.92
145	T14-39	0.04	0.01	0.24	98.98	0.01	<0.007	0.02	0.13	0.16	<0.010	99.60
146	T14-39	0.03	0.01	0.05	98.83	0.02	<0.007	0.03	0.17	0.14	<0.010	99.27
147	T14-39	0.93	0.02	0.24	97.73	0.04	0.01	0.02	0.35	0.24	<0.010	99.57
148	T14-39	0.04	0.03	0.08	98.92	0.01	0.01	0.08	0.15	0.12	<0.010	99.42
149	T14-29	0.50	0.01	0.05	98.09	0.01	<0.007	0.02	0.51	0.09	0.02	99.29
150	T14-29	0.51	0.17	0.01	95.95	0.06	0.01	0.38	1.10	0.09	0.08	98.37
151	T14-29	0.05	0.01	0.04	99.20	0.03	<0.007	0.03	0.53	0.15	0.03	100.07
152	T14-29	0.61	0.03	0.06	97.82	0.01	0.01	0.05	0.45	0.10	0.04	99.19
153	T14-29	0.49	0.07	0.02	97.53	0.06	0.04	0.15	0.87	0.14	0.09	99.46
154	T14-29	0.17	0.16	0.11	98.95	0.01	0.01	0.29	0.40	0.29	<0.010	100.38
155	T14-29	0.01	0.01	<0.003	101.37	0.07	<0.007	0.03	0.32	0.21	0.01	102.03
156	T14-29	0.05	0.01	0.08	99.41	0.02	<0.007	0.05	0.53	0.06	0.02	100.25
157	T14-29	0.27	0.15	0.03	94.42	0.07	<0.007	0.30	3.31	0.06	0.04	98.63
158	T14-29	0.12	0.01	0.09	98.61	0.12	<0.007	0.02	0.40	0.71	<0.010	100.08
159	T14-29	0.11	0.07	0.05	98.72	0.04	0.02	0.22	0.43	0.32	0.02	100.00
160	T14-29	0.35	0.01	0.04	97.90	0.06	0.08	0.03	0.62	0.09	0.02	99.17
161	T14-29	0.21	0.18	0.06	95.38	0.06	0.01	0.75	1.76	0.07	0.02	98.49
162	T14-29	0.12	0.03	0.05	98.15	0.02	0.01	0.07	0.54	0.14	<0.010	99.11
163	T14-29	0.14	0.05	0.02	96.87	<0.005	0.01	0.13	0.94	0.05	0.02	98.23
164	T14-29	0.10	0.01	0.07	98.34	0.02	<0.007	0.01	0.43	0.12	<0.010	99.11
165	T14-29	0.41	0.01	0.03	98.92	0.04	0.01	0.02	0.35	0.20	0.01	99.99
166	T14-29	0.10	0.01	0.10	98.96	0.02	0.01	0.03	0.23	0.24	<0.010	99.69
167	T14-29	0.12	0.18	0.16	96.42	0.12	0.01	0.28	0.43	0.34	<0.010	98.06
168	T14-29	1.26	0.01	0.03	96.76	0.03	0.02	0.02	1.18	0.16	0.10	99.56
169	T14-29	0.17	0.01	0.17	98.84	0.02	0.02	0.02	0.24	0.35	0.02	99.85
170	T14-29	0.17	<0.002	0.31	98.22	0.27	<0.007	0.01	0.16	0.60	0.01	99.75
171	T14-29	0.52	0.01	0.07	97.10	0.12	0.02	0.03	0.34	0.23	0.02	98.46
172	T14-29	0.31	0.03	0.01	98.15	0.01	0.01	0.06	0.55	0.19	<0.010	99.34
173	T14-29	0.54	0.04	0.12	97.59	0.15	<0.007	0.21	0.39	0.32	0.04	99.39
174	T14-29	0.40	0.17	<0.003	96.10	0.06	0.01	0.46	1.04	0.10	0.05	98.38
175	T14-29	0.11	0.16	0.01	97.10	0.31	<0.007	0.81	0.70	0.04	0.01	99.24
176	T14-29	0.28	0.01	0.02	97.77	0.03	<0.007	0.06	0.62	0.10	<0.010	98.89
177	T14-29	0.17	0.01	0.57	97.74	0.15	0.01	0.04	0.35	0.44	0.03	99.52
178	T14-29	<0.007	0.01	0.36	99.44	0.01	<0.007	0.02	0.11	0.13	<0.010	100.08

Table C.4: Operating conditions for EMPA

Rutile	***Acc. voltage: 25 kV***	***Beam Diameter: 10 µm***	***Beam current: 80 nA***
Spectrometer	**Element (line)**	**Count time**	**Backgr.**	**Standard**
1 PETJ	Nb (Lα)	200	100	Nb_metallic
2 TAP	Si (Kα)	100	50	$ZrSiO_4$
5 PETH	Zr (Lα)	200	100	$ZrSiO_4$
1 PETJ	Sn (Lα)	100	50	Cassiterite
2 TAP	Al (Kα)	200	100	Al_2O_3
4 LIF	V (Kα)	200	100	V_metallic
3 LIF	Cr (Kα)	200	100	Cr_2O_3
3 LIF	Fe (Kα)	100	50	Hematite